Ecological vectors of carbon and biomineral export in the Southern Ocean

Mathieu Rembauville

Université Pierre et Marie Curie

Ecole Doctorale des Sciences de l'Environnement d'Ile-de-France

Laboratoire d'Océanographie Microbienne (UMR 7621)

Ecological vectors of carbon and biomineral export in the Southern Ocean
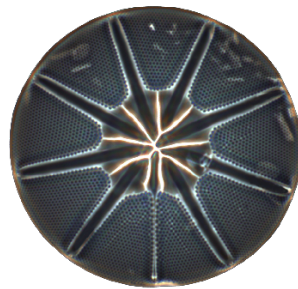
Par **Mathieu Rembauville**

Thèse de Doctorat en Océanographie Biogéochimique

Dirigée par **Ian Salter** et **Stéphane Blain**

Présentée et soutenue publiquement le 20 Septembre 2016

Devant un jury composé de:

Stephanie Henson	NOC, Southampton, Angleterre	Rapporteur
Christine Klaas	AWI, Bremerhaven, Allemagne	Rapporteur
Damien Cardinal	LOCEAN, Paris, France	Président
Tom Trull	CSIRO, Hobart, Australie	Examinateur
Bernard Quéguiner	MIO, Marseille, France	Examinateur
Ian Salter	AWI, Bremerhaven, Allemagne	Directeur de thèse
Stéphane Blain	LOMIC, Banyuls, France	Directeur de thèse

Remerciements

J'adresse mes sincères remerciements au jury de thèse qui a bien voulu évaluer mon travail. Thanks to Christine Klaas and Stephanie Henson for examining the manuscript. Merci à Bernard Quéguiner et Tom Trull qui ont suivi l'avancée de mon travail au cours des comités de thèse et ont toujours été de très bon conseil, ouvrant systématiquement de nouvelles pistes de réflexion. Merci à Damien Cardinal qui suit mes avancées depuis le master et qui a accepté de présider le jury de thèse.

J'ai bénéficié pendant ces trois années de thèse d'un encadrement optimal qui aura toujours entretenu ma motivation et une part de challenge. Réunissez l'expérience d'un professeur en océanographie et le dynamisme d'un jeune chercheur, et vous obtenez le meilleur mélange qu'un étudiant de thèse puisse espérer. Stéphane, merci pour ta grande expérience, ton écoute, tes conseils, ton franc-parler qui fait avancer les choses. Ian, thank you for your efficiency, your numerous ideas s^{-1}, and your continuous support throughout these 3 years. Distance has never been an issue! Ian and Stéphane, it was a real pleasure to learn so much from you.

Ce travail de thèse n'aurait jamais été possible sans les multiples collaborations fructueuses qui l'ont jalonné. Claire, merci de m'avoir accueilli et encadré au sein de l'équipe OISO le temps d'une campagne dans l'Océan Austral. Bernard, merci de m'avoir reçu à Marseille et de m'avoir appris à compter mes premières diatomées. Leanne, thank you for passing on your passion for diatoms to me, I hope I learned at least few percents of your taxonomic skills. Patrizia, thank you for your warm welcome in your wonderful lab in Barcelona. My visits were short but definitively productive. Ralph, it was a pleasure to work in your lab in Angers. Thank you for your precious time. Clara, thank you for your confidence, it was a great opportunity to work on the South Georgia samples. I sincerely hope that I'll have the opportunity to work again with all of you in the future.

Quand il s'agit de mettre les mains dans la science, les ingénieurs et techniciens sont la source intarissable d'un savoir-faire essentiel. Nathalie, c'est avec toi que j'ai passé mes premiers échantillons de piège au CHN dès le stage M1. Merci pour ta gentillesse et ta patience. Merci Louise, experte dans l'analyse des sels nutritifs, de m'avoir transmis une partie de tes connaissances. Merci Jocelyne, d'avoir enduré avec moi les 6 mètres de creux à bord du Suroît et d'avoir toujours été disponible pour la moindre question au labo. Merci Isabelle pour les conseils de traitements CTD et l'aide dans les calculs de turbulence. Merci Olivier, de m'avoir laissé jouer avec le vieux et susceptible Skalar. Merci Audrey, toujours de bon conseil, d'être allé récupérer ces pièges au milieu de l'Austral. Merci à tous de m'avoir guidé dans les différents laboratoires qui semblent souvent hermétiques de prime abord.

Enfin, il y a les thésards, qui font la recherche pour pas cher. Merci Marine pour tes nombreux conseils concernant la taxonomie des diatomées. Merci Ivia, mademoiselle silicium, dompteuse de spectromètre de masse. Merci Julie pour m'avoir accueilli à Angers,

et tant appris sur les foraminifères. Merci Lucile de m'avoir prêté un coin de ta chambre étudiante à Saint-Denis de la Réunion, c'était un véritable luxe après un mois et demi en mer.

Et puis, les copains. Ceux qui ont usé leur jeans d'étudiants sur les bancs de la fac en licence avec moi : Camille, Lucile, Baptiste, Julien. Vous m'avez permis de sortir du cadre banyulenc et de respirer à la faveur d'une visite d'Istanbul, de vacances dans le Jura, de week-end à Avignon, d'ascension mémorable du mont Ventoux (Baptiste, je te la dois celle-là). Ceux qui ont usé leur abonnement SNCF entre les différentes stations marines du master: Nicolas, Fabio, Simon merci pour votre accueil dans la méga-collocation villefranchoise. Ceux qui ont usé leurs neurones pour leur thèse à Banyuls : Sandrine, Mariana, Marine, Tatiana (pas taper !), Claire, Amandine, Matthias, Hugo L, Hugo B., Daniel, Marc. Pour les nombreux barbecues, pour les soirées sur la plage, pour les gaming nights, pour les pauses café. Hugo L., mention spéciale pour les sorties chasse sous-marine sous l'orage. Hugo B., merci pour les week-end chez les brebis. Marc, une pensée particulière pour nos soirées métal-gastronomie-géopolitique-philosophie. Ton adoration des chinchillas n'a d'égale que ta foi en la société humaine.

Quand on parle d'une thèse à Banyuls, il faut comprendre ce que ça signifie. Ca signifie s'évader en randonnées mémorables, s'épuiser dans des courses allant des chemins littoraux aux petites montagnes, avaler les kilomètres à vélo dans les plaines, envoyer du braquet pour gravir la Madeloc, aller dans l'eau en fin de journée pour en sortir moult sars, dentis, barracudas, mulets et sérioles qui auront ravi les papilles de mes visiteurs. C'est une somme de choses qui permettent de trouver un équilibre dans la thèse.

Merci à mes parents qui m'ont fait pas trop bête et ont suivi mes travaux avec intérêt. Merci de prouver que l'enseignement publique ça peut marcher du début à la fin. Je dédie ce manuscrit à ma grand-mère Jeanine et mon grand-père René qui, s'ils n'ont respectivement pas réussi à révolutionner le système socio-politique français et à résoudre le mouvement perpétuel (pourtant, ça tourne !), ont toujours été intéressés par ce que je fais.

Enfin, et surtout, merci à toi d'avoir accepté tous ces sacrifices.

Pluralitas non est ponenda sine necessitate.

Résumé

La biosphère océanique module la concentration de CO_2 atmosphérique via deux processus majeurs: la pompe biologique (transfert vertical de carbone organique particulaire - POC - depuis l'océan de surface vers l'océan profond) et la contre-pompe des carbonates (émission de CO_2 lors de la précipitation du carbone inorganique particulaire - PIC). Si les flux de POC et PIC sont généralement précisément quantifiés, les études estimant la contribution des groupes planctoniques à ces flux restent rares. La pompe biologique est considérée comme peu efficace dans l'océan Austral du fait de la limitation de la production primaire par le fer. Cependant peu d'études ont présenté des flux d'export à échelle annuelle. Cette thèse a pour but (1) d'identifier la contribution de différents groupes planctoniques à l'export de POC et PIC à échelle annuelle dans des zones naturellement fertilisées de l'océan Austral et (2) de comprendre comment cette diversité planctonique influence la stoechimétrie et la labilité du matériel exporté.

Des déploiements de pièges à particules à proximité des plateaux insulaires de Kerguelen et de la Géorgie du Sud ont permis de d'estimer la contribution relative des diatomées et des pelottes fécales à l'export de POC dans des environnements de productivité contrastée. Dans chacun des sites productifs, l'export de annuel de carbone reste faible au regard de la production communautaire nette. Nos résultats suggèrent que si la fertilisation naturelle augmente l'intensité des flux de POC, elle n'augmente pas l'efficacité de l'export. Un mécanisme écologique pilote une fraction importante (40-60 %) de l'export annuel de POC dans chacun des sites productifs: la formation de spore de résistance par les diatomées. La quantification des cellules pleines et des frustules vides de diatomées mène à l'identification de groupes consistants associés à des stratégies écologiques qui impactent la séquestration préférentielle du carbone ou du silicium. Au cours d'une campagne estivale, nous identifions l'abondance relative de diatomées et dinoflagellés comme un facteur majeur influençant la stoichiométrie N:P de la matière organique. De plus, nous soulignons l'importance de la couche de transition pour le découplage du C et Si résultant de processus écologiques (broutage par le zooplancton) et physiologiques (découplage de la fixation de C et Si). La comparaison de la composition en lipides de l'export à Kerguelen, Crozet et en Géorgie du Sud nous permet d'identifier les spores de diatomées comme des vecteurs de matière organique contenant des acides gras riches en énergie. Cet apport de matière organique labile est susceptible de modifier la production et la diversité des communautés benthiques de l'océan profond. A Kerguelen, nous rapportons une dominance des coccolithophoridés dans l'export de PIC. La comparaison avec les communautés de calcifiants exportées à Crozet suggère qu'un changement majeur du type de plancton calcifiant (foraminifère versus coccolithophoridé) ainsi qu'un changement dans les assemblages d'espèces de foraminifères au Sud du Front Polaire induit une contre-pompe des carbonates moins intense. D'une manière générale cette thèse fournit un lien quantitatif entre entre les vecteurs écologiques et la composition chimique des flux d'export. Elle met

en lumière le besoin d'une approche ecosystème-centré pour une meilleure compréhension du fonctionnement de la pompe biologique.

Abstract

The marine biosphere impacts atmospheric CO_2 concentrations by two main processes: the biological pump (vertical transfer of particulate organic carbon - POC - from the surface to the deep ocean) and the carbonate counter pump (CO_2 production during particulate inorganic - PIC - precipitation). Although POC and PIC export are generally well quantified, studies defining the specific contribution of plankton groups to these fluxes remain scare. In the Southern Ocean, the biological pump is considered inefficient due to a limitation of primary production by iron. However, very few studies have reported annual export fluxes in these environments. The objectives of this PhD are (1) to identify the relative contribution of different plankton groups to POC and PIC export over a complete seasonal cycle in naturally iron-fertilized areas of the Southern Ocean and (2) to understand how planktonic diversity impacts the elemental stoichiometry and lability of the exported material.

To address these objectives, annual sediment trap deployments were conducted in the vicinity of the Kerguelen and South Georgia island plateaus. In the productive regimes of these island systems, annual carbon export was moderate compared to estimates of net community production. Therefore, natural iron fertilization may increase the strength but not the efficiency of the biological carbon pump. A detailed examination of the samples enabled a quantitative description of diatom- and faecal pellet-derived carbon to total POC export in contrasting productivity regimes. The export of diatom resting spores accounted for a similarly important fraction (40-60 %) of annual POC fluxes in the productive sites. The separate quantification of full and empty diatom frustules enabled the identification of consistent diatom functional groups across the Subantarctic islands systems that impact the preferential export of carbon or silicon. During a summer cruise in the Indian sector of the Southern Ocean, the relative abundance of diatoms and dinoflagellates was identified as the primary factor influencing the N:P stoichiometry of particulate organic matter. Furthermore, comparison of water column and sediment trap analyses revealed that the ratio of empty to full diatom frustules exerted a first order control on Si:C export stoichiometry. Transition layers were identified as a place where carbon and silicon cycles become decoupled as a result of ecological (grazing pressure) and physiological (uncoupled C and Si fixation) processes. The comparison of lipid fluxes across Southern Ocean island systems (Kerguelen, Crozet and South Georgia) was conducted to elucidate the impact of ecological flux vectors on the geochemical composition of export. These analyses highlighted the strong association of diatom resting spores with labile fatty acids. The supply of labile organic matter is likely to impact the biomass and diversity of deep-sea benthic communities. At Kerguelen, a dominance of coccolithophore-derived PIC flux was observed. A comparison with calcifying plankton communities exported at Crozet suggests that a switch in the dominant calcifying plankton (foraminifer versus coccolithophore), together with a change in the foraminifer species assemblage south of

the Polar Front, regulates the extent to which the carbonate counter pump can impact the sequestration efficiency of the soft-tissue pump. More generally the results of this thesis provide a quantitative framework linking ecological flux vectors to the magnitude and composition particle flux in the Southern Ocean. Furthermore it highlights the need for an ecosystem-centered approach in studying the function of the biological carbon pump.

Table of contents

List of Figures

List of publications

1. **Rembauville, M.**, Salter, I., Leblond, N., Gueneugues, A. and Blain, S.: Export fluxes in a naturally iron-fertilized area of the Southern Ocean – Part 1: Seasonal dynamics of particulate organic carbon export from a moored sediment trap, *Biogeosciences*, 12, 3153–3170, doi:10.5194/bg-12-3153-2015, URL www.biogeosciences.net/12/3153/2015/, 2015.

2. **Rembauville, M.**, Blain, S., Armand, L., Quéguiner, B. and Salter, I.: Export fluxes in a naturally iron-fertilized area of the Southern Ocean – Part 2: Importance of diatom resting spores and faecal pellets for export, *Biogeosciences*, 12, 3171–3195, doi:10.5194/bg-12-3171-2015, URL www.biogeosciences.net/12/3171/2015/, 2015.

3. **Rembauville, M.**, Manno, C., Tarling, G. A., Blain, S., and Salter, I.: Strong contribution of diatom resting spores to deep-sea carbon transfer in naturally iron-fertilized waters downstream of South Georgia, *Deep Sea Research Part I*, 115, 22-35, doi:10.1016/j.dsr.2016.05.002, URL http://www.sciencedirect.com/science/article/pii/S0967063716300036, 2016.

4. **Rembauville, M.**, Blain, S., Caparros, J. and Salter, I.: Particulate matter stoichiometry driven by microplankton community structure in summer in the Indian sector of the Southern Ocean, *Limnology and Oceanography*, doi:10.1002/lno.10291, URL http://onlinelibrary.wiley.com/doi/10.1002/lno.10291/full, 2016.

5. **Rembauville, M.**, Meilland, J., Ziveri, P., Schiebel, R., Blain, S. and Salter, I.: Planktic foraminifer and coccolith contribution to carbonate export fluxes over the central Kerguelen Plateau, *Deep Sea Research Part I*, 111, 91-101, doi:10.1016/j.dsr.2016.02.017, URL http://www.sciencedirect.com/science/article/pii/S0967063715301837, 2016.

List of communications

1. **Rembauville, M.**, Salter, I. and Blain, S.: EXPLAIN: EXport of PLankton functional types from Austral Island blooms Naturally fertilized by Iron. Talk a the LEFE-CYBER meeting, Bordeaux, June 2016.

2. **Rembauville, M.**, Salter, I. and Blain, S.: Diatom resping spore formation and carbon export in the Southern Ocean. Talk at the Ocean Sciences Meeting 2016, New Orleans, February 2016.

3. **Rembauville, M.**, Salter, I. and Blain, S.: Modelling diatom resting spore formation and contribution to carbon export fluxes: first approach. Talk at the LEFE-CYBER modelling workshop, Marseille, November 2015.

4. **Rembauville, M.**, Salter, I. and Blain, S.: Diatom life cycles and the export of carbon and biominerals in the Southern Ocean. Talk at the conference "7è colloque de l'association francophone d'écologie microbienne". Anglet, November 2015.

5. Blain, S., Claustre, H., Speich, S., Uitz, J., Poteau, A., Obolensky, G. and **Rembauville, M.**: Autonomous observation with bio-argo floats in the Southern Ocean. Poster at the conference "Our Common Future Under Climate Change", Paris, June 2015.

6. **Rembauville, M.**, Salter, I. and Blain, S.: Ecological vectors of carbon and biogenic silicon over the naturally fertilized Kerguelen Plateau. Poster at the ASLO Ocean Science Meeting, Granada, February 2015.

1 | Introduction

Contents

1.1 The global carbon cycle

1.1.1 Carbon cycle and climate

Carbon is the 15th most abundant element of the Earth's crust (Cox, 1989) and plays a major role in the Earth's functioning by cycling between different reservoirs (Fig. 1.1). The Earth system carbon cycle can be divided into two domains defined by their turnover time. The slow domain includes the huge reservoirs of carbon stored in rocks and sediments. The main processes characterizing this domain are volcanic emissions of CO_2, silicate weathering, and carbon burial in marine and land sediments associated with turnover times of $> 10\,000$ years to a million years (Sundquist, 1986). The fast domain includes the atmosphere, land and ocean biomass stocks and the oceanic dissolved inorganic carbon reservoir. Processes such as biological carbon fixation and remineralization, river export and air-sea exchange are associated with short turnover times (few years for the atmosphere to millennia for large oceanic reservoirs). During the Holocene (11 700 years ago to present), the fast domain was close to steady state as suggested by the constant CO_2 concentration observed in ice cores (Petit et al., 1999). However, since the beginning of the industrial revolution (1750), human activities have provided a link between the slow and fast domains, notably by injecting carbon stored as fossil fuels into the atmosphere (IPCC, 2013). The increase in atmospheric CO_2 over the last centuries was diagnosed from ice cores and atmospheric measurements, starting at 278 ppm in 1750 and increasing gradually to reach 400 ppm in 2015 (Conway and Tans, 2015). However, of the $9.3\,\mathrm{Pg\,yr^{-1}}$ of carbon emitted due to anthropogenic activity, only half of it accumulates in the atmosphere and the remaining part is taken up by the sum of land and ocean sinks (Le Quéré et al., 2013). The oceans have played a major role as a sink for one-third of the global anthropogenic emissions since the industrial revolution (Raven and Falkowski, 1999; Khatiwala et al., 2009).

CO_2 and other gases of anthropogenic origin (N_2O, CH_4, SF_6, chlorofluorocarbons and halogenated species) accumulate in the atmosphere and affect radiative forcing: a net change in the earth system energy balance. More specifically, greenhouse gases absorb and emit infrared radiations toward the Earth. From 1750 to 2011, CO_2 emissions have played a major role ($2\,\mathrm{W\,m^{-2}}$) in the total ($2.3\,\mathrm{W\,m^{-2}}$) anthropogenic-induced radiative forcing (IPCC, 2013). During the same period, the average temperature on Earth's surface has increased by $1\,^{\circ}\mathrm{C}$ due to greenhouse gases from anthropogenic origin (Forster et al., 2013), and global climate models forecast further temperature increases of $2\,^{\circ}\mathrm{C}$ to $4\,^{\circ}\mathrm{C}$ over the 21st century (IPCC, 2013). Global climate change is associated with a rise in sea level ($+0.4$ to $1\,\mathrm{m}$) and changes to ocean chemistry. A decrease in surface ocean pH (up to -0.4 pH unit) and CO_3^{2-} (Orr et al., 2005), particularly pronounced in mid latitudes (Feely et al., 2009), is expected to occur alongside a decrease in mesopelagic ocean oxygenation
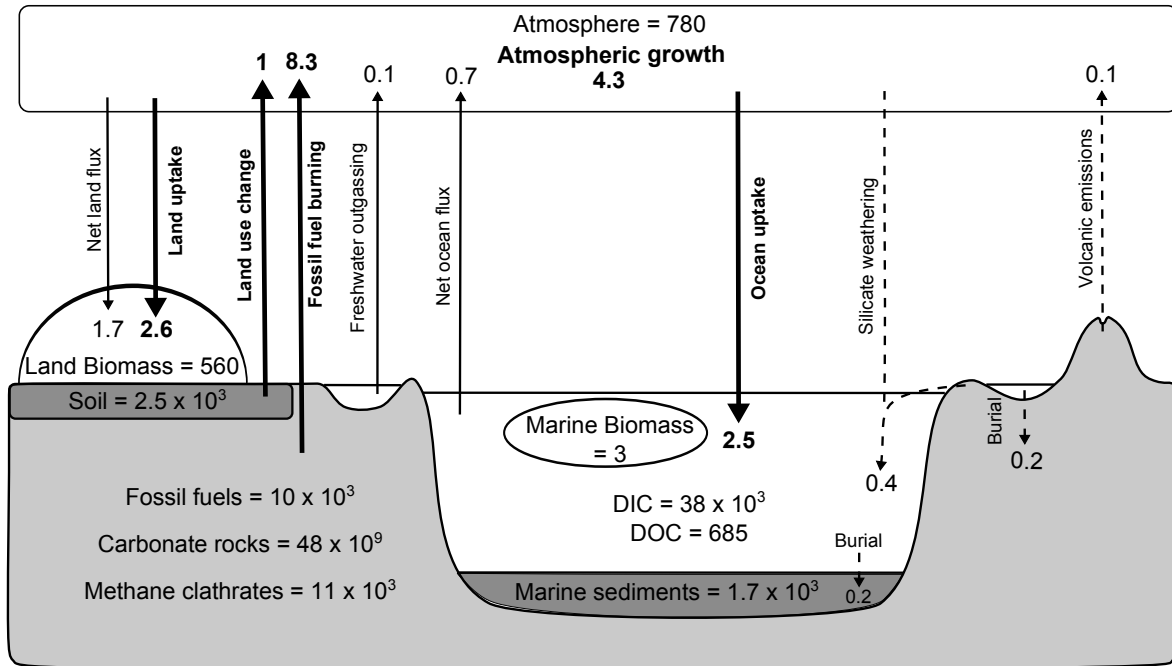
Figure 1.1: Global carbon stocks and fluxes (arrows). Slow, fast and anthropogenic fluxes are represented by dashed, thin and bold arrows, respectively. Stocks and fluxes from the pre-industrial era are from IPCC (2013). Fluxes induced by anthropogenic activities are from Le Quéré et al. (2013). Dissolved inorganic carbon (DIC) and dissolved organic carbon (DOC) oceanic stocks are from (Hansell, 2001). Stocks are expressed as Pg and fluxes as $Pg\,yr^{-1}$.

due to higher stratification and lower oxygen solubility (Keeling et al., 2010). The sum of these changes are likely to induce major changes in carbon cycling, marine production, trophic interactions and species habitat distribution (e. g. Sala et al., 2000; Fabry et al., 2008; Thackeray et al., 2010; Kroeker et al., 2013; Beaugrand et al., 2015). Understanding processes responsible for CO_2 sequestration in the ocean is therefore of critical importance to better constrain future changes in the Earth system functioning.

1.1.2 Distribution of oceanic carbon stocks

The ocean represents the second most important carbon reservoir on Earth ($\sim 4 \times 10^4$ $Pg\,yr^{-1}$), after carbonate rocks ($\sim 5 \times 10^{10}$ $Pg\,yr^{-1}$). Carbon is present in the ocean predominantly as dissolved inorganic carbon (DIC = $[CO_{2diss}]$ + $[H_2CO_3]$ + $[HCO_3^-]$ + $[CO_3^{2-}]$) and to a lesser extent as dissolved organic carbon (DOC) (Fig. 1.1). The vertical distribution of DIC in the ocean is highly heterogeneous (Fig. 1.2a). A strong gradient of $\sim 300\,\mu mol\,kg^{-1}$ is observed between the surface and the deep ocean. Oceanic DIC content can be modulated by air-sea CO_2 exchange as a function of CO_2 solubility, the difference in the air and the sea CO_2 partial pressure, and a gas transfer coefficient (Weiss, 1974; Takahashi et al., 2002). Additionally, photosynthesis and respiration by marine organisms modulates DIC concentration ($6CO_2$ + $6H_2O$ $\leftrightarrow$ $C_6H_{12}O_6$ + $6O_2$). The

solubility effect alone (higher solubility in cold deep waters) can only account for a small proportion of the observed vertical DIC gradient (Fig. 1.2a). The remaining gradient is due to biological activity that transfers carbon from the surface to the deep ocean, acting as a biological carbon pump (Volk and Hoffert, 1985). DOC oceanic stock is comparable to the atmospheric carbon stock and is the net result of autotrophic production by marine phytoplankton and heterotrophic microbial remineralization (Hansell, 2001). The DOC pool is a heterogeneous mixture of compounds with varying levels of reactivity that are characterized as functional categories. Turnover times range from few days to weeks for labile DOC (LDOC) to 16 000 years for refractory DOC (RDOC) (Hansell, 2013). The vertical distribution of DOC in the ocean displays a pronounced gradient between the mixed layer and the deep ocean, with values decreasing in the deep-ocean (Fig. 1.2b). During the productive season, the production of labile DOC in the mixed layer exceeds heterotrophic remineralization, resulting in an accumulation of semi-labile DOC (SLDOC). In the upper mesopelagic ocean, remineralization is the dominant process leading to the accumulation of semi-refractory DOC (SRDOC). The deep ocean contains a quasi constant RDOC concentration of $44\,\mu\mathrm{mol\,kg^{-1}}$that appears largely unaffected by biological activity. The observed gradients of DIC and DOC highlight the fundamental role of biology in the vertical distribution of carbon stocks in the ocean. This is an important feature of the global carbon cycle as it determines the time scales over which oceanic and atmospheric reservoirs interact (the sequestration time, Boyd and Trull, 2007) and thus partly regulates the atmospheric CO_2 content (Kwon et al., 2009).
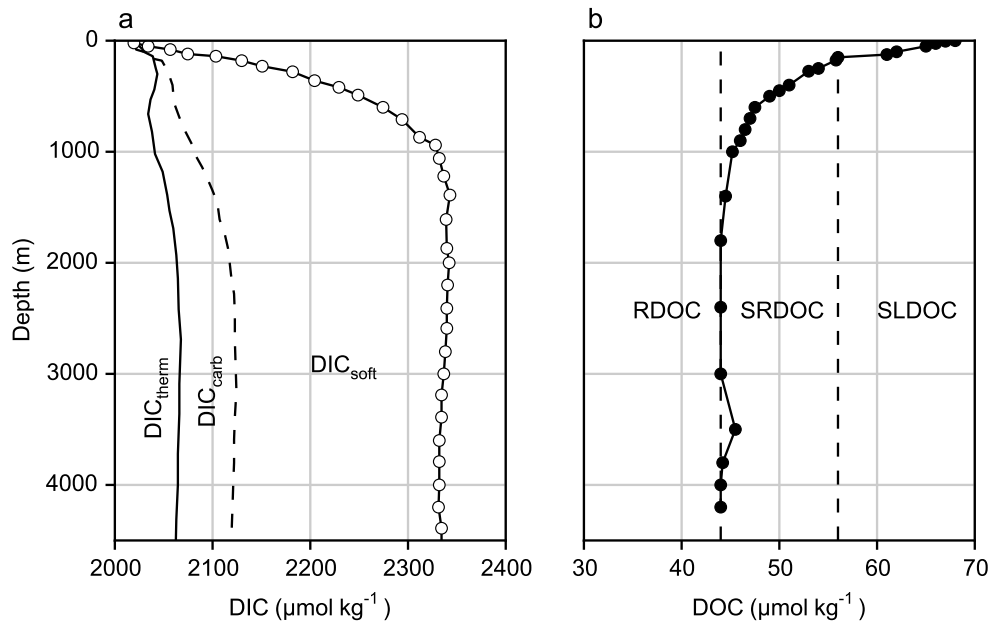
Figure 1.2: **a.** Globally averaged vertical DIC profile (white dots) and relative contribution of the solubility pump (DIC_{therm}, continuous line), carbonate pump (DIC_{carb}, dashed line) and soft tissue pump (DIC_{soft}). Redrawn from Sarmiento and Gruber (2006). **b.** Vertical DOC profile in the Sargasso Sea with contribution from refractory DOC (RDOC), semi-refractory DOC (SRDOC), semi-labile DOC (SLDOC). Redrawn from Hansell (2013).

1.2 Oceanic carbon pumps

The ocean plays a key role in absorbing atmospheric CO_2 and thus has the potential to partly mitigate the rise in atmospheric CO_2 concentration. The oceanic carbon sink has been classically divided into three main components, also referred to as carbon "pumps" (Volk and Hoffert, 1985): the solubility pump, the soft tissue pump, and the carbonate pump (Fig. 1.3). More recently, additional concepts of the microbial carbon pump and the lithogenic carbon pump have been introduced into this general scheme.

1.2.1 Solubility, carbonate, microbial and lithogenic carbon pumps

The *solubility pump* results from the increased solubility of CO_2 in cold waters that equilibrates with the atmosphere pCO_2 and is subducted to the deep ocean due to their density (Volk and Hoffert, 1985). This sink is particularly important at high latitudes where deep water formation takes place such as the Subpolar North Atlantic (Karleskind et al., 2011) and the Subantarctic Southern Ocean (Sallée et al., 2012). Modelling studies suggest that water mass subduction is responsible for the gross DIC export of $265\,\mathrm{Pg\,yr^{-1}}$ out of the mixed layer (Levy et al., 2013), which makes the solubility pump by far the most important carbon export pathway. However when obduction is taken into account,
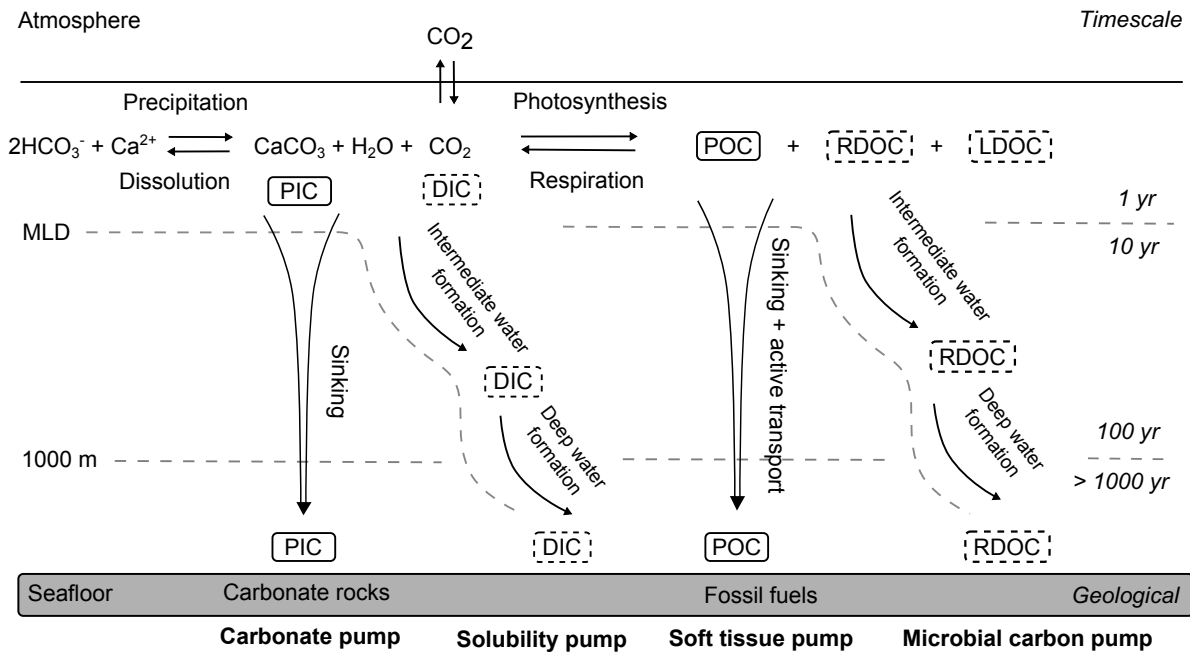
Figure 1.3: The four main oceanic carbon pumps. MLD: mixed layer depth, POC: particulate organic carbon, PIC: particulate inorganic carbon. Timescales from Boyd and Trull (2007).

the net effect of physical transport is a DIC input of $11\,\mathrm{Pg\,yr^{-1}}$ to the mixed layer. The solubility pump plays a limited role in the vertical gradient of DIC in the Ocean (Fig. 1.2).

The *carbonate pump* results from the production and export of PIC by calcifying organisms (foraminifera, coccolithophores, calcareous dinophytes and pteropods). Given that seawater alkalinity is dominated by its carbonate components (Alk $\sim [\mathrm{HCO_3^-}] + 2[\mathrm{CO_3^{2-}}]$), the carbonate pump is often referred to as an alkalinity pump that transfers alkalinity from the surface ocean to the deep ocean when PIC dissolves below the lysocline (Fig. 1.3). It is responsible for one third of the observed vertical DIC gradient (Fig. 1.2a). Global estimate of the carbonate pump from the surface ocean is $0.90\,\mathrm{Pg\,yr^{-1}}$ but only $0.16\,\mathrm{Pg\,yr^{-1}}$ reaches the seafloor due to PIC dissolution in the water column (Battaglia et al., 2016). Foraminifera are the major contributors to this downward PIC flux ($>30\%$, Schiebel, 2002), followed by coccolithophores (12%, Bramlette, 1958; Beaufort and Heussner, 1999), pteropods (10%, Fabry, 1990) and calcareous dinophytes (3.5%, Schiebel, 2002). The calcification process in the mixed layer decreases DIC and Alk with a ratio 1:2 and counter-intuitively increases $p\mathrm{CO_2}$ (Frankignoulle et al., 1994). If PIC is exported below the permanent thermocline, it represents a net source of $\mathrm{CO_2}$ from the ocean to the atmosphere over $\sim 1\,000$ year timescale (Zeebe, 2012). This process, also known as the carbonate counter pump, decreases the effect of the other oceanic carbon pumps on the atmospheric $\mathrm{CO_2}$ drawdown. It was suggested that "switching-off" of calcification in the ocean would lead to a 40 ppmv decrease in atmospheric $p\mathrm{CO_2}$ (Wolf-

Gladrow et al., 1999). More recently, Salter et al. (2014) reported that the carbonate counter pump can reduce the effective sequestration of atmospheric CO_2 in deep ocean by up to 30% in the naturally fertilized waters downstream of the Crozet Plateau.

The *microbial carbon pump* defines the long-term sequestration of refractory dissolved organic carbon resulting from microbial food-web processes (Jiao et al., 2010). The refractory character of the exported DOC results in long turnover times and sequestration over significant timescales. Despite the potential importance of the microbial carbon pump, it is an emerging concept. The paucity of observations thus render it difficult to compare its significance with the more classically defined carbon pumps. However, recent estimates suggest it could account for $0.2\,\mathrm{Pg\,yr^{-1}}$ in the present day ocean (Legendre et al., 2015). The analysis of sediment biomarkers and isotopic records appear to support the idea of intensive microbial carbon pump processes in the Proterozoic (2 500 to 542 million years ago, Jiao et al., 2014). Additional experimental, field and modelling studies are required to estimate the past, present, and future importance of the microbial carbon pump.

Another recent concept to emerge is that of the *lithogenic carbon pump*. It suggests that the addition of lithogenic material, such as atmospheric dust, to the surface ocean could result in the adsorption of dissolved organic matter (DOM) onto the lithogenic particles. Due to their density, the lithogenic particles associated with this organic matter could act to export organic carbon that would otherwise remain in the dissolved pool. This concept has been formulated based on in situ observations (Ternon et al., 2010) and mesocosm experiments (Bressac et al., 2014). To date, very few studies have focused on the lithogenic carbon pump, and little is known about the processes regulating the adsorption of DOM onto lithogenic particles. However, preliminary evidence seems to suggest the quality of DOM strongly influences its affinity with lithogenic mineral phases (Desboeufs et al., 2014). Currently there is no estimation of the global significance of the lithogenic carbon pump. Quantifying the lithogenic carbon pump is further complicated by the difficulty in discriminating a fertilization effect associated with atmospheric dust events (stimulation of the new production and subsequent soft tissue pump) and the direct DOM adsorption onto lithogenic particles (Guieu et al., 2014).

1.2.2 Focus on the soft tissue pump

The *soft tissue pump* is defined as the vertical transfer of particulate organic carbon originating from photosynthesis in the upper ocean to the deep ocean (Volk and Hoffert, 1985). Is is distinguished from the biological pump (*sensu lato*) as is does not explicitly consider dissolved organic forms. The soft tissue pump is a complex process that involves many ecological pathways linking CO_2 fixation by autotrophic plankton in the euphotic layer to the burial of POC in the seafloor. The process is conceptually divided in two steps: (i) the export of POC from the production layer and (ii) the transfer from the

upper ocean to the deep ocean. The efficiency of each step can be quantified by two variables: the particle export efficiency (PE_{eff}=POC flux at the base of the productive layer / net primary production, Dunne et al., 2005) and the transfer efficiency (T_{eff}= POC flux at 2000 m / POC flux at the base of the productive layer, Francois et al., 2002). Initial studies suggested that over long time and space scales, the PE_{eff} was equal to the ratio of new to total primary production (f-ratio, Dugdale and Goering, 1967). In line with this hypothesis, Legendre and le Fèvre (1989) have proposed a theoretical scheme where areas of strong physico-chemical seasonal gradients would support a high level of new production and hence high exported production. Conversely, areas of weakly variable physico-chemical conditions would result in a regenerated production system that supports low export production.

Direct measurements of meso- and bathypelagic POC fluxes show a strong decrease of flux with depth (Martin et al., 1987) that is frequently described with a power law equation known as the Martin curve:

$$POCflux_z = POCflux_{z0} \times \left(\frac{z}{z0} \right)^{-b} \tag{1.1}$$

In this formulation, the b exponent summarizes the processes responsible for POC flux attenuation with depth and many related formulations have been proposed (Boyd and Trull, 2007). The attenuation of POC depends on the initial composition of the productive community (phytoplankton size and/or association with biominerals, Boyd and Newton, 1995) but also on the magnitude of remineralization by heterotrophic bacteria (Herndl and Reinthaler, 2013), particle consumption by zooplankton (Jackson, 1993; Steinberg et al., 2008; Robinson et al., 2010; Cavan et al., 2015) and/or packaging into larger aggregates (Francois et al., 2002; Stemmann et al., 2004; Burd and Jackson, 2009).

The first global-scale compilations demonstrated that the b value was not constant and varied geographically (Francois et al., 2002; Honjo et al., 2008). It was first hypothesized that the geographical variability of T_{eff} was due to the association of POC with ballast minerals (from lithogenic or biological origin) that result in different particle sinking speeds and protection from remineralization due to associations with mineral phases (Ittekkot, 1993; Armstrong et al., 2002; Klaas and Archer, 2002; Francois et al., 2002). More recent compilations of shallow and deep export fluxes have demonstrated strong latitudinal patterns in the distribution of PE_{eff}, T_{eff} and b (Henson et al., 2012; Guidi et al., 2015). Low latitude ecosystems exhibit low PE_{eff} and high T_{eff} (and therefore low b) and the opposite is observed in high latitude ecosystems (Fig. 1.4). In low latitude ecosystems, it was suggested that the low PE_{eff} was due to low levels of new production (low f-ratio) under macronutrient limitation, characterized by phytoplankton communities dominated by small cells with low sinking rates (Henson et al., 2012). In these conditions, much of the organic carbon is remineralized within the mixed layer and the

POC exported is mostly refractory and likely to be packaged into strong and fast-sinking faecal pellets resulting in a high T_{eff} (Francois et al., 2002). Conversely, in high latitude ecosystems, macronutrient availability sustains the new production of large phytoplankton mainly represented by diatoms with high sinking speeds, leading to high PE_{eff} (Boyd and Newton, 1995, 1999; Buesseler, 1998). However, the POC exported from the surface with this phytoplankton community is considered more labile, and it therefore undergoes enhanced remineralization below the productive layer which is manifested as a low T_{eff}. These ideas are supported by global scale analyses that highlight the negative relationship between T_{eff} and the biogenic silica (BSi) content of exported particles (Francois et al., 2002; Henson et al., 2012) and the positive relationship between the fraction of microphytoplankton and the b attenuation coefficient (Guidi et al., 2015).
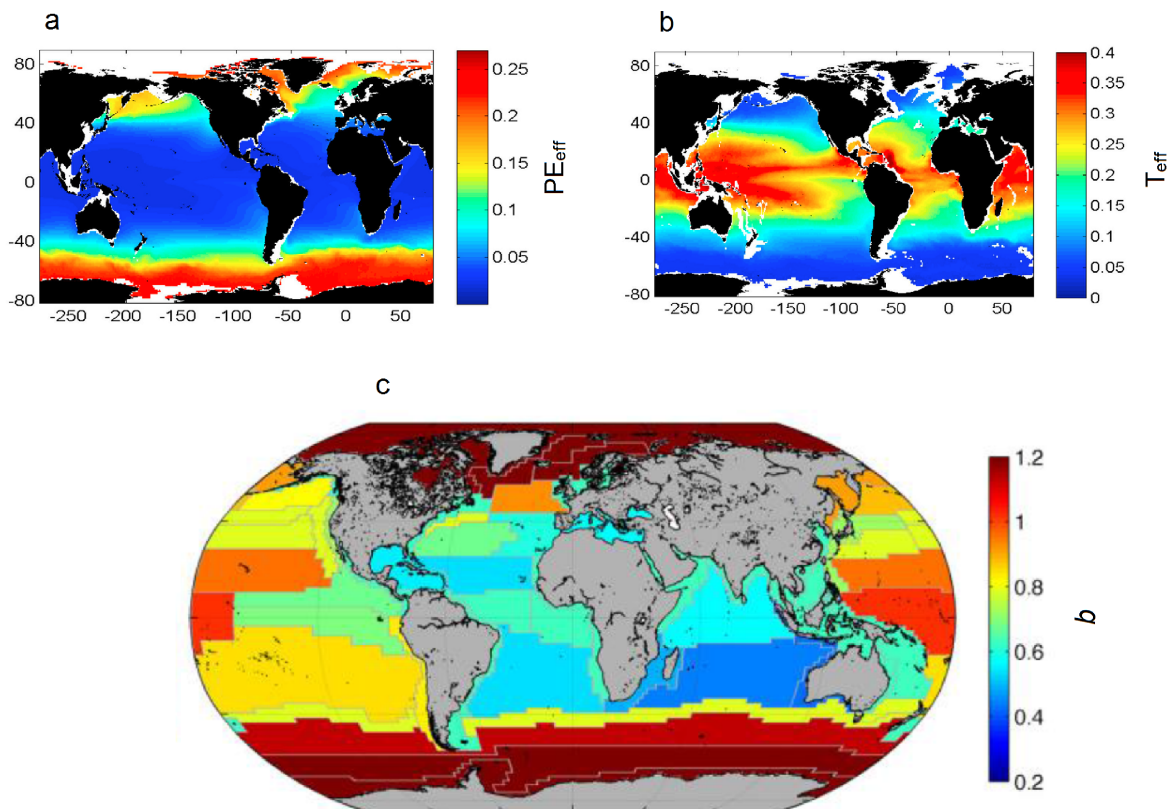
Figure 1.4: Global distribution of **a.** PE_{eff} and **b.** T_{eff} from Henson et al. (2012). **c.** Regionalized b values in Longhurst biological provinces from Guidi et al. (2015).

General conclusions from these global-scale analyses are however not always consistent with short term observations observations from regional studies. Rivkin et al. (1996) have demonstrated that the relationship between the f-ratio and the PE_{eff} was invalid over short time scales. A more recent study even showed an inverse relationship between net primary production and PE_{eff} in the Southern Ocean (Maiti et al., 2013). Additionally, numerous process-oriented studies have identified ecological processes responsible for the formation of fast-sinking particles: algal aggregation (Jackson et al., 2005; Burd and Jackson, 2009),

plankton faecal pellet production (Lampitt et al., 1990; Wilson et al., 2008; Lampitt et al., 2009; Wilson et al., 2013), diatom resting spore formation (Salter et al., 2012; Rynearson et al., 2013), or active transport by vertically migration zooplankton (Jackson and Burd, 2001; Steinberg et al., 2008; Davison et al., 2013). Moreover, physical processes such as eddy-driven subduction of non sinking POC (Omand et al., 2015) have been demonstrated to play a substantial role in global POC export from the mixed layer. These studies highlighted important subtleties likely to explain why local observations diverge from the patterns identified at global scale. In this context the hypothesis of a ballasting effect has been heavily debated (Thomalla et al., 2008; Sanders et al., 2010). Certain authors suggest the correlation between POC and mineral fluxes might not be causal and should be considered as an indicator of the ecosystem structure and functioning that ultimately determines the functioning of the biological pump (Lam et al., 2011; Henson et al., 2012).

POC export at the base of the productive layer estimated from observations and global numerical models is reported to range from 5 to $13\,\mathrm{Pg\,yr^{-1}}$ (Lima et al., 2014, and references therein). It is generally accepted that only $\sim 0.2\,\mathrm{Pg\,yr^{-1}}$ reaches a depth >2000 m (Lutz et al., 2007; Lima et al., 2014) but a recent estimate suggests a three-fold increase to $\sim 0.7\,\mathrm{Pg\,yr^{-1}}$ (Guidi et al., 2015). First studies based on box models of the global carbon cycle have reported that an ocean without biological pump would result in an increase in atmospheric pCO_2 of up to 200 ppm (Sarmiento and Toggweiler, 1984; Sarmiento et al., 1988). More recent studies using global circulation models suggest a much more moderate impact (Archer et al., 2000b). However, the biological pump remains one of the most important biological mechanisms in the Earth's system allowing the transfer of carbon from the fast climate cycle ($\sim$ decades to centuries) to the geological cycles (IPCC, 2013). The uncertainty in both the shallow and deep export fluxes at global scale reflects the difficulty to represent poorly documented ecological processes in numerical models (Francois et al., 2002; Boyd and Trull, 2007; Lam et al., 2011; Henson et al., 2012; Guidi et al., 2015). Therefore describing biological and ecological factors responsible for POC export out of the mixed layer and transfer to the deep ocean is still a fundamental goal in Earth system science and is the focus of the present thesis.

1.2.3   Biological components of the export fluxes

There is the life of the plankton in almost endless variety; there are the many kinds of fish, both surface and bottom living; there are the hosts of different invertebrate creatures on the sea-floor; and there are those almost grotesque forms of pelagic life in the oceans depths. - Sir Alister Hardy, 1956.

A recent large scale sampling of the ocean and DNA sequencing suggests that $\sim$ 150 000 operational taxonomic units of eukaryotes exist in the euphotic zone (de Vargas et al., 2015), and models converge to a theoretical total number of 2.2 million eukaryotic marine species (Mora et al., 2011). For prokaryotes, the concept of species is even more complicated (Rosselló-Mora and Amann, 2001), and 6000 species of prokaryotes have been formally described so far and 360 new prokaryotic taxa are submitted to Genbank every year (Pedrós-Alió, 2006). Such a phylogenetic diversity is associated with metabolic and physiological diversities that impact the biogeochemical cycles (Fig. 1.5).

Most of the bacteria and archaebacteria are heterotrophs that oxidize organic matter to CO_2, converting labile organic matter to more refractory compounds. However, some bacteria are phototrophs and part of them (cyanobacteria) are able to fix atmospheric nitrogen. This process has a potential significance for the biological pump not only by introducing new nitrogen to the mixed layer, but also through the direct collapse and export of the cyanobacteria bloom (Bar-Zeev et al., 2013). Some bacteria lineages are able to fix inorganic carbon into organic matter in the dark ocean (chemolithoautotrophy, e.g. Swan et al., 2011). Metazoarian organisms (here mesozooplankton) are strict heterotrophs. Nevertheless, their ability to produce dense and fast-sinking faecal pellets is likely to increase the POC export fluxes (Lampitt et al., 1990; Turner, 2002). Additionally, zooplankton actively transfer organic matter to the mesopelagic ocean during diel vertical migration patterns (Steinberg et al., 2002). The diversity of the physiological and ecological strategies make the calculation of the carbon budget in the deep ocean complicated (Burd et al., 2010).

An important fraction of marine protists (unicellular eukaryotes) are autotrophs that produce organic matter that has a potential for export. This is notably the case for diatoms (Bacillariophyceae). However, numerous protists exhibit mixotrophy depending on the phase of their life cycle and/or the availability of food. The most common example is dinoflagellates (Stoecker, 1999; Jeong et al., 2010), but it is also frequently observed among ciliates (Stoecker et al., 1989). This metabolic plasticity has a potential impact on the biological pump, because it allows access to organic forms of nutrients for mixotrophic protists (Mitra et al., 2014). Finally the symbiotic association of heterotrophic and autotrophic organisms (e.g. foraminifera with dinoflagellates or acantharia with *Phaeocystis*, Gast and Caron, 2001; Decelle et al., 2012) increases the difficulty to fully understand the role of plankton diversity and associated physiology in carbon fluxes. Recent trait-based
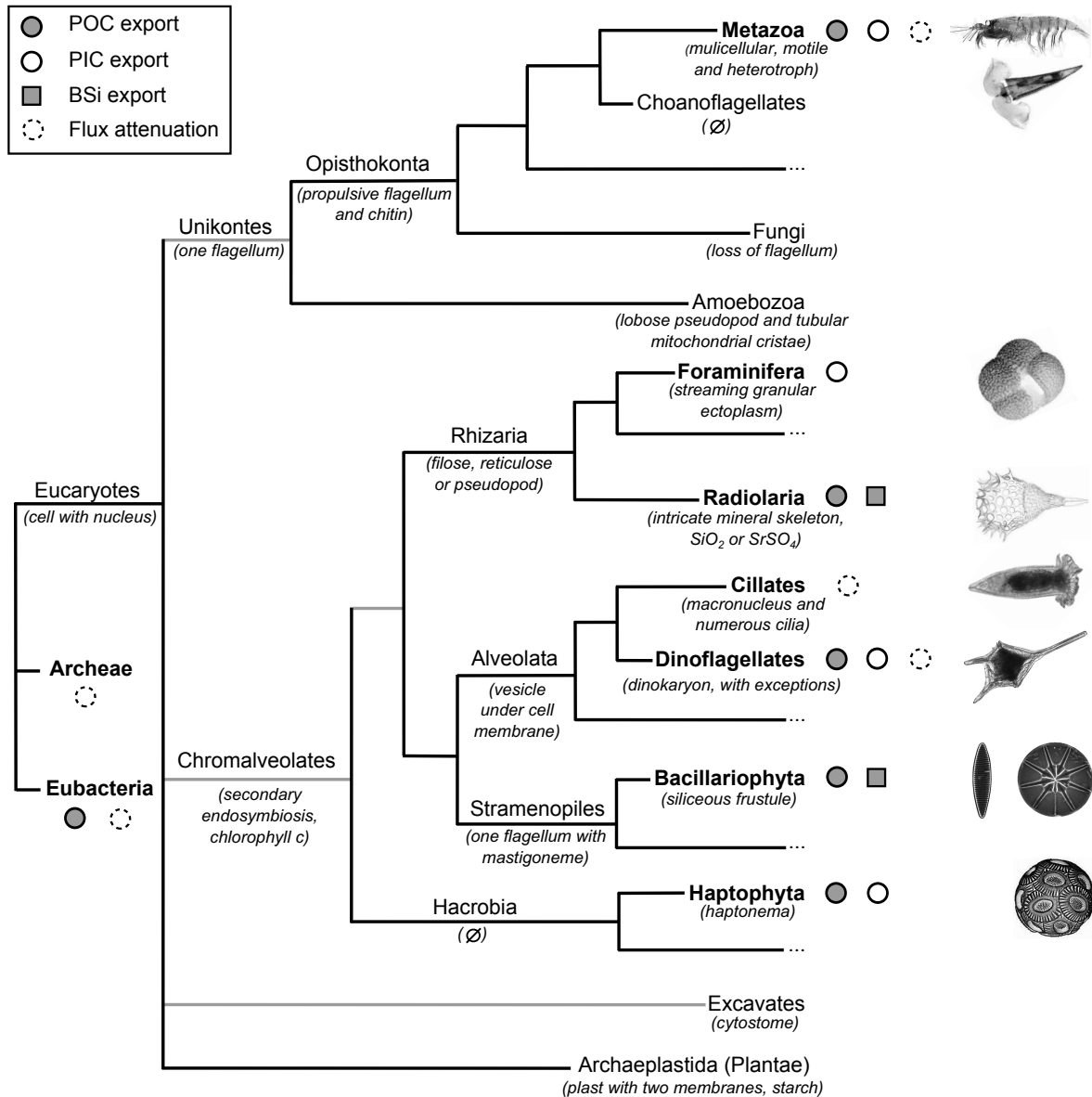
Figure 1.5: Phylogeny of eukaryotic plankton (based on the Tree Of Life consensus http://tolweb.org) and its role on export fluxes. Grey branches may not be monophyletic. Although the present clustering is based on genetic, some characteristics of the taxa (synapomorphic characters) are written in italic.

models of unicellular organisms integrate a continuum of size and trophic strategy, rather than discrete classes of size and trophic interactions (Andersen et al., 2015). Adding such trophic plasticity into biogeochemical models might increase the ability to predict export fluxes in a dynamic and changing environment.

Plankton diversity is also associated with variability in organic matter stoichiometry. A recent compilation of particulate organic carbon, nitrogen (PON) and phosphorus (POP) at global scale demonstrates strong latitudinal patterns in the molar ratios of these elements (Martiny et al., 2013a). The observed changes in organic matter stoichiometry reflect changes in the intrinsic stoichiometry of plankton (at the species level) as well as the result of food web processes and ecological strategy (Klausmeier et al., 2004). For example, diatoms usually display a lower PON:POP ratio than dinoflagellates (Ho et al., 2003). However, ecological strategies (competitive equilibrium versus exponential growth) and environmental factors (temperature) can influence the nature of resource allocation at a cellular level and thereby impact the stoichiometry of phytoplankton populations (Klausmeier et al., 2004; Toseland et al., 2013). Thus plankton diversity and associated food web processes have an impact on the degree of coupling of major elements (C, N, P, Si) in biogeochemical cycles. Plankton communities synthesise lipid compounds used for cell structure or energy storage (Chuecas and Riley, 1969; Lee et al., 1971). The specificity of lipid classes to certain planktonic taxa or metabolisms make them good trophic markers for the study of food web structure in the pelagic environment (Dalsgaard et al., 2003). Moreover, lipid export flux represents a source of energy for the deep ocean whose lability depends on the lipid composition (Wakeham et al., 1997, 2009). Thus, the lipid composition of export fluxes is an important factor for the pelagic/benthic coupling and is likely to influence the composition of the benthic community structure (Ruhl and Smith, 2004; Wolff et al., 2011).

1.2.4 Biological processes contributing to export

The sinking speed (w) of an idealized small, slow-sinking spherical particle (Reynold number Re <0.5) in a quiescent fluid is described by Stokes' law:

$$w = \frac{g \; \Delta\rho \; d^2}{18 \; \mu} \tag{1.2}$$

Where g is the gravitational acceleration, $\Delta\rho$ is the density difference between the particle and the fluid, d is the particle diameter and μ is the dynamic viscosity of the fluid. For large particles with higher sinking velocities (Re >0.5), the drag forces increase strongly with speed, and a different formulation has been proposed by Alldredge and Gotschalk (1988):

$$w = \left[\frac{4}{3} \frac{g \; \Delta\rho \; d}{c_d \; \rho_{sw}} \right]^{1/2} \tag{1.3}$$

In this formulation, ρ_{sw} is the seawater density and c_d is the drag coefficient, an empirical coefficient depending on the shape of the particle.

In both formulations, the sinking speed is dependent on two essential characteristics of the particle : the diameter and the density. Particle size in the ocean results from the equilibrium of disaggregation and coagulation. Models suggest aggregation is always occurring in phytoplankton populations and that this process is concentration-dependent (Jackson, 1990). When phytoplankton reaches a "critical concentration" , cells are supposed to collide and attach to each other to form large phytodetrital aggregates (Jackson and Kiørboe, 2008; Burd and Jackson, 2009), a phenomenon enhanced by the presence of exopolymeric substances (Logan et al., 1995; Engel, 2000). Aggregated particles $>0.5\,\mathrm{mm}$ are referred-to as "marine snow" and associated with a high sinking speed $>100\,\mathrm{m\,s^{-1}}$ (Alldredge and Gotschalk, 1988). In this context, aggregation and sinking of phytoplankton populations have been suggested as an important process exporting carbon from the surface ocean (Burd and Jackson, 2009). However, observations of aggregation and sinking of phytoplankton in the ocean are rare (Kiørboe et al., 1994; Jackson and Kiørboe, 2008), and it appears that concurrent disaggregation occurs in the mesopelagic ocean due to bacterial remineralization and zooplankton feeding on sinking material (Stemmann et al., 2004). Moreover, a recent compilation of particle size and sinking speed data demonstrates that there is no robust relationship between the two variables (Laurenceau-Cornec et al., 2015b). These studies emphasize the importance of the shape and biological composition of the particles that influences the density and drag coefficient and ultimately the sinking speed.

Although small particles dominate numerically the particle standing stock in the ocean, very large particles such as faecal pellets (FP) have been identified as important contributors to export fluxes (McCave, 1975; Lampitt et al., 1990; Turner, 2002). Zooplankton FP are dense particles, in some case protected by a peritrophic membrane (Gauld, 1957). These properties confer a high sinking speed ranging from 30 to $3000\,\mathrm{m\,d^{-1}}$ (Turner, 2002), and a degree of protection from bacterial degradation (Poulsen and Iversen, 2008). For these reasons, zooplankton FP have been long considered as the main vector of POC export to the deep ocean (Lampitt et al., 1990; Turner, 2002). The relative contribution of zooplankton FP to total POC flux is highly variable vertically and geographically. Data compilations suggest that the relative contribution of faecal pellet to bathy- and abyssopelagic carbon flux is higher during low POC flux periods (Wilson et al., 2013; Manno et al., 2015). Wilson et al. (2013) have concluded that high export fluxes to the abyssal ocean originated from lower trophic levels. Additionally, FP from different origins can have different shapes (spherical, ovoid, ellipsoid, cylindrical and tabular) associated with different sinking speed. For example, the sinking speed of small spherical FP produced by small copepods ($\sim$20 m d^{-1}, Yoon et al., 2001) is two orders of magnitude lower than that of large tabular FP produced by salps ($\sim$2700 m d^{-1}, Madin, 1982). Because

the faecal pellet flux depends on the surface ocean phyto- and zooplankton community structure as well as heterotrophic activity in the deep ocean (bacterial remineralization and consumption/fragmentation by flux-feeders), it is very difficult to predict the relative contribution of FP to deep ocean POC fluxes (Turner, 2002).

Zooplankton is involved in another process likely to contribute to the export of carbon in the mesopelagic ocean. At night, zooplankton swim to the surface and feed in the productive euphotic layer. Before sunrise, many metazoarian organisms swim to the depth, presumably to escape from their large visual predators (Haren and Compton, 2013). This diel vertical migration is ubiquitous in the marine environment, and the migration depth ranges 200-1000 m (Bianchi et al., 2013a). Excretion, FP production and mortality at depth result in an active transfer of carbon and nutrient to the mesopelagic ocean. Moreover, zooplankton feeding is sometimes considered as "sloppy feeding" that produces dissolved or slowly-sinking suspended organic matter in the mesopelagic ocean likely to be consumed by bacterial communities (Giering et al., 2014). It was suggested that the energy supply attributed to diel vertical migration was necessary to meet the demand of the mesopelagic ecosystem and close the carbon budget (Steinberg et al., 2008; Burd et al., 2010; Giering et al., 2014). Models suggest that diel vertical migration can account for 15-40 % of the POC flux in the mesopelagic ocean (Bianchi et al., 2013b).

1.2.5 Diatoms and their significance for biogeochemical cycles

Diatoms (Bacillariophyta) are freshwater and marine protists producing a siliceous frustule (Fig. 1.5). Diatoms account for >40 % of marine primary production (Nelson et al., 1995). This is equivalent to 20 % of the net primary production on Earth, exceeding the contribution of all the rainforests (Field et al., 1998). Because of their silica frustule, diatoms are generally denser than the surrounding water and consequently have a tendency to sink out of the photic zone (Smetacek, 1985). However, diatoms can modulate their density by exchanging high for low molecular weight ions (Boyd and Gradmann, 2002; Anderson and Sweeney, 1978), making the prediction of the sinking speed at the cellular level difficult (Miklasz and Denny, 2010). Some species are even capable of positive buoyancy (Villareal, 1988, 1992; Moore and Villareal, 1996), complicating the use of size-sinking speed relationships for this phytoplankton group. Due to their generally large size (~10-2000 μm), the low surface:volume ratio imposes lower affinity for nutrients than pico and nanoplankton (Pahlow et al., 1997; Sarthou et al., 2005; Sunda and Hardison, 2010). Therefore diatoms are preferentially found in nutrient-rich waters of upwelling areas or high latitude oceans (Patrick, 1948; Margalef, 1958; Alvain et al., 2008) where they have developed a strategy to cope with low iron availability and light levels (Strzepek et al., 2012). Moreover, their success in iron-poor regions could be due to their capability to produce ferritin, a protein involved in iron storage within the cell (Marchetti et al., 2009).

Diatoms store carbon products from photosynthesis as chrysolaminarin (hydrophilic glucose polymer) and unsaturated fatty acids (Müller-Navarra et al., 2000), which make them an energy-rich food source. Therefore diatom production is not only important for the biogeochemical cycle of carbon and silicon, but also essential for carbon transfer to zooplankton grazers and pelagic fish (Ryther, 1969; Walsh, 1981; Ainley et al., 2015).

The rise of oceanic diatoms during the Cenozoic (66 million years ago to present) might be due to increased continental erosion and increased silicic acid concentration in the global ocean (Cermeño et al., 2015). The large size, the strong frustule, sometimes with numerous setae, and the ability to form chains confer to diatoms a mechanical resistance to mesozooplankton grazing pressure (Smetacek et al., 2004; Friedrichs et al., 2013). This watery arm race (Smetacek, 2001), together with the blooming strategy, has implications on the export of carbon and silica (Assmy et al., 2013) and thereby shapes the biogeochemical cyles of these two elements (Boyd and Newton, 1995; Nelson and Brzezinski, 1997; Smetacek, 1999). For example, diatoms may have contributed to higher export fluxes during the Paleocene-Eocene transition (55 million years ago) (Ma et al., 2014), leading to important climate feedback (lowering air temperature) driven by the soft tissue pump (Bowen, 2013). In this context, the evolution of biogenic silica production not only had an impact on the trophic interactions, but also on the chemical and probably climatic changes of the Earth system. In the modern ocean, diatom biogeography strongly constrains the accumulation of silica into siliceous oozes in the Southern Ocean, connecting the short (silica production/dissolution) and long (sediment burial) time scales of the silicon cycle (Tréguer et al., 1995).

Diatom life cycles are characterized by vegetative divisions during which each valve becomes the epivalve of the future cell, reducing the cell size at each generation (Fig. 1.6). When the cell reaches a minimum size, meiosis occurs resulting in sexual reproduction. This strategy ensures that meiosis occurs at regular intervals, balancing the cost of sexual reproduction with the advantage of genetic mixing (Lewis, 1984). Sexual reproduction can be extremely regular with little impact from external abiotic factors (D'Alelio et al., 2010). Several types of gametes exist (oogamy, anisogamy, free gametes or direct contact of the vegetative cells). After fertilization, the zygote (or auxospore) produces the largest cell called the initial cell. To ensure survival in adverse conditions, formation of a resting stage can occur (Fig. 1.6). It can take the form of a resting spore (morphologically very different to the vegetative cell and containing storage bodies), resting cell (morphologically similar to the vegetative stage but with physiological and cytoplasmic changes) or winter stage (similar to the spore but without energy storage bodies, only observed for *Eucampia antarctica* var. *antarctica*, Fryxell and Prasad, 1990). Resting spores have a thicker frustule than the vegetative cell, larger vesicles where lipids are stored (Doucette and Fryxell, 1983; Kuwata et al., 1993), and show reduced metabolic rates (20 % respiration and 4 % photosynthetic rates compared to vegetative cells, Kuwata et al., 1993). Due to

their small size and strong frustule, resting spores are quite resistant to grazing and have even been observed to lower copepod grazing rates (Kuwata and Tsuda, 2005). Resting stage can be released from the parent frustule (exogenous), attached to the parent frustule (semi-endogenous), or remain within the two valves of the frustule (endogenous). During resting spore formation, silicic acid uptake rates increase to build a thick, resistant frustule around the spore (Kuwata and Takahashi, 1990; Oku and Kamatani, 1995). Resting spores exhibit sinking speeds up to 30 times higher than the vegetative stage (McQuoid and Hobson, 1996). The formation of resting spores can occur rapidly, for example a whole community of *Chaetoceros pseudocurvisetus* can form spores within 48 hours (Kuwata et al., 1993).
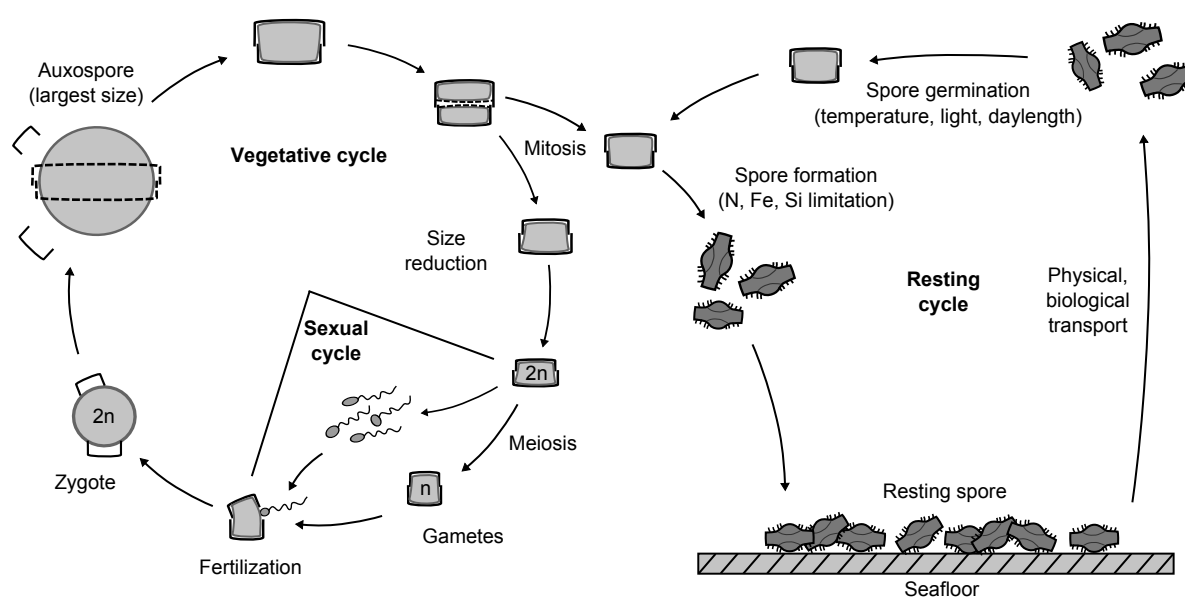
Figure 1.6: Schematic of a diatom life cycle, drawn after Hasle and Syvertsen (1997) and Round et al. (2007)

Numerous triggering factors have been invoked for resting spore formation such as temperature, salinity and pH stress, light and nutrient limitation. A compilation of *in situ* and culture experiments concluded that nitrogen limitation was the most important triggering factor (McQuoid and Hobson, 1996). Micronutrient limitation, such as iron, was also evoked, although the authors concluded it indirectly lowered the nitrogen cell content which was the ultimate triggering factor (Sugie and Kuma, 2008). Finally, resting spore formation by *Thalassiosira antarctica* was observed in Southern Ocean waters without particular nutrient or light limitation (von Bodungen et al., 1987), suggesting that interactions between factors might trigger spore formation. Resting spore formation by neritic diatom populations was interpreted as a way to persist regionally in places where favourable growth conditions occur seasonally. Resting spore sinking transfers the resting stages into deep, cold and dark waters were non-growing cells have been shown

to survive longer (Peters and Thomas, 1996), and allows them to potentially initiate the spring diatom bloom in neritic areas (Smetacek, 1985). This concept implies a mechanism that brings spores back to the euphotic zone, which is most of the time poorly documented (vertical currents, active transport). Spores might also be exported in one area and reseed another area after lateral advection (Leventer, 1991). This could explain why resting spores are found in very deep sediments remote from neritic areas along the Antarctic circumpolar current (Crosta et al., 1997). Light seems to be a critical factor for spore germination, in terms of both photoperiod (Hobson, 1981) and intensity (French and Hargraves, 1985). During spore germination, the cell undergoes reverse physiological processes that occur during spore formation (organelles and cytoplasm proliferation, reduction of storage lipids) and ultimately undergo mitosis (Anderson, 1975). The fraction of germinating spores decreases with increasing resting time. Resting spores can survive for a very long time (up to 100 years) in appropriate conditions such as anoxic sediments (Härnström et al., 2011). Given their low sensitivity to grazing, their high carbon content, and their important sinking speed, diatom resting stages are good candidates to drive efficient carbon export from the mixed layer to the seafloor (Smetacek, 1985; Salter et al., 2012; Rynearson et al., 2013).

1.3 Quantifying export fluxes

Deep-sea organisms are nourished by a "rain" of organic detritus from overlying surface waters. - Alexander Agassiz (1888).

The soft tissue pump appears to be responsible for the majority of the vertical DIC gradient in the ocean (Fig 1.2a) and therefore plays a major role in the air-sea CO_2 fluxes. Quantifying the downward flux of POC has been a central question in oceanography for nearly 40 years (McCave, 1975; Eppley and Peterson, 1979; Suess, 1980; Martin et al., 1987; Boyd and Trull, 2007). Several methods based on direct and indirect measurements as well as budget calculations have been used to constrain the POC export fluxes.

1.3.1 Budget calculations

A first approach to quantify the magnitude of carbon export from the mixed layer is to build a seasonal carbon budget at local scale based on pCO_2, DIC, POC and DOC measurements. This concept introduced by Emerson et al. (1997) was notably applied by Jouandet et al. (2008) for the central Kerguelen Plateau bloom. The first step is to calculate seasonal net community production (NCP = net primary production - heterotrophic respiration). The NCP equals the seasonal DIC consumption in the mixed layer corrected from atmospheric, vertical and horizontal fluxes.

$$NCP = \Delta DIC + F_{atm} + F_{vert} + F_{horiz} \tag{1.4}$$

$$NCP = \int_0^h (DIC_w - DIC_s) + \int_0^t kK_0 \, \Delta pCO_2 \, dt + \int_0^t K_z \, \frac{dDIC}{dz} \, dt + \int_0^t K_h \, \frac{dDIC}{dh} \, dt \tag{1.5}$$

DIC_w and DIC_s are respectively the mean winter and summer DIC concentration within the mixed layer, h the mixed layer depth, k the transfer velocity, K_0 the CO_2 solubility, ΔpCO_2 the difference in the air-sea pCO_2, K_z and K_h the vertical and horizontal diffusivity coefficients that multiplies the vertical and horizontal DIC gradients (the horizontal formulation was simplified here). Seasonal carbon export is then calculated from NCP corrected for summer POC and DOC accumulation in the mixed layer.

$$C_{exp} = NCP - \Delta POC - \Delta DOC \tag{1.6}$$

$$C_{exp} = NCP - \int_0^h (POC_s - POC_w) - \int_0^h (DOC_s - DOC_w) \tag{1.7}$$

This approach can be particularly useful in areas rarely visited, such as Southern Ocean blooms and provides and estimate of carbon export over an entire seasonal cycle. It is highly sensitive to the choice of diffusion coefficients (Jouandet et al., 2008) that may strongly vary across the season. Moreover it does not take into account carbon removal by vertically-migrating organisms or highly motile predators. A more recent formulation of carbon budget taking into account DOC export and zooplankton migration and respiration to depth was proposed by Emerson (2014).

Over large temporal and spatial scales, the efficiency of the biological pump can be quantified as the fraction of mixed layer nutrient inventory that is annually transferred to depth by the biology (Sarmiento et al., 2004). It can be calculated from climatological fields of nutrients (World Ocean Atlas 2013, Garcia et al., 2013).

$$Efficiency = \frac{< \mathrm{NO_3}^- >_{100-200m} - < \mathrm{NO_3}^- >_{0-100m}}{< \mathrm{NO_3}^- >_{100-200m}} \qquad (1.8)$$

$<\mathrm{NO_3}^->$ is the mean nitrate concentration within each layer. The result at global scale is shown in Figure 1.7. Efficiency is 100 % when organisms completely deplete surface nutrients, and is 0 % when there is no removal of upwelled nutrients. The major result is that the high latitude ocean, and more specifically the Southern Ocean, displays a very low biological pump efficiency (<25 %). Therefore the ecological and physical processes responsible for the efficiency of the biological pump are not constant but highly variable geographically. Several reasons are invoked for the low efficiency of the present day Southern Ocean (iron limitation, deep summer mixed layer, low light levels, phytoplankton self-shading and high nutrient supply) and are detailed in section 1.4.
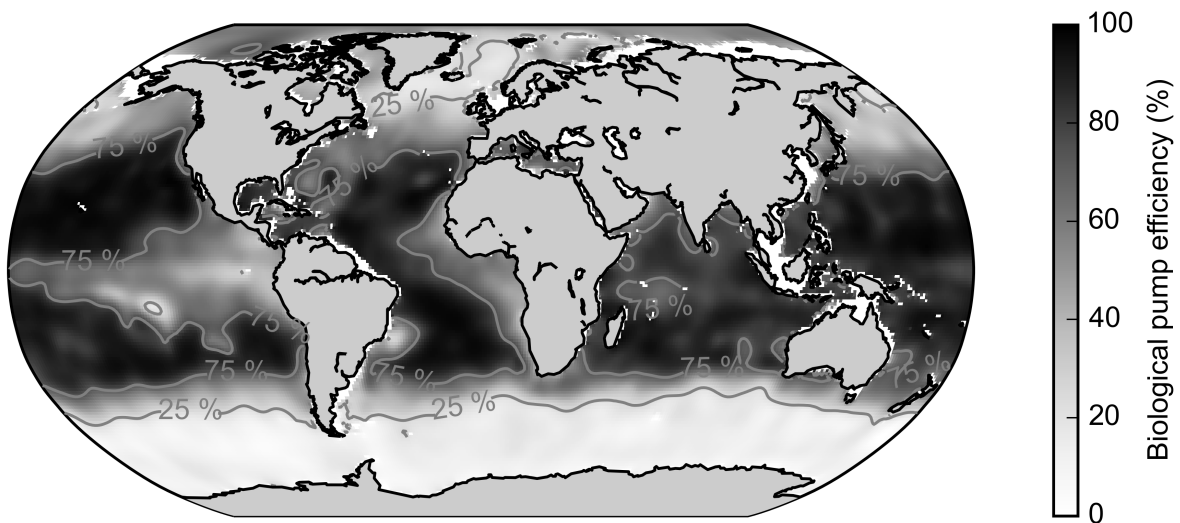
Figure 1.7: Global distribution of the biological pump efficiency calculated from climatological $\mathrm{NO_3}^-$ field (World Ocean Atlas 2013, Garcia et al., 2013)

Budget calculations based on relatively simple oceanographic parameters are highly useful to scale the magnitude and efficiency of export fluxes over long temporal and spatial scales. However, they do not allow the examination of the ecological and environmental mechanisms responsible for variations in the function of the biological carbon pump.

1.3.2 Geochemical proxies

In the late 1980s, the analytical measurements of radioisotopes characterizing the uranium decay chain (^{238}U $\rightarrow$ ^{234}Th $\rightarrow$ ^{234}Pa $\rightarrow$ ^{234}U $\rightarrow$ ...) have been significantly improved (Cochran and Masqué, 2003). All of these elements decay by alpha emissions and are therefore measurable by alpha spectrometry. Early measurements of ^{234}Th demonstrated its affinity for particles (Bhat et al., 1968), whereas its parent element ^{238}U is soluble in seawater and directly related to salinity (Chen et al., 1986). The properties of the ^{238}U-^{234}Th radionuclide pairing enables particle export models based on the ^{238}U/^{234}Th distribution in the sea (Savoye et al., 2006). In the simplest one box model, ^{234}Th activity is a result of a balance between its production from ^{238}U, its radioactive decay, its removal on sinking particles and its advection/diffusion into or out of the box:

$$\frac{dA_{Th}}{dt} = \lambda A_U - \lambda A_{Th} - P + V \tag{1.9}$$

where λ is the decay constant of ^{234}Th ($0.028\,76\,\mathrm{d}^{-1}$), A are the radioisotopes activities, P the removal on particles and V the advection/diffusion term. Under steady-state conditions ($\frac{dA_{Th}}{dt} = 0$), and assuming negligible advection/diffusion processes, the net ^{234}Th flux at the base of a layer (P) equals the depth-integrated total ^{234}Th activity deficit relative to ^{238}U multiplied by the decay constant λ:

$$P = \lambda \int_0^z (A_U - A_{Th}) \tag{1.10}$$

The ^{234}Th flux ($\mathrm{dpm\,m^{-2}\,d^{-1}}$) is then multiplied by a POC:^{234}Th ratio ($\mathrm{mmol\,dpm^{-1}}$) to obtain a particulate organic carbon flux ($\mathrm{mmol\,m^{-2}\,d^{-1}}$) at the base of disequilibrium integration depth. The ^{234}Th half life of 24.1 days allows to study the integrated export over a time scale of $\sim$three weeks prior to the measurement. Other models taking into account non steady-state conditions ($\frac{dA_{Th}}{dt} \neq 0$) were developed and require two consecutive visits of the same station (Savoye et al., 2006). Finally, models taking into account advection were developed for areas where horizontal velocities cannot be neglected (Benitez-Nelson et al., 2000). Because the ^{234}Th method is logistically simpler and less expensive than the deployment of a sediment trap, this proxy constitutes the most abundant database of particle export from the upper ocean (Le Moigne et al., 2013a). The ^{234}Th proxy is now accepted as a reference to study the particulate export and, when coupled with NPP measurements, provides a direct estimate of PE$_{\mathrm{eff}}$ (Henson et al., 2012; Le Moigne et al.,

2013a; Maiti et al., 2013). Alternatively, another radionuclide pair, the ^{210}Pb/^{210}Po, with similar properties can be used to estimate export fluxes (Cochran and Masqué, 2003; Le Moigne et al., 2013b).

Many uncertainties are associated with radionuclide budgets. Firstly, a strong uncertainty exists in C:^{234}Th ratio that can temporally vary 60-fold at a single location (Buesseler et al., 2006). The POC:^{234}Th ratio is strongly influenced by particle size and composition, although little is known of its dependence on these two variables. Some studies have tried to address this issue using a size-fractionated POC:^{234}Th ratio (e.g. Jacquet et al., 2011). Moreover, the ^{234}Th deficit occurs over a time scale equal to its half life (24.1 days), whereas the POC:^{234}Th is an instantaneous ratio only representative of the sampling conditions. The integration of the ^{234}Th also complicates the comparison of ^{234}Th-derived export with daily NPP measurements. Finally, the assumption that the entirety of the ^{234}Th deficit is due to export might not be true in an ecosystem with a very short food web where energy and matter is efficiently transferred to highly motile higher trophic levels (Huntley et al., 1991). This might lead to an overestimation of export fluxes. This question has not been addressed to date.

1.3.3   Optical methods

Bulk particulate matter distribution in the ocean can be tracked optically using a transmissiometer (Gardner et al., 1990). This instrument emits an optical signal (usually at 660 nm) and measures the fraction of the signal that is absorbed during its path in the water. When corrected for the attenuation due to pure water, the measurement provides an attenuation coefficient attributed to particles (c_p). Strong empirical relationships between c_p and POC concentration have been identified (Loisel and Morel, 1998; Cetinić et al., 2012) and the recent integration of transmissiometers with Argo floats and sea gliders facilitates the study of POC distribution at high temporal and spatial resolution (e.g. Bishop and Wood, 2009; Xing et al., 2014). Another optical property, the backscattering coefficient (b_{bp}, ~1 % of the total particulate scattering b_p) has been mechanistically linked to the concentration of small particles ($< 20\,\mu$m), positively correlated to chlorophyll a concentration (Loisel and Morel, 1998) and to a lesser extent POC concentration (Cetinić et al., 2012). A modified version of an upward-looking transmissiometer was used to study particle export during the SOFEX artificial fertilization experiment (Coale et al., 2004). In the Norwegian Sea, Dall'Olmo and Mork (2014) used b_{bp} from an Argo float to calculate the variation of POC stocks in constant depth intervals and derived POC export from this optical measurement. Such instruments can provide data at very high frequency (several profiles per day) but cannot document important qualitative aspects of particulate material that may drive export processes. However, recent efforts to link optical properties with the composition of the phytoplanktonic community (Cetinić et al.,

2015) may represent a way to address such limitations.

Concomitantly, other instruments have been developed to study particulate matter distribution. The underwater Vision Profiler (UVP, Picheral et al., 2010) takes pictures of particles $> 52\,\mu m$ at high frequency ($6\,Hz$) during vertical downcasts. The particle equivalent spherical diameter (d) is calculated from the pixel area of each particle. The UVP represents a significant step forward in studying particle distribution and particle size spectra in the ocean (Gorsky et al., 2000; Stemmann et al., 2004). Guidi et al. (2008) compiled a global database of particle d and POC fluxes from short term sediment trap deployments. The authors derived a power relationship between d and the POC flux:

$$POC_{flux}\ (mg\ m^{-2}\ d^{-1}) = 12.5d\ (mm)^{3.81}\ \ (n = 118,\ R^2 = 0.73) \qquad (1.11)$$

This empirical relationship has been used to derive POC fluxes at local (Jouandet et al., 2011; Martin et al., 2013; Jouandet et al., 2014) and global scale (Guidi et al., 2008, 2015). The calibration performed at global scale assumes that particle sinking velocity and organic carbon content (the two properties setting the POC flux) are directly related to particle diameter. Any increase in particle content is therefore translated to an increase in POC flux, which might be misleading in the case of carbon-poor particles (e.g. empty diatom frustule aggregates or nepheloid layers). Moreover laboratory measurements suggest there is no single relationship between particle equivalent spherical diameter and sinking speed (see the data compilation by Laurenceau-Cornec et al., 2015b). Moreover recent studies suggest that shape is as important as diameter in driving the sinking velocity of marine snow (McDonnell and Buesseler, 2010; Laurenceau-Cornec et al., 2015b). The lower end of size range recorded by the UVP ($52\,\mu m$) ignores the contribution of small particles (e.g. single phytoplankton cells) to total export (Durkin et al., 2015). Alternative optical tools such as the video Plankton Recorder (VPR) have also been used to assess POC export fluxes (McDonnell and Buesseler, 2012).

1.3.4 Sediment traps

Another approach to estimate POC export flux is to directly catch sinking particles. The development of moored sediment traps (conical funnel catching the sinking material in sample cups) in the late 1970s allowed the collection of biogenic particles over time scales of days, weeks and years (Berger, 1971; Honjo, 1976). Having direct access to the exported material brings valuable information on essential particle characteristics likely to influence POC export such as the size (Suess, 1980), the chemical composition (Ittekkot, 1993; Armstrong et al., 2002; Ragueneau et al., 2006; Honjo et al., 2008) and biological composition (Gersonde and Wefer, 1987; Wilson et al., 2008; Salter et al., 2012). However, early studies also demonstrated that hydrodynamics around moored sediment traps might introduce a strong bias in the trapping efficiency (Buesseler et al., 2007, for a review).

Firstly, the trap itself introduces turbulence at small scale likely to modify the composition of particles through aggregation/disaggregation processes (Baker et al., 1988). Secondly, because horizontal velocities relative to the trap might (1) bend the sediment trap line, modifying the collecting area and (2) select the size of the particles collected by the trap (Hawley, 1988). In this context, it was proposed that moored sediment traps should not be used in shallow areas subjected to strong velocities, with an upper limit of $12\,\mathrm{cm\,s^{-1}}$ (Baker et al., 1988). Additionally, it was demonstrated that the higher the aspect ratio (height to diameter ratio) of the trap funnel, the lower the hydrodynamic bias.

To overcome hydrodynamic bias, surface-tethered sediment traps were developed. These shallow traps are attached to a surface buoy and drift in a quasi-Lagrangian way (e.g. Buesseler et al., 2000; Nodder et al., 2001). The horizontal current velocities relative to the trap are thus reduced (except in the case of stong current shear with depth), but vertical movements remain problematic. A more recent development is the use of neutrally buoyant sediment traps (NBST). A NBST is generally composed of a profiling float associated with a trap funnel. It can be programmed to remain on fixed isopycnal levels until trap retrieval (Buesseler et al., 2000; Salter et al., 2007; Lampitt et al., 2008). NBSTs have proven to be less prone to hydrodynamic biases, but as for surface-tethered sediment traps, vertical movements are unavoidable and logistical constraints limit the extent of the deployment period.

Another possible bias occurring in shallow sediment traps are zooplankton organisms that may actively enter the collection funnel. This can manifest itself in an overestimation of POC flux or underestimation if significant feeding on particles within the trap occurs. Furthermore there is no standard protocol to remove swimmers from passively sinking material (Buesseler et al., 2007), or indeed to distinguish between swimmers actively or passively entering the trap. Some authors sieve the bulk trapped material on $1\,\mathrm{mm}$, whilst others manually pick swimmers according to the preservation of the organic material. The swimmer issue is strongly reduced in the case of deep sediment traps ($>1000\,\mathrm{m}$). Another potential bias occurring during long term deployments of moored sediment traps is the degree of particle solubilization in the sampling cups. The two main preservatives used in sediment trap studies are mercuric chloride ($HgCl_2$) and formaldehyde. $HgCl_2$ acts as a poison to inhibit microbial activity whereas the formaldehyde also fixes biological membranes. Antia (2005) and O'Neill et al. (2005) studied particle solubilization in sediment traps samples and demonstrated that despite the preservative effect, up to 60 % of the particulate organic phosphorous and 30 % of the POC could be dissolved during an annual deployment. Such a bias inevitably leads to an underestimation of trap-derived particulate export fluxes. It is in theory possible to correct for particle leaching by measuring dissolved organic carbon and nutrients in the preservative solutions before and after the deployment. However, this is rarely carried out and carbon solubilization can only be corrected in $HgCl_2$ poisoned traps. An unfortunate consequence of these uncertainties is

that comparisons of export fluxes measured by different methods are challenging.

The biases described above should be taken into account when studying particle fluxes with sediment traps. They can be constrained for example by a careful examination of the hydrodynamical environment (coupling current meters to the sediment trap), an efficient swimmer sorting procedure, and appropriate corrections for particle solubilization. Despite these uncertainties, annual deployments of moored sediment traps have provided highly valuable data to better understand seasonal and regional differences in export fluxes (Lutz et al., 2002, 2007) and the biological components contributing to these fluxes (e.g. Romero and Armand, 2010). A detailed description of up-to-date chemical and biological export fluxes derived from moored sediment traps in the Southern Ocean is provided in section 1.4.3.

Another type of sediment trap has been developed to study the composition of the exported particles. These small cylindrical traps contain a polyacrilamide gel that collects and conserves the shape of marine particles as they sink in the water column (Lundsgaard, 1994; Waite et al., 2000; Ebersbach and Trull, 2008; McDonnell and Buesseler, 2010; Laurenceau-Cornec et al., 2015a). It avoids physical disruption of aggregates or the modification of original particle properties (size, shape) that occurs during the processing of traditional sediment trap samples (splitting, sieving, swimmers sorting). High resolution pictures of the particles trapped by the gel are taken, and particle volume can be converted to organic carbon using appropriate C:volume ratios. These traps enable a detailed study of particle size spectra and determination of the relative contribution of phytoplankton aggregates or faecal pellets to the export fluxes. Similar to surface-tethered and neutrally-buoyant sediment traps, the gel traps are currently only deployed for short periods of time to avoid overloading gels with particulate material.

1.4   The Southern Ocean case

1.4.1   Importance of the Southern Ocean in global biogeochemical cycles

The Southern Ocean surrounds the Antarctic continent, covers a surface corresponding to 20 % of the global ocean, and interconnects the three other oceanic basins (Atlantic, Pacific and Indian, Fig. 1.8a). It is the only unbounded ocean and is often defined by a dynamic geographical limit: the eastward-flowing Antarctic Circumpolar Current (ACC) generated by westerlies. This ACC is composed of dynamic meridional fronts characterized by increased velocities (Fig. 1.8b). These fronts delineate major oceanographic zones from North to South: the warm Subtropical Zone (STZ), the Subantarctic Zone (SAZ) with important atmospheric forcing inducing very deep winter mixed layers, the Polar Frontal Zone (PFZ) where significant downwelling occurs and the Antarctic Zone (AAZ) characterized by a remaining temperature minimum layer of $\sim 2\,^{\circ}\mathrm{C}$. The AAZ contains the Permanently Open Ocean Zone (POOZ) and the Seasonal Ice Zone (SIZ), under the influence of the sea ice in winter. The meridional circulation of the Southern Ocean can be schematically viewed as two convective cells located on each side of the Antarctic divergence (Fig. 1.9b). Ekman drift along the ACC is responsible for the upwelling of North Atlantic Deep Water (NADW) and Upper Circumpolar Deep Water (UCDW) and the northward advection of modal waters: the Antarctic Intermediate Waters (AAIW) and Subantarctic Mode Water (SAMW). Conversely, the westward katabatic winds along the Antarctic coasts drive the subduction of Antarctic Bottom Water (AABW).

This "great mix-master of the world ocean" (Broecker, 1991) is responsible for the exchange of heat, salt, nutrient and gases between the oceanic basins. The upwelling of old DIC-rich deep water results in the outgassing of natural (pre-industrial) CO_2 from the ocean to the atmosphere (Mikaloff Fletcher et al., 2007; Takahashi et al., 2009). Conversely, the strong solubility pump associated with AAIW and SAMW formation represents an important sink of anthropogenic CO_2 from the atmosphere (Marshall and Speer, 2012). Over the last century, 40% of the oceanic uptake of anthropogenic CO_2 occurred south of 40°S (Sabine et al., 2004; Mikaloff Fletcher et al., 2006; Khatiwala et al., 2009; Frölicher et al., 2014). However the anthropogenic carbon is not stored in the Southern Ocean but is advected northward in the southern hemisphere subtropical thermocline (Sabine et al., 2004; Sallée et al., 2012). All of the CMIP5 (Coupled Model Intercomparison Project Phase 5) models agree on a warming and freshening of the Southern Ocean waters over the 21$^{\mathrm{st}}$ century (Meijers, 2014). However the impact of these changes on the CO_2 sink is still unclear. Some studies suggest a weakening of the CO_2 sink due to (1) increased stratification and weakening of the deep water formation (Sarmiento et al., 1998) and (2) intensification of westerly winds that increases the upwelling of carbon-rich deep
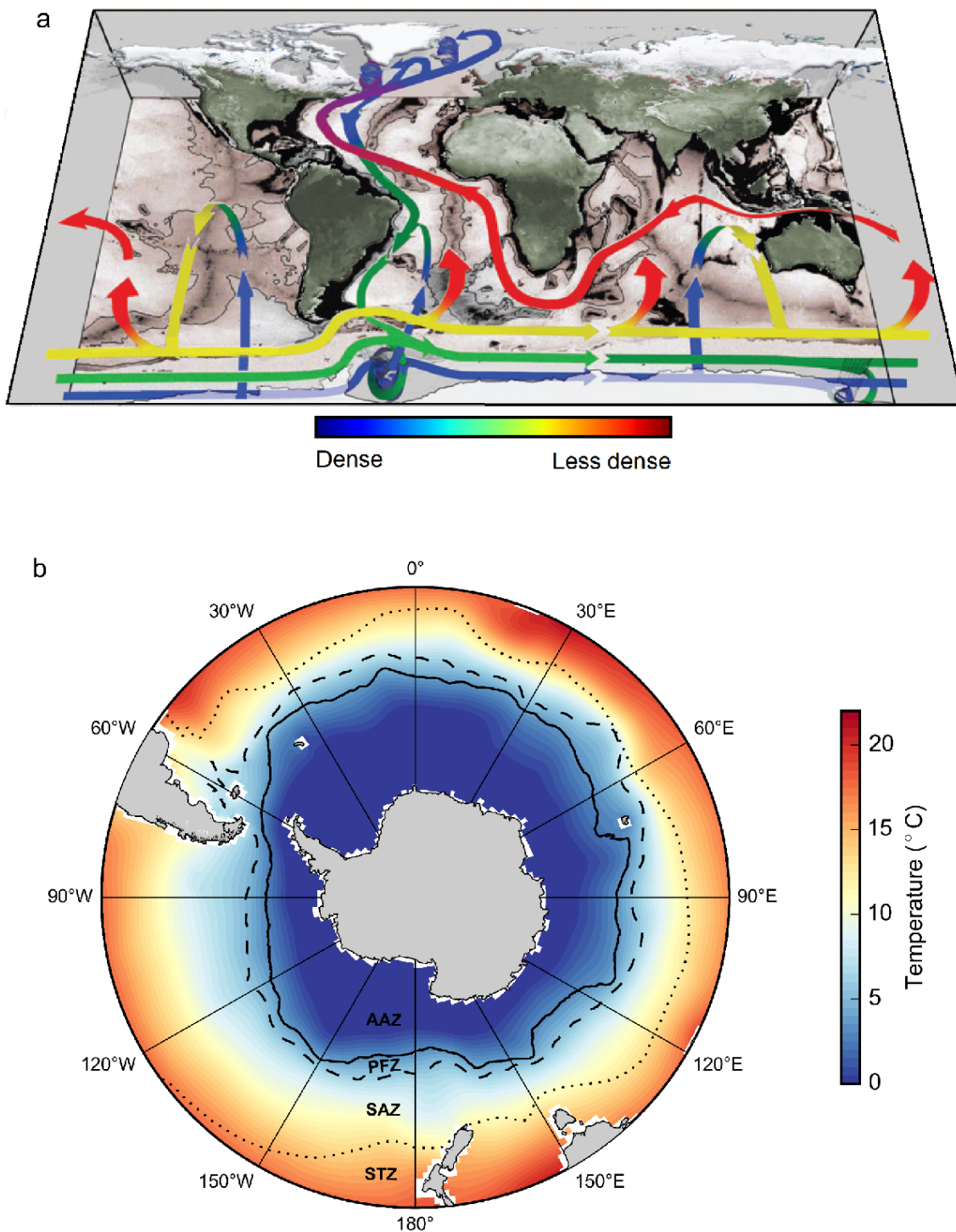
Figure 1.8: **a.** The recent view of the meridional overturning circulation adapted from Broecker (1991) by Marshall and Speer (2012) that details the upwelling processes in the Southern Ocean that now balance the deep water formation in the Atlantic. Figure adapted from Marshall and Speer (2012). **b.** Sea surface temperature in the Southern Ocean (World Ocean Atlas 2013) and major fronts (dotted line : Subtropical front from Orsi et al. (1995), dashed line: Subantarctic front and continuous line: Polar front front from Sallée et al. (2008)) that delimit Southern Ocean zones (STZ: Subtropical Zone, SAZ: Subantarctic Zone, PFZ: Polar Frontal Zone, AAZ: Antarctic Zone).

waters (le Quéré et al., 2007; Lovenduski et al., 2013). Other studies suggest an increase in the future CO_2 sink due to (1) increased wind-driven circulation that should enhance the equatorward transport of anthropogenic carbon (Ito et al., 2010; Sallée et al., 2012) and (2) weakening of the deep water ventilation leading to a decrease in CO_2 outgasing from deep waters of the Southern Ocean (Ito et al., 2015). To date, spatial and temporal coverage of air and sea pCO_2 measurements in the Southern Ocean are inadequate to detect significant trends in its capability to absorb atmospheric CO_2 (Lovenduski et al., 2015). To overcome this issue, robust interpolation methods (neural network and MLD budget-based interpolation) were used to derive continuous air-sea CO_2 fluxes spatially and temporally (Landschützer et al., 2015). Based on this approach, the authors concluded a reduction in the Southern Ocean sink from 1990-2000 occured followed by a strong increase from 2000 to present. This would be due to a more zonally asymmetric atmospheric forcing in the Southern Ocean over the last decade.

Most of the Southern Ocean waters are remote from the coasts and display low contents of the micronutrient iron. The lack of iron, despite high macronutrient availability (Martin et al., 1990; de Baar et al., 1995), together with low surface irradiance and deep mixed layers (Boyd, 2002; Boyd et al., 2007; Venables and Moore, 2010) limit primary production and make the Southern Ocean one of the largest High Nutrient, Low Chlorophyll (HNLC, Minas et al., 1986) areas of the global ocean (Martin, 1990; Minas and Minas, 1992). However, phytoplankton blooms are observed in areas where iron is delivered to surface water such as frontal systems (Moore and Abbott, 2002), downstream of islands plateaus (Blain et al., 2001), in areas influenced by melting glaciers (Gerringa et al., 2012), in seasonally ice-covered zones (Smith and Nelson, 1985, 1986), in coastal polynyas (Arrigo and van Dijken, 2003) and in areas influenced by atmospheric dust deposition (Mahowald et al., 2005). These conditions generally lead to the development of massive, diatom-dominated phytoplankton blooms (Quéguiner, 2013) that strongly decrease DIC concentration in the mixed layer and generate air-to-sea CO_2 fluxes (Merlivat et al., 2015).

The Southern Ocean have played an important role in the glacial-interglacial atmospheric CO_2 variability. Martin (1990) highlighted the inverse relationship between iron concentration and pCO_2 in Vostok ice core over the last 160 kyr, with higher iron concentration and lower pCO_2 during ice ages. It was suggested that higher atmospheric dust deposition during glacial periods would enhance phytoplankton production and the subsequent carbon sequestration to the deep ocean, lowering the atmospheric pCO_2 (the "Iron Hypothesis"). This process could account for ∼30-50 ppmv of the ∼80 ppmv difference in atmospheric pCO_2 between the pre-industrial era and the last glacial maximum (LGM, 25 000 - 18 000 years ago, Bopp et al., 2003; Kohfeld et al., 2005; Wolff et al., 2006). Additional biological mechanisms to lower atmospheric pCO_2 were proposed such as an increase in the carbon to nitrogen ratio of export (Broecker, 1982) and a change in
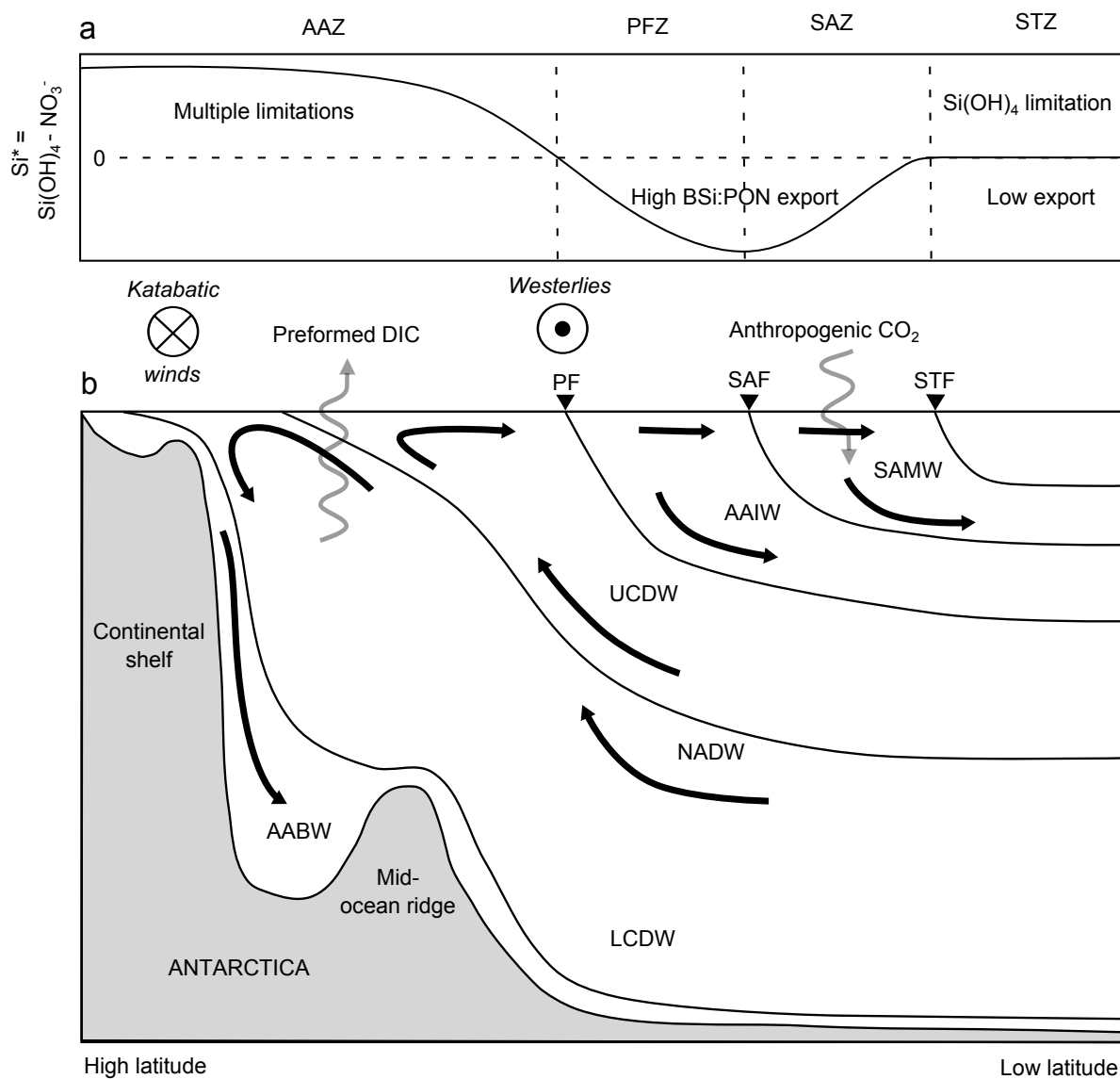
Figure 1.9: **a.** Surface water Si* distribution along a meridional transect in the Southern Atlantic (modified from Sarmiento et al., 2004). **b.** Corresponding vertical section of major circulation pathways and associated water masses. Major ACC fronts (STF: Subtropical Front, SAF: Subantarctic Front, PF: Polar Front) delimit the Southern Ocean hydrological zones (STZ: Subtropical Zone, SAZ: Subantarctic Zone, PFZ: Polar Frontal Zone). Modified from Speer et al. (2000).

the dominant phytoplankton type from calcifyiers to silicifiers (Archer and Maier-Reimer, 1994). Finally, changes in oceanic circulation were also suggested to play an important role in air-sea CO_2 fluxes such as increased stratification that reduces the ventilation of DIC-rich deep waters (Francois et al., 1997; Toggweiler, 1999; Sigman et al., 2010), an increased area of ice-covered waters reducing the CO_2 outgassing (Stephens and Keeling, 2000), and a change in the location and intensity of deep water formation (Toggweiler et al., 2003).

Diatom $Si(OH)_4$ to NO_3^- uptake ratio increases in response to iron limitation (Takeda, 1998; Hutchins and Bruland, 1998). Moreover, the remineralization of N occurs at faster rates than Si, leading to an increase in BSi to particulate organic nitrogen (PON) ratio in exported particles with depth (Ragueneau et al., 2006). For these reasons the Southern Ocean is a place of preferential export and trapping of silicon relative to phosphorus and nitrogen (Holzer et al., 2014). These processes impose negative Si* values (Si* = $Si(OH)_4$-NO_3^-) in productive areas where modal and intermediate water formation takes place (Fig. 1.9a). Given that diatoms are usually thought to drive intense POC export (Boyd and Newton, 1995; Buesseler, 1998), the northward advection of water with low $SiOH_4$ relative to NO_3^- strongly constrains the production of siliceous plankton in the low latitude ocean, with potentially important implications for the exported production (Sarmiento et al., 2004). It has been proposed that a decrease in the $Si(OH)_4$ to NO_3^- uptake ratio in response to increased iron availability during the LGM would have resulted in an increased supply of $Si(OH)_4$ to the low latitude ocean and an increase in primary production at global scale (Brzezinski et al., 2002; Matsumoto et al., 2002). This "Silicic Acid Leakage Hypothesis" (SALH) directly links the stoichiometry of the biological pump in the Southern Ocean to the atmospheric pCO_2 at long time scale. In this context, understanding the ecological factors that are responsible for the stoichiometry of the biological pump in the Southern Ocean remains a fundamental question.

1.4.2   Iron availability and carbon export in the Southern Ocean

High macronutrient concentration in surface waters of the modern-day Southern Ocean suggests that the biological pump is currently inefficient (Fig. 1.7, Volk and Hoffert, 1985; Sarmiento and Orr, 1991). Following Martin (1990) "Iron Hypothesis", numerous programs have studied the impact of natural and artificial iron fertilization on the biological pump in the Southern Ocean (Table 1.1, Fig. 1.10a).

In artificial fertilization experiments, iron sulfate ($FeSO_4$) is delivered to HNLC surface waters together with sulfur hexafluoride (Sf_6) as a conservative tracer. The impact of iron addition on the ocean biogeochemistry is typically studied over short time (weeks) and space ($\sim 100\,km$) scales. As reviewed by de Baar et al. (2005), all of the artificial fertilization experiments to date lead to a decrease in mixed layer DIC inventories

accompanied with an increase in chlorophyll *a*. The significant relationship between maximum chlorophyll *a* concentration and the mixed layer depth suggested an iron-light colimitation. Phytoplankton communities that responded to the iron availability were mostly large diatoms during SOIREE (*Fragilariopsis kerguelensis*, *Trichotoxon reinboldii*, Boyd et al., 2000), SOFEX-S (*F. kerguelensis*, *Thalassiothrix antarctica*, Coale et al., 2004) and EIFEX (*F. kerguelensis*, *Chaetoceros dichaeta*, *T. antarctica*, Smetacek et al., 2012). However, small diatoms (*Pseudo-nitzschia* and *Chaetoceros hyalochaete*), haptophytes/prasinophytes, and other picoeukaryotes were the major groups to respond to iron addition during the EisenEx (Assmy et al., 2007), SAGE (Peloquin et al., 2011), and LOHAFEX (Martin et al., 2013) experiments, respectively. These varied responses demonstrate the importance of initial conditions (notably $Si(OH)_4$ availability) for bloom development and the subsequent export of POC to depth in response to iron addition (Table 1.1). Negligible export was observed in experiments where grazer biomass was high enough to take advantage of the increased phytoplankton biomass and efficiently recycle carbon within the mixed layer (Martin et al., 2013).

Artificial fertilization experiments have provided important information on the ecological and chemical interactions during the initiation, development and fate of phytoplankton blooms in HNLC waters (factors controlling growth rate, nutrient uptake ratio, sensitivity to grazing, export triggering, Boyd et al., 2007, and references therein). However the variability in carbon export and the technical constraints raised questions about the ability of large scale fertilization to fulfil its initial objective and lower atmospheric pCO$_2$ (Chisholm et al., 2001; Zeebe and Archer, 2005). Additionally, numerical models demonstrated that side-effects of artificial fertilization would not balance the benefits. Sarmiento and Orr (1991) reported an anoxia of deep waters at global scale, Aumont and Bopp (2006) suggested that most of the iron added would be lost to the sediments by scavenging and Law (2008) described an increase in greenhouse gases emissions (N_2O, DMS, CH_4) with a potentially positive feedback on global warming. Such cumulative uncertainties on the impact of global scale fertilization cannot be solved short term and spatially limited experiments. Other geoengineering tools such as direct air capture and enhanced silicate weathering are now considered to mitigate the atmospheric increase of CO$_2$ (IPCC, 2013).

We suggest that ocean fertilization, in the open seas or territorial waters, should never become eligible for carbon credits - Chisholm et al. (2001).

The concept of "natural laboratory" evolved concomitantly with artificial fertilization studies. In these studies the biogeochemical functioning of areas naturally fertilized with iron is compared with surrounding HNLC waters. The input of iron from sediments and glacial melt water downstream of the subantarctic islands leads to large scale ($10^4 - 10^5$km^2) and long lasting (few months) phytoplankton blooms (Westberry et al.,

Experiment	Change in POC export	Method	Reference
Artificial fertilization experiments			
SOIREE	No	^{234}Th	Charette and Buesseler (2000)
	No	drifting trap	Nodder and Waite (2001)
SOFEX	×3	^{234}Th	Buesseler et al. (2004)
	×6	optical ARGO	Bishop et al. (2004)
EIFEX	×3	POC stocks	Smetacek et al. (2012)
LOHAFEX	No	drifting trap	Martin et al. (2013)
Natural fertilization experiments			
KEOPS1	×2	^{234}Th	Blain et al. (2007)
CROZEX	×3	moored trap	Pollard et al. (2009)
SAZ-SENSE	÷4	^{234}Th	Jacquet et al. (2011)
DISCOVERY	×2	moored trap	Manno et al. (2015)
BWZ	×3	^{234}Th	Charette (unpublished)

Table 1.1: Effect of natural or artificial fertilization experiments performed in the Southern Ocean on POC export. The change in POC export is the ratio between POC export in the fertilized area compared to the control area. See Fig. 1.10a for the location of the studies.

2013) that were studied by multidisciplinary programs such as KEOPS1 (Blain et al., 2007), KEOPS2, CROZEX (Pollard et al., 2009), and DISCOVERY (Tarling et al., 2012) (Fig. 1.10). Other natural fertilization processes such as upwelling of iron-rich deep waters (BWZ, Zhou et al., 2013), aerosol iron deposition (SAZ-SENSE, Bowie et al., 2011) and sea-ice melting in coastal polynias (DynaLiFe, Arrigo and Alderkamp, 2012) have also been studied. Most of these studies reported an increase in POC export in response to fertilization that was comparable to artificial experiments (Table 1.1). The major difference was the fertilization efficiency: the excess of carbon export per excess of iron added (excess refers to the difference between the fertilized and control site). In artificial fertilization experiments, the efficiency was of the order of magnitude $\sim 10^3 - 10^4$ (mole of C per mole Fe) whereas it reached values $> 10^5$ in natural fertilizations studies (Chever et al., 2010). This is notably due to the mode of iron addition and its bioavailability. Pulsed and intense inputs of iron during artificial fertilization lead to significant dilution and losses (de Baar et al., 2005) whereas slow and continuous natural inputs are more efficiently utilized (Blain et al., 2008b). Additionally, natural iron inputs deliver key ligands maintaining iron available to biology whereas most of the artificial addition of $FeSO_4$ precipitates (Gerringa et al., 2008; Thuróczy et al., 2012). One of the key characteristic of both natural and artificial fertilization studies is their short duration imposed by logistical reasons (e.g. ship availability). This does not allow to study the effect of iron addition at long time scale. Therefore, carbon export is most of the time studied at short time scale using the ^{234}Th technique or drifting traps (Table 1.1). As a consequence, robust estimates of the fertilization efficiency over an entire seasonal cycle are not possible.

Two studies reported the export of material to deep waters over an annual cycle using moored sediment traps in the vicinity of Subantarctic islands. Manno et al. (2015) highlighted the importance of zooplankton faecal pellets for carbon export in the vicinity of South Georgia. Based on faecal pellet types, the authors identified a switch from herbivorous to detritivorous zooplankton from spring to summer in the fertilized waters. In the HNLC waters upstream of the island, detritivorous zooplankton faecal pellets were dominant. At Crozet, Salter et al. (2012) identified resting spores of *Eucampia antarctica* as a potentially efficient vector of carbon export in the fertilized waters. Moreover, the authors described how changes in diatom community between sites were likely to shape the preferential export of silicon and/or carbon. Diatom species with large and/or strong frustules (*F. kerguelensis*, *Corethron pennatum*, *Dactyliosolen antarcticus*) were dominant in the HNLC waters where the BSi:POC export ratio was twofold higher when compared to the productive site. These two studies demonstrated how valuable sediment trap data are to better understand ecological factors driving carbon and biomineral export at annual scales. Such ecological characteristics might explain , for example, why export was four times lower in the iron rich waters during SAZ-SENSE (Table 1.1, Jacquet et al., 2011). The authors invoke a stronger grazer response in the productive site leading to

higher carbon recycling within the mixed layer. This phenomenon was also reported by (Cavan et al., 2015) downstream of South Georgia where the lowest PE$_{\text{eff}}$ was measured. Interestingly, this observation was also reported during artificial fertilization experiments (Martin et al., 2013).

1.4.3 Global distribution of export in the Southern Ocean

Distribution of sediment trap-derived annual records of POC, BSi and PIC export in the Southern Ocean is shown in Fig. 1.10b (black crosses, updated database from Salter et al., 2014). In order to compare the characteristics of export fluxes in different oceanic zones of the Southern Ocean, data were grouped according to their zonal location (SAZ, PFZ, POOZ and SIZ). POC fluxes were normalized to 250 m using the Martin curve and a b value of -1 (a robust value for the Southern Ocean, Guidi et al., 2015). Molar BSi:POC and PIC:POC ratios were also calculated on raw data without any depth normalization. Results are shown as boxplots in Figure 1.11. The annual POC flux normalized to 250 m is significantly lower in the POOZ compared to the SAZ and SIZ and no significant difference can be found between the PFZ and the POOZ. The SAZ, PFZ and SIZ display no significant difference in the BSi:POC ratio and the POOZ shows a significantly higher BSi:POC ratio than the three other oceanographic zones. Finally, the PIC:POC ratio significantly decreases southward with highest values observed in the SAZ and lowest values in the POOZ and SIZ.

Significantly different annual POC fluxes are found depending on the hydrological zone. However, the latitudinal pattern of POC flux does not simply follow the one observed for primary production (Moore and Abbott, 2000). The positive relationship between primary production and export production observed at global scale (Laws et al., 2011) appears not to be valid in the Southern Ocean. More recently, Maiti et al. (2013) compiled short term measurements of NPP and export and demonstrated the inverse relationship between primary production and export efficiency in the Southern Ocean. These results suggest that production itself cannot explain zonal patterns in POC export and that other ecological factors (probably different in each hydrological zone) must be taken into account. The variability in the BSi:POC export ratio probably derives from different contribution of diatom to the exported community, together with a change in diatom silicification level imposed by shift in diatom species and/or modification of the Si:N uptake ratio in response to iron limitation (Hutchins and Bruland, 1998; Takeda, 1998). Lam et al. (2011) have compiled POC concentration profiles in the global ocean and showed that diatom-dominated ecosystems transfer a lower fraction of carbon from the mixed layer to the mesopelagic ocean. A more recent compilation of UVP-derived POC fluxes came to a similar conclusion (Guidi et al., 2015). Lam and Bishop (2007) introduced the concept of "High Biomass, Low Export" regime in which a major part of the large
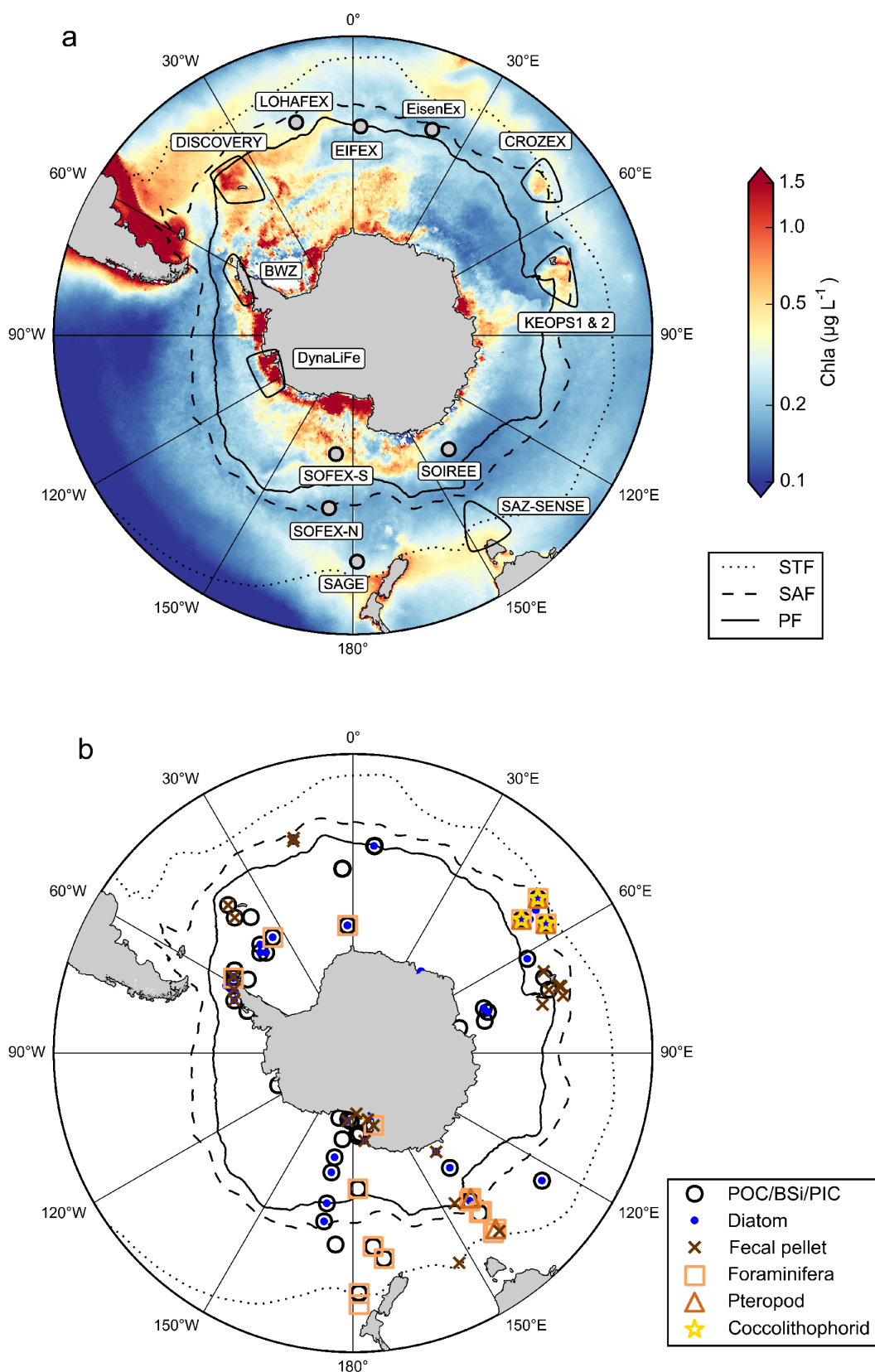
Figure 1.10: **a.** Location of artificial iron fertilization experiments (white dots) and natural fertilization studies (encircled areas) in the Southern Ocean. Background color represents the climatological surface chlorophyll *a* concentration (MODIS full mission). **b.** Distribution of the sediment trap data in the Southern Ocean (black circles). Coloured symbols represent studies where the fluxes of each biological constituent have been reported.

particles produced in the productive upper ocean are fragmented and remineralized by a highly active heterotrophic community of efficient grazers. Results from the SAZ-SENSE project (Table 1.1) are consistent with the HBLE theory (Jacquet et al., 2011). Before the concept of HBLE was proposed, Huntley et al. (1991) suggested with a box model that the elevated biomass of top predators observed in productive Antarctic ecosystems would take advantage of enhanced food availability and respire a significant fraction (up to 22 %) of the primary production.

... respiration of air-breathing predators will be most concentrated relatively near the antarctic continent and few polar islands (...) This phenomenon may be a characteristic feature of especially productive Antarctic marine ecosystems caused by seasonally intensive feeding and respiration of highly concentrated birds and mammals. We conclude that the CO_2 respired by birds and mammals may represents a significant inefficiency in the ability of the Southern Ocean to act as a carbon sink. - (Huntley et al., 1991).

Grazing pressure was also suggested to exert a strong control on the decoupling of the POC and BSi export. Smetacek et al. (2004) proposed that under iron-sufficient conditions, small and lightly silcified diatom would preferentially export carbon while under iron-limiting conditions, the high grazing pressure of copepods would results in the accumulation of large and heavily silicified diatom exporting preferentially silicon. This hypothesis was verified during the EIFEX artificial fertilization experiment (Assmy et al., 2013). Authors identified a "silica sinker" community composed of robust, highly silicified species like *F. kerguelensis* and a "carbon sinker" community made of small, lightly silicified "bloom-and-bust" species characteristic of productive areas such as *Chaetoceros dichaeta*. A preferential export of "silica sinkers" in the POOZ would explain the higher BSi:POC export ratio. A detailed description of the exported plankton community remains necessary to better understand what are the ecological processes impacting the intensity and stoichiometry of export fluxes.

Previous studies have provided a description of some of the biological components of export (Fig. 1.10b). Highest diatom fluxes recorded by sediment traps ($>1 \times 10^9$ valve m^{-2} d^{-1}) were observed in the SIZ near Prydz Bay and Adélie Land and were dominated by *F. kerguelensis* and smaller *Fragilariopsis* species (Suzuki et al., 2001; Pilskaln et al., 2004). In the POOZ, highest diatom fluxes were 2 orders of magnitude lower (1×10^7 valve m^{-2} d^{-1} Abelmann and Gersonde, 1991; Salter et al., 2012; Grigorov et al., 2014). Despite a generally positive correlation between POC fluxes and diatom export fluxes over a seasonal cycle (Romero and Armand, 2010; Salter et al., 2012; Rigual-Hernández et al., 2015b), a quantitative estimation of diatom contribution to carbon export fluxes in the Southern Ocean has been poorly studied. In contrast, the contribution of faecal pellets to POC fluxes has received wide attention. It is typically higher in shelf regions (Schnack-Schiel and Isla, 2005), with highest numerical fluxes and a contribution to POC flux >90%
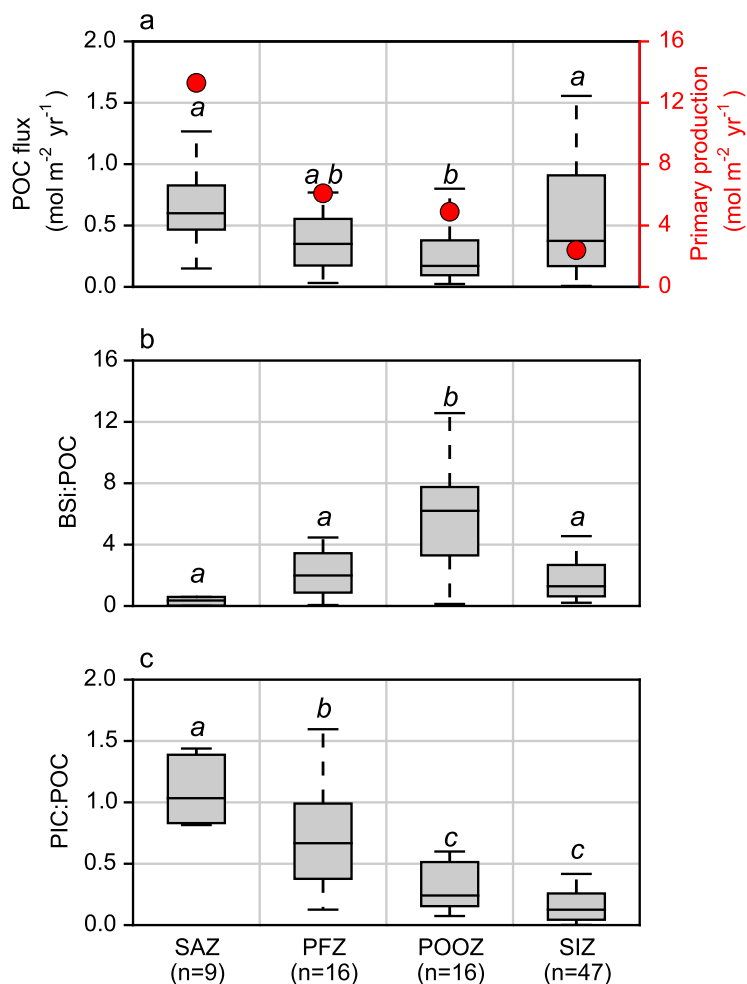
Figure 1.11: Export properties in different Southern Ocean oceanographic zones. **a.** POC flux from annual sediment trap records in the Southern Ocean normalized to 250 m using a b value of -1. Red dots represent the average annual primary production for each hydrological zone (Moore and Abbott, 2000).**b.** BSi:POC ratio. **c.** PIC:POC ratio. Italic letters correspond to significantly homogeneous groups as determined by a Kruskall-Wallis test followed by a post-hoc Tuckey test (p=0.05).

observed in the Bransfield Strait (Bodungen, 1986; Wefer et al., 1988). Authors have attributed these faecal pellets to the massive Antarctic krill (*Euphausia superba*) populations in the marginal ice zone of the Scotia Sea.

Although the Southern Ocean has been typically considered as a diatom dominated system, more recent work has established the significance of calcifying communities. Satellite-derived PIC concentrations have been used to describe a "great calcite belt" located in the PFZ and SAZ (Balch et al., 2005, 2011) that has been attributed to coccolithophores. It is now clear that coccolithophores are present in the Southern Ocean, even south of the Polar Front (Winter et al., 2014). Coccolithophore abundance decreases southward and they are mainly represented by the cosmopolitan species *Emiliania huxleyi* (Cubillos et al., 2007; Saavedra-Pellitero et al., 2014). This zonal pattern is consistent with the southward decrease in the PIC:POC export ratio (Fig. 1.11c). However, coccolithophores are not necessarily the dominant calcifying plankton in the Southern Ocean, and foraminifera and pteropods have to be taken into account. Highest planktic foraminifera fluxes of $1 \times 10^4\,\mathrm{individual\,m^{-2}\,d^{-1}}$ were reported in the SAZ south of Tasmania (King and Howard, 2003). Authors reported a southward decrease in the foraminifera export fluxes accompanied by a switch from temperate (*Globigerina bulloides*) to cold-water species (*Neoglobiquadrina pachyderma*). In a review, Hunt et al. (2008) have compiled pteropods abundance in the Southern Ocean and reported a switch from a dominance of *Limacina retroversa australis* north of the PF to *Limacina helicina antarctica* south of the PF. Salter et al. (2014) quantified the role of each calcifying organism on the carbonate counter pump in the vicinity of the Crozet Islands. Strong foraminifera response to phytoplankton biomass in the naturally fertilized region in the PFZ was responsible for a major part of the intense PIC fluxes that drove a carbonate counter pump representing 10-30 % of the POC flux. This study emphasized the need to take into account the carbonate counter pump effect to calculate a robust carbon budget. To date, it is the only study that quantified and partitioned the carbonate counter-pump among the calcifying planktonic organisms.

... despite early warnings sent by ecologists (Banse, 1990; Wassmann, 1997), our community of biogeochemists has tried to understand the functionning of the biological pump from a too extreme "flux-oriented" perspective and most importantly, probably looking at the wrong temporal and spacial scales. - (Ragueneau et al., 2006).

1.5 Thesis structure and objectives

This PhD thesis is based on seven scientific articles, published (five) or in preparation (two) that aim to increase our present understanding of mechanisms regulating the intensity and stoichiometry of export fluxes in the Southern Ocean. It is organised in four chapters that address the following specific objectives:

- **Chapter 2.** Provides a detailed description of diatom and faecal pellet contribution to POC export over an annual cycle in the two island systems of Southern Ocean: the Kerguelen Islands (**article 1, 2 and 3**) and the South Georgia Island (**article 4**). The articles describe how diatom ecological strategies (e.g. resting spore formation, protection by a thick frustule or a large size) influence the preferential export of carbon and silicon (**article 2, 3 and 4**).

- **Chapter 3.** Describes how plankton diversity regulates particulate matter stoichiometry and composition. Firstly, how microplankton community structure constrains the particulate matter C:N:P:Si stoichiometry in summer around the Crozet and Kerguelen Plateaus. What are the physiological and ecological processes leading to the observed particulate matter stoichiometry and what are the implications for C and Si export (**article 5**) ? Secondly, the lipid composition of export will be compared in three Southern Ocean island systems (Kerguelen, Crozet, and South Georgia). The link between the lipids composition of export fluxes and the biological constituents of export is be investigated to understand how they shape the lability of the exported matter (**manuscript in preparation**).

- **Chapter 4.** Estimates the carbonate counter pump intensity over the Kerguelen Plateau and partitioning of PIC fluxes among the major calcifying organisms. The article evaluates the influence of diversity of calcifying organisms and their morphological characteristics (e. g. size-normalized test weight) to the intensity of PIC fluxes (**article 6**).

- **Perspectives.** Introduces new variables and tools to study the biological pump. Firstly it proposes additional variables to quantify in sediment trap studies. Secondly, using a compilation of bio-optical data from the KEOPS cruises and the SOCLIM bio-argo floats, it describes the seasonal evolution of biomass distribution and attenuation with depth and identify parameters likely to influence these variables. Finally, a simple numerical model is developed that builds on the observational data acquired during the thesis to consider ecological processes such as resting spore formation. Simulations are compared with the observed export.

2 | Ecological vectors of export fluxes

Contents

2.1   Export fluxes over the Kerguelen Plateau (articles 1 and 2)

The **first article** provides a detailed description of the physical environment of a sediment trap moored over the central Kerguelen Plateau during the KEOPS2 cruise. The reliability of the sediment trap data is discussed in the hydrological context and compared with concomitant short term estimates of POC export during KEOPS2 and previous estimates from KEOPS 1. It appears that the POC flux reported by the trap at 289 m is much lower than estimates at 200 m in spring, summer and at annual scale. The favourable hydrodynamical conditions do not support a hydrodynamical bias, but the hypothesis of zooplankton feeding on the trap funnel cannot be neglected. However, strong carbon export attenuation due to efficient grazers and possibly mesopelagic fish activity is also likely to explain the low POC export fluxes observed at annual scale below the winter mixed layer. Thus the central plateau would also be, as other productive sites of the Southern Ocean, a high biomass-low export environment.

Sediment trap samples processing, swimmer sorting, mass flux and POC/PON analyses were performed by the author. Raw physical data were provided by the Direction Technique de l'INSU (CNRS).

The **second article** describes the diatom and faecal pellet contribution to the POC fluxes collected from the trap introduced in the **article 1**. Contrary to previous studies, the diatom were enumerated using a simple biological method that allows the differentiation of full and empty cells. Thereby the accurate quantification of diatom contribution to POC flux is possible. At annual scale, the export of *Chaetoceros Hyalochaete* and *Thalassiosira antarctica* resting spores drives >60 % of the POC flux, whereas faecal pellets contribution is lower (36 %). It is hypothesized that diatom resting spores are able to bypass the strong grazing pressure responsible for the low POC flux observed at annual scale. A strong relationship between the BSi:POC ratio and the empty:full cell ratio suggests that the ecological processes regulating the abundance of empty frustules (e.g. grazing, viral lysis) impose a first order control on the export stoichiometry. Moreover, the empty:full cell ratio is species-specific, appears consistent with previous classification of species as preferential "silica sinkers" or "carbon sinkers".

BSi analyses, phytoplankton identification and biomass calculation, faecal pellet imaging and measurements were performed by the author.

Biogeosciences

Export fluxes in a naturally iron-fertilized area of the Southern Ocean – Part 1: Seasonal dynamics of particulate organic carbon export from a moored sediment trap

M. Rembauville[1,2], **I. Salter**[1,2,3], **N. Leblond**[4,5], **A. Gueneugues**[1,2], and **S. Blain**[1,2]

[1]Sorbonne Universités, UPMC Univ Paris 06, UMR7621, LOMIC, Observatoire Océanologique, Banyuls-sur-Mer, France
[2]CNRS, UMR7621, LOMIC, Observatoire Océanologique, Banyuls-sur-Mer, France
[3]Alfred Wegener Institute for Polar and Marine Research, Bremerhaven, Germany
[4]Sorbonne Universités, UPMC Univ Paris 06, LOV, UMR7093, Observatoire Océanologique, Villefranche-sur-Mer, France
[5]CNRS-INSU, LOV, UMR7093, Observatoire Océanologique, Villefranche-sur-Mer, France

Correspondence to: M. Rembauville (rembauville@obs-banyuls.fr)

Abstract. A sediment trap moored in the naturally iron-fertilized Kerguelen Plateau in the Southern Ocean provided an annual record of particulate organic carbon and nitrogen fluxes at 289 m. At the trap deployment depth, current speeds were typically low ($\sim 10\,\mathrm{cm\,s^{-1}}$) and primarily tidal-driven (M2 tidal component). Although advection was weak, the sediment trap may have been subject to hydrodynamical and biological (swimmer feeding on trap funnel) biases. Particulate organic carbon (POC) flux was generally low ($< 0.5\,\mathrm{mmol\,m^{-2}\,d^{-1}}$), although two episodic export events (< 14 days) of $1.5\,\mathrm{mmol\,m^{-2}\,d^{-1}}$ were recorded. These increases in flux occurred with a 1-month time lag from peaks in surface chlorophyll and together accounted for approximately 40 % of the annual flux budget. The annual POC flux of $98.2 \pm 4.4\,\mathrm{mmol\,m^{-2}\,yr^{-1}}$ was low considering the shallow deployment depth but comparable to independent estimates made at similar depths ($\sim 300\,\mathrm{m}$) over the plateau, and to deep-ocean ($> 2\,\mathrm{km}$) fluxes measured from similarly productive iron-fertilized blooms. Although undertrapping cannot be excluded in shallow moored sediment trap deployment, we hypothesize that grazing pressure, including mesozooplankton and mesopelagic fishes, may be responsible for the low POC flux beneath the base of the winter mixed layer. The importance of plankton community structure in controlling the temporal variability of export fluxes is addressed in a companion paper.

1 Introduction

The biological carbon pump is defined as the downward transfer of biologically fixed carbon from the ocean surface to the ocean interior (Volk and Hoffert, 1985). Global estimates of particulate organic carbon (POC) export cluster between $5\,\mathrm{Pg\,C\,yr^{-1}}$ (Moore et al., 2004; Lutz et al., 2007; Honjo et al., 2008; Henson et al., 2011; Lima et al., 2014) and $10\,\mathrm{Pg\,C\,yr^{-1}}$ (Laws et al., 2000; Schlitzer, 2004; Gehlen et al., 2006; Boyd and Trull, 2007; Dunne et al., 2007; Laws et al., 2011). The physical transfer of dissolved inorganic carbon to the ocean interior during subduction of water masses is 2 orders of magnitude higher ($> 250\,\mathrm{Pg\,C\,yr^{-1}}$; Karleskind et al., 2011; Levy et al., 2013). The global ocean represents a net annual CO_2 sink of $2.5\,\mathrm{Pg\,C\,yr^{-1}}$ (Le Quéré et al., 2013), slowing down the increase in the atmospheric CO_2 concentration resulting from anthropogenic activity. Although the Southern Ocean (south of 44° S) plays a limited role in the net air–sea CO_2 flux (Lenton et al., 2013), it is a key component of the global anthropogenic CO_2 sink representing one-third the global oceanic sink ($\sim 1\,\mathrm{Pg\,C\,yr^{-1}}$) while covering 20 % of its surface (Gruber et al., 2009). The solubility pump is considered to be the major component of this sink, whereas the biological carbon pump is considered to be inefficient in the Southern Ocean and sensitive to iron supply.

Following "the iron hypothesis" in the 1990s (Martin, 1990), iron limitation of high-nutrient, low-chlorophyll (HNLC) areas, including the Southern Ocean, has been tested

in bottle experiments (de Baar et al., 1990) and through in situ artificial fertilization experiments (de Baar et al., 2005; Boyd et al., 2007). Results from these experiments are numerous and essentially highlight that the lack of iron limits macronutrient (N, P, Si) utilization (Boyd et al., 2005; Hiscock and Millero, 2005) and primary production (Landry et al., 2000; Gall et al., 2001; Coale et al., 2004) in these vast HNLC areas of the Southern Ocean. Due to a large macronutrient repository, the biological carbon pump in the Southern Ocean is considered to be inefficient in its capacity to transfer atmospheric carbon to the ocean interior (Sarmiento and Gruber, 2006). In the context of micronutrient limitation, sites enriched in iron by natural processes have also been studied and include the Kerguelen Islands (Blain et al., 2001, 2007), the Crozet Islands (Pollard et al., 2007), the Scotia Sea (Tarling et al., 2012) and the Drake Passage (Measures et al., 2013). Enhanced primary producer biomass in association with natural iron supply (Korb and Whitehouse, 2004; Seeyave et al., 2007; Lefèvre et al., 2008) strongly support trace-metal limitation. Furthermore, indirect seasonal budgets constructed from studies of naturally fertilized systems have been capable of demonstrating an increase in the strength of the biological carbon pump (Blain et al., 2007; Pollard et al., 2009), although strong discrepancies in carbon to iron sequestration efficiency exist between systems. To date, direct measurements of POC export over seasonal cycles from naturally fertilized blooms in the Southern Ocean are limited to the Crozet Plateau (Pollard et al., 2009; Salter et al., 2012). The HNLC Southern Ocean represents a region where changes in the strength of the biological pump may have played a role in the glacial–interglacial CO_2 cycles (Bopp et al., 2003; Kohfeld et al., 2005) and have some significance to future anthropogenic CO_2 uptake (Sarmiento and Le Quéré, 1996). In this context, additional studies that directly measure POC export from naturally iron-fertilized blooms in the Southern Ocean are necessary.

POC export can be estimated at short timescales (days to weeks) using the ^{234}Th proxy (Coale and Bruland, 1985; Buesseler et al., 2006; Savoye et al., 2006), by optical imaging of particles (e.g. Picheral et al., 2010, Jouandet et al., 2011) or by directly collecting particles into surface-tethered sediment traps (e.g. Maiti et al., 2013 for a compilation in the Southern Ocean) or neutrally buoyant sediment traps (e.g. Salter et al., 2007; Rynearson et al., 2013). Temporal variability of flux in the Southern Ocean precludes extrapolation of discrete measurements to estimate seasonal or annual carbon export. However, seasonal export of POC can be derived from biogeochemical budgets (Blain et al., 2007; Jouandet et al., 2011; Pollard et al., 2009) or be directly measured by moored sediment traps (e.g. Salter et al., 2012). Biogeochemical budgets are capable of integrating over large spatial and temporal scales but may incorporate certain assumptions and lack information about underlying mechanisms. Direct measurement by sediment traps rely on fewer assumptions but their performance is strongly related to prevailing hydrody-

namic conditions (Buesseler et al., 2007a), which can be particularly problematic in the surface ocean. Measuring the hydrological conditions characterizing mooring deployments is therefore crucial to address issues surrounding the efficiency of sediment trap collection.

The ecological processes responsible for carbon export remain poorly characterized (Boyd and Trull, 2007). There is a strong requirement for quantitative analysis of the biological components of export to elucidate patterns in carbon and biomineral fluxes to the ocean interior (Francois et al., 2002; Salter et al., 2010; Henson et al., 2012; Le Moigne et al., 2012; Lima et al., 2014). Long-term deployment of moored sediment traps in areas of naturally iron-fertilized production, where significant macro- and micronutrient gradients seasonally structure plankton communities, can help to establish links between ecological succession and carbon export. For example, sediment traps around the Crozet Plateau (Pollard et al., 2009) identified the significance of *Eucampia antarctica* var. *antarctica* resting spores for carbon transfer to the deep ocean, large empty diatom frustules for Si : C export stoichiometry (Salter et al., 2012) and heterotrophic calcifiers for the carbonate counter pump (Salter et al., 2014).

The increase in primary production resulting from natural fertilization might not necessarily lead to significant increases in carbon export. The concept of "high-biomass, low-export" (HBLE) environments was first introduced in the Southern Ocean (Lam and Bishop, 2007). This concept is partly based on the idea that a strong grazer response to phytoplankton biomass leads to major fragmentation and remineralization of particles in the twilight zone, shallowing the remineralization horizon (Coale et al., 2004). In these environments, the efficient utilization and reprocessing of exported carbon by zooplankton leads to faecal-pellet-dominated, low-POC fluxes (Ebersbach et al., 2011). A synthesis of short-term sediment trap deployments, ^{234}Th estimates of upper ocean POC export, and in situ primary production measurements in the Southern Ocean by Maiti et al. (2013) highlighted the inverse relationship between primary production and export efficiency, verifying the HBLE status of many productive areas in the Southern Ocean. The iron-fertilized bloom above the Kerguelen Plateau exhibits strong remineralization in the mixed layer compared to the mesopelagic (Jacquet et al., 2008) and high bacterial carbon demand (Obernosterer et al., 2008), features consistent with a HBLE regime. Moreover, an inverse relationship between export efficiency and zooplankton biomass in the Kerguelen Plateau region supports the key role of grazers in the HBLE scenario (Laurenceau-Cornec et al., 2015). Efficient grazer responses to phytoplankton biomass following artificial iron fertilization of HNLC regions also demonstrate increases in net community production that are not translated to an increase in export fluxes (Lam and Bishop, 2007; Tsuda et al., 2007; Martin et al., 2013; Batten and Gower, 2014).

POC flux attenuation with depth results from processes occurring in the euphotic layer (setting the particle export

efficiency, Henson et al., 2012) and processes occurring in the twilight zone between the euphotic layer and ~ 1000 m (Buesseler and Boyd, 2009), setting the transfer efficiency (Francois et al., 2002). These processes are mainly biologically driven (Boyd and Trull, 2007) and involve a large diversity of ecosystem components from bacteria (Rivkin and Legendre, 2001; Giering et al., 2014), protozooplankton (Barbeau et al., 1996), mesozooplankton (Dilling and Alldredge, 2000; Smetacek et al., 2004) and mesopelagic fishes (Davison et al., 2013; Hudson et al., 2014). The net effect of these processes is summarized in a power-law formulation of POC flux attenuation with depth proposed by Martin et al. (1987) that is still commonly used in data and model applications. The b exponent in this formulation has been reported to range from 0.4 to 1.7 (Buesseler et al., 2007b; Lampitt et al., 2008; Henson et al., 2012) in the global ocean. Nevertheless, a change in the upper mesopelagic community structure (Lam et al., 2011) and, more precisely, an increasing contribution of mesozooplankton (Lam and Bishop, 2007; Ebersbach et al., 2011) could lead to a shift toward higher POC flux attenuation with depth.

In this paper, we provide the first annual description of the POC and PON export fluxes below the mixed layer within the naturally fertilized bloom of the Kerguelen Plateau, and we discuss the reliability of these measurements considering the hydrological and biological context. A companion paper (Rembauville et al., 2015) addresses our final aim: to identify the ecological vectors that explain the intensity and the stoichiometry of the fluxes.

2 Material and methods

2.1 Trap deployment and mooring design

As part of the KEOPS2 multidisciplinary programme, a mooring line was deployed at station A3 (50°38.3 S–72°02.6 E) in the Permanently Open Ocean Zone (POOZ), south of the polar front (PF; Fig. 1). The mooring line was instrumented with a Technicap PPS3 (0.125 m² collecting area, 4.75 aspect ratio) sediment trap and inclinometer (NKE S2IP) at a depth of 289 m (seafloor depth 527 m; Fig. 2). A conductivity–temperature–pressure (CTD) sensor (Sea-Bird SBE 37) and a current meter (Nortek Aquadopp) were placed on the mooring line 30 m beneath the sediment trap (319 m). The sediment trap collection period started on 21 October 2011 and continued until 7 September 2012. The sediment trap was composed of 12 rotating sample cups (250 mL) filled with a 5 % formalin hypersaline solution buffered with sodium tetraborate at pH = 8. Rotation of the carousel was programmed to sample short intervals (10–14 days) between October and February to optimize the temporal resolution of export from the bloom, and long intervals (99 days) between February and September. All instruments had a 1 h recording interval. The current meter failed on 7 April 2012.
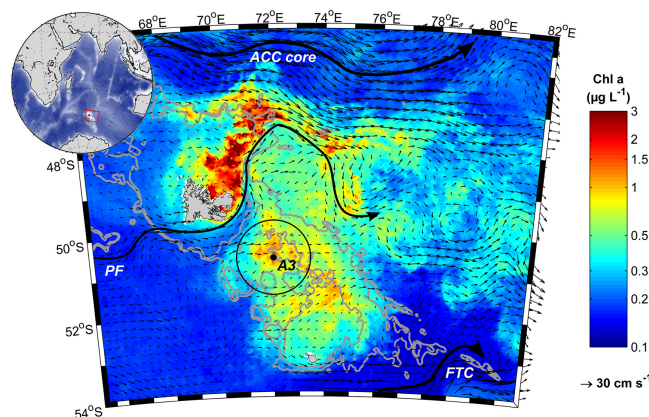
Figure 1. Localization of the Kerguelen Plateau in the Indian sector of the Southern Ocean and detailed map of the satellite-derived surface chlorophyll a concentration (MODIS level 3 product) averaged over the sediment trap deployment period. Sediment trap location at station A3 is represented by a black dot, whereas the black circle represents the 100 km radius area used to average the surface chlorophyll a time series. Arrows represent surface geostrophic circulation derived from the absolute dynamic topography (AVISO product). Positions of the Antarctic Circumpolar Current core (AAC core), the polar front (PF) and the Fawn Trough Current (FTC) are shown by thick black arrows. Grey lines are 500 and 1000 m isobaths.

2.2 Surface chlorophyll data

The MODIS AQUA level 3 (4 km grid resolution, 8-day averages) surface chlorophyll a product was extracted from the NASA website (http://oceancolor.gsfc.nasa.gov/) for the sediment trap deployment period. An annual climatology of surface chlorophyll a concentration, based on available satellite products (1997–2013), was calculated from the multisatellite GlobColour product. The GlobColour level 3 (case 1 waters, 4.63 km resolution, 8-day averages) product merging SeaWiFS, MODIS and MERIS data with GSM merging model (Maritorena and Siegel, 2005) was accessed via http://www.globcolour.info. Surface chlorophyll a concentrations derived from GlobColour (climatology) and MODIS data (deployment year) were averaged across a 100 km radius centred on the sediment trap deployment location (Fig. 1).

2.3 Time series analyses of hydrological parameters

Fast Fourier transform (FFT) analysis was performed on the annual time series data obtained from the mooring, depth and potential density anomaly (σ_θ) that were derived from the CTD sensor. Significant peaks in the power spectrum were identified by comparison to red noise, a theoretical signal in which the relative variance decreases with increasing frequency (Gilman et al., 1963). The red noise signal was considered as a null hypothesis, and its power spectrum was scaled to the 99th percentile of χ^2 probability. Power peaks higher than 99 % red noise values were considered to be sta-
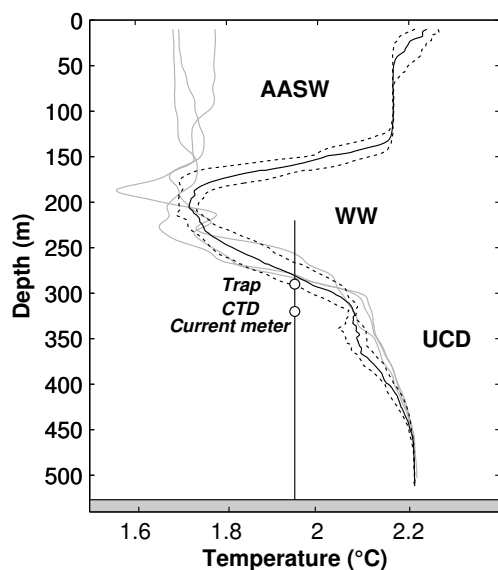
Figure 2. Schematic of the instrumented mooring line against vertical temperature profiles. The sediment trap and the current meter/CTD sensor location on the mooring line are shown by white circles. Temperature profiles performed during the sediment trap deployment (20 October 2011) are represented by grey curves. The solid black curve is the median temperature profile from 12 casts realized on the 16 November 2011. Dashed black lines are the first and third quartiles from these casts. The grey rectangle represents the Kerguelen Plateau seafloor. The different water masses are Antarctic Surface Water (AASW), Winter Water (WW) and Upper Circumpolar Deep Water (UCDW).

tistically significant (Schulz and Mudelsee, 2002), enabling the identification of periods of major variability in time series. In order to identify the water masses surrounding the trap, temperature and salinity recorded by the mooring CTD were placed in context to previous CTD casts conducted at station A3 during KEOPS1 (39 profiles, 23 January 2005–13 February 2005) and KEOPS2 (12 profiles, from 15 to 17 November).

2.4 Sediment trap material analyses

Upon recovery of the sediment trap the pH of the supernatant was measured in every cup and 1 mL of 37 % formalin buffered with sodium tetraborate (pH = 8) was added. After allowing the particulate material to settle to the base of the sample cup (~ 24 h), 60 mL of supernatant was removed with a syringe and stored separately. The samples were transported in the dark at 4 °C (JGOFS Sediment Trap Methods, 1994) and stored under identical conditions upon arrival at the laboratory until further analysis. Nitrate, nitrite, ammonium and phosphate in the supernatant were analysed colorimetrically (Aminot and Kerouel, 2007) to check for possible leaching of dissolved inorganic nitrogen and phosphorus from the particulate phase.

Samples were first transferred to a Petri dish and examined under stereomicroscope (Leica MZ8, $\times 10$ to $\times 50$ magnification) to determine and isolate swimmers (i.e. organisms that actively entered the cup). All swimmers were carefully sorted, cleaned (rinsed with preservative solution), enumerated and removed from the cups for further taxonomic identification. The classification of organisms as swimmers remains subjective, and there is no standardized protocol. We classified zooplankton organisms as swimmers if organic material and preserved structures could be observed. Empty shells, exuvia (exoskeleton remains) and organic debris were considered part of the passive flux. Sample preservation prevented the identification of smaller swimmers (mainly copepods), but, where possible, zooplankton were identified following Boltovskoy (1999).

Following the removal of swimmers, samples were quantitatively split into eight aliquots using a Jencons peristaltic splitter. A splitting precision of 2.9 % (coefficient of variation) was determined by weighing the particulate material obtained from each of four 1/8th aliquots (see below). Aliquots for chemical analyses were centrifuged (5 min at 3000 rpm) with the supernatant being withdrawn after this step and replaced by Milli-Q-grade water to remove salts. Milli-Q rinses were compared with ammonium formate. Organic carbon content was not statistically different even though nitrogen concentrations were significantly higher; as a consequence, Milli-Q rinses were routinely performed. The rinsing step was repeated three times. The remaining pellet was freeze-dried (SGD-SERAIL, 0.05–0.1 mbar, -30 to 30 °C, 48 h run) and weighed three times (Sartorius MC 210 P balance, precision $\times 10^{-4}$ g) to calculate the total mass. The particulate material was ground to a fine powder and used for measurements of particulate constituents.

For particulate organic carbon (POC) and particulate organic nitrogen (PON) analyses, 3 to 5 mg of the freeze-dried powder was weighed directly into pre-combusted (450 °C, 24 h) silver cups. Samples were decarbonated by adding 20 µL of 2 M analytical-grade hydrochloric acid (Sigma-Aldrich). Acidification was repeated until no bubbles could be seen, ensuring all particulate carbonate was dissolved (Salter et al., 2010). Samples were dried overnight at 50 °C. POC and PON were measured with a CHN analyser (Perkin Elmer 2400 Series II CHNS/O elemental analyser) calibrated with glycine. Samples were analysed in triplicate with an analytical precision of less than 0.7 %. Due to the small amount of particulate material in sample cups #5 and #12, replicate analyses were not possible. Uncertainty propagation for POC and PON flux was calculated as the quadratic sum of errors on mass flux and POC/PON content in each sample. The annual flux ($\pm$ standard deviation) was calculated as the sum of the time-integrated flux.
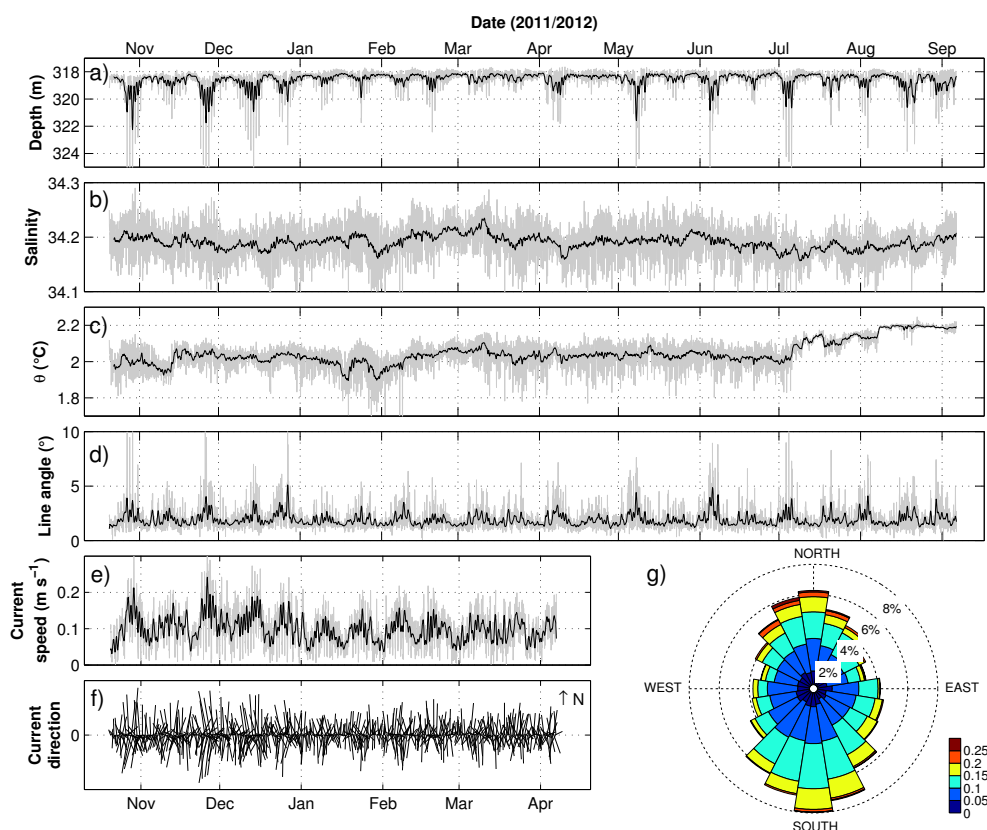
Figure 3. Hydrological properties recorded by the instrument mooring at station A3. (a) Depth of the CTD sensor, (b) salinity, (c) potential temperature, (d) line angle, and (e) current speed. In (a)–(e), grey lines are raw data, and black lines are low-pass-filtered data with a Gaussian filter (40 h window as suggested by the spectral analysis). (f) Direction and speed of currents represented by vectors (undersampled with a 5 h interval) and (g) wind rose plot of current direction and intensities (dotted circles are directions relatives frequencies and colours refer to current speed (m s^{-1})).
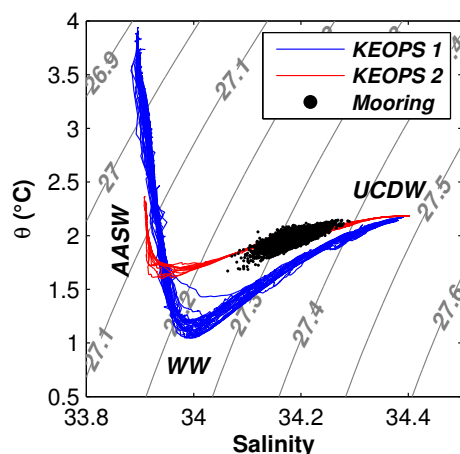
Figure 4. Potential temperature–salinity diagram at station A3. Data are from the moored CTD (black dots), KEOPS1 (blue line) and KEOPS2 (red line). Grey lines are potential density anomaly. The different water masses are Antarctic Surface Water (AASW), Winter Water (WW) and Upper Circumpolar Deep Water (UCDW).

3   Results

3.1   Physical conditions around trap

The sediment trap was deployed in the upper layers of Upper Circumpolar Deep Water (UCDW), beneath seasonally mixed Winter Water (WW; Fig. 2). The depth of the CTD sensor varied between 318 and 322 m (1 and 99 % quantiles), with rare deepening to 328 m (Fig. 3a). Variations in tilt angle of the sediment trap were also low, mostly between 1 and 5°, and occasionally reaching 13° (Fig. 3d). Current speed amplitude varied between 4 and 23 cm s^{-1} (1 and 99 % quantiles), with a maximum value of 33 cm s^{-1} and a mean value of 9 cm s^{-1} (Fig. 3e). Horizontal flow vectors were divided between northward and southward components with strongest current speeds observed to flow northward (Fig. 3f and g).

The range in potential temperature and salinity was 1.85–2.23 °C and 34.12–34.26 (1–99 % quantiles; Fig. 3b and c). From July to September 2012, a mean increase of 0.2 °C in potential temperature was associated with a strong diminution of high-frequency noise, suggesting a drift of the
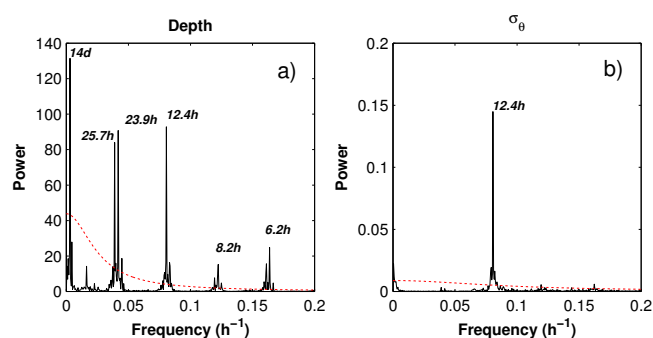
Figure 5. Power spectrum of the spectral analysis of (a) depth time series and (b) potential density anomaly time series. Pure red noise (null hypothesis) is represented by red dashed lines for each variable. The period corresponding to a significant power peak (power peak higher than the red noise) is written.

Figure 6. Progressive vector diagram (integration of the current vectors all along the current meter record) calculated from current meter data at 319 m. The colour scale refers to date.

temperature sensor. Consequently these temperature data were rejected from the time series analysis. The potential temperature–salinity diagram is compared to KEOPS1 and KEOPS2 CTD downcast at station A3 (Fig. 4). The CTD sensor recorded the signature of the UCDW, and no intrusion of overlying WW could be detected.

The power spectrum of vertical sediment trap displacements identified six significant peaks corresponding to frequencies of 6.2, 8.2, 23.9 and 25.7 h and 14 days (Fig 5a). Concomitant peaks of depth, angle and current speed were also observed with a period of 14 days. However, spectral analysis of the potential density anomaly σ_θ revealed only one significant major power peak corresponding to a frequency of 12.4 h (Fig. 5b). Isopycnal displacements were driven by the unique tidal component (M2, 12.4 h period) and trap displacements resulted from a complex combination of multiple tidal components. The power spectrum analysis suggested that a 40 h window was relevant to filter out most of the short-term variability (black line in Fig. 3a–e).

A pseudo-Lagrangian trajectory was calculated by cumulating the instantaneous current vectors (Fig. 6). Over short timescales (hours to day) the trajectory displays numerous tidal ellipses. The flow direction is mainly to the southeast in October 2011 to December 2011 and northeast from December 2011 to April 2012. For the entire current meter record (6 months) the overall displacement followed a 120 km northeasterly, anticlockwise trajectory with an effective eastward current speed of approximately 1 cm s^{-1}.

3.2 Seasonality of surface chlorophyll *a* concentration above trap location

The seasonal variations of surface chlorophyll *a* concentration for the sediment trap deployment period differed significantly from the long-term climatology (Fig. 7a). The bloom started at the beginning of November 2011, 10 days after the start of the sediment trap deployment. Maximum sur-

face chlorophyll *a* values of 2.5 µg L^{-1} occurred on the first week of November and subsequently declined rapidly to 0.2 µg L^{-1} in late December 2011. A second increase in surface chlorophyll *a* up to 1 µg L^{-1} occurred in January 2012, and values decreased to winter levels of 0.2 µg L^{-1} in February 2012. A short-term increase of 0.8 µg L^{-1} occurred in mid-April 2012.
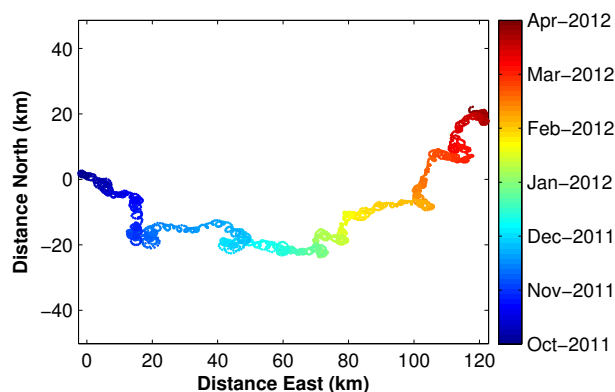
3.3 Swimmer abundances

No swimmers were found in cups #3 and #5 (Table 2). Total swimmer numbers were highest in winter (1544 individuals in cup #12). When normalized to cup opening time, swimmer intrusion rates were highest between mid-December 2011 and mid-February 2012 (from 26 to 55 individuals per day) and lower than 20 individuals per day for the remainder of the year. Swimmers were numerically dominated by copepods throughout the year, but elevated amphipod and pteropod abundances were observed at the end of January and February 2012 (Table 2). There was no significant correlation between mass flux, POC and PON fluxes and total swimmer number or intrusion rate (Spearman's correlation test, $p > 0.01$). Copepods were essentially small cyclopoid species. Amphipods were predominantly represented by the hyperidean *Cyllopus magellanicus* and *Themisto gaudichaudii*. Pteropods were represented by *Clio pyramidata*, *Limacina helicina* forma *antarctica* and *Limacina retroversa* subsp. *australis*. Euphausiids were only represented by the genus *Thysanoessa*. One *Salpa thompsoni* salp (aggregate form) was found in the last winter cup #12.

3.4 Seasonal particulate organic carbon and nitrogen fluxes

Particulate organic carbon flux ranged from 0.15 to 0.55 mmol m^{-2} d^{-1} during the productive period except during two short export events of 1.6 ± 0.04 and 1.5 ± 0.04 mmol m^{-2} d^{-1} sampled in cups #4 (2 to 12 De-
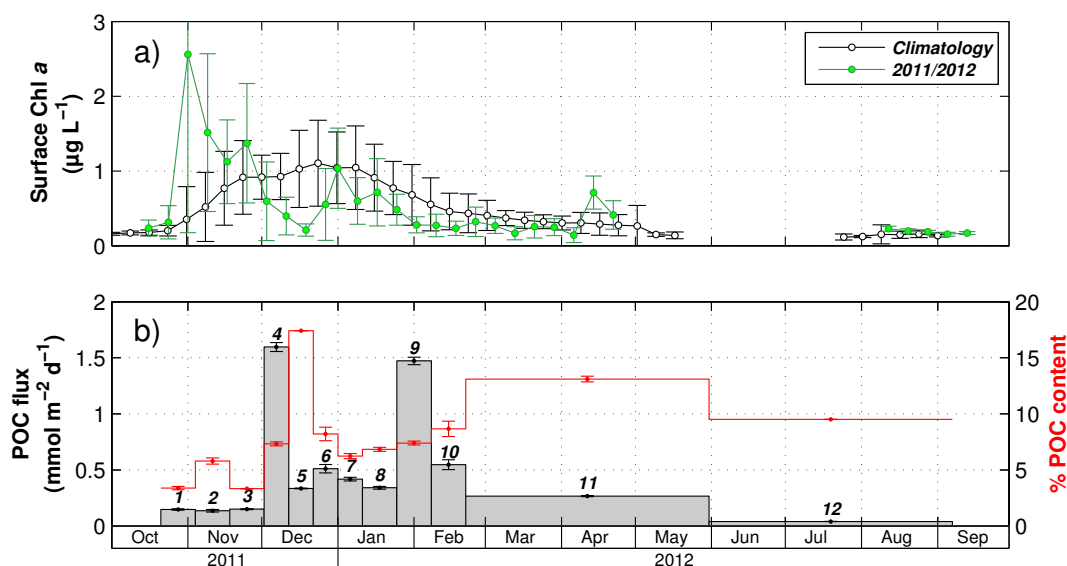
Figure 7. Seasonal variations of surface chlorophyll *a* and particulate organic carbon (POC) export. **(a)** Seasonal surface chlorophyll concentration and 16-year climatology (GlobColour) averaged in a 100 km radius around station A3. The black line represents the climatology calculated for the period 1997/2013, whilst the green line corresponds to the sediment trap deployment period (2011/2012). **(b)** POC flux (grey bars) and mass percentage of POC (red dotted line). Error bars are standard deviations from triplicates, and bold italic numbers refer to cup number.

cember 2011) and #9 (25 January to 8 February 2012), respectively (Fig. 7b). The two flux events occurred with an approximate time lag of 1 month compared to peaks in surface chlorophyll *a* values. A modest value of 0.27 ± 0.01 mmol m^{-2} d^{-1} was observed in autumn (cup #11, 22 February to 30 May 2012). The lowest POC flux was measured during winter (0.04 mmol m^{-2} d^{-1}, cup #12, 31 May to 7 October). Assuming that POC export was negligible from mid-September to mid-October, the annually integrated POC flux was 98.2 ± 4.4 mmol m^{-2} yr^{-1} (Table 1). The two short (< 14 days) export events accounted for 16.2 ± 0.5 % (cup #4) and 21.0 ± 0.6 % (cup #9) of the annual carbon export out of the mixed layer (Table 1). Mass percentage of organic carbon ranged from 3.3 to 17.4 % (Fig. 7b). Values were slightly higher in autumn and winter (respectively 13.1 ± 0.2 and 11 ± 2.1 % in cups #11 and #12) than in the summer, with the exception of cup #5, where the highest value of 17.4 % was observed. PON fluxes followed the same seasonal patterns as POC. This resulted in a relatively stable POC : PON ratio that varied between 6.1 and 7.4, except in autumn cup #11, where it exceeded 8.1 (Table 1).

4 Discussion

4.1 Physical conditions of trap deployment

Moored sediment traps can be subject to hydrodynamic biases that affect the accuracy of particle collection (Bues-

seler et al., 2007a). The aspect ratio, tilt and horizontal flow regimes are important considerations when assessing sediment trap performance. Specifically, the line angle and aspect ratio of cylindrical traps can result in oversampling (Hawley, 1988). Horizontal current velocities of 12 cm s^{-1} are often invoked as a critical threshold over which particles are no longer quantitatively sampled (Baker et al., 1988). During the sediment trap deployment period we observed generally low current speeds (mean < 10 cm s^{-1}), with 75% of the recorded data lower than 12 cm s^{-1}. Despite the high aspect ratio of the PPS3 trap (4.75), and the small mooring line angle deviations, it is likely that episodic increases in current velocities (> 12 cm s^{-1}) impacted collection efficiency. When integrated over the entire current meter record (October 2011 to April 2012), the resulting flow is consistent with the annual northeastward, low-velocity (~ 1 cm s^{-1}) geostrophic flow previously reported over the central part of the Kerguelen Plateau (Park et al., 2008b).

The depth of the winter mixed layer (WML) on the Kerguelen Plateau is usually shallower than 250 m (Park et al., 1998; Metzl et al., 2006). The sediment trap deployment depth of ~ 300 m was selected to sample particle flux exiting the WML. The moored CTD sensor did not record any evidence of a winter water incursion during the deployment period, confirming that the WML did not reach the trap depth. The small depth variations observed during the deployment period resulted from vertical displacement of the trap. Variations in σ_θ may have resulted from both vertical displacement of the CTD sensor and possible isopycnal displacements due to strong internal waves that can occur with an

Table 1. Dynamics of carbon and nitrogen export fluxes at station A3 collected by the sediment trap at 289 m.

			Fluxes (mmol m^{-2} d^{-1})			Contribution to annual export (%)	
Cup	Start	Stop	POC	PON	POC : PON	POC	PON
1	21/10/2011	04/11/2011	0.15 ± 0.01	0.02 ± 0.00	6.80 ± 0.56	2.11 ± 0.06	2.30 ± 0.01
2	04/11/2011	18/11/2011	0.14 ± 0.01	0.02 ± 0.00	6.09 ± 0.67	1.94 ± 0.16	2.27 ± 0.15
3	18/11/2011	02/12/2011	0.15 ± 0.01	0.02 ± 0.00	7.33 ± 0.31	2.12 ± 0.06	1.99 ± 0.06
4	02/12/2011	12/12/2011	1.60 ± 0.04	0.23 ± 0.01	6.95 ± 0.29	16.18 ± 0.45	16.48 ± 0.07
5	12/12/2011	22/12/2011	0.34 ± 0.00	0.05 ± 0.00	6.87 ± 0.08	3.41 ± 0.03	3.64 ± 0.03
6	22/12/2011	01/01/2012	0.51 ± 0.04	0.08 ± 0.01	6.70 ± 0.78	4.82 ± 0.76	5.50 ± 0.39
7	01/01/2012	11/01/2012	0.42 ± 0.02	0.06 ± 0.00	6.73 ± 0.46	4.23 ± 0.14	4.65 ± 0.42
8	11/01/2012	25/01/2012	0.34 ± 0.01	0.05 ± 0.00	6.94 ± 0.38	4.83 ± 0.18	4.84 ± 0.11
9	25/01/2012	08/02/2012	1.47 ± 0.03	0.20 ± 0.01	7.38 ± 0.26	20.98 ± 0.57	21.07 ± 0.05
10	08/02/2012	22/02/2012	0.55 ± 0.04	0.08 ± 0.00	6.97 ± 0.88	7.83 ± 0.64	8.36 ± 0.57
11	22/02/2012	31/05/2012	0.27 ± 0.01	0.03 ± 0.00	8.09 ± 0.22	26.84 ± 0.47	24.12 ± 0.20
12	31/05/2012	07/09/2012	0.04 ± 0.00	0.01 ± 0.00	6.06 ± 0.17	4.71 ± 0.90	4.78 ± 0.09
Annual export (mmol m^{-2} yr^{-1})			98.24 ± 4.35	13.59 ± 0.30			

amplitude of > 50 m at this depth (Park et al., 2008a). Our measurements demonstrate that isopycnal displacements are consistent with the M2 (moon 2, 12.4 h period) tidal forcing described in physical modelling studies (Maraldi et al., 2009, 2011). Spectral analysis indicates that high-frequency tidal currents are the major circulation components. Time-integrated currents suggest that advection is weak and occurs over a longer timescale (months). Assuming the current flow measured at the sediment trap deployment depth is representative of the prevailing current under the WML, more than three months are required for particles to leave the plateau from station A3, a timescale larger than the bloom duration itself. Therefore we consider that the particles collected in the sediment trap at station A3 were produced in the surface waters located above the plateau during bloom conditions.

4.2 Swimmers and particle solubilization

Aside from the hydrodynamic effects discussed above, other potential biases characterizing sediment trap deployments, particularly those in shallow waters, are the presence of swimmers and particle solubilization. Swimmers can artificially increase POC fluxes by entering the cups and releasing particulate organic matter or decrease the flux by feeding in the trap funnel (Buesseler et al., 2007a). Some studies have focused specifically on swimmer communities collected in shallow sediment traps (Matsuno et al., 2014, and references therein), although trap collection of swimmers is probably selective and therefore not quantitative. Total swimmer intrusion rate was highest in cups #6 to #9 (December 2011 to February 2012) generally through the representation of copepods and amphipods (Table 2). The maximum swimmer intrusion rate in mid-summer as well as the copepod dominance is consistent with the 4-fold increase in mesozooplankton abundance observed from winter to summer (Carlotti et

al., 2015). Swimmer abundance was not correlated with mass flux, POC or PON fluxes, suggesting that their presence did not systematically affect particulate fluxes inside the cups. Nevertheless such correlations cannot rule out the possibility of swimmers feeding in the trap funnel modifying particle flux collection.

Particle solubilization in preservative solutions may also lead to an underestimation of total flux measured in sediment traps. Previous analyses from traps poisoned with mercuric chloride suggest that ∼ 30 % of total organic carbon flux can be found in the dissolved phase and much higher values of 50 and 90 % may be observed for nitrogen and phosphorous, respectively (Antia, 2005; O'Neill et al., 2005). Unfortunately the use of a formaldehyde-based preservative in our trap samples precludes any direct estimate of excess of dissolved organic carbon in the sample cup supernatant. Furthermore, corrections for particle leaching have been considered problematic in the presence of swimmers since a fraction of the leaching may originate from the swimmers themselves (Antia, 2005), potentially leading to overcorrection. Particle solubilization may have occurred in our samples, as evidenced by excess PO_4^{3-} in the supernatant. However the largest values were measured in sample cups where total swimmers were abundant (cups #8 to #12; data not shown). Consequently, it was not possible to discriminate solubilization of P from swimmers and passively settling particles, and it therefore remains difficult to quantify the effect of particle leaching. However, leaching of POC should be less problematic in formalin-preserved samples because aldehydes fix organic matter, in addition to poisoning microbial activity.

4.3 Seasonal dynamics of POC export

The sediment trap record obtained from station A3 provides the first direct estimate of POC export covering an entire sea-

Table 2. Number of swimmer individuals found in each cup and swimmer intrusion rate (number per day, bold numbers) for each taxa and for the total swimmers.

Cup	Copepod	Pteropod	Euphausid	Ostracod	Amphipod	Cnidarian	Polychaete	Ctenophore	Siphonophore	Salp	Total
1	166	13	1	2	1	0	0	0	0	0	183
	12	**1**	**< 1**	**< 1**	**< 1**	**0**	**0**	**0**	**0**	**0**	**13**
2	55	0	0	0	0	0	0	0	0	0	55
	4	**0**	**0**	**0**	**0**	**0**	**0**	**0**	**0**	**0**	**4**
3	0	0	0	0	0	0	0	0	0	0	0
	0	**0**	**0**	**0**	**0**	**0**	**0**	**0**	**0**	**0**	**0**
4	113	0	0	0	0	0	0	0	0	0	113
	11	**0**	**0**	**0**	**0**	**0**	**0**	**0**	**0**	**0**	**11**
5	0	0	0	0	0	0	0	0	0	0	0
	0	**0**	**0**	**0**	**0**	**0**	**0**	**0**	**0**	**0**	**0**
6	540	0	1	0	2	5	1	4	1	0	554
	54	**0**	**< 1**	**0**	**< 1**	**< 1**	**0**	**0**	**0**	**0**	**55**
7	583	0	0	0	0	2	2	3	0	0	590
	58	**0**	**0**	**0**	**0**	**< 1**	**< 1**	**< 1**	**0**	**0**	**58**
8	686	33	2	2	8	5	1	4	0	0	741
	49	**2**	**< 1**	**< 1**	**1**	**< 1**	**< 1**	**< 1**	**0**	**0**	**52**
9	392	14	4	3	121	4	2	0	0	0	540
	28	**1**	**< 1**	**< 1**	**9**	**< 1**	**< 1**	**0**	**0**	**0**	**38**
10	264	69	1	2	18	11	0	2	0	0	367
	19	**5**	**< 1**	**< 1**	**1**	**1**	**0**	**< 1**	**0**	**0**	**26**
11	54	0	0	0	29	4	1	0	0	0	88
	1	**0**	**0**	**0**	**< 1**	**< 1**	**< 1**	**0**	**0**	**0**	**1**
12	1481	44	5	7	2	3	2	0	0	1	1544
	15	**< 1**	**< 1**	**< 1**	**< 1**	**< 1**	**< 1**	**0**	**0**	**< 1**	**15**

son over the naturally fertilized Kerguelen Plateau. We observed a temporal lag of 1 month between the two surface chlorophyll a peaks and the two export events. Based on a compilation of annual sediment trap deployments, Lutz et al. (2007) reported that export quickly follows primary production at low latitudes, whereas a time lag up to 2 months could occur at higher latitudes. A 1–2-month lag was observed between production and export in the pacific sector of the Southern Ocean (Buesseler et al., 2001), as well as along 170° W (Honjo et al., 2000) and in the Australian sector of the Subantarctic Zone (Rigual-Hernández et al., 2015). The temporal lag between surface production and measured export in deep traps can originate from ecological processes in the upper ocean (e.g. carbon retention in the mixed layer) as well as slow sinking velocities (Armstrong et al., 2009), and one cannot differentiate the two processes from a single deep trap signal. A global-scale modelling study suggests that the strongest temporal decoupling between production and export (more than 1 month) occurs in areas characterized by a strong seasonal variability in primary production (Henson et al., 2014). The study attributes this decoupling to differences in phenology of phytoplankton and zooplankton and evokes zooplankton ejection products as major contributors to fast-sinking particles sedimenting post-bloom.

On the Kerguelen Plateau there is evidence that a significant fraction of phytoplankton biomass comprising the two chlorophyll peaks is remineralized by a highly active heterotrophic microbial community (Obernosterer et al., 2008;

Christaki et al., 2014). Another fraction is likely channelled toward higher trophic levels through the intense grazing pressure that supports the observed increase in zooplankton biomass (Carlotti et al., 2008, 2015). Therefore an important fraction of phytoplankton biomass increases observed by satellite may not contribute to export fluxes. Notably, the POC : PON ratio measured in our trap material is close to values reported for marine diatoms (7.3 ± 1.2; Sarthou et al., 2005) compared to the C : N ratio of zooplankton faecal pellets, which is typically higher (7.3 to > 15, Gerber and Gerber, 1979; Checkley and Entzeroth, 1985; Morales, 1987). Simple mass balance would therefore suggest a significant contribution of phytoplanktonic cells to the POC export, which is indeed corroborated by detailed microscopic analysis (Rembauville et al., 2015).

Although we observed increasing contributions of faecal pellet carbon post-bloom (Rembauville et al., 2015), in line with the model output of Henson et al. (2014), differences in phytoplankton and zooplankton phenology do not fully explain the seasonality of export on the Kerguelen Plateau. Considering the shallow trap depth (289 m) and typical sinking speed of $100 \, \text{m} \, \text{d}^{-1}$ for phyto-aggregates (Allredge and Gotschalk, 1988; Peterson et al., 2005; Trull et al., 2008a), aggregate-driven export following bloom demise would suggest a short lag of a few days between production and export peaks. The temporal lag of 1 month measured in the present study suggests either slow sinking rates ($< 5 \, \text{m} \, \text{d}^{-1}$) characteristic of single phytoplanktonic cells or faster-sinking par-

ticles that originate from subsurface production peaks un-detected by satellite. It is generally accepted that satellite detection depth is 20–50 m (Gordon and McCluney, 1975), and can be less than 20 m when surface chlorophyll a exceeds $0.2\,\mu g\,L^{-1}$ (Smith, 1981), which prevents the detection of deep phytoplanktonic biomass structures (Villareal et al., 2011). Although subsurface chlorophyll maxima located around 100 m have been observed over the Kerguelen Plateau at the end of the productive period, they have been interpreted to result from the accumulation of surface production at the base of the mixed layer rather than subsurface productivity features (Uitz et al., 2009). In support of this, detailed taxonomic analysis of the exported material highlights diatom resting spores as major contributors to the two export fluxes rather than a composite surface community accumulated at the base of the mixed layer. The hypothesis of a mass production of nutrient-limited resting spores post-bloom with high settling rates explains the temporal patterns of export we observed (Rembauville et al., 2015). However a better knowledge of the dynamics of factors responsible for resting spore formation by diatoms remains necessary to fully validate this hypothesis.

4.4 Evidence for significant flux attenuation over the Kerguelen Plateau

The Kerguelen Plateau annual POC export $(98.2 \pm 4.4\,\text{mmol}\,\text{m}^{-2}\,\text{yr}^{-1})$ approaches the median global ocean POC export value comprising shallow and deep sediment traps $(83\,\text{mmol}\,\text{m}^{-2}\,\text{yr}^{-1}$; Lampitt and Antia, 1997), but is also close to values observed in HNLC areas of the POOZ $(11–43\,\text{mmol}\,\text{m}^{-2}\,\text{yr}^{-1}$ at 500 m; Fischer et al., 2000). Moreover, the magnitude of annual POC export measured at ~ 300 m on the Kerguelen Plateau is comparable to deep-ocean $(> 2\,\text{km})$ POC fluxes measured from the iron-fertilized Crozet $(60\,\text{mmol}\,\text{m}^{-2}\,\text{yr}^{-1}$; Salter et al., 2012) and South Georgia blooms $(180\,\text{mmol}\,\text{m}^{-2}\,\text{yr}^{-1}$; Manno et al., 2015).

We first compared the sediment trap export fluxes with short-term estimates at 200 m in spring (KEOPS2) and summer (KEOPS1). The POC flux recorded in the moored sediment trap represents only a small fraction $(3–8\,\%)$ of the POC flux measured at the base of the winter mixed layer (200 m) by different approaches during the spring KEOPS2 cruise (Table 3). The same conclusion can be drawn when considering the comparison with different estimates made at the end of summer during KEOPS1. Moreover, the annual POC export of $\sim 0.1\,\text{mol}\,\text{m}^{-2}\,\text{yr}^{-1}$ at 289 m (Table 1) represents only 2 % of the indirect estimate of POC export $(5.1\,\text{mol}\,\text{m}^{-2}\,\text{yr}^{-1})$ at the base of the WML (200 m) on the Kerguelen Plateau based on a seasonal dissolved inorganic carbon (DIC) budget (Blain et al., 2007). The short-term estimates are derived from a diverse range of methods. The ^{234}Th proxy is based on the ^{234}Th deficit relative to the ^{238}U due to its adsorption on particles, and its subsequent con-

version to carbon fluxes using measured POC : ^{234}Th ratios. (Coale and Bruland, 1985; Buesseler et al., 2006; Savoye et al., 2006). The UVP (underwater video profiler) provides high-resolution images of particles $(> 52\,\mu m)$, and the particle size distribution is then converted to carbon fluxes using an empirical relationship (Guidi et al., 2008; Picheral et al., 2010). Drifting gel traps allow for the collection, preservation and imaging of sinking particles $(> 71\,\mu m)$ that are converted to carbon fluxes using empirical volume–carbon relationship (Ebersbach and Trull, 2008; Ebersbach et al., 2011; Laurenceau-Cornec et al., 2015). Finally, drifting sediment traps are conceptually similar to moored sediment traps but avoid most of the hydrodynamic biases associated with this technique (Buesseler et al., 2007a). The diversity of the methods and differences in depth where the POC flux was estimated render quantitative comparisons challenging. Nevertheless, POC fluxes measured at 289 m with the moored sediment trap are considerably lower than other estimates made at 200 m. This result indicates either extremely rapid attenuation of flux between 200 and 300 m or significant sampling bias by the sediment trap.

We note that low carbon export fluxes around 300 m have been previously reported on the Kerguelen Plateau. In spring 2011, UVP-derived estimates of POC export at 350 m were 0.1 to $0.3\,\text{mmol}\,\text{m}^{-2}\,\text{d}^{-1}$ (Table 3), values close to our reported value of $0.15\,\text{mmol}\,\text{m}^{-2}\,\text{d}^{-1}$. In summer 2005, POC export at 330 m from a gel trap was $0.7\,\text{mmol}\,\text{m}^{-2}\,\text{d}^{-1}$ (Ebersbach and Trull 2008), which is also close to our value of $1.5\,\text{mmol}\,\text{m}^{-2}\,\text{d}^{-1}$. Using the Jouandet et al. (2014) data at 200 m $(1.9\,\text{mmol}\,\text{m}^{-2}\,\text{d}^{-1})$ and 350 m $(0.3\,\text{mmol}\,\text{m}^{-2}\,\text{d}^{-1})$ and the Ebersbach and Trull (2008) data at 200 m $(5.2\,\text{mmol}\,\text{m}^{-2}\,\text{d}^{-1})$ and 330 m $(0.7\,\text{mmol}\,\text{m}^{-2}\,\text{d}^{-1})$ leads to Martin power-law exponent values of 3.3 and 4, respectively. These values are high when compared to the range of 0.4–1.7 that was initially compiled for the global ocean (Buesseler et al., 2007b). However, there is increasing evidence in support of much higher b values in the Southern Ocean that fall in the range of 0.9–3.9 (Lam and Bishop, 2007; Henson et al., 2012; Cavan et al., 2015). Our calculations are thus consistent with emerging observations of significant POC flux attenuation in the Southern Ocean.

Using the aforementioned b values (3.3 and 4) and the POC flux derived from ^{234}Th deficit at 200 m in spring (Planchon et al., 2014), we estimate POC fluxes at 289 m of 0.7 to $1.1\,\text{mmol}\,\text{m}^{-2}\,\text{d}^{-1}$. The flux measured in our sediment trap $(0.15\,\text{mmol}\,\text{m}^{-2}\,\text{d}^{-1})$ data represents 14 to 21 % of this calculated flux. Very similar percentages (21 to 27 %) are found using the POC fluxes derived from the ^{234}Th deficit in summer (Savoye et al., 2008). Therefore we consider that the moored sediment trap collected $\sim 15–30\,\%$ of the ^{234}Th-derived particle flux equivalent throughout the year. Trap-derived particle fluxes can represent 0.1 to > 3 times the ^{234}Th-derived particles in shallow sediment traps (Buesseler, 1991; Buesseler et al., 1994; Coppola et al., 2002; Gustafsson et al., 2004), and this difference is largely attributed to the

Table 3. Summary of estimates of POC fluxes at the base of, or under, the mixed layer at station A3 from the KEOPS cruises.

Author	Method	Period	Depth (m)	POC flux (mmol m^{-2} d^{-1})
		KEOPS1		
Savoye et al. (2008)	^{234}Th deficit	23 Jan–12 Feb 2005	100	23 ± 3.6
			150	25.7 ± 3.6
			200	24.5 ± 6.8
Ebersbach and Trull (2008)	Drifting gel trap, optical measurements, and both constant and power-law C conversion factor	4 Feb 2005	200	23.9
		12 Feb 2005	100	5.3
			200	5.2
			330	0.7
			430	1
Jouandet et al. (2008)	Annual DIC budget	Annual	MLD base	85
Trull et al. (2008b)	Drifting sediment trap	4 Feb 2005	200	7.3–10
		12 Feb 2005	200	3–3.1
Jouandet et al. (2011)	In situ optical measurement (UVP) and power function C conversion factor	22 Jan 2005	200	72.4
			330	27.2
			400	21.6
		23 Jan 2005	200	29.8
			330	26.8
			400	15.9
		12 Feb 2005	200	4.8
			330	5.6
			400	7.9
		KEOPS2		
Planchon et al. (2014)	^{234}Th deficit, steady-state model	20 Oct 2011	100	3.5 ± 0.9
			150	3.9 ± 0.9
			200	3.7 ± 0.9
		16 Nov 2011	100	4.6 ± 1.5
			150	7.1 ± 1.5
			200	3.1 ± 0.6
	^{234}Th deficit, non-steady-state model	16 Nov 2011	100	7.3 ± 1.8
			150	8.4 ± 1.8
			200	3.8 ± 0.8
Laurenceau-Cornec et al. (2015)	Drifting gel trap, optical measurement of particles	16 Nov 2011	210	5.5
	Drifting sediment trap		210	2.2
Jouandet et al. (2014)	In situ optical measurement (UVP) and power function C conversion factor	21 Oct 2011	200	0.2
			350	0.1
		16 Nov 2011	200	1.9
			350	0.3

sum of hydrodynamic biases and swimmer activities (Buesseler, 1991), although it probably also includes the effect of post-collection particle solubilization. In the Antarctic Peninsula, ^{234}Th-derived POC export was 20 times higher than the fluxes collected by a shallow, cylindrical, moored sediment trap at 170 m (Buesseler et al., 2010). The present deployment context is less extreme (depth of 289 m, mean current speed < 10 cm s^{-1}, low tilt angle, high aspect ratio of the cylindrical PPS3 trap) but we consider that hydrodynamics (current speed higher than 12 cm s^{-1} during short tidal-driven events) and possible zooplankton feeding on the trap funnel are potential biases that may explain in part the low fluxes recorded by the moored sediment trap. Therefore the low fluxes observed likely result from a combined effect of collection bias (hydrodynamics and swimmers) and attenuation of the POC flux between the base of the WML and

300 m. However, it is not possible with the current data set to isolate a specific explanation for low flux values.

Strong POC flux attenuation over the Kerguelen Plateau compared to the open ocean is also reported by Laurenceau-Cornec et al. (2015), who associated this characteristic with an HBLE scenario and invoked the role of mesozooplankton in the carbon flux attenuation. Between October and November 2011, mesozooplankton biomass in the mixed layer doubled (Carlotti et al., 2014) and summer biomass was a further 2-fold higher (Carlotti et al., 2008). These seasonal patterns are consistent with the maximum swimmer intrusion rate and swimmer diversity observed in summer (Table 2). It has previously been concluded that zooplankton biomass is more tightly coupled to phytoplankton biomass on the plateau compared to oceanic waters, leading to higher secondary production on the plateau (Carlotti et al., 2008, 2014). The findings of Cavan et al. (2015) that document the lowest export ratio (exported production/primary production) in the most productive, naturally fertilized area downstream of South Georgia provide further support linking zooplankton dynamics to HBLE environments of iron-fertilized blooms. Another important ecosystem feature associated with the HBLE environment of the Kerguelen Plateau, and likely shared by other island-fertilized blooms in the Southern Ocean, is the presence of mesopelagic fish (myctophid spawning and larvae foraging site; Koubbi et al., 1991, 2001). Mesopelagic fish can be tightly coupled to lower trophic levels (Saba and Steinberg, 2012) and can play a significant role in carbon flux attenuation (Davison et al., 2013). Although important for carbon budgets, mesopelagic fish represents a compartment often neglected due to the challenge of quantitative sampling approaches. We suggest that the HBLE scenario and large attenuation of carbon flux beneath the WML at Kerguelen may reflect the transfer of carbon biomass to higher and mobile trophic groups that fuel large mammal and bird populations rather than the classical remineralization-controlled attenuation characterizing open-ocean environments. Although technically challenging, testing this hypothesis should be a focus for future studies in this and similar regions.

5   Conclusions

We report the seasonal dynamics of particulate organic carbon (POC) export under the winter mixed layer (289 m) of the naturally iron-fertilized and productive central Kerguelen Plateau. Annual POC flux was remarkably low (98 mmol m^{-2}) and occurred primarily during two episodic (< 14 days) flux events exported with a 1-month lag following two surface chlorophyll a peaks. Analysis of the hydrological conditions and a comparison with different estimates of POC fluxes in spring and summer at the same station suggests that the sediment trap was subject to possible hydrodynamic and biological biases leading to under-collection of particle flux. Nevertheless, the low POC export was close to

other estimates of deep (> 300 m) POC export at the same station and is consistent with high attenuation coefficients reported from other methods. We invoke heterotrophic microbial activity and mesozooplankton and mesopelagic fish activity as possible explanations for efficient carbon flux attenuation and/or transfer to higher trophic levels which results in a high-biomass, low-export environment.

The biogenic silicon, diatoms assemblages and faecal pellet fluxes are reported in a companion paper that identifies the primary ecological vectors regulating the magnitude of POC export and seasonal patterns in BSi : POC export (Rembauville et al., 2015).

Edited by: T. Trull

References

Allredge, A. L. and Gotschalk, C.: In situ settling behavior of marine snow, Limnol. Oceanogr., 33, 339–351, 1988.

Aminot, A. and Kerouel, R.: Dosage automatique des nutriments dans les eaux marines: méthodes en flux continu, Ifremer, Plouzané, France, 2007.

Antia, A. N.: Solubilization of particles in sediment traps: revising the stoichiometry of mixed layer export, Biogeosciences, 2, 189–204, doi:10.5194/bg-2-189-2005, 2005.

Armstrong, R. A., Peterson, M. L., Lee, C., and Wakeham, S. G.: Settling velocity spectra and the ballast ratio hypothesis, Deep-Sea Res. Pt. II, 56, 1470–1478, doi:10.1016/j.dsr2.2008.11.032, 2009.

Baker, E. T., Milburn, H. B., and Tennant, D. A.: Field assessment of sediment trap efficiency under varying flow conditions, J. Mar. Res., 46, 573–592, doi:10.1357/002224088785113522, 1988.

Barbeau, K., Moffett, J. W., Caron, D. A., Croot, P. L., and Erdner, D. L.: Role of protozoan grazing in relieving iron limitation of phytoplankton, Nature, 380, 61–64, doi:10.1038/380061a0, 1996.

Batten, S. D. and Gower, J. F. R.: Did the iron fertilization near Haida Gwaii in 2012 affect the pelagic lower trophic level ecosystem?, J. Plankton Res., 36, 925–932, doi:10.1093/plankt/fbu049, 2014.

Blain, S., Tréguer, P., Belviso, S., Bucciarelli, E., Denis, M., Desabre, S., Fiala, M., Martin Jézéquel, V., Le Fèvre, J., Mayzaud, P., Marty, J.-C., and Razouls, S.: A biogeochemical

study of the island mass effect in the context of the iron hypothesis: Kerguelen Islands, Southern Ocean, Deep-Sea Res. Pt. I, 48, 163–187, doi:10.1016/S0967-0637(00)00047-9, 2001.

Blain, S., Quéguiner, B., Armand, L., Belviso, S., Bombled, B., Bopp, L., Bowie, A., Brunet, C., Brussaard, C., Carlotti, F., Christaki, U., Corbière, A., Durand, I., Ebersbach, F., Fuda, J.-L., Garcia, N., Gerringa, L., Griffiths, B., Guigue, C., Guillerm, C., Jacquet, S., Jeandel, C., Laan, P., Lefèvre, D., Lo Monaco, C., Malits, A., Mosseri, J., Obernosterer, I., Park, Y.-H., Picheral, M., Pondaven, P., Remenyi, T., Sandroni, V., Sarthou, G., Savoye, N., Scouarnec, L., Souhaut, M., Thuiller, D., Timmermans, K., Trull, T., Uitz, J., van Beek, P., Veldhuis, M., Vincent, D., Viollier, E., Vong, L., and Wagener, T.: Effect of natural iron fertilization on carbon sequestration in the Southern Ocean, Nature, 446, 1070–1074, doi:10.1038/nature05700, 2007.

Boltovskoy, D.: South Atlantic zooplankton, Backhuys, 1999.

Bopp, L., Kohfeld, K. E., Le Quéré, C., and Aumont, O.: Dust impact on marine biota and atmospheric CO_2 during glacial periods, Paleoceanography, 18, 1046, doi:10.1029/2002PA000810, 2003.

Boyd, P. W. and Trull, T. W.: Understanding the export of biogenic particles in oceanic waters: Is there consensus?, Prog. Oceanogr., 72, 276–312, doi:10.1016/j.pocean.2006.10.007, 2007.

Boyd, P. W., Law, C. S., Hutchins, D. A., Abraham, E. R., Croot, P. L., Ellwood, M., Frew, R. D., Hadfield, M., Hall, J., Handy, S., Hare, C., Higgins, J., Hill, P., Hunter, K. A., LeBlanc, K., Maldonado, M. T., McKay, R. M., Mioni, C., Oliver, M., Pickmere, S., Pinkerton, M., Safi, K., Sander, S., Sanudo-Wilhelmy, S. A., Smith, M., Strzepek, R., Tovar-Sanchez, A., and Wilhelm, S. W.: FeCycle: Attempting an iron biogeochemical budget from a mesoscale SF6 tracer experiment in unperturbed low iron waters, Glob. Biogeochem. Cy., 19, GB4S20, doi:10.1029/2005GB002494, 2005.

Boyd, P. W., Jickells, T., Law, C. S., Blain, S., Boyle, E. A., Buesseler, K. O., Coale, K. H., Cullen, J. J., Baar, H. J. W. de, Follows, M., Harvey, M., Lancelot, C., Levasseur, M., Owens, N. P. J., Pollard, R., Rivkin, R. B., Sarmiento, J., Schoemann, V., Smetacek, V., Takeda, S., Tsuda, A., Turner, S., and Watson, A. J.: Mesoscale Iron Enrichment Experiments 1993-2005: Synthesis and Future Directions, Science, 315, 612–617, doi:10.1126/science.1131669, 2007.

Buesseler, K. O.: Do upper-ocean sediment traps provide an accurate record of particle flux?, Nature, 353, 420–423, doi:10.1038/353420a0, 1991.

Buesseler, K. O. and Boyd, P. W.: Shedding light on processes that control particle export and flux attenuation in the twilight zone of the open ocean, Limnol. Oceanogr., 54, 1210–1232, doi:10.4319/lo.2009.54.4.1210, 2009.

Buesseler, K. O., Michaels, A. F., Siegel, D. A., and Knap, A. H.: A three dimensional time-dependent approach to calibrating sediment trap fluxes. Glob. Biogeochem. Cy., 8, 179–193, doi:10.1029/94GB00207, 1994.

Buesseler, K. O., Ball, L., Andrews, J., Cochran, J. K., Hirschberg, D. J., Bacon, M. P., Fleer, A., and Brzezinski, M.: Upper ocean export of particulate organic carbon and biogenic silica in the Southern Ocean along 170° W, Deep-Sea Res. Pt. II, 48, 4275–4297, doi:10.1016/S0967-0645(01)00089-3, 2001.

Buesseler, K. O., Benitez-Nelson, C. R., Moran, S. B., Burd, A., Charette, M., Cochran, J. K., Coppola, L., Fisher, N. S., Fowler,

S. W., Gardner, W. D., Guo, L. D., Gustafsson, Ö., Lamborg, C., Masque, P., Miquel, J. C., Passow, U., Santschi, P. H., Savoye, N., Stewart, G., and Trull, T.: An assessment of particulate organic carbon to thorium-234 ratios in the ocean and their impact on the application of 234Th as a POC flux proxy, Future Applications of 234Th in Aquatic Ecosystems (FATE), Mar. Chem., 100, 213–233, doi:10.1016/j.marchem.2005.10.013, 2006.

Buesseler, K. O., Antia, A. N., Chen, M., Fowler, S. W., Gardner, W. D., Gustafsson, Ö., Harada, K., Michaels, A. F., Rutgers V. D. Loeff, M., Sarin, M., Steinberg, D. K., and Trull, T.: An assessment of the use of sediment traps for estimating upper ocean particle fluxes, J. Mar. Res., 65, 345–416, 2007a.

Buesseler, K. O., Lamborg, C. H., Boyd, P. W., Lam, P. J., Trull, T. W., Bidigare, R. R., Bishop, J. K. B., Casciotti, K. L., Dehairs, F., Elskens, M., Honda, M., Karl, D. M., Siegel, D. A., Silver, M. W., Steinberg, D. K., Valdes, J., Mooy, B. V., and Wilson, S.: Revisiting Carbon Flux Through the Ocean's Twilight Zone, Science, 316, 567–570, doi:10.1126/science.1137959, 2007b.

Buesseler, K. O., McDonnell, A. M. P., Schofield, O. M. E., Steinberg, D. K., and Ducklow, H. W.: High particle export over the continental shelf of the west Antarctic Peninsula, Geophys. Res. Lett., 37, L22606, doi:10.1029/2010GL045448, 2010.

Carlotti, F., Thibault-Botha, D., Nowaczyk, A., and Lefèvre, D.: Zooplankton community structure, biomass and role in carbon fluxes during the second half of a phytoplankton bloom in the eastern sector of the Kerguelen Shelf (January–February 2005), Deep-Sea Res. Pt. II, 55, 720–733, doi:10.1016/j.dsr2.2007.12.010, 2008.

Carlotti, F., Jouandet, M.-P., Nowaczyk, A., Harmelin-Vivien, M., Lefèvre, D., Guillou, G., Zhu, Y., and Zhou, M.: Mesozooplankton structure and functioning during the onset of the Kerguelen phytoplankton bloom during the Keops2 survey, Biogeosciences Discuss., 12, 2381–2427, doi:10.5194/bgd-12-2381-2015, 2015.

Cavan, E. L., Le Moigne, F. A. C., Poulton, A. J., Tarling, G. A., Ward, P., Daniels, C. J., Fragoso, G., and Sanders, R. J.: Zooplankton fecal pellets control the attenuation of particulate organic carbon flux in the Scotia Sea, Southern Ocean, Geophys. Res. Lett., GL062744, doi:10.1002/2014GL062744, 2015.

Checkley, D. M. and Entzeroth, L. C.: Elemental and isotopic fractionation of carbon and nitrogen by marine, planktonic copepods and implications to the marine nitrogen cycle, J. Plankton Res., 7, 553–568, doi:10.1093/plankt/7.4.553, 1985.

Christaki, U., Lefèvre, D., Georges, C., Colombet, J., Catala, P., Courties, C., Sime-Ngando, T., Blain, S., and Obernosterer, I.: Microbial food web dynamics during spring phytoplankton blooms in the naturally iron-fertilized Kerguelen area (Southern Ocean), Biogeosciences, 11, 6739–6753, doi:10.5194/bg-11-6739-2014, 2014.

Coale, K. H. and Bruland, K. W.: ^{2}34Th: 6238U Disequilibria Within the California Current, Limnol. Oceanogr., 30, 22–33, 1985.

Coale, K. H., Johnson, K. S., Chavez, F. P., Buesseler, K. O., Barber, R. T., Brzezinski, M. A., Cochlan, W. P., Millero, F. J., Falkowski, P. G., Bauer, J. E., Wanninkhof, R. H., Kudela, R. M., Altabet, M. A., Hales, B. E., Takahashi, T., Landry, M. R., Bidigare, R. R., Wang, X., Chase, Z., Strutton, P. G., Friederich, G. E., Gorbunov, M. Y., Lance, V. P., Hilting, A. K., Hiscock, M. R., Demarest, M., Hiscock, W. T., Sullivan, K. F., Tanner, S. J., Gordon, R. M., Hunter, C. N., Elrod, V. A., Fitzwater, S. E.,

Jones, J. L., Tozzi, S., Koblizek, M., Roberts, A. E., Herndon, J., Brewster, J., Ladizinsky, N., Smith, G., Cooper, D., Timothy, D., Brown, S. L., Selph, K. E., Sheridan, C. C., Twining, B. S., and Johnson, Z. I.: Southern Ocean Iron Enrichment Experiment: Carbon Cycling in High- and Low-Si Waters, Science, 304, 408–414, doi:10.1126/science.1089778, 2004.

Coppola, L., Roy-Barman, M., Wassmann, P., Mulsow, S., and Jeandel, C.: Calibration of sediment traps and particulate organic carbon export using ^{234}Th in the Barents Sea, Mar. Chem., 80, 11–26, doi:10.1016/S0304-4203(02)00071-3, 2002.

Davison, P. C., Checkley Jr., D. M., Koslow, J. A., and Barlow, J.: Carbon export mediated by mesopelagic fishes in the northeast Pacific Ocean, Prog. Oceanogr., 116, 14–30, doi:10.1016/j.pocean.2013.05.013, 2013.

De Baar, H. J. W., Buma, A. G. J., Nolting, R. F., Cadée, G. C., Jacques, G., and Tréguer, P.: On iron limitation of the Southern Ocean: experimental observations in the Weddell and Scotia Seas, Mar. Ecol.-Prog. Ser. 65, 105–122, doi:10.3354/meps065105, 1990.

De Baar, H. J. W., Boyd, P. W., Coale, K. H., Landry, M. R., Tsuda, A., Assmy, P., Bakker, D. C. E., Bozec, Y., Barber, R. T., Brzezinski, M. A., Buesseler, K. O., Boyé, M., Croot, P. L., Gervais, F., Gorbunov, M. Y., Harrison, P. J., Hiscock, W. T., Laan, P., Lancelot, C., Law, C. S., Levasseur, M., Marchetti, A., Millero, F. J., Nishioka, J., Nojiri, Y., van Oijen, T., Riebesell, U., Rijkenberg, M. J. A., Saito, H., Takeda, S., Timmermans, K. R., Veldhuis, M. J. W., Waite, A. M., and Wong, C.-S.: Synthesis of iron fertilization experiments: From the Iron Age in the Age of Enlightenment, J. Geophys. Res.-Oceans, 110, C09S16, doi:10.1029/2004JC002601, 2005.

Dilling, L. and Alldredge, A. L.: Fragmentation of marine snow by swimming macrozooplankton: A new process impacting carbon cycling in the sea, Deep-Sea Res. Pt. I, 47, 1227–1245, doi:10.1016/S0967-0637(99)00105-3, 2000.

Dunne, J. P., Sarmiento, J. L., and Gnanadesikan, A.: A synthesis of global particle export from the surface ocean and cycling through the ocean interior and on the seafloor, Glob. Biogeochem. Cy., 21, GB4006, doi:10.1029/2006GB002907, 2007.

Ebersbach, F. and Trull, T. W.: Sinking particle properties from polyacrylamide gels during the KErguelen Ocean and Plateau compared Study (KEOPS): Zooplankton control of carbon export in an area of persistent natural iron inputs in the Southern Ocean, Limnol. Oceanogr., 53, 212–224, doi:10.4319/lo.2008.53.1.0212, 2008.

Ebersbach, F., Trull, T. W., Davies, D. M., and Bray, S. G.P: Controls on mesopelagic particle fluxes in the Sub-Antarctic and Polar Frontal Zones in the Southern Ocean south of Australia in summer–Perspectives from free-drifting sediment traps, Deep-Sea Res. Pt. II, 58, 2260–2276, doi:10.1016/j.dsr2.2011.05.025, 2011.

Fischer, G., Ratmeyer, V., and Wefer, G.: Organic carbon fluxes in the Atlantic and the Southern Ocean: relationship to primary production compiled from satellite radiometer data, Deep-Sea Res. Pt. II, 47, 1961–1997, doi:10.1016/S0967-0645(00)00013-8, 2000.

Francois, R., Honjo, S., Krishfield, R., and Manganini, S.: Factors controlling the flux of organic carbon to the bathypelagic zone of the ocean, Glob. Biogeochem. Cy., 16, 1087, doi:10.1029/2001GB001722, 2002.

Gall, M. P., Strzepek, R., Maldonado, M., and Boyd, P. W.: Phytoplankton processes, Part 2: Rates of primary production and factors controlling algal growth during the Southern Ocean Iron RElease Experiment (SOIREE), Deep-Sea Res. Pt. II, The Southern Ocean Iron Release Experiment (SOIREE), 48, 2571–2590, doi:10.1016/S0967-0645(01)00009-1, 2001.

Gehlen, M., Bopp, L., Emprin, N., Aumont, O., Heinze, C., and Ragueneau, O.: Reconciling surface ocean productivity, export fluxes and sediment composition in a global biogeochemical ocean model, Biogeosciences, 3, 521–537, doi:10.5194/bg-3-521-2006, 2006.

Gerber, R. P. and Gerber, M. B.: Ingestion of natural particulate organic matter and subsequent assimilation, respiration and growth by tropical lagoon zooplankton, Mar. Biol., 52, 33–43, doi:10.1007/BF00386855, 1979.

Giering, S. L. C., Sanders, R., Lampitt, R. S., Anderson, T. R., Tamburini, C., Boutrif, M., Zubkov, M. V., Marsay, C. M., Henson, S. A., Saw, K., Cook, K., and Mayor, D. J..: Reconciliation of the carbon budget in the ocean/'s twilight zone, Nature, 507, 480–483, doi:10.1038/nature13123, 2014.

Gilman, D. L., Fuglister, F. J., and Mitchell, J. M.: On the Power Spectrum of "Red Noise.", J. Atmospheric Sci., 20, 182–184, doi:10.1175/1520-0469(1963)020<0182:OTPSON>2.0.CO;2, 1963.

Gordon, H. R. and McCluney, W. R.: Estimation of the depth of sunlight penetration in the sea for remote sensing, Appl. Opt., 14, 413–416, 1975.

Gruber, N., Gloor, M., Mikaloff Fletcher, S. E., Doney, S. C., Dutkiewicz, S., Follows, M. J., Gerber, M., Jacobson, A. R., Joos, F., Lindsay, K., Menemenlis, D., Mouchet, A., Müller, S. A., Sarmiento, J. L., and Takahashi, T.: Oceanic sources, sinks, and transport of atmospheric CO_2, Glob. Biogeochem. Cy., 23, GB1005, doi:10.1029/2008GB003349, 2009.

Guidi, L., Jackson, G. A., Stemmann, L., Miquel, J. C., Picheral, M., and Gorsky, G.: Relationship between particle size distribution and flux in the mesopelagic zone, Deep-Sea Res. Pt. I, 55, 1364–1374, doi:10.1016/j.dsr.2008.05.014, 2008.

Gustafsson, O., Andersson, P., Roos, P., Kukulska, Z., Broman, D., Larsson, U., Hajdu, S., and Ingri, J.: Evaluation of the collection efficiency of upper ocean sub-photic-layer sediment traps: A 24-month in situ calibration in the open Baltic Sea using ^{234}Th, Limnol. Oceanogr.-Methods, 2, 62–74, doi:10.4319/lom.2004.2.62, 2004.

Hawley, N.: Flow in Cylindrical Sediment Traps, J. Great Lakes Res., 14, 76–88, doi:10.1016/S0380-1330(88)71534-8, 1988.

Henson, S. A., Sanders, R., Madsen, E., Morris, P. J., Le Moigne, F., and Quartly, G. D.: A reduced estimate of the strength of the ocean's biological carbon pump, Geophys. Res. Lett., 38, L04606, doi:10.1029/2011GL046735, 2011.

Henson, S. A., Sanders, R., and Madsen, E.: Global patterns in efficiency of particulate organic carbon export and transfer to the deep ocean, Glob. Biogeochem. Cy., 26, GB1028, doi:10.1029/2011GB004099, 2012.

Henson, S. A., Yool, A., and Sanders, R.: Variability in efficiency of particulate organic carbon export: A model study, Glob. Biogeochem. Cy., 29, GB4965, doi:10.1002/2014GB004965, 2014.

Hiscock, W. T. and Millero, F. J.: Nutrient and carbon parameters during the Southern Ocean iron experiment (SOFeX), Deep-Sea Res. Pt. I, 52, 2086–2108, doi:10.1016/j.dsr.2005.06.010, 2005.

Honjo, S., Francois, R., Manganini, S., Dymond, J., and Collier, R.: Particle fluxes to the interior of the Southern Ocean in the Western Pacific sector along 170° W, Deep-Sea Res. Pt. II, 47, 3521–3548, doi:10.1016/S0967-0645(00)00077-1, 2000.

Honjo, S., Manganini, S. J., Krishfield, R. A., and Francois, R.: Particulate organic carbon fluxes to the ocean interior and factors controlling the biological pump: A synthesis of global sediment trap programs since 1983, Prog. Oceanogr., 76, 217–285, doi:10.1016/j.pocean.2007.11.003, 2008.

Hudson, J. M., Steinberg, D. K., Sutton, T. T., Graves, J. E., and Latour, R. J.: Myctophid feeding ecology and carbon transport along the northern Mid-Atlantic Ridge, Deep-Sea Res. Pt. I, 93, 104–116, doi:10.1016/j.dsr.2014.07.002, 2014.

Jacquet, S. H. M., Dehairs, F., Savoye, N., Obernosterer, I., Christaki, U., Monnin, C., and Cardinal, D.: Mesopelagic organic carbon remineralization in the Kerguelen Plateau region tracked by biogenic particulate Ba, Deep-Sea Res. Pt. II, 55, 868–879, doi:10.1016/j.dsr2.2007.12.038, 2008.

JGOFS: Sediment Trap Methods, in: Protocols for the Joint Global Ocean Flux Study (JGOFS) Core Measurements, Intergovernmental Oceanographic Commission, Scientific Committee on Oceanic Research Manual and Guides, UNESCO, 157–164, 1994.

Jouandet, M. P., Blain, S., Metzl, N., Brunet, C., Trull, T. W., and Obernosterer, I.: A seasonal carbon budget for a naturally iron-fertilized bloom over the Kerguelen Plateau in the Southern Ocean, Deep-Sea Res. Pt. II, KEOPS: Kerguelen Ocean and Plateau compared Study, 55, 856–867, doi:10.1016/j.dsr2.2007.12.037, 2008.

Jouandet, M.-P., Trull, T. W., Guidi, L., Picheral, M., Ebersbach, F., Stemmann, L., and Blain, S.: Optical imaging of mesopelagic particles indicates deep carbon flux beneath a natural iron-fertilized bloom in the Southern Ocean, Limnol. Oceanogr., 56, 1130–1140, doi:10.4319/lo.2011.56.3.1130, 2011.

Jouandet, M.-P., Jackson, G. A., Carlotti, F., Picheral, M., Stemmann, L., and Blain, S.: Rapid formation of large aggregates during the spring bloom of Kerguelen Island: observations and model comparisons, Biogeosciences, 11, 4393–4406, doi:10.5194/bg-11-4393-2014, 2014.

Karleskind, P., Lévy, M., and Memery, L.: Subduction of carbon, nitrogen, and oxygen in the northeast Atlantic, J. Geophys. Res.-Oceans, 116, C02025, doi:10.1029/2010JC006446, 2011.

Kohfeld, K. E., Quéré, C. L., Harrison, S. P., and Anderson, R. F.: Role of Marine Biology in Glacial-Interglacial CO_2 Cycles, Science, 308, 74–78, doi:10.1126/science.1105375, 2005.

Korb, R. E. and Whitehouse, M.: Contrasting primary production regimes around South Georgia, Southern Ocean: large blooms versus high nutrient, low chlorophyll waters, Deep-Sea Res. Pt. I, 51, 721–738, doi:10.1016/j.dsr.2004.02.006, 2004.

Koubbi, P., Duhamel, G., and Hebert, C.: Seasonal relative abundance of fish larvae inshore at Îles Kerguelen, Southern Ocean. Antarct. Sci., 13, 385–392, doi:10.1017/S0954102001000542, 2001.

Koubbi, P., Ibanez, F., and Duhamel, G.: Environmental influences on spatio-temporal oceanic distribution of ichthyoplankton around the Kerguelen Islands (Southern Ocean), Mar. Ecol.-Prog. Ser., 72, 225–238, 1991.

Lam, P. J. and Bishop, J. K. B.: High biomass, low export regimes in the Southern Ocean, Deep-Sea Res. Pt. II, 54, 601–638, doi:10.1016/j.dsr2.2007.01.013, 2007.

Lam, P. J., Doney, S. C., and Bishop, J. K. B.: The dynamic ocean biological pump: Insights from a global compilation of particulate organic carbon, $CaCO_3$, and opal concentration profiles from the mesopelagic, Glob. Biogeochem. Cy., 25, GB3009, doi:10.1029/2010GB003868, 2011.

Lampitt, R. S. and Antia, A. N.: Particle flux in deep seas: regional characteristics and temporal variability, Deep-Sea Res. Pt. I, 44, 1377–1403, doi:10.1016/S0967-0637(97)00020-4, 1997.

Lampitt, R. S., Boorman, B., Brown, L., Lucas, M., Salter, I., Sanders, R., Saw, K., Seeyave, S., Thomalla, S. J., and Turnewitsch, R.: Particle export from the euphotic zone: Estimates using a novel drifting sediment trap, 234Th and new production, Deep-Sea Res. Pt. I, 55, 1484–1502, doi:10.1016/j.dsr.2008.07.002, 2008.

Landry, M. R., Constantinou, J., Latasa, M., Brown, S. L., Bidigare, R. R., and Ondrusek, M. E.: Biological response to iron fertilization in the eastern equatorial Pacific (IronEx II), III. Dynamics of phytoplankton growth and microzooplankton grazing, Mar. Ecol.-Prog. Ser., 201, 57–72, doi:10.3354/meps201057, 2000.

Laurenceau-Cornec, E. C., Trull, T. W., Davies, D. M., Bray, S. G., Doran, J., P lanchon, F., Carlotti, F., Jouandet, M.-P., Cavagna, A.-J., Waite, A. M., and Blain, S.: The relative importance of phytoplankton aggregates and zooplankton fecal pellets to carbon export: insights from free-drifting sediment trap deployments in naturally iron-fertilised waters near the Kerguelen Plateau, Biogeosciences, 12, 1007–1027, doi:10.5194/bg-12-1007-2015, 2015.

Laws, E. A., Falkowski, P. G., Smith, W. O., Ducklow, H., and McCarthy, J. J.: Temperature effects on export production in the open ocean, Glob. Biogeochem. Cy. 14, 1231–1246, doi:10.1029/1999GB001229, 2000.

Laws, E. A., D'Sa, E., and Naik, P.: Simple equations to estimate ratios of new or export production to total production from satellite-derived estimates of sea surface temperature and primary production, Limnol. Oceanogr.-Methods, 593–601, doi:10.4319/lom.2011.9.593, 2011.

Lefèvre, D., Guigue, C., and Obernosterer, I.: The metabolic balance at two contrasting sites in the Southern Ocean: The iron-fertilized Kerguelen area and HNLC waters, Deep-Sea Res. Pt. II, KEOPS: Kerguelen Ocean and Plateau compared Study, 55, 766–776, doi:10.1016/j.dsr2.2007.12.006, 2008.

Le Moigne, F. A. C., Sanders, R. J., Villa-Alfageme, M., Martin, A. P., Pabortsava, K., Planquette, H., Morris, P. J., and Thomalla, S. J.: On the proportion of ballast versus non-ballast associated carbon export in the surface ocean, Geophys. Res. Lett., 39, L15610, doi:10.1029/2012GL052980, 2012.

Lenton, A., Tilbrook, B., Law, R. M., Bakker, D., Doney, S. C., Gruber, N., Ishii, M., Hoppema, M., Lovenduski, N. S., Matear, R. J., McNeil, B. I., Metzl, N., Mikaloff Fletcher, S. E., Monteiro, P. M. S., Rödenbeck, C., Sweeney, C., and Takahashi, T.: Sea-air CO_2 fluxes in the Southern Ocean for the period 1990–2009, Biogeosciences, 10, 4037–4054, doi:10.5194/bg-10-4037-2013, 2013.

Le Quéré, C., Andres, R. J., Boden, T., Conway, T., Houghton, R. A., House, J. I., Marland, G., Peters, G. P., van der Werf, G. R., Ahlström, A., Andrew, R. M., Bopp, L., Canadell, J. G., Ciais,

P., Doney, S. C., Enright, C., Friedlingstein, P., Huntingford, C., Jain, A. K., Jourdain, C., Kato, E., Keeling, R. F., Klein Goldewijk, K., Levis, S., Levy, P., Lomas, M., Poulter, B., Raupach, M. R., Schwinger, J., Sitch, S., Stocker, B. D., Viovy, N., Zaehle, S., and Zeng, N.: The global carbon budget 1959–2011, Earth Syst. Sci. Data, 5, 165–185, doi:10.5194/essd-5-165-2013, 2013.

Levy, M., Bopp, L., Karleskind, P., Resplandy, L., Ethe, C., and Pinsard, F.: Physical pathways for carbon transfers between the surface mixed layer and the ocean interior, Glob. Biogeochem. Cy., 27, 1001–1012, doi:10.1002/gbc.20092, 2013.

Lima, I. D., Lam, P. J., and Doney, S. C.: Dynamics of particulate organic carbon flux in a global ocean model, Biogeosciences, 11, 1177–1198, doi:10.5194/bg-11-1177-2014, 2014.

Lutz, M. J., Caldeira, K., Dunbar, R. B., and Behrenfeld, M. J.: Seasonal rhythms of net primary production and particulate organic carbon flux to depth describe the efficiency of biological pump in the global ocean, J. Geophys. Res.-Oceans, 112, C10011, doi:10.1029/2006JC003706, 2007.

Maiti, K., Charette, M. A., Buesseler, K. O., and Kahru, M.: An inverse relationship between production and export efficiency in the Southern Ocean, Geophys. Res. Lett., 40, 1557–1561, doi:10.1002/grl.50219, 2013.

Manno, C., Stowasser, G., Enderlein, P., Fielding, S., and Tarling, G. A.: The contribution of zooplankton faecal pellets to deep-carbon transport in the Scotia Sea (Southern Ocean), Biogeosciences, 12, 1955–1965, doi:10.5194/bg-12-1955-2015, 2015.

Maraldi, C., Mongin, M., Coleman, R., and Testut, L.: The influence of lateral mixing on a phytoplankton bloom: Distribution in the Kerguelen Plateau region, Deep-Sea Res. Pt. I, 56, 963–973, doi:10.1016/j.dsr.2008.12.018, 2009.

Maraldi, C., Lyard, F., Testut, L., and Coleman, R.: Energetics of internal tides around the Kerguelen Plateau from modeling and altimetry, J. Geophys. Res.-Oceans, 116, C06004, doi:10.1029/2010JC006515, 2011.

Maritorena, S. and Siegel, D. A.: Consistent merging of satellite ocean color data sets using a bio-optical model, Remote Sens. Environ., 94, 429–440, doi:10.1016/j.rse.2004.08.014, 2005.

Martin, J. H.: Glacial-interglacial CO_2 change: The Iron Hypothesis, Paleoceanography, 5, 1–13, doi:10.1029/PA005i001p00001, 1990.

Martin, J. H., Knauer, G. A., Karl, D. M., and Broenkow, W. W.: VERTEX: carbon cycling in the northeast Pacific, Deep-Sea Res. Pt. I, 34, 267–285, doi:10.1016/0198-0149(87)90086-0, 1987.

Martin, P., van der Loeff, M. R., Cassar, N., Vandromme, P., d'Ovidio, F., Stemmann, L., Rengarajan, R., Soares, M., González, H. E., Ebersbach, F., Lampitt, R. S., Sanders, R., Barnett, B. A., Smetacek, V., and Naqvi, S. W. A.: Iron fertilization enhanced net community production but not downward particle flux during the Southern Ocean iron fertilization experiment LOHAFEX, Glob. Biogeochem. Cy., 27, 871–881, doi:10.1002/gbc.20077, 2013.

Matsuno, K., Yamaguchi, A., Fujiwara, A., Onodera, J., Watanabe, E., Imai, I., Chiba, S., Harada, N., and Kikuchi, T.: Seasonal changes in mesozooplankton swimmers collected by sediment trap moored at a single station on the Northwind Abyssal Plain in the western Arctic Ocean, J. Plankton Res., 36, 490–502, doi:10.1093/plankt/fbt092, 2014.

Measures, C. I., Brown, M. T., Selph, K. E., Apprill, A., Zhou, M., Hatta, M., and Hiscock, W. T.: The influence of shelf processes in delivering dissolved iron to the HNLC waters of the

Drake Passage, Antarctica, Deep-Sea Res. Pt. II, 90, 77–88, doi:10.1016/j.dsr2.2012.11.004, 2013.

Metzl, N., Brunet, C., Jabaud-Jan, A., Poisson, A., and Schauer, B.: Summer and winter air–sea CO_2 fluxes in the Southern Ocean, Deep-Sea Res. Pt. I, 53, 1548–1563, doi:10.1016/j.dsr.2006.07.006, 2006.

Moore, J. K., Doney, S. C., and Lindsay, K.: Upper ocean ecosystem dynamics and iron cycling in a global three-dimensional model, Glob. Biogeochem. Cy., 18, GB4028, doi:10.1029/2004GB002220, 2004.

Morales, C. E.: Carbon and nitrogen content of copepod faecal pellets: effect of food concentration and feeding behaviour, Mar. Ecol.-Prog. Ser., 36, 107–114, 1987.

Obernosterer, I., Christaki, U., Lefèvre, D., Catala, P., Van Wambeke, F., and Lebaron, P.: Rapid bacterial mineralization of organic carbon produced during a phytoplankton bloom induced by natural iron fertilization in the Southern Ocean, Deep-Sea Res. Pt. II, 55, 777–789, doi:10.1016/j.dsr2.2007.12.005, 2008.

O'Neill, L. P., Benitez-Nelson, C. R., Styles, R. M., Tappa, E., and Thunell, R. C.: Diagenetic effects on particulate phosphorus samples collected using formalin poisoned sediment traps, Limnol. Oceanogr.-Methods, 3, 308–317, doi:10.4319/lom.2005.3.308, 2005.

Park, Y.-H., Charriaud, E., Pino, D. R., and Jeandel, C.: Seasonal and interannual variability of the mixed layer properties and steric height at station KERFIX, southwest of Kerguelen, J. Mar. Syst., 17, 571–586, doi:10.1016/S0924-7963(98)00065-7, 1998.

Park, Y.-H., Fuda, J.-L., Durand, I., and Naveira Garabato, A. C.: Internal tides and vertical mixing over the Kerguelen Plateau, Deep-Sea Res. Pt. II, 55, 582–593, doi:10.1016/j.dsr2.2007.12.027, 2008a.

Park, Y.-H., Roquet, F., Durand, I., and Fuda, J.-L.: Large-scale circulation over and around the Northern Kerguelen Plateau, Deep-Sea Res. Pt. II, 55, 566–581, doi:10.1016/j.dsr2.2007.12.030, 2008b.

Peterson, M. L., Wakeham, S. G., Lee, C., Askea, M. A., and Miquel, J. C.: Novel techniques for collection of sinking particles in the ocean and determining their settling rates, Limnol. Oceanogr.-Methods, 3, 520–532, doi:10.4319/lom.2005.3.520, 2005.

Picheral, M., Guidi, L., Stemmann, L., Karl, D. M., Iddaoud, G., and Gorsky, G.: The Underwater Vision Profiler 5: An advanced instrument for high spatial resolution studies of particle size spectra and zooplankton, Limnol. Oceanogr.-Methods, 8, 462–473, doi:10.4319/lom.2010.8.462, 2010.

Planchon, F., Ballas, D., Cavagna, A.-J., Bowie, A. R., Davies, D., Trull, T., Laurenceau, E., Van Der Merwe, P., and Dehairs, F.: Carbon export in the naturally iron-fertilized Kerguelen area of the Southern Ocean based on the 234Th approach, Biogeosciences Discuss., 11, 15991–16032, doi:10.5194/bgd-11-15991-2014, 2014.

Pollard, R., Sanders, R., Lucas, M., and Statham, P.: The Crozet Natural Iron Bloom and Export Experiment (CROZEX), Deep-Sea Res. Pt. II, 54, 1905–1914, doi:10.1016/j.dsr2.2007.07.023, 2007.

Pollard, R. T., Salter, I., Sanders, R. J., Lucas, M. I., Moore, C. M., Mills, R. A., Statham, P. J., Allen, J. T., Baker, A. R., Bakker, D. C. E., Charette, M. A., Fielding, S., Fones, G. R., French, M., Hickman, A. E., Holland, R. J., Hughes, J. A., Jickells, T.

D., Lampitt, R. S., Morris, P. J., Nédélec, F. H., Nielsdóttir, M., Planquette, H., Popova, E. E., Poulton, A. J., Read, J. F., Seeyave, S., Smith, T., Stinchcombe, M., Taylor, S., Thomalla, S., Venables, H. J., Williamson, R., and Zubkov, M. V.: Southern Ocean deep-water carbon export enhanced by natural iron fertilization, Nature, 457, 577–580, doi:10.1038/nature07716, 2009.

Rembauville, M., Blain, S., Armand, L., Quéguiner, B., and Salter, I.: Export fluxes in a naturally iron-fertilized area of the Southern Ocean – Part 2: Importance of diatom resting spores and faecal pellets for export, Biogeosciences, 12, 3171–3195, doi:10.5194/bg-12-3171-2015, 2015.

Rigual-Hernández, A. S., Trull, T. W., Bray, S. G., Closset, I., and Armand, L. K.: Seasonal dynamics in diatom and particulate export fluxes to the deep sea in the Australian sector of the southern Antarctic Zone, J. Mar. Syst., 142, 62–74, doi:10.1016/j.jmarsys.2014.10.002, 2015.

Rivkin, R. B. and Legendre, L.: Biogenic carbon cycling in the upper ocean: effects of microbial respiration, Science, 291, 2398–2400, doi:10.1126/science.291.5512.2398, 2001.

Rynearson, T. A., Richardson, K., Lampitt, R. S., Sieracki, M. E., Poulton, A. J., Lyngsgaard, M. M., and Perry, M. J.: Major contribution of diatom resting spores to vertical flux in the sub-polar North Atlantic, Deep-Sea Res. Pt. I, 82, 60–71, doi:10.1016/j.dsr.2013.07.013, 2013.

Saba, G. K. and Steinberg, D. K.: Abundance, Composition, and Sinking Rates of Fish Fecal Pellets in the Santa Barbara Channel, Sci. Rep., 2, doi:10.1038/srep00716, 2012.

Salter, I., Lampitt, R. S., Sanders, R., Poulton, A., Kemp, A. E. S., Boorman, B., Saw, K., and Pearce, R.: Estimating carbon, silica and diatom export from a naturally fertilised phytoplankton bloom in the Southern Ocean using PELAGRA: A novel drifting sediment trap, Deep-Sea Res. Pt. II, The Crozet Natural Iron Bloom and Export Experiment CROZEX, 54, 2233–2259, doi:10.1016/j.dsr2.2007.06.008, 2007.

Salter, I., Kemp, A. E. S., Lampitt, R. S., and Gledhill, M.: The association between biogenic and inorganic minerals and the amino acid composition of settling particles, Limnol. Oceanogr., 55, 2207–2218, doi:10.4319/lo.2010.55.5.2207, 2010.

Salter, I., Kemp, A. E. S., Moore, C. M., Lampitt, R. S., Wolff, G. A., and Holtvoeth, J.: Diatom resting spore ecology drives enhanced carbon export from a naturally iron-fertilized bloom in the Southern Ocean, Glob. Biogeochem. Cy., 26, GB1014, doi:10.1029/2010GB003977, 2012.

Salter, I., Schiebel, R., Ziveri, P., Movellan, A., Lampitt, R., and Wolff, G. A.: Carbonate counter pump stimulated by natural iron fertilization in the Polar Frontal Zone, Nat. Geosci., 7, 885–889, doi:10.1038/ngeo2285, 2014.

Sarmiento, J. L. and Gruber, N.: Ocean Biogeochemical Dynamics, Princeton University Press, Princeton, 2006.

Sarmiento, J. L. and Le Quéré, C.: Oceanic Carbon Dioxide Uptake in a Model of Century-Scale Global Warming, Science, 274, 1346–1350, 1996.

Sarthou, G., Timmermans, K. R., Blain, S., and Tréguer, P.: Growth physiology and fate of diatoms in the ocean: a review, J. Sea Res., Iron Resources and Oceanic Nutrients – Advancement of Global Environmental Simulations, 53, 25–42, doi:10.1016/j.seares.2004.01.007, 2005.

Savoye, N., Benitez-Nelson, C., Burd, A. B., Cochran, J. K., Charette, M., Buesseler, K. O., Jackson, G. A., Roy-Barman, M.,

Schmidt, S., and Elskens, M.: ^{234}Th sorption and export models in the water column: A review, Mar. Chem., 100, 234–249, doi:10.1016/j.marchem.2005.10.014, 2006.

Savoye, N., Trull, T. W., Jacquet, S. H. M., Navez, J., and Dehairs, F.: 234Th-based export fluxes during a natural iron fertilization experiment in the Southern Ocean (KEOPS), Deep-Sea Res. Pt. II, KEOPS: Kerguelen Ocean and Plateau compared Study, 55, 841–855, doi:10.1016/j.dsr2.2007.12.036, 2008.

Schlitzer, R.: Export production in the Equatorial and North Pacific derived from dissolved oxygen, nutrient and carbon data, J. Oceanogr., 60, 53–62, 2004.

Schulz, M. and Mudelsee, M.: REDFIT: estimating red-noise spectra directly from unevenly spaced paleoclimatic time series, Comput. Geosci., 28, 421–426, doi:10.1016/S0098-3004(01)00044-9, 2002.

Seeyave, S., Lucas, M. I., Moore, C. M., and Poulton, A. J.: Phytoplankton productivity and community structure in the vicinity of the Crozet Plateau during austral summer 2004/2005, The Crozet Natural Iron Bloom and Export Experiment CROZEX, Deep-Sea Res. Pt. II, 54, 2020–2044, doi:10.1016/j.dsr2.2007.06.010, 2007.

Smetacek, V., Assmy, P., and Henjes, J.: The role of grazing in structuring Southern Ocean pelagic ecosystems and biogeochemical cycles, Antarct. Sci., 16, 541–558, doi:10.1017/S0954102004002317, 2004.

Smith, R. C:. Remote sensing and depth distribution of ocean chlorophyll, Mar. Ecol.-Prog. Ser., 5, 359–361, 1981.

Tarling, G. A., Ward, P., Atkinson, A., Collins, M. A., and Murphy, E. J.: DISCOVERY 2010: Spatial and temporal variability in a dynamic polar ecosystem, Deep-Sea Res. Pt. II, 59–60, 1–13, doi:10.1016/j.dsr2.2011.10.001, 2012.

Trull, T. W., Bray, S. G., Buesseler, K. O., Lamborg, C. H., Manganini, S., Moy, C., and Valdes, J.: In situ measurement of mesopelagic particle sinking rates and the control of carbon transfer to the ocean interior during the Vertical Flux in the Global Ocean (VERTIGO) voyages in the North Pacific, Deep-Sea Res. Pt. II, 55, 1684–1695, doi:10.1016/j.dsr2.2008.04.021, 2008a.

Trull, T. W., Davies, D., and Casciotti, K.: Insights into nutrient assimilation and export in naturally iron-fertilized waters of the Southern Ocean from nitrogen, carbon and oxygen isotopes, Deep-Sea Res. Pt. II, 55, 820–840, doi:10.1016/j.dsr2.2007.12.035, 2008b.

Tsuda, A., Takeda, S., Saito, H., Nishioka, J., Kudo, I., Nojiri, Y., Suzuki, K., Uematsu, M., Wells, M.L., Tsumune, D., Yoshimura, T., Aono, T., Aramaki, T., Cochlan, W.P., Hayakawa, M., Imai, K., Isada, T., Iwamoto, Y., Johnson, W. K., Kameyama, S., Kato, S., Kiyosawa, H., Kondo, Y., Levasseur, M., Machida, R. J., Nagao, I., Nakagawa, F., Nakanishi, T., Nakatsuka, S., Narita, A., Noiri, Y., Obata, H., Ogawa, H., Oguma, K., Ono, T., Sakuragi, T., Sasakawa, M., Sato, M., Shimamoto, A., Takata, H., Trick, C.G., Watanabe, Y. W., Wong, C. S., and Yoshie, N.: Evidence for the grazing hypothesis: Grazing reduces phytoplankton responses of the HNLC ecosystem to iron enrichment in the western subarctic pacific (SEEDS II), J. Oceanogr., 63, 983–994, doi:10.1007/s10872-007-0082-x, 2007.

Uitz, J., Claustre, H., Griffiths, F. B., Ras, J., Garcia, N., and Sandroni, V.: A phytoplankton class-specific primary production model applied to the Kerguelen Islands region (Southern Ocean),

Deep-Sea Res. Pt. I, 56, 541–560, doi:10.1016/j.dsr.2008.11.006, 2009.

Villareal, T. A., Adornato, L., Wilson, C., and Schoenbaechler, C. A.: Summer blooms of diatom-diazotroph assemblages and surface chlorophyll in the North Pacific gyre: A disconnect, J. Geophys. Res.-Oceans, 116, C03001, doi:10.1029/2010JC006268, 2011.

Volk, T. and Hoffert, M. I.: Ocean carbon pumps: Analysis of relative strengths and efficiencies in ocean-driven atmospheric CO_2 changes, in: Geophysical Monograph Series, edited by:: Sundquist, E. T. and Broecker, W. S., American Geophysical Union, Washington, D. C., 99–110, 1985.

Biogeosciences

Open Access

Export fluxes in a naturally iron-fertilized area of the Southern Ocean – Part 2: Importance of diatom resting spores and faecal pellets for export

M. Rembauville[1,2], S. Blain[1,2], L. Armand[3], B. Quéguiner[4], and I. Salter[1,2,5]

[1]Sorbonne Universités, UPMC Univ Paris 06, UMR7621, LOMIC, Observatoire Océanologique, Banyuls-sur-Mer, France
[2]CNRS, UMR7621, LOMIC, Observatoire Océanologique, Banyuls-sur-Mer, France
[3]Department of Biological Sciences and Climate Futures, Macquarie University, New South Wales, Australia
[4]Aix-Marseille Université, Université de Toulon, CNRS/INSU, IRD, MIO, UM110, Marseille, France
[5]Alfred Wegener Institute for Polar and Marine Research, Bremerhaven, Germany

Correspondence to: M. Rembauville (rembauville@obs-banyuls.fr)

Abstract. The biological composition of the material exported to a moored sediment trap located under the winter mixed layer of the naturally fertilized Kerguelen Plateau in the Southern Ocean was studied over an annual cycle. Despite iron availability in spring, the annual particulate organic carbon (POC) export ($98.2 \, \mathrm{mmol \, m^{-2}}$) at 289 m was low, but annual biogenic silica export was significant ($114 \, \mathrm{mmol \, m^{-2}}$). This feature was related to the abundance of empty diatom cells and the ratio of full to empty cells exerted a first-order control in BSi : POC export stoichiometry of the biological pump. *Chaetoceros Hyalochaete* spp. and *Thalassiosira antarctica* resting spores were responsible for more than 60 % of the annual POC flux that occurred during two very short export events of < 14 days in spring–summer. Relatively low diatom fluxes were observed over the remainder of the year. Faecal pellet contribution to annual carbon flux was lower (34 %) and reached its seasonal maximum in autumn and winter (> 80 %). The seasonal progression of faecal pellet types revealed a clear transition from small spherical shapes (small copepods) in spring, to larger cylindrical and ellipsoid shapes in summer (euphausiids and large copepods) and finally to large tabular shapes (salps) in autumn and winter. We propose in this high-biomass, low-export (HBLE) environment that small but highly silicified and fast-sinking resting spores are able to bypass the intense grazing pressure and efficient carbon transfer to higher trophic levels that are responsible for the low fluxes observed the during the remainder of the year. More generally our study also provides a statistical framework linking the ecological succession of diatom and zooplankton communities to the seasonality of carbon and silicon export within an iron-fertilized bloom region in the Southern Ocean.

1 Introduction

The Southern Ocean is the place of exposure of old upwelled waters to the atmosphere and the formation of mode waters, thereby ventilating an important part of the global ocean and playing a central role in distributing heat, carbon and nutrients in the global ocean (Sarmiento et al., 2004; Takahashi et al., 2012; Sallée et al., 2012). Silicon trapping occurs in the Southern Ocean because silicon is stripped out of the euphotic zone more efficiently than phosphorus and nitrogen (Holzer et al., 2014). It is generally acknowledged that regional variations in plankton community structure are responsible for variations in nutrient stoichiometry in the Southern Ocean (Jin et al., 2006; Weber and Deutsch, 2010) and that the biological pump is a central process regulating this stoichiometry (Ragueneau et al., 2006; Salter et al., 2012; Primeau et al., 2013). These characteristics emphasize the importance of biological processes in the Southern Ocean waters for the availability of silicic acid and nitrate (Sarmiento et al., 2004; Dutkiewicz et al., 2005) as well as

phosphate (Primeau et al., 2013) at lower latitudes, thereby regulating part of the productivity of the global ocean. It has been proposed that change in the uptake ratio of silicate and nitrate by Southern Ocean phytoplankton in response to increased iron availability during the Last Glacial Maximum could have played a substantial role in varying atmospheric CO_2 (Brzezinski et al., 2002; Matsumoto et al., 2002).

Primary production in the Southern Ocean is regulated by macro- and micronutrient availability (Martin et al., 1990; J. K. Moore et al., 2001; Nelson et al., 2001; C. M. Moore et al., 2013) and light levels as modulated by insolation and surface layer mixing (Venables and Moore, 2010; Blain et al., 2013). The complex interaction of these factors introduces strong spatial heterogeneity in the distribution of primary producer biomass (Arrigo et al., 1998; Thomalla et al., 2011). In particular, high-nutrient, low-chlorophyll (HNLC) areas in the open ocean contrast strongly with highly productive, naturally fertilized blooms located downstream of island systems such as the Kerguelen Plateau (Blain et al., 2001, 2007), Crozet Islands (Pollard et al., 2002) and South Georgia (Park et al., 2010; Tarling et al., 2012). The diatom-dominated phytoplankton blooms characteristic of these island systems are the product of multiple environmental conditions favourable for their rapid growth (Quéguiner, 2013), which appear to promote POC export from the mixed layer (Nelson et al., 1995; Buesseler, 1998). However the ecological traits of certain species can impact the BSi : POC export stoichiometry (Crawford, 1995; Salter et al., 2012), and may therefore control the biogeochemical function of a particular region of the Southern Ocean (Smetacek et al., 2004; Assmy et al., 2013).

Among the numerous ecological characteristics of plankton communities, algal aggregation (Jackson et al., 2005; Burd and Jackson, 2009), mesozooplankton faecal pellets (Lampitt et al., 1990; Wilson et al., 2008, 2013), vertical migrations of zooplankton (Jackson and Burd, 2001; Steinberg et al., 2002; Davison et al., 2013), radiolarian faecal pellets (Lampitt et al., 2009) and diatom resting spore formation (Salter et al., 2012; Rynearson et al., 2013) have all been highlighted as efficient vectors of carbon export out of the surface mixed layer. The challenge in describing the principal ecological processes regulating POC export fluxes is the requirement to have direct access to sinking particles. Many of the processes described occur in the upper layers of the ocean, where circulation can strongly influence the reliability of sediment trap collections (Baker et al., 1988; Buesseler et al., 2007). Short-term deployments of free-drifting sediment traps can be an efficient solution to minimize the hydrodynamic bias (Buesseler et al., 2000; Lampitt et al., 2008), but spatial and temporal decoupling of production and export needs to be considered (Salter et al., 2007; Rynearson et al., 2013). In regions characterized by relatively weak circulation, moored sediment trap observations in areas of naturally fertilized production can track temporal succession of exported material from long-term (several-month)

blooms (Westberry et al., 2013). Such an approach can partially resolve how ecological processes in plankton communities regulate POC and biomineral export out of the mixed layer (Salter et al., 2012, 2014), although selective processes during export may modify original surface features.

The central Kerguelen Plateau is a good environment to study the ecological vectors of export with sediment traps due to the naturally fertilized recurrent bloom (Blain et al., 2007) and shallow bathymetry that breaks the strong Antarctic Circumpolar Current flow (Park et al., 2008, 2014). As reported in the companion paper (Rembauville et al., 2015), annual POC export measured by the sediment trap deployment at 289 m beneath the southeastern iron-fertilized Kerguelen bloom was 98 ± 4 mmol m^{-2} yr^{-1}. This downward flux of carbon may account for as little as ~ 1.5 % of seasonal net community carbon production (6.6 ± 2.2 mol m^{-2}; Jouandet et al., 2008) and < 2 % of seasonally integrated POC export estimated at 200 m from a dissolved inorganic carbon budget (5.1 mol C m^{-2}; Blain et al., 2007). Although hydrodynamical and biological biases related to the shallow moored sediment trap deployment may partly explain the low POC fluxes we report, independent measurements of low POC fluxes (> 300 m) at the same station (Ebersbach and Trull, 2008; Jouandet et al., 2014) are consistent with the hypothesis of flux attenuation below the winter mixed layer. These observations suggest a "high-biomass, low-export" (HBLE; Lam and Bishop, 2007) status characterizing the productive Kerguelen Plateau. HBLE status appears to be a common feature of other productive sites of the Southern Ocean (Lam and Bishop, 2007; Ebersbach et al., 2011; Lam et al., 2011; Maiti et al., 2013; Cavan et al., 2015). Describing the temporal succession of POC and BSi flux vectors from the Kerguelen Plateau is of interest to increase our understanding of the ecological processes characterizing HBLE environments.

Numerous studies have described diatom fluxes from sediment trap records in the Southern Ocean (Leventer and Dunbar, 1987; Fischer et al., 1988, 2002; Abelmann and Gersonde, 1991; Leventer, 1991; Gersonde and Zielinski, 2000; Pilskaln et al., 2004; Ichinomiya et al., 2008; Salter et al., 2012). Highest diatom fluxes recorded by sediment traps (> 10^9 valves m^{-2} d^{-1}) were observed in the seasonal ice zone (SIZ) near Prydz Bay and Adélie Land and were dominated by *Fragilariopsis kerguelensis* and smaller *Fragilariopsis* species such as *Fragilariopsis curta* and *Fragilariopsis cylindrus* (Suzuki et al., 2001; Pilskaln et al., 2004). These high fluxes occurred in summer and were associated with the melting of sea ice. Changes in light availability and melt water input appear to establish favourable conditions for the production and export of phytoplankton cells (Romero and Armand, 2010). In the Permanently Open Ocean Zone (POOZ), highest diatom fluxes recorded were 2 orders of magnitude lower, $\sim 10^7$ valves m^{-2} d^{-1} (Abelmann and Gersonde, 1991; Salter et al., 2012; Grigorov et al., 2014), and typically represented by *F. kerguelensis* and *Thalassionema nitzschioides*. One notable exception is the naturally iron-

fertilized waters downstream of the Crozet Plateau, where resting spores of *Eucampia antarctica* var. *antarctica* dominated the diatom export assemblage (Salter et al., 2012).

Other studies have reported faecal pellet contribution to POC fluxes in the Southern Ocean (Dunbar, 1984; G. Wefer et al., 1988; G. G. Wefer et al., 1990; Wefer and Fisher, 1991; Dubischar and Bathmann, 2002; Suzuki et al., 2001, 2003; Accornero and Gowing, 2003; Schnack-Schiel and Isla, 2005; Gleiber et al., 2012), with a particular emphasis on shelf environments where faecal pellet contribution to POC flux was typically higher than in the oceanic regions (Wefer et al., 1990; Wefer and Fischer, 1991; Schnack-Schiel and Isla, 2005). In the Ross Sea, a northward decreasing contribution to carbon flux of 59, 38 and 15 % for southern, central and northern areas was reported from 235 m sediment traps deployments (Schnack-Schiel and Isla, 2005). Faecal pellets in the Ross Sea were generally represented by larger shapes, with only 2 to 3 % of them present as small spherical or ellipsoid shapes, and total faecal pellet flux was slightly higher than 10^3 pellets $m^{-2} d^{-1}$. High faecal pellet contributions to carbon fluxes (> 90 %) have been observed in the Bransfield Strait and the marginal ice zone of the Scotia Sea, and have been linked to the abundance of the Antarctic krill *Euphausia superba*, resulting in maximum recorded fluxes of $> 5 \times 10^5$ pellets $m^{-2} d^{-1}$ (von Bodungen, 1986; von Bodungen et al., 1987; Wefer et al., 1988). The strong contribution of krill faecal pellets to carbon flux in the western Antarctic Peninsula was confirmed over several years of observations, with the highest contributions to carbon flux succeeding the phytoplankton bloom in January and February (Gleiber et al., 2012).

In the present study, particulate material exported from the mixed layer in the naturally fertilized Permanently Open Ocean Zone (POOZ) of the Kerguelen Plateau is described from an annual sediment trap mooring. To develop our understanding of seasonal variability in the ecological flux vectors and particle biogeochemistry, we investigate the link between the chemical (POC, PON, BSi) and biological (diatom species and faecal pellet types) components of exported particles. Furthermore, we advance the limitations of previous studies by explicitly distinguishing between full and empty diatom cells in the exported material and thereby determine species-specific roles for carbon and silica export.

2 Materials and methods

As part of the multidisciplinary research programme KEOPS2, a moored sediment trap (Technicap PPS3) was deployed at 289 m (seafloor depth: 527 m) at the representative bloom station A3 (50°38.3′ S, 72°02.6′ E) for a period of 321 days (21 October 2011 to 7 September 2012). The sediment trap mooring was located within an iron-fertilized bloom site on the southern part of the Kerguelen Plateau (Blain et al., 2007). The cup rotation dates of the sediment trap are listed in Table 1. Details of sediment trap design, hydrological conditions, sample processing, POC and PON analyses, and surface chlorophyll *a* data extraction are described in a companion paper (Rembauville et al., 2015). Comparison with thorium-based estimates of carbon export suggests a trapping efficiency of 15–30 % relative to the proxy, although strong particle flux attenuation between 200 m and the trap depth (289 m) might also contribute to the low fluxes. We therefore interpret our results to accurately reflect the relationships between the biological and geochemical signals of the material caught by the sediment trap, which we acknowledge may not necessarily represent the entire particle export at 289 m.

2.1 Biogenic and lithogenic silicon analyses

For the analysis of biogenic silica (BSi) and lithogenic silica (LSi), 2 to 8 mg of freeze-dried material was weighed (Sartorius precision balance, precision 10^{-4} g) and placed into Falcon tubes. The extraction of silicon from biogenic and lithogenic particle phases was performed following the Ragueneau et al. (2005) triple NaOH/HF extraction procedure. Silicic acid ($Si(OH)_4$) resulting from NaOH extractions was measured automatically on a Skalar 5100 autoanalyser, whereas $Si(OH)_4$ resulting from HF extraction was measured manually on a Milton Roy Spectronic 401 spectrophotometer. $Si(OH)_4$ analyses were performed colorimetrically following Aminot and Kerouel (2007). Standards for the analysis of samples from the HF extraction were prepared in an HF/H_3BO_4 matrix, ensuring the use of an appropriate calibration factor that differs from Milli-Q water. The contribution of LSi to the first leaching was determined by using Si : Al ratios from a second leaching step (Ragueneau et al., 2005). Aluminium concentrations were measured by spectrophotometry (Howard et al., 1986). The triple extraction procedure is optimized for samples with a BSi content < 10 μmol. For some samples (cups #3, #4, #6, #7, #8, #9 and #10) the Si : Al molar ratio in the second leachate was high (> 10), indicating the incomplete dissolution of BSi. For these samples it was not possible to use Si : Al ratios to correct for LSi leaching. A crustal Si : Al mass ratio of 3.74 (Taylor and McClennan, 1986) was therefore used and applied to all the samples for consistency. Precision (estimated from measurement of 25 independent samples) was 13 nmol mg^{-1}, which represents < 1 % of the BSi content in all samples and 14 % of the mean LSi content. Blank triplicates from each extraction were below the detection limit. BSi results from this method were compared to the kinetic method from DeMaster (1981). There was an excellent agreement between the two methods (Spearman rank correlation, $n = 12$, $p < 0.001$, $BSi_{kinetic} = 1.03 BSi_{triple extraction} - 0.08$; data not shown). To estimate the contribution of opal to total mass flux, we assumed an opal composition of SiO_2 0.4 H_2O (Mortlock and Froelich, 1989).

In order to correct for the dissolution of BSi during deployment and storage, $Si(OH)_4$ excess was analysed in the over-

Table 1. Sediment bulk flux and composition results.

Cup	Cup opening date	Cup closing date	Collection time (days)	Season	Mass flux (mg m^{-2} d^{-1})*	POC flux (mmol m^{-2} d^{-1})*	PON flux (mmol m^{-2} d^{-1})*	BSi Flux (mmol m^{-2} d^{-1})	LSi flux (μmol m^{-2} d^{-1})	% opal	POC : PON	BSi : POC
1	21/10/2011	04/11/2011	14	Spring	52.2	0.15	0.02	0.51	26.6	65.6	6.80	3.46
2	04/11/2011	18/11/2011	14	Spring	28.1	0.14	0.02	0.30	18.0	70.8	6.09	2.18
3	18/11/2011	02/12/2011	14	Spring	54.1	0.15	0.02	0.51	13.0	63.9	7.33	3.43
4	02/12/2011	12/12/2011	10	Summer	261.3	1.60	0.23	2.60	20.9	66.9	6.95	1.63
5	12/12/2011	22/12/2011	10	Summer	23.1	0.34	0.05	0.21	4.4	62.4	6.87	0.64
6	22/12/2011	01/01/2012	10	Summer	74.8	0.51	0.08	0.37	8.2	32.9	6.70	0.72
7	01/01/2012	11/01/2012	10	Summer	80.5	0.42	0.06	0.55	8.9	46.0	6.73	1.32
8	11/01/2012	25/01/2012	14	Summer	59.8	0.34	0.05	0.50	5.4	56.5	6.94	1.48
9	25/01/2012	08/02/2012	14	Summer	238.7	1.47	0.20	2.19	7.2	61.7	7.38	1.49
10	08/02/2012	22/02/2012	14	Summer	75.8	0.55	0.08	0.72	6.1	64.2	6.97	1.32
11	22/02/2012	31/05/2012	99	Autumn	24.4	0.27	0.03	0.08	1.5	21.5	8.09	0.29
12	31/05/2012	07/09/2012	99	Winter	5.1	0.04	0.01	0.03	2.2	35.0	6.06	0.66
	Annual export**		322		14 438	98.2	13.6	114	1.85	53.1	7.2	1.2

* Data from Rembauville et al. (2015). ** Values assume no flux during the unsampled portion of the year.

lying preservative solution. Particulate BSi fluxes were corrected for dissolution assuming that excess silicic acid originated only from the dissolution of BSi phases. Si(OH)$_4$ excess was always < 10 % of total (dissolved + particulate) Si concentrations. Error propagation for POC, PON, BSi fluxes and molar ratios was calculated as the quadratic sum of the relative error from triplicate measurements of each variable.

2.2 Diatom identification, fluxes and biomass

Many sediment trap studies reporting diatom fluxes in the Southern Ocean use a micropalaeontological protocol that oxidizes organic material (KMnO$_4$, HCl, H$_2$O$_2$), thereby facilitating the observation of diatom valves (see Romero et al., 1999, 2000, for a description). In the present manuscript, our specific aim was to separately enumerate full and empty diatom cells captured by the sediment trap to identify key carbon or silicon exporters amongst the diatom species. We therefore used a biological method following a similar protocol to that of Salter et al. (2007, 2012). To prepare samples for counting, 2 mL of a gently homogenized one-eighth wet aliquot was diluted in a total volume of 20 mL of artificial seawater ($S = 34$). In order to minimize the exclusion and/or breaking of large or elongated diatom frustules (e.g. *Thalassiothrix antarctica*), the pipette tip used for sub-sampling was modified to increase the tip aperture to > 2 mm. The diluted and homogenized sample was placed in a Sedgewick Rafter counting chamber (Pyser SGE S52, 1 mL chamber volume). Each sample was observed under an inverted microscope (Olympus IX71) with phase contrast at 200× and 400× magnification. Diatom enumeration and identification was made from one-quarter to one-half of the counting chamber (depending on cell abundance). The total number of diatoms counted was > 400 in all the cups, with the exception of the winter cup #12 (May–September 2012), where the diatom abundance was low (< 100 diatoms counted). Diatoms species were identified following the recommendations of Hasle and Syvertsen (1997). All whole, intact and recognizable frustules were enumerated. Full and empty cells

were counted separately, following suggestions in Assmy et al. (2013).

Due to the lower magnification used and preserved cell contents sometimes obscuring taxonomic features on the valve face, taxonomic identification to the species level was occasionally difficult and necessitated the categorizing of diatom species to genus or taxa groupings in the following manner: *Chaetoceros* species of the subgenus *Hyalochaete* resting spores (CRS) were not differentiated into species or morphotypes but were counted separately from the vegetative cells; *Fragilariopsis separanda* and *Fragilariopsis rhombica* were grouped as *Fragilariopsis separanda/rhombica*; *Membraneis imposter* and *Membraneis challengeri* and species of the genera *Banquisia* and *Manguinea* were denominated as *Membraneis* spp. (Armand et al., 2008a); diatoms of the genus *Haslea* and *Pleurosigma* were grouped as *Pleurosigma* spp.; all *Pseudo-nitzschia* species encountered were grouped as *Pseudo-nitzschia* spp.; *Rhizosolenia antennata* and *Rhizosolenia styliformis* were grouped as *Rhizosolenia antennata/styliformis*; large and rare *Thalassiosira oliverana* and *Thalassiosira tumida* were grouped as *Thalassiosira* spp.; *Thalassiosira antarctica* resting spores (TRS) were identified separately from the vegetative cells; small centric diatoms (< 20 μm) represented by *Thalassiosira gracilis* and other *Thalassiosira* species were designated as small centrics (< 20 μm); and finally large and rare centrics, including *Azpeitia tabularis*, *Coscinodiscus* spp. and *Actinocyclus curvatulus*, were grouped as large centrics (> 20 μm). Full and empty frustules of each species or taxa grouping were distinguished and enumerated separately. The cell flux for each diatom species or taxa grouping was calculated according to Eq. (1):

$$\text{Cell flux} = N_{\text{diat}} \cdot d \cdot 8 \cdot V_{\text{cup}} \cdot \frac{1}{0.125} \cdot \frac{1}{\text{days}} \cdot \text{chamber fraction}, \quad (1)$$

where Cell flux is in valves m^{-2} d^{-1}, N_{diat} is the number of cells enumerated for each diatom classification, d is the dilution factor from the original wet aliquot, 8 is the total number of wet aliquots comprising one sample cup, V_{cup} is the volume of each wet aliquot, 0.125 is the Technicap PPS/3 sedi-

ment trap collecting area (m²), days is the collecting period, and chamber fraction is the surface fraction of the counting chamber that was observed (one-quarter or one-half). The annually integrated full and empty diatom flux for each species was calculated as follows:

$$\text{Annual flux}_{(x)} = \sum_{i=1}^{12} \left(\text{Flux}_{(x)i} \cdot \text{days}_i \right), \qquad (2)$$

where Annual flux$_{(x)}$ is the annually integrated flux of a full or empty diatom species x (cell m^{-2} yr^{-1}), Flux$_{(x)i}$ is the full or empty flux of this species in the cup number i (cell m^{-2} d^{-1}) and days$_i$ is the collecting time for the cup number i (d). The calculations assume that negligible export occurred during the month of September, which was not sampled by the sediment trap. We consider this assumption reasonable based on the preceding flux profile and low concentration of satellite-derived chlorophyll a (Rembauville et al., 2015).

We directly compared the micropalaeontological (as used in Rigual-Hernández et al. (2015) and biological counting techniques in our sediment trap samples and noted the loss of several species (*Chaetoceros decipiens, Chaetoceros dichaeta, Corethron pennatum, Corethron inerme, Guinardia cylindrus* and *Rhizosolenia chunii*) under the micropalaeontological technique. We attribute this to the aggressive chemical oxidation techniques used to "clean" the samples as well as the centrifugation steps, which may also selectively destroy or dissolve certain frustules. For the species that were commonly observed by both techniques, total valve flux was in good agreement (Spearman rank correlation, $n = 12$, $\rho = 0.91$, $p < 0.001$; data not shown) although consistently lower with the micropalaeontolgical technique, probably due to the loss of certain frustules described above. Full details of this method comparison are in preparation for a separate submission.

Diatoms species that contributed to more than 1 % of total full cell flux were converted to carbon flux. For *E. antarctica* var. *antarctica, Fragilariopsis kerguelensis, Fragilariopsis separanda/rhombica, Pseudo-nitzschia* spp. and *Thalassionema nitzschioides* spp., we used published cell-specific carbon content (Cell$_C$, pg C cell^{-1}) for diatoms communities of the Kerguelen Plateau from Cornet-Barthaux et al. (2007). As *Chaetoceros Hyalochaete* resting spores (CRS) and *Thalassiosira antarctica* resting spores (TRS) largely dominated the full diatom fluxes (> 80 %), an appropriate estimation of their carbon content based on the specific sizes observed in our data set was required for accurate quantification of their contribution to carbon fluxes. Biomass calculations for both CRS and TRS were determined from > 50 randomly selected complete resting spores observed in splits from cups #4 to #11 (December 2011 to May 2012). Morphometric measurements (pervalvar and apical axis) were made using the Fiji image processing package (available at http://fiji.sc/Fiji) on images taken with an Olympus DP71 cam-

era. Cell volumes followed appropriate shape-designated calculations from Hillebrand et al. (1999; Table 2). The cell volume coefficient of variation was 46 and 54 % for CRS and TRS, respectively. CRS carbon content was estimated from the derived cell volume using the volume-to-carbon relationship of 0.039 pmol C µm^{-3} established from the resting spore of *Chaetoceros pseudocurvisetus* (Kuwata et al., 1993), leading to a mean Cell$_C$ value of 227 pg C cell^{-1} (Table 2). There is currently no volume-to-carbon relationship for *Thalassiosira antarctica* resting spores described in the literature; therefore, the allometric relationship for vegetative diatoms (Menden-Deuer and Lessard, 2000) was used to calculate our TRS carbon content, giving a mean Cell$_C$ value of 1428 pg C cell^{-1} (Table 2). Full diatom fluxes were converted to carbon fluxes as follows:

$$\text{C flux}_{(x)} = \frac{\text{Flux}_{(x)} \cdot \text{Cell}_{C(x)}}{M_{12C} \cdot 10^9}, \qquad (3)$$

where C flux$_{(x)}$ is the carbon flux carried by each diatom species x (mmol C m^{-2} d^{-1}), Flux$_{(x)}$ is the full cell numerical flux of species x (cell m^{-2} d^{-1}), Cell$_{C(x)}$ is the carbon content of species x (pg C cell^{-1}), M_{12C} is the molecular weight of ^{12}C (12 g mol^{-1}) and 10^9 is a conversion factor from pmol to mmol.

2.3 Faecal pellet composition and fluxes

To enumerate faecal pellets, an entire one-eighth aliquot of each sample cup was placed in a gridded Petri dish and observed under a stereomicroscope (Zeiss Discovery V20) coupled to a camera (Zeiss Axiocam ERc5s) at 10× magnification. Photographic images (2560 × 1920 pixels, 3.49 µm pixel^{-1}) covering the entire surface of the Petri dish were acquired. Following Wilson et al. (2013), faecal pellets were classified into five types according to their shape: spherical, ovoid, cylindrical, ellipsoid and tabular. The flux of each faecal pellet class (nb m^{-2} d^{-1}) was calculated as follows:

$$\text{Faecal pellet flux} = N_{\text{FP}} \cdot 8 \cdot \frac{1}{0.125} \cdot \frac{1}{\text{days}}, \qquad (4)$$

where N_{FP} is the number of pellets within each class observed in the one-eight aliquot. The other constants are as described in Eq. (1). Individual measurements of the major and minor axis for each faecal pellet were performed with the Fiji software. The total number of spherical, ovoid, cylindrical, ellipsoid and tabular faecal pellets measured was 4041, 2047, 1338, 54 and 29, respectively. Using these dimensions, faecal pellet volume was determined using the appropriate shape equation (e.g. sphere, ellipse, cylinder, ovoid/ellipse) and converted to carbon using a factor of 0.036 mg C mm^{-3} (Gonzalez and Smetacek, 1994). Due to the irregularity of the tabular shapes preventing the use of a single equation to calculate their volume, a constant value of 119 µg C pellet^{-1}, representing a mid-range value for tabular shapes (Madin, 1982), was applied to tabular faecal pellets (Wilson et al.,

Table 2. *Chaetoceros* resting spores (CRS) and *Thalassiosira antarctica* resting spores (TRS) measurement and biomass data from station A3 sediment trap. The range and the mean value (bold) are reported for each variable.

Spore type	Number measured	Pervalvar axis (µm)	Apical axis (µm)	Shape[a]	Cell volume (µm^3)	Volume–carbon relationship	Cell carbon content (pmol C cell^{-1})	Cell carbon content (pg C cell^{-1})
CRS	63	3.1–8.5 **6**	7.2–17.4 **12.1**	Cylinder + two cones	116.9–1415 **483**	0.039 pmol C µm^{-3}[b]	5–55 **19**	55–662 **227**
TRS	57	10.2–26 **20.8**	25.6–35.3 **32.6**	Cylinder + two half-spheres	14035–48477 **35502**	$C = 0.582 \times V^{0.811}$[c]	56–153 **119**	672–1839 **1428**

[a] As defined in Hillebrand et al. (1999). [b] Data representative of *Chaetoceros pseudocurvisetus* resting spore (Kuwata et al. 1993). [c] Equation from Menden-Deuer and Lessard (2000), where C is the carbon content (pg C) and V is the cell volume (µm^3).

2013). This value was appropriate because the observed tabular faecal pellets were within the size range reported in Madin (1982). Ranges and mean values of faecal pellet volumes and carbon content are reported in Table 3. Faecal fluff and disaggregated faecal pellets were not considered in these calculations because quantitative determination of their volume is difficult. We acknowledge that fragmentation of larger pellets may represent an artifact of the sample-splitting procedure. Alternatively, their presence may also result from natural processes within the water column, although dedicated sampling techniques (e.g. polyacrylamide gel traps) are required to make this distinction (Ebersbach et al., 2014, 2011; Ebersbach and Trull, 2008; Laurenceau-Cornec et al., 2015). Consequently our present quantification of faecal pellet carbon flux should be considered as lower-end estimates.

The precision of our calculations depends on the reliability of carbon–volume conversion factors of faecal pellets, which vary widely in the literature, as well as variability in diatom resting spore volumes (Table 2). To constrain the importance of this variability on our quantitative estimation of C flux, we calculated upper and lower error bounds using a constant scaling of the conversion factors (± 50 %).

2.4   Statistical analyses

Correspondence analysis was performed to summarize the seasonality of diatom export assemblages. This approach projects the original variables (here full and empty cells) onto a few principal axes that concentrate the information of the chi-squared (χ^2) distance between both observations and variables (Legendre and Legendre, 1998). χ^2 distance is very sensitive to rare events. Consequently, only species with an annual mean flux higher than 10 % of the mean annually integrated flux of all the species were retained in the correspondence analysis. This selection was performed separately on full and empty cell fluxes.

Partial least-squares regression (PLSR) analysis was used to examine the relationships between ecological flux vectors (full and empty diatom cells and faecal pellet fluxes as columns of the X matrix, cups being the rows) and bulk geochemical properties (POC flux, PON flux, BSi flux, POC : PON and BSi : POC molar ratio and columns in the

Y matrix) of the exported material. The principle of PLSR is to decompose both the X and Y matrix into their principal components using principal component analysis and then use these principal components to regress Y in X (Abdi, 2010). PLSR is capable of modelling response variables from a large set of predictors. The same filter as for the correspondence analysis (full and empty cell fluxes > 10 % of the total mean flux) was applied.

3   Results

3.1   Chemical composition of the settling material

Time series of the chemical signature of the settling material are presented in Fig. 1, and export fluxes are reported in Table 1. POC and PON fluxes are also reported and discussed in the companion paper (Rembauville et al., 2015). BSi fluxes exhibited the same seasonal pattern as POC fluxes (Fig. 1c) with low fluxes (< 1 mmol m^{-2} d^{-1}) except during the two intense events (2.60 ± 0.03 and 2.19 ± 0.10 mmol m^{-2} d^{-1}, mean $\pm$ standard deviation). LSi fluxes were highest in spring (> 10 µmol m^{-2} d^{-1} in cups #1 to #4, October to December 2011, Table 1). The contribution of LSi to total particulate Si was 5 and 10 %, respectively, in cups #1 (October/November 2011) and #12 (May to September 2012) and lower than 3 % the remainder of the year. The BSi : POC molar ratio was highest at the beginning of the season (between 2.18 ± 0.19 and 3.46 ± 0.16 in the first three cups from October to December 2011, blue line in Fig. 1c) and dropped to 0.64 ± 0.06 in cup #5 (end of December 2011), following the first export event. BSi : POC ratios were close in the two export events (1.62 ± 0.05 and 1.49 ± 0.08). The lowest BSi : POC ratio was observed in autumn in cup #11 (0.29 ± 0.01, February to May 2012). Similarly, the opal contribution to total mass flux was highest in spring (70.8 % in cup #2, November 2011) and lowest in autumn (21.5 % in cup #11, February to May 2012).

Table 3. Faecal pellet measurement and biomass estimations from the station A3 sediment trap. For each variable, the range and the mean value (bold) are reported.

Faecal pellet shape	Number measured	Major axis (μm) (a)	Minor axis (μm) (b)	Volume equation	Volume (μm^3)	Volume–carbon relationship	Faecal pellet carbon content (μmol C pellet^{-1})	Faecal pellet carbon content (μg C pellet^{-1})
Spherical	4041	11–1069 **150**		$4/3\,\pi\,(a/2)^3$	697–6.39×10^8 **1.77 $\times 10^6$**	0.036 mg C mm^{-3} *	2.09×10^{-6}–1.91 **5.3 10^{-3}**	2.51×10^{-5}–23 **0.06**
Ovoid	2047	85–1132 **314**	10–802 **154**	$4/3\,\pi\,(a/2)\,(b/2)^2$	4.45×10^3–3.81×10^8 **3.90 $\times 10^6$**		1.34×10^{-5}–1.14 **11.7 $\times 10^{-3}$**	1.60×10^{-4}–13.72 **0.14**
Cylindrical	1338	106–6152 **981**	14–547 **136**	$\pi\,(b/2)^2\,a$	1.63×10^4–1.45×10^9 **1.43 $\times 10^7$**		4.89×10^{-4}–4.35 **0.04**	5.87×10^{-4}–52 **0.51**
Ellipsoid	54	301–3893 **1329**	51–1051 **413**	$4/3\,\pi\,(a/2)\,(b/2)^2$	4.10×10^5–2.25×10^9 **1.19 $\times 10^8$**		1.2×10^{-3}–6.75 **0.36**	0.01–81 **4.28**
Tabular	29	Highly variable shapes; see text				Constant, 119 μg C pellet^{-1}**	9.92	119

* Conversion factor from Gonzalez and Smetacek (1994). ** Conversion factor from Wilson et al. (2013).
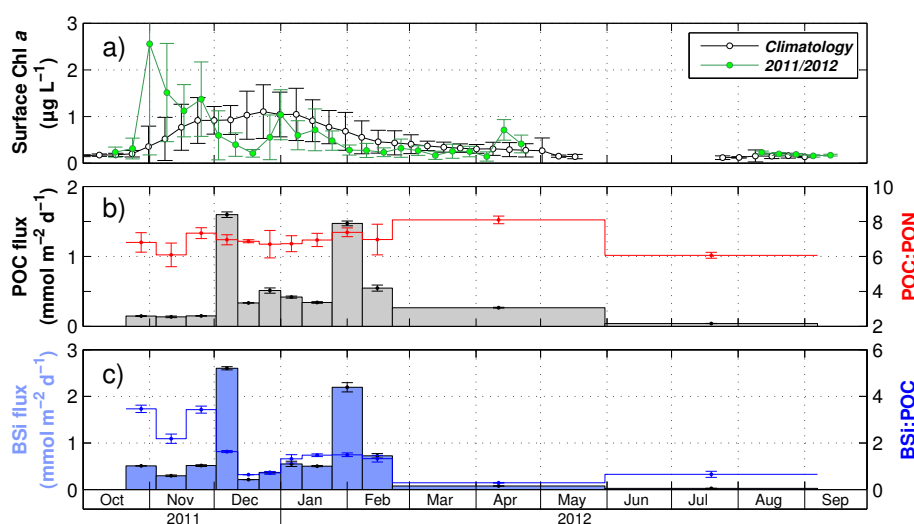
Figure 1. (a) Time series of the surface chlorophyll a concentration averaged in a 100 km radius around the trap location. The black line represents the climatology calculated for the period 1997/2013, whilst the green line corresponds to the sediment trap deployment period (2011/2012). **(b)** POC fluxes (grey bars) and C / N molar ratio (red line) of the exported material, **(c)** BSi flux (light-blue bars) and BSi : POC ratio (blue line). Error bars are standard deviations on triplicates.

3.2 Diatom fluxes

Diatoms from 33 taxa were identified and their fluxes determined across the 11-month time series. Fluxes are reported in Tables 4 and 5 for full and empty cells, respectively. Full and empty cell fluxes for the total community and for the taxa that are the major contributors to total diatom flux (eight taxa that account for > 1 % of total cells annual export) are presented in Fig. 2. The full and empty cell fluxes for each diatom species or taxa are reported in Tables 4 and 5, respectively.

During spring (cups #1 to #3, October to December 2011) and autumn/winter (cups #11 and #12, February to September 2012) the total flux of full cells was $< 5 \times 10^6$ cells m^{-2} d^{-1} (Fig. 2a). The total flux of full cells increased to 5.5 and 9.5×10^7 cells m^{-2} d^{-1} (cups #4

and #9, December and end of January, respectively) during two episodic (< 14 days) sedimentation events. The two largest flux events (cups #4 and #9) were also associated with significant export of empty cells with respectively 6.1×10^7 and 2.9×10^7 cells m^{-2} d^{-1} (Fig. 2a). For *Chaetoceros Hyalochaete* spp. resting spores (CRS), full cell fluxes of 4×10^7 and 7.8×10^7 cells m^{-2} d^{-1} accounted for 76 and 83 % of the total full cell flux during these two events, respectively (Fig. 2b), whereas a smaller contribution of *Thalassiosira antarctica* resting spores (TRS; 2.7×10^6 cells m^{-2} d^{-1}, 5 % of total full cells) was observed during the first event (Fig. 2h). CRS also dominated (79–94 %) the composition of full cells in the intervening period (cups #5 to #8, December 2011 to January 2012), although the magnitude of cell flux was moderate (9×10^6–2.5×10^7 cells m^{-2} d^{-1}) by comparison (Fig. 2b). In cup
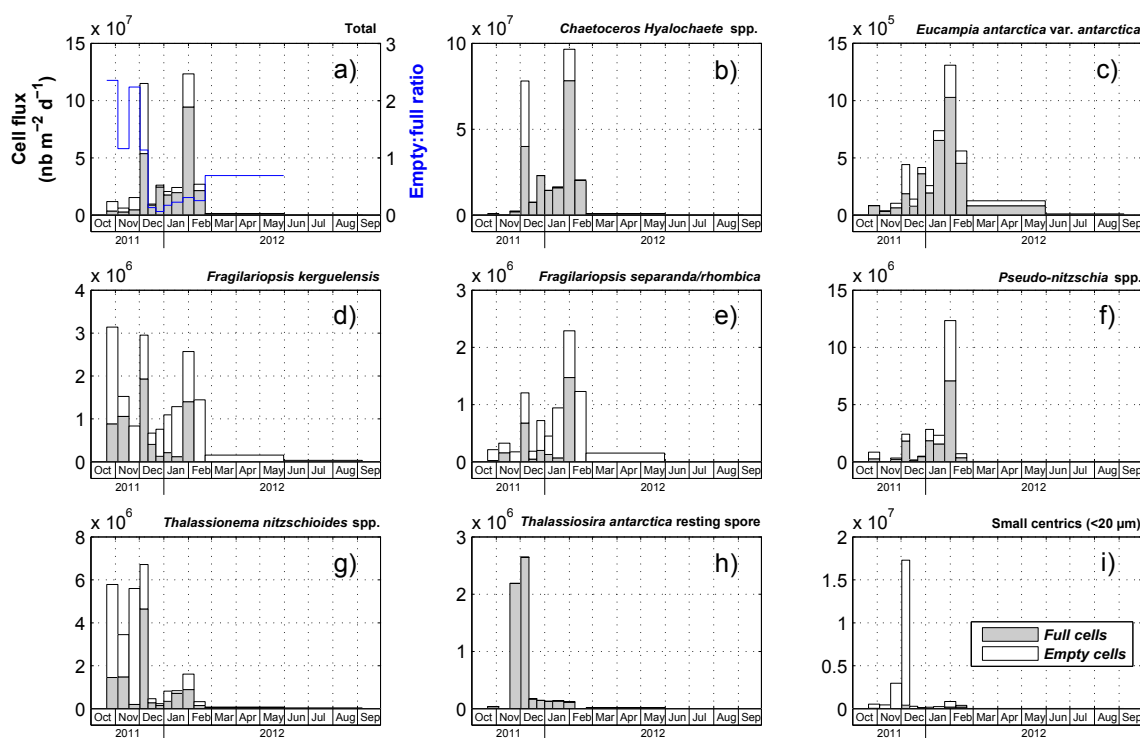
Figure 2. (a) Total diatom cell fluxes (bars, left axis) and total empty : full cell ratio (blue line, right axis). **(b–h)** Fluxes of diatom cells from selected species identified as major contributors to diatom fluxes ($> 1\,\%$ of total diatom fluxes). In **(b)**, full cells are *Chaetoceros Hyalochaete* resting spores and empty cells are the vegetative stage. Full cell fluxes are represented by grey bars, whereas empty cell fluxes are represented by white bars.

#4 (December 2011), the empty cell flux contained 61 % *Chaetoceros Hyalochaete* spp. vegetative empty cells and 27 % unidentified small centrics ($< 20\,\mu$m) empty cells. In cup #9 (end of January 2012), the total empty cell flux contained 60 % *Chaetoceros Hyalochaete* spp. vegetative stage and only 2 % small centrics ($< 20\,\mu$m) empty cells.

Fragilariopsis kerguelensis and *Fragilariopsis separanda/rhombica* (Fig. 2d and e) were mostly exported from spring through the end of summer (cups #1 to #10, October 2011 to February 2012) with total (full + empty) fluxes $< 3 \times 10^6$ cells m^{-2} d^{-1}, a value ~ 20 times lower than the highest CRS fluxes recorded. During this time, these species were represented by $> 50\,\%$ of empty cells. In autumn and winter (cups #10 and #11, February to May 2012), these species were only represented by low fluxes ($< 0.5 \times 10^{-6}$ cells m^{-2} d^{-1}) of empty cells. *Thalassionema nitzschioides* spp. fluxes were highest in spring and early summer (cups #1 to #4, October to December 2011), with total fluxes comprising between 3.5×10^6 and 6.7×10^6 cells m^{-2} d^{-1} (Fig. 2g). The remainder of the year, total flux was $< 2 \times 10^6$ cells m^{-2} d^{-1} and was essentially represented by full cells. *Pseudo-nitzschia* spp. were mostly represented by full cells (Fig. 2f) with the highest flux of 1.2×10^7 cells m^{-2} d^{-1} observed in the second intense export event (cup #9, end of January 2012). *Eucampia antarc-*

tica var.*antarctica* total fluxes were always represented by $> 50\,\%$ of full cells (Fig. 2c). Total cell fluxes of *Eucampia antarctica* var. *antarctica* gradually increased from $< 1 \times 10^5$ to 1.3×10^6 cells m^{-2} d^{-1} from spring to summer (cups #1 to #9, October 2011 to January 2012) and then decreased to a negligible flux in winter (cup #12, May to September 2012). This species was observed as both the lightly silicified, chain-forming, vegetative form and the highly silicified winter growth stage form. Both forms were observed throughout the year without a specific seasonal pattern. Small centric species ($< 20\,\mu$m) were essentially represented by empty cells (Fig. 2i). Their total fluxes were $< 4 \times 10^6$ cells m^{-2} d^{-1}, except in the first export event (cup #4, December 2011), where their flux represented a considerable export of 1.7×10^7 cells m^{-2} d^{-1}.

Diatoms and sampling cup projection on the first two axes from the correspondence analysis is presented in Fig. 3. χ^2 distance in the correspondence analysis is based on frequency distribution; therefore the results of the analysis must be considered as representative of the community composition as opposed to cell flux. The first two factors accounted for the majority (75.6 %) of total explained variance. Early in the season (cups #1 to #3, October to mid-December 2011), during the period of biomass accumulation in the surface (Fig. 1a), diatom fluxes were characterized by empty cells

Table 4. Full diatoms cells flux ($10^6 \, \mathrm{m}^{-2} \, \mathrm{d}^{-1}$) from the station A3 sediment trap.

Species – taxa group	1	2	3	4	5	6	7	8	9	10	11	12	Contribution to annual full cells flux (%)
Asteromphalus spp.	0	0.01	0	0.03	0	0	0	0	0.12	0	0	0	0.1
Chaetoceros atlanticus Cleve	0	0	0	0	0	0	0	0	0.07	0	0	0	0.0
Chaetoceros atlanticus f. *bulbosus* Ehrenberg	0	0	0	0	0	0	0	0	0	0	0	0	0.0
Chaetoceros decipiens Cleve	0	0	0.02	0	0	0	0	0	0.07	0	0	0	0.0
Chaetoceros dichaeta Ehrenberg	0	0	0	0.07	0	0	0	0	0.26	0	0	0	0.1
Chaetoceros Hyalochaete spp.*	0.70	0	1.95	39.92	7.42	23.04	14.37	15.88	78.29	20.24	0.68	0	80.2
Corethron inerme Karsten	0	0	0	0	0	0	0	0	0.23	0	0	0	0.1
Corethron pennatum Grunow	0	0	0	0	0	0	0	0	0	0	0	0	0.0
Dactyliosolen antarcticus Castracane	0	0	0	0.05	0	0	0	0	0.02	0	0	0	0.0
Eucampia antarctica var. antarctica (Castracane) Mangin	0.08	0.03	0.06	0.19	0.08	0.36	0.19	0.65	1.03	0.45	0.08	0.01	1.6
Fragilariopsis kerguelensis (O'Meara) Hustedt	0.88	1.06	0	1.93	0.40	0.13	0.21	0.12	1.40	0	0	0	2.4
Fragilariopsis separanda/rhombica group	0.02	0.16	0	0.68	0.05	0.20	0.13	0.07	1.47	0	0	0	1.1
Guinardia cylindrus (Cleve) Hasle	0	0	0	0	0	0	0	0	0.07	0	0	0	0.0
Leptocylindrus sp.	0	0	0	0.03	0	0	0	0	0	0	0	0	0.0
Membraneis spp.	0.04	0.01	0	0.19	0	0	0.02	0.02	0.02	0	0	0	0.1
Navicula spp.	0	0	0.04	0.64	0	0	0	0.29	0.58	0	0	0	0.6
Odontella weissflogii (Grunow) Grunow	0	0	0	0.08	0	0	0	0	0.05	0	0	0	0.0
Pleurosigma spp.	0.01	0	0	0.22	0.02	0.02	0	0.03	0.96	0.04	0	0	0.5
Proboscia alata (Brightwell) Sundröm	0	0	0	0	0	0	0	0	0.09	0	0	0	0.0
Proboscia inermis (Castracane) Jordan & Ligowski	0	0	0	0.03	0	0	0	0	0.33	0	0	0	0.2
Proboscia truncata (Karsten) Nöthig & Ligowski	0	0	0	0	0	0	0	0	0	0	0	0	0.0
Pseudo-nitzschia spp.	0.26	0.02	0.21	1.81	0.08	0.45	1.85	1.56	7.08	0.36	0.02	0	5.6
Rhizosolenia antennata/styliformis group	0	0	0	0	0	0	0	0	0.05	0	0	0	0.0
Rhizosolenia chunii Karsten	0	0	0	0	0.05	0	0	0.03	0.07	0	0	0	0.1
Rhizosolenia crassa Schimper in Karsten	0	0	0	0	0	0	0	0	0	0	0	0	0.0
Rhizosolenia simplex Karsten	0	0	0	0	0	0	0	0	0.07	0	0	0	0.0
Thalassionema nitzschioides spp. Pergallo & Pergallo	1.45	1.48	0.20	4.65	0.28	0.14	0.34	0.72	0.89	0.14	0.05	0.01	4.0
Thalassiosira lentiginosa (Janisch) Fryxell	0.01	0	0	0	0	0	0	0	0	0	0	0	0.0
Thalassiosira spp.	0	0.05	0	0.05	0	0	0	0	0.12	0.05	0	0	0.1
Thalassiosira antarctica resting spore (TRS) Comber	0.04	0	2.19	2.65	0.17	0.14	0.13	0.14	0.12	0	0.01	0	2.1
Thalassiothrix antarctica Schimper ex Karsten	0	0	0	0.02	0.05	0.04	0.34	0.14	0.70	0	0	0	0.5
Small centrics ($<20\,\mu\mathrm{m}$)	0.05	0	0	0.41	0	0	0	0	0.19	0.18	0	0	0.3
Large centrics ($>20\,\mu\mathrm{m}$)	0	0	0.05	0.08	0	0	0	0	0.05	0	0	0	0.1
Total full cells	35.39	28.20	47.18	537.38	85.85	245.20	175.89	196.56	943.88	214.65	8.46	0.22	

* Full cells of *Chaetoceros Hyalochaete* spp. were only found as resting spores.

of *T. nitzschioides* spp. and *F. kerguelensis*. Full TRS cells were observed in cup #3 (end of November 2011) following the initial bloom decline. The first major flux event (cup #4, December 2011) contained mostly TRS, empty small centrics ($<20\,\mu\mathrm{m}$) cells and empty *Chaetoceros Hyalochaete* spp. cells. The summer flux period (cups #5 to #8, December 2011 to January 2012) primarily consisted of CRS, although *E. antarctica* var. *antarctica*, *Pseudo-nitzschia* spp. and *Thalassiothrix antarctica* were present as full cells and *Plagiotropis* spp., *Membraneis* spp., *Pseudo-nitzschia* spp. as empty cells. The second major flux event (cup #9, end of January 2012) was tightly associated with CRS and full *Pseudo-nitzschia* spp. cells. Subsequent cups (#10 and #11, February to May 2012) were characterized by full cells of *E. antarctica* var. *antarctica* and *Thalassiothrix antarctica* and empty cells of *Corethron inerme*, *P. alata*, *F. separanda/rhombica* and *F. kerguelensis*. Winter fluxes (cup #12, May to September 2012) were similar to the initial three cups characterized pri-

marily by empty cells of small diatom taxa. The centralized projection in Fig. 3 of full *F. kerguelensis* and *T. nitzschioides* spp. highlights their constant presence throughout the annual record.

The total empty : full cell ratio is presented in Fig. 2a (blue line). This ratio was highest in spring and early summer (cups #1 to #4, October to December 2011), ranging between 1.1 and 2.4, suggesting more empty cells to full cells. The ratio was lowest, representing considerably more full cells to empty cells in cups #5 to #10 (December 2011 to February 2012) with values between 0.1 and 0.4. In autumn (cup #11, February to May 2012), the empty : full ratio increased to 0.7. In the winter cup #12 (May to September 2012), the total amount of full diatom cells was very low and therefore we could not calculate a robust empty : full ratio. Across the time series, certain diatom taxa were observed exclusively as empty cells, notably *Chaetoceros atlanticus* f. *bulbosus* and *Corethron pennatum*. For diatom

Table 5. Empty diatoms cells flux (10^6 m^{-2} d^{-1}) from the station A3 sediment trap.

Species – taxa group	1	2	3	4	5	6	7	8	9	10	11	12	Contribution to annual empty cells flux (%)
Asteromphalus spp.	0.02	0.02	0.09	0.08	0	0.05	0	0.03	0.05	0	0	0	0.3
Chaetoceros atlanticus Cleve	0	0	0	0	0	0	0	0	0	0	0	0	0.0
Chaetoceros atlanticus f. *bulbosus* Ehrenberg	0.01	0	0	0	0	0	0	0.02	0	0.02	0	0	0.0
Chaetoceros decipiens Cleve	0	0	0.02	0.24	0	0	0	0	0	0	0	0	0.2
Chaetoceros dichaeta Ehrenberg	0	0	0.06	0.07	0	0	0	0	0.05	0	0.01	0	0.2
Chaetoceros Hyalochaete spp.	0	0	0.45	38.19	0	0	0	0.60	18.23	0.18	0	0	41.2
Corethron inerme Karsten	0.01	0.01	0.04	0	0	0.02	0	0	0.23	0.31	0.06	0	0.9
Corethron pennatum Grunow	0	0	0.02	0	0	0	0	0.02	0	0	0.01	0	0.1
Dactyliosolen antarcticus Castracane	0	0	0	0.05	0	0	0	0.07	0.02	0.05	0	0	0.2
Eucampia antarctica var. antarctica (Castracane) Mangin	0	0	0.04	0.25	0.06	0.05	0.06	0.09	0.28	0.11	0.04	0	1.0
Fragilariopsis kerguelensis (O'Meara) Hustedt	2.25	0.46	0.84	1.02	0.26	0.63	0.88	1.17	1.17	1.45	0.16	0.03	9.4
Fragilariopsis separanda/rhombica group	0.19	0.17	0.18	0.53	0.14	0.52	0.32	0.87	0.82	1.23	0.15	0	5.0
Guinardia cylindrus (Cleve) Hasle	0	0	0	0	0	0	0	0	0	0	0	0	0.0
Leptocylindrus sp.	0	0	0	0	0	0	0	0	0	0	0	0	0.0
Membraneis spp.	0	0	0.02	0.05	0.02	0.04	0.02	0.07	0.14	0.07	0.01	0	0.4
Navicula spp.	0	0	0.13	0.36	0	0	0	0.12	0.12	0	0	0	0.5
Odontella weissflogii (Grunow) Grunow	0	0	0.02	0.10	0	0	0	0.02	0	0.02	0	0	0.1
Pleurosigma spp.	0.18	0.06	0.08	0.41	0.08	0	0.09	0.12	0.93	0.38	0.03	0	2.1
Proboscia alata (Brightwell) Sundröm	0	0	0	0	0	0	0	0.03	0.05	0.34	0.01	0	0.5
Proboscia inermis (Castracane) Jordan & Ligowski	0	0	0.01	0.08	0	0	0	0.03	0.05	0.13	0.01	0	0.3
Proboscia truncata (Karsten) Nöthig & Logowski	0	0	0.02	0	0	0	0	0	0	0.02	0	0	0.0
Pseudo-nitzschia spp.	0.59	0	0.12	0.59	0.09	0.04	0.99	0.75	5.26	0.34	0.02	0	7.4
Rhizosolenia antennata/styliformis group	0	0	0	0	0	0	0	0.02	0.02	0.13	0	0	0.2
Rhizosolenia chunii Karsten	0	0	0	0.03	0	0	0	0.02	0.02	0.20	0.02	0	0.4
Rhizosolenia crassa Schimper in Karsten	0	0	0	0	0	0	0	0	0	0.04	0	0	0.0
Rhizosolenia simplex Karsten	0	0	0	0	0	0	0	0.02	0	0	0	0	0.0
Thalassionema nitzschioides spp. Pergallo & Pergallo	4.33	1.97	5.39	2.07	0.19	0.09	0.47	0.12	0.72	0.18	0.03	0.01	13.2
Thalassiosira lentiginosa (Janisch) Fryxell	0.25	0.06	0.10	0	0	0	0	0	0	0	0	0	0.4
Thalassiosira spp.	0.02	0.06	0.01	0	0	0	0	0	0	0	0	0	0.1
Thalassiosira antarctica resting spore (TRS) Comber	0	0	0	0	0	0	0	0	0	0	0	0	0.0
Thalassiothrix antarctica Schimper ex Karsten	0	0	0	0	0	0.02	0	0	0	0.04	0	0	0.0
Small centrics (< 20 µm)	0.48	0.44	2.96	16.87	0.28	0.13	0.17	0.24	0.65	0.20	0.03	0.02	15.7
Large centrics (> 20 µm)	0	0.03	0.01	0.20	0	0	0	0	0.16	0.04	0	0	0.3
Total empty cells	8.34	3.28	10.57	61.20	1.12	1.59	3.01	4.43	28.98	5.46	0.59	0.07	

taxa present as full and empty cells we calculated an annually integrated empty : full ratio (Fig. 4) and arbitrarily defined threshold values of 2 (representing species mainly observed as empty cells) and 0.5 (representing species mainly observed as full cells). In decreasing order, the diatom taxa exhibiting empty : full ratios > 2 were *Thalassiosira lentiginosa*, small centrics (< 20 µm), *Proboscia alata, Rhizosolenia antennata/styliformis, Chaetoceros decipiens, Corethron inerme, Dactyliosolen antarcticus*, large centrics (> 20 µm), and *Asteromphalus* spp. The diatom taxa displaying an empty : full ratio < 0.5 were *Thalassiothrix antarctica, Rhizosolenia simplex* CRS, *Eucampia antarctica* var. *antarctica, Thalassiosira* spp. and *Navicula* spp. Species or grouped taxa with ratio values falling between the thresholds < 2 and > 0.5 (*R. chunii*, through to *C. dichaeta* in Fig. 4) were perceived

as being almost equally represented by full and empty cells when integrated annually across the time series.

3.3 Faecal pellet fluxes

The seasonal flux of faecal pellet type, and volume and their estimated carbon flux are summarized in Fig. 5 and Table 6. Total faecal pellet flux was $< 2 \times 10^3$ pellets m^{-2} d^{-1} in spring (cups #1 to #3, October to December 2011). Cups #4 and #5 (December 2011) were characterized by the highest fluxes of 21.8×10^3 and 5.1×10^3 pellets m^{-2} d^{-1} (Fig. 5a, Table 6). Faecal pellet numerical flux decreased gradually from mid-summer (cup #5, December 2011) to reach a minimal value in winter (140 pellets m^{-2} d^{-1} in cup #12, May to September 2012). In spring (cups #1 to #3, October to December 2011), spherical and cylindrical shapes dominated the numerical faecal pellet fluxes. Ellipsoid and tab-
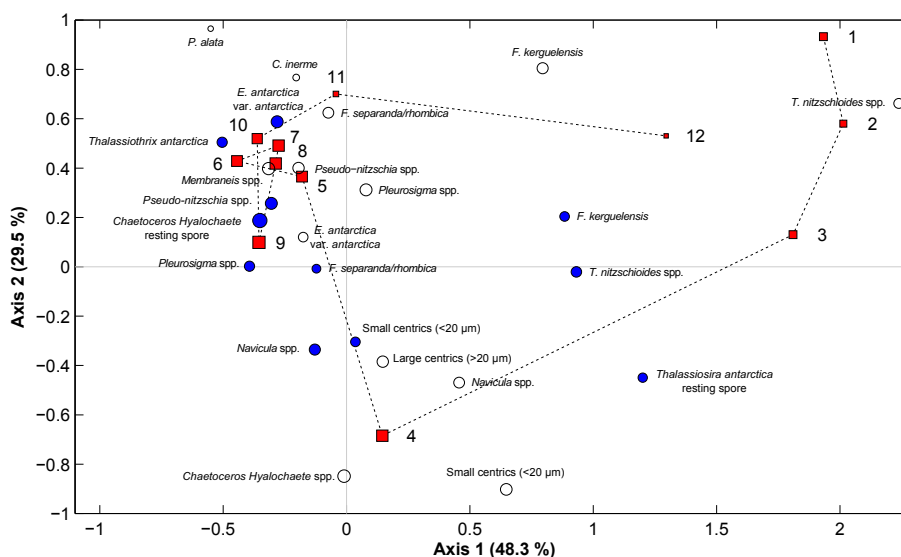
Figure 3. Factorial map constituted by the first two axes of the correspondence analysis performed on the full and empty diatom cell fluxes. Red squares are cup projections with cup numbers specified, blue circles are full cell projections and white circles are empty cell projections. The size of the markers is proportional to their representation quality in this factorial map.
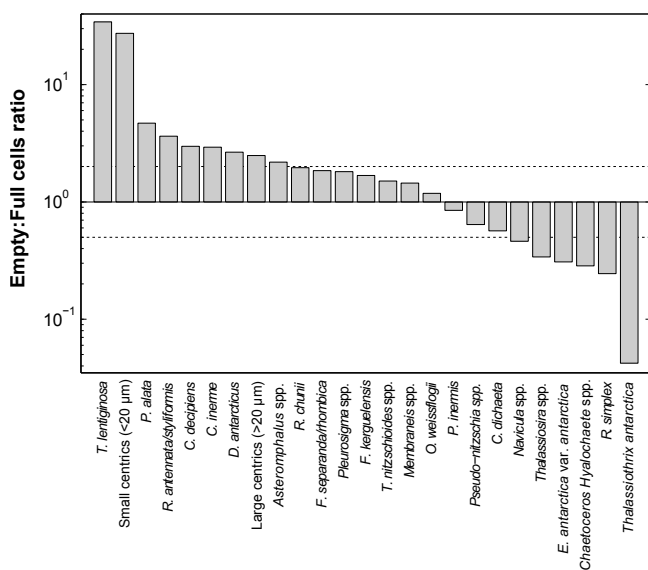
Figure 4. Annual ratio of empty to full cells for species observed as both forms. The dashed lines are the 0.5 and 2 ratio values. *Chaetoceros Hyalochaete* spp. full cells were only observed as resting spores.

ular shapes were absent from these spring cups. The first export event (cup #4, December 2011) was numerically dominated by the spherically shaped pellets; however the remainder of the summer (cups #5 to #10, December 2011 to February 2012) contained spherical, ovoid and cylindrical shapes in comparable proportions. Ellipsoid shapes were observed from mid-summer to autumn (cups #7 to #11, January to May 2012), but their overall contribution to pellet flux was

low (< 6 %, Table 6). Rare tabular shapes were observed in summer (cups #6 and #8, December and January 2012) and their contribution to numerical fluxes was highest in autumn and winter (cups #11 and #12, February to September 2012).

The median faecal pellet volume showed a seasonal signal, with a maximum peak $> 5.5 \times 10^6$ μm^3 in mid-summer (cups # 6 to #8, mid-December to January 2012) and values $< 4 \times 10^6$ μm^3 the remainder of the year (Fig. 5b). Concomitantly with the highest median volume, the largest variance in faecal pellet size was also observed in the summer (highest interquartile values in Fig. 5b).

Total faecal pellet carbon flux was lowest in spring (< 0.05 mmol C m^{-2} d^{-1} in cups #1 to #3, October to December 2011, Fig. 5c, Table 6). The highest total faecal pellet carbon flux of nearly 0.5 mmol C m^{-2} d^{-1} was observed during the first export event in cup #4 (December 2011) and was essentially composed of spherical shapes (83 %, Table 6). For the remainder of the summer (cups #5 to #10, December 2011 to February 2012), total faecal pellet carbon flux was between 0.03 and 0.15 mmol C m^{-2} d^{-1}, with a dominant contribution of cylindrical, ellipsoid and tabular shapes. In autumn and winter (cups #11 and #12, February to September 2012), faecal pellet carbon fluxes of 0.13 and 0.06 mmol C m^{-2} d^{-1} were strictly dominated by tabular shapes (> 90 % to total faecal pellet carbon fluxes, Table 6).

3.4 Statistical analysis of biological and biogeochemical signatures

The β correlation coefficients of standardized variables obtained from the PLSR analysis are presented as a heat map in Fig. 6. The full cell fluxes of all diatom taxa, in addition

Table 6. Faecal pellet numerical fluxes (normal text) and contribution to faecal pellet carbon fluxes (bold) from the station A3 sediment trap.

			Contribution (%)				
Cup	Total FP flux (nb m^{-2} d^{-1}) $\times 10^3$	Total FP carbon flux (mmol m^{-2} d^{-1})	Median volume (10^6 μm^3)	Spherical	Ovoid	Cylindrical	Ellipsoid	Tabular
1	1.39	0.02	2.07	53.3	19.7	27.0	0.0	0.0
				36.8	**18.6**	**44.6**	**0.0**	**0.0**
2	1.75	0.04	3.55	36.5	29.7	33.9	0.0	0.0
				22.4	**21.3**	**56.3**	**0.0**	**0.0**
3	0.72	<0.01	0.95	62.7	37.3	0.0	0.0	0.0
				54.5	**45.5**	**0.0**	**0.0**	**0.0**
4	21.81	0.48	1.91	76.4	22.8	0.8	0.0	0.0
				83.1	**15.3**	**1.6**	**0.0**	**0.0**
5	5.10	0.12	3.71	26.6	35.0	38.3	0.1	0.0
				13.8	**18.3**	**67.4**	**0.5**	**0.0**
6	2.69	0.15	5.67	28.8	33.1	37.9	0.0	0.2
				4.6	**10.9**	**43.1**	**0.0**	**41.3**
7	2.46	0.12	6.71	15.6	45.5	37.1	1.8	0.0
				2.5	**16.1**	**56.0**	**25.3**	**0.0**
8	2.06	0.20	6.18	37.6	15.5	44.2	2.2	0.4
				1.9	**2.1**	**34.6**	**15.8**	**45.5**
9	1.36	0.09	3.59	40.4	20.5	35.4	3.7	0.0
				2.8	**4.9**	**27.9**	**64.4**	**0.0**
10	1.22	0.03	2.34	56.0	22.4	21.3	0.4	0.0
				17.7	**9.1**	**69.9**	**3.3**	**0.0**
11	0.27	0.13	2.10	38.9	30.8	20.3	5.7	4.3
				0.4	**0.7**	**2.5**	**3.9**	**92.6**
12	0.14	0.06	2.41	18.4	57.6	20.3	0.0	3.7
				0.4	**2.6**	**5.3**	**0.0**	**91.8**
	Annually integrated contribution			53.8	27.3	17.8	0.7	0.4
	to faecal pellet flux			**17.9**	**6.6**	**17.3**	**7.7**	**50.4**

to spherical and ovoid and ellipsoid faecal pellet fluxes were positively correlated with POC and PON fluxes. By contrast, empty cell fluxes of *F. kerguelensis*, *P. alata*, *T. nitzschioides* spp. and *T. lentiginosa* as well as cyclindrical, ellipsoid and tabular pellet fluxes were either uncorrelated or negatively correlated with POC and PON fluxes. Full and empty cell fluxes of all diatom taxa were positively correlated with BSi fluxes, although this correlation was notably weak for empty cells of *C. inerme*, *P. alata* and *T. lentiginosa*. Only spherical and ovoid faecal pellets were positively correlated with BSi fluxes. Full cell fluxes of CRS and *E. antarctica* var. *antarctica* were the most negatively correlated with BSi : POC molar ratio, whereas TRS, *F. kerguelensis*, *T. nitzschioides* spp. and *T. lentiginosa* full cell fluxes were positively correlated. Spherical and ovoid faecal pellets were weakly and negatively correlated with the BSi : POC molar ratio, whereas the cylindrical, ellipsoid and tabular shapes were more strongly negatively correlated with the BSi : POC molar ratio. All the biological components exhibited weak or no correlations to the POC : PON molar ratio.

The first two latent vectors of the PLSR accounted for 61.3 and 74.1 % of cumulative variance in *X* (full and empty di-atom and pellet fluxes) and *Y* (biogeochemical properties). In order to show how the seasonal succession of flux vectors was related to the bulk geochemical properties of particles, the sampling cups, biological and chemical factors were projected on the first two latent factors of the PLSR analysis (Fig. 7). Positively projected on the first axis are the POC, PON and BSi fluxes, close to the export events sampled in cups #4 (December 2011) and #9 (end of January 2012). The closest biological components comprise a complex assemblage of full and empty cells and spherical and ovoid faecal pellet shapes. All the other cups are projected far from these two export events. Spring cups (#1 to #3, October to mid-December 2011) are opposite to the autumn (#11, February to May 2012) and winter (#12, May to September 2012) cups on the second axis. Empty frustules of *F. kerguelensis*, *T. lentiginosa* and *T. nitzschioides* spp. are projected close to the spring cups (#1 to #3, October to mid-December 2011) together with the BSi : POC molar ratio, whereas autumn (#11, February to May 2012) and winter cups (#12, May to September 2012) are projected far from the BSi : POC molar ratio and close to the tabular and cylindrical faecal pellet shapes.
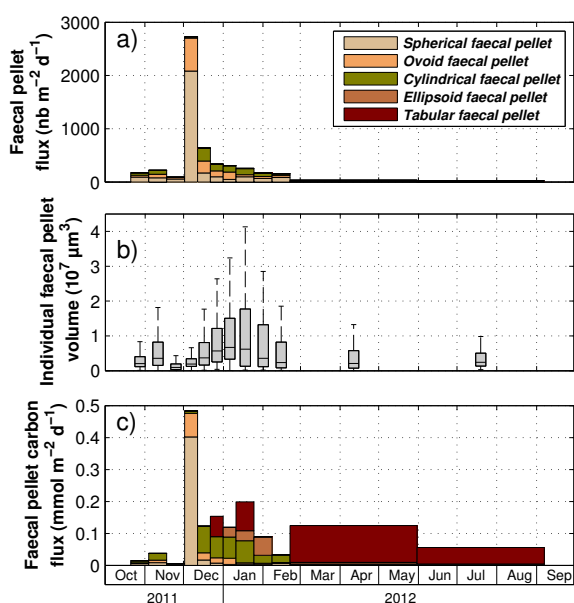
Figure 5. (a) Faecal pellet numerical fluxes partitioned among faecal pellet types and **(b)** box plot of faecal pellet volume. On each box, the central mark is the median, the edges of the box are the first and third quartiles, and the whiskers extend to the most extreme data points comprised in 1.5 times the interquartile distance. **(c)** Faecal pellet carbon fluxes partitioned between the five faecal pellet types. The two arrows represent the two strong POC export events (cup #4 and #9, December 2011 and end of January 2012, respectively).

		POC	PON	BSi	POC:PON	BSi:POC
ⓐ	CRS	0.07	0.07	0.06	0.02	−0.04
ⓑ	*E. antarctica*	0.05	0.05	0.03	0.02	−0.04
ⓒ	*F. kerguelensis*	0.05	0.05	0.07	0	0.07
ⓓ	*F. separanda/rhombica*	0.06	0.06	0.06	0.02	−0.01
ⓔ	*Navicula* spp.	0.07	0.07	0.07	0.02	0
ⓕ	*Pleurosigma* spp.	0.06	0.06	0.05	0.02	−0.01
ⓖ	*Pseudo−nitzschia* spp.	0.06	0.05	0.05	0.02	−0.01
ⓗ	*T. nitzschioides* spp.	0.04	0.04	0.06	0	0.07
ⓘ	TRS	0.03	0.03	0.05	−0.01	0.1
ⓙ	*Thalassiothrix antarctica*	0.04	0.04	0.03	0.01	−0.03
ⓚ	Small centrics (<20 µm)	0.06	0.06	0.07	0.01	0.01
ⓐ	*Chaetoceros Hyalochaete* spp.	0.07	0.07	0.07	0.02	0
ⓑ	*C. inerme*	0.03	0.03	0.02	0.01	−0.03
ⓒ	*E. antarctica*	0.08	0.07	0.06	0.02	−0.04
ⓓ	*F. kerguelensis*	0	0.01	0.05	−0.02	0.17
ⓔ	*F. separanda/rhombica*	0.04	0.04	0.03	0.01	−0.03
ⓕ	*Membraneis* spp.	0.06	0.06	0.05	0.02	−0.04
ⓖ	*Navicula* spp.	0.05	0.05	0.06	0.01	0.05
ⓗ	*Pleurosigma* spp.	0.06	0.06	0.06	0.01	0.01
ⓘ	*P. alata*	0.01	0.01	0	0.01	−0.03
ⓙ	*Pseudo−nitzschia* spp.	0.05	0.05	0.05	0.01	0
ⓚ	*T. nitzschioides* spp.	−0.03	−0.02	0.04	−0.04	0.24
ⓛ	*T. lentiginosa*	−0.04	−0.04	0.02	−0.04	0.22
ⓜ	Small centrics (<20 µm)	0.05	0.05	0.06	0.01	0.04
ⓝ	Large centrics (>20 µm)	0.07	0.07	0.07	0.02	0.01
Ⓢ	Spherical faecal pellet	0.05	0.05	0.05	0.01	0.01
Ⓞ	Ovoid faecal pellet	0.05	0.05	0.04	0.01	−0.02
Ⓒ	Cylindrical faecal pellet	0	0	−0.02	0.01	−0.08
Ⓔ	Ellipsoid faecal pellet	0.03	0.03	0.01	0.01	−0.06
Ⓣ	Tabular faecal pellet	−0.01	−0.01	−0.05	0.02	−0.15

Figure 6. Heat map representation of β correlation coefficients between the biological variables (empty and full cell diatom and faecal pellet type fluxes) and the chemical variables (POC, PON, BSi, POC : PON and BSi : POC) resulting from the partial least-squares regression. Blue circles represent full diatom cells, and white circles are empty diatom cells. Brown circles represent the faecal pellet type fluxes. The alphabetical labels within the circles are used to identify the variable projections shown in Fig. 7. CRS: *Chaetoceros Hyalochaete* resting spores; TRS: *Thalassiosira antarctica* resting spores.

3.5 Partitioning carbon fluxes among ecological vectors

We estimated the contribution of resting spores and faecal pellets to carbon flux, calculated their cumulative values and compared them to measured values (Fig. 8a and b). A highly significant correlation (Spearman rank correlation, $n = 36$, $\rho = 0.84$, $p < 0.001$) was evident between calculated and measured carbon flux, suggesting that the main ecological flux vectors observed in the sample were capable of explaining the seasonal variation in total POC flux. Table 7 lists the contribution of each vector to the calculated flux. In cup #1 (October to mid-November 2011), CRS and other diatoms dominated the calculated POC fluxes, with respectively 25.3 and 38.6 %. Diatoms other than spores dominated the calculated carbon flux (35.4 %) together with cylindrical faecal pellets (36.4 %) in cup #2 (November 2011). TRS dominated the POC fluxes (85.1 %) in cup #3 (November/December 2011). CRS strictly dominated the calculated POC fluxes in summer (cups #4 to #10, December 2011 to February 2012), with a contribution ranging from 46.8 to 88.1 %. During the autumn and winter (cups #11 and #12, February to September 2012), POC fluxes were almost exclusively associated with tabular faecal pellets, 81 and 93.3 %, respectively. At annual scale, diatom's resting spores (CRS and TRS), other diatoms and faecal pellets respectively ac-
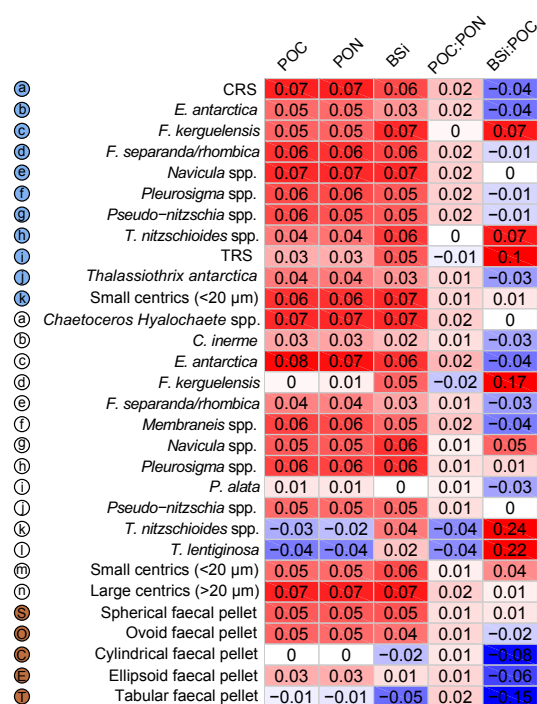
counted for 60.7, 5 and 34.3 % of the calculated POC fluxes. Annual POC fluxes estimated from ecological vectors considered here were slightly less than measured values (93.1 versus 98.2 mmol m^{-2}).
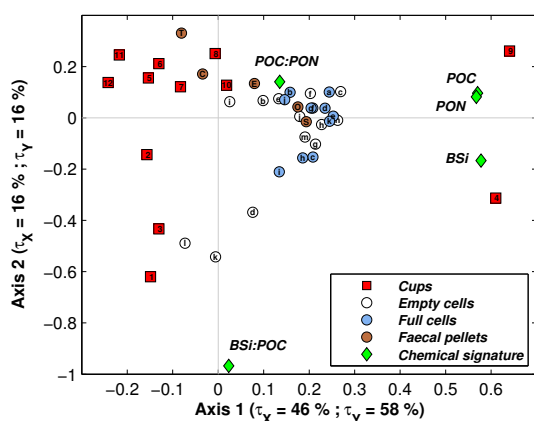
4   Discussion

4.1   The significance of resting spores for POC flux

Generally POC fluxes were < 0.5 mmol m^{-2} d^{-1}, with the notable exception of two pulsed (< 14 days) export events of ~ 1.5 mmol m^{-2} d^{-1} that accounted for ~ 40 % of annual POC export. These two flux events were characterized by a noticeable increase and general dominance of diatom resting spores. During both of these pulsed export events, cumulative *Chaetoceros Hyalochaete* spp. resting spore (CRS and *Thalassiosira antarctica* resting spore (TRS) fluxes accounted for 66 and 88 % of the measured POC flux, whereas total faecal pellet flux accounted for 29 and 5.2 %, respectively (Table 7). The combination of CRS and TRS was responsible for

Table 7. Measured and calculated POC fluxes as well as POC flux partitioning among the major identified ecological vectors of carbon exported out of the mixed layer at station A3.

				Contribution to calculated POC flux (%)						
Cup	Measured POC flux (mmol m^{-2} d^{-1})[a]	Calculated POC flux (mmol m^{-2} d^{-1})	CRS[b]	TRS[c]	Other diatoms	Spherical faecal pellet	Ovoid faecal pellet	Cylindrical faecal pellet	Ellipsoid faecal pellet	Tabular faecal pellet	Total faecal pellet
1	0.15	0.05	25.3	8.1	38.6	10.3	5.2	12.5	0.0	0.0	28.0
2	0.14	0.06	0.0	0.0	35.4	14.5	13.7	36.4	0.0	0.0	64.6
3	0.15	0.31	12.1	85.1	1.4	0.8	0.6	0.0	0.0	0.0	1.4
4	1.60	1.62	46.8	19.4	3.9	24.8	4.6	0.5	0.0	0.0	29.8
5	0.34	0.29	48.0	6.9	3.3	5.8	7.7	28.2	0.2	0.0	41.8
6	0.51	0.63	69.7	2.7	3.2	1.1	2.7	10.5	0.0	10.1	24.4
7	0.42	0.43	63.1	3.5	5.8	0.7	4.4	15.4	7.0	0.0	27.5
8	0.34	0.56	54.4	2.9	6.8	0.7	0.8	12.4	5.7	16.3	35.9
9	1.47	1.71	86.8	0.8	7.2	0.1	0.3	1.4	3.3	0.0	5.2
10	0.55	0.44	88.1	0.0	4.3	1.4	0.7	5.4	0.3	0.0	7.7
11	0.27	0.14	9.1	1.2	2.2	0.3	0.6	2.2	3.4	81.0	87.5
12	0.04	0.06	0.0	0.0	0.5	0.4	2.6	5.2	0.0	91.3	99.5
	Contribution to annual calculated POC flux (%	52.1	8.6	5.0	5.1	2.0	5.2	2.2	19.8	34.3

[a] Data from Rembauville et al. (2015). [b] CRS: *Chaetoceros Hyalochaete* resting spores. [c] TRS: *Thalassiosira antarctica* resting spores.

Figure 7. Projection of the cups (red squares), the biological factors (circles) and the chemical factors (green diamonds) in the first two latent vectors of the partial least-squares regression. Circled labels refer to the full and empty species listed in Fig. 6.

anism through which carbon, and to a lesser extent silicon, is exported from the surface.

Numerous sediment trap studies have reported a strong contribution, if not dominance, of CRS to diatom fluxes at depth in various oceanographic regions: firstly, in coastally influenced regions, e.g. the Antarctic Peninsula (Leventer, 1991), Bransfield Strait (Abelmann and Gersonde, 1991), Gulf of California (Sancetta, 1995), the Omura Bay (Kato et al., 2003), Santa Barbara basin (Lange, 1997), North Pacific Ocean (Chang et al., 2013) and the Artic (Onodera et al., 2015); secondly in upwelling-influenced regions (eastern equatorial Atlantic (Treppke et al., 1996); and finally in the open ocean in the subarctic Atlantic (Rynearson et al., 2013). Similar to sediment trap observations, CRS are reported as dominant in surface sediments of coastal regions (peri-Antarctic shelf and Antarctic sea ice (Crosta et al., 1997; Zielinski and Gersonde, 1997; Armand et al., 2005), the North Scotia Sea (Allen et al., 2005) and east of the Kerguelen Islands (Armand et al., 2008b), as well as in upwelling-influenced regions (e.g. the northeast Pacific; Grimm et al., 1996; Lopes et al., 2006) and finally in the open ocean (the North Atlantic; Bao et al., 2000). Moreover, the annual POC export from the A3 station sediment trap at 289 m (98.2 ± 4.4 mmol m^{-2} yr^{-1}) falls near annual estimates from deep sediment traps (> 2000 m) located in the naturally fertilized area downstream of the Crozet Islands (37–60 and 40–42 mmol m^{-2} yr^{-1}; Salter et al., 2012), where fluxes were considered as mainly driven by resting spores of *Eucampia antarctica* var. *antarctica*. Diatom resting spores are frequently observed in blooms heavily influenced by the proximity of the coast. Major resting spores' contribution to carbon fluxes was observed in only one study in the open North Atlantic Ocean (Rynearson et al., 2013), but they are generally absent or very rare in open ocean sediment trap studies (Fischer et al., 2002; Grigorov et al., 2014; Rigual-Hernández et al., 2015). The frequent occurrence and
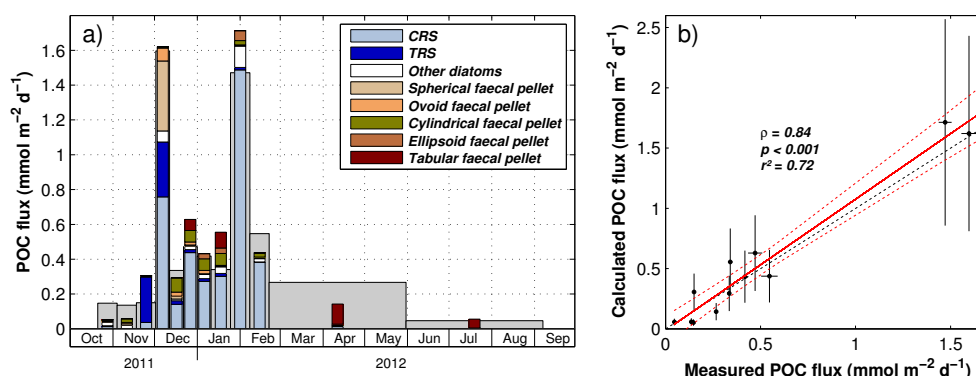
60.7 % of the annual calculated POC flux, a value 10 times higher than the contribution of other diatoms (5 %). We did not observe any full cells of the vegetative stage of *Chaetoceros Hyalochaete*, a feature possibly related to its high susceptibility to grazing pressure in the mixed layer (Smetacek et al., 2004; Quéguiner, 2013; Assmy et al., 2013). Empty *Chaetoceros Hyalochaete* spp. cells were vegetative stages different in shape from the resting spores. These empty frustules may be the remnants of vegetative stages following spore formation. Alternatively, dissolution of the lightly silicified valves or girdle bands of the vegetative cell could result in the rapid consumption of the cellular organic material in the upper water column, and this may also explain the absence of full vegetative cells in the sediment trap record. Our flux data reveal that small (10 to 30 µm) and highly silicified resting spores bypass the intense grazing pressure characterizing the base of the mixed layer, and are the primary mech-

Figure 8. (a) Grey bars in the background are measured POC fluxes, and coloured bars in the foreground are calculated POC fluxes partitioned among the main ecological vectors identified. **(b)** Regression ($r^2 = 0.72$) between the measured and calculated POC fluxes. The correlation is highly significant (Spearman rank correlation, $n = 36$, $\rho = 0.84$, $p < 0.001$). Error bars were generated by increasing/decreasing the carbon/volume conversion factors by 50 %. Black dashed line is the 1 : 1 relation, red line is the regression line, and red dashed lines denotes the 99 % confidence interval. CRS *Chaetoceros Hyalochaete* resting spores; TRS: *Thalassiosira antarctica* resting spores.

widespread distribution of a diatom's resting spores in the neritic or coastally influenced ocean suggest their pivotal role in the efficient transfer of carbon to depth in these areas.

Chaetoceros resting spores have been reported to contain up to 10 times more carbon than the vegetative forms (Kuwata et al., 1993) with no vacuole and high contents of lipids and carbohydrates (Doucette and Fryxell, 1983; Kuwata et al., 1993). Moreover, CRS resist grazing and have been found to lower copepods grazing pressure (Kuwata and Tsuda, 2005). We suggest that diatom resting spores gather three essential characteristics for effective POC export to the deep ocean: (1) they efficiently bypass the grazing pressure near the mixed layer due to their morphological characteristics such as very robust frustules (CRS) or numerous spines (TRS; high export efficiency), (2) they are efficiently transferred to depth due to the thick and dense frustule increasing sinking velocity and (3) their high carbon content is protected from microbial degradation by the thick frustules (these last two points result in a high transfer efficiency). The spatial distribution and formation of resting spores may therefore be an integral ecological component defining the strength and efficiency of the biological pump in specific regions. Nutrient depletion has been shown to trigger resting spore formation in *Chaetoceros Hyalochaete* laboratory cultures (Garrison, 1981; Sanders and Cibik, 1985; Kuwata et al., 1993; Oku and Kamatani, 1997) over relatively rapid timescales (6 to 48 h; McQuoid and Hobson, 1996). Although Si(OH)$_4$ depletion appears to be the most likely biogeochemical trigger at the Kerguelen Plateau (from 24 μmol L^{-1} in early spring to 2 μmol L^{-1} in summer (Mosseri et al., 2008; Closset et al., 2014), other environmental factors (iron or light availability) could influence resting spore formation. Notably, dissolved iron concentration in the mixed layer rapidly decreases to $\sim$ 0.1 to 0.2 nmol L^{-1} after the beginning of the spring bloom at A3; however the vertical entrainment is much weaker in

summer compared to spring (Bowie et al., 2014). Rynearson et al. (2013) reported the absence of spores in the mixed layer despite a strict dominance of the trap samples. Resting spore formation at some depth below the summer mixed layer (possibly implying a light control) could explain the temporal decoupling between the surface production tracked by the satellite in the surface layer (first $\sim$ 20 m) and the export events. Further work to establish seasonal dynamics of factors linked to diatom life cycles and specifically the formation of resting spores is necessary.

4.2 Contribution of faecal pellets to POC flux

Although diatom resting spores are the primary vector for POC flux below the mixed layer, faecal pellets were also important and accounted for 34.3 % of annual export. It has been hypothesized that faecal pellets are the dominant flux component in high-biomass, low-export (HBLE) environments, where biomass is routed to higher trophic levels (Lam and Bishop, 2007; Ebersbach et al., 2011). However, this hypothesis does not appear to be true for the bloom of the central Kerguelen Plateau, suggesting that faecal material is efficiently reprocessed in the mixed layer, or that a significant part of the pellet flux is excreted below the trap depth by vertically migrating zooplankton. Small spherical faecal pellets dominated the annual numerical faecal pellet flux (53.8 %, Table 6). The short and intense export of small spherical faecal pellets was concomitant with the first strong POC export in cup #4 (December 2011, Table 6). The significance of small spherical faecal pellets to POC flux is somewhat uncharacteristic in comparison to other sediment trap records in shallow areas of the Southern Ocean (Schnack-Schiel and Isla, 2005). They are possibly produced by small cyclopoid copepods, like *Oithona similis*, that are abundant in the POOZ (Fransz and Gonzalez, 1995; Pinkerton et al., 2010). More specifically, *O. similis* represents > 50 % of mesozoo-

plankton abundance at A3 in spring (Carlotti et al., 2015) and has been observed at station A3 in summer (Carlotti et al., 2008). *Oithona* species are known to be coprophagous and play an important role in flux reprocessing (Gonzalez and Smetacek, 1994), which may partially contribute to the rapid flux attenuation observed by efficiently retaining carbon in the mixed layer. This reprocessing feeding strategy might also explain the low faecal pellet flux we observed (highest value of 21.8×10^3 pellet m^{-2} d^{-1}), which was 2 orders of magnitude lower than the $> 5 \times 10^5$ pellet m^{-2} d^{-1} observed in neritic areas where euphausiids dominate the mesozooplankton community (von Bodungen, 1986; von Bodungen et al., 1987; Wefer et al., 1988).

There were notable differences in faecal pellet types over the course of the season. The transition from spherical and ovoid pellets in spring to larger cylindrical and tabular pellets in summer presumably reflects shifts in dominant zooplankton species from small cyclopoid copepods towards larger calanoid copepods, euphausiids and salps (e.g. Wilson et al., 2013). Carlotti et al. (2015) report that mesozooplankton biomass doubled between October and November 2011 and was 3-fold higher in January 2005 (Carlotti et al., 2008). In spring, Carlotti et al. (2015) observed that the small size fraction (300–500 µm) was numerically dominated by *Oithona similis* (50 % of the total mesozooplankton assemblage), although the larger size fractions dominated the mesozooplankton biomass (dominated by *Clausocalanus citer* and *Rhicalanus gigas*). This is consistent with the dominance of small spherical faecal pellets and the lower contribution of cylindrical shapes we observed in spring and early summer (cups #1 to #4, October to December 2011, Table 6). In summer (January 2005), the mesozooplankton community was more diversified and comprised 21 % small individuals (*Oithona* sp. and *Oncea* sp.), 20 % medium-sized individuals (*Clausocalanus* sp. and *Microcalanus* sp.) and 21 % large individuals (*Calanus* sp., *Metrida* sp., *Paraeuchaeta* sp., *Pleuromamma* sp. and *Rhincalanus* sp.; Carlotti et al., 2008). As the median size of faecal pellets increases, so does their relative contribution to carbon flux (Fig. 5b and d, Table 6). Our observation of an increasing contribution of cylindrical faecal pellet shapes in summer (cups #5 to #10, December 2011 to February 2012, Table 6) is consistent with the increasing contribution of large calanoid copepods to the mesozooplankton assemblages. We note that pteropods showed the highest contribution to mesozooplankton assemblages at station A3 in summer (16 % of total abundance; Carlotti et al., 2008). We associate this observation with the large ellipsoid faecal pellet shape that was first observed in the sediment trap in cup #5 (end of December 2011) and represented the highest contribution to faecal pellet carbon fluxes in cup #9 (January/February 2012, Table 7). Tabular faecal pellets dominated the low POC fluxes observed in the autumn and winter, when chlorophyll *a* concentration was reduced to background levels, although this interpretation should be treated with caution since a constant and high carbon con-

tent was used for this shape. The increase in organic carbon content and negative correlation between the abundance of cylindrical, ellipsoid and tabular faecal pellets fluxes and the BSi : POC molar ratio suggests that large zooplankton producing these tabular pellets (large copepods, euphausiids and salps) was not feeding directly on diatoms. During the autumn and winter, microbial components other than diatoms must sustain the production of these large zooplankton. Direct observation of faecal pellet content is beyond the scope of the present study but would help in elucidating how seasonal trends of zooplankton feeding ecology influence carbon and biomineral export. Moreover, dedicated studies are still needed to document the seasonal dynamic of euphausiid and salp abundances over the Kerguelen Plateau to compare them with our reported faecal pellet fluxes.

4.3 Diatom fluxes

The diatom fluxes (sum of empty and full cells) observed at the central Kerguelen Plateau reached their maximum value of 1.2×10^8 cells m^{-2} d^{-1} during the two short export events, which is equivalent to 2.4×10^8 valves m^{-2} d^{-1}. This latter value falls between the highest values observed in POOZ ($\sim 10^7$ valves m^{-2} d^{-1}; Abelmann and Gersonde, 1991; Salter et al., 2012; Grigorov et al., 2014) and the SIZ ($> 10^9$ valves m^{-2} d^{-1}; Suzuki et al., 2001; Pilskaln et al., 2004). The diatom fluxes over the Kerguelen Plateau are similar to the $2.5–3.5 \times 10^8$ valves m^{-2} d^{-1} measured at 200 m depth in a coastal station of the Antarctic Peninsula, where CRS represented ~ 80 % of the phytoplankton assemblage (Leventer, 1991). Previous studies report the presence of a resting spore formation strategy in diatom species as typically associated with neritic areas (Smetacek, 1985; Crosta et al., 1997; Salter et al., 2012). During the summer KEOPS1 cruise, a shift in plankton community composition was observed at station A3 between January and February. The surface community initially dominated by *Chaetoceros Hyalochaete* vegetative chains gave way to one dominated by *Eucampia antarctica* var. *antarctica*, concomitant with increasing CRS abundance in the mixed layer (Armand et al., 2008a). The abundance of dead cells (within chains or as empty single cells and half-cells) in the surface water column also increased from January to February, suggesting intense heterotrophic activity. Surface sediments at station A3 contain, in decreasing abundance, *F. kerguelensis*, CRS and *T. nitzschioides* spp. cells (Armand et al., 2008b). These sedimentary distributions are consistent with the dominant species observed in the sediment trap, *F. kerguelensis* and *T. nitzschioides* spp. being present throughout the year and mostly represented by empty cells, whereas CRS are exported during short and intense events.

Eucampia antarctica var. *antarctica* resting spores dominated the deep (2000 m) sediment trap diatom assemblages in the naturally fertilized area close to the Crozet Islands with fluxes $> 10^7$ cells m^{-2} d^{-1} (Salter et al., 2012). We ob-

served highest *Eucampia antarctica* var. *antarctica* full cell fluxes of $\sim 10^6$ cells m^{-2} d^{-1} in summer, which represents $< 10\%$ of the total cell flux. Both vegetative and resting stages were observed. Our results suggest that *Eucampia antarctica* var. *antarctica* are unlikely to be a major driving vector for carbon fluxes to depth over the central Kerguelen Plateau, in part because the community was not forming massive highly silicified, fast-sinking resting spores, contrary to observations near the Crozet Islands. Moreover their biogeographic abundance distribution from sea floor observations suggests they are not dominant in this region of the plateau (Armand et al., 2008b). The iron-fertilized Crozet bloom is north of the polar front and dissolved Si(OH)$_4$ concentrations were depleted to 0.2 µmol L^{-1} (Salter et al., 2007) compared to ~ 2 µmol L^{-1} on the Kerguelen Plateau (Mosseri et al., 2008). It is possible, along with differences in iron dynamics between the two plateaus, that differences in nutrient stoichiometry favour bloom dynamics and resting spore formation of *Chaetoceros Hyalochaete* populations surrounding the Kerguelen Islands. Nevertheless, the increasing full cell flux of *Eucampia antarctica* var. *antarctica* from spring to summer in the sediment trap time series is consistent with the observations of an increasing abundance in the mixed layer at the station A3 in summer (Armand et al., 2008a).

Highest *Pseudo-nitzschia* spp. full cell fluxes were observed in summer, concomitantly with the second export peak (cup #9, end of January 2012). *Pseudo-nitzschia* species are rarely found in deep sediment trap studies and are absent from sediment diatom assemblages, presumably due to their susceptibility to water column dissolution (Grigorov et al., 2014; Rigual-Hernández et al., 2015). The species *Pseudo-nitzschia hemii* has been reported to accumulate in summer in deep chlorophyll maximum in the Polar Frontal Zone (Kopczynska et al., 2001). Such deep biomass accumulation is hypothesized to benefit from nutrient diffusion through the pycnocline (Parslow et al., 2001). These general observations are consistent with the peaks in *Pseudo-nitzschia* spp. fluxes we report in summer over the Kerguelen Plateau.

Although their fluxes were very low, species of the *Rhizosolenia* and *Proboscia* genera were mostly exported as empty cells at the end of summer and during autumn (cups #8 to #11, end of January to May 2012), occurring in parallel with the full cell fluxes of the giant diatom *Thalassiothrix antarctica* (Table 4). It has been suggested that these species belong to a group of "deep shade flora" that accumulate at the subsurface chlorophyll maxima in summer, with their large frustules protecting them from grazing pressure in stratified waters (Kemp and Villareal, 2013). Interestingly these species were also found in deep sediment traps located in an HNLC area south of the Crozet Plateau (Salter et al., 2012), as well as in subsurface chlorophyll maximum in HNLC waters of the Southern Ocean (Parslow et al., 2001; Holm-Hansen et al., 2004; Gomi et al., 2010). A subsurface chlorophyll maximum has previously been observed at 120 m on the Kerguelen Plateau (also station A3) during summer

(Uitz et al., 2009) and appears to correspond to an accumulation of particles consisting of aggregates of large diatom species (Jouandet et al., 2011). The fact that *Rhizosolenia* spp. and *Proboscia* spp. were observed as empty cells whereas *Thalassiothrix antarctica* was mostly represented by full cells suggests species-specific grazing on these communities. There appears to be ecological differentiation within the "deep shade flora" that precludes describing a single effect on export stoichiometry. Moreover, on the Kerguelen Plateau, these species are not exported in "massive" proportions as the "fall-dump" hypothesis suggests (Kemp et al., 2000). The physical and biogeochemical factors responsible for their production and export are still to be determined, and should be investigated thoroughly given the potential importance that these species might have for export fluxes on a global scale (Kemp et al., 2000; Richardson et al., 2000; Kemp and Villareal, 2013).

4.4 Preferential carbon and silica sinkers

Unlike most previous sediment trap studies in the Southern Ocean, we used a counting technique that facilitated the identification of carbon and siliceous components of exported material. Although we lost a small degree of taxonomic resolution with this approach (see Methods), it allowed us to avoid unnecessary assumptions concerning carbon content of exported diatoms and directly constrain the role of different species for carbon and silica export.

The annual BSi : POC ratio of the exported material (1.16) is much higher than the usual ratio proposed for marine diatoms of 0.13 (Brzezinski, 1985). Moreover, the BSi : POC ratio of the exported material in spring (2.1 to 3.4, cups #1 to #3, October to mid-December 2011) is significantly higher than the BSi : POC ratio of 0.3 to 0.7 in the mixed layer of the same station during spring (Lasbleiz et al., 2014; Trull et al., 2015). Numerous chemical, physical, biological and ecological factors can impact BSi : POC ratios of marine diatoms (e.g. Ragueneau et al., 2006). However, the 10-fold differences in BSi : POC ratios of exported particles between spring and summer is unlikely to result only from physiological constraints set during diatoms growth (Hutchins and Bruland, 1998; Takeda, 1998). Previous comparisons in natural and artificially iron-fertilized settings have highlighted the importance of diatom community structure for carbon and silica export (Smetacek et al., 2004; Salter et al., 2012; Quéguiner, 2013; Assmy et al., 2013). The presence of different diatom species and their characteristic traits (e.g. susceptibility to grazing, apoptosis, viral lysis) are all likely to influence the flux of full and empty cells. Therefore, the net BSi : POC export ratio results from the net effect of species-specific Si : C composition (Sackett et al., 2014) and the subsequent species-specific mortality pathway and dissolution. A significant correlation between BSi : POC and empty : full cell ratio (Spearman rank correlation, $n = 12$, $\rho = 0.78$, $p < 0.05$) suggests the latter acts as a first-order

control on the silicon and organic carbon export stoichiometry. Differences in BSi : POC ratios between the mixed layer suspended particle stock and particles exported out of the mixed layer may be explained by the dominant sedimentation of empty diatom frustules that results from the grazing pressure by the zooplankton community and the intense carbon utilization by heterotrophic microbial communities (Christaki et al., 2014).

We classified species that were observed exclusively as empty cells, or sinking with an integrated empty : full ratio > 2, as predominantly silica exporters, and these included *C. bulbosus*, *C. pennatum*, *P. truncata*, *R. antennata/styliformis*, *A. hookeri*, *A. hyalinus*, *C. decipiens*, *C. inerme*, *D. antarcticus*, *P. alata*, *T. nitzschioides* spp., *T. lentiginosa* and small centric species (< 20 µm). Although *F. kerguelensis*, *T. nitzschioides spp.* and *T. lentiginosa* were present through the entire season, their fluxes were highly correlated with BSi : POC ratios (Fig. 6), identifying these species as significant contributors to silica export. However, resting spores and species that sink with a major contribution of full cells (integrated empty : full ratio < 0.5) were identified as belonging to the preferential carbon sinkers: *Chaetoceros Hyalochaete* spp., *E. antarctica* var. *antarctica, R. simplex* and *Thalassiothrix antarctica*. Among them, CRS and *E. antarctica* var. *antarctica* were the most negatively correlated with the BSi : POC ratio and were identified as key species for carbon export (Fig. 6). These observations are consistent with a previous study of natural iron fertilization that identified *C. pennatum*, *D. antarcticus* and *F. kerguelensis* as major silica sinkers and CRS and *E. antarctica* var. *antarctica* resting spores as major carbon sinkers downstream of the Crozet Islands (Salter et al., 2012). During the EIFEX artificial fertilization experiment, *Chaetoceros Hyalochaete* vegetative stages were identified as a major carbon sinker, whereas *F. kerguelensis* was considered as a strong silica sinker (Assmy et al., 2013). Notably, resting spore formation was not observed in the artificial experiment performed in the open ocean remote from coastal influence, and carbon export was attributed to mass mortality and aggregation of algal cells (Assmy et al., 2013). Nevertheless, a more detailed analysis of species-specific carbon and silica content in the exported material is necessary to fully elucidate their respective roles on carbon and silica export.

4.5   Seasonal succession of ecological flux vectors over the Kerguelen Plateau

Although sediment trap records integrate cumulative processes of production in the mixed layer and selective losses during export, they provide a unique insight into the temporal succession of plankton functional types and resultant geochemical properties of exported particles characterizing the biological pump. The seasonal cycle of ecological vectors and associated export stoichiometry is summarized in Fig. 7. The robustness of the relationship between measured

and calculated POC fluxes (Fig. 8b) suggests that the main ecological flux vectors described from the samples are capable of predicting seasonal patterns of total POC fluxes. At an annual scale the calculated POC fluxes slightly underestimate the measured fluxes (93.1 vs. 98.2 mmol m^{-2}). This might result from the minor contribution of full cells other than the diatoms species considered, aggregated material, organic matter sorbed to the exterior of empty cells and faecal fluff that was difficult to enumerate.

A scheme of phytoplankton and zooplankton communities succession in naturally fertilized areas of the Southern Ocean was proposed by Quéguiner (2013). Spring phytoplankton communities are characterized by small, lightly silicified, fast-growing diatoms associated with small microphagous copepods. In summer, the phytoplankton community progressively switches toward large, highly silicified, slow-growing diatoms resistant to grazing by large copepods. In this scheme carbon export occurs mostly in the end of summer through the fall dump. The species succession directly observed in our sediment trap samples differs somewhat to the conceptual model proposed by Quéguiner (2013), although the general patterns are similar. The diatom species exported in spring were *F. kerguelensis* and *T. nitzschioides* spp. and small centric species (< 20 µm), whilst in summer the comparatively very large (> 200 µm) species of *Proboscia* sp., *Rhizosolenia* sp. *and Thalassiothrix antarctica* were observed. However we observe that these species constituting the spring fluxes are exported almost exclusively as empty cells. The abundance of small spherical and ovoid faecal pellet suggests an important role of small copepods in the zooplankton (Yoon et al., 2001; Wilson et al., 2013), which was corroborated by the finding of dominant *Oithona similis* abundances in the spring mesozooplankton assemblages at station A3 (Carlotti et al., 2015). Therefore, our data suggest that spring export captured by the sediment trap was the remnants of a diatom community subject to efficient grazing and carbon utilization in, or at the base of, the mixed layer, resulting in a BSi : POC export ratio > 2 (Table 1).

The main difference in our observations and the conceptual scheme of Quéguiner (2013) is the dominance of *Chaetoceros Hyalochaete* resting spores to diatom export assemblages and their contribution to carbon fluxes out of the mixed layer in summer. Resting spores appear to efficiently bypass the "carbon trap" represented by grazers and might also physically entrain small faecal pellets in their downward flux. In mid-summer, faecal pellet carbon export is dominated by the contribution of cylindrical shapes. This appears to be consistent with an observed shift toward a higher contribution of large copepods and euphausiids to the mesozooplankton community in the mixed layer (Carlotti et al., 2008). However, CRS still dominate the diatom exported assemblage. The corresponding BSi : POC ratio decreases with values between 1 and 2 (Table 1). The fact that there are two discrete resting spore export events might be explained by a

mixing event that injected $Si(OH)_4$ into the surface, allowing the development of a secondary $Si(OH)_4$ limitation.

In the autumn and winter, diatom fluxes are very low and faecal pellet carbon export is dominated by cylindrical and tabular contributions consistent with a supposed shift to zooplankton communities dominated by large copepods, euphausiids and salps (Wilson et al., 2013). The low BSi : POC ratios characterizing export at this time suggest that these communities feed primarily on suspended particles (in the case of salps) and on micro- and mesozooplankton or small diatoms, although direct measurements of faecal pellet content would be necessary to confirm this.

5   Conclusions

We report the chemical (particulate organic carbon and nitrogen, biogenic silica) and biological (diatom cells and faecal pellets) composition of material exported beneath the winter mixed layer (289 m) in a naturally iron-fertilized area of the Southern Ocean. Annually integrated organic carbon export from the iron-fertilized bloom was low (98 mmol m^{-2}), although biogenic silicon export was significant (114 mmol m^{-2}). *Chaetoceros Hyalochaete* and *Thalassiosira antarctica* resting spores accounted for more than 60 % of the annual POC flux. The high abundance of empty cells and the lower contribution of faecal pellets to POC flux (34 %) suggest efficient carbon retention occurs in or at the base of the mixed layer. We propose that, in this HBLE environment, carbon-rich and fast-sinking resting spores bypass the intense grazing pressure otherwise responsible for the rapid attenuation of flux. The seasonal succession of diatom taxa groups was tightly linked to the stoichiometry of the exported material. Several species were identified as primarily "silica sinkers" (e.g. *Fragilariopsis kerguelensis* and *Thalassionema nitzschioides* spp.) and others as preferential "carbon sinkers" (e.g. resting spores of *Chaetoceros Hyalochaete* and *Thalassiosira antarctica*, *Eucampia antarctica* var. *antarctica* and the giant diatom *Thalassiothrix antarctica*). Faecal pellet types described a clear transition from small spherical shapes (small copepods) in spring, larger cylindrical an ellipsoid shapes in summer (euphausiids and large copepods) and large tabular shape (salps) in autumn. Their contribution to carbon fluxes increased with the presence of larger shapes.

The change in biological productivity and ocean circulation cannot explain the ~ 80 ppmv atmospheric $p\mathrm{CO}_2$ difference between the pre-industrial era and the Last Glacial Maximum (Archer et al., 2000; Bopp et al., 2003; Kohfeld et al., 2005; Wolff et al., 2006). Nevertheless, a simple switch in "silica sinker" versus "carbon sinker" relative abundance would have a drastic effect on carbon sequestration in the Southern Ocean and silicic acid availability at lower latitudes (Sarmiento et al., 2004; Boyd, 2013). The results presented here emphasize the compelling need for similar studies in

other locations of the global Ocean that will allow for identification of key ecological vectors that set the magnitude and the stoichiometry of the biological pump.

The Supplement related to this article is available online at doi:10.5194/bg-12-3171-2015-supplement.

References

Abdi, H.: Partial least squares regression and projection on latent structure regression (PLS Regression), Wiley Interdiscip. Rev. Comput. Stat., 2, 97–106, doi:10.1002/wics.51, 2010.

Abelmann, A. and Gersonde, R.: Biosiliceous particle flux in the Southern Ocean, Mar. Chem., 35, 503–536, doi:10.1016/S0304-4203(09)90040-8, 1991.

Allen, C. S., Pike, J., Pudsey, C. J., and Leventer, A.: Submillennial variations in ocean conditions during deglaciation based on diatom assemblages from the southwest Atlantic, Paleoceanography, 20, PA2012, doi:10.1029/2004PA001055, 2005.

Aminot, A. and Kerouel, R.: Dosage automatique des nutriments dans les eaux marines: methodes en flux continu, Ifremer, Plouzané, France, 2007.

Archer, D., Winguth, A., Lea, D., and Mahowald, N.: What caused the glacial/interglacial atmospheric $p\mathrm{CO}_2$ cycles?, Rev. Geophys., 38, 159–189, doi:10.1029/1999RG000066, 2000.

Armand, L. K., Crosta, X., Romero, O., and Pichon, J.-J.: The biogeography of major diatom taxa in Southern Ocean sediments: 1. Sea ice related species, Palaeogeogr. Palaeoecl., 223, 93–126, doi:10.1016/j.palaeo.2005.02.015, 2005.

Armand, L. K., Crosta, X., Quéguiner, B., Mosseri, J., and Garcia, N.: Diatoms preserved in surface sediments of the northeastern Kerguelen Plateau, Deep-Sea Res. Pt. II, 55, 677–692, doi:10.1016/j.dsr2.2007.12.032, 2008a.

Armand, L. K., Cornet-Barthaux, V., Mosseri, J., and Quéguiner, B.: Late summer diatom biomass and community structure on and around the naturally iron-fertilised Kerguelen Plateau in the Southern Ocean, Deep-Sea Res. Pt. II, 55, 653–676, doi:10.1016/j.dsr2.2007.12.031, 2008b.

Arrigo, K. R., Worthen, D., Schnell, A., and Lizotte, M. P.: Primary production in Southern Ocean waters, J. Geophys. Res.-Oceans, 103, 15587–15600, doi:10.1029/98JC00930, 1998.

Assmy, P., Smetacek, V., Montresor, M., Klaas, C., Henjes, J., Strass, V. H., Arrieta, J. M., Bathmann, U., Berg, G. M., Breitbarth, E., Cisewski, B., Friedrichs, L., Fuchs, N., Herndl, G. J., Jansen, S., Krägefsky, S., Latasa, M., Peeken, I., Röttgers, R., Scharek, R., Schüller, S. E., Steigenberger, S., Webb, A., and Wolf-Gladrow, D.: Thick-shelled, grazer-protected diatoms decouple ocean carbon and silicon cycles in the iron-limited Antarctic Circumpolar Current, P. Natl. Acad. Sci., 110, 20633–20638, doi:10.1073/pnas.1309345110, 2013.

Baker, E. T., Milburn, H. B., and Tennant, D. A.: Field assessment of sediment trap efficiency under varying flow conditions, J. Mar. Res., 46, 573–592, doi:10.1357/002224088785113522, 1988.

Bao, R., Stigter, H. D., and Weering, T. C. E. V.: Diatom fluxes in surface sediments of the Goban Spur continental margin, NE Atlantic Ocean, J. Micropalaeontol., 19, 123–131, doi:10.1144/jm.19.2.123, 2000.

Blain, S., Tréguer, P., Belviso, S., Bucciarelli, E., Denis, M., Desabre, S., Fiala, M., Martin Jézéquel, V., Le Fèvre, J., Mayzaud, P., Marty, J.-C., and Razouls, S.: A biogeochemical study of the island mass effect in the context of the iron hypothesis: Kerguelen Islands, Southern Ocean, Deep-Sea Res. Pt. I, 48, 163–187, doi:10.1016/S0967-0637(00)00047-9, 2001.

Blain, S., Quéguiner, B., Armand, L., Belviso, S., Bombled, B., Bopp, L., Bowie, A., Brunet, C., Brussaard, C., Carlotti, F., Christaki, U., Corbière, A., Durand, I., Ebersbach, F., Fuda, J.-L., Garcia, N., Gerringa, L., Griffiths, B., Guigue, C., Guillerm, C., Jacquet, S., Jeandel, C., Laan, P., Lefèvre, D., Lo Monaco, C., Malits, A., Mosseri, J., Obernosterer, I., Park, Y.-H., Picheral, M., Pondaven, P., Remenyi, T., Sandroni, V., Sarthou, G., Savoye, N., Scouarnec, L., Souhaut, M., Thuiller, D., Timmermans, K., Trull, T., Uitz, J., van Beek, P., Veldhuis, M., Vincent, D., Viollier, E., Vong, L., and Wagener, T.: Effect of natural iron fertilization on carbon sequestration in the Southern Ocean, Nature, 446, 1070–1074, doi:10.1038/nature05700, 2007.

Blain, S., Renaut, S., Xing, X., Claustre, H., and Guinet, C.: Instrumented elephant seals reveal the seasonality in chlorophyll and light-mixing regime in the iron-fertilized Southern Ocean, Geophys. Res. Lett., 40, 6368–6372, doi:10.1002/2013GL058065, 2013.

Bopp, L., Kohfeld, K. E., Le Quéré, C., and Aumont, O.: Dust impact on marine biota and atmospheric CO_2 during glacial periods, Paleoceanography, 18, 1046, doi:10.1029/2002PA000810, 2003.

Bowie, A. R., van der Merwe, P., Quéroué, F., Trull, T., Fourquez, M., Planchon, F., Sarthou, G., Chever, F., Townsend, A. T., Obernosterer, I., Sallée, J.-B., and Blain, S.: Iron budgets for three distinct biogeochemical sites around the Kerguelen archipelago (Southern Ocean) during the natural fertilisation experiment KEOPS-2, Biogeosciences Discuss., 11, 17861–17923, doi:10.5194/bgd-11-17861-2014, 2014.

Boyd, P. W.: Diatom traits regulate Southern Ocean silica leakage, P. Natl. Acad. Sci., 110, 20358–20359, doi:10.1073/pnas.1320327110, 2013.

Brzezinski, M. A.: The Si:C:N ratio of marine diatoms: interspecific variability and the effect of some environmental variables,

J. Phycol., 21, 347–357, doi:10.1111/j.0022-3646.1985.00347.x, 1985.

Brzezinski, M. A., Pride, C. J., Franck, V. M., Sigman, D. M., Sarmiento, J. L., Matsumoto, K., Gruber, N., Rau, G. H., and Coale, K. H.: A switch from $Si(OH)_4$ to NO_3 depletion in the glacial Southern Ocean, Geophys. Res. Lett., 29, 1564, doi:10.1029/2001GL014349, 2002.

Buesseler, K. O.: The decoupling of production and particulate export in the surface ocean, Glob. Biogeochem. Cy., 12, 297–310, doi:10.1029/97GB03366, 1998.

Buesseler, K. O., Steinberg, D. K., Michaels, A. F., Johnson, R. J., Andrews, J. E., Valdes, J. R., and Price, J. F.: A comparison of the quantity and composition of material caught in a neutrally buoyant versus surface-tethered sediment trap, Deep-Sea Res. Pt. I, 47, 277–294, doi:10.1016/S0967-0637(99)00056-4, 2000.

Buesseler, K. O., Antia, A. N., Chen, M., Fowler, S. W., Gardner, W. D., Gustafsson, Ö., Harada, K., Michaels, A. F., Rutgers v. d. Loeff, M., Sarin, M., Steinberg, D. K., and Trull, T.: An assessment of the use of sediment traps for estimating upper ocean particle fluxes, J. Mar. Res., 65, 345–416, 2007.

Burd, A. B. and Jackson, G. A.: Particle Aggregation, Annu. Rev. Mar. Sci., 1, 65–90, doi:10.1146/annurev.marine.010908.163904, 2009.

Carlotti, F., Thibault-Botha, D., Nowaczyk, A., and Lefèvre, D.: Zooplankton community structure, biomass and role in carbon fluxes during the second half of a phytoplankton bloom in the eastern sector of the Kerguelen Shelf (January–February 2005), Deep-Sea Res. Pt. II, 55, 720–733, doi:10.1016/j.dsr2.2007.12.010, 2008.

Carlotti, F., Jouandet, M.-P., Nowaczyk, A., Harmelin-Vivien, M., Lefèvre, D., Guillou, G., Zhu, Y., and Zhou, M.: Mesozooplankton structure and functioning during the onset of the Kerguelen phytoplankton bloom during the Keops2 survey, Biogeosciences Discuss., 12, 2381–2427, doi:10.5194/bgd-12-2381-2015, 2015.

Cavan, E. L., Le Moigne, F. A. C., Poulton, A. J., Tarling, G. A., Ward, P., Daniels, C. J., Fragoso, G., and Sanders, R. J.: Zooplankton fecal pellets control the attenuation of particulate organic carbon flux in the Scotia Sea, Southern Ocean, Geophys. Res. Lett., GL062744, doi:10.1002/2014GL062744, 2015.

Chang, A. S., Bertram, M. A., Ivanochko, T., Calvert, S. E., Dallimore, A., and Thomson, R. E.: Annual record of particle fluxes, geochemistry and diatoms in Effingham Inlet, British Columbia, Canada, and the impact of the 1999 La Niña event, Mar. Geol., 337, 20–34, doi:10.1016/j.margeo.2013.01.003, 2013.

Christaki, U., Lefèvre, D., Georges, C., Colombet, J., Catala, P., Courties, C., Sime-Ngando, T., Blain, S., and Obernosterer, I.: Microbial food web dynamics during spring phytoplankton blooms in the naturally iron-fertilized Kerguelen area (Southern Ocean), Biogeosciences, 11, 6739–6753, doi:10.5194/bg-11-6739-2014, 2014.

Closset, I., Lasbleiz, M., Leblanc, K., Quéguiner, B., Cavagna, A.-J., Elskens, M., Navez, J., and Cardinal, D.: Seasonal evolution of net and regenerated silica production around a natural Fe-fertilized area in the Southern Ocean estimated with Si isotopic approaches, Biogeosciences, 11, 5827–5846, doi:10.5194/bg-11-5827-2014, 2014.

Cornet-Barthaux, V., Armand, L., and Quéguiner, B.: Biovolume and biomass estimates of key diatoms in the Southern Ocean,

Aquat. Microb. Ecol., 48, 295–308, doi:10.3354/ame048295, 2007.

Crawford, R.: The role of sex in the sedimentation of a marine diatom bloom, Limnol. Oceanogr., 40, 200–204, 1995.

Crosta, X., Pichon, J.-J., and Labracherie, M.: Distribution of Chaetoceros resting spores in modern peri-Antarctic sediments, Mar. Micropaleontol., 29, 283–299, doi:10.1016/S0377-8398(96)00033-3, 1997.

Davison, P. C., Checkley Jr., D. M., Koslow, J. A., and Barlow, J.: Carbon export mediated by mesopelagic fishes in the northeast Pacific Ocean, Prog. Oceanogr., 116, 14–30, doi:10.1016/j.pocean.2013.05.013, 2013.

DeMaster, D. J.: The supply and accumulation of silica in the marine environment, Geochim. Cosmochim. Ac., 45, 1715–1732, doi:10.1016/0016-7037(81)90006-5, 1981.

Doucette, G. J. and Fryxell, G. A.: Thalassiosira antarctica: vegetative and resting stage chemical composition of an ice-related marine diatom, Mar. Biol., 78, 1–6, doi:10.1007/BF00392964, 1983.

Dubischar, C. D. and Bathmann, U. V.: The occurrence of faecal material in relation to different pelagic systems in the Southern Ocean and its importance for vertical flux, Deep-Sea Res. Pt. II, 49, 3229–3242, doi:10.1016/S0967-0645(02)00080-2, 2002.

Dunbar, R. B.: Sediment trap experiments on the Antarctic continental margin., Antarct. J. US, 70–71, 1984.

Dutkiewicz, S., Follows, M. J., and Parekh, P.: Interactions of the iron and phosphorus cycles: A three-dimensional model study, Glob. Biogeochem. Cy., 19, GB1021, doi:10.1029/2004GB002342, 2005.

Ebersbach, F. and Trull, T. W.: Sinking particle properties from polyacrylamide gels during the KErguelen Ocean and Plateau compared Study (KEOPS): Zooplankton control of carbon export in an area of persistent natural iron inputs in the Southern Ocean, Limnol. Oceanogr., 53, 212–224, doi:10.4319/lo.2008.53.1.0212, 2008.

Ebersbach, F., Trull, T. W., Davies, D. M., and Bray, S. G.: Controls on mesopelagic particle fluxes in the Sub-Antarctic and Polar Frontal Zones in the Southern Ocean south of Australia in summer-Perspectives from free-drifting sediment traps, Deep-Sea Res. Pt. II, 58, 2260–2276, doi:10.1016/j.dsr2.2011.05.025, 2011.

Ebersbach, F., Assmy, P., Martin, P., Schulz, I., Wolzenburg, S., and Nöthig, E.-M.: Particle flux characterisation and sedimentation patterns of protistan plankton during the iron fertilisation experiment LOHAFEX in the Southern Ocean, Deep-Sea Res. Pt. I, 89, 94–103, doi:10.1016/j.dsr.2014.04.007, 2014.

Fischer, G., Fütterer, D., Gersonde, R., Honjo, S., Ostermann, D., and Wefer, G.: Seasonal variability of particle flux in the Weddell Sea and its relation to ice cover, Nature, 335, 426–428, doi:10.1038/335426a0, 1988.

Fischer, G., Gersonde, R., and Wefer, G.: Organic carbon, biogenic silica and diatom fluxes in the marginal winter sea-ice zone and in the Polar Front Region: interannual variations and differences in composition, Deep-Sea Res. Pt. II, 49, 1721–=1745, doi:10.1016/S0967-0645(02)00009-7, 2002.

Fransz, H. G. and Gonzalez, S. R.: The production of Oithona similis (Copepoda: Cyclopoida) in the Southern Ocean, ICES, J. Mar. Sci. J. Cons., 52, 549–555, doi:10.1016/1054-3139(95)80069-7, 1995.

Garrison, D. L.: Monterey Bay Phytoplankton. II. Resting Spore Cycles in Coastal Diatom Populations, J. Plankton Res., 3, 137–156, doi:10.1093/plankt/3.1.137, 1981.

Gersonde, R. and Zielinski, U.: The reconstruction of late Quaternary Antarctic sea-ice distribution-the use of diatoms as a proxy for sea-ice, Palaeogeogr. Palaeoecl., 162, 263–286, doi:10.1016/S0031-0182(00)00131-0, 2000.

Gleiber, M. R., Steinberg, D. K., and Ducklow, H. W.: Time series of vertical flux of zooplankton fecal pellets on the continental shelf of the western Antarctic Peninsula, Mar. Ecol. Prog. Ser., 471, 23–36, doi:10.3354/meps10021, 2012.

Gomi, Y., Fukuchi, M., and Taniguchi, A.: Diatom assemblages at subsurface chlorophyll maximum layer in the eastern Indian sector of the Southern Ocean in summer, J. Plankton Res., 32, 1039–1050, doi:10.1093/plankt/fbq031, 2010.

Gonzalez, H. E. and Smetacek, V.: The possible role of the cyclopoid copepod Oithona in retarding vertical flux of zooplankton faecal material, Mar. Ecol.-Prog. Ser., 113, 233–246, 1994.

Grigorov, I., Rigual-Hernandez, A. S., Honjo, S., Kemp, A. E. S., and Armand, L. K.: Settling fluxes of diatoms to the interior of the Antarctic circumpolar current along 170° W, Deep-Sea Res. Pt. I, 93, 1–13, doi:10.1016/j.dsr.2014.07.008, 2014.

Grimm, K. A., Lange, C. B., and Gill, A. S.: Biological forcing of hemipelagic sedimentary laminae; evidence from ODP Site 893, Santa Barbara Basin, California, J. Sediment. Res., 66, 613–624, doi:10.1306/D42683C4-2B26-11D7-8648000102C1865D, 1996.

Hasle, G. R. and Syvertsen, E. E.: Chapter 2 – Marine Diatoms, in: Identifying Marine Phytoplankton, edited by: C. R. Tomas, 5–385, Academic Press, San Diego, 1997.

Hillebrand, H., Dürselen, C.-D., Kirschtel, D., Pollingher, U., and Zohary, T.: Biovolume Calculation for Pelagic and Benthic Microalgae, J. Phycol., 35, 403–424, doi:10.1046/j.1529-8817.1999.3520403.x, 1999.

Holm-Hansen, O., Kahru, M., Hewes, C. D., Kawaguchi, S., Kameda, T., Sushin, V. A., Krasovski, I., Priddle, J., Korb, R., Hewitt, R. P., and Mitchell, B. G.: Temporal and spatial distribution of chlorophyll-a in surface waters of the Scotia Sea as determined by both shipboard measurements and satellite data, Deep-Sea Res. Pt. II, 51, 1323–1331, doi:10.1016/j.dsr2.2004.06.004, 2004.

Holzer, M., Primeau, F. W., DeVries, T., and Matear, R.: The Southern Ocean silicon trap: Data-constrained estimates of regenerated silicic acid, trapping efficiencies, and global transport paths, J. Geophys. Res.-Oceans, 119, 313–331, doi:10.1002/2013JC009356, 2014.

Howard, A. G., Coxhead, A. J., Potter, I. A., and Watt, A. P.: Determination of dissolved aluminium by the micelle-enhanced fluorescence of its lumogallion complex, Analyst, 111, 1379–1382, doi:10.1039/AN9861101379, 1986.

Hutchins, D. A. and Bruland, K. W.: Iron-limited diatom growth and Si:N uptake ratios in a coastal upwelling regime, Nature, 393, 561–564, doi:10.1038/31203, 1998.

Ichinomiya, M., Gomi, Y., Nakamachi, M., Honda, M., Fukuchi, M., and Taniguchi, A.: Temporal variations in the abundance and sinking flux of diatoms under fast ice in summer near Syowa Station, East Antarctica, Polar Sci., 2, 33–40, doi:10.1016/j.polar.2008.01.001, 2008.

Jackson, G. A. and Burd, A. B.: A model for the distribution of particle flux in the mid-water column controlled by subsurface biotic interactions, Deep-Sea Res. Pt. II, 49, 193–217, doi:10.1016/S0967-0645(01)00100-X, 2001.

Jackson, G. A., Waite, A. M., and Boyd, P. W.: Role of algal aggregation in vertical carbon export during SOIREE and in other low biomass environments, Geophys. Res. Lett., 32, L13607, doi:10.1029/2005GL023180, 2005.

Jin, X., Gruber, N., Dunne, J. P., Sarmiento, J. L., and Armstrong, R. A.: Diagnosing the contribution of phytoplankton functional groups to the production and export of particulate organic carbon, $CaCO_3$, and opal from global nutrient and alkalinity distributions, Glob. Biogeochem. Cy., 20, GB2015, doi:10.1029/2005GB002532, 2006.

Jouandet, M.-P., Blain, S., Metzl, N., Brunet, C., Trull, T. W., and Obernosterer, I.: A seasonal carbon budget for a naturally iron-fertilized bloom over the Kerguelen Plateau in the Southern Ocean, Deep-Sea Res. Pt. II, 55, 856–867, doi:10.1016/j.dsr2.2007.12.037, 2008.

Jouandet, M.-P., Trull, T. W., Guidi, L., Picheral, M., Ebersbach, F., Stemmann, L., and Blain, S.: Optical imaging of mesopelagic particles indicates deep carbon flux beneath a natural iron-fertilized bloom in the Southern Ocean, Limnol. Oceanogr., 56, 1130–1140, doi:10.4319/lo.2011.56.3.1130, 2011.

Jouandet, M.-P., Jackson, G. A., Carlotti, F., Picheral, M., Stemmann, L., and Blain, S.: Rapid formation of large aggregates during the spring bloom of Kerguelen Island: observations and model comparisons, Biogeosciences, 11, 4393–4406, doi:10.5194/bg-11-4393-2014, 2014.

Kato, M., Tanimura, Y., Matsuoka, K., and Fukusawa, H.: Planktonic diatoms from sediment traps in Omura Bay, western Japan with implications for ecological and taphonomic studies of coastal marine environments, Quat. Int., 105, 25–31, doi:10.1016/S1040-6182(02)00147-7, 2003.

Kemp, A. E. S. and Villareal, T. A.: High diatom production and export in stratified waters – A potential negative feedback to global warming, Prog. Oceanogr., 119, 4–23, doi:10.1016/j.pocean.2013.06.004, 2013.

Kemp, A. E. S., Pike, J., Pearce, R. B., and Lange, C. B.: The "Fall dump" – a new perspective on the role of a "shade flora" in the annual cycle of diatom production and export flux, Deep-Sea Res. Pt. II, 47, 2129–2154, doi:10.1016/S0967-0645(00)00019-9, 2000.

Kohfeld, K. E., Quéré, C. L., Harrison, S. P., and Anderson, R. F.: Role of Marine Biology in Glacial-Interglacial CO_2 Cycles, Science, 308, 74–78, doi:10.1126/science.1105375, 2005.

Kopczynska, E. E., Dehairs, F., Elskens, M., and Wright, S.: Phytoplankton and microzooplankton variability between the Subtropical and Polar Fronts south of Australia: Thriving under regenerative and new production in late summer, J. Geophys. Res.-Oceans, 106, 31597–31609, doi:10.1029/2000JC000278, 2001.

Kuwata, A. and Tsuda, A.: Selection and viability after ingestion of vegetative cells, resting spores and resting cells of the marine diatom, Chaetoceros pseudocurvisetus, by two copepods, J. Exp. Mar. Biol. Ecol., 322, 143–151, doi:10.1016/j.jembe.2005.02.013, 2005.

Kuwata, A., Hama, T., and Takahashi, M.: Ecophysiological characterization of two life forms, resting spores and resting cells, of

a marine planktonic diatom, Mar. Ecol. Prog. Ser., 102, 245–255, 1993.

Lampitt, R. S., Noji, T., and Bodungen, B. von: What happens to zooplankton faecal pellets? Implications for material flux, Mar. Biol., 104, 15–23, doi:10.1007/BF01313152, 1990.

Lampitt, R. S., Boorman, B., Brown, L., Lucas, M., Salter, I., Sanders, R., Saw, K., Seeyave, S., Thomalla, S. J., and Turnewitsch, R.: Particle export from the euphotic zone: Estimates using a novel drifting sediment trap, 234Th and new production, Deep-Sea Res. Pt. I, 55, 1484–1502, doi:10.1016/j.dsr.2008.07.002, 2008.

Lampitt, R. S., Salter, I., and Johns, D.: Radiolaria: Major exporters of organic carbon to the deep ocean, Glob. Biogeochem. Cy., 23, GB1010, doi::10.1029/2008GB003221, 2009.

Lam, P. J. and Bishop, J. K. B.: High biomass, low export regimes in the Southern Ocean, Deep-Sea Res. Pt. II, 54, 601–638, doi:10.1016/j.dsr2.2007.01.013, 2007.

Lam, P. J., Doney, S. C., and Bishop, J. K. B.: The dynamic ocean biological pump: Insights from a global compilation of particulate organic carbon, CaCO3, and opal concentration profiles from the mesopelagic, Glob. Biogeochem. Cy., 25, GB3009, doi:10.1029/2010GB003868, 2011.

Lange, C. B., Weinheimer, A. L., Reid, F. M. H,. and Thunell, R. C.: Sedimentation patterns of diatoms, radiolarians, and silicoflagellates in Santa Barbara Basin, California, Calif. Coop. Ocean. Fish. Investig. Rep., 38, 161–170, 1997.

Lasbleiz, M., Leblanc, K., Blain, S., Ras, J., Cornet-Barthaux, V., Hélias Nunige, S., and Quéguiner, B.: Pigments, elemental composition (C, N, P, and Si), and stoichiometry of particulate matter in the naturally iron fertilized region of Kerguelen in the Southern Ocean, Biogeosciences, 11, 5931–5955, doi:10.5194/bg-11-5931-2014, 2014.

Laurenceau-Cornec, E. C., Trull, T. W., Davies, D. M., Bray, S. G., Doran, J., Planchon, F., Carlotti, F., Jouandet, M.-P., Cavagna, A.-J., Waite, A. M., and Blain, S.: The relative importance of phytoplankton aggregates and zooplankton fecal pellets to carbon export: insights from free-drifting sediment trap deployments in naturally iron-fertilised waters near the Kerguelen Plateau, Biogeosciences, 12, 1007–1027, doi:10.5194/bg-12-1007-2015, 2015.

Legendre, P. and Legendre, F. J. L.: Numerical Ecology, Édition : 2., Elsevier Science, Amsterdam, New York, 1998.

Leventer, A.: Sediment trap diatom assemblages from the northern Antarctic Peninsula region, Deep-Sea Res. Pt. I, 38, 1127–1143, doi:10.1016/0198-0149(91)90099-2, 1991.

Leventer, A. and Dunbar, R. B.: Diatom flux in McMurdo Sound, Antarctica, Mar. Micropaleontol., 12, 49–64, doi:10.1016/0377-8398(87)90013-2, 1987.

Lopes, C., Mix, A. C., and Abrantes, F.: Diatoms in northeast Pacific surface sediments as paleoceanographic proxies, Mar. Micropaleontol., 60, 45–65, doi:10.1016/j.marmicro.2006.02.010, 2006.

Madin, L. P.: Production, composition and sedimentation of salp fecal pellets in oceanic waters, Mar. Biol., 67, 39–45, doi:10.1007/BF00397092, 1982.

Maiti, K., Charette, M. A., Buesseler, K. O., and Kahru, M.: An inverse relationship between production and export efficiency in the Southern Ocean, Geophys. Res. Lett., 40, 1557–1561, doi:10.1002/grl.50219, 2013.

Martin, J. H., Gordon, R. M., and Fitzwater, S. E.: Iron in Antarctic waters, Nature, 345, 156–158, doi:10.1038/345156a0, 1990.

Matsumoto, K., Sarmiento, J. L., and Brzezinski, M. A.: Silicic acid leakage from the Southern Ocean: A possible explanation for glacial atmospheric pCO$_2$, Glob. Biogeochem. Cy., 16, 5–1, doi:10.1029/2001GB001442, 2002.

McQuoid, M. R. and Hobson, L. A.: Diatom Resting Stages, J. Phycol., 32, 889–902, doi:10.1111/j.0022-3646.1996.00889.x, 1996.

Menden-Deuer, S. and Lessard, E. J.: Carbon to volume relationships for dinoflagellates, diatoms, and other protist plankton, Limnol. Oceanogr., 45, 569–579, doi:10.4319/lo.2000.45.3.0569, 2000.

Moore, C. M., Mills, M. M., Arrigo, K. R., Berman-Frank, I., Bopp, L., Boyd, P. W., Galbraith, E. D., Geider, R. J., Guieu, C., Jaccard, S. L., Jickells, T. D., La Roche, J., Lenton, T. M., Mahowald, N. M., Marañón, E., Marinov, I., Moore, J. K., Nakatsuka, T., Oschlies, A., Saito, M. A., Thingstad, T. F., Tsuda, A., and Ulloa, O.: Processes and patterns of oceanic nutrient limitation, Nat. Geosci., 6, 701–710, doi:10.1038/ngeo1765, 2013.

Moore, J. K., Doney, S. C., Glover, D. M., and Fung, I. Y.: Iron cycling and nutrient-limitation patterns in surface waters of the World Ocean, Deep-Sea Res., 49, 463–507, doi:10.1016/S0967-0645(01)00109-6, 2001.

Mortlock, R. A. and Froelich, P. N.: A simple method for the rapid determination of biogenic opal in pelagic marine sediments, Deep-Sea Res. Pt. I, 36, 1415–1426, doi:10.1016/0198-0149(89)90092-7, 1989.

Mosseri, J., Quéguiner, B., Armand, L., and Cornet-Barthaux, V.: Impact of iron on silicon utilization by diatoms in the Southern Ocean: A case study of Si/N cycle decoupling in a naturally iron-enriched area, Deep-Sea Res. Pt. II, 55, 801–819, doi:10.1016/j.dsr2.2007.12.003, 2008.

Nelson, D. M., Tréguer, P., Brzezinski, M. A., Leynaert, A., and Quéguiner, B.: Production and dissolution of biogenic silica in the ocean: Revised global estimates, comparison with regional data and relationship to biogenic sedimentation, Glob. Biogeochem. Cy., 9, 359–372, doi:10.1029/95GB01070, 1995.

Nelson, D. M., Brzezinski, M. A., Sigmon, D. E., and Franck, V. M.: A seasonal progression of Si limitation in the Pacific sector of the Southern Ocean, Deep-Sea Res. Pt. II, 48, 3973–3995, doi:10.1016/S0967-0645(01)00076-5, 2001.

Oku, O. and Kamatani, A.: Resting spore formation of the marine planktonic diatom Chaetoceros anastomosans induced by high salinity and nitrogen depletion, Mar. Biol., 127, 515–520, doi:10.1007/s002270050040, 1997.

Onodera, J., Watanabe, E., Harada, N., and Honda, M. C.: Diatom flux reflects water-mass conditions on the southern Northwind Abyssal Plain, Arctic Ocean, Biogeosciences, 12, 1373–1385, doi:10.5194/bg-12-1373-2015, 2015.

Park, J., Oh, I.-S., Kim, H.-C., and Yoo, S.: Variability of SeaWiFs chlorophyll-a in the southwest Atlantic sector of the Southern Ocean: Strong topographic effects and weak seasonality, Deep-Sea Res. Pt. I, 57, 604–620, doi:10.1016/j.dsr.2010.01.004, 2010.

Park, Y.-H., Roquet, F., Durand, I., and Fuda, J.-L.: Large-scale circulation over and around the Northern Kerguelen Plateau, Deep-Sea Res. Pt. II, 55, 566–581, doi:10.1016/j.dsr2.2007.12.030, 2008.

Park, Y.-H., Durand, I., Kestenare, E., Rougier, G., Zhou, M., d'Ovidio, F., Cotté, C., and Lee, J.-H.: Polar Front around the Kerguelen Islands: An up-to-date determination and associated circulation of surface/subsurface waters, J. Geophys. Res.-Oceans, 119, 6575–6592, doi:10.1002/2014JC010061, 2014.

Parslow, J. S., Boyd, P. W., Rintoul, S. R., and Griffiths, F. B.: A persistent subsurface chlorophyll maximum in the Interpolar Frontal Zone south of Australia: Seasonal progression and implications for phytoplankton-light-nutrient interactions, J. Geophys. Res.-Oceans, 106, 31543–31557, doi:10.1029/2000JC000322, 2001.

Pilskaln, C. H., Manganini, S. J., Trull, T. W., Armand, L., Howard, W., Asper, V. L., and Massom, R.: Geochemical particle fluxes in the Southern Indian Ocean seasonal ice zone: Prydz Bay region, East Antarctica, Deep-Sea Res. Pt. I, 51, 307–332, doi:10.1016/j.dsr.2003.10.010, 2004.

Pinkerton, M. H., Smith, A. N. H., Raymond, B., Hosie, G. W., Sharp, B., Leathwick, J. R., and Bradford-Grieve, J. M.: Spatial and seasonal distribution of adult Oithona similis in the Southern Ocean: Predictions using boosted regression trees, Deep-Sea Res. Pt. I, 57, 469–485, doi:10.1016/j.dsr.2009.12.010, 2010.

Pollard, R., Lucas, M., and Read, J.: Physical controls on biogeochemical zonation in the Southern Ocean, Deep-Sea Res. Pt. II, 49, 3289–3305, doi:10.1016/S0967-0645(02)00084-X, 2002.

Primeau, F. W., Holzer, M., and DeVries, T.: Southern Ocean nutrient trapping and the efficiency of the biological pump, J. Geophys. Res.-Oceans, 118, 2547–2564, doi:10.1002/jgrc.20181, 2013.

Quéguiner, B.: Iron fertilization and the structure of planktonic communities in high nutrient regions of the Southern Ocean, Deep-Sea Res. Pt. II, 90, 43–54, doi:10.1016/j.dsr2.2012.07.024, 2013.

Ragueneau, O., Savoye, N., Del Amo, Y., Cotten, J., Tardiveau, B., and Leynaert, A.: A new method for the measurement of biogenic silica in suspended matter of coastal waters: using Si:Al ratios to correct for the mineral interference, Cont. Shelf Res., 25, 697–710, doi:10.1016/j.csr.2004.09.017, 2005.

Ragueneau, O., Schultes, S., Bidle, K., Claquin, P., and Moriceau, B.: Si and C interactions in the world ocean: Importance of ecological processes and implications for the role of diatoms in the biological pump, Glob. Biogeochem. Cy., 20, GB4S02, doi:10.1029/2006GB002688, 2006.

Rembauville, M., Salter, I., Leblond, N., Gueneugues, A., and Blain, S.: Export fluxes in a naturally iron-fertilized area of the Southern Ocean – Part 1: Seasonal dynamics of particulate organic carbon export from a moored sediment trap, Biogeosciences, 12, 3153–3170, doi:10.5194/bg-12-3153-2015, 2015.

Richardson, K., Visser, A. W., and Pedersen, F. B.: Subsurface phytoplankton blooms fuel pelagic production in the North Sea, J. Plankton Res., 22, 1663–1671, doi:10.1093/plankt/22.9.1663, 2000.

Rigual-Hernández, A. S., Trull, T. W., Bray, S. G., Closset, I.,fWe directly compared and Armand, L. K.: Seasonal dynamics in diatom and particulate export fluxes to the deep sea in the Australian sector of the southern Antarctic Zone, J. Mar. Syst., 142, 62–74, doi:10.1016/j.jmarsys.2014.10.002, 2015.

Romero, O. E. and Armand, L.: Marine diatoms as indicators of modern changes in oceanographic conditions. In: 2nd Edition The Diatoms: Applications for the Environmental and Earth Sciences, Camb. Univ. Press, 373–400, 2010.

Romero, O. E., Lange, C. B., Fisher, G., Treppke, U. F., and Wefer, G.: Variability in export prodution documented by downward

fluxes and species composition of marine planktonic diatoms: observations from the tropical and equatorial Atlantic, in: The Use of Proxies in Paleoceanography, Examples from the South Atlantic, 365–392, Heidelberg, Berlin, 1999.

Romero, O. E., Fischer, G., Lange, C. B., and Wefer, G.: Siliceous phytoplankton of the western equatorial Atlantic: sediment traps and surface sediments, Deep-Sea Res. Pt. II, 47, 1939–1959, doi:10.1016/S0967-0645(00)00012-6, 2000.

Rynearson, T. A., Richardson, K., Lampitt, R. S., Sieracki, M. E., Poulton, A. J., Lyngsgaard, M. M., and Perry, M. J.: Major contribution of diatom resting spores to vertical flux in the sub-polar North Atlantic, Deep-Sea Res. Pt. I, 82, 60–71, doi:10.1016/j.dsr.2013.07.013, 2013.

Sackett, O., Armand, L., Beardall, J., Hill, R., Doblin, M., Connelly, C., Howes, J., Stuart, B., Ralph, P., and Heraud, P.: Taxon–specific responses of Southern Ocean diatoms to Fe enrichment revealed by synchrotron radiation FTIR microspectroscopy, Biogeosciences, 11, 5795–5808, doi:10.5194/bg-11-5795-2014, 2014.

Sallée, J.-B., Matear, R. J., Rintoul, S. R., and Lenton, A.: Localized subduction of anthropogenic carbon dioxide in the Southern Hemisphere oceans, Nat. Geosci., 5, 579–584, doi:10.1038/ngeo1523, 2012.

Salter, I., Lampitt, R. S., Sanders, R., Poulton, A., Kemp, A. E. S., Boorman, B., Saw, K., and Pearce, R.: Estimating carbon, silica and diatom export from a naturally fertilised phytoplankton bloom in the Southern Ocean using PELAGRA: A novel drifting sediment trap, Deep-Sea Res. Pt. II, 54, 2233–2259, doi:10.1016/j.dsr2.2007.06.008, 2007.

Salter, I., Kemp, A. E. S., Moore, C. M., Lampitt, R. S., Wolff, G. A., and Holtvoeth, J.: Diatom resting spore ecology drives enhanced carbon export from a naturally iron-fertilized bloom in the Southern Ocean, Glob. Biogeochem. Cy., 26, GB1014, doi:10.1029/2010GB003977, 2012.

Sancetta, C.: Diatoms in the Gulf of California: Seasonal flux patterns and the sediment record for the last 15 000 years, Paleoceanography, 10, 67–84, doi:10.1029/94PA02796, 1995.

Sanders, J. G. and Cibik, S. J.: Reduction of growth rate and resting spore formation in a marine diatom exposed to low levels of cadmium, Mar. Environ. Res., 16, 165–180, doi:10.1016/0141-1136(85)90136-9, 1985.

Sarmiento, J. L., Gruber, N., Brzezinski, M. A., and Dunne, J. P.: High-latitude controls of thermocline nutrients and low latitude biological productivity, Nature, 427, 56–60, doi:10.1038/nature02127, 2004.

Schnack-Schiel, S. B. and Isla, E.: The role of zooplankton in the pelagic-benthic coupling of the Southern Ocean, Sci. Mar., 69, 39–55, 2005.

Smetacek, V., Assmy, P., and Henjes, J.: The role of grazing in structuring Southern Ocean pelagic ecosystems and biogeochemical cycles, Antarct. Sci., 16, 541–558, doi:10.1017/S0954102004002317, 2004.

Smetacek, V. S.: Role of sinking in diatom life-history cycles: ecological, evolutionary and geological significance, Mar. Biol., 84, 239–251, doi:10.1007/BF00392493, 1985.

Steinberg, D. K., Goldthwait, S. A., and Hansell, D. A.: Zooplankton vertical migration and the active transport of dissolved organic and inorganic nitrogen in the Sargasso Sea, Deep-Sea

Res. Pt. I, 49, 1445–1461, doi:10.1016/S0967-0637(02)00037-7, 2002.

Suzuki, H., Sasaki, H., and Fukuchi, M.: Short-term variability in the flux of rapidly sinking particles in the Antarctic marginal ice zone, Polar Biol., 24, 697–705, doi:10.1007/s003000100271, 2001.

Suzuki, H., Sasaki, H., and Fukuchi, M.: Loss Processes of Sinking Fecal Pellets of Zooplankton in the Mesopelagic Layers of the Antarctic Marginal Ice Zone, J. Oceanogr., 59, 809–818, doi:10.1023/B:JOCE.0000009572.08048.0d, 2003.

Takahashi, T., Sweeney, C., Hales, B., Chipman, D., Newberger, T., Goddard, J., Iannuzzi, R., and Sutherland, S.: The Changing Carbon Cycle in the Southern Ocean, Oceanography, 25, 26–37, doi:10.5670/oceanog.2012.71, 2012.

Takeda, S.: Influence of iron availability on nutrient consumption ratio of diatoms in oceanic waters, Nature, 393, 774–777, doi:10.1038/31674, 1998.

Tarling, G. A., Ward, P., Atkinson, A., Collins, M. A., and Murphy, E. J.: DISCOVERY 2010: Spatial and temporal variability in a dynamic polar ecosystem, Deep-Sea Res. Pt. II, 59–60, 1–13, doi:10.1016/j.dsr2.2011.10.001, 2012.

Taylor, S. R., and McClennan, S. M.: The continental crust: Its composition and evolution, Geol. J., 21, 85–86, doi:10.1002/gj.3350210116, 1986.

Thomalla, S. J., Fauchereau, N., Swart, S., and Monteiro, P. M. S.: Regional scale characteristics of the seasonal cycle of chlorophyll in the Southern Ocean, Biogeosciences, 8, 2849–2866, doi:10.5194/bg-8-2849-2011, 2011.

Treppke, U. F., Lange, C. B., and Wefer, G.: Vertical fluxes of diatoms and silicoflagellates in the eastern equatorial Atlantic, and their contribution to the sedimentary record, Mar. Micropaleontol., 28, 73–96, doi:10.1016/0377-8398(95)00046-1, 1996.

Trull, T. W., Davies, D. M., Dehairs, F., Cavagna, A.-J., Lasbleiz, M., Laurenceau-Cornec, E. C., d'Ovidio, F., Planchon, F., Leblanc, K., Quéguiner, B., and Blain, S.: Chemometric perspectives on plankton community responses to natural iron fertilisation over and downstream of the Kerguelen Plateau in the Southern Ocean, Biogeosciences, 12, 1029–1056, doi:10.5194/bg-12-1029-2015, 2015.

Uitz, J., Claustre, H., Griffiths, F. B., Ras, J., Garcia, N., and Sandroni, V.: A phytoplankton class-specific primary production model applied to the Kerguelen Islands region (Southern Ocean), Deep-Sea Res. Pt. I, 56, 541–560, doi:10.1016/j.dsr.2008.11.006, 2009.

Venables, H. and Moore, C. M.: Phytoplankton and light limitation in the Southern Ocean: Learning from high-nutrient, high-chlorophyll areas, J. Geophys. Res.-Oceans, 115, C02015, doi:10.1029/2009JC005361, 2010.

Von Bodungen, B.: Phytoplankton growth and krill grazing during spring in the Bransfield Strait, Antarctica – Implications from sediment trap collections, Polar Biol., 6, 153–160, doi:10.1007/BF00274878, 1986.

Von Bodungen, B., Fischer, G., Nöthig, E.-M., and Wefer, G.: Sedimentation of krill faeces during spring development of phytoplankton in Bransfield Strait, Antarctica, Mitt Geol Paläont Inst Univ Hambg. SCOPE/UNEP Sonderbd, 62, 243–257, 1987.

Weber, T. S. and Deutsch, C.: Ocean nutrient ratios governed by plankton biogeography, Nature, 467, 550–554, doi:10.1038/nature09403, 2010.

Wefer, G. and Fischer, G.: Annual primary production and export flux in the Southern Ocean from sediment trap data, Mar. Chem., 35, 597–613, doi:10.1016/S0304-4203(09)90045-7, 1991.

Wefer, G., Fischer, G., Füetterer, D., and Gersonde, R.: Seasonal particle flux in the Bransfield Strait, Antartica, Deep-Sea Res. Pt. I, 35, 891–898, doi:10.1016/0198-0149(88)90066-0, 1988.

Wefer, G. G., Fisher, D. K., Futterer, R., Gersonde, R., Honjo, S., and Ostermann, D.: Particle sedimentation and productivity in Antarctic waters of the Atlantic sector, in: Geological history of the polar oceans?, Arctic versus Antarctic, 363–379, Kluwer Academic Publishers, The Netherlands, 1990.

Westberry, T. K., Behrenfeld, M. J., Milligan, A. J., and Doney, S. C.: Retrospective satellite ocean color analysis of purposeful and natural ocean iron fertilization, Deep-Sea Res. Pt. I, 73, 1–16, doi:10.1016/j.dsr.2012.11.010, 2013.

Wilson, S. E., Steinberg, D. K., and Buesseler, K. O.: Changes in fecal pellet characteristics with depth as indicators of zooplankton repackaging of particles in the mesopelagic zone of the subtropical and subarctic North Pacific Ocean, Deep-Sea Res. Pt. II, 55, 1636–1647, doi:10.1016/j.dsr2.2008.04.019, 2008.

Wilson, S., E., Ruhl, H. A., and Smith Jr, K. L.: Zooplankton fecal pellet flux in the abyssal northeast Pacific: A 15 year time-series study, Limnol. Oceanogr., 58, 881–892, doi:10.4319/lo.2013.58.3.0881, 2013.

Wolff, E. W., Fischer, H., Fundel, F., Ruth, U., Twarloh, B., Littot, G. C., Mulvaney, R., Röthlisberger, R., de Angelis, M., Boutron, C. F., Hansson, M., Jonsell, U., Hutterli, M. A., Lambert, F., Kaufmann, P., Stauffer, B., Stocker, T. F., Steffensen, J. P., Bigler, M., Siggaard-Andersen, M. L., Udisti, R., Becagli, S., Castellano, E., Severi, M., Wagenbach, D., Barbante, C., Gabrielli, P., and Gaspari, V.: Southern Ocean sea-ice extent, productivity and iron flux over the past eight glacial cycles, Nature, 440, 491–496, doi:10.1038/nature04614, 2006.

Yoon, W., Kim, S., and Han, K.: Morphology and sinking velocities of fecal pellets of copepod, molluscan, euphausiid, and salp taxa in the northeastern tropical Atlantic, Mar. Biol., 139, 923–928, doi:10.1007/s002270100630, 2001.

Zielinski, U. and Gersonde, R.: Diatom distribution in Southern Ocean surface sediments (Atlantic sector): Implications for paleoenvironmental reconstructions, Palaeogeogr. Palaeoecl., 129, 213–250, doi:10.1016/S0031-0182(96)00130-7, 1997.

2.2 Export from one sediment trap sample at E1

A second sediment trap was moored at the station E1 (48°27'S - 72°11'E) at 1900 m over a depth of 2700 m (Fig. 2.1). The carousel rotation stopped after the first sampling cup. Therefore only one sample is available. It corresponds to a 15-days sampling period from the 23 October 2011 to the 6 November 2011. The flux collected by this sample equals $4.4\,\mathrm{mmol\,m^{-2}\,d^{-1}}$, which is three time higher than the highest resting spore driven flux observed at A3 ($1.5\,\mathrm{mmol\,m^{-2}\,d^{-1}}$). The BSi:POC ratio export ratio equals 2.8. The sample is characterized by the absence of faecal material and is very similar in appearance that the ones containing resting spores from the A3 sediment trap. Diatom community composition was studied using the same methodology than for the A3 sediment trap. Results are presented as pie chart in figure 2.2.
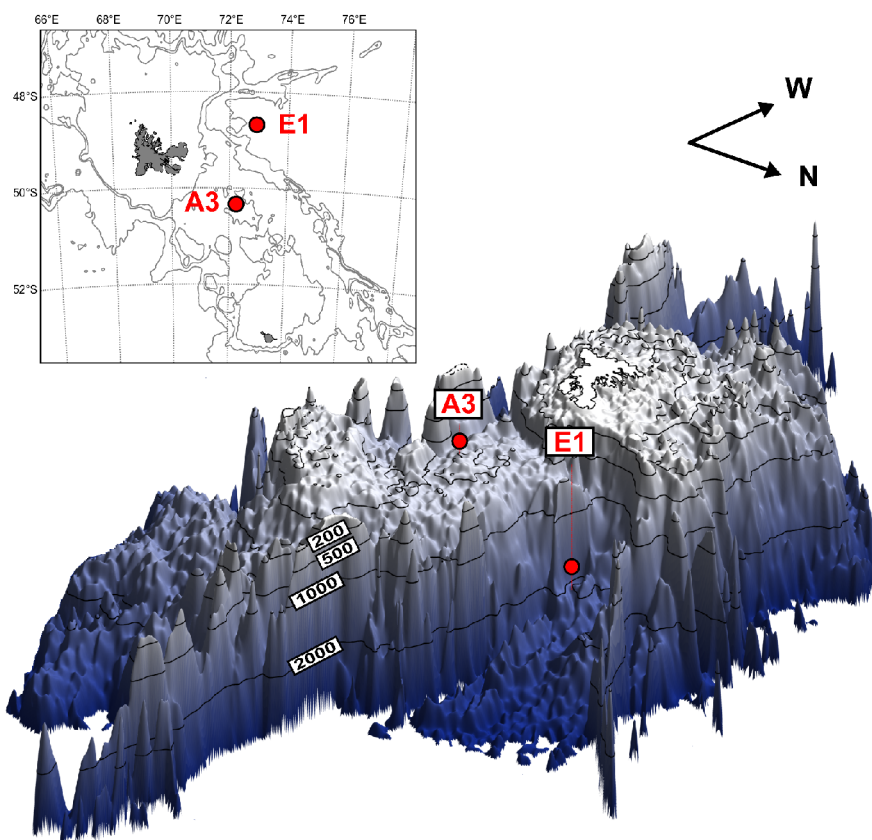

Figure 2.1: Location of the A3 and E1 stations where sediment traps have been deployed. The 3D view of the Kerguelen Plateau highlights the particular bathymetry around the E1 station with a semi-enclosed structure and an abrupt plateau flank.

The exported diatom community is characterized by a dominance of full *Chaetoceros Hyalochaete* resting spores (58 %) followed by Fragilariopsis (18 %) mainly exported as empty frustules. The total diatom cell flux equals $3.8 \times 10^8\,\mathrm{cell\,m^{-2}\,d^{-1}}$, a value again three times higher than the highest flux at A3 ($1.2 \times 10^8\,\mathrm{cell\,m^{-2}\,d^{-1}}$). When converted to carbon flux, the *Chaetoceros* resting spores (CRS) represent a flux of $4.2\,\mathrm{mmol\,m^{-2}\,d^{-1}}$.
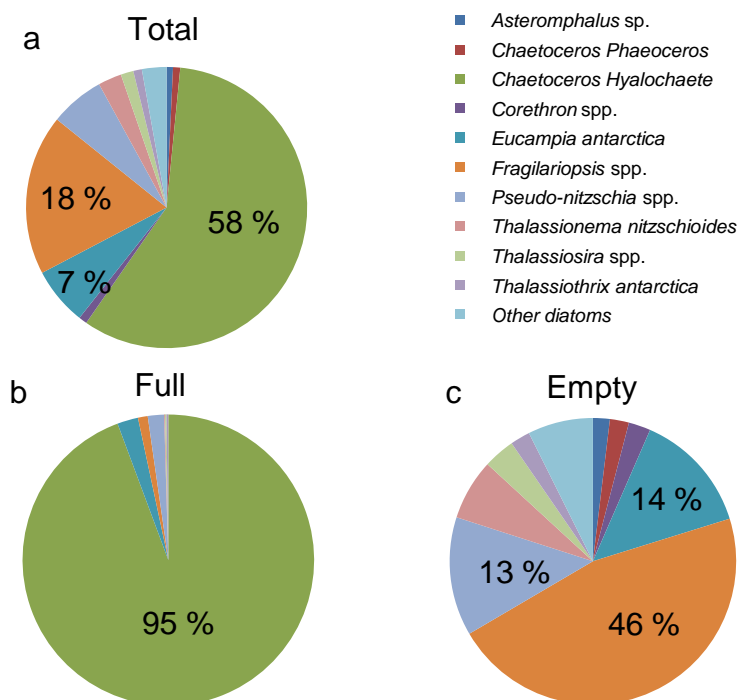
Figure 2.2: Composition of **a.** the total, **b.** full, and **c.** empty diatom community exported at E1 from the 23 October to the 6 November 2011.

This value is close to the $4.4\,\mathrm{mmol\,m^{-2}\,d^{-1}}$ measured. This suggests that CRS export is again dominating the carbon export, and gives confidence in the carbon content calculated for CRS at A3. However, species of the *Chaetoceros Hyalochaete* subgenus are a minor component of the mixed layer diatom community at this moment (Lasbleiz, pers. comm.), and no spores where observed at this site during the cruise (Lasbleiz, personal communication). The hypothesis of a resting spore formation at the E1 site is therefore not relevant. Given the abrupt flank of the Kerguelen Plateau, and the dominant eastward circulation, it is likely that the CRS found in the trap at E1 are coming from the shallow central plateau. It is difficult, however, to estimate if the spores found in the trap at E1 come from the mixed layer or from the accumulated sediments on the shallow plateau at A3. The rest of the diatom community is mainly composed of empty cells of *Fragilariopsis* (mostly *F. kerguelensis* and to a lesser extent *Eucampia antarctica*. The importance of empty diatom frutules leads to a high BSi:POC ratio (2.8), which is comparable with the spring values observed at A3 ($\sim$3) where empty cells dominate the export fluxes. The empty cells assemblage is comparable with the composition of surface sediments of the central plateau (Armand et al., 2008b) and supports the hypothesis of an eastward advection of surface sediments.

2.3   Export fluxes at KERFIX (article 3)

The first two **articles** described carbon export in the productive waters of the central Kerguelen Plateau (station A3). The low annual carbon export at $300\,m$ compared to the net community production raised questions about the efficiency of a naturally fertilized system in exporting carbon out of the mixed layer. A comparison with a less productive system is necessary to draw conclusion on the relationship between the biological pump efficiency and the natural iron-fertilization. In this manuscript, we present an unpublished dataset of biogechemical and diatom export flux collected during KERFIX project (1993-1995). The KERFIX (Kerguelen - point fixe, P.I. Catherine Jeandel) station was located in HNLC waters on the western flank of the Kerguelen Plateau. A sediment trap moored at $300\,m$ collected sinking material for nearly one year (mid February 1994 - January 1995).

At KERFIX, diatom enumeration from sediment trap samples was performed using a micropaleontological technique, preventing the quantification of the full- and empty diatom cells and therefore the calculation of diatom contribution to carbon export (see **Appendix 2**). However, hierarchical clustering based on the seasonality of diatom taxa reveals consistent diatom groups with specific export seasonality. We obtain a positive (or negative) association of certain diatom species with carbon export, consistent with their classification as "carbon (or silicon) sinkers" previously suggested at A3 and in other studies. The contribution of *Chaetoceros Hyalochaete* resting spore to total diatom community is low (5%). We explain this by their low contribution to mixed layer phytoplankton community previously described for these HNLC waters, together with $Si(OH)_4$ concentrations that do not reach limiting values in summer. Finally, the comparison of annual net community production (NCP) estimates and annual carbon export at $300\,m$ at KERFIX (HNLC) and A3 (productive) suggests that a low fraction of NCP is exported at both sites (1.7 and 1.5 %, respectively). Therefore natural iron fertilization increases primary production and export but does not increase PE_{eff}. A low export efficiency seems to be an intrinsic property of the Southern Ocean imposed by the food web structure rather than iron availability.

BSi analyses were performed by the author. POC analyses were previously analysed by J. C. Miquel, PIC analyses by F. Dehairs, and diatom identification and enumeration by J. J. Pichon.

Annual particulate matter and diatom export in an HNLC regime upstream of the Kerguelen Plateau in the Southern Ocean (station KERFIX)

M. Rembauville[1], I. Salter[1,2], F. Dehairs[3] , J-C. Miquel[4] and S. Blain[1].

[1]Sorbonne Universités, UPMC Univ Paris 06, CNRS, Laboratoire d'Océanographie Microbienne (LOMIC), Observatoire Océanologique, F-66650, Banyuls/mer, France

[2]Alfred Wegener Institute, Helmholtz Centre for Polar and Marine Research, Am Handelshafen 12, 27570 Bremerhaven, Germany

[3]Analytical, Environmental and Geo – Chemistry; Earth System Sciences Research Group, Vrije Universiteit Brussel, Belgium

[4]International Atomic Energy Agency, Environment Laboratories, 4, quai Antoine 1er, 98000 Monaco

Manuscript in preparation.

Abstract

Upper ocean plankton assemblages are known to influence the export of carbon and biominerals from the mixed layer. However, relationships between plankton community structure and the magnitude and stoichiometry of export remain poorly characterized. We present data on biogeochemical and diatom export fluxes from the annual deployment of a sediment trap in a High Nutrient, Low Chlorophyll (HNLC) area upstream of the Kerguelen Plateau (KERFIX station). The weak and tidal-driven circulation provided favorable conditions for a quantitative analysis of export processes. Particulate organic carbon (POC) fluxes were highest in spring and summer. Biogenic silica (BSi) fluxes displayed similar seasonal patterns, although BSi:POC ratios were elevated in winter. *Fragilariopsis kerguelensis* dominated the annual diatom export assemblage (59.8 %). A cluster comprised of *F. kerguelensis* and *Thalassionema nitzschioides* displayed highest relative abundances in winter and was negatively correlated to POC flux. In contrast, a second cluster composed notably of *Chaetoceros Hyalochaete* resting spores, *Eucampia antarctica* (vegetative), *Navicula directa* and *Thalassiothrix antarctica* was positively correlated with POC flux. Our results show that the differential role of certain diatom species for carbon export, previously identified from iron-fertilized productive areas, is also valid in HNLC regimes. A comparison with previously published work demonstrates that the fraction of seasonal net community production exported below the mixed layer was similarly low in HNLC (1.7 %) and iron-fertilized productive area (1.5 %). These findings suggest that natural iron fertilization in the Southern Ocean does not increase the efficiency of carbon export from the mixed layer.

Introduction

The Southern Ocean is the largest high nutrient, low chlorophyll (HNLC, Minas et al., 1986) area of the Global Ocean (Martin et al., 1990; Minas and Minas, 1992). In open ocean areas of the Southern Ocean HNLC regime, the low primary production is mainly attributable to iron limitation (Martin et al., 1990; de Baar et al., 1990, 1995). However, in the vicinity of subantarctic islands and plateau regions, iron inputs from shelf sediments and glacial melt represent a natural fertilization mechanism that can sustain long-lasting (several months) phytoplankton blooms (Blain et al., 2001, 2007; Pollard et al., 2007; Tarling et al., 2012). These blooms are associated with strong air to sea CO_2 fluxes (Jouandet et al., 2008; Merlivat et al., 2015). The fate of this carbon entering the ocean has been studied in relation to the physical and biogeochemical characteristics during multidisciplinary cruises such as the KEOPS1 and KEOPS2 cruises near the Kerguelen Islands (Blain et al., 2008a). In spring and summer, short term measurement of carbon export using the ^{234}Th proxy indicates a two-fold increase in carbon export in naturally fertilized water compared to HNLC waters (Blain et al., 2007; Savoye et al., 2008; Planchon et al., 2015). An annual deployment of a moored sediment trap just below the mixed layer at the productive station A3 (50°38 S – 72°02 E, Fig. 2.3) reported a low annual particulate organic carbon (POC) flux of $98.2\,\mathrm{mmol\,m^{-2}\,d^{-1}}$ (Rembauville et al., 2015b) with a major contribution (>60 %) of diatom resting spores to carbon export (Rembauville et al., 2015a).

Conceptual schemes linking diatom community structure to export fluxes have been proposed (Boyd and Newton, 1995, 1999; Quéguiner, 2013). Detailed descriptions of diatom export assemblages from iron fertilized blooms have highlighted the importance of diatom life cycle ecology for the regulation of carbon and silicon export (Smetacek et al., 2004, 2012; Salter et al., 2007, 2012; Assmy et al., 2013; Rembauville et al., 2015b). However, despite significant levels of biomass production, low values of POC export have raised questions concerning the efficiency of such systems to transfer carbon to depth through the biological pump (Lam and Bishop, 2007; Jacquet et al., 2011; Rembauville et al., 2015a). Indeed, the positive relationship between production and export efficiency observed in most of the global ocean (Laws et al., 2000, 2011) appears to be invalid in the Southern Ocean (Maiti et al., 2013). Furthermore, a recent global analysis comparing the fraction of microphytoplankton with POC flux attenuation shows that highest attenuation coefficients occur in high latitude regions (Guidi et al., 2015). These recent observations are consistent with the concept of high biomass, low export (HBLE) regimes identified in certain regions of the Southern Ocean (Lam and Bishop, 2007), and thereafter other locations of the global ocean (Lam et al., 2011). It has been suggested that in HBLE regimes, iron availability does not necessarily lead to higher carbon export but rather results in enhanced POC fragmentation, remineralization (Obernosterer et al., 2008), and/or transfer to higher trophic levels (Huntley et al., 1991). Certain regional studies support this

scenario. For example, in a naturally fertilized and diatom-dominated productive system downstream of South Georgia, highest zooplankton biomass is associated with the lowest particle export efficiency (Cavan et al., 2015). Although these snapshots offer intriguing insights into ecosystem function, comparative studies linking chemical fluxes to ecological vectors over seasonal and annual timescales remain necessary to compare export efficiencies of HNLC and productive systems.

KERFIX (Kerguelen fixed station) was a five year observation program that ran from 1991 to 1995 (Jeandel et al., 1998) and was established as a component of the international JGOFS program. The KERFIX station is located on the southwestern flank of the Kerguelen Plateau. A key objective of the program was to describe the factors responsible for low primary production in a region of the Antarctic Zone (AAZ) characterized by high macronutrient concentrations. The monthly sampling program included hydrological variables (Jeandel et al., 1998; Park et al., 1998), dissolved inorganic carbon and alkalinity (Louanchi et al., 2001) as well as biological (Fiala et al., 1998; Razouls et al., 1998; Kopczyńska et al., 1998) and geochemical parameters (Dehairs et al., 1996). These data were used to build and calibrate numerical models to explain how the diatom spring bloom contributed to intense silicon trapping despite an overall dominance of nanoplankton in these HNLC waters (Pondaven et al., 1998, 2000).

During the last two years of the KERFIX program, sediment traps were deployed below the mixed layer with the aim of providing a coupled description of production and export. Ternois et al. (1998) have reported particulate organic carbon and lipid export fluxes from a shallow sediment trap (175 m) over a 10-months time series (April 1993 to January 1994). A high contribution of fresh (i. e. labile) marine material was recorded during the summer and autumn months. During the winter months an unresolved and complex mixture characterized the organic composition of particles and was linked to zooplankton grazing. Despite these valuable insights, missing samples and location of the sediment trap within the winter mixed layer (182 m, Park et al., 1998) prevented a quantitative analysis of the export processes. A second sediment trap deployment was carried out the following year at a slightly deeper position of 280 m covering a nearly complete annual cycle. These samples provide a valuable opportunity to study the link between the diatom flux assemblages and the intensity and stoichiometry of export in iron-limited HNLC waters located 200 km upstream of the productive central Kerguelen Plateau.

In the present study, we report the biogeochemical fluxes (POC, particulate inorganic carbon - PIC, biogenic silica - BSi) and diatom community composition of material collected by a moored sediment trap deployed below the mixed layer in a low productivity area and covering an entire annual cycle. Our aims are (1) to assess the reliability of the collected fluxes by analyzing the physical environment of the deployment, (2) to investigate how diatom community composition influences the magnitude of the POC flux and
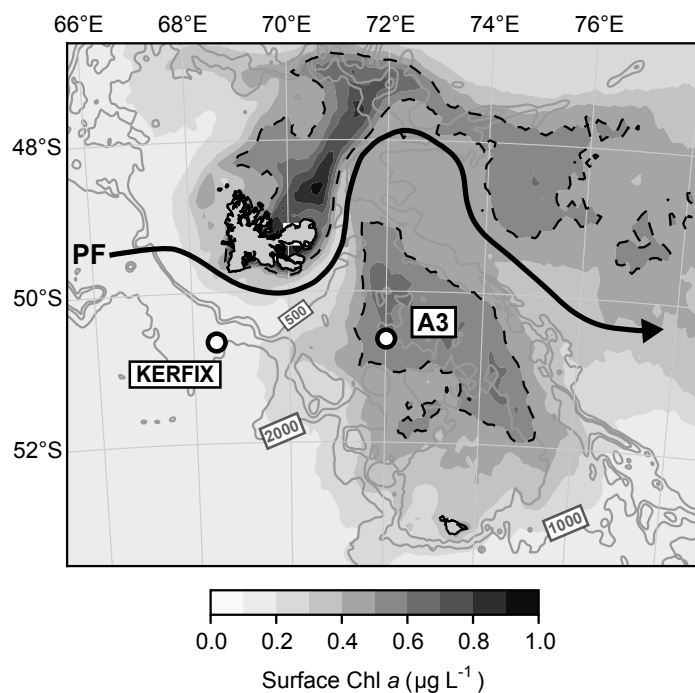
Figure 2.3: Map of the Kerguelen Plateau showing the location of the KERFIX station and A3 station where annual sediment trap deployments were carried out. Grey scale corresponds to a 15-year climatology (1997-2013) of satellite-derived chlorophyll a (Globcolour). The dashed line represents a $0.5\,\mu g\,L^{-1}$ value and highlights difference between the productive central Kerguelen Plateau and HNLC area to the West. The grey contour lines are the 500, 1000 and 2000 m isobaths, thick arrow denotes the approximate Polar Front (PF) location.

(3) compare the fluxes from this HNLC area with previously published sediment trap data from the productive central Kerguelen Plateau to examine the efficiency of both systems in exporting carbon from the mixed layer.

Material and methods

Sediment trap deployment and chemical analyses

As part of the KERFIX program (Jeandel et al., 1998), a sediment trap was moored at the HNLC station (50°40 S – 68°25 E), south of the Polar Front in the AAZ. The KERFIX station is characterized by low phytoplankton biomass (Fiala et al., 1998; Kopczyńska et al., 1998) in comparison to the productive central Kerguelen Plateau (Fig. 2.3). The sediment trap (Technicap PPS5, $1\,m^2$ collecting area) was moored at 280 m with a bottom depth of 2300 m. To prevent the intrusion of macrozooplankton and mesopelagic fish, the trap funnel was equipped with a baffle (8 mm diameter cells) with an aspect ratio (height/diameter) of 6.2. A current meter (Anderaa RCM7) was placed 20 m below the sediment trap and recorded current speed, pressure and temperature with a 2 h period. The sediment trap contained a 24-sample carousel. Sample cups (250 mL) were filled with a preservative solution of hyper saline seawater and 5 % formalin buffered to pH

8 with filtered (0.2 µm) sodium tetraborate. The collection period was from the 19th February 1994 to the 22nd January 1995 (total = 337 days). Sampling intervals were programmed to reflect anticipated flux patterns with the highest temporal resolution in spring and summer (7-10 days) and the lowest in winter (30 days). Following the recovery of the sediment trap, 50 mL of supernatant was withdrawn from the sample and 1 mL of buffered preservative solution was added. Samples were sieved through a 1.5 mm mesh and both fractions were examined under binoculars to manually remove swimmers (organisms actively entering the trap). After the swimmers were removed, both size fractions were combined and the samples were split into 1/8 aliquots using a Folsom splitter (McEwen et al., 1954) with a precision of <5 % (Sell and Evans, 1982).

Prior to chemical analysis, wet aliquots were centrifuged and rinsed with milli-Q water (10 minutes at 5000 rpm, three times) to remove excess salt and formalin. The supernatant was withdrawn and the resulting pellet freeze-dried (FTS systems DURA DRY). Mass flux was determined from the weight of the lyophilized pellet (Mettler-Toledo AE163 balance, 10 µg precision). For POC, of freeze-dried pellet (Sartorius M3P balance, 1 µg precision) was placed in silver cups and phosphoric acid (1 N) added in excess to dissolve $CaCO_3$. POC content was measured with a CHN analyzer (Heraeus CHN-O-Rapid) calibrated with acetanilide (Miquel et al., 1994). The precision derived from repeat measurements of carbon on the acetanilide standard was 1.4 %. For BSi, a kinetic method (DeMaster, 1981) was used as described in Mosseri et al. (2008). Briefly, of freeze-dried material was weighed and placed in centrifuge tubes with 40 mL of ultrapure NaOH (0.2 N). The samples were placed in a water bath at 95 °C and 200 µL of solution were removed after 1, 2, 3 and 4 h and placed into scintillation vials and made up to 10 mL with milli-Q water. Silicic acid concentrations were determined colorimetrically on a Skalar autoanalyser following Aminot and Kerouel (2007). The BSi content was determined by fitting a linear regression to silicic acid concentration as a function of extraction time. The intercept of this relationship is taken as BSi content without interference of silicon leaching from lithogenic material (DeMaster, 1981). Particulate inorganic carbon (PIC) was determined from direct measurement of calcium (Ca). 5 mg of freeze-dried material was mineralized in Teflon vials by adding 0.5 mL of 65 % HNO_3 and 0.5 mL of 40 % HF. Samples were ultrasonicated and dried at 40 °C overnight. This residue was dissolved in 10 mL of 0.1 N HNO_3 and the calcium concentrations determined by coupled plasma-optical emission spectrometry (ICP-OES, HORIBA Jobin Yvon 48 and 38). The flux for the unsampled month (February 1995) was estimated by calculating the mean flux of the time series to compute the annually integrated POC, PIC and BSi fluxes.

Slides preparation and diatom taxonomy

Samples for diatom taxonomy were prepared using a micropaleontological oxidative method as previously described in Romero et al. (1999). Briefly, a 1/8 wet aliquot was placed

in a beaker and oxidized with potassium permanganate ($20 \, \text{mL}$, $65 \, \text{g} \, \text{L}^{-1}$), hydrochloric acid ($50 \, \text{mL}$, 37 %) and hydrogen peroxide ($40 \, \text{mL}$, H_2O_2 35 %) at $95 \, °\text{C}$. Samples were then rinsed with milli-Q water and centrifugated several times to raise the pH to the one of the milli-Q water. Three slides were prepared per sample using a random settling method (Bárcena and Abrantes, 1998). Slides were observed under an inverted microscope with phase contrast (Olympus BH2) at 400 and 1000 x magnification. A minimum of 400 valves were enumerated per sample following Schrader and Gersonde (1978) recommandations. Diatoms were identified to the species level following (Hasle and Syvertsen, 1997). Diatom counts were not possible in the last two sample cups (January 1995) due to the very low quantity of material. Contrary to the direct observation of untreated samples (Salter et al., 2007, 2012; Rembauville et al., 2015b), the micropaleontological technique prevents the distinction between full or empty cells comprising the export assemblage. The micropaleontological method was originally developed for samples originating from sediment cores. The oxidation and multiple centrifugation steps remove organic cell contents and separate diatom cells into valves. Consequently the contribution of individual diatom species to total POC export fluxes cannot be quantified. However the absence of organic material allows a detailed observation of frustule characteristics that enables precise and detailed taxonomic analyses of the diatom community. The biogeochemical and diatom taxonomy data are accessible at http://www.obs-vlfr.fr/cd_rom_dmtt/OTHER/KERFIX/trapdata/.

Numerical and statistical analyses

To identify the major periods of current speed variations, current speed data was analyzed using fast Fourier transform (FFT). The resulting power spectrum was compared to a red noise, a theoretical signal in which the amplitude decreases with increasing frequency. The red noise was considered as a null hypothesis and scaled to the power spectrum to identify periods that differ significantly from a random distribution (Schulz and Mudelsee, 2002).

To categorize diatom groups that were exported with similar seasonality, a clustering analysis was performed on the relative abundance of diatom taxa within each sample cup. The Euclidian distance was calculated between taxa and the distance matrix was used to build a dendrogram based on Ward's agglomerative method (Ward, 1963). The relative contribution of each cluster to the total diatom assemblage was then calculated by summing the contribution of all species belonging to one cluster.

Results

Hydrological context

Hydrological properties recorded by the instruments moored together with the sediment trap are shown in Figure 2.4. The trap depth gradually decreased by 4 meter (284 m to 280
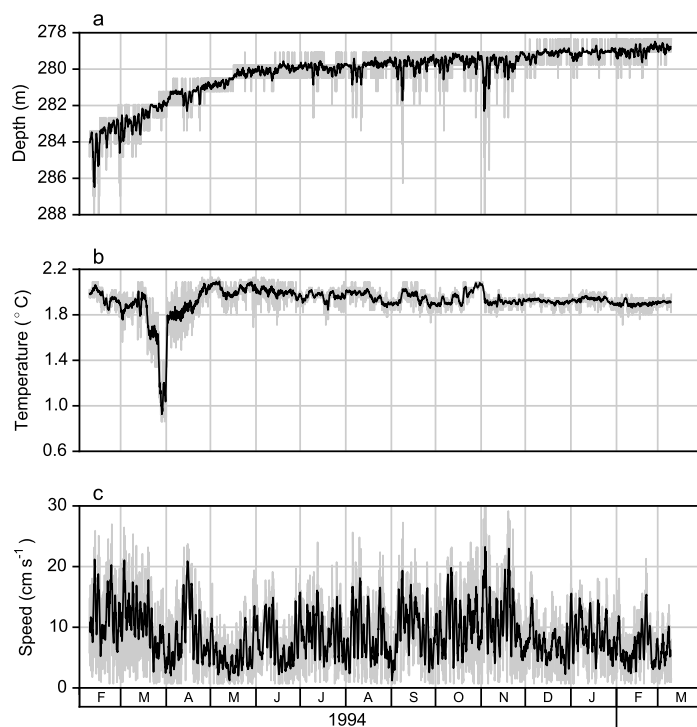
Figure 2.4: Hydrological properties recorded by the moored instruments deployed on the sediment trap mooring: **a.** Trap depth variation, **b.** temperature and **c.** current speed. Grey lines are raw data, black lines are filtered data using a moving average with a 24 h window

m) from February to June 1994 and remained at 280 m until the recovery. No strong depth oscillation was observed except during two short deepening events (4-6 m amplitude) that occurred in February and September 1994. Temperature remained mostly constant between 1.8 and 2.2 °C except during one short event from 20 to 30 March 1994 where temperature decreased to 1 °C. This event was not associated with any particular depth or current speed variation. Current speed ranged from <1 to 30 cm s^{-1} and displayed a highly variable signal over short time scales. There were no obvious seasonal patterns in current speed distribution and 74 % of the current speed data was <12 cm s^{-1}.

The progressive vector diagram displayed numerous tidal ellipses over short time scales (hours to days, Fig. 2.5a). The integrated displacement over one year corresponds to a 450 km northward advection. Higher frequencies were observed for northwestward flow when current speeds exceeded 20 cm s^{-1} (2.5b). Conversely, the southwestward flow displayed lower frequencies and was mainly characterized by speeds <10 cm s^{-1}. Six significant peaks corresponding to tidal components were observed (2.5c). Short time scale peaks (6.2 h and 6.8 h period) corresponded to a combination of tidal components of longer periods. The moon 2 (M2, 12.4 h period) component was present, and long-term components (3 d and 14 d period) were also observed.

Biogeochemical fluxes
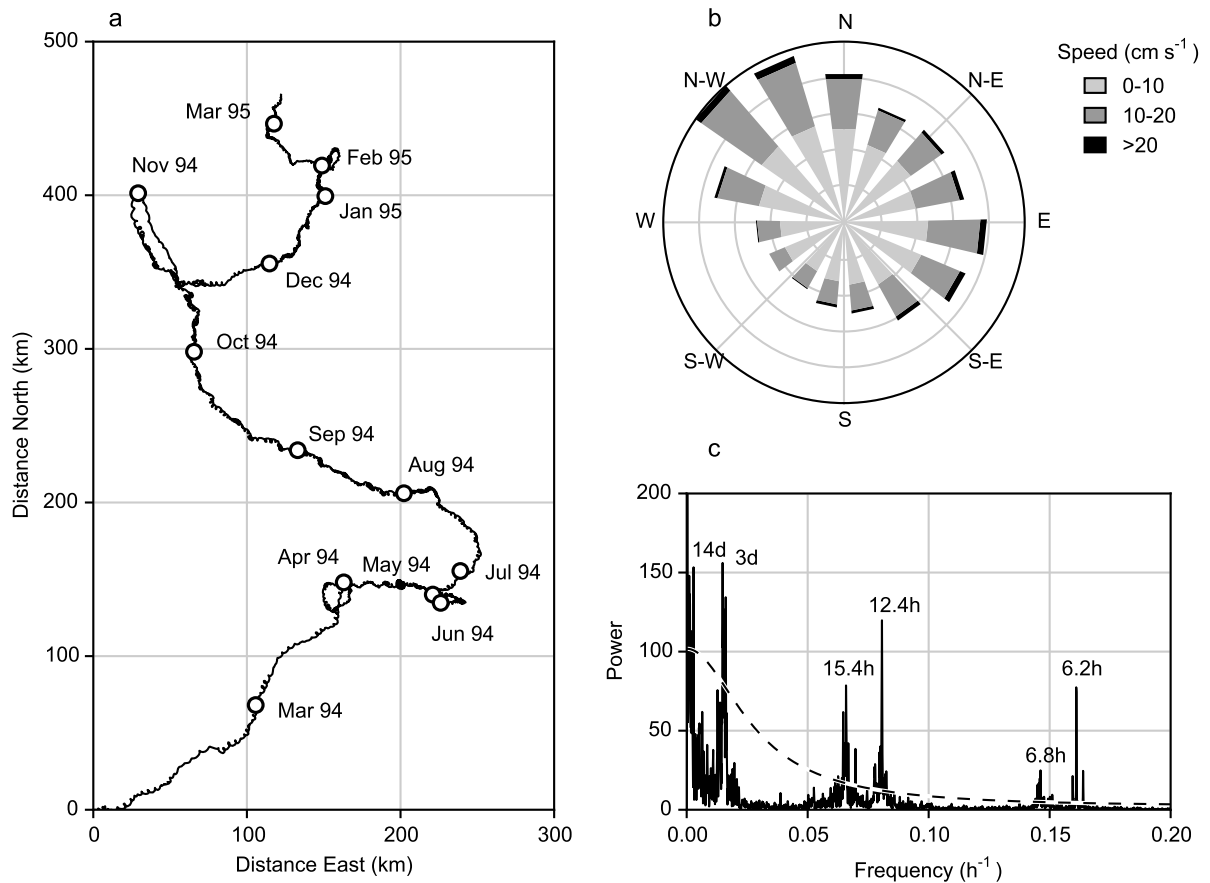
Figure 2.5: Hydrodynamics at the sediment trap deployment location. **a.** Progressive vector diagram showing water displacement integrated over the sediment trap deployment period. **b.** Wind rose plot of current speed and direction. Grey circles are the probability distribution drawn every 2 % from 0 to 10 %. **c.** Power spectrum resulting from the spectral analysis of the current speed. Dotted line represents 99 % probability threshold for a random red noise distribution.

Cup	Opening	Closing	Mass flux $(\mathrm{mg\,m^{-2}\,d^{-1}})$	POC	BSi $(\mathrm{\mu mol\,m^{-2}\,d^{-1}})$	PIC	Total valves $(10^6 \mathrm{\ valve\,m^{-2}\,d^{-1}})$
1	19/02/94	28/02/94	207	930	2144	67	131
2	28/02/94	10/03/94	132	604	1214	25	64
3	10/03/94	20/03/94	113	367	1026	14	68
4	20/03/94	31/03/94	64	241	589	15	39
5	31/03/94	30/04/94	74	262	710	18	42
6	30/04/94	31/05/94	69	176	665	1	29
7	31/05/94	30/06/94	25	74	264	1	16
8	30/06/94	31/07/94	6	29	40	2	2
9	31/07/94	31/08/94	2	14	10	1	1
10	31/08/94	30/09/94	2	22	8	1	1
11	30/09/94	11/10/94	2	29	9	4	1
12	11/10/94	21/10/94	2	19	4	0	1
13	21/10/94	31/10/94	2	25	3	0	0
14	31/10/94	08/11/94	2	16	2	1	2
15	08/11/94	16/11/94	6	39	20	9	1
16	16/11/94	23/11/94	7	38	13	76	0
17	23/11/94	30/11/94	7	45	7	57	1
18	30/11/94	08/12/94	12	136	45	112	2
19	08/12/94	16/12/94	15	116	99	46	3
20	16/12/94	24/12/94	23	122	182	50	21
21	24/12/94	31/12/94	29	129	229	90	32
22	31/12/94	08/01/95	42	233	343	165	6

Table 2.1: Sampling cups collecting period, biogeochemical fluxes and total diatom valves flux from the KERFIX sediment trap.

Chlorophyll a concentrations started to increase in October 1993 from $0.2\,\mathrm{\mu g\,L^{-1}}$ to reach $1\,\mathrm{\mu g\,L^{-1}}$ in mid December 1993 when MLD was the shallowest (60 m, Fig. 2.6a). A significant proportion of the phytoplankton biomass (70 %) was located below the MLD. The MLD gradually decreased to $185\,\mathrm{m}$ in August 1994 concomitantly with a decrease in chlorophyll a to $0.2\,\mathrm{\mu g\,L^{-1}}$. A second spring bloom occurred in November 1994 reaching a maximum of $1.2\,\mathrm{\mu g\,L^{-1}}$ in December and was also associated with a shoaling of the MLD.

POC flux was highest in late summer (February 1994) following the sediment trap deployment ($0.9\,\mathrm{mmol\,m^{-2}\,d^{-1}}$) and decreased to 0.10 - $0.25\,\mathrm{mmol\,m^{-2}\,d^{-1}}$ in autumn (Table 2.3, Fig. 2.6b). Winter fluxes were negligible ($<0.1\,\mathrm{mmol\,m^{-2}\,d^{-1}}$ from July to October 1994). A small increase in POC flux of up to $0.25\,\mathrm{mmol\,m^{-2}\,d^{-1}}$ occurred concomitantly with the phytoplankton bloom in November-December 1994. Annual POC export flux was estimated at $51.6\,\mathrm{mmol\,m^{-2}\,yr^{-1}}$. PIC fluxes were low in late summer (25 - $75\,\mathrm{\mu mol\,m^{-2}\,d^{-1}}$, Table 2.3, Fig. 2.6b), negligible in winter, and increased to 50 – $160\,\mathrm{\mu mol\,m^{-2}\,d^{-1}}$ during the spring bloom (November-December 1994). The annual PIC export flux was estimated at $7.7\,\mathrm{mmol\,m^{-2}\,yr^{-1}}$.

BSi flux showed a similar seasonal pattern to POC with highest fluxes in late summer (1 - $2\,\mathrm{mmol\,m^{-2}\,d^{-1}}$ in February – March 1994), moderate fluxes in autumn ($\sim0.5\,\mathrm{mmol\,m^{-2}\,d^{-1}}$), and negligible fluxes in winter (Fig. 2.6c). A small but noticeable increase was observed
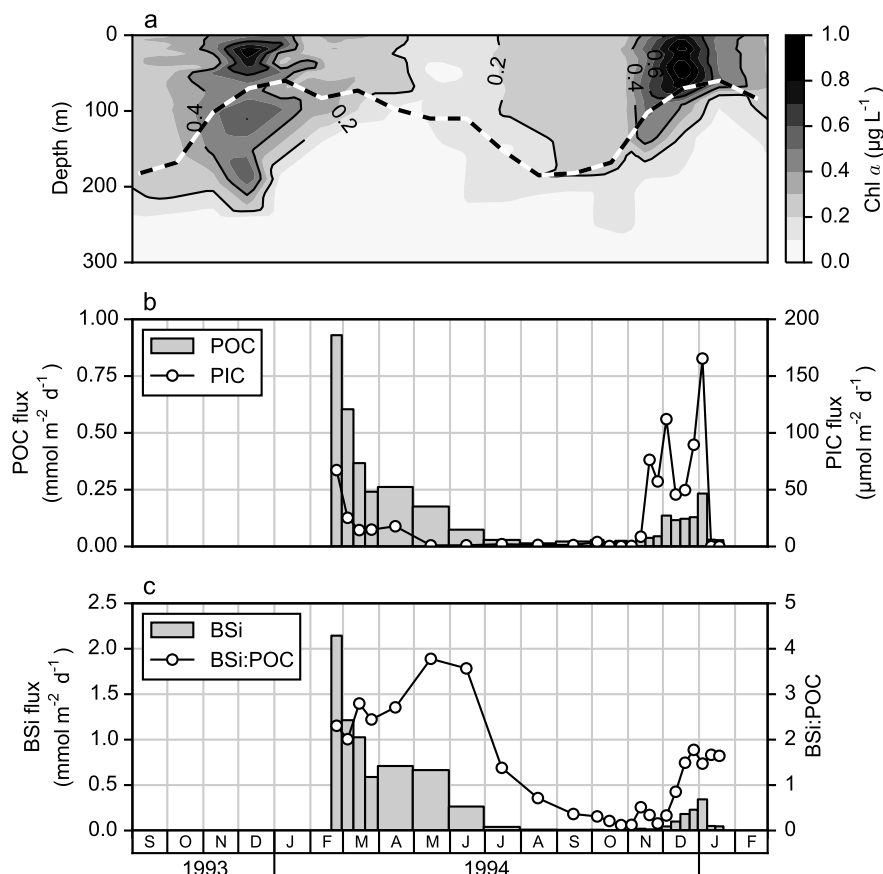
Figure 2.6: Phytoplankton biomass and particulate export. **a.** Chlorophyll *a* concentration in the upper 300 m at the KERFIX station (monthly measurements, redrawn from Fiala et al., 1998). Dotted line denotes the mixed layer depth from Park et al. (1998). **b.** Particulate organic carbon (POC) and inorganic carbon (PIC) fluxes recorded by the sediment trap at 280 m. **c.** Biogenic silica (BSi) and BSi:POC molar ratio in the exported particles.

during the spring bloom (up to $0.4\,\mathrm{mmol\,m^{-2}\,d^{-1}}$). The BSi:POC molar ratio displayed a clear seasonal pattern with a value close to 2 in late summer, increasing to 3.9 in autumn. Winter values were <0.5, increasing to ~ 1.8 during the spring bloom. The annually integrated BSi:POC ratio was 2.2.

Diatom fluxes

The seasonal pattern of total diatom valve flux mirrored that of POC with the highest flux observed in the first sample cup (1.3×10^8 valve $\mathrm{m^{-2}\,d^{-1}}$, Fig. 2.7a), decreasing gradually in autumn to reach very low values in winter (1×10^6 valve $\mathrm{m^{-2}\,d^{-1}}$). Total diatom valve flux increased again during the spring bloom to 3.5×10^7 valve $\mathrm{m^{-2}\,d^{-1}}$.

Fragilariopsis kerguelensis dominated the diatom export assemblage at an annual scale (59.8 %), with the highest relative contribution in winter ($> 70\,\%$ of the diatom assemblage in August). This species presented a notable export peak in summer (6×10^7 valve $\mathrm{m^{-2}\,d^{-1}}$, Fig. 2.7b) and lower values during spring (1×10^7 valve $\mathrm{m^{-2}\,d^{-1}}$). A similar pattern
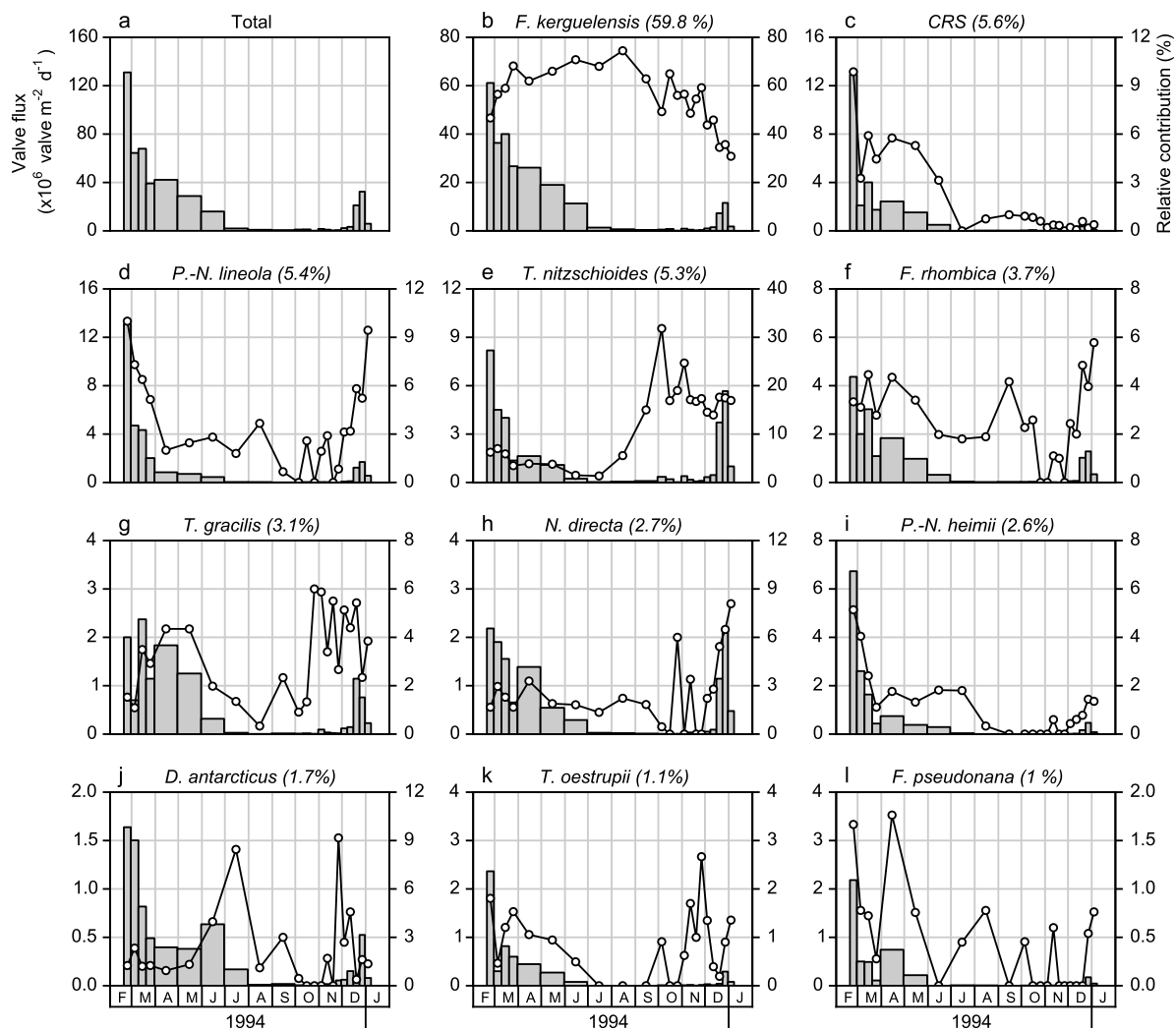
Figure 2.7: Diatom export fluxes measured in the sediment trap. **a.** Total diatom valve flux and **b.-l.** diatom valve flux for species accounting for >1 % of the annually-integrated diatom valve flux (grey bars). Numbers in bracket refer to the relative contribution of each species to total diatom valves following integration over the deployment period. The relative contribution of each species to the diatom assemblage is shown by dots and lines.

of preferential summer export peaks was also evident for the following diatom species: *Chaetoceros Hyalochaete* resting spores (10 % of the diatom assemblage in February), *Pseudo-nitzschia lineola* (10 %), *Pseudo-nitzschia heimii* (5 %), *Fragilariopsis rhombica* (3 %), *Thalassiosira oestrupii* (2 %) and *Fragilariopsis pseudonana* (1.7 %). In contrast, other diatom species displayed export peaks during both spring and summer such as *Thalassionema nitzschiodes* (16 % of the diatom community in November), *Thalassiosira gracilis* (4 %), *Navicula directa* (6 %) and *Dactyliosolen antarcticus* (9 %).

Three distinct clusters were identified based on the relative abundance of diatoms in each sediment trap sample cup (Fig. 2.8). Cluster A was comprised of the dominant *F. kerguelensis* and *T. nitzschioides*. Cluster B primarily contained diatoms that had a relatively minor contribution to the integrated annual export assemblage. Notably large diatoms (>100 µm) such as *Corethron criophilum*, *Rhizosolenia hebetata* f. *hebetata*, *R. antennata* f. *semispina*, *Coscinodiscus curvatulus* and *Proboscia inermis* belonged to this cluster. Finally, cluster C was comprised of abundant species (2-5 % of the exported diatom community) such as *Chaetoceros Hyalochaete* resting spores, *Pseudo-nitzschia* species, *N. directa* and the giant diatom *Thalassiothrix antarctica*.

Cluster A was the dominant component throughout the year (Fig. 2.9a). Its relative abundance increased from 50 % in late summer (February 1994) to 80 % in winter (August 1994) when the total diatom flux was lowest (Fig. 2.7a). In spring, the relative contribution of cluster A decreased to 50 % in summer (January 1995). Cluster B exhibited the lowest contribution with values <5 % in winter doubling to 10 % in spring. Cluster C had lowest contributions of <25 % in winter with a marked increase of up to 50 % in spring (November 1994 to January 1995). The total relative abundance of diatoms in clusters A and C exhibited a significant correlation with POC flux (Pearson test on log-transformed data, p <0.05, Fig. 2.9b). Regression analysis indicated a positive relationship in the case of cluster C and a negative one for cluster A.

Discussion

Hydrological context and sediment trap record reliability

The mean temperature of ~2 ° observed over the course of the year is consistent with the temperature of water masses just below the winter water (WW) reported at the same station (Park et al., 1998). The abrupt decrease in temperature to 1 ° at the end of March is unusual considering the lowest recorded temperature of WW is 1.8 ° (Park et al., 1998). Nevertheless, Park et al. (1998) reported the largest steric height negative anomaly during the same period (February - March 1994). Such a major and abrupt change in water mass circulation could entrain very cold WW northward and explain the observed temperature decrease. Although the exact reason for this temperature change remains unresolved, it did not affect the sediment trap depth and was not associated with any change in current speed. Therefore it seems unlikely that it significantly impacted the sediment
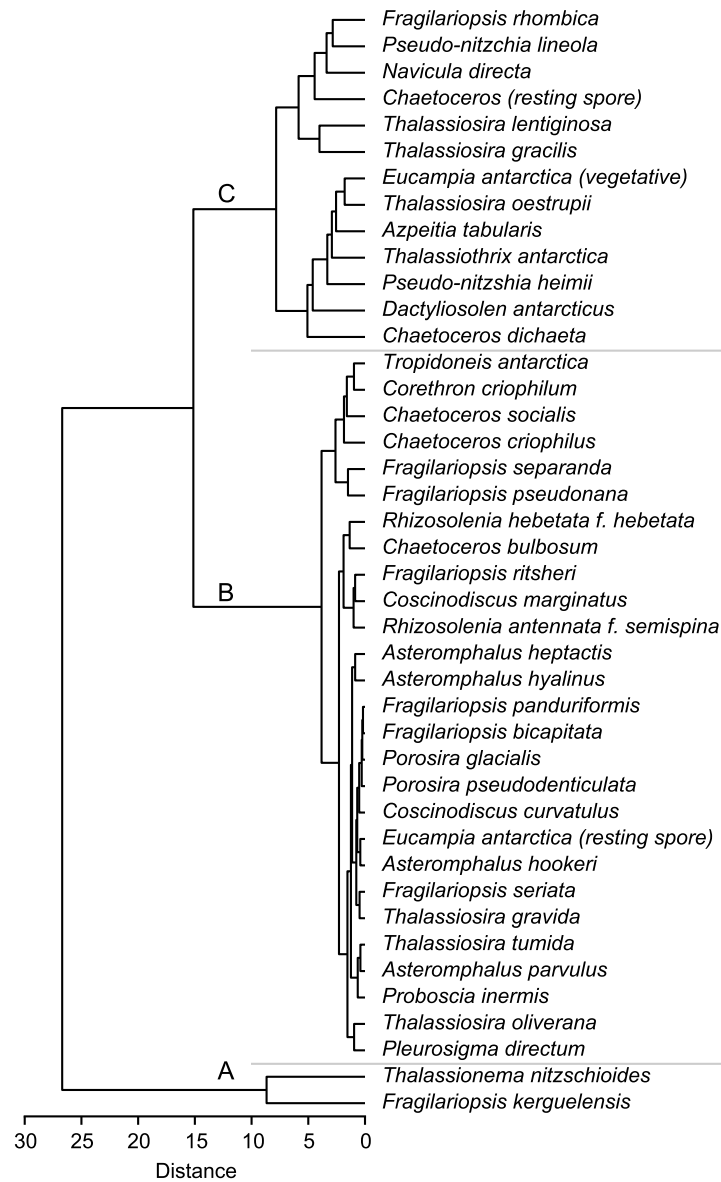
Figure 2.8: Dendrogram resulting from the clustering of diatom species based on the relative abundance in each sediment trap cup (Euclidian distance, Ward aggregation method). Clusters A, B and C were defined using the largest distance after the first node of the dendrogram.

trap collection efficiency.

The KERFIX sediment trap deployment location was characterized by a major north-westward flow. As the Antarctic Circumpolar Current (ACC) encounters the Kerguelen Plateau, most of the surface water continues an eastward flow over the central plateau, although deeper currents appear to exhibit a northward inflection when they meet the western flank of the plateau at the KERFIX location (Park et al., 2008b). The pseudo-Lagrangian view of the progressive vector diagram is therefore consistent with the current understanding of circulation in the study area. The 450 km northward displacement in one year corresponds to advection with a mean speed of $1.4\,\mathrm{cm\,s^{-1}}$. This is comparable to the range of sinking speeds reported for marine particles in the region of 0.01 - $1.1\,\mathrm{cm\,s^{-1}}$ (Laurenceau-Cornec et al., 2015b), and thus advection should not have transported particles far away from the overlying surface before they reach the shallow trap depth (280 m).

Current speed variations were associated with tidal components (Fig. 2.5c). A similar finding was found on the central Kerguelen Plateau, with a major contribution of the M2 tidal component (Rembauville et al., 2015a). At KERFIX, the tidal components are more diverse and contain components of diurnal and semi-diurnal waves. The additional complexity may arise from the proximity of the plateau flank where most of the tidal energy is dissipated (Maraldi et al., 2011). Overall, the observations are entirely consistent with short-term observations of tidal-driven water mass displacement (Park et al., 2008a) and emphasize the importance of tides for circulation around the Kerguelen Plateau.

It is widely acknowledged that shallow sediment trap deployments are prone to hydrodynamic artifacts (Gardner, 1980; Buesseler et al., 2007). A current speed of $12\,\mathrm{cm\,s^{-1}}$ is often invoked as an upper limit for the reliability of moored sediment trap (Baker et al., 1988). In the present deployment 74 % of the current speed data observed is below this threshold. The circulation patterns are mainly tidal-driven and advection is low over long time scales. These data would suggest that the sediment trap was not subject to major hydrodynamic biases beyond the normal conditions for shallow deployments (Gardner, 1980; Baker et al., 1988). The sediment trap used in the present study was equipped with an 8 mm baffle (aspect ratio of the baffle: 6.2). This design is typically considered to prevent the intrusion of large organisms (e.g. fishes) into sediment traps, but has no effect on smaller swimmers intrusion (Nodder and Alexander, 1999). However, the low aspect ratio (1.7) and conical funnel shape of the PPS5 could render this design more susceptible to hydrodynamic and biological artifacts(Hawley, 1988; Buesseler et al., 2007). Unfortunately with the present dataset we cannot explicitly address trapping efficiencies as has been carried out in previous studies (Coppola et al., 2002; Buesseler et al., 2010).

Export seasonality and diatom export assemblage

The annual record presented in this study covers a period from summer 1994 to summer
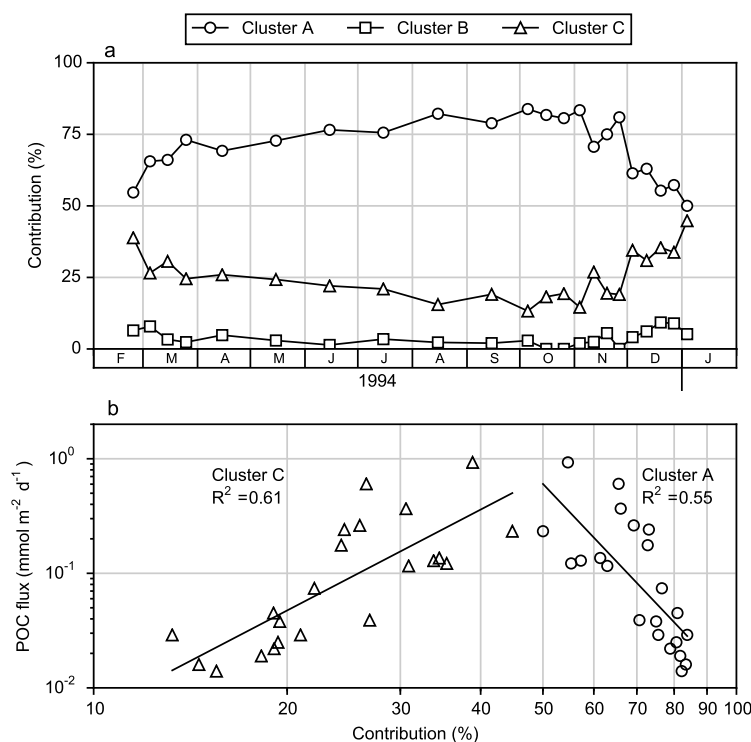
Figure 2.9: Seasonality of diatom clusters and their relationship with POC flux. **a.** Seasonal variation of the relative abundance of each diatom cluster defined from the dendrogram. **b.** Relationship between the relative abundance of cluster A and C and POC flux. Regressions are performed on log-transformed data.

1995 and is therefore considered representative of the main seasonal transitions at the KERFIX site. Both POC and BSi fluxes display clear late-summer maxima. It seems probable that any export production originating from the 1993 phytoplankton bloom would have occurred during the summer prior to the sediment trap deployment. However, the export in spring that occurs concomitantly with the 1994 bloom appears moderate and the bloom dynamics are similar in 1993 and 1994. The timing of the export in spring 1994 is closely associated to the development of the spring phytoplankton bloom. The tight temporal coupling between production and export observed at the HNLC KERFIX station is in stark contrast with the one month lag observed at the productive A3 station of the central Kerguelen Plateau (Rembauville et al., 2015a). We previously attributed the temporal lag at A3 to the formation and export of diatom resting spores that dominate POC flux (60-80 %) during export events that occur 1 month later than surface chlorophyll *a* peaks (Rembauville et al., 2015b). The tight coupling between production and export at the KERFIX site suggests export vectors aside from diatom spore formation may be important in a HNLC regime.

Chaetoceros Hyalochaete resting spores represent a minor contribution to the exported diatom community at the KERFIX station (5.6 %), whereas they were the dominant component (70 %) at the productive A3 station (Rembauville et al., 2015b). These results are

consistent with the observation of a strict dominance of *Eucampia antarctica* var. *antarctica* resting spores to the diatom export assemblage in the productive stations downstream os the Crozet Islands and negligible contribution in the upstream HNLC area (Salter et al., 2012). The vegetative stages of *Chaetoceros Hyalochaete* are a minor fraction of the mixed layer diatom assemblage at KERFIX (Fiala et al., 1998). Additionally, it was hypothesized that a strong decrease in silicic acid concentration in late summer in naturally fertilized and productive areas could trigger the diatom resting spore formation (Salter et al., 2012; Rembauville et al., 2015b). The silicic acid concentration in the mixed layer never reaches values lower than $9\,\mu mol\,L^{-1}$ in summer at KERFIX (Jeandel et al., 1998) whereas it is almost depleted ($\sim$$1\,\mu mol\,L^{-1}$) over the central Kerguelen Plateau (Mosseri et al., 2008). Very similar observations were made at Crozet with the absence of spore-forming diatoms in the HNLC waters together with much lower silicic acid utilization in summer when compared to iron-fertilized waters (Moore et al., 2007; Salter et al., 2007).

The exported diatom assemblage at the KERFIX station was strictly dominated by *F. kerguelensis* (59.8 %), consistent with its dominance of the mixed layer diatom assemblage (Fiala et al., 1998; Kopczyńska et al., 1998). *Fragilariopsis* species typically dominate diatom export assemblages in the vast HNLC areas of the Southern Ocean (Romero and Armand, 2010; Grigorov et al., 2014; Rigual-Hernández et al., 2015b,a), and it is the most abundant species in the silica ooze under the ACC (Zielinski and Gersonde, 1997). Its strong and thick frustules, together with its ability to form long chains, might protect this species from grazing pressure in the AAZ and contribute towards its ecological success (Hamm et al., 2003; Smetacek et al., 2004).

Clustering analysis delineates groups of diatom species that were exported with a specific seasonality. For example *F. kerguelensis* and *T. nitzschioides* (cluster A) were present in export assemblages throughout the year but displayed a higher relative contribution to fluxes in winter. The significant negative correlation between the relative abundance of cluster A and POC flux suggests a minor contribution towards carbon export. In support of this, *Fragilariopsis* species are frequently observed as empty frustules in both natural and artificial fertilization experiments (Smetacek et al., 2004; Salter et al., 2012; Assmy et al., 2013). A detailed quantitative analysis of exported diatom assemblages from the productive waters of the central Kerguelen Plateau shows empty cells of *F. kerguelensis* and *T. nitzschioides* dominating spring export fluxes coinciding with the lowest POC flux (Rembauville et al., 2015b). However, at KERFIX, there was no significant relationship between the seasonal dynamics of cluster A and the BSi:POC ratio suggesting that *F. kerguelensis* flux dynamics did not exert a first-order control on Si-C export stoichiometry. Other diatom species with specific empty:full cell ratio may impact BSi:POC export ratio (Rembauville et al., 2015b), but this cannot be addressed with the present dataset. Contrary to the diatom-dominated, productive central Kerguelen Plateau, the phytoplankton community at KERFIX is dominated by small flagellates (2-10 μm) comprising Prasino-

phyceae and Cryptophyceae and showing the highest relative abundance in winter (Fiala et al., 1998; Kopczyńska et al., 1998). Therefore, contrary to a diatom-dominated system, the seasonality of the BSi:POC ratio at KERFIX is likely to be influenced by processes that are not quantified here (e. g. faecal pellet and/or non-diatom phytoplankton export).

The total relative abundance of cluster C was positively correlated to POC flux. This cluster was comprised of *Chaetoceros Hyalochate* resting spores (CRS), *Chaetoceros dichaeta*, *E. antarctica*, *N. directa* as well as the very large species *T. antarctica*. All these species were found to be preferentially exported as full cells in the productive area of the Kerguelen Plateau (Rembauville et al., 2015b). The positive correlation between this diatom group and POC flux at the KERFIX site indicates they play a similarly important role as a carbon export vector in HNLC-like waters. Consistent with that, several species of cluster C (*Pseudo-nitzschia lineola*, *T. gracilis*, *N directa*), were also positively associated with POC flux in a deeper (800 m) sediment trap in the Polar Frontal Zone south of Tasmania (Rigual-Hernández et al., 2015b). However, a precise quantification of the fraction of full and empty cells (Assmy et al., 2013), together with the contribution of non-diatom cells and faecal pellet material is necessary to fully quantify their relative contributions to POC flux (Rembauville et al., 2015b).

Calcifying planktonic organisms were not quantified in the export assemblages as part of the present study. Nevertheless, the seasonality of the PIC signal can be compared with the abundance of calcifying communities from the mixed layer time series. The marked increase in coccolithophore biomass in the mixed layer (Fiala et al., 1998; Kopczyńska et al., 1998) occurs concomitantly with the highest PIC flux observed in the sediment trap (from November 1994 to January 1995). Pteropods are a minor component (<7 %) of the zooplankton assemblage at KERFIX in summer (Carlotti et al., 2008) and low foraminifera abundances are typical for the AAZ (Mortyn and Charles, 2003; Bergami et al., 2009; Lombard et al., 2011). Coccolithophore-derived $CaCO_3$ has been recently shown to dominate (85 %) PIC export at the productive A3 station (Rembauville et al., 2016b). The co-occurrence of enhanced coccolithopore abundance in the mixed layer and PIC export in the sediment trap implies a significant contribution of this calcifying group to PIC export also occurs under HNLC conditions, although a more detailed analysis is required to confirm this hypothesis.

Comparison with the iron-fertilized productive central Kerguelen Plateau
An upper limit of $1\,\mu g\,L^{-1}$ for chlorophyll *a* concentration has been suggested as a threshold to define HNLC conditions (Tyrrell et al., 2005). Under this definition, the KERFIX station lies in the upper limit of what is considered as HNLC conditions. We carried out a comparison of water column and sediment trap data from the KERFIX (HNLC) and nearby A3 site (productive) in an attempt to elucidate the impact of iron availability on production and export processes around the Kerguelen Plateau (Table 2.2).

Site	KERFIX	A3
	(50°40' S - 68°25' E)	(50°38' S - 72°0.2' E)
Trap depth (m)	280	289
Seasonal net community production ($mol\,m^{-2}$)	3.1 ± 0.9[a]	6.6 ± 2.2[b]
Maximum net primary production ($mmol\,m^{-2}\,d^{-1}$)	42[c]	180[d]
Annual POC export ($mmol\,m^{-2}\,yr^{-1}$)	51.6	98.2[e]
Maximum POC export ($mmol\,m^{-2}\,d^{-1}$)	0.9	1.5[e]
Annual BSi:POC (mol:mol)	2.3	1.2[f]
Annual PIC export ($mmol\,m^{-2}\,yr^{-1}$)	7.7	6.6[g]
Major diatom	*Fragilariopsis kerguelensis* (59.8 %)	*Chaetoceros Hyalochaete* resting spore (80 %)[f]

[a]Louanchi et al. (2001)
[b]Jouandet et al. (2008)
[c]Pondaven et al. (2000)
[d]Cavagna et al. (2015)
[e]Rembauville et al. (2015a)
[f]Rembauville et al. (2015b)
[g]Rembauville et al. (2016b)

Table 2.2: Comparison of production and export terms between the HNLC station KER-FIX (this study) and the iron-fertilized productive site A3.

One major difference we observed between the two sites is a two-fold higher annual BSi:POC ratio under HNLC conditions. This is remarkably similar to the 2-3.5 fold difference in BSi:POC ratio found in deep sediment traps (>2000 m) between HNLC and iron-fertilized productive waters around the Crozet Plateau (Salter et al., 2012). At KERFIX the maximum fluxes of *F. kerguelensis* are one order of magnitude higher than at A3 and they dominate the diatom assemblage (60 %) at this HNLC site compared to a lower contribution (10 %) at A3 (Rembauville et al., 2015b). *F. kerguelensis* is a strongly silicified species (Smetacek et al., 2004; Assmy et al., 2013) that likely contributes to the higher BSi:POC export ratio on seasonal and annual time scales (Rembauville et al., 2015b). Similar observations were made at Crozet where the fluxes of heavily silicified and/or large species (*F. kerguelensis*, *C. pennatum* and *Dactyliosolen antarcticus*) were enhanced under HNLC conditions (Salter et al., 2012). Although non-diatom components may influence POC fluxes, it is apparent that iron limitation favors the ecological selection of large and heavily silicified diatoms with a measurable and consistent effect on Si:C export stoichiometry.

Annual PIC export is similar at the KERFIX and A3 stations ($\sim$ 7 mmol m^{-2} d^{-1}). This is in stark contrast to the Crozet Plateau where deep-ocean PIC fluxes were 7-10 are higher at the iron-fertilized productive site (Salter et al., 2014). These differences are likely related to the position of the two plateaus relative to the Polar and Subantarctic Fronts. Foraminifera are a dominant component of PIC fluxes at the Crozet Plateau north of the Polar Front and pteropod aragonite fluxes are notably enhanced (Salter et al., 2014). In contrast, *Emiliania huxleyi* coccoliths dominate the PIC export at A3 south of the Polar Front (Rembauville et al., 2016b) and it seems probable that they also contributed to PIC export at KERFIX. South of the Polar Front, the cosmopolitan species *E. huxleyi* dominates the coccolithophore community composition (Saavedra-Pellitero et al., 2014; Winter et al., 2014). This species is known to prevail under low iron concentrations (Brand et al., 1983; Muggli and Harrison, 1997) and coccolithophore blooms are strongly temperature-dependant in the high latitude ocean (Sadeghi et al., 2012). Therefore the similarity in nitrate and phosphate concentrations (Blain et al., 2015) and summer temperature may explain the similarity of PIC flux mechanisms at both KERFIX and A3. These results further support the idea that the response of calcifying communities to Southern Ocean iron fertilization and the ensuing carbonate counter pump effect displays a strong regional component linked to the major hydrological fronts (Salter et al., 2014; Rembauville et al., 2016b).

The seasonal net community production (NCP, net primary production minus heterotrophic respiration integrated during the productive period) derived from DIC budgets is two-fold higher at A3 compared to KERFIX, although maximum primary production levels are four-fold higher at A3 (Table 2.2). Similar to NCP, annual POC export is two-fold higher at A3. A conclusion that may be drawn from this comparison is that the

fraction of net community production exported annually from the mixed layer is similar at the productive station A3 (1.5 %) and the HNLC station KERFIX (1.7 %). However, it must be stressed that estimates of seasonal NCP rely on DIC distribution and are associated with important uncertainties (Jouandet et al., 2008), and potentially strong inter annual variability (Louanchi et al., 2001). The annual sediment trap records are separated by 17 years and may be influenced by inter annual variability and long-term trends that are difficult to quantify. Furthermore, the sediment traps deployed at KERFIX and A3 were different models (Technicap PPS5 and PPS3, respectively) that differ in their funnel shape and aspect ratio. We cannot eliminate the possibility that these designs may have been subject to different hydrodynamic and biological biases that alter the collection efficiency of sinking particles (Hawley, 1988; Buesseler et al., 2007). Nevertheless, the low and tidal-driven circulation observed at both KERFIX and A3 (Rembauville et al., 2015a) instills a certain degree of confidence that there is value in comparing the two flux records.

Assuming a 2-fold uncertainty on both NCP and export estimates, we calculate that the HNLC environment exports a similarly low fraction of seasonal NCP (<10 %) when compared to a productive iron-fertilized regime (A3 station, Rembauville et al., 2015a). Our findings suggest that natural iron fertilization in the Southern Ocean has a limited capacity to increase the efficiency of carbon export from the mixed layer.

2.4 Export fluxes at South Georgia (article 4)

The shallow sediment trap deployment (300 m) over the central Kerguelen Plateau (station A3, Antarctic Zone) demonstrated the importance of diatom resting spore for carbon export in a naturally iron-fertilized area (**article 2**). A similar mechanism has been already reported in the naturally fertilized waters of the Polar Frontal Zone downstream of the Crozet islands (Salter et al., 2012). Conversely, contribution of resting spore to the exported diatom community was much lower at the HNLC station KERFIX (**article 3**). Given its importance for the functioning of the biological pump, it is necessary to know if this ecological strategy is also observed in other Subantarctic islands systems of the Southern Ocean. In this **article**, we present particulate organic carbon (POC), biogenic silicon (BSi), and diatom export fluxes from a third naturally-fertilized island system in the Atlantic sector of the Southern Ocean: the South Georgia islands. Sediment trap samples were provided by the British Antarctic Survey. We compare deep sediment trap records at annual scale from a productive (P3, 2000 m) and HNLC (P2, 1500 m) site South of the Polar Front.

The POC export is twice as high in the productive site ($40\,\mathrm{mmol\,m^{-2}\,yr^{-1}}$) compared to the HNLC site ($26\,\mathrm{mmol\,m^{-2}\,yr^{-1}}$), an observation consistent with what was observed at Kerguelen. A similar mechanism of resting spore formation by *Chaetoceros Hyalochaete* in late summer explains most of the difference in the annual carbon export between the two sites, whereas the remainder of the diatom community is similar in the two sites. These results demonstrate that regardless of the depth, productive areas of the Southern Ocean export a low amount of organic carbon, and that diatom resting spores contribute to a high proportion of this export. At the productive site P3, a comparison of the mixed layer, sediment trap (2000 m) and surface sediment (3750 m) diatom community demonstrates that the relative contribution of *Chaetoceros Hyalochaete* resting spores increases with depth. This observation confirms their high transfer efficiency that was hypothesized in the previous papers. Finally, the quantification of full- and empty diatom cells collected in the trap allows to identify taxa exported with a similar empty:full ratio and relative abundance than at Kerguelen.

Diatom identification and enumeration was performed by the author. Sediment trap samples were provided as wet aliquots by C. Manno and G. Tarling. POC and BSi analyses were performed by C. Manno.

Contents lists available at ScienceDirect

Deep-Sea Research I

journal homepage: www.elsevier.com/locate/dsri

CrossMark

Strong contribution of diatom resting spores to deep-sea carbon transfer in naturally iron-fertilized waters downstream of South Georgia

M. Rembauville [a,*], C. Manno [b], G.A. Tarling [b], S. Blain [a], I. Salter [a,c]

[a] Sorbonne Universités, UPMC Univ Paris 06, CNRS, Laboratoire d'Océanographie Microbienne (LOMIC), Observatoire Océanologique, F-66650 Banyuls/mer, France
[b] British Antarctic Survey, Natural Environmental Research Council, High Cross, Madingley Road, Cambridge CB3 0ET, UK
[c] Alfred-Wegener-Institute for Polar and Marine research, Bremerhaven, Germany

ARTICLE INFO

ABSTRACT

Biogeochemical and diatom export fluxes are presented from two bathypelagic sediment trap deployments in the Antarctic Zone of the Southern Ocean. One of the sediment traps was deployed in very productive, naturally iron-fertilized waters downstream of South Georgia (P3, 2000 m) and compared to a deployment in moderately productive waters upstream of the island system (P2, 1500 m). At both sites significant diatom export events occurred in spring (November) and contained mostly empty cells that were associated with low particulate organic carbon (POC) fluxes. A summer export pulse occurred one month later at P2 (end February/March) compared to P3 (end January). Diatom fluxes at P3 were one order of magnitude higher than at P2, a difference mainly attributed to the short and intense export of resting spores from *Chaetoceros Hyalochaete* and *Thalassiosira antarctica* species. Aside from these resting spores, diatom export assemblages at both sites were dominated by empty *Fragilariopsis kerguelensis* frustules. The fraction of diatoms exported as empty frustules was considerably lower at P3 (52%) than P2 (91%). This difference was related to the flux of intact diatom resting spores at P3 and may partially explain the lower Si:C export stoichiometry observed at P3 (1.1) compared to P2 (1.5). Through the enumeration of full diatom frustules and subsequent biomass calculations we estimate that diatom resting spores account for 42% of annual POC flux in the productive waters downstream of South Georgia. At both sites the contribution of diatom vegetative stages to POC fluxes was considerably lower ($< 5\%$). From these analyses we conclude that resting spore export contributes towards the slightly higher bathypelagic (POC) flux at P3 (40.6 mmol m^{-2} y^{-1}) compared to P2 (26.4 mmol m^{-2} y^{-1}). We compared our sediment trap records with previously published diatom assemblage data from the mixed layer and surface sediments (3760 m) around South Georgia. The relative proportion of diatom resting spores within diatom assemblages increases as a function of depth and is explained by selective preservation of their robust frustules. Our study highlights the significance of diatom resting spore export as a carbon vector out of the mixed layer. Furthermore, the contribution or resting spores to POC flux in the bathypelagic ocean and sediments suggests they play a particularly important role in sequestering biologically fixed CO$_2$ over climatically relevant timescales.

1. Introduction

The Southern Ocean (SO) is generally considered as the largest high nutrient, low chlorophyll (HNLC) area of the global ocean, where primary production is limited by iron availability (Martin, 1990; de Baar et al., 1990, 1995). Downstream of island plateaus, such as those at Kerguelen (Blain et al., 2001, 2007), Crozet (Pollard et al., 2009) and South Georgia (Whitehouse et al., 1996; Korb and Whitehouse, 2004), shelf sediments and glacial melt waters are a natural source of iron. These naturally-fertilized waters contrast strongly with surrounding HNLC conditions and display large scale phytoplankton blooms that can persist for several months (Westberry et al., 2013). In addition to the island mass effect (Blain et al., 2001), trace metal inputs into surface waters can sustain notable primary production (Moore and Abbott, 2000; Whitehouse et al., 2012) from upwelling associated with major fronts of the Antarctic Circumpolar Current (Loscher et al., 1997), atmospheric dust deposition (Meskhidze et al., 2007), sea

ice melt (van der Merwe et al., 2011), glacial runoff (Hawkings et al., 2014; van der Merwe et al., 2015) and melting icebergs (Duprat et al., 2016). Primary production downstream of sub-antarctic island systems is typically dominated by diatoms (Smetacek et al., 2004; Quéguiner, 2013), a microphytoplankton group generally considered to promote carbon export out of the mixed layer directly by sinking (Smetacek, 1985; Boyd and Newton, 1995, 1999) or indirectly by sustaining faecal pellet-productive food webs (Smetacek et al., 2004; Manno et al., 2014).

Maiti et al. (2013) demonstrated an inverse relationship between primary production and export efficiency in the Southern Ocean, contrasting with the positive relationship between primary production and export prevailing in most of the global ocean (Laws et al., 2011). These so called high biomass, low export regimes (HBLE, Lam and Bishop, 2007; Lam et al., 2011) appear to be characterized by enhanced heterotrophic microbial activity (Obernosterer et al., 2008; Christaki et al., 2014) and intense re-processing and fragmentation of particulate matter by zoo-plankton. On the Kerguelen Plateau for example, net community production (NCP) was estimated to be 6.6 mol m^{-2} yr^{-1} (Jouandet et al., 2008), although only a small fraction of this NCP was exported out of the mixed layer (Rembauville et al., 2015b). Annual records of particulate organic carbon (POC) export fluxes derived from moored sediment traps have been published for productive, naturally-fertilized waters downstream of Crozet (Salter et al., 2012), Kerguelen (Rembauville et al., 2015a,b) and South Georgia (Manno et al., 2015). Irrespective of depth (300–2000 m), annual POC export from these island systems exhibits low variability and is typically < 100 mmol C m^{-2} yr^{-1}. This finding contrasts with the high levels of productivity associated with these naturally fertilized systems. Identifying the dominant export vectors from such systems is therefore necessary to advance our understanding of the mechanistic relationships between production and export in the Southern Ocean.

A significant positive relationship between POC fluxes and *Eucampia antarctica* var. *antarctica* winter stages highlighted its important role as a carbon export vector from the Crozet bloom (Salter et al., 2012). Similarly, quantification of diatom and carbon fluxes from the Kerguelen bloom indicated that 60% of annual carbon export was due to short term (< 2 week) export events of *Chaetoceros Hyalochaete* and *Thalassiosira antarctica* resting spores (Rembauville et al., 2015a). Moreover, Salter et al. (2012) and Rembauville et al. (2015a) observed that species-specific diatom ecology (spore formation, protection from grazing through the acquisition of a thick frustule) impacts not only the magnitude of carbon fluxes, but also the Si:C export stoichiometry over annual scales, corroborating previous suggestions (Smetacek, 1985; Smetacek et al., 2004; Salter et al., 2012; Assmy et al., 2013). Downstream of South Georgia, faecal pellets were reported to dominate ($\sim 60\%$) the second POC export peak often observed in March-April (Manno et al., 2015). However, the contribution of diatoms to bathypelagic POC flux at South Georgia has yet to be addressed.

The waters downstream South Georgia exhibit a large and recurrent phytoplankton bloom (Ward et al., 2002; Borrione and Schlitzer, 2013) characterized by interannual variability in the seasonal pattern (unimodal versus bimodal chlorophyll *a* peaks, Park et al., 2010; Borrione and Schlitzer, 2013). The bloom is dominated by microplankton diatoms (Korb and Whitehouse, 2004) with a major contribution of *Fragilariopsis kerguelensis*, *Chaetoceros Hyalochaete*, *Pseudo-nitzschia* spp., *Eucampia antarctica* var. *antarctica* and *Corethron* (Korb et al., 2008, 2010). The productive waters downstream of South Georgia support a very large biomass of mesozooplankton (Ward et al., 2012), macro-zooplankton (Atkinson et al., 2008, 2009), mesopelagic fish (Collins et al., 2012) and top predators (Boyd et al., 1994), with significant implications for the amount of POC export out of the

mixed layer (Huntley et al., 1991). Upstream of South Georgia, the lack of iron limits phytoplankton growth and phytoplankton biomass is one order of magnitude lower than that is observed downstream of the island (Korb et al., 2008). Although the contribution of naked dinoflagellates to microplankton biomass is higher than in naturally-fertilized waters, the diatom species *Fragilariospsis kerguelensis*, *Pseudo-nitzschia* spp., small *Thalassionema nitzschioides* and *Chaetoceros Hyalochaete* species still dominate the microplankton assemblage (Korb et al., 2010). Korb et al. (2012) hypothesized that differences in diatom community structure upstream and downstream of South Georgia would impact the magnitude of POC export. However, these hypotheses have yet to be addressed by a detailed analysis of diatom export assemblages and elemental fluxes around South Georgia.

In the present study we report diatom and biogeochemical fluxes from two annual sediment trap deployments in varying productivity regimes upstream and downstream of South Georgia. The objectives are (i) to describe spatial and temporal patterns of diatom export assemblages, (ii) to differentiate full and empty frustules to estimate the contribution of specific diatom groups to carbon fluxes and Si:C export stoichiometry and (iii) to compare mixed layer, sediment trap and surface sediment data to describe changes in diatom assemblages as a function of depth.

2. Materials and methods

2.1. Trap deployments and chemical analyses

Bottom-tethered moorings were deployed at two sites (P2 and P3) for periods of approximately 12 months between January and November 2012. P2 was located upstream of South Georgia (55°11.99S, 41°07.42W), and P3 downstream (52°43.40S, 40°08.83W) (Fig. 1). Each sediment trap (McLane Parflux conical sediment traps, 0.5 m^2 surface collecting area, McLane Labs, Falmouth, MA, USA) was equipped with 12 sample cups and fitted with a plastic baffle mounted in the opening to prevent the entrance of large organisms. Prior to deployment, the sample cups were filled with a preservative seawater solution of NaCl-buffered HgCl$_2$. Traps were deployed at a depth of 1500 m (P2, water depth 3200 m) and 2000 m (P3, water depth 3800 m), and the sample carousel was programmed to rotate at intervals of 15 days in austral summer and 30 days in austral winter (Table 1). Sample cups for April, July, October (P2) and August (P3) were missing on recovery (unscrewed from the carrousel). Prior to splitting, "swimmers" (i.e. zooplankton organisms that can enter the receiving cups while alive) were carefully removed: samples were first wet-sieved through a 1 mm nylon mesh and the remaining swimmers were hand-picked under a dissecting microscope. Large aggregates, fragments of moults and empty tests retained by the mesh were returned to the sample. Samples were split in replicate fractions using a McLane rotary sample splitter (McLane Labs, Falmouth, MA, USA). Replicate fractions were vacuum-filtered through preweighed and precalcinated (450 °C, 4 h) Whatman GF/F filters for POC analyses. Salt content was removed from the filters by a short distilled water rinse and they were dried at 60 °C. For POC determination, filters were treated with 2 N H$_3$PO$_4$ and 1 N HCl to dissolve the carbonate fraction. POC was measured by combustion in an elemental analyser (CHN). For biogenic silica (BSi) analyses, replicate fractions were vacuum-filtered through 0.4 μm Nuclepore filters. Prior to BSi extraction, the material was pretreated with 10% H$_2$O$_2$ and 1 N HCl to remove organic particle coatings (Mortlock and Froelich, 1989). BSi was determined by a time-series extraction experiment in a 0.5 M NaOH solution at 85 °C for 5 h (DeMaster, 1981). An aliquot of each sample was taken for silicic acid analysis every hour and the BSi content was
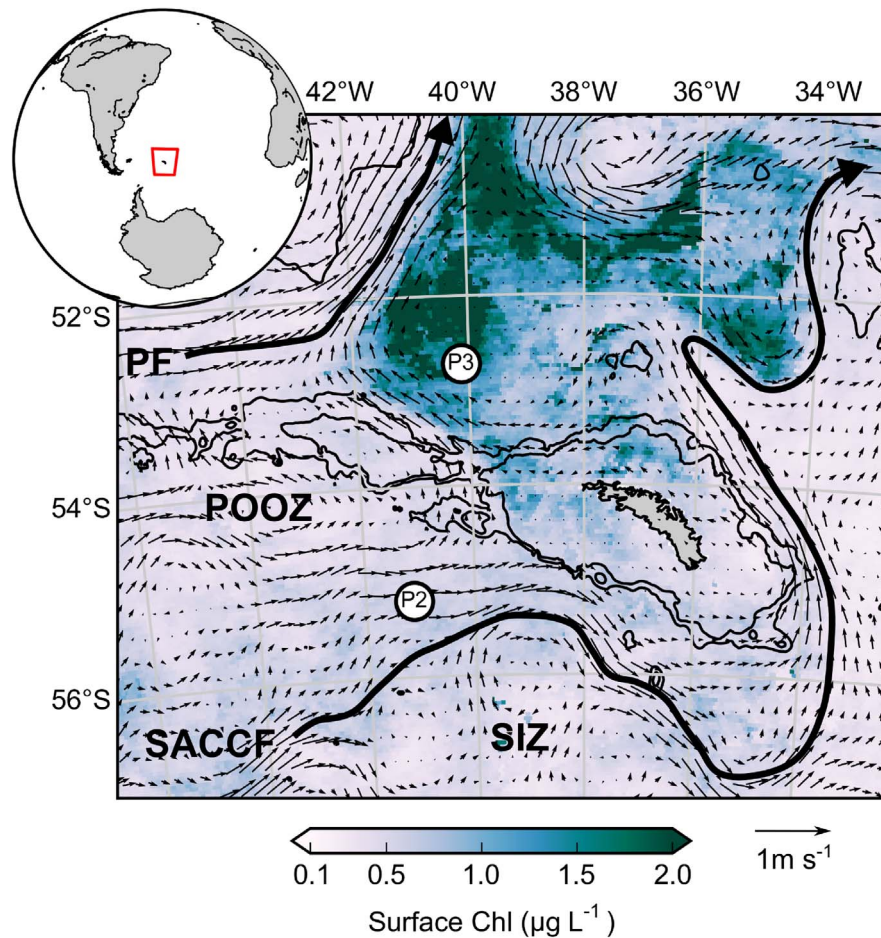
Fig. 1. Location of the South Georgia Plateau in the Atlantic sector of the Southern Ocean and location of the two sediment traps (P2, P3). Colors represent the satellite-derived chlorophyll *a* concentration (MODIS) and arrows the altimetry-derived geostrophic velocities (AVISO) averaged over the sediment trap deployment period (January to December 2012). Thick arrows denote the mean fronts positions during the deployment (PF: Polar Front, SACCF: Southern ACC Front) arbitrarily defined by enhanced geostrophic velocities, (Moore et al., 1999; Thorpe et al., 2002). POOZ: Permanently Open Ocean Zone, SIZ: Seasonal ice Zone. Black isolines are the 1000 m and 2000 m isobaths. (For interpretation of the references to color in this figure, the reader is referred to the web version of this article.)

estimated from the intercept of the extraction time-series (De-Master, 1981).

2.2. Remote sensing and derived oceanographic variables

Satellite-derived surface chlorophyll *a* concentration (MODIS Aqua, 4 km, 8-days composite, level 3 product) for the sediment trap deployment period was accessed at http://oceancolor.gsfc.nasa.gov/cms/. Altimetry-derived geostrophic velocities (AVISO MADT, 1/4°, daily product) were extracted at http://www.aviso.altimetry.fr/. For sea surface temperature (SST) data, the NOAA 1/4° daily Optimum Interpolation Sea Surface Temperature (OISST) was accessed at http://www.esrl.noaa.gov/psd/data/gridded/data.noaa.oisst.v2.html (Reynolds et al., 2002). Time series of chlorophyll *a* concentration and SST were calculated by averaging the data in a 100 km radius centered on each sediment trap location. Averages of chlorophyll *a* concentration and geostrophic velocities were calculated for the sediment trap deployment period of January to December 2012 (Fig. 1).

2.3. Diatom enumeration, identification and biomass

Diatom enumeration and identification was performed using a biological counting technique that does not include any chemical treatment before counting (Salter et al., 2012) and thereby allows the separate enumeration of full and empty cells (Rembauville

et al., 2015a). A 1/8 aliquot of each sample was gently homogenized and 2 mL withdrawn and diluted in a final volume of 20 mL of artificial seawater (salinity=34 PSU). A modified pipette tip with a large aperture was used to avoid breakage of larger species such as *Thalassiothrix antarctica*. The diluted sample was placed in a Sedgewick-Rafter counting chamber (Pyser-SGI S52, 1 mL volume). One quarter to one half of the chamber (depending on diatom abundance) was observed with an inverted microscope with phase contrast (Olympus IX70) at $400 \times$ magnification.

Diatoms were identified to the lowest possible taxonomic level following Hasle and Syvertsen (1997). The relatively low magnification imposed by the counting technique and presence of organic material occasionally obscuring the valve face limited species-level identification for some taxa. Consequently certain species were classified as follows: *Fragilariopsis separanda* and *Fragilariopsis rhombica* were grouped as *Fragilariopsis separanda/rhombica*; all the *Pseudo-nitzschia* species (mainly *Pseudo-nitzschia lineola* and *Pseudo-nitzschia heimii*) were grouped as *Pseudo-nitzschia* spp.; the genera *Haslea* and *Pleurosigma* were grouped as *Pleurosigma*; species of the genera *Banquisia* and *Manguinea* and *Membraneis challengeri* and *Membraneis imposter* were grouped as *Membraneis*. Unidentifiable centric species $< 20\,\mu m$ and large centric species were denominated as Small centric ($< 20\,\mu m$) and Large centric ($> 20\,\mu m$), respectively. This arbitrary size classification was chosen to differentiate small centric species, typically attributable to the *Thalassiosira* genus, from genera such as

Table 1
Total mass flux (TMF), particulate organic carbon (POC), biogenic silica (BSi) fluxes and BSi:POC molar ratio of material collected by sediment traps upstream (P2, 1500 m) and downstream (P3, 2000 m) of South Georgia.

Site	Cup collection period (2012)		TMF	POC	BSi	BSi:POC
	Opening	Closing	(mg m^{-2} d^{-1})	(μmol m^{-2} d^{-1})	(μmol m^{-2} d^{-1})	(mol:mol)
P2	15/01	01/02	24.1	38	61	1.6
	01/02	15/02	8.3	40	25	0.6
	15/02	01/03	49.7	172	267	1.5
	01/03	01/04	60.7	101	289	2.9
	01/04	01/05	Lost			
	01/05	01/06	17.5	205	83	0.4
	01/06	01/07	13.8	84	18	0.2
	01/07	01/08	Lost			
	01/08	01/09	10.1	78	26	0.3
	01/09	01/10	9.7	97	73	0.8
	01/10	01/11	Lost			
	01/11	01/12	58.2	174	606	3.5
P3	15/01	01/02	146.0	904	765	0.8
	01/02	15/02	42.5	164	191	1.2
	15/02	01/03	22.3	73	60	0.8
	01/03	01/04	25.0	156	145	0.9
	01/04	01/05	9.5	86	20	0.2
	01/05	01/06	9.0	65	18	0.3
	01/06	01/07	8.9	46	10	0.2
	01/07	01/08	15.1	70	17	0.3
	01/08	01/09	Lost			
	01/09	01/10	17.8	110	44	0.4
	01/10	01/11	39.3	90	349	3.9
	01/11	01/12	70.3	92	344	3.7

Azpeitia and *Actinocyclus* comprising the large centric species. All of the whole, intact and recognizable frustules were counted (Supplementary Fig. 1). For each sample, > 300 cells were counted, except in sample cups #1, 2, 7 and 8 from the less productive site P2 where only ~ 100 cells were counted. Full and empty cells were enumerated separately (e.g. Assmy et al., 2013; Rembauville et al., 2015a). We considered cells as full when plasts were clearly visible and intact (Supplementary Fig. 1). The empty:full export ratio of a given species was defined as the ratio of empty cells to full cells following integration over the complete sediment trap record. Although broken frustules and debris were present (Supplementary Fig. 1), they were not enumerated in the samples. We estimate that the relative abundance of broken frustules is $< 15\%$. Diatom export assemblages were compared between the two sites using Shannon's diversity index ($H' = \sum_{i=1}^{n} p_i ln(p_i)$, where n is the total number of species and p_i the proportion of individuals of species i) and Pielou's evenness index ($J' = H'/H'_{max}$, where H'_{max} is the maximal possible value of H', equal to $ln(n)$). Both indexes were calculated on total (empty and full) cell numbers following integration over the complete sediment trap record.

Full diatom fluxes were converted to carbon fluxes using previously published species-specific biomass values for diatoms in the vicinity of the Kerguelen Plateau (Cornet-Barthaux et al., 2007) which were considered as a good analogue for South Georgia diatom populations. For species not listed in Cornet-Barthaux et al. (2007), 10 representative individuals of each species were measured and biovolume was calculated following Hillebrand et al. (1999). Carbon content was then calculated using the Menden-Deuer and Lessard (2000) equation for diatoms ($C = 0.288 \times V^{0.811}$). For *Chaetoceros Hyalochaete* resting spores (CRS) and *Thalassiosira antarctica* resting spores (TRS), 100 randomly selected individuals were measured. Biovolume was calculated and carbon content was estimated using the Kuwata et al. (1993) carbon:volume relationship for CRS and the Menden-Deuer and Lessard (2000) formulation for TRS. The mean carbon content ($\pm$ standard deviation) was 240 ± 101 pgC cell^{-1} and 1018 ± 460 pgC cell^{-1} for

CRS and TRS, respectively. The list of diatom species and the corresponding carbon content is reported in Table 3.

To describe the change in diatom assemblage with depth, we compared the annual sediment trap record from P3 with mixed layer diatom assemblage from multiple summer surveys (February 2002, 2003 and January 2005) at the P3 trap location (Korb et al., 2008) and surface sediment diatom assemblage from a core located very close to the trap (42°09.2′S–41°10.7′W, 3760 m, Allen et al., 2005).

3. Results

3.1. Biogeochemical fluxes

At P2, highest surface chlorophyll *a* concentration (1.5 µg L^{-1}) was observed in February, associated with the highest SST in summer (3.5 °C, Fig. 2a). Chlorophyll *a* concentration remained low in spring (< 1 µg L^{-1} from October to December) when SST increased from 0 to 2 °C. At P3, SST followed the same seasonal signal but was 1 °C warmer. Chlorophyll *a* concentration was close to P2 values in summer (1.5–2 µg L^{-1}) but was much higher in spring, reaching values > 6 µg L^{-1} in December.

POC fluxes at P2 were < 0.2 mmol m^{-2} d^{-1} throughout the year, with the highest value observed in May (Table 1 and Fig. 2b). At P3, POC fluxes were highest at the beginning of the sediment trap record in January (0.9 mmol m^{-2} d^{-1}) and < 0.2 mmol m^{-2} d^{-1} for the remainder of the year. POC export integrated across the sediment trap deployment record was ~ 1.7 times greater at P3 compared to P2 (40.6 vs. 26.4 mmol m^{-2}, Table 2). At P2, the highest BSi flux of 0.6 mmol m^{-2} d^{-1} was observed in spring (November), and decreased in summer (February to March) to 0.3 mmol m^{-2} d^{-1} (Table 1 and Fig. 2c). BSi fluxes were < 0.1 mmol m^{-2} d^{-1} the remaining of the year. At P3, the highest BSi flux of 0.8 mmol m^{-2} d^{-1} was concomitant with the highest POC flux at the end January. Winter values (April to
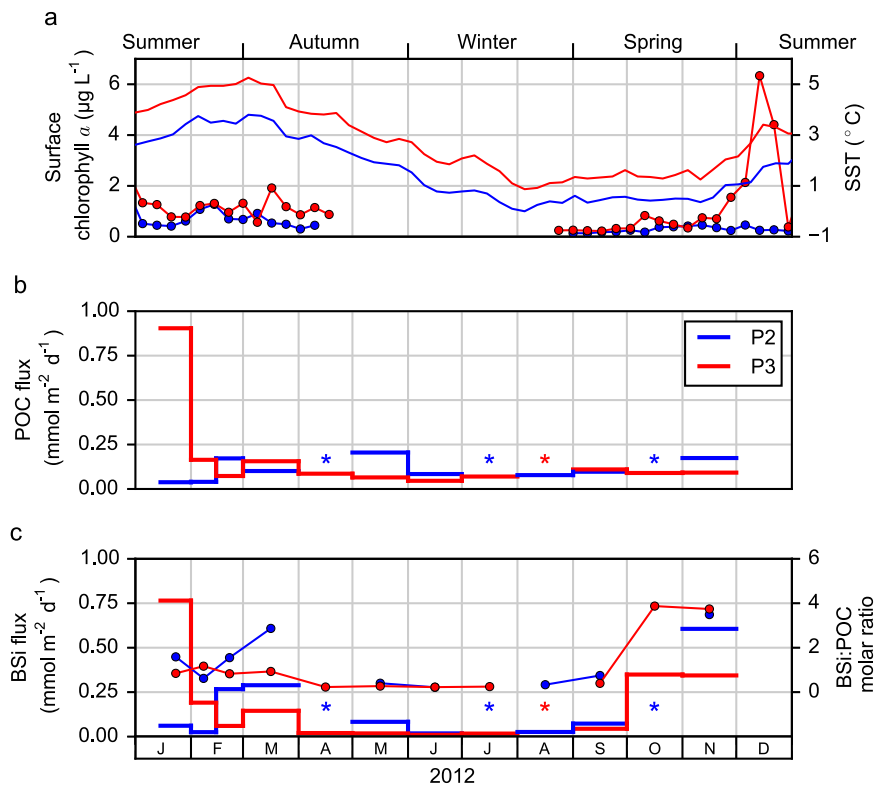
Fig. 2. Oceanographic parameters and biogeochemical fluxes. (a) Satellite-derived surface chlorophyll *a* (dots) and sea surface temperature (SST, continuous lines) averaged over an area with a 100 km radius centered on P2 (blue) and P3 (red). (b) Particulate organic carbon (POC) fluxes collected by sediment traps at P2 (1500 m, blue) and P3 (2000 m, red). (c) Biogenic silica (BSi) fluxes (bold lines) and BSi:POC ratio (dots). Asterisks denote missing cups. (For interpretation of the references to color in this figure legend, the reader is referred to the web version of this article.)

Table 2
Annually integrated fluxes of particulate organic carbon (POC), biogenic silica (BSi) and corresponding BSi:POC molar ratio. Fraction of total empty diatoms, diversity (Shannon's H′) and evenness (Pielou's J′) indexes and contribution of each vector to measured carbon fluxes.

Site	Annual flux (mmol m^{-2} or g m^{-2})				BSi:POC raw (mol: mol)	Empty diatom (%)	H′	J′	Contribution to measured POC fluxes (%)	
	POC raw	POC interpolated	BSi raw	BSi interpolated					Diatom resting spores	Other diatoms
P2	26.4	35.8	38.6	55.2	1.5	91.1	1.97	0.59	0	1.9
	0.32	*0.46*	*2.59*	*3.71*						
P3	40.6	43.3	45.5	46.4	1.1	51.5	1.70	0.48	41.7	3.9
	0.49	*0.52*	*3.06*	*3.12*						

September) were < 0.1 mmol m^{-2} d^{-1}. Winter BSi:POC ratio was similar at P2 and P3 with low values < 0.5. The BSi:POC ratio in spring was also similar at the two sites with the highest values observed (3.5–4) in October and November. The main difference between the two sites was in summer, when values of 1.5–3 were observed at P2 whereas the BSi:POC ratio remained ∼1 at P3. The integrated BSi fluxes were lower at P2 than P3 (38.6 versus 45.5 mmol m^{-2}, Table 2) and the annual BSi:POC ratio was higher at P2 (1.5 versus 1.1).

3.2. Diatom fluxes and contribution to carbon fluxes

At P2, the total diatom flux showed two peaks: the first occurring in summer (3.5 × 10^6 cell m^{-2} d^{-1}) and a second in the following spring (7 × 10^6 cell m^{-2} d^{-1}, Fig. 3a). During winter total diatom fluxes were < 1 × 10^6 cell m^{-2} d^{-1}. Diatom fluxes in spring (November) were characterized by *Fragilariopsis kerguelensis* (39% of total cells), *Fragilariopsis separanda/rhombica* (50%), *Thalassiosira lentiginosa* (12%), *Pseudo-nitzschia* spp. (10%) and *Dactyliosolen antarcticus* (2%). Summer fluxes contained mainly *F. kerguelensis* (41% of total cells), *Thalassionema nitzschioides* (16%),

and *Thalassiosira gracilis* (7%, Fig. 3b–h). When integrated over the deployment period, empty diatoms constituted 91.1% of the total diatom flux at P2 (Table 2). *F. kerguelensis* dominated (> 40%) the empty, full and total diatom export assemblage (Table 3). Almost all species were preferentially exported as empty cells (empty:full ratio > 1) with the exception of *Eucampia antarctica* var. *antarctica* and *Navicula* sp. that exhibited empty:full ratios close to 1 (Table 3).

At P3, total diatom flux displayed highest values in spring (November) and summer (January). The highest flux of 6 × 10^7 cell m^{-2} d^{-1} observed at the end of January was one order of magnitude higher than the corresponding maxima at P2 (Fig. 4). In spring, the total cell flux of 8 × 10^6 cell m^{-2} d^{-1} was close to that observed at P2 during the same period. Diatom fluxes were dominated by full cells of CRS, mainly exported during one short event in mid January (3.8 × 10^7 cell m^{-2} d^{-1}, Fig. 4b). CRS accounted for 42.7% of the total diatom export integrated over the complete record at P3 (Table 3). Concomitant to the significant flux of CRS in January (63% of total cells in this sample), a noticeable export peak of *Eucampia antarctica* (3%), *Navicula* sp. (3%) and TRS (1%) was also observed
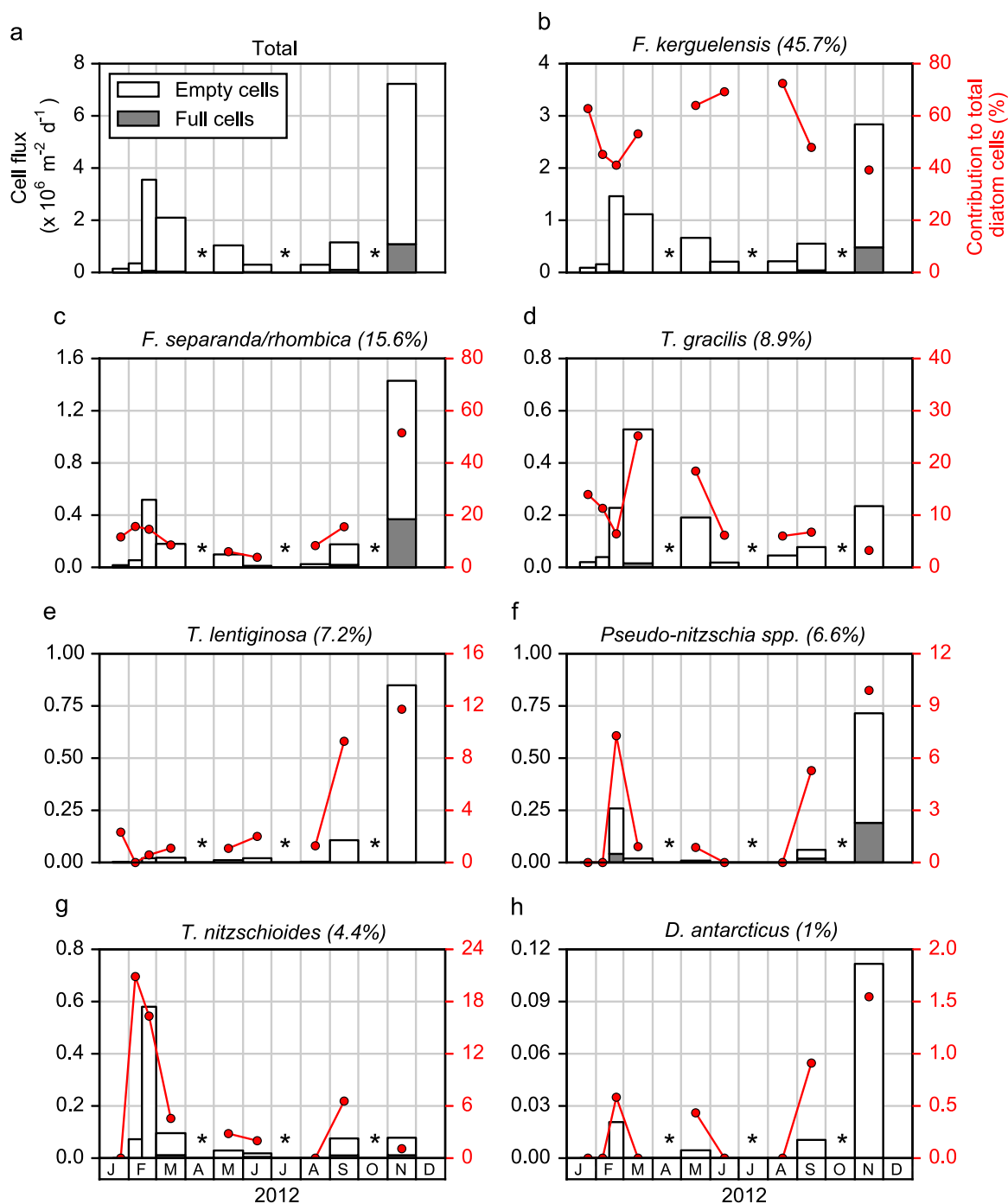
Fig. 3. Diatom fluxes at P2. Empty (white bars) and full (grey bars) diatom fluxes (left axis) for (a) the total diatom community and (b-h) the diatom species/groups contributing to > 1% of the annual diatom flux. The relative contribution of each diatom species/group (empty + full) to the total diatom assemblage is shown as red dots (right axis). The number in brackets is the relative contribution to the total diatom flux integrated over the deployment period and includes full and empty cells. Asterisks denote missing cups.(For interpretation of the references to color in this figure legend, the reader is referred to the web version of this article.)

(Fig. 4b, f, g, and l). However, their relative contribution to annual diatom export was much lower (< 3%). Some species were observed in both spring and summer such as *F. kerguelensis*, *T. nitzschioides*, *F. separanda/rhombica*, *Pseudo-nitzschia* spp., *T. gracilis*, and *T. lentiginosa* (Fig. 4c, d, e, i, j and k). Conversely, other species were observed primarily in summer such as CRS, *E. antarctica* var. *antarctica*, *Navicula* sp. and TRS (Fig. 4b, f, g, and l).

At P3 approximately half (51.5%) of the diatoms were exported as empty cells when integrated over the deployment period, lower than the corresponding value at P2 (91%). The diatom assemblage

of full cells at P3 was dominated by CRS (87.9%, Table 3). Empty cells were mostly represented by *F. kerguelensis* (55.6%), followed by *T. nitzschioides* (15.9%) and *F. separanda/rhombica* (5%) (Table 3). Only CRS were exported with an empty:full ratio < 1, although *E. antarctica* var. *antarctica* also showed a comparatively low empty: full ratios (1.8). *F. kerguelensis* was exported with an empty:full ratio of 10.6, a value similar to the one observed at P2 (Table 3).

At P2, diatoms comprised a minor contribution to measured POC fluxes (1.9%, Table 2). Conversely, diatoms represented 41.7% of measured POC fluxes at P3 with CRS alone accounting for 38.6% of POC flux integrated over the deployment period. At both sites

Table 3

Contribution of each diatom species/group to the annual full, empty, and total diatom flux integrated over the entire record for each sediment trap. Values higher than 5% are highlighted in bold. Total integrated empty:full ratio. Carbon content used to calculate diatom contribution to carbon export.

Species/group	P2				P3				C content (pgC cell^{-1})
	Annual contribution (%)			Empty:full	Annual contribution (%)			Empty:full	
	Full	Empty	Total		Full	Empty	Total		
Asteromphalus hookeri Ehrenberg	0	0.4	0.4		0	0.3	0.2		1900[a]
Asteromphalus hyalinus Karsten	0	0.6	0.6		0	0.5	0.2		365[a]
Asteromphalus parvulus Karsten	0	0.1	0.1		0	0.1	0.1		365[a]
Chaetoceros atlanticus Cleve	0	0.9	0.8		0	0	0		217[b]
Chaetoceros bulbosus (Ehrenberg) Heiden	0	0.2	0.1		0	0	0		222[a]
Chaetoceros dichaeta Ehrenberg	0	0.5	0.5		0	0.1	0		303[b]
Chaetoceros Hyalochaete (spore) group	0	0	0		**87.9**	0.1	**42.7**	0.0	240[c]
Chaetoceros peruvianus Brightwell	0	0	0		0	< 0.1	< 0.1		356[b]
Corethron inerme Karsten	0	0.9	0.8		0	1.6	0.8		1097[a]
Corethron pennatum (Grunow) Ostenfeld	0	1.0	0.9		0	0.6	0.3		1097[a]
Coscinodiscus group	0	0	0		0	< 0.1	< 0.1		244[a]
Dactyliosolen antarcticus Castracane	0	1.1	1.0		0	0.4	0.2		700[a]
Eucampia antarctica var. *antarctica* (Castracane) Mangin	1.9	0.2	0.3	1.0	1.5	2.6	2.1	1.8	416[a]
Fragilariopsis kerguelensis (O'Meara) Hustedt	**42.4**	**46.0**	**45.7**	11.2	**5.6**	**55.6**	**31.4**	10.6	158[a]
Fragilariopsis separanda/rhombica (group)	**30.7**	14.2	**15.6**	4.7	0.2	**5.0**	2.6	30.3	128[a]
Guinardia cylindrus (Cleve) Hasle	0	0	0		0	< 0.1	< 0.1		495[a]
Membraneis group	0	0.4	0.4		0	0.3	0.2		3225[a]
Navicula sp.	2.7	0.2	0.4	0.8	0.8	2.8	1.8	3.5	126[a]
Odontella weissflogii (Grunow) Grunow	0	0.3	0.3		0	0.9	0.5		1939[a]
Pleurosigma group	0	0.5	0.5		0	0.8	0.4		469[a]
Proboscia alata (Brightwell) Sundström	0	0.6	0.6		0	0.1	0.1		3686[a]
Proboscia inermis (Castracane) Jordan & Ligowski	0	0.8	0.7		0	0.1	0.1		2898[a]
Proboscia truncata (Karsten) Nöthig & Ligowski	0	0	0		0	< 0.1	< 0.1		2898[a]
Pseudo-nitzschia spp. group	**18.2**	5.4	**6.6**	3.1	0.7	2.4	1.6	3.7	127[a]
Rhizosolenia antenata f. *semispina* Sundström	0	0.4	0.4		0	0.2	0.1		1382[a]
Rhizosolenia chunii Karsten	0	0.7	0.6		0	0.1	0.1		1382[a]
Rhizosolenia simplex Karsten	0	0.4	0.3		0	0	0		1382[a]
Rhizosolenia styliformis Brightwell	0	0	0		0	0.1	0.1		1382[a]
Thalassionema nitzschioides (Grunow) Mereschkowsky	3.0	4.5	4.4	15.4	1.4	**15.9**	**8.9**	11.8	30[a]
Thalassiosira antarctica (spore)	0	0	0		1.7	0.4	1.0		1018[b]
Thalassiosira gracilis Karsten Hustedt	1.3	**9.6**	**8.9**	78.9	0	2.5	1.3	122.4	93[a]
Thalassiosira lentiginosa (Janisch) Fryxell	0	**7.9**	**7.2**		0.1	2.0	1.1	20.0	3119[a]
Thalassiosira tumida (Janisch) Hasle	0	0	0		0	0	0		379[a]
Thalassiotrix antarctica Schimper	0	0.7	0.6		0	0.6	0.3		3556[a]
Small centric (< 20 μm) group	0	0.7	0.6		0.1	3.2	1.7	59.0	93[a]
Large centric (> 20 μm) group	0	0.7	0.7		0	0.4	0.2	10.4	365[a]

[a] Species-specific biomass taken from Cornet-Barthaux et al. (2007).

[b] Individuals were measured in the sediment trap samples. Biovolume was calculated from Hillebrand et al. (1999) and carbon:volume relationship from Menden-Deuer and Lessard (2000) was applied.

[c] Individuals were measured in the sediment trap samples. Biovolume was calculated from Hillebrand et al. (1999) and carbon:volume relationship from Kuwata et al. (1993) was applied.
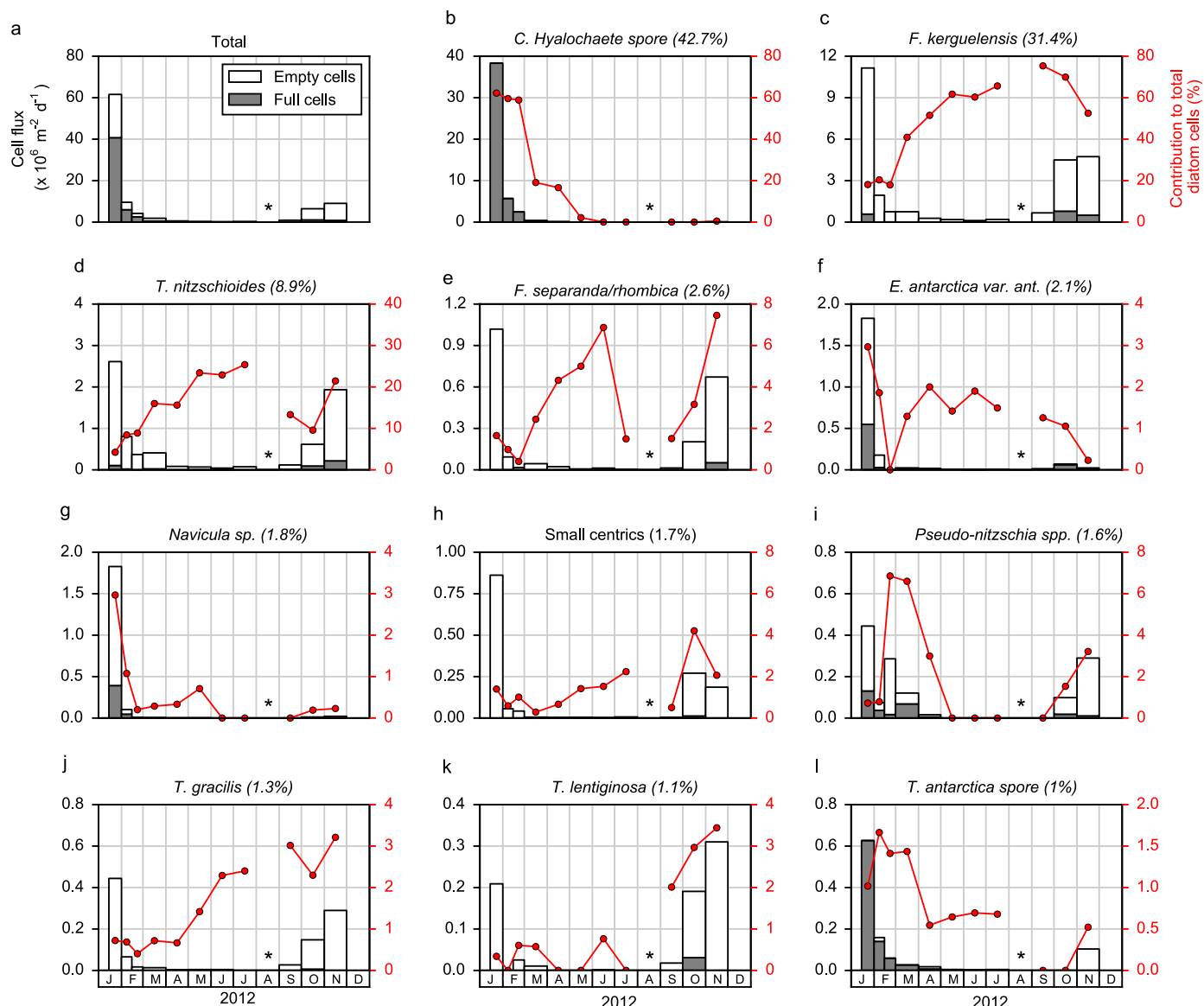
Fig. 4. Diatom fluxes at P3. Empty (white bars) and full (grey bars) diatoms fluxes for (a) the total diatom community and (b-l) the diatom species/groups contributing to more than 1% of the annual diatom flux. The relative contribution of each diatom species/group (empty+full) to the total diatom assemblage is shown as red dots (right axis). The number in brackets is the relative contribution to the total diatom flux integrated over the deployment period and includes full and empty cells. Asterisks denote missing cups. (For interpretation of the references to color in this figure legend, the reader is referred to the web version of this article.)

diatom vegetative stages accounted for a low proportion of POC flux, amounting to 3.9% at P3 and 1.9% at P2 (Table 2).

3.3. Change in diatom assemblages through the water column

At P3, the mean summer mixed layer diatom assemblages (Korb et al., 2008) are dominated by *F. kerguelensis* (30%), followed by *Pseudo-nitzschia* (20%) and *C. Hyalochaete* vegetative stage (10%, Fig. 5). Between the mixed layer and the sediment trap depth (2000 m) there are notable decreases in the contribution of *Pseudo-nitzschia* (20–2%), *Thalassiothrix antarctica* (10–1%) and *E. antarctica* (8–2.5%). Conversely, *F. kerguelensis* relative abundance is similar between the mixed layer and the sediment trap depth (30%), while the contribution of *C. Hyalochaete* increases (11–42%) and is present as resting spores in the trap samples. In surface sediments (Allen et al., 2005), CRS represents 80% of the diatom assemblage, followed by *F. kerguelensis* (10%) and TRS (3%).
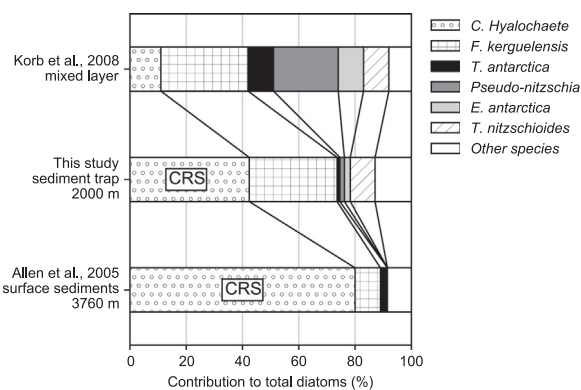

Fig. 5. Evolution of diatom assemblages with depth at P3. Mixed layer data from Korb et al. (2008) are summer averages from February 2002, 2003 and January 2005. *Chaetoceros Hyalochaete* is present as vegetative stage in the mixed layer and as resting spore (CRS: *Chaetoceros Hyalochaete* resting spore) in the sediment trap and surface sediment (Allen et al., 2005) assemblages.

4. Discussion

4.1. Magnitude of particle fluxes

POC export at station P3 is higher than that observed at station P2 (40.6 mmol m^{-2} yr^{-1} vs. 26.4 mmol m^{-2} yr^{-1}). The omission of flux data from sample cups lost during recovery introduces some uncertainty in equating the integrated POC fluxes to annual values. If the missing values are estimated by linear interpolation (affecting the mean value of two windowing samples to the missing sample) resulting POC export is still higher at P3 and the annual BSi:POC ratio remains similar (Table 2). The missing samples are from a period of low background flux with no notable surface chlorophyll *a* features (Fig. 2). Consequently we decided not to include the linear interpolation of missing samples and present integrated fluxes of chemical and biological constituents as a conservative approximation of annual flux.

At P3, the sediment trap deployment location is positioned in the center of a cyclonic circulation feature originating from the northern South Georgia shelf (Meredith et al., 2003). The area downstream of South Georgia is fertilized by continuous benthic iron supply from the South Georgia shelf system, resulting in higher dissolved iron concentration when compared to the waters upstream of the island (0.3 nM versus < 0.05 nM in spring, Nielsdóttir et al., 2012). This natural iron fertilization mechanism has been suggested to support the large and recurrent phytoplankton blooms observed downstream of South Georgia (Fig. 1, Ward et al., 2002; Borrione and Schlitzer, 2013). The regional differences we report in deep-ocean POC fluxes at P2 and P3 are therefore consistent with the varying levels of chlorophyll *a* biomass observed around South Georgia resulting from differences in iron supply.

Deep-ocean POC fluxes at the productive P3 site lag the strong surface chlorophyll *a* peak (6 µg L^{-1}) by one month and exhibit no notable peaks in the time preceding surface biomass maxima. Time lags of 1–2 month between production and export have been observed previously in the Southern Ocean (Honjo et al., 2000; Buesseler et al., 2001; Rigual-Hernández et al., 2015a,b). During a shallow sediment trap deployment (289 m) over the central Kerguelen Plateau (Rembauville et al., 2015b), CRS also dominated carbon export and was exported one month after the surface chlorophyll *a* peak, a pattern very similar to what we observe at P3 despite a much deeper sediment trap depth (2000 m). Highest BSi:POC ratio was observed in spring (September/October) at both sites. Very similar patterns in export stoichiometry have been observed in other naturally fertilized area of the Southern Ocean and were attributed to changes in the diatom community structure across the season (Rembauville et al., 2015a; Salter et al., 2012).

There are no comparable peaks in either surface biomass (< 2 µg L^{-1} throughout the year) or deep ocean POC flux at station P2 upstream of South Georgia. Despite strong differences in surface phytoplankton biomass, primarily mediated by iron supply (Nielsdóttir et al., 2012; Borrione and Schlitzer, 2013), the amount of POC reaching the deep-ocean differs by a factor of < 2 between the two sites. This is consistent with a scenario of enhanced carbon remineralization downstream of South Georgia (Cavan et al., 2015; Le Moigne et al., 2016). The annual POC fluxes observed at South Georgia are remarkably similar (< 100 mmol m^{-2} yr^{-1}) to those measured at other naturally iron-fertilized sites in the Southern Ocean (Salter et al., 2012; Rembauville et al., 2015b). These fluxes are also comparable to the ones recorded during annual deployments of deep sediment traps in other non-fertilized areas of the Permanently Open Ocean Zone (POOZ, 33 mmol m^{-2} y^{-1} at 2200 m, Fischer et al., 2002; 35 mmol m^{-2} y^{-1} at 1300 m, Tesi et al., 2012; 102 mmol m^{-2} y^{-1} at 2000 m, Rigual-Hernández et al., 2015a,b ; 180 mmol m^{-2} y^{-1} at 1031 m, Honjo et al., 2000). The homogeneity of the deep ocean POC fluxes, despite contrasted surface primary production, highlights the inverse relationship between primary production and export efficiency in the Southern Ocean (Maiti et al., 2013).

4.2. Seasonality of diatom fluxes

The majority of studies examining diatom export fluxes in the Southern Ocean have used a micropaleontological technique, originally developed for sediment samples (Funkhouser and Evitt, 1959). To remove organic and detrital material the micropaleontological technique includes a chemical oxidation step to "clean" and isolate the diatom frustules. This treatment separates all frustules into single valves and may selectively damage and dissolve the frustules of certain species. Furthermore, the micropaleontological technique generally considers broken frustules (Schrader and Gersonde, 1978). In the present study a direct observation of samples was favoured to meet the objective of distinguishing full and empty frustules (e.g. Armand et al., 2008; Assmy et al., 2013; Rembauville et al., 2015a) in order to calculate the relative contribution of different diatom species to total POC flux. The two techniques are likely to give slightly different results (Abrantes et al., 2005; Rembauville et al., 2015a) and therefore the comparison of diatom flux data between studies must take into account these different analytical approaches.

Despite the methodological considerations described above, a comparison of diatom export fluxes from different oceanographic zones reveals quite consistent patterns. The highest total diatom flux at P2 equals 1.4 × 10^7 valves m^{-2} d^{-1} (frustules converted to valves with a factor 2), similar to previous findings in low productivity waters of the POOZ ($\sim$10^7 valves m^{-2} d^{-1}, Abelmann and Gersonde, 1991; Grigorov et al., 2014). At P3, highest total diatom flux is one order of magnitude higher with 1.2 × 10^8 valves m^{-2} d^{-1}. This flux is comparable to the 2.4 × 10^8 valves m^{-2} d^{-1} found in a shallower (289 m) sediment trap at the central Kerguelen Plateau (station A3, Rembauville et al., 2015a), and a deep sediment trap (2000 m) also located in the POOZ (4 × 10^8 valves m^{-2} d^{-1}, Rigual-Hernández et al., 2015a, b). Despite the high primary production levels at these naturally-fertilized sites (P3 and A3), diatom valve fluxes remain lower than those reported in the Seasonal Ice Zone (SIZ) with fluxes of $\sim$10^9 valves m^{-2} d^{-1} (Suzuki et al., 2001; Pilskaln et al., 2004). These massive diatom export fluxes in the SIZ are attributed to changes in light availability and melt waters input during sea ice retreat that favors production and export of POC by diatoms (Smith and Nelson, 1986; Annett et al., 2009; Romero and Armand, 2010). In addition to iron supply, silicic acid availability also plays an important role in diatom productivity (Mengelt et al., 2001; Poulton et al., 2007). Lower diatom fluxes of 2.5 × 10^7 valves m^{-2} d^{-1} were observed (Salter et al., 2012) in the iron-fertilized productive waters downstream of Crozet (Polar Frontal Zone, PFZ) and may be explained by the lower silicic acid concentration and higher temperature north of the Polar Front (Pondaven et al., 2000; Whitehouse et al., 2012).

The similarity of diatom export assemblages observed in sediment traps is in stark contrast with the observed differences in surface waters assemblages. In the surface lightly silicified species (e.g. *Chaetoceros Hyalochaete, Pseudo-nitzschia* spp.) are dominant upstream of South Georgia, compared to more robust and highly silicified species (*Corethron pennatum, Thalassiothrix antarctica, Eucampia antarctica* var. *antarctica*) downstream (Korb et al., 2010, 2012). In the sediment traps, with the notable exception of resting spores and neritic species (*Chaetoceros Hyalochaete, E. antarctica* var. *antarctica* and *Navicula* sp.), the diatom species export assemblage is comparable at both sites. The slightly lower evenness

at P3 (Table 2) reflects the dominant contribution of CRS to the total diatom flux. *Fragilariopsis kerguelensis*, *Pseudo-nitzschia* spp., *Thalassiosira gracilis*, *Thalassiosira lentiginosa* and *Thalassionema nitzschioides* are abundant at both sites (Table 3). All of these species (with the exception of *Pseudo-nitzschia* spp.) are considered to have robust and highly silicified frustules. Preferential grazing pressure on lightly-silicified species in the upper ocean (e.g. Smetacek et al., 2004; Assmy et al., 2013) and mesopelagic BSi dissolution (Nelson et al., 1995; Ragueneau et al., 2000, 2006) may explain the dominance of highly-silicified species to bathypelagic diatom flux assemblages. Additionally, horizontal advection could homogenize variability in the surface signal (Siegel and Deuser, 1997; van Sebille et al., 2015). The absence of *Chaetoceros Hyalochaete* vegetative stages from the sediment trap record at both sites despite its presence in the mixed layer in summer (Korb et al., 2010, 2008) could be explained by the preferential dissolution of the weakly silicified vegetative frustules and/or conversion into resting spore below the mixed layer at P3 (Rynearson et al., 2013).

4.3. Si:C export stoichiometry

It has been suggested previously that diatom species-specific sensitivity to grazing pressure and the presence of certain life cycle stages can impact the Si:C export stoichiometry through the differential export of full or empty cells (Smetacek et al., 2004; Salter et al., 2012; Assmy et al., 2013). In the South Georgia trap samples resting spores were almost exclusively exported as full cells. Culture experiments suggest CRS are poorly grazed by copepods, and may even lower the grazing rate (Kuwata and Tsuda, 2005), potentially contributing to their export from the mixed layer as full cells. *Navicula* sp., *E. antarctica* var. *antarctica* and *Pseudo-nitzschia* spp. were exported with relatively low empty:full of < 5, in good agreement with previous findings from the Kerguelen Plateau (Rembauville et al., 2015a). These species were also associated with highest POC fluxes in the PFZ in the Australian sector of the Southern Ocean (Rigual-Hernández et al., 2015a,b), highlighting their potential role in carbon export.

With the exception of the resting spore export event at the end of summer, the dominance of empty *F. kerguelensis* in spring, autumn and winter at South Georgia and Kerguelen confirms its key role in the silicon pump (Smetacek et al., 2004; Salter et al., 2012; Assmy et al., 2013). The seasonal evolution of the BSi:POC ratio is similar at P2 and P3 (except in summer) and reflects comparable diatom community composition. However, the lower BSi:POC ratio in summer at P3 can be attributed to the sinking of carbon-rich diatom resting spores containing neutral lipids (Doucette and Fryxell, 1983; Kuwata et al., 1993). These findings support an emerging view (Salter et al., 2012; Rembauville et al., 2015a) that the flux of carbon rich resting spores/stages are of particular importance in setting the Si:C export stoichiometry characterizing naturally-fertilized island systems in the Southern Ocean.

Certain species that were preferentially exported as full cells at 289 m at Kerguelen were only found as empty cells at both P2 and P3 sites (*Thalassiothrix antarctica*, *Chaetoceros dichaeta* and *Proboscia inermis*). These species are either very large (*T. antarctica*, *P. inermis*), or exhibit spiny setae (*C. dichaeta*), which are thought to confer some protection from grazing (Smetacek et al., 2004). Other processes such as microbial degradation of the cellular content during sinking (Grossart and Ploug, 2001; Twining et al., 2014) might contribute to the high empty:full ratio observed for these species in deeper samples. Alternatively, the more abundant krill population at South Georgia (Atkinson et al., 2008), which is able to feed on larger phytoplankton species (Granĺi et al., 1993), might explain the higher empty:full ratio observed for these species when compared to Kerguelen. These findings suggest that differences in upper trophic level ecosystem structure modulate the role

a particular diatom species plays in carbon and BSi flux, limiting species-level generalizations between regions.

4.4. Resting spore formation and carbon transfer to the seafloor

Resting spores comprising bathypelagic (> 1500 m) flux around South Georgia were present almost entirely as full cells and accounted for 41.7% of the annual POC flux. Similar observations were made at 289 m over the Kerguelen Plateau (Rembauville et al., 2015a). These findings suggest that their importance as a POC vector persists throughout the water column. To examine changes in the occurrence of CRS as a function of depth upstream of South Georgia we combined our sediment trap dataset with mixed layer (Korb et al., 2008) and sediment (Allen et al., 2005) assemblage data (Fig. 5). We make these comparisons cautiously for several reasons: (i) mixed layer data are from January and February, averaged over three years (Korb et al., 2008), and are unlikely to represent seasonal integrals of diatom communities, (ii) surface sediments integrate over several years, averaging any inter-annual variability, and (iii) different diatom counting techniques were used. Given the considerations described above these data comparisons should be considered only as a semi-quantitative analysis of the relative importance of CRS at different depth horizons. There is a significant increase in the proportion of *Chaetoceros Hyalochaete* from the mixed layer to sediment (10–80%). *Chaetoceros Hyalochaete* species were only observed as vegetative stages in the mixed layer and resting spores below 1500 m. This could be due to either (i) resting spore formation had not occurred at the time of the sampling in the Korb et al. (2008, 2010) studies or (ii) resting spore formation occurs below the mixed layer (e.g. Rynearson et al., 2013). The increase in CRS through the mesopelagic and into the sediments supports a scenario whereby they become increasingly important vectors of carbon through selective preservation of their robust frustules.

Considering the significance of resting spores as a deep-ocean carbon vector upstream of South Georgia, it is of interest to assess the factors triggering spore formation. Numerous experimental studies have demonstrated the role of macronutrient and trace metal limitation for resting spore formation in diatoms in laboratory experiments (Garrison, 1981; Sanders and Cibik, 1985; Kuwata et al., 1993; Oku and Kamatani, 1997, Sugie et al., 2010). *Chaetoceros Hyalochaete* vegetative stages were observed in the summer upstream and downstream of South Georgia (Korb et al., 2010, 2008), although only present in export assemblages downstream. A difference in nutrient utilization at the two sites could explain the difference level of resting spore formation. It is generally reported that nitrogen limitation is the most important factor driving resting spore formation (McQuoid and Hobson, 1996, Sugie et al., 2008), although these observations were only made for low latitude diatom populations where nitrate is seasonally depleted. In the Southern Ocean, and more specifically south of the Polar Front, nitrate concentration is always > 20 μmol L^{-1} in summer, even in very productive areas (Nielsdóttir et al., 2012; Whitehouse et al., 2012; Blain et al., 2015). It therefore seems unlikely that nitrate limitation can explain the regional differences in resting spore formation.

Downstream of South Georgia, silicic acid drawdown over the summer ranges between 20 and 35 μmol L^{-1} and summer mixed layer values are < 5 μmol L^{-1} (Whitehouse et al., 2000; Nielsdóttir et al., 2012; Whitehouse et al., 2012; Borrione and Schlitzer, 2013). In contrast, upstream of South Georgia mixed layer concentrations remain at ~ 20 μmol L^{-1} upstream (Korb et al., 2008; Nielsdóttir et al., 2012) despite substantial silicic acid utilization. The P3 site is also characterized by low dissolved iron concentration in the mixed layer in spring (0.06–0.07 nmol L^{-1}) compared to waters below the thermocline (0.25–0.43 nmol L^{-1} at 1000 m)

(Nielsdóttir et al., 2012) suggesting a scenario whereby a formerly iron-replete community moves into limitation. The limitation by silicic acid and iron in summer has already been observed in two other naturally-fertilized systems of the Southern Ocean where resting spore formation is an important process for the export of carbon out of the mixed layer: the Crozet Plateau (Salter et al., 2012) and the Kerguelen Plateau (Rembauville et al., 2015a). These data suggest that iron and/or silicic acid limitation in summer might trigger resting spore formation in high latitude diatoms species, although this hypothesis requires further investigations.

4.5. Possible limitations of the present dataset

Partitioning carbon export across diatom species vectors is dependent on carbon:volume relationships (e.g. Rynearson et al., 2013), which can exhibit variability among species (Menden-Deuer and Lessard, 2000) and life cycle stages (Kuwata et al., 1993). In the present study we tried to minimize this artifact by using species-specific relationships and where necessary distinct values for vegetative and resting stages (for *Chaetoceros Hyalochaete* and *Thalassiosira antarctica*). The variability of the biovolume among individuals of a given species and the uncertainty on the carbon:volume relationship result in a coefficient of variation for resting spore carbon content of 40%. This certainly affects the precision of our estimates. However, it is unlikely to alter our main conclusion that *Chaetoceros Hyalochaete* resting spores contribute to a significant fraction of bathypelagic carbon fluxes downstream of South Georgia.

The calculated diatom contribution to carbon export accounts for < 50% of the measured carbon flux at P3 and only 2% at P2. This indicates that flux vectors not quantified here contribute significantly to carbon export at both sites. Faecal pellets (Manno et al., 2015) and/or other plankton groups (e.g. radiolarians Lampitt et al., 2009) are likely to be important components of carbon flux budgets. Nevertheless, we outline that the export of diatom spores makes a significant contribution to POC export at P3. At this same site, annual POC export in 2010 was ~ 100 mmol m^{-2} y^{-1} (Manno et al., 2015), approximately two times higher than what we report for the 2012. This highlight the need to address inter annual variability of deep ocean POC fluxes (e.g. Salter et al., 2010; Nodder et al., 2016) before robust conclusions can be drawn about a particular system.

We associate the BSi:POC ratio with diatom community composition and empty:full cell ratio based on co-occurrence patterns. An accurate partitioning of biogenic silica fluxes amongst diatom species would require knowledge of the BSi content per frustule for different species and these data are currently unavailable (Jungandreas et al., 2012). Additionally, broken frustules and debris, as well as other siliceous plankton (radiolarian, silicoflagellates) were not quantified here and certainly contribute to BSi fluxes (Supplementary Figure 1). However, despite the technical difficulties, partitioning elemental fluxes across species vectors (e.g. Salter et al., 2014; Rembauville et al. 2016) is an important endeavor for establishing the links between biological diversity and biogeochemical fluxes. However, despite the technical difficulties, partitioning elemental fluxes across species vectors (e.g. Salter et al., 2014; Rembauville et al. 2016) is an important endeavor for establishing the links between biological diversity and biogeochemical fluxes.

5. Conclusion

Diatom export fluxes over a complete seasonal cycle are now available from the three major naturally iron-fertilized Southern Ocean island systems: South Georgia (this study), Crozet (Salter et al., 2012) and Kerguelen (Rembauville et al., 2015a). Despite strong regional differences in bloom dynamics and sediment trap deployment depths (289–3160 m), annual POC export is of the same order of magnitude at each site (40–100 mmol m^{-2} d^{-1}). A similar mechanism of diatom resting spore formation and subsequent export to depth is observed at all three sites. In the naturally fertilized sites of South Georgia and Kerguelen, partitioning carbon fluxes across diatom species indicates that 40–60% of annual POC export beneath the mixed layer can be attributed to resting spore-driven export. Furthermore, consistent seasonal patterns of diatom export assemblages emerge from the comparison of these systems that appear to exert significant control on Si: C export stoichiometry. Silicon-rich fluxes consisting of empty *Fragilariopsis* species ("silica sinkers") are observed throughout the year with highest relative abundance in winter and spring. Conversely, carbon-rich fluxes are observed in summer and contain resting spores and other species exported with a high proportion of full cells such as *Eucampia antarctica* var. *antarctica*, and *Navicula* sp. ("carbon sinkers"). The selective preservation of the robust resting spore frustules as a function of depth highlights the increasing importance of resting spores as carbon vector into the bathypelagic ocean and ultimately the sediments. They may thus play a critical role in sequestering atmospheric CO_2 from these naturally iron fertilized systems over climatically relevant timescales. The exact environmental triggers for resting spore formation, and their subsequent export to depth, requires further investigation.

Appendix A. Supporting information

Supplementary data associated with this article can be found in the online version at doi:10.1016/j.dsr.2016.05.002.

References

Abelmann, A., Gersonde, R., 1991. Biosiliceous particle flux in the Southern Ocean. Mar. Chem. 35, 503–536. http://dx.doi.org/10.1016/S0304-4203(09)90040-8.

Abrantes, F., Gil, I., Lopes, C., Castro, M., 2005. Quantitative diatom analyses—a faster cleaning procedure. Deep Sea Res. Part I: Oceanogr. Res. Pap. 52, 189–198. http://dx.doi.org/10.1016/j.dsr.2004.05.012.

Allen, C.S., Pike, J., Pudsey, C.J., Leventer, A., 2005. Submillennial variations in ocean conditions during deglaciation based on diatom assemblages from the southwest Atlantic. Paleoceanography 20, PA2012. http://dx.doi.org/10.1029/2004PA001055.

Annett, A.L., Carson, D.S., Crosta, X., Clarke, A., Ganeshram, R.S., 2009. Seasonal progression of diatom assemblages in surface waters of Ryder Bay, Antarctica. Polar Biol. 33, 13–29. http://dx.doi.org/10.1007/s00300-009-0681-7.

Armand, L.K., Cornet-Barthaux, V., Mosseri, J., Quéguiner, B., 2008. Late summer diatom biomass and community structure on and around the naturally iron-fertilised Kerguelen Plateau in the Southern Ocean. Deep Sea Res. Part II: Top. Stud. Oceanogr. 55, 653–676. http://dx.doi.org/10.1016/j.dsr2.2007.12.031.

Assmy, P., Smetacek, V., Montresor, M., Klaas, C., Henjes, J., Strass, V.H., Arrieta, J.M., Bathmann, U., Berg, G.M., Breitbarth, E., Cisewski, B., Friedrichs, L., Fuchs, N., Herndl, G.J., Jansen, S., Krägefsky, S., Latasa, M., Peeken, I., Röttgers, R., Scharek, R., Schüller, S.E., Steigenberger, S., Webb, A., Wolf-Gladrow, D., 2013. Thick-shelled, grazer-protected diatoms decouple ocean carbon and silicon cycles in

the iron-limited Antarctic Circumpolar. Curr. Proc. Natl. Acad. Sci. 110, 20633–20638. http://dx.doi.org/10.1073/pnas.1309345110.

Atkinson, A., Siegel, V., Pakhomov, E.A., Jessopp, M.J., Loeb, V., 2009. A re-appraisal of the total biomass and annual production of Antarctic krill. Deep Sea Res. Part I: Oceanogr. Res. Pap. 56, 727–740. http://dx.doi.org/10.1016/j.dsr.2008.12.007.

Atkinson, A., Siegel, V., Pakhomov, E.A., Rothery, P., Loeb, V., Ross, R.M., Quetin, L.B., Schmidt, K., Fretwell, P., Murphy, E.J., Tarling, G.A., Fleming, A.H., 2008. Oceanic circumpolar habitats of Antarctic krill. Mar. Ecol. Prog. Ser. 362, 1–23. http://dx.doi.org/10.3354/meps07498.

Blain, S., Capparos, J., Guéneuguès, A., Obernosterer, I., Oriol, L., 2015. Distributions and stoichiometry of dissolved nitrogen and phosphorus in the iron-fertilized region near Kerguelen (Southern Ocean). Biogeosciences 12, 623–635. http://dx.doi.org/10.5194/bg-12-623-2015.

Blain, S., Quéguiner, B., Armand, L., Belviso, S., Bombled, B., Bopp, L., Bowie, A., Brunet, C., Brussaard, C., Carlotti, F., Christaki, U., Corbière, A., Durand, I., Ebersbach, F., Fuda, J.–L, Garcia, N., Gerringa, L., Griffiths, B., Guigue, C., Guillerm, C., Jacquet, S., Jeandel, C., Laan, P., Lefèvre, D., Lo Monaco, C., Malits, A., Mosseri, J., Obernosterer, I., Park, Y.-H., Picheral, M., Pondaven, P., Remenyi, T., Sandroni, V., Sarthou, G., Savoye, N., Scouarnec, L., Souhaut, M., Thuiller, D., Timmermans, K., Trull, T., Uitz, J., van Beek, P., Veldhuis, M., Vincent, D., Viollier, E., Vong, L., Wagener, T., 2007. Effect of natural iron fertilization on carbon sequestration in the Southern Ocean. Nature 446, 1070–1074. http://dx.doi.org/10.1038/nature05700.

Blain, S., Tréguer, P., Belviso, S., Bucciarelli, E., Denis, M., Desabre, S., Fiala, M., Martin Jézéquel, V., Le Fèvre, J., Mayzaud, P., Marty, J.-C., Razouls, S., 2001. A biogeochemical study of the island mass effect in the context of the iron hypothesis: Kerguelen Islands Southern Ocean. Deep Sea Res. Part I: Oceanogr. Res. Pap. 48, 163–187. http://dx.doi.org/10.1016/S0967-0637(00)00047-9.

Borrione, I., Schlitzer, R., 2013. Distribution and recurrence of phytoplankton blooms around South Georgia, Southern Ocean. Biogeosciences 10, 217–231. http://dx.doi.org/10.5194/bg-10-217-2013.

Boyd, I.L., Arnbom, T.A., Fedak, M.A., 1994. Biomass and energy consumption of the South Georgia population of southern elephant seals, in: Proceedings of Elephant Seals: Population Ecology, Behavior, and Physiology, pp. 98–117.

Boyd, P., Newton, P., 1995. Evidence of the potential influence of planktonic community structure on the interannual variability of particulate organic carbon flux. Deep Sea Res. Part I: Oceanogr. Res. Pap. 42, 619–639. http://dx.doi.org/10.1016/0967–0637(95)00017-Z.

Boyd, P.W., Newton, P.P., 1999. Does planktonic community structure determine downward particulate organic carbon flux in different oceanic provinces? Deep Sea Res. Part I: Oceanogr. Res. Pap. 46, 63–91. http://dx.doi.org/10.1016/S0967-0637(98)00066-1.

Buesseler, K.O., Ball, L., Andrews, J., Cochran, J.K., Hirschberg, D.J., Bacon, M.P., Fleer, A., Brzezinski, M., 2001. Upper ocean export of particulate organic carbon and biogenic silica in the Southern Ocean along 170°W. Deep Sea Res. Part II: Top. Stud. Oceanogr. 48, 4275–4297. http://dx.doi.org/10.1016/S0967-0645(01)00089-3.

Cavan, E.L., Le Moigne, F.A.C., Poulton, A.J., Tarling, G.A., Ward, P., Daniels, C.J., Fragoso, G., Sanders, R.J., 2015. Zooplankton fecal pellets control the attenuation of particulate organic carbon flux in the Scotia Sea, Southern Ocean. Geophys. Res. Lett. . http://dx.doi.org/10.1002/2014GL062744

Christaki, U., Lefèvre, D., Georges, C., Colombet, J., Catala, P., Courties, C., Sime-Ngando, T., Blain, S., Obernosterer, I., 2014. Microbial food web dynamics during spring phytoplankton blooms in the naturally iron-fertilized Kerguelen area (Southern Ocean). Biogeosciences 11, 6739–6753. http://dx.doi.org/10.5194/bg-11-6739-2014.

Collins, M.A., Stowasser, G., Fielding, S., Shreeve, R., Xavier, J.C., Venables, H.J., Enderlein, P., Cherel, Y., Van de Putte, A., 2012. Latitudinal and bathymetric patterns in the distribution and abundance of mesopelagic fish in the Scotia Sea. Deep Sea Res. Part II: Top. Stud. Oceanogr. 59–60, 189–198. http://dx.doi.org/10.1016/j.dsr2.2011.07.003 (DISCOVERY 2010: Spatial and Temporal Variability in a Dynamic Polar Ecosystem).

Cornet-Barthaux, V., Armand, L., Quéguiner, B., 2007. Biovolume and biomass estimates of key diatoms in the Southern Ocean. Aquat. Microb. Ecol. 48, 295–308. http://dx.doi.org/10.3354/ame048295.

de Baar, H.J.W., Buma, A.G.J., Nolting, R.F., Cadée, G.C., Jacques, G., Tréguer, P., 1990. On iron limitation of the Southern Ocean: experimental observations in the Weddell and Scotia Seas. Mar. Ecol. Prog. Ser. 65, 105–122. http://dx.doi.org/10.3354/meps065105.

de Baar, H.J.W., de Jong, J.T.M., Bakker, D.C.E., Löscher, B.M., Veth, C., Bathmann, U., Smetacek, V., 1995. Importance of iron for plankton blooms and carbon dioxide drawdown in the Southern Ocean. Nature 373, 412–415. http://dx.doi.org/10.1038/373412a0.

DeMaster, D.J., 1981. The supply and accumulation of silica in the marine environment. Geochim. Cosmochim. Acta 45, 1715–1732. http://dx.doi.org/10.1016/0016-7037(81)90006-5.

Doucette, G.J., Fryxell, G.A., 1983. Thalassiosira antarctica: vegetative and resting stage chemical composition of an ice-related marine diatom. Mar. Biol. 78, 1–6. http://dx.doi.org/10.1007/BF00392964.

Duprat, L.P.A.M., Bigg, G.R., Wilton, D.J., 2016. Enhanced Southern Ocean marine productivity due to fertilization by giant icebergs. Nat. Geosci. 9, 219–221. http://dx.doi.org/10.1038/ngeo2633.

Fischer, G., Gersonde, R., Wefer, G., 2002. Organic carbon, biogenic silica and diatom fluxes in the marginal winter sea-ice zone and in the Polar Front Region: interannual variations and differences in composition. Deep Sea Res. Part II: Top. Stud. Oceanogr. 49, 1721–1745. http://dx.doi.org/10.1016/S0967-0645(02)00009-7.

Funkhouser, J.W., Evitt, W.R., 1959. Preparation techniques for acid-insoluble microfossils. Micropaleontology 5, 369–375. http://dx.doi.org/10.2307/1484431.

Garrison, D.L., 1981. Monterey bay phytoplankton. II. Resting spore cycles in coastal diatom populations. J. Plankton Res. 3, 137–156. http://dx.doi.org/10.1093/plankt/3.1.137.

Granĺí, E., Granéli, W., Rabbani, M.M., Daugbjerg, N., Fransz, G., Roudy, J.C., Alder, V. A., 1993. The influence of copepod and krill grazing on the species composition of phytoplankton communities from the Scotia Weddell sea. Polar Biol. 13, 201–213. http://dx.doi.org/10.1007/BF00238930.

Grigorov, I., Rigual-Hernandez, A.S., Honjo, S., Kemp, A.E.S., Armand, L.K., 2014. Settling fluxes of diatoms to the interior of the Antarctic circumpolar current along 170W. Deep Sea Res. Part I: Oceanogr. Res. Pap. 93, 1–13. http://dx.doi.org/10.1016/j.dsr.2014.07.008.

Grossart, H.-P., Ploug, H., 2001. Microbial degradation of organic carbon and nitrogen on diatom aggregates. Limnol. Oceanogr. 46, 267–277. http://dx.doi.org/10.4319/lo.2001.46.2.0267.

Hasle, G.R., Syvertsen, E.E., 1997. Chapter 2 – marine diatoms. In: Tomas, C.R. (Ed.), Identifying Marine Phytoplankton. Academic Press, San Diego, pp. 5–385.

Hawkings, J.R., Wadham, J.L., Tranter, M., Raiswell, R., Benning, L.G., Statham, P.J., Tedstone, A., Nienow, P., Lee, K., Telling, J., 2014. Ice sheets as a significant source of highly reactive nanoparticulate iron to the oceans. Nat. Commun. 5, 3929. http://dx.doi.org/10.1038/ncomms4929.

Hillebrand, H., Dürselen, C.-D., Kirschtel, D., Pollingher, U., Zohary, T., 1999. Biovolume calculation for pelagic and benthic microalgae. J. Phycol. 35, 403–424. http://dx.doi.org/10.1046/j.1529-8817.1999.3520403.x.

Honjo, S., Francois, R., Manganini, S., Dymond, J., Collier, R., 2000. Particle fluxes to the interior of the Southern Ocean in the Western Pacific sector along 170°W. Deep Sea Res. Part II: Top. Stud. Oceanogr. 47, 3521–3548. http://dx.doi.org/10.1016/S0967-0645(00)00077-1.

Huntley, M.E., Lopez, M.D., Karl, D.M., 1991. Top predators in the Southern ocean: a major leak in the biological carbon pump. Science 253, 64–66. http://dx.doi.org/10.1126/science.1905841.

Jouandet, M.P., Blain, S., Metzl, N., Brunet, C., Trull, T.W., Obernosterer, I., 2008. A seasonal carbon budget for a naturally iron-fertilized bloom over the Kerguelen Plateau in the Southern Ocean. Deep Sea Res. Part II: Top. Stud. Oceanogr. 55, 856–867. http://dx.doi.org/10.1016/j.dsr2.2007.12.037.

Jungandreas, A., Wagner, H., Wilhelm, C., 2012. Simultaneous measurement of the silicon content and physiological parameters by FTIR spectroscopy in diatoms with siliceous cell walls. Plant Cell Physiol. 53, 2153–2162. http://dx.doi.org/10.1093/pcp/pcs144.

Korb, R.E., Whitehouse, M., 2004. Contrasting primary production regimes around South Georgia, Southern Ocean: large blooms versus high nutrient, low chlorophyll waters. Deep Sea Res. Part I: Oceanogr. Res. Pap. 51, 721–738. http://dx.doi.org/10.1016/j.dsr.2004.02.006.

Korb, R.E., Whitehouse, M.J., Atkinson, A., Thorpe, S.E., 2008. Magnitude and maintenance of the phytoplankton bloom at South Georgia: a naturally ironreplete environment. Mar. Ecol. Prog. Ser. 368, 75–91. http://dx.doi.org/10.3354/meps07525.

Korb, R.E., Whitehouse, M.J., Gordon, M., Ward, P., Poulton, A.J., 2010. Summer microplankton community structure across the Scotia Sea: implications for biological carbon export. Biogeosciences 7, 343–356. http://dx.doi.org/10.5194/bg-7-343-2010.

Korb, R.E., Whitehouse, M.J., Ward, P., Gordon, M., Venables, H.J., Poulton, A.J., 2012. Regional and seasonal differences in microplankton biomass, productivity, and structure across the Scotia Sea: implications for the export of biogenic carbon. Deep Sea Res. Part II: Top. Stud. Oceanogr. 59–60, 67–77. http://dx.doi.org/10.1016/j.dsr2.2011.06.006.

Kuwata, A., Hama, T., Takahashi, M., 1993. Ecophysiological characterization of two life forms, resting spores and resting cells, of a marine planktonic diatom. Mar. Ecol. Prog. Ser. 102, 245–255.

Kuwata, A., Tsuda, A., 2005. Selection and viability after ingestion of vegetative cells, resting spores and resting cells of the marine diatom, Chaetoceros pseudocurvisetus, by two copepods. J. Exp. Mar. Biol. Ecol. 322, 143–151. http://dx.doi.org/10.1016/j.jembe.2005.02.013.

Lampitt, R.S., Salter, I., Johns, D., 2009. Radiolaria: major exporters of organic carbon to the deep ocean. Glob. Biogeochem. Cycles 23, GB1010. http://dx.doi.org/10.1029/2008GB003221.

Lam, P.J., Bishop, J.K.B., 2007. High biomass, low export regimes in the Southern Ocean. Deep Sea Res. Part II: Top. Stud. Oceanogr. 54, 601–638. http://dx.doi.org/10.1016/j.dsr2.2007.01.013.

Lam, P.J., Doney, S.C., Bishop, J.K.B., 2011. The dynamic ocean biological pump: Insights from a global compilation of particulate organic carbon, $CaCO_3$, and opal concentration profiles from the mesopelagic. Glob. Biogeochem. Cycles 25, GB3009. http://dx.doi.org/10.1029/2010GB003868.

Laws, E.A., D'Sa, E., Naik, P., 2011. Simple equations to estimate ratios of new or export production to total production from satellite-derived estimates of sea surface temperature and primary production. Limnol. Oceanogr. Methods 9, 593–601. http://dx.doi.org/10.4319/lom.2011.9.593.

Le Moigne, F.A.C., Henson, S.A., Cavan, E., Georges, C., Pabortsava, K., Achterberg, E. P., Ceballos-Romero, E., Zubkov, M., Sanders, R.J., 2016. What causes the inverse relationship between primary production and export efficiency in the Southern Ocean? Geophys. Res. Lett. . http://dx.doi.org/10.1002/2016GL068480

Loscher, B.M., De Baar, H.J.W., De Jong, J.T.M., Veth, C., Dehairs, F., 1997. The distribution of Fe in the antarctic circumpolar current. Deep Sea Res. Part II: Top. Stud. Oceanogr. 44, 143–187. http://dx.doi.org/10.1016/S0967-0645(96)00101-4.

Maiti, K., Charette, M.A., Buesseler, K.O., Kahru, M., 2013. An inverse relationship between production and export efficiency in the Southern Ocean. Geophys. Res. Lett. 40, 1557–1561. http://dx.doi.org/10.1002/grl.50219.

Manno, C., Stowasser, G., Enderlein, P., Fielding, S., Tarling, G.A., 2015. The contribution of zooplankton faecal pellets to deep-carbon transport in the Scotia Sea (Southern Ocean). Biogeosciences 12, 1955–1965. http://dx.doi.org/10.5194/bg-12-1955-2015.

Manno, C., Stowasser, G., Enderlein, P., Fielding, S., Tarling, G.A., 2014. The contribution of zooplankton faecal pellets to deep carbon transport in the Scotia Sea (Southern Ocean). Biogeosci. Discuss 11, 16105–16134. http://dx.doi.org/10.5194/bgd-11-16105-2014.

Martin, J.H., 1990. Glacial-interglacial CO_2 change: the iron hypothesis. Paleoceanography 5, 1–13. http://dx.doi.org/10.1029/PA005i001p00001.

McQuoid, M.R., Hobson, L.A., 1996. Diatom Resting Stages. J. Phycol. 32, 889–902. http://dx.doi.org/10.1111/j.0022-3646.1996.00889.x.

Menden-Deuer, S., Lessard, E.J., 2000. Carbon to volume relationships for dinoflagellates, diatoms, and other protist plankton. Limnol. Oceanogr. 45, 569–579. http://dx.doi.org/10.4319/lo.2000.45.3.0569.

Mengelt, C., Abbott, M.R., Barth, J.A., Letelier, R.M., Measures, C.I., Vink, S., 2001. Phytoplankton pigment distribution in relation to silicic acid, iron and the physical structure across the Antarctic Polar Front, 170°W, during austral summer. Deep Sea Res. Part II: Top. Stud. Oceanogr. 48, 4081–4100. http://dx.doi.org/10.1016/S0967-0645(01)00081-9.

Meredith, M.P., Watkins, J.L., Murphy, E.J., Cunningham, N.J., Wood, A.G., Korb, R., Whitehouse, M.J., Thorpe, S.E., Vivier, F., 2003. An anticyclonic circulation above the Northwest Georgia Rise, Southern Ocean. Geophys. Res. Lett. 30, 2061. http://dx.doi.org/10.1029/2003GL018039.

Meskhidze, N., Nenes, A., Chameides, W.L., Luo, C., Mahowald, N., 2007. Atlantic Southern Ocean productivity: Fertilization from above or below? Glob. Biogeochem. Cycles 21, GB2006. http://dx.doi.org/10.1029/2006GB002711.

Moore, J.K., Abbott, M.R., 2000. Phytoplankton chlorophyll distributions and primary production in the Southern Ocean. J. Geophys. Res. Oceans 105, 28709–28722. http://dx.doi.org/10.1029/1999JC000043.

Moore, J.K., Abbott, M.R., Richman, J.G., 1999. Location and dynamics of the Antarctic Polar Front from satellite sea surface temperature data. J. Geophys. Res. Oceans 104, 3059–3073. http://dx.doi.org/10.1029/1998JC900032.

Mortlock, R.A., Froelich, P.N., 1989. A simple method for the rapid determination of biogenic opal in pelagic marine sediments. Deep Sea Res. Part I: Oceanogr. Res. Pap. 36, 1415–1426. http://dx.doi.org/10.1016/0198-0149(89)90092-7.

Nelson, D.M., Tréguer, P., Brzezinski, M.A., Leynaert, A., Quéguiner, B., 1995. Production and dissolution of biogenic silica in the ocean: revised global estimates, comparison with regional data and relationship to biogenic sedimentation. Glob. Biogeochem. Cycles 9, 359–372. http://dx.doi.org/10.1029/95GB01070.

Nielsdóttir, M.C., Bibby, T.S., Moore, C.M., Hinz, D.J., Sanders, R., Whitehouse, M., Korb, R., Achterberg, E.P., 2012. Seasonal and spatial dynamics of iron availability in the Scotia Sea. Mar. Chem. 130–131, 62–72. http://dx.doi.org/10.1016/j.marchem.2011.12.004.

Nodder, S.D., Chiswell, S.M., Northcote, L.C., 2016. Annual cycles of deep-ocean biogeochemical export fluxes in subtropical and subantarctic waters, southwest Pacific Ocean. J. Geophys. Res. Oceans . http://dx.doi.org/10.1002/2015JC011243.

Obernosterer, I., Christaki, U., Lefèvre, D., Catala, P., Van Wambeke, F., Lebaron, P., 2008. Rapid bacterial mineralization of organic carbon produced during a phytoplankton bloom induced by natural iron fertilization in the Southern Ocean. Deep Sea Res. Part II: Top. Stud. Oceanogr. 55, 777–789. http://dx.doi.org/10.1016/j.dsr2.2007.12.005.

Oku, O., Kamatani, A., 1997. Resting spore formation of the marine planktonic diatom Chaetoceros anastomosans induced by high salinity and nitrogen depletion. Mar. Biol. 127, 515–520. http://dx.doi.org/10.1007/s002270050040.

Park, J., Oh, I.-S., Kim, H.-C., Yoo, S., 2010. Variability of SeaWiFs chlorophyll-a in the southwest Atlantic sector of the Southern Ocean: strong topographic effects and weak seasonality. Deep Sea Res. Part I: Oceanogr. Res. Pap. 57, 604–620. http://dx.doi.org/10.1016/j.dsr.2010.01.004.

Pilskaln, C.H., Manganini, S.J., Trull, T.W., Armand, L., Howard, W., Asper, V.L., Massom, R., 2004. Geochemical particle fluxes in the Southern Indian Ocean seasonal ice zone: Prydz Bay region East Antarctica. Deep Sea Res. Part I: Oceanogr. Res. Pap. 51, 307–332. http://dx.doi.org/10.1016/j.dsr.2003.10.010.

Pollard, R.T., Salter, I., Sanders, R.J., Lucas, M.I., Moore, C.M., Mills, R.A., Statham, P.J., Allen, J.T., Baker, A.R., Bakker, D.C.E., Charette, M.A., Fielding, S., Fones, G.R., French, M., Hickman, A.E., Holland, R.J., Hughes, J.A., Jickells, T.D., Lampitt, R.S., Morris, P.J., Nédélec, F.H., Nielsdóttir, M., Planquette, H., Popova, E.E., Poulton, A. J., Read, J.F., Seeyave, S., Smith, T., Stinchcombe, M., Taylor, S., Thomalla, S., Venables, H.J., Williamson, R., Zubkov, M.V., 2009. Southern Ocean deep-water carbon export enhanced by natural iron fertilization. Nature 457, 577–580. http://dx.doi.org/10.1038/nature07716.

Pondaven, P., Ragueneau, O., Tréguer, P., Hauvespre, A., Dezileau, L., Reyss, J.L., 2000. Resolving the "opal paradox" in the Southern Ocean. Nature 405, 168–172. http://dx.doi.org/10.1038/35012046.

Poulton, A.J., Mark Moore, C., Seeyave, S., Lucas, M.I., Fielding, S., Ward, P., 2007. Phytoplankton community composition around the Crozet Plateau, with emphasis on diatoms and Phaeocystis. Deep Sea Res. Part II: Top. Stud. Oceanogr. 54, 2085–2105. http://dx.doi.org/10.1016/j.dsr2.2007.06.005.

Quéguiner, B., 2013. Iron fertilization and the structure of planktonic communities in high nutrient regions of the Southern Ocean. Deep Sea Res. Part II: Top. Stud. Oceanogr. 90, 43–54. http://dx.doi.org/10.1016/j.dsr2.2012.07.024.

Ragueneau, O., Schultes, S., Bidle, K., Claquin, P., Moriceau, B., 2006. Si and C interactions in the world ocean: importance of ecological processes and

implications for the role of diatoms in the biological pump. Glob. Biogeochem. Cycles 20, GB4S02. http://dx.doi.org/10.1029/2006GB002688.

Ragueneau, O., Tréguer, P., Leynaert, A., Anderson, R.F., Brzezinski, M.A., DeMaster, D.J., Dugdale, R.C., Dymond, J., Fischer, G., François, R., Heinze, C., Maier-Reimer, E., Martin-Jézéquel, V., Nelson, D.M., Quéguiner, B., 2000. A review of the Si cycle in the modern ocean: recent progress and missing gaps in the application of biogenic opal as a paleoproductivity proxy. Glob. Planet Change 26, 317–365. http://dx.doi.org/10.1016/S0921-8181(00)00052-7.

Rembauville, M., Blain, S., Armand, L., Quéguiner, B., Salter, I., 2015a. Export fluxes in a naturally iron-fertilized area of the Southern Ocean – Part 2: importance of diatom resting spores and faecal pellets for export. Biogeosciences 12, 3171–3195. http://dx.doi.org/10.5194/bg-12-3171-2015.

Rembauville, M., Meilland, J., Ziveri, P., Schiebel, R., Blain, S., Salter, I., 2016. Planktic foraminifer and coccolith contribution to carbonate export fluxes over the central Kerguelen Plateau. Deep Sea Res. Part I: Oceanogr. Res. Pap. 111, 91–101. http://dx.doi.org/10.1016/j.dsr.2016.02.017.

Rembauville, M., Salter, I., Leblond, N., Gueneugues, A., Blain, S., 2015b. Export fluxes in a naturally iron-fertilized area of the Southern Ocean – Part 1: seasonal dynamics of particulate organic carbon export from a moored sediment trap. Biogeosciences 12, 3153–3170. http://dx.doi.org/10.5194/bg-12-3153-2015.

Reynolds, R.W., Rayner, N.A., Smith, T.M., Stokes, D.C., Wang, W., 2002. An improved in situ and satellite SST analysis for climate. J. Clim. 15, 1609–1625. http://dx.doi.org/10.1175/1520-0442(2002)015 < 1609:AIISAS > 2.0.CO;2.

Rigual-Hernández, A.S., Trull, T.W., Bray, S.G., Closset, I., Armand, L.K., 2015a. Seasonal dynamics in diatom and particulate export fluxes to the deep sea in the Australian sector of the southern Antarctic Zone. J. Mar. Syst. 142, 62–74. http://dx.doi.org/10.1016/j.jmarsys.2014.10.002.

Rigual-Hernández, A.S., Trull, T.W., Bray, S.G., Cortina, A., Armand, L.K., 2015b. Latitudinal and temporal distributions of diatom populations in the pelagic waters of the Subantarctic and Polar Frontal zones of the Southern Ocean and their role in the biological pump. Biogeosciences 12, 5309–5337. http://dx.doi.org/10.5194/bg-12-5309-2015.

Romero, O.E., Armand, L., 2010. Marine diatoms as indicators of modern changes in oceanographic conditions, The Diatoms: Applications for the Environmental and Earth Sciences, 2nd Ed. Camb. Univ. Press, pp. 373–400.

Rynearson, T.A., Richardson, K., Lampitt, R.S., Sieracki, M.E., Poulton, A.J., Lyngsgaard, M.M., Perry, M.J., 2013. Major contribution of diatom resting spores to vertical flux in the sub-polar North Atlantic. Deep Sea Res. Part I: Oceanogr. Res. Pap. 82, 60–71. http://dx.doi.org/10.1016/j.dsr.2013.07.013.

Salter, I., Kemp, A.E.S., Lampitt, R.S., Gledhill, M., 2010. The association between biogenic and inorganic minerals and the amino acid composition of settling particles. Limnol. Oceanogr. 55, 2207–2218. http://dx.doi.org/10.4319/lo.2010.55.5.2207.

Salter, I., Kemp, A.E.S., Moore, C.M., Lampitt, R.S., Wolff, G.A., Holtvoeth, J., 2012. Diatom resting spore ecology drives enhanced carbon export from a naturally iron-fertilized bloom in the Southern Ocean. Glob. Biogeochem. Cycles 26, GB1014. http://dx.doi.org/10.1029/2010GB003977.

Salter, I., Schiebel, R., Ziveri, P., Movellan, A., Lampitt, R., Wolff, G.A., 2014. Carbonate counter pump stimulated by natural iron fertilization in the Polar Frontal Zone. Nat. Geosci. 7, 885–889. http://dx.doi.org/10.1038/ngeo2285.

Sanders, J.G., Cibik, S.J., 1985. Reduction of growth rate and resting spore formation in a marine diatom exposed to low levels of cadmium. Mar. Environ. Res. 16, 165–180. http://dx.doi.org/10.1016/0141-1136(85)90136-9.

Schrader, H.J., Gersonde, R., 1978. Diatoms and silicofagellates. Micropaleontological counting methods and techniques: an exercise on an eight metres section of the Lower Pliocene of Capo Rosello, Sicily. Utrecht Micropaleontol. Bull., 129–176.

Siegel, D.A., Deuser, W.G., 1997. Trajectories of sinking particles in the Sargasso Sea: modeling of statistical funnels above deep-ocean sediment traps. Deep Sea Res. Part I: Oceanogr. Res. Pap. 44, 1519–1541. http://dx.doi.org/10.1016/S0967-0637(97)00028-9.

Smetacek, V., Assmy, P., Henjes, J., 2004. The role of grazing in structuring Southern Ocean pelagic ecosystems and biogeochemical cycles. Antarct. Sci. 16, 541–558. http://dx.doi.org/10.1017/S0954102004002317.

Smetacek, V.S., 1985. Role of sinking in diatom life-history cycles: ecological, evolutionary and geological significance. Mar. Biol. 84, 239–251. http://dx.doi.org/10.1007/BF00392493.

Smith Jr., W.O., Nelson, D.M., 1986. Importance of ice edge phytoplankton production in the Southern Ocean. BioScience 36, 251–257. http://dx.doi.org/10.2307/1310215.

Sugie, K., Kuma, K., 2008. Resting spore formation in the marine diatom Thalassiosira nordenskioeldii under iron- and nitrogen-limited conditions. J. Plankton Res. 30, 1245–1255. http://dx.doi.org/10.1093/plankt/fbn080.

Sugie, K., Kuma, K., Fujita, S., Ikeda, T., 2010. Increase in Si:N drawdown ratio due to resting spore formation by spring bloom-forming diatoms under Fe- and N-limited conditions in the Oyashio region. J. Exp. Mar. Biol. Ecol. 382, 108–116. http://dx.doi.org/10.1016/j.jembe.2009.11.001.

Suzuki, H., Sasaki, H., Fukuchi, M., 2001. Short-term variability in the flux of rapidly sinking particles in the Antarctic marginal ice zone. Polar Biol. 24, 697–705. http://dx.doi.org/10.1007/s003000100240.

Tesi, T., Langone, L., Ravaioli, M., Giglio, F., Capotondi, L., 2012. Particulate export and lateral advection in the Antarctic Polar Front (Southern Pacific Ocean): one-year mooring deployment. J. Mar. Syst. 105–108, 70–81. http://dx.doi.org/10.1016/j.jmarsys.2012.06.002.

Thorpe, S.E., Heywood, K.J., Brandon, M.A., Stevens, D.P., 2002. Variability of the

southern Antarctic Circumpolar Current front north of South Georgia. J. Mar. Syst. Phys. Biol. Ocean Fronts 37, 87–105. http://dx.doi.org/10.1016/S0924-7963 (02)00197-5.

Twining, B.S., Nodder, S.D., King, A.L., Hutchins, D.A., LeCleir, G.R., DeBruyn, J.M., Maas, E.W., Vogt, S., Wilhelm, S.W., Boyd, P.W., 2014. Differential remineralization of major and trace elements in sinking diatoms. Limnol. Oceanogr. 59, 689–704. http://dx.doi.org/10.4319/lo.2014.59.3.0689.

van der Merwe, P., Bowie, A.R., Quéroué, F., Armand, L., Blain, S., Chever, F., Davies, D., Dehairs, F., Planchon, F., Sarthou, G., Townsend, A.T., Trull, T.W., 2015. Sourcing the iron in the naturally fertilised bloom around the Kerguelen Plateau: particulate trace metal dynamics. Biogeosciences 12, 739–755. http://dx. doi.org/10.5194/bg-12-739-2015.

van der Merwe, P., Lannuzel, D., Bowie, A.R., Meiners, K.M., 2011. High temporal resolution observations of spring fast ice melt and seawater iron enrichment in East Antarctica. J. Geophys. Res. Biogeosci. 116, G03017. http://dx.doi.org/ 10.1029/2010JG001628.

van Sebille, E., Scussolini, P., Durgadoo, J.V., Peeters, F.J.C., Biastoch, A., Weijer, W., Turney, C., Paris, C.B., Zahn, R., 2015. Ocean currents generate large footprints in marine palaeoclimate proxies. Nat. Commun. 6, 6521. http://dx.doi.org/10.1038/ ncomms7521.

Ward, P., Atkinson, A., Venables, H.J., Tarling, G.A., Whitehouse, M.J., Fielding, S., Collins, M.A., Korb, R., Black, A., Stowasser, G., Schmidt, K., Thorpe, S.E., Enderlein, P., 2012. Food web structure and bioregions in the Scotia Sea: a

seasonal synthesis. Deep Sea Res. Part II: Top. Stud. Oceanogr. 59–60, 253–266. http://dx.doi.org/10.1016/j.dsr2.2011.08.005.

Ward, P., Whitehouse, M., Meredith, M., Murphy, E., Shreeve, R., Korb, R., Watkins, J., Thorpe, S., Woodd-Walker, R., Brierley, A., Cunningham, N., Grant, S., Bone, D., 2002. The Southern Antarctic circumpolar current front: physical and biological coupling at South Georgia. Deep Sea Res. Part I: Oceanogr. Res. Pap. 49, 2183–2202. http://dx.doi.org/10.1016/S0967-0637(02)00119-X.

Westberry, T.K., Behrenfeld, M.J., Milligan, A.J., Doney, S.C., 2013. Retrospective satellite ocean color analysis of purposeful and natural ocean iron fertilization. Deep Sea Res. Part I: Oceanogr. Res. Pap. 73, 1–16. http://dx.doi.org/10.1016/j. dsr.2012.11.010.

Whitehouse, M.J., Atkinson, A., Korb, R.E., Venables, H.J., Pond, D.W., Gordon, M., 2012. Substantial primary production in the land-remote region of the central and northern Scotia Sea. Deep Sea Res. Part II: Top. Stud. Oceanogr. 59–60, 47–56. http://dx.doi.org/10.1016/j.dsr2.2011.05.010 (DISCOVERY 2010: Spatial and Temporal Variability in a Dynamic Polar Ecosystem).

Whitehouse, M.J., Priddle, J., Brandon, M.A., 2000. Chlorophyll/nutrient characteristics in the water masses to the north of South Georgia, Southern Ocean. Polar Biol. 23, 373–382. http://dx.doi.org/10.1007/s003000050458.

Whitehouse, M.J., Priddle, J., Symon, C., 1996. Seasonal and annual change in seawater temperature, salinity, nutrient and chlorophyll a distributions around South Georgia, South Atlantic. Deep Sea Res. Part I: Oceanogr. Res. Pap. 43, 425–443. http://dx.doi.org/10.1016/0967-0637(96)00020-9.
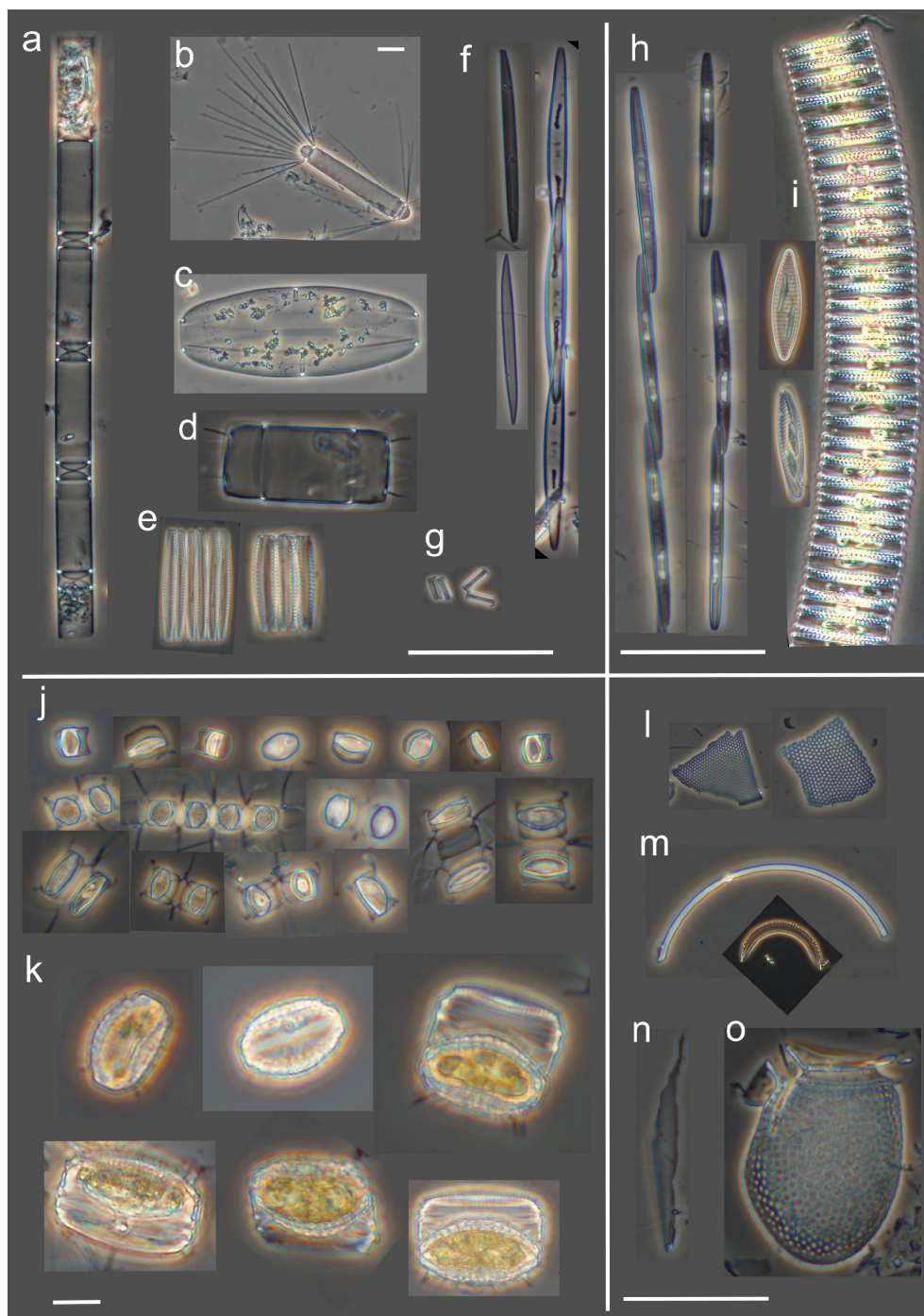
Figure 2.10: **Supplementary Figure.** Plate with light microscopy micrographs of some diatoms found in the sediment traps. Upper left panel: examples of empty cells. **a.** Chain of *Corethron inerme*, **b.** *Corethron pennatum*, **c.** *Membraneis*, **d.** *Odontella weissflogii*, **e.** *Fragilariopsis kerguelensis*, **f.** *Pseudo-nitzschia* spp., **g.** *Thalassionema nitzschioides*. Scale bars are 50 µm. Upper right panel: examples of cells considered as full due to the presence of plasts. **h.** *Pseudo-nitzschia* spp., **i.** *F. kerguelensis*. Scale bar is 50 µm. Lower left panel: examples of resting spores. **j.** *Chaetoceros Hyalochaete* resting spores. The multiple morphologies suggest different species at the origin of the spore. **k.** *Thalassiosira antarctica* resting spores. Scale bar is 10 µm. Lower right panel: examples of particles not quantified in this study. **l.** Frustule debris, **m.** centric diatom girdle band (broken) and *Dactyliosolen antarcitucs* girdle band, **n.** frustule debris probably belonging to *Pleurosigma*, **o.** Dinoflagellate theca belonging to the Dinophysiaceae family. Scale bar is 50 µm.

3 | Plankton diversity and particulate matter stoichiometry
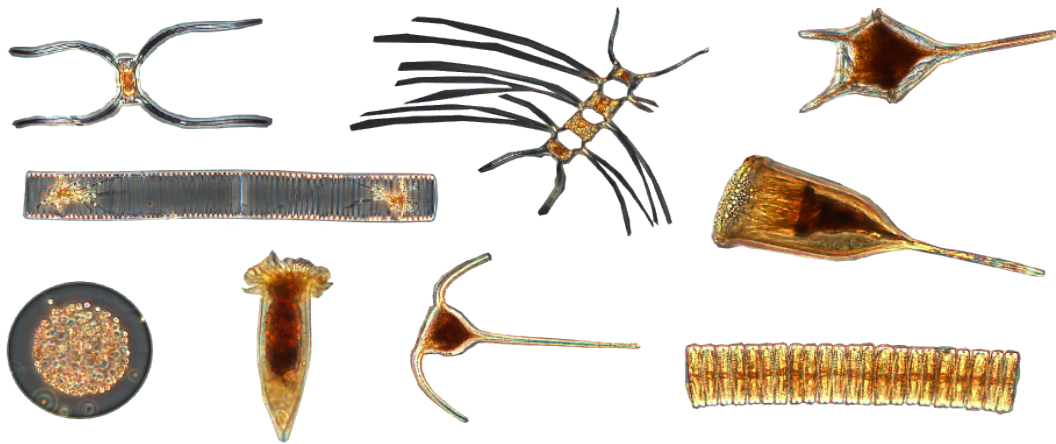
Contents

3.1 Summer microplankton community structure in the Indian Sector of the Southern Ocean (article 5)

Previous **articles 1-4** mainly focussed on the importance of diatom life strategies for the intensity of particulate organic carbon (POC) and biogenic silicon (BSi) export, but nitrogen and phosphorous stoichiometry was poorly considered. A compilation of particulate carbon, nitrogen (PON) and phosphorous (POP) at global scale showed strong latitudinal patterns in particulate stoichiometry likely to reflect the imprint of different plankton communities (Martiny et al., 2013b,a). This study revealed the scarcity of data on particulate stoichiometry in the Southern Ocean, and emphasized the compelling need to couple the description of the plankton community together with the particulate matter stoichiometry to be able to explain the observed geographical patterns. Additionally, the sediment trap studies suggested an uncoupling of plankton communities and BSi:POC stoichoimetry between the mixed layer and the upper mesopelagic ocean. Sediment trap records themselves do not allow to identify where the uncoupling occurs in the water column, nor the reasons for this uncoupling. The OISO23 cruise (January-February 2014) was the opportunity to document the relationship between microplankton community structure and particulate matter C, N, P, and Si stoichiometry in a diversity of hydrological conditions around the Crozet and Kerguelen island plateaus.

In summer, the diatom versus dinoflagellate dominance of the micropankton community exerts a first order control on the PON:POP ratio. In the Antarctic zone, an important part of the chlorophyll a (Chl) is located below the euphotic and mixed layer. Elevated Chl:POC ratios in the transiton layer (density gradient below the mixed layer) suggests photoacclimatation of a diatom community comparable in terms of structure to the one of mixed layer. However, the fraction of empty diatom frustules shows an abrupt increase within the transition layer with a predominance of *Fragilariopsis kerguelensis*. We suggest Si and C decoupling occurs within the transition layer and results from intense grazing on diatoms and a possible silicification sustained by strong diapycnal $Si(OH)_4$ diffusive fluxes that alleviate silicon limitation in the mixed layer. Finally, one sample from the upper mesopelagic ocean (250 m at the A3 station - location of the sediment trap in **articles 1 and 2**) display a dominance of *Chaetoceros Hyalochaete* resting spore to microplankton biomass, confirming its ability to exit the mixed layer and bypass the grazing pressure within the transition layer.

All data collected and analysed by the author except chlorophyll a analyses performed by C. Lo Monaco.

Particulate matter stoichiometry driven by microplankton community structure in summer in the Indian sector of the Southern Ocean

M. Rembauville,*[1] S. Blain,[1] J. Caparros,[1] I. Salter[1,2]

[1]Sorbonne Universités, UPMC Univ Paris 06, CNRS, Laboratoire d'Océanographie Microbienne (LOMIC), Observatoire Océanologique, Banyuls/mer, France
[2]Alfred Wegener Institute, Helmholtz Centre for Polar and Marine Research, Bremerhaven, Germany

Abstract

Microplankton community structure and particulate matter stoichiometry were investigated in a late summer survey across the Subantarctic and Polar Front in the Indian sector of the Southern Ocean. Microplankton community structure exerted a first order control on PON:POP stoichiometry with diatom-dominated samples exhibiting much lower ratios (4–6) than dinoflagellate and ciliate-dominated samples (10–21). A significant fraction of the total chlorophyll *a* (30–70%) was located beneath the euphotic zone and mixed layer and sub-surface chlorophyll features were associated to transition layers. Although microplankton community structure and biomass was similar between mixed and transition layers, the latter was characterized by elevated Chl:POC ratios indicating photoacclimation of mixed layer communities. Empty diatom frustules, in particular of *Fragilariopsis kerguelensis* and *Pseudo-nitzschia*, were found to accumulate in the Antarctic Zone transition layer and were associated to elevated BSi:POC ratios. Furthermore, high $Si(OH)_4$ diffusive fluxes (>1 mmol m^2 d^{-1}) into the transition layer appeared likely to sustain silicification. We suggest transition layers as key areas of C and Si decoupling through (1) physiological constraints on carbon and silicon fixation (2) as active foraging sites for grazers that preferentially remineralize carbon. On the Kerguelen Plateau, the dominant contribution of *Chaetoceros Hyalochaete* resting spores to microplankton biomass resulted in a three-fold enhancement of POC concentration at 250 m, compared to other stations. These findings further highlight the importance of diatom resting spores as a significant vector of carbon export through the intense remineralization horizons characterising Southern Ocean ecosystems.

The Southern Ocean connects the three major Ocean basins and is important for heat and carbon exchange with the atmosphere, representing a critical conduit by which anthropogenic CO_2 enters the ocean (Sabine et al. 2004; Khatiwala et al. 2009). Modeling studies have suggested that nutrients exiting the Southern Ocean, through the formation of mode water, may constrain primary production in vast areas of the global Ocean (Sarmiento et al. 2004; Dutkiewicz et al. 2005). The efficiency and stoichiometry of surface nutrient depletion by the biological pump in the Southern Ocean can thus have major implications for global Ocean productivity (Primeau et al. 2013). A large fraction of present-day Southern Ocean surface waters are referred to as "High-Nutrient, Low-Chlorophyll" areas (HNLC, Minas et al. 1986) where low trace-metal concentrations, in particular

iron, can limit primary production (de Baar et al. 1990; Martin 1990) and result in a weaker biological pump (e.g., Salter et al. 2012). Regional trace metal inputs from shelf sediments and glacial melt-water can sustain large scale (>100 km) and long lasting (several months) phytoplankton blooms in proximity to island systems such as South Georgia, Crozet and Kerguelen plateaus (Whitehouse et al. 2000; Blain et al. 2001; Pollard et al. 2007).

Many studies of phytoplankton blooms in the Southern Ocean usually focus on the euphotic zone and studies using satellite data (e.g., Park et al. 2010; Borrione and Schlitzer 2013) are restricted to the surface. However, subsurface chlorophyll maxima (SCM) deeper than the euphotic zone at the base of the mixed layer are recurrent in late summer in the HNLC waters of the Southern Ocean (Parslow et al. 2001, Holm-Hansen and Hewes 2004; Holm-Hansen et al. 2005). Sub-surface chlorophyll features were also observed over the productive central Kerguelen Plateau in late summer (February) with chlorophyll *a* concentrations >2.5 μg L^{-1} (Uitz et al. 2009), suggesting that SCM are not strictly

*Correspondence: rembauville@obs-banyuls.fr

restricted to the HNLC waters. These sub-surface biomass features are observed around 100 m and thus escape satellite detection depth (∼20 m in productive areas; Gordon and McCluney 1975). This region of the water column, also called the "transition layer," is defined as the interface between the stratified ocean interior and the highly turbulent surface mixed layer (Johnston and Rudnick 2009).

Diatoms typically dominate spring/summer phytoplankton blooms in the Southern Ocean (Korb and Whitehouse 2004; Armand et al. 2008; Quéguiner 2013), and the subsurface chlorophyll maximum is also characterized by a dominance of diatom biomass (Kopczynska et al. 2001; Armand et al. 2008; Gomi et al. 2010). Both studies from Armand et al. (2008) and Gomi et al. (2010) described a similarity between the mixed layer and deep diatom communities. However, Kopczynska et al. (2001) reported a difference between the mixed layer and the subsurface phytoplankton diatom assemblage with a dominance of larger species in the deeper samples. Additionally, high regional and interannual variability of diatom assemblages in the SCM is reported from two consecutive summer surveys in the Polar Frontal Zone (PFZ) and the Seasonal Ice Zone in the Indian Sector of the Southern Ocean (Gomi et al. 2010).

It has been proposed that the development of sub-surface biomass features in the Southern Ocean is linked to iron depletion in the mixed layer (Parslow et al. 2001). Under these conditions, phytoplankton accumulates in temperature minimum layers that are frequently associated to the pycnocline and/or nutricline (Holm-Hansen and Hewes 2004). The similarity that is frequently observed between mixed layer and the SCM diatom communities supports this hypothesis (Armand et al. 2008; Gomi et al. 2010). It is presently unclear, however, if the SCM phytoplankton communities are predominantly senescent and/or poorly active (Parslow et al. 2001; Armand et al. 2008) or productive communities with low growth rates sustained by nutrient diffusion through the pycnocline (Holm-Hansen and Hewes 2004; Quéguiner 2013). Irrespective of photosynthetic production levels, it has been suggested previously that the transition layer could be an important foraging site for various micro- and mesozooplanktonic grazers (Kopczynska et al. 2001; Gomi et al. 2010). A coupled study of microplankton assemblages and particulate matter stoichiometry is therefore of particular importance to gain a better understanding of SCM formation and their impact on carbon and biomineral cycling through transition layers in the Southern Ocean.

Redfield (1958) first described the homogeneity of deep water N and P stoichiometry and its coherence with plankton stoichiometry and the resulting "Redfield-ratio" has been a central tenet in modern oceanography. The quantity of particulate matter data has increased substantially in recent years and stoichiometric nutrient ratios are commonly observed to derivate from Redfield values. A recent large scale data synthesis demonstrated that PON:POP ratios are not homogeneous at a global scale and may reflect latitudinal patterns related to plankton community composition (Martiny et al. 2013). Diatoms, for example, are known to have a lower N:P ratio than dinoflagellates or chlorophyceae (Ho et al. 2003; Quigg et al. 2003; Sarthou et al. 2005).

There are alternative explanations for latitudinal trends in particulate matter stoichiometry. The growth rate hypothesis (Elser et al. 1996) suggests that among one phytoplankton taxa, changes in physiological status affects the allocation of nutrients to various macromolecular pools with different N:P stoichiometry. For example, competitive equilibrium in nutrient limiting conditions will lead to the synthesis of N-rich proteins required for nutrient acquisition. During exponential growth, there is an increased demand for the synthesis of P-rich ribosomes which are required for cell component synthesis. (Elser et al. 1996; Sterner and Elser 2002; Klausmeier et al. 2004). This general scheme might be modulated by local availability of nutrients, and phytoplankton for example have been reported to synthesize nonphosphorous lipids in oligotrophic, low P environments (Van Mooy et al. 2009). Temperature has also been identified as a factor strongly influencing the N:P ratios and Southern Ocean diatoms contain more P-rich rRNA at low temperatures (Toseland et al. 2013). These observations reinforce the need of a joint description of plankton community structure and stoichiometry to document how plankton biogeography might impact Southern Ocean nutrient stoichiometry at local scale (Weber and Deutsch 2010).

In this study, we report data acquired late summer in the Subantarctic Zone (SAZ), the PFZ, and the Antarctic Zone (AAZ) in the Indian Sector of the Southern Ocean. Our objectives are (1) to assess whether patterns in sub-surface chlorophyll features are linked to biomass accumulation at physical interfaces, (2) to compare microplankton assemblages between the mixed layer and transition layer and identify physiological changes and potential ecological processes occurring within the transition layer, (3) investigate the statistical relationship between microplankton community structure and particulate matter stoichiometry in contrasting hydrological environments, and (4) to assess how biogeochemical processes within the transition layer modulate the intensity and stoichiometry of the particulate matter transfer from the mixed layer to the mesopelagic ocean.

Material and procedures

OISO23 cruise and sampling strategy

The OISO23 cruise took place onboard the R/V *Marion Dufresne* in the Indian sector of the Southern Ocean from the 06 January 2014 to the 23 February 2014. The biogeochemical study presented here is focused on 11 stations located on a latitudinal transect in the SAZ, PFZ, and AAZ, linking the two island systems of Crozet and Kerguelen (Fig. 1; Table 1). Conductivity-Temperature-Depth (CTD,
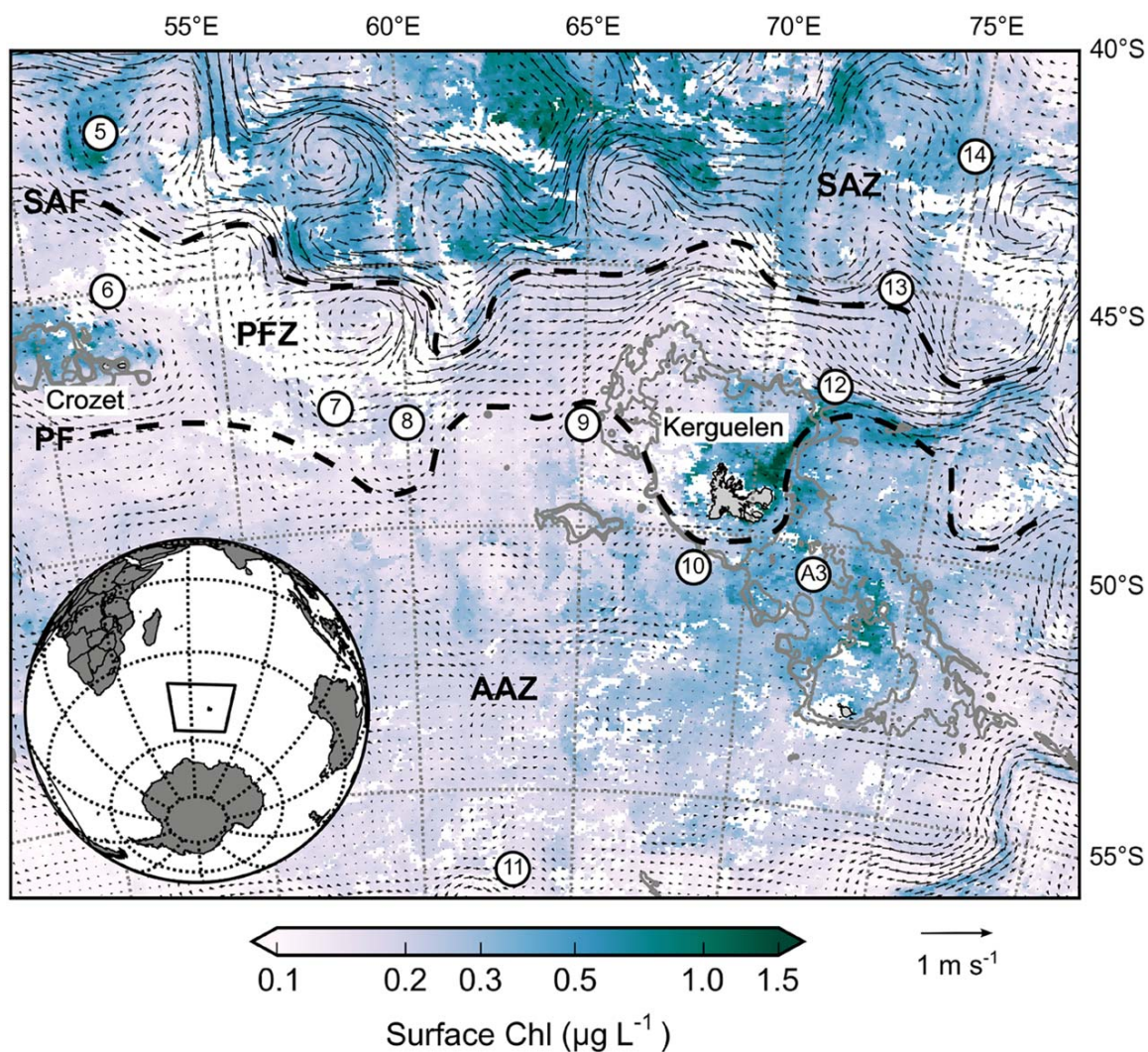
Fig. 1. Location of the study in the Indian sector of the Southern Ocean and station map. Satellite-derived surface chlorophyll *a* (MODIS level 3 product, 8 d composite) was averaged from 09 January 2013 to 10 February 2014. Arrows correspond to altimetry-derived geostrophic velocities (AVISO MA-DT daily product) averaged over the same period. Grey lines represent the 500 m and 1000 m isobaths. SAF, Subantarctic Front; PF, Polar Front; SAZ, Subantarctic Zone; PFZ, Polar Frontal Zone; AAZ, Antarctic Zone. [Color figure can be viewed in the online issue, which is available at wileyonlinelibrary.com.]

Seabird SBE 911 plus) casts were performed at each station. Samples for nutrients and chlorophyll *a* (Chl *a*) analyses were taken at 20 fixed depths. Precise sampling depths for particulate matter and microplankton abundance were chosen at each station following a preliminary analysis of the down-cast temperature, salinity, and fluorescence profiles. Samples were taken in the mixed layer, in the strong density gradient beneath the mixed layer (transition layer) and at a constant depth of 250 m. The last depth was chosen as a reference depth located under the annual upper mixed layer for this sector of the Southern Ocean (Park et al. 1998; de Boyer Montégut et al. 2004).

Derived hydrological parameters

The turbulent diffusivity coefficient was computed with the Thorpe scale method using the Shih et al. (2005) parameterization as previously described in Park et al. (2014). The robustness of the Thorpe scale calculation using this indirect method depends on the level of CTD processing prior to the computation (Park et al. 2014). The diffusivity coefficient (Kz in $m^2\ s^{-1}$) was calculated as follows:

$$Kz = 1.6\ v^{1/2}\ L_t\ N^{1/2} \tag{1}$$

where v is the cinematic viscosity of seawater (1.5–$1.8\ 10^{-6}$ $m^2\ s^{-1}$ for $T = 0$–$5°C$), L_t is the Thorpe scale (vertical density

Table 1. Stations labels, date and locations and attributed hydrological zone. Mixed layer depth (MLD), depth of the euphotic layer (Ze), depth of the fluorescence-derived chlorophyll maximum (Chl$_{max}$), and percentage of chlorophyll *a* located under the mixed layer depth.

Station	Date	Location	Zone	MLD (m)	Ze (m)	Depth of Chl$_{max}$ (m)	% Chl under MLD
5	11 Jan 14	42°30′S 52°29′E	SAZ	35	35	20	39
6	12 Jan 14	44°60′S 52°06′E	PFZ	52	53	75	73
7	14 Jan 14	47°40′S 58°00′E	PFZ	59	58	46	54
8	16 Jan 14	48°00′S 60°00′E	PFZ	63	44	44	46
9	17 Jan 14	48°30′S 65°01′E	AAZ	70	42	77	58
10	19 Jan 14	50°40′S 68°25′E	AAZ	76	38	48	28
11	21 Jan 14	56°30′S 62°59′E	AAZ	71	66	61	65
A3	23 Jan 14	50°38′S 72°05′E	AAZ	78	37	50	53
12	06 Feb 14	46°60′S 72.01°E	PFZ	56	58	70	69
13	06 Feb 14	44.60°S 73.20°E	SAZ	39	44	47	50
14	08 Feb 14	42.28°S 74.54°E	SAZ	38	49	50	70

overturning scale, in m) and N is the Brunt-Väisalä buoyancy frequency (s^{-1}) defined as:

$$N = \left(-\frac{g}{\rho_e} \times \frac{d\rho}{dz} \right)^{1/2} \quad (2)$$

where g is the gravitational acceleration (9.81 m s^{-1}), ρ_e is a constant reference density for seawater, ρ is the seawater density and z is the depth (m). Brunt-Väisalä buoyancy frequency was used to quantify the water column stability and the strength of the physical interface associated with the transition layer. Each Kz profile was averaged in 10 m bins. The Thorpe scale method cannot resolve overturns smaller than 20 cm, consequently Kz values $< 10^{-5}$ m^2 s^{-1} were set to this minimal value based on in situ measurements around the Kerguelen plateau with a Turbo MAP profiler (Park et al. 2014).

The mixed layer depth (MLD) was calculated using a 0.02 kg m^{-3} density-difference criterion relative to the density at 20 m (Park et al. 1998). The depth of the euphotic layer (Ze, 1% of the surface irradiance, in m) was calculated from the vertical profile of fluorescence-derived Chl *a* using Morel and Berthon (1989) formulation:

$$Ze = 568.2 \left(\int_0^z \text{chla } dz \right)^{-0.746} \quad (3)$$

where chla is the Chl *a* concentration (mg m^{-3}) derived from the calibrated CTD fluorometer (WET Labs ECO FL, see below for calibration method). The calculation was performed iteratively downward from the surface until $z = Ze$.

Biogeochemical analyses

Particulate matter: particulate organic carbon (POC), nitrogen (PON), phosphorous (POP), biogenic silica (BSi) and Chl **a** *analysis*

For POC and PON, 2 L of seawater were filtered on precalcinated (450°C, 24 h) 25 mm Whatman GF/F filters stored in precalcinated glass vials and dried overnight at 60°C. Filters were decarbonated by fumigating pure HCl (Merck) during 10 h. POC and PON were measured on a Perkin Elmer C,H,N 2400 autoanalyser calibrated with acetanelyde. Detection limits were defined as the mean blank plus three times the standard deviation of the blanks and were 0.17 μmol L^{-1} and 0.04 μmol L^{-1} for POC and PON, respectively. For POP, 500 mL of seawater was filtered on precalcinated GF/F filters. POP was analyzed following a wet oxidation procedure (Pujo-Pay and Raimbault 1994). Extracts were filtered through two precalcinated GF/F filters prior to spectrophotometric analysis of PO$_4^{3-}$ on a Skalar autoanalyser following the method of Aminot and Kerouel (2007). The detection limit for POP was 0.01 μmol L^{-1}.

For BSi, 1 L of seawater was filtered on 25 mm nuclepore filter of 0.2 μm porosity. Filters were placed in cryotubes and dried at 60°C overnight. BSi was estimated by the triple NaOH/ HF extraction procedure allowing correction of lithogenic silica (LSi, Ragueneau et al. 2005). Filters were digested two times with 0.2 N NaOH at 95°C during 45 min. At the end of both extractions, aliquots were taken for silicic acid (Si(OH)$_4$) and aluminum (Al) concentration measurements. A third extraction was performed with 2.9 N HF over 48 h at ambient temperature ($\sim$20°C). Si(OH)$_4$ was determined colorimetrically on a Skalar autoanalyser following Aminot and Kerouel (2007) and Al was determined fluorimetrically using the Lumogallion complex (Howard et al. 1986). The detection limit for BSi was 0.02 μmol L^{-1}. The LSi correction was most important in the vicinity of the plateaus (e.g., at A3, 250 m the LSi represented 17% of the total particulate Si).

For Chl *a* analysis, 2 L of seawater were collected in opaque bottles, filtered onto GF/F filters and immediately placed in cryotubes at -80°C. Pigments were extracted in 90% acetone solution and analyzed using 24 fluorescence excitation and emission wavelengths with a Hitachi F-4500 fluorescence spectrophotometer according to Neveux and Lantoine (1993). These Chl *a* concentrations measured from niskin bottles were used to calibrate the CTD fluorescence profiles by linear regression ($R^2 = 0.8$).

Dissolved nutrients analysis and calculation of diffusive fluxes

For the analysis of major nutrients (NO$_3^-$, NO$_2^-$, Si(OH)$_4$, PO$_4^{3-}$), 20 mL of filtered (0.2 μm cellulose acetate filters) seawater was sampled into scintillation vials and poisoned with 100 μL of 100 mg L^{-1} HgCl$_2$. Nutrient concentrations were determined colorimetrically on a Skalar autoanalyzer following Aminot and Kerouel (2007). Nutrient gradients were calculated at each sampling depth for particulate matter and microplankton based on the three nutrient concentrations (*C*) windowing this depth. Nutrient diffusive fluxes (N_{diff} in μmol m^{-2} s^{-1}) in the transition layer were calculated as follow:

$$N_{diff} = Kz \frac{dC}{dz} \quad (4)$$

Kz profiles are highly variable over short time scales (days to hour), whereas nutrient gradients result from nutrient consumption occurring at longer timescales (weeks to month). To minimize the bias caused by short term Kz variability, nutrient diffusive fluxes were calculated using the average Kz profile from the study region (Supporting Information Fig. S1). A characteristic value of 4.5×10^{-5} m^2 s^{-1} in the transition layer was derived from the mean Kz profile.

Microplankton abundance, identification and biomass calculation

Seawater samples for microplankton identification and enumeration were collected in 125 mL amber glass bottles

and immediately fixed with acid Lugol solution (1% final concentration). Samples were maintained in the dark at ambient temperature until counting (performed within 3 months after the sampling). Microplankton cells were enumerated from either a 50 mL (mixed layer and transition layer) or 100 mL (250 m) subsample after settling for 24 h (dark) in an Utermöhl counting chamber. Taxonomic identification was performed under an inverted microscope (Olympus IX71) with phase contrast at $\times$200 and $\times$400 magnification. One half of the counting chamber (mixed layer and transition layer) or the entire surface (250 m samples) was used to enumerate the microplankton. The total number of cells counted was > 200 except in sample 13 at 250 m. Ciliates and tintinnids were enumerated but not classified into taxa. Dinoflagellates were identified to the genus level, and diatoms were identified to species level when possible, following the recommendations of Hasle and Syvertsen (1997). Full and empty diatoms frustules were enumerated separately. Half or broken frustules were not considered. Due to the preserved cell contents sometimes obscuring taxonomic features on the valve face, taxonomic identification of diatoms to the species level was occasionally difficult and necessitated the categorizing of diatom species to genus or taxa as previously described in Rembauville et al. (2015a). The microplankton cell counts and empty diatom cell counts are provided in Supporting Information Tables S2 and S3, respectively.

The composition of living diatom biomass was estimated from the abundance of full cells using a species-specific carbon content for diatoms in the Indian sector of the Southern Ocean (Cornet-Barthaux et al. 2007). For species absent from this reference, > 20 individuals were measured from microscopic images using the imageJ software. Cell volume for the appropriate shape was calculated following Hillebrand et al. (1999) and carbon content was calculated using a diatom-specific carbon:volume relationship (Menden-Deuer and Lessard 2000). The same procedure was used for dinoflagellates and ciliates. For *Chaetoceros Hyalochaete* resting spores (CRS), the carbon content for spores over the Kerguelen plateau calculated in Rembauville et al. (2015a) was used. A complete list of microplankton categories and their respective carbon content is provided in Supporting Information Table S1.

Statistical analyses

To compare microplankton community structure between samples, Bray-Curtis distance was calculated based on raw microplankton abundances. Samples were clustered using the unweighted pair group method with arithmetic mean (UPGMA). To link microplankton community structure with biogeochemical factors (particulate matter stoichiometry and nutrient diffusive fluxes), a canonical correspondence analysis (CCA) was performed (Legendre and Legendre 1998). Prior to the CCA, microplankton abundances were sorted into groups to facilitate the ecological interpretation of the analysis. For example, a distinction is often made between
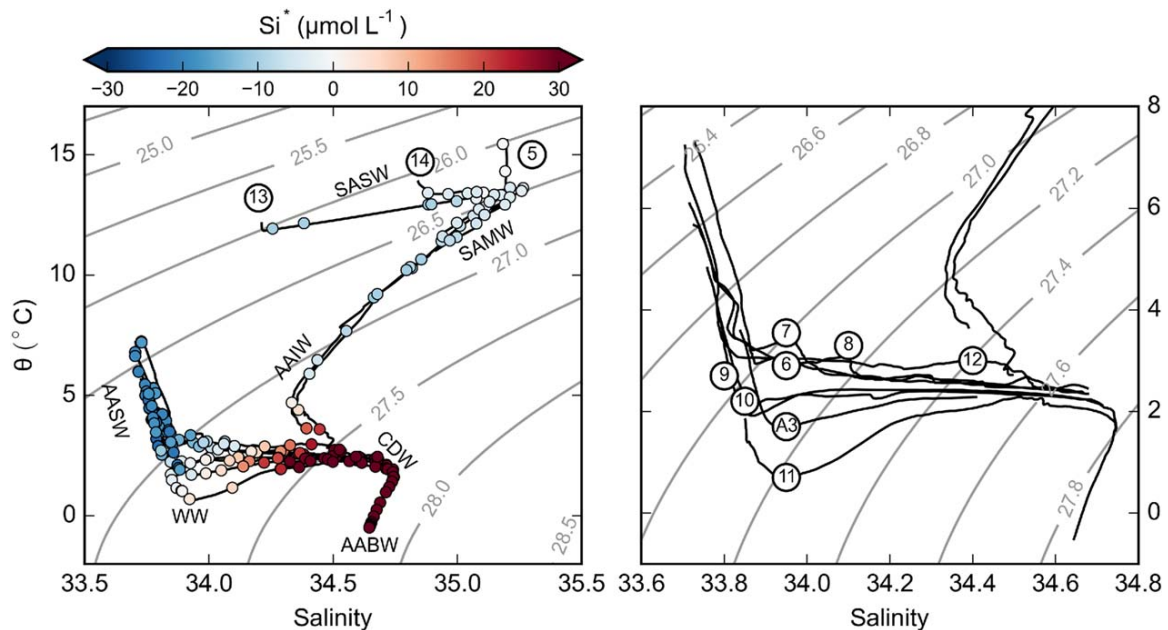
Fig. 2. Potential temperature/salinity diagram. (a) Colored points denote Si* ($Si(OH)_4 - NO_3^-$) distribution. Circled labels refer to stations. The main water masses identified are specified: SASW, Subantarctic Surface Water; SAMW, Subantarctic Mode Water; AAIW, Antarctic Intermediate Water; AASW, Antarctic Surface Water; WW, Winter Water; CDW, Circumpolar Deep Water; AABW, Antarctic Bottom Water. (b) Detailed view for stations of the PFZ and AAZ. [Color figure can be viewed in the online issue, which is available at wileyonlinelibrary.com.]

small and large diatoms that are thought to occupy different niches of nutrient and light availability, and have different sensitivity to grazing in the Southern Ocean (Smetacek et al. 2004; Quéguiner 2013). "Large diatoms (>100 μm)" comprised the following genera: *Corethron*, *Dactyliosolen*, *Membraneis*, *Pleurosigma*, *Proboscia*, *Rhizosolenia* and *Thalassiothrix*. "Small diatoms (<100 μm)" referred to the other diatom genera. Armored dinoflagellates (*Prorocentrum, Ceratium, Brachidinium*, *Dinophysis, Oxytoxum, Podolampas*, and *Protoperidinium)* were differentiated from naked dinoflagellates (*Gymnodinium* and *Gyrodinium*).

Results

Hydrological characteristics and nutrients diffusive flux

During the study (11 January to 08 February), the north Crozet bloom had terminated and partly advected by mesoscale features of the Subantarctic Front (SAF) associated with strong geostrophic velocities (Fig. 1). Surface waters of the PFZ displayed very low Chl *a* concentration (<0.3 μg L^{-1}) and the bloom of the central Kerguelen plateau was also declining ($\sim$0.8 μg L^{-1}). East of Kerguelen Island, on the northern flank of the PF, a Chl *a* plume originating from coastal waters was advected eastward as the PF merged with the SAF. A potential temperature-salinity diagram (Fig. 2) was used to classify the different stations into discrete hydrological zones, summarized in Table 1. The SAZ displayed the highest surface temper-

atures (>10°C, stations 5, 13, and 14). The PFZ exhibited a clear decrease in surface salinity (<34, stations 6, 7, 8, and 12) and the AAZ was characterized by the presence of a temperature minimum layer ($\sim$1.8°C; stations 9, 10, 11, and A3). The Si* ($= Si(OH)_4 - NO_3^-$) in intermediate and winter waters was homogeneous ($\sim$0 μmol L^{-1}) at all stations. Therefore, the Si* signature of surface waters was used as a tracer for $Si(OH)_4$ uptake relative to nitrate in the productive layer, rather than differences in preformed nutrients. In the SAZ, Si* was similar in surface water and intermediate waters (0 μmol L^{-1}) whereas in the PFZ and the AAZ, Si* in surface waters was strongly negative (<-20 μmol L^{-1}).

At all stations, 30–70% of the vertically integrated Chl *a* occurred deeper than the MLD (Table 2). However, only stations 6, 9, 12, 13, and 14 exhibited a maximum Chl *a* concentration deeper than the MLD. Brunt-Väisälä frequencies (*N*) were highest in the transition layer and ranged from 4.5 cycles h^{-1} to 8.2 cycles h^{-1}, with high values associated with frontal (e.g., station 13 close to SAF) or bathymetric (station 6 near the Crozet plateau) structures. At stations located close to the Kerguelen plateau (9, 10 and A3), Ze was shallower than the MLD. Station 9 displayed a characteristic subsurface chlorophyll maximum where Chl *a* shows a steep increase under the MLD (70 m) and a gradual decrease in the pycnocline down to 150 m (Fig. 3). Kz values peak at 9.5 $\times$ 10^{-5} m^2 s^{-1} in the mixed layer but display a second maximum associated with the pycnocline, nutriclines, and

Table 2. Sample code (M: mixed layer, T: transition layer, D: 250 m), sampling depth and concentrations of particulate organic carbon (POC), nitrogen (PON), and phosphorous (POP). Nutrient diffusive flux was calculated using a K_z value of 4.5×10^{-5} m^2 s^{-1} in the transition layer (see materials and methods).

Sample	Depth (m)	Particulate stock (μmol L^{-1})				Chlorophyll *a* (μg L^{-1})	Nutrient gradient (μmol m^{-4})			Nutrient diffusive flux (μmol m^{-2} d^{-1})			Brunt-Väisälä Frequency (cycle h^{-1})
		POC	PON	POP	BSi		$Si(OH)_4$	NO_3^-	PO_4^{3-}	$Si(OH)_4$	NO_3^-	PO_4^{3-}	
5M	20	18.60	2.34	0.19	1.07	1.26	0	78	7	—	—	—	3.1
5T	57	3.30	0.47	0.06	0.25	0.20	46	94	1	178	367	6	4.8
5D	250	1.10	0.15	0.02	0.02	0.01	15	35	2	—	—	—	2.3
6M	30	6.00	0.93	0.09	0.17	0.50	0	20	1	—	—	—	2.7
6T	71	5.53	0.85	0.05	0.25	0.67	100	89	7	390	345	25	8.2
6D	250	1.48	0.18	0.02	0.19	0.02	133	37	2	—	—	—	2.5
7M	39	4.85	0.72	0.10	0.16	0.40	37	0	4	—	—	—	2.9
7T	74	2.66	0.41	0.02	0.20	0.41	108	61	2	419	236	8	6.5
7D	249	1.27	0.18	0.02	0.17	0.02	81	20	2	—	—	—	2.2
8M	32	4.56	0.64	0.08	0.10	0.73	18	0	5	—	—	—	1.9
8T	100	4.93	0.80	0.04	0.26	0.37	69	49	3	269	191	10	5.1
8D	250	1.29	0.13	0.02	0.18	0.02	107	15	2	—	—	—	2.8
9M	50	7.25	1.10	0.17	3.19	0.83	27	8	0	—	—	—	2.2
9T	110	5.01	0.73	0.09	4.35	1.04	241	22	4	935	86	16	6.9
9D	250	1.36	0.18	0.02	1.02	0.04	168	37	3	—	—	—	2.9
10M	49	7.79	1.09	0.15	4.91	1.00	12	0	1	—	—	—	2.1
10T	99	3.45	0.42	0.06	3.14	0.69	342	71	6	1328	274	24	5.8
10D	248	1.36	0.17	0.02	0.57	0.03	156	19	2	—	—	—	2.4
11M	49	4.14	0.59	0.15	1.84	0.51	25	31	2	—	—	—	2.7
11T	119	3.46	0.43	0.09	1.52	0.63	143	15	3	556	58	10	4.4
11D	250	0.97	0.10	0.02	0.53	0.03	163	22	1	—	—	—	2.1
12M	40	4.57	0.62	0.07	0.24	0.49	21	18	0	—	—	—	3.3
12T	70	2.96	0.41	0.06	0.29	0.55	64	35	4	250	135	15	6.5
12D	250	1.46	0.15	0.02	0.21	0.03	109	40	1	—	—	—	2.6
13M	21	10.60	1.52	0.13	0.28	0.73	0	0	0	—	—	—	3.4
13T	46	6.77	0.95	0.08	0.37	0.82	71	24	0	277	93	0	8.2
13D	251	1.90	0.25	0.04	0.09	0.02	14	27	1	—	—	—	2.1
14M	20	10.49	1.59	0.15	0.33	0.62	0	0	3	—	—	—	4.1
14T	55	6.81	1.04	0.10	0.65	0.94	64	34	2	251	133	7	6.3
14D	250	1.85	0.20	0.03	0.09	0.04	2	22	1	—	—	—	2.1
A3M	41	9.36	1.47	0.25	4.71	1.10	1	15	0	—	—	—	2.0
A3T	110	8.19	1.31	0.18	5.08	1.20	426	83	6	1655	322	22	6.1
A3D	250	3.39	0.54	0.06	1.50	0.21	142	19	3	—	—	—	2.3

elevated Chl *a* values of 1.1 μg L^{-1}. The gradient between 150 m and the mixed layer was much higher for $Si(OH)_4$ (20 μmol L^{-1} to < 2 μmol L^{-1}) than for NO_3^- (27 μmol L^{-1} to 23 μmol L^{-1}) and PO_4^{3-} (2.2 μmol L^{-1} to 1.5 μmol L^{-1}).

Nutrient gradients estimated for the three different layers covered two order of magnitude and were generally larger for $Si(OH)_4$ (Table 2). Highest $Si(OH)_4$ gradients (>200 μmol m^{-4}) were observed in the transition layer in stations of the AAZ close to the Kerguelen plateau (stations 9, 10, A3), leading to large $Si(OH)_4$ diffusive fluxes ($\geq$ 1 mmol m^{-2} d^{-1}). Highest NO_3^- gradients (~100 μmol m^{-4}) were found in the transition layer of stations 5 and 6 close to the Crozet Island,

associated with the highest NO_3^- diffusive fluxes (>300 μmol m^{-2} d^{-1}). PO_4^{3-} gradients were at least one order of magnitude lower (<10 μmol m^{-4}) than nitrate gradient, resulting in negligible diffusive fluxes.

Particulate matter stocks and stoichiometry

POC concentrations generally decreased with depth with highest values found in the mixed layer of the SAZ (>10 μmol L^{-1}), followed by the AAZ (4.4–9.1 μmol L^{-1}) and PFZ (4.5–6.0 μmol L^{-1}, Table 2). The largest value of 18.6 μmol L^{-1} at station 5 corresponded to a biomass patch in a meander of the SAF (Fig. 1). POC concentrations in the transition
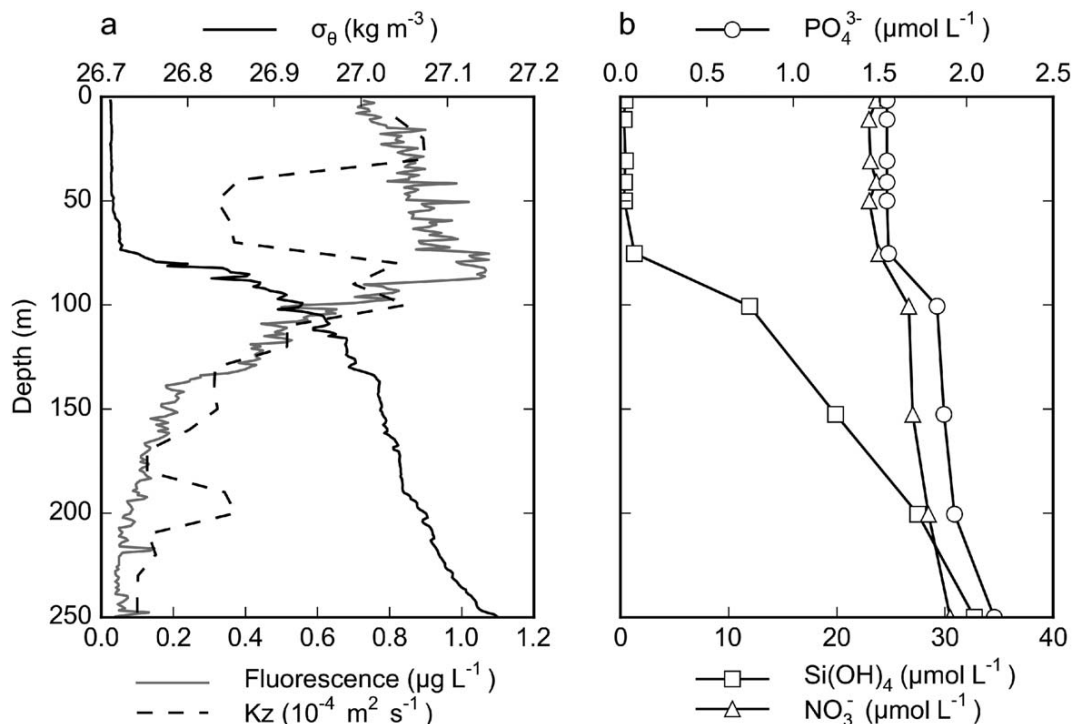
Fig. 3. Example of vertical profiles for station 9. (a) Potential density anomaly (σ_θ, black line), fluorescence-derived chlorophyll *a* (grey line) and turbulent diffusion coefficient (Kz, black dashed line). (b) Vertical profile of nitrate (triangles), phosphate (circles) and silicate (square).
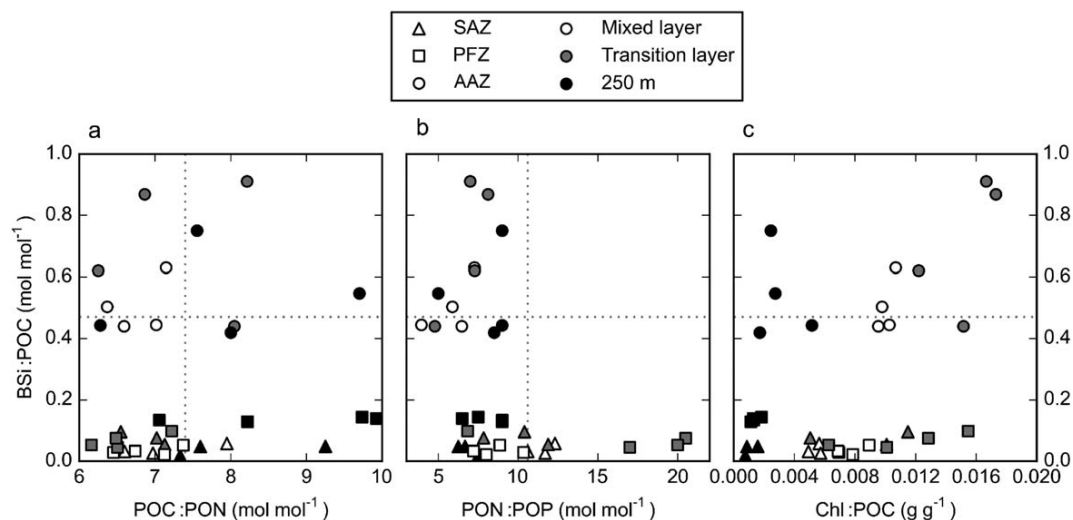
Fig. 4. Particulate matter stoichiometry. (a) POC:PON vs. BSi:POC. (b) PON:POP vs. BSi:POC. (c) Chl:POC vs. BSi:POC. Horizontal dashed line is the mean BSi:POC ratio from Quéguiner and Brzezinski (2002) for the Polar Frontal Zone in the Indian sector of the Southern Ocean (0.47). Vertical dashed line are the mean POC:PON and PON:POP ratios for the Southern Ocean from Martiny et al. (2013) (7.4 and 10.6, respectively).

layer ranged from 2.7 μmol L^{-1} to 8.2 μmol L^{-1} with the highest value observed over the Kerguelen plateau (Station A3). At the reference depth of 250 m POC concentrations were relatively uniform (1.4 $\pm$ 0.3 μmol L^{-1}), although on the Kerguelen plateau (Station A3) they were notably higher (3.4 μmol L^{-1}).

Table 3. Total microplankton cells abundances, total microplankton POC, and relative contribution of each microplanktonic group to the total abundance.

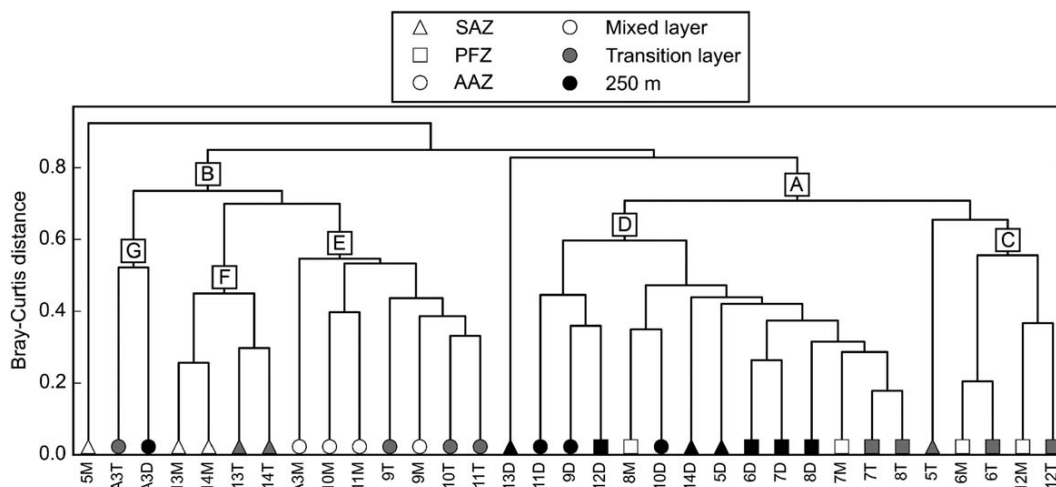| Sample	Total cell abundance (10³ L⁻¹)	Total microplankton POC (µmol L⁻¹)	Empty diatoms (>100 µm)	Empty diatoms (<100 µm)	Full diatoms (>100 µm)	Full diatoms (<100 µm)	CRS	Naked dinoflagellate	Prorocentrum	Other armored dinoflagellates	Naked ciliates	Tintinnids	Total diatoms	Total dinoflagellates	Total ciliates
5M	527	13.50	0	2	0	90	0	1	5	0	2	0	92	6	2
5T	25	1.34	1	3	1	60	0	4	25	1	4	1	65	30	5
5D	3	0.19	0	0	0	0	0	5	60	2	34	0	0	66	34
6M	49	3.23	0	5	1	19	0	9	38	0	28	1	24	47	28
6T	40	2.34	0	5	1	23	0	6	41	0	23	1	30	46	24
6D	5	0.16	0	48	0	4	0	3	33	1	11	0	52	37	11
7M	5	1.83	0	4	2	20	0	14	36	0	25	0	25	50	25
7T	8	1.26	0	22	2	20	0	6	34	0	15	0	45	40	15
7D	8	0.13	0	52	0	4	0	3	29	1	12	0	56	32	12
8M	12	2.29	0	1	1	17	0	24	24	0	33	0	19	49	33
8T	10	2.07	0	29	1	23	0	5	28	0	14	0	53	32	15
8D	6	0.14	0	15	0	0	0	5	59	1	20	0	15	65	20
9M	89	4.46	1	19	6	57	0	7	7	0	3	0	83	14	3
9T	104	3.41	1	32	3	51	0	4	6	0	2	0	87	10	2
9D	12	0.19	2	50	0	18	0	12	15	0	3	0	70	27	3
10M	145	4.38	1	18	7	67	0	4	3	0	1	0	92	7	1
10T	77	2.36	2	44	7	34	0	5	6	1	2	0	86	11	2
10D	11	0.11	0	38	0	1	0	16	18	0	26	0	39	34	26
11M	114	2.82	1	17	4	71	0	2	1	0	2	0	94	4	2
11T	75	1.50	1	52	2	33	0	5	4	0	2	0	89	9	2
11D	22	0.14	2	82	0	1	0	8	8	0	0	0	84	16	0
12M	24	2.28	0	15	12	35	0	5	28	0	5	1	61	33	5
12T	16	1.24	0	16	5	28	0	3	32	0	16	0	49	35	16
12D	13	0.14	3	63	1	8	0	1	18	0	6	0	75	19	6
13M	149	6.72	0	4	1	24	0	21	39	1	9	0	30	61	9
13T	77	4.31	0	3	1	48	0	9	26	4	8	0	53	39	8
13D	2	0.23	0	0	0	0	0	17	78	0	6	0	0	94	6
14M	103	6.15	1	0	4	23	0	12	42	7	11	1	28	61	12
14T	72	3.50	1	3	8	63	0	10	15	0	0	0	74	26	0
14D	4	0.13	1	5	2	4	0	18	68	1	1	1	12	87	2
A3M	108	7.29	2	17	13	60	0	3	3	1	2	0	91	7	2
A3T	234	5.75	0	13	8	66	8	1	2	0	1	0	95	3	2
A3D	110	2.89	1	17	0	37	39	2	2	0	1	0	94	4	1

Fig. 5. Dendrogram of the hierarchical clustering (UPGMA agglomeration) based on the Bray-Curtis distance calculated on raw microplankton abundances. Capital letters categorize the groups referred to in the text.

The highest Chl *a* concentration was observed in the warm mixed layer of station 5 (1.26 μg L^{-1}). Stations in the PFZ exhibited the lowest mixed layer Chl *a* concentrations (0.40–0.50 μg L^{-1}), intermediate values were found in the SAZ (0.60–0.90 μg L^{-1}) and highest values in the AAZ ($\sim$1 μg L^{-1}). Unlike POC, Chl *a* values in the transition layer frequently exceeded those in the mixed layer, with the largest value of 1.20 μg L^{-1} observed at the Kerguelen plateau station A3. Similarly the largest 250 m Chl *a* concentration of 0.21 μg L^{-1} was observed at station A3, compared to negligible values of < 0.05 μg L^{-1} at all other stations.

All the samples from the SAZ and PFZ displayed BSi:POC ratios < 0.2 (Fig. 4). Conversely, in the AAZ, BSi:POC values were between 0.4 and 0.9 with highest values found in the transition layers. POC:PON ratios generally displayed a typical increase with depth with a notable exception at station A3 (Kerguelen plateau) where the POC:PON ratio was vertically homogeneous (6.3). PON:POP ratios demonstrated more variability than POC:PON. In the AAZ, PON:POP mixed layer ratios were between 4 and 8, increasing with depth. Mixed layer values in the PFZ (stations 6–10) were slightly higher than the AAZ (6–9), and SAZ samples were notably larger with values > 10. The highest values of 16–21 were found in transition layer PFZ samples located between the Crozet and Kerguelen Islands (stations 6, 7, and 8). Chl:POC ratio (g g^{-1}) were generally highest in the transition layer and lowest in 250 m samples. The largest Chl:POC ratios of 0.016–0.018 were observed in the transition layer of the AAZ.

Microplankton abundance and distribution

The largest microplankton cell abundance (527 $\times$ 10^3 cell L^{-1}) was observed in the mixed layer of station 5 and corresponded to a community dominated ($>90\%$) by *Bacterias-*

trum spp. (Table 3), constituting the external branch of the dendrogram based on Bray-Curtis distance (Fig. 5). The low biomass group A ($<50 \times 10^3$ cell L^{-1}) contained the subgroup C which represented mixed layer and transition layer of PFZ stations 6 and 12 characterized by an equal proportion of full diatoms (>100 μm), *Prorocentrum* and naked ciliates. Subgroup D contained all of the 250 m samples (except A3) and transition layer samples from the PFZ stations 7 and 8, the latter characterized in decreasing order by empty diatoms (<100 μm), *Prorocentrum* and naked ciliates. Group B (high abundance) contained three subgroups, E, F, and G. Subgroup E represented the majority of surface and transition layer samples from the AAZ and was characterized by a strict dominance of full diatoms (<100 μm). Subgroup F constituted samples from the mixed and transition layer of SAZ stations 13 and 14 with an assemblage of *Prorocentrum* and full diatoms (<100 μm). Finally, subgroup G contained samples from the transition layer and deep layer at A3 dominated by CRS and full diatoms (<100 μm). It is generally stated that bottle sampling might under-sample large and rare diatoms (Armand et al. 2008). Therefore our data might underestimate the contribution of large diatoms to the total microplankton assemblage.

The fraction of empty diatoms generally increased with depth (up to 90% at 250 m in the PFZ), with the notable exception of station A3 where it remained $\sim$20%. *Fragilariopsis kerguelensis* dominated ($>60\%$) the empty diatoms in all the samples of the AAZ and PFZ at any depth, with the exception of station A3 (Fig. 6). Station 5 was mostly characterized by empty *Bacteriastrum* spp. cells. In stations 13 and 14 (SAZ) the mixed layer empty diatom community was dominated by *Pseudo-nitzschia* spp., *Thalassiothrix antarctica* and *Chaetoceros Hyalochaete* (vegetative). Mixed layer sample
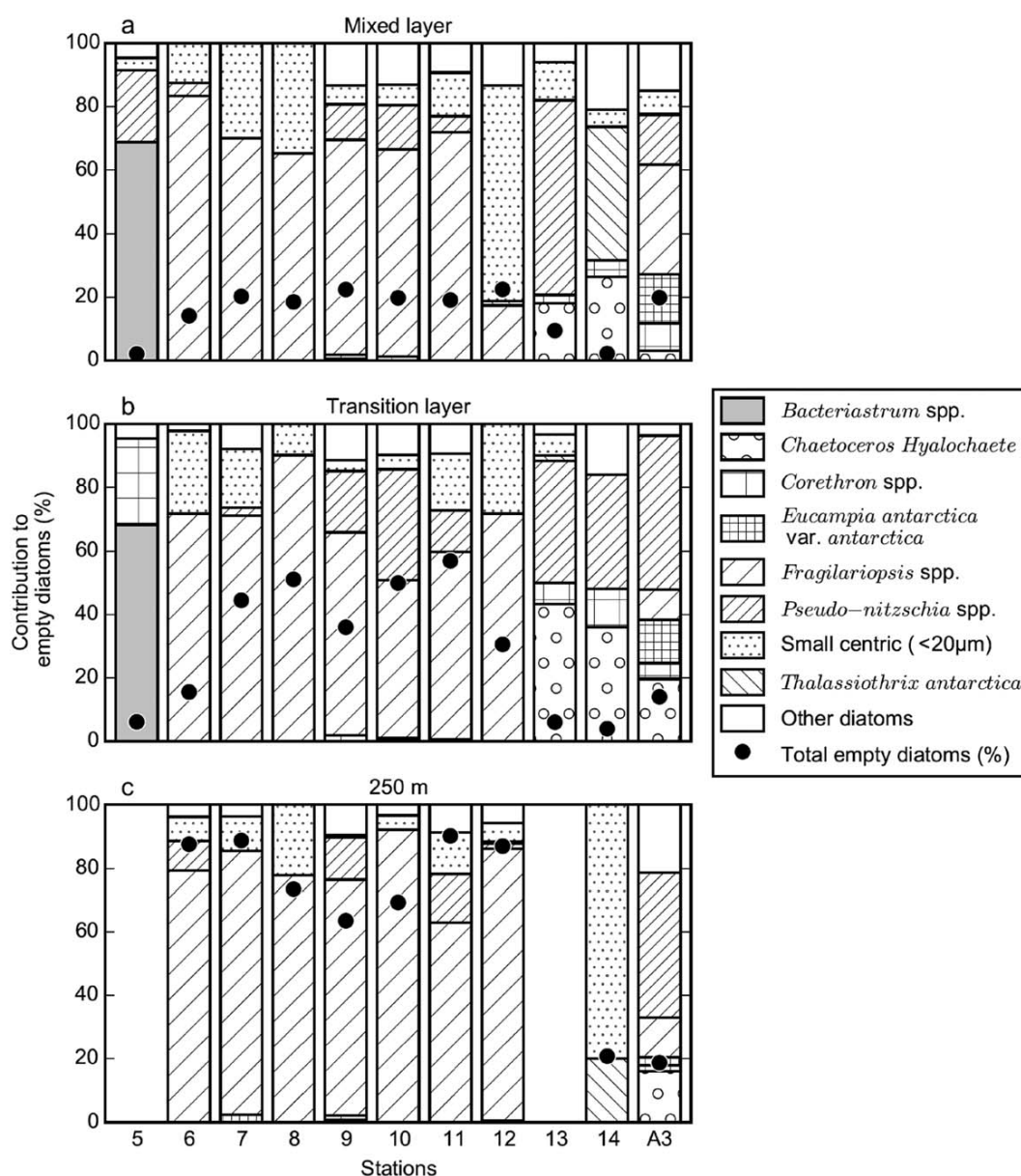
Fig. 6. Fraction of empty diatoms for (a) mixed layer samples, (b) transition layer samples, and (c) 250 m samples. Black dots represent the fraction of total empty diatoms to the sum of full and empty diatom frustules. Patterned bars refer to the fraction of a diatom group as specified in the legend.

at A3 contained in decreasing abundance empty cells of *F. kerguelensis*, *Pseudo-nitzschia* spp., *Eucampia antarctica* var. *antarctica* and *Corethron* spp. In the transition layer of stations 13 and 14 (SAZ), empty diatoms were dominated by *C. Hyalochaete* (vegetative) and *Pseudo-nitzschia* spp. At A3, empty diatoms in the transition layer were dominated by *Pseudo-nitzschia* spp. (50%), followed by *C. Hyalochaete* (vegetative) and *E. antarctica* var. *antarctica*. Finally, empty *Pseudo-nitzschia* (45%), *C. Hyalochaete* (vegetative, 18%) and *F. kerguelensis* (12%) were observed at 250 m at A3.

Microplankton POC partitioning

A highly significant linear correlation (Spearman, $n = 33$, $\rho = 0.88$, $p < 0.01$) was found between the measured POC (Table 2) and the calculated total microplankton POC (POC-$_{micro}$, Table 3). The regression slope (0.7), and significant intercept (~ 1 μmol L^{-1}), suggested that the microplankton biomass calculation underestimated the total POC. At station 5, the mixed layer sample was dominated by *Bacteriastrum* spp. (>60%, Fig. 7). At stations 6 to 8 (PFZ between Crozet and Kerguelen), naked ciliates (>40%) and dinoflagellates
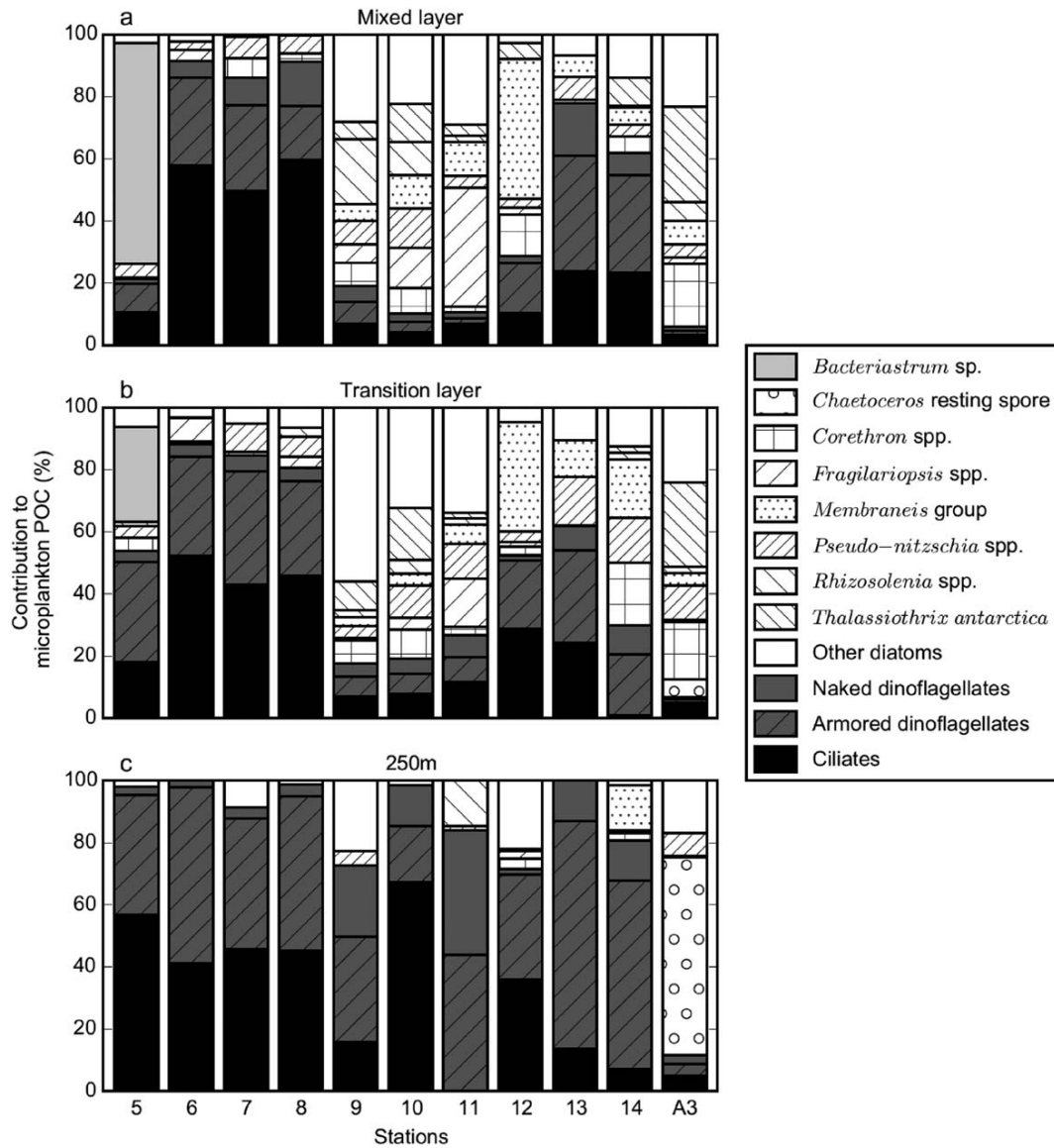
Fig. 7. Microplankton POC partitioning for (a) mixed layer samples, (b) transition layer samples, and (c) 250 m samples. Patterned bars refer to the contribution of a microplankton group as specified in the legend.

were the main contributors to POC$_{micro}$ at any depth. In the mixed layer samples of stations 13 and 14 (SAZ) dinoflagellates dominated (>50%) the POC$_{micro}$. In the AAZ, diatoms dominated POC$_{micro}$ at all stations, with a major contribution of the assemblage of large diatoms (>100 μm): *Rhizosolenia* spp., *Corethron* spp., *T. antarctica*, *Membraneis* and *F. kerguelensis* (<100 μm). The same pattern of dominant taxa was also observed in the transition layer of the AAZ. At stations 12, 13, and 14 (north of Kerguelen), dinoflagellates followed by *Membraneis* and *Pseudo-nitzschia* spp. were the main contributors to POC$_{micro}$. In the deep samples, POC$_{micro}$ was dominated by the contribution of dinoflagellates (mainly

Prorocentrum) and ciliate biomass with a noticeable exception at station A3 with the presence of *C. Hyalochaete* resting spores (>60% POC$_{micro}$).

Particulate matter signature and microplankton assemblages

The first two axes of the CCA accounted for ∼88% of the variability within the dataset (Fig. 8). Axis 1 opposed AAZ and SAZ stations characterized by a dominance of diatoms and high BSi:POC stoichiometry to the PFZ stations dominated by dinoflagellates and ciliates and a high PON:POP ratio. Axis 2 globally opposed surface samples with marked
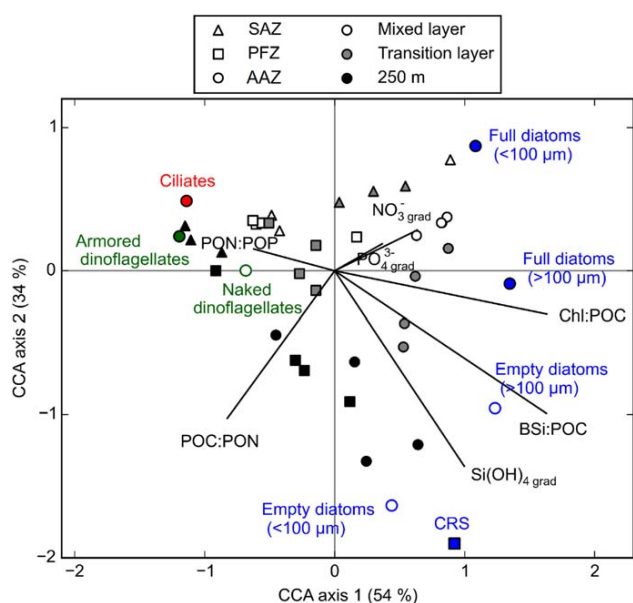
Fig. 8. Projection of samples, main microplankton groups and biogeochemical factors (particulate matter stoichiometry and major nutrients diffusive fluxes) on the first two axes of the canonical correspondence analysis (CCA). [Color figure can be viewed in the online issue, which is available at wileyonlinelibrary.com.]

NO_3^- and PO_4^{3-} gradients associated with full diatoms (<100 μm) to the 250 m samples with a high POC:PON ratio associated with empty diatoms (<100 μm). Full diatoms (>100 μm) were projected close to the Chl:POC ratio and the AAZ transition layer samples. Finally, empty diatoms (>100 μm) were projected close to the $Si(OH)_4$ gradient, the BSi:POC ratio and the transition layer samples and deep samples of the AAZ.

Discussion

Microplankton community and physiology in the transition layer

During our study (January–February), the period of maximum productivity had already occurred (Supporting Information animation). The North Crozet bloom ended and was partly advected eastward in the SAF, and the central Kerguelen plateau bloom was also in decline. Large and negative Si* values in the PFZ and AAZ (Fig. 2) suggested intense $Si(OH)_4$ utilization compared to nitrate utilization associated to bloom features. This can result from a dominance of diatoms in phytoplankton populations together with an increase in Si:N uptake ratio in response to iron limitation (Hutchins and Bruland 1998; Takeda 1998; Moore et al. 2007). Low concentrations of $Si(OH)_4$ (1.8 μmol L^{-1}; Mosseri et al. 2008) and dissolved iron (~0.1 nmol L^{-1} Blain et al. 2008) over

the central Kerguelen plateau in summer suggest that both elements may limit diatom growth in summer mixed layers.

The subsurface chlorophyll maximum is a recurrent feature in the oligotrophic ocean (Venrick et al. 1973; Letelier et al. 2004; Mignot et al. 2014), the North Sea (Weston et al. 2005), and the Arctic (Martin et al. 2010). The SCM can be associated with a phytoplankton biomass maximum (Martin et al. 2010), or the two structures can be uncoupled, suggesting that the vertical distribution of chlorophyll is strongly determined by photoacclimation (Fennel and Boss 2003). In the Southern Ocean, it has been proposed that the development of sub-surface biomass features is linked to such nutrient depletion, in particular iron in the mixed layer (Parslow et al. 2001). Under these conditions, phytoplankton accumulates in temperature minimum layers that are frequently associated to the pycnocline and/or nutricline (Holm-Hansen and Hewes 2004). In this study, a large fraction of integrated Chl *a* was observed below the mixed layer and the euphotic layer in the SAZ, PFZ and AAZ in the vicinity of the Crozet and Kerguelen plateaus. The transition layer constitutes a physical interface of increased water column stability, as diagnosed by maximum Brunt-Väisälä frequencies (Table 2). However, although POC and POC$_{micro}$ concentrations were higher in the transition layer relative to the deep-reference samples, they were notably lower than those of the mixed layer (Tables 2, 3), not indicative of biomass accumulation on this physical interface. Furthermore, examples of significant sub-surface biomass accumulation in the Southern Ocean have been associated to divergent diatom communities with an accumulation of larger diatoms at depth (Kopczynska et al. 2001). In our regional survey, mixed layer and transition layer diatom communities were similar, consistent with more localised studies (Armand et al. 2008; Gomi et al. 2010). The data presented above suggests that subsurface chlorophyll features are not necessarily associated with biomass accumulation in the Southern ocean and this is consistent across a broad spatial scale.

In the PFZ and AAZ, the highest Chl:POC ratios were observed in the transition layer and we suggest this is linked to photoacclimation. It is known that Chl:POC ratios of phytoplankton can cover more than one order of magnitude (0.003–0.055 g g^{-1}; Cloern et al. 1995) and due to photoacclimation vary fourfold among single diatom species (Anning et al. 2000). The CCA results highlight the association of high Chl:POC ratios with full and large (>100 μm) diatom cells in the transition layer of the AAZ. Southern Ocean diatoms have developed an acclimation strategy to low light and iron levels by increasing the amount of light-harvesting pigments on photosynthetic units, rather than multiplying the number of photosynthetic units (Strzepek et al. 2012).

It has been suggested previously that nutrient diffusion through the pycnocline could sustain phytoplankton production in a transition layer when mixed layer nutrient concentrations reach limiting levels (Holm-Hansen and Hewes

2004; Johnston and Rudnick 2009; Quéguiner 2013). There was no evidence of oxygen accumulation in the transition layer (data not shown) suggesting minimal photosynthetic production, although diffusion and heterotrophic respiration may have dampened an already low signal. Unfortunately no carbon fixation data is available to validate the hypothesis of negligible photosynthetic rates below the euphotic layer. However, production in the transition layer would also require iron diffusion but ferriclines can be significantly deeper than mixed layers and transition layers. On the Kerguelen plateau, although the transition layer occurs at 110 m, the ferricline is located at 175 m in summer (Blain et al. 2008). This is a pattern generally applicable to the Southern Ocean as a whole, where summer ferricline horizons appear to be systematically deeper than MLDs (Tagliabue et al. 2014) and thus significant carbon fixation by transition layer communities appears unlikely. Our data suggests that sub-surface chlorophyll features can be attributed to photoacclimatation of mixed layer communities within the transition layer, rather than production and subsequent biomass accumulation at this interface.

Late summer transition layers as a site for carbon and silicon decoupling

We propose Southern Ocean transition layers as a key location in the water column where carbon and silicon elemental cycles are decoupled. A notable biogeochemical feature of late summer transition layers in our study region is elevated BSi:POC ratios compared to mixed layer samples (Fig. 4). In contrast to the deep water-column (250 m), mixed layer and transition layer diatom communities are quite similar. This indicates that differences in diatom community structure, (i.e., shifts to larger diatoms in sub-surface communities, Kopczynska et al. 2001) does not act as a major control in driving the patterns in BSi:POC ratios as a function of depth. In contrast, the proportion of empty diatom frustules in the transition layer is markedly increased compared to the mixed layer (Fig. 6). Specifically, we observed an accumulation of empty *F. kerguelensis* and *Pseudo-nitzschia* cells associated to high BSi:POC ratios. Programmed cell death, viral lysis and grazing pressure have all been proposed as mechanisms that could lead to the accumulation of empty frustules (Assmy et al. 2013). In this context, transition layers have been identified as grazing hotspots for micro- and meso-zooplankton (Holm-Hansen and Hewes 2004; Gomi et al. 2010). A high BSi:POC ratio is an inherent property to the iron-limited ACC characterized by the dominance of heavily silicified diatoms (Smetacek et al. 2004), our results suggest it might be enhanced within the transition layer transitional layer due to elevated heterotrophic activity and zooplankton grazing. Additionally, transition layers in the SAZ and at A3 displayed a low fraction of empty frustules and a high abundance of large *Corethron* spp. or very large *Thalassiothrix antarctica*. The large size of these diatom might confer them a resistance to

grazing (Smetacek et al. 2004), resulting in a low proportion of empty frustules for these species.

In the AAZ, we observed high $Si(OH)_4$ diffusive fluxes in the transition layer, mainly driven by a strong $Si(OH)_4$ gradient generated by the intense silicon utilization by diatoms in surface waters in summer, and to a lesser extent by an increased Kz within the transition layer. Carbon fixation relies on iron-dependent photosynthesis whereas Si fixation depends on energy from respiration (Martin-Jézéquel et al. 2000) and may thus occur independent of light (Chisholm et al. 1978; Martin-Jézéquel et al. 2000). Silicification may be sustained by vertical diffusion of $Si(OH)_4$ (Table 2) and, even at low levels, may partly contribute to the increase in BSi:POC ratios in AAZ transition layers. Consequently the transition layer may represent a location in the water column where carbon and silicon fixation can become physiologically decoupled, although direct measurements of carbon and silicon uptake (e.g., Closset et al. 2014) would be necessary to confirm this hypothesis.

Regional patterns in microplankton diversity and particulate matter stoichiometry

The hierarchical clustering and the CCA suggest strong regional patterns in microplankton community structure relative to the frontal location and the depth. The dominance of the sub-tropical diatom *Bacteriastrum* in the warm surface water waters (15°C) in the SAZ is likely to result from the southward advection of a the Subtropical Front meander. In general mixed layer communities in the SAZ and PFZ were dominated by the dinoflagellate *Prorocentrum*, in terms of both abundance and biomass. A major contribution of dinoflagellates to late summer phytoplankton biomass was also observed in the SAZ of the Crozet Basin (Kopczyńska and Fiala 2003), although flagellates and coccolithophorids dominated the numerical assemblage (Fiala et al. 2004), consistent with the regional pattern of coccolith sedimentation (Salter et al. 2014). Poulton et al. (2007) reported that post-bloom phytoplankton communities in the PFZ, North of the Crozet plateau, were dominated by the nanoplanktonic *Phaeocystis antarctica*, with a low contribution by the small diatom *Thalassionema nitzschioides*. The low contribution of diatoms to late summer biomass in the mixed layer of the SAZ and PFZ is consistent with the commonly observed succession of diatoms to dinoflagellates from spring to summer (Margalef 1978; Barton et al. 2013). Ciliates significantly contributed to phytoplankton biomass in the mixed layer of the PFZ, indicative of nutrient limitation driving a switch towards a more heterotrophic food-web as often observed at a global scale (Margalef 1958; Landry and Calbet 2004) and during artificial (Gall et al. 2001; Henjes et al. 2007) and natural (Poulton et al. 2007) iron-fertilization studies in the Southern Ocean.

In contrast to the patterns described above, diatoms still heavily dominated AAZ microplankton communities at the

Rembauville et al.   *Particulate matter stoichiometry*

time of sampling (>80% abundance, >70% biomass), notably through the contribution of large diatoms such as *Membraneis*, *Corethron* and *Rhizosolenia*. A dominance of the large diatom *Corethron pennatum* to the total biomass was previoulsy reported in late summer in the AAZ south of Crozet Islands (Poulton et al. 2007). In the AAZ west of South Georgia, diatoms also dominate phytoplankton biomass in late summer with a strong contribution of *Pseudo-nitzschia*, *T. antarctica*, and *E. antarctica* var. *antarctica* (Korb and Whitehouse 2004; Korb et al. 2008, 2010). We observed a strong contribution of the very large diatom *Thalassiothrix antarctica* together with *Corethron* spp. to the total biomass at the central Kerguelen plateau station A3. This is consistent with previous observations at the same station in summer during KEOPS1, although in the latter *E. antarctica* dominated diatom biomass (Armand et al. 2008). On the Kerguelen plateau dinoflagellates contribution to biomass and abundance was lower (mainly though the representation of the genera *Gyrodinium* and *Prorocentrum*) and similar to observations made during KEOPS1 (>20% microplankton biomass; Sarthou et al. 2008). Over the Kerguelen plateau, diapycnal iron diffusive flux in summer (Blain et al. 2008; Chever et al. 2010) might sustain diatom production and explain why the microplankton community has not shifted to a dominance of dinoflagellates and ciliates.

Regional patterns in PON:POP stoichiometry of particulate matter were strongly correlated with the distribution of major microplankton groups across frontal zones and at different depth horizons. The CCA highlights the general association of elevated PON:POP ratios with dinoflagellates and ciliates. Furthermore, PON:POP ratios were lowest in the mixed layer of the AAZ (4–7) and transition layer of the AAZ (5–8) where biomass is dominated by diatoms (>70%). In culture, N:P ratios of ∼10 for the dinoflagellates *Gymnodinium dominans* and *Oxyrhhis marina* and 10–15 for the ciliate *Euplotes* have been reported (Golz et al. 2015). Under optimal growth conditions *O. marina* exhibits high N:P ratios of 25 (Malzahn et al. 2010). Similarly several studies have reported low N:P ratio from diatom cultures (<10; Ho et al. 2003; Quigg et al. 2003). During the EIFEX artificial-iron fertilization experiment, *F. kerguelensis* was reported to grow with an N:P ratio of 3–4 (Hoffmann et al. 2007). During KEOPS2, N:P ratio of 6–15 was found in the high biomass stations of the PFZ east of Kerguelen Islands (Lasbleiz et al. 2014). In agreement with these previous studies, our results suggest that broad-scale shifts in microplankton community composition in the Southern Ocean can modulate particulate matter stoichiometry and are consistent with the major latitudinal trends observed globally (Martiny et al. 2013).

There are some notable subtleties to the general trends presented above. SAZ mixed layer particles exhibit relatively high PON:POP ratios (10–12) even if the community was dominated by diatoms (e.g., Station 5; >75% *Bacteriastrum* sp.). Resource allocation in Southern Ocean diatoms is

known to be highly sensitive to temperature with more P-rich ribosomes being required for protein synthesis under low temperature resulting in a lower N:P ratio (Toseland et al. 2013). Mixed layer waters of the SAZ are notably warmer (10–15°C) than the AAZ (2–4°C), which may result in higher PON:POP ratio for diatom-dominated communities of the SAZ compared to the AAZ. Iron-limitation is an additional plausible mechanism that may modulate PON:POP ratios. Iron limitation decreases nitrate uptake (Price et al. 1994) and nitrate reductase activity (Timmermans et al. 1994), leading to lower N:P ratio in iron-limited diatom cultures (Price 2005). Furthermore, Hoffmann et al. (2006) reported a strong N:P increase (4 to 16) in the >20 μm fraction following iron addition in iron-limited cultures. The dissolved iron concentration is <0.15 nmol L^{-1} in the mixed layer in the AAZ over the central Kerguelen plateau in February (Blain et al. 2008) and therefore iron limitation may have lowered PON:POP ratios observed in the diatom-dominated AAZ samples. In conclusion microplankton community structure appears to exert a first order control on PON:POP stoichiometry in late summer in this sector of the Southern Ocean. Physiological constraints linked to environmental factors, such as temperature and iron limitation, are also able to modulate this ratio.

Implications for carbon and silicon export

A recent compilation of carbon export estimates over the Kerguelen plateau (station A3) indicates a strong POC flux attenuation between the mixed layer and 300 m (Rembauville et al. 2015b). In this region we observed similarly high BSi:POC ratios in the transition layer (∼0.8) compared to sediment trap samples (0.7–1.5) at the end of summer (Rembauville et al. 2015a). *F. kerguelensis* was mostly present in the form of empty frustules in the transition layer, consistent with its classification as a preferential "silica sinker" (Smetacek et al. 2004; Assmy et al. 2013) that has been confirmed by sediment trap studies (Salter et al. 2012; Rembauville et al. 2015a; Rigual-Hernández et al. 2015). In contrast, the large *Rhizosolenia* spp. (∼500 μm) and very large *T. antarctica* (up to 3–4 mm) were present as full cells within the transition layer, an observation consistent with their recent quantification as a "carbon sinker" over the central Kerguelen plateau (Rembauville et al. 2015a). However, the large frustule of these species confers a resistance to grazing (e.g., Smetacek et al. 2004) and high Si:C ratio that may drive a significant contribution to silicon sinking.

It is generally stated that diatom-dominated ecosystems are more efficient in exporting carbon from the mixed layer compared to more recycling systems dominated by dinoflagellates and ciliates (Smetacek 1985; Legendre and Le Fèvre 1989; Boyd and Newton 1995, 1999; Legendre and Rivkin 2015). However, despite a dominance of diatoms in the mixed layer microplankton assemblage in the AAZ, the deep (250 m) POC concentrations in the AAZ were comparable to

the PFZ and SAZ (0.9–1.36 μmol L^{-1} vs. 1.10–1.90 μmol L^{-1}) where dinoflagelates and ciliates dominated the microplankton assemblage. Although one must be cautious in equating standing stocks to fluxes these data suggest that in late summer in the Southern Ocean, a higher proportion of diatoms in the mixed layer does not consistently lead to a higher transfer of carbon at 250 m. Intense zooplankton grazing of diatom biomass in the transition layer, as evidenced by the increased proportion of empty cells relative to the mixed layer, presumably results in the efficient consumption and recycling of exportable biomass reducing diatom-mediated carbon transfer into the ocean interior. This has been suggested previously as an explanation for High biomass Low Export Environments (Lam and Bishop 2007; Lam et al. 2011; Jacquet et al. 2011). Moreover, a strong response of heterotrophic microbial communities to the high primary production levels (Obernosterer et al. 2008) and the association of specific bacterial communities with deep biomass features (Obernosterer et al. 2011) might also strongly contribute to the remineralization of POC over the Kerguelen plateau. An efficient response of both microbial and mesozooplanktonic communities to POC availability is consistent with the inverse relationship between diatom-dominated primary production and export efficiency observed in the Southern Ocean (Maiti et al. 2013). Furthermore we observed a progressive increase of diatoms present as empty frustules through the water column and a significantly higher contribution of dinoflagellates and ciliates to total microplankton POC at 250 m compared to the transition layer. These data show the importance of zooplankton grazing in modulating diatom export production during late summer Southern Ocean ecosystems and highlight the potential importance of ciliates and dinoflagellates to the biological carbon pump at these specific times.

A notable exception to the patterns described above are the observations from station A3, on the Kerguelen plateau, where deep microplankton POC is dominated by *Chaetoceros Hyalochaete* resting spores (80%), leading to POC concentrations that are ~3 times higher than mean values at 250 m in the AAZ, PFZ and SAZ. This observation is broadly consistent with a recent sediment trap study which documented *C. Hyalochaete* resting spores as the dominant contributor to the annual carbon export (>60%) mediated through two rapid flux events occurring at the end of summer (Rembauville et al. 2015a). If the transition layer is a place of intense grazing pressure then our results consolidate the idea that resting spores are a specific ecological vector for carbon export through intense remineralization horizons. Indeed, small and highly silicified CRS have been demonstrated to lower copepod grazing pressure in culture (Kuwata and Tsuda 2005). In line with recent sediment trap results, the present study supports the pivotal role of diatom resting spores for carbon export from natural iron fertilized blooms in the Southern Ocean (Salter et al. 2007, 2012; Rembauville et al. 2015a). The

net impact of diatom-dominated communities on carbon export strongly depends on the ecology of the species present. Preferential silicon sinking species poorly contribute to carbon export contrary to carbon sinking species, such as diatoms that form resting spores. A coupled description of mixed layer properties (nutrient dynamics and phytoplankton communities) and export out of the mixed layer over an entire productive cycle remains necessary to better understand processes responsible for resting spore formation.

References

Aminot, A., and R. Kerouel. 2007. Dosage automatique des nutriments dans les eaux marines: Méthodes en flux continu. Ifremer.

Anning, T., H. L. MacIntyre, S. M. Pratt, P. J. Sammes, S. Gibb, and R. J. Geider. 2000. Photoacclimation in the marine diatom *Skeletonema costatum*. Limnol. Oceanogr. **45**: 1807–1817. doi:10.4319/lo.2000.45.8.1807

Armand, L. K., V. Cornet-Barthaux, J. Mosseri, and B. Quéguiner. 2008. Late summer diatom biomass and community structure on and around the naturally iron-fertilised Kerguelen Plateau in the Southern Ocean. Deep Sea Res. Part II Top. Stud. Oceanogr. **55**: 653–676. doi:10.1016/j.dsr2.2007.12.031

Assmy, P., and others. 2013. Thick-shelled, grazer-protected diatoms decouple ocean carbon and silicon cycles in the iron-limited Antarctic Circumpolar Current. Proc. Natl. Acad. Sci. U. S. A. **110**: 20633–20638. doi:10.1073/pnas.1309345110

Barton, A. D., Z. V. Finkel, B. A. Ward, D. G. Johns, and M. J. Follows. 2013. On the roles of cell size and trophic strategy in North Atlantic diatom and dinoflagellate communities. Limnol. Oceanogr. **58**: 254–266. doi:10.4319/lo.2013.58.1.0254

Blain, S., and others. 2001. A biogeochemical study of the island mass effect in the context of the iron hypothesis: Kerguelen Islands, Southern Ocean. Deep Sea Res. Part I Oceanogr. Res. Pap. **48**: 163–187. doi:10.1016/S0967-0637(00)00047-9

Blain, S., G. Sarthou, and P. Laan. 2008. Distribution of dissolved iron during the natural iron-fertilization experiment KEOPS (Kerguelen Plateau, Southern Ocean). Deep Sea Res. Part II Top. Stud. Oceanogr. **55**: 594–605. doi:10.1016/j.dsr2.2007.12.028

Borrione, I., and R. Schlitzer. 2013. Distribution and recurrence of phytoplankton blooms around South Georgia, Southern Ocean. Biogeosciences **10**: 217–231. doi:10.5194/bg-10-217-2013

Boyd, P., and P. Newton. 1995. Evidence of the potential influence of planktonic community structure on the interannual variability of particulate organic carbon flux. Deep Sea Res. Part I Oceanogr. Res. Pap. **42**: 619–639. doi:10.1016/0967-0637(95)00017-Z

Boyd, P. W., and P. P. Newton. 1999. Does planktonic community structure determine downward particulate organic carbon flux in different oceanic provinces? Deep Sea Res. Part I Oceanogr. Res. Pap. **46**: 63–91. doi:10.1016/S0967-0637(98)00066-1

Chever, F., G. Sarthou, E. Bucciarelli, S. Blain, and A. R. Bowie. 2010. An iron budget during the natural iron fertilisation experiment KEOPS (Kerguelen Islands, Southern Ocean). Biogeosciences **7**: 455–468. doi:10.5194/bg-7-455-2010

Chisholm, S. W., F. Azam, and R. W. Eppley. 1978. Silicic acid incorporation in marine diatoms on light:dark cycles: Use as an assay for phased cell division 1. Limnol. Oceanogr. **23**: 518–529. doi:10.4319/lo.1978.23.3.0518

Cloern, J. E., C. Grenz, and L. Vidergar-Lucas. 1995. An empirical model of the phytoplankton chlorophyll : Carbon ratio-the conversion factor between productivity and growth rate. Limnol. Oceanogr. **40**: 1313–1321. doi:10.4319/lo.1995.40.7.1313

Closset, I., and others. 2014. Seasonal evolution of net and regenerated silica production around a natural Fe-fertilized area in the Southern Ocean estimated with Si isotopic approaches. Biogeosciences **11**: 5827–5846. doi:10.5194/bg-11-5827-2014

Cornet-Barthaux, V., L. Armand, and B. Quéguiner. 2007. Biovolume and biomass estimates of key diatoms in the Southern Ocean. Aquat. Microb. Ecol. **48**: 295–308. doi:10.3354/ame048295

de Baar, H. J. W., A. G. J. Buma, R. F. Nolting, G. C. Cadée, G. Jacques, and P. Tréguer. 1990. On iron limitation of the Southern Ocean: Experimental observations in the Weddell and Scotia Seas. Mar. Ecol. Prog. Ser. **65**: 105–122. doi:10.3354/meps065105

de Boyer Montégut, C., G. Madec, A. S. Fischer, A. Lazar, and D. Iudicone. 2004. Mixed layer depth over the global ocean: An examination of profile data and a profile-based climatology. J. Geophys. Res. Oceans **109**: C12003. doi:10.1029/2004JC002378

Dutkiewicz, S., M. J. Follows, and P. Parekh. 2005. Interactions of the iron and phosphorus cycles: A three-dimensional model study. Global Biogeochem. Cycles **19**: GB1021. doi:10.1029/2004GB002342

Elser, J. J., D. R. Dobberfuhl, N. A. MacKay, and J. H. Schampel. 1996. Organism size, life history, and N:P stoichiometry. BioScience **46**: 674–684. doi:10.2307/1312897

Fennel, K., and E. Boss. 2003. Subsurface maxima of phytoplankton and chlorophyll: Steady-state solutions from a simple model. Limnol. Oceanogr. **48**: 1521–1534. doi:10.4319/lo.2003.48.4.1521

Fiala, M., E. E. Kopczynska, L. Oriol, and M.-C. Machado. 2004. Phytoplankton variability in the Crozet Basin frontal zone (Southwest Indian Ocean) during austral summer. J. Mar. Syst. **50**: 243–261. doi:10.1016/j.jmarsys.2004.01.008

Gall, M. P., P. W. Boyd, J. Hall, K. A. Safi, and H. Chang. 2001. Phytoplankton processes. Part 1: Community structure during the Southern Ocean Iron RElease Experiment (SOIREE). Deep Sea Res. Part II Top. Stud. Oceanogr. **48**: 2551–2570. doi:10.1016/S0967-0645(01)00008-X

Golz, A.-L., A. Burian, and M. Winder. 2015. Stoichiometric regulation in micro- and mesozooplankton. J. Plankton Res. **37**: 293–305. doi:10.1093/plankt/fbu109

Gomi, Y., M. Fukuchi, and A. Taniguchi. 2010. Diatom assemblages at subsurface chlorophyll maximum layer in the eastern Indian sector of the Southern Ocean in summer. J. Plankton Res. **32**: 1039–1050. doi:10.1093/plankt/fbq031

Gordon, H. R., and W. R. McCluney. 1975. Estimation of the depth of sunlight penetration in the sea for remote sensing. Appl. Opt. **14**: 413–416. doi:10.1364/AO.14.000413

Hasle, G. R., and E. E. Syvertsen. 1997. Chapter 2—marine diatoms, p. 5–385. In C. R. Tomas [ed.], Identifying marine phytoplankton. Academic Press.

Henjes, J., P. Assmy, C. Klaas, P. Verity, and V. Smetacek. 2007. Response of microzooplankton (protists and small copepods) to an iron-induced phytoplankton bloom in the Southern Ocean (EisenEx). Deep Sea Res. Part I Oceanogr. Res. Pap. **54**: 363–384. doi:10.1016/j.dsr.2006.12.004

Hillebrand, H., C.-D. Dürselen, D. Kirschtel, U. Pollingher, and T. Zohary. 1999. Biovolume calculation for pelagic and benthic microalgae. J. Phycol. **35**: 403–424. doi:10.1046/j.1529-8817.1999.3520403.x

Ho, T.-Y., A. Quigg, Z. V. Finkel, A. J. Milligan, K. Wyman, P. G. Falkowski, and F. M. M. Morel. 2003. The elemental composition of some marine phytoplankton. J. Phycol. **39**: 1145–1159. doi:10.1111/j.0022-3646.2003.03-090.x

Hoffmann, L. J., I. Peeken, K. Lochte, P. Assmy, and M. Veldhuis. 2006. Different reactions of Southern Ocean phytoplankton size classes to iron fertilization. Limnol. Oceanogr. **51**: 1217–1229. doi:10.4319/lo.2006.51.3.1217

Hoffmann, L. J., I. Peeken, and K. Lochte. 2007. Effects of iron on the elemental stoichiometry during EIFEX and in the diatoms Fragilariopsis kerguelensis and Chaetoceros dichaeta. Biogeosciences **4**: 569–579. doi:10.5194/bg-4-569-2007

Holm-Hansen, O., and C. D. Hewes. 2004. Deep chlorophyll-a maxima (DCMs) in Antarctic waters. I. Relationships between DCMs and the physical, chemical, and optical conditions in the upper water column. Polar Biol. **27**: 699–710. doi:10.1007/s00300-004-0641-1

Holm-Hansen, O., M. Kahru, and C. Hewes. 2005. Deep chlorophyll a maxima (DCMs) in pelagic Antarctic waters. II. Relation to bathymetric features and dissolved iron concentrations. Mar. Ecol. Prog. Ser. **297**: 71–81. doi:10.3354/meps297071

Howard, A. G., A. J. Coxhead, I. A. Potter, and A. P. Watt. 1986. Determination of dissolved aluminium by the micelle-enhanced fluorescence of its lumogallion

complex. Analyst **111**: 1379–1382. doi:10.1039/AN9861101379

Hutchins, D. A., and K. W. Bruland. 1998. Iron-limited diatom growth and Si:N uptake ratios in a coastal upwelling regime. Nature **393**: 561–564. doi:10.1038/31203

Jacquet, S. H., P. J. Lam, T. Trull, and F. Dehairs. 2011. Carbon export production in the Subantarctic zone and polar front zone south of Tasmania. Deep Sea Res. Part II Top. Stud. Oceanogr. **58**: 2277–2292. doi:10.1016/j.dsr2.2011.05.035

Johnston, T. M. S., and D. L. Rudnick. 2009. Observations of the Transition Layer. J. Phys. Oceanogr. **39**: 780–797. doi:10.1175/2008JPO3824.1

Khatiwala, S., F. Primeau, and T. Hall. 2009. Reconstruction of the history of anthropogenic CO_2 concentrations in the ocean. Nature **462**: 346–349. doi:10.1038/nature08526

Klausmeier, C. A., E. Litchman, T. Daufresne, and S. A. Levin. 2004. Optimal nitrogen-to-phosphorus stoichiometry of phytoplankton. Nature **429**: 171–174. doi:10.1038/nature02454

Kopczynska, E. E., F. Dehairs, M. Elskens, and S. Wright. 2001. Phytoplankton and microzooplankton variability between the Subtropical and Polar Fronts south of Australia: Thriving under regenerative and new production in late summer. J. Geophys. Res. Oceans **106**: 31597–31609. doi:10.1029/2000JC000278

Kopczyńska, E. E., and M. Fiala. 2003. Surface phytoplankton composition and carbon biomass distribution in the Crozet Basin during austral summer of 1999: Variability across frontal zones. Polar Biol. **27**: 17–28. doi:10.1007/s00300-003-0564-2

Korb, R. E., and M. Whitehouse. 2004. Contrasting primary production regimes around South Georgia, Southern Ocean: Large blooms versus high nutrient, low chlorophyll waters. Deep Sea Res. Part I Oceanogr. Res. Pap. **51**: 721–738. doi:10.1016/j.dsr.2004.02.006

Korb, R. E., M. J. Whitehouse, A. Atkinson, and S. E. Thorpe. 2008. Magnitude and maintenance of the phytoplankton bloom at South Georgia: A naturally iron-replete environment. Mar. Ecol. Prog. Ser. **368**: 75–91. doi:10.3354/meps07525

Korb, R. E., M. J. Whitehouse, M. Gordon, P. Ward, and A. J. Poulton. 2010. Summer microplankton community structure across the Scotia Sea: Implications for biological carbon export. Biogeosciences **7**: 343–356. doi:10.5194/bg-7-343-2010

Kuwata, A., and A. Tsuda. 2005. Selection and viability after ingestion of vegetative cells, resting spores and resting cells of the marine diatom, Chaetoceros pseudocurvisetus, by two copepods. J. Exp. Mar. Biol. Ecol. **322**: 143–151. doi:10.1016/j.jembe.2005.02.013

Lam, P. J., and J. K. B. Bishop. 2007. High biomass, low export regimes in the Southern Ocean. Deep Sea Res. Part

II Top. Stud. Oceanogr. **54**: 601–638. doi:10.1016/j.dsr2.2007.01.013

Lam, P. J., S. C. Doney, and J. K. B. Bishop. 2011. The dynamic ocean biological pump: Insights from a global compilation of particulate organic carbon, CaCO3, and opal concentration profiles from the mesopelagic. Global Biogeochem. Cycles **25**: GB3009. doi:10.1029/2010GB003868

Landry, M. R., and A. Calbet. 2004. Microzooplankton production in the oceans. ICES J. Mar. Sci. J. Cons. **61**: 501–507. doi:10.1016/j.icesjms.2004.03.011

Lasbleiz, M., K. Leblanc, S. Blain, J. Ras, V. Cornet-Barthaux, S. Hélias Nunige, and B. Quéguiner. 2014. Pigments, elemental composition (C, N, P, and Si), and stoichiometry of particulate matter in the naturally iron fertilized region of Kerguelen in the Southern Ocean. Biogeosciences **11**: 5931–5955. doi:10.5194/bg-11-5931-2014

Legendre, L., and J. Le Fèvre. 1989. Hydrodynamical singularities as controls of recycled versus export production in oceans, p. 49–63. In W. H. Berger, V. S. Smetacek, G. Wefer [eds.], Productivity of the oceans: Present and past. John Wiley & Sons.

Legendre, P., and L. Legendre. 1998. Numerical ecology, 2nd ed. Elsevier Science.

Legendre, L., and R. B. Rivkin. 2015. Flows of biogenic carbon within marine pelagic food webs: Roles of microbial competition switches. Mar. Ecol. Prog. Ser. **521**: 19–30. doi:10.3354/meps11124

Letelier, R. M., D. M. Karl, M. R. Abbott, and R. R. Bidigare. 2004. Light driven seasonal patterns of chlorophyll and nitrate in the lower euphotic zone of the North Pacific Subtropical Gyre. Limnol. Oceanogr. **49**: 508–519. doi:10.4319/lo.2004.49.2.0508

Maiti, K., M. A. Charette, K. O. Buesseler, and M. Kahru. 2013. An inverse relationship between production and export efficiency in the Southern Ocean. Geophys. Res. Lett. **40**: 1557–1561. doi:10.1002/grl.50219

Malzahn, A. M., F. Hantzsche, K. L. Schoo, M. Boersma, and N. Aberle. 2010. Differential effects of nutrient-limited primary production on primary, secondary or tertiary consumers. Oecologia **162**: 35–48. doi:10.1007/s00442-009-1458-y

Margalef, R. 1958. Temporal succession and spatial heterogeneity in phytoplankton, p. 323–349. In A. A. Buzzati-Traverso [eds.], Perspective in marine biology. University of California.

Margalef, R. 1978. Life-forms of phytoplankton as survival alternatives in an unstable environment. Oceanol. Acta **1**: 493–509.

Martin, J. H. 1990. Glacial-interglacial CO_2 change: The Iron Hypothesis. Paleoceanography **5**: 1–13. doi:10.1029/PA005i001p00001

Martin, J., and others. 2010. Prevalence, structure and properties of subsurface chlorophyll maxima in Canadian

Rembauville et al.   *Particulate matter stoichiometry*

Arctic waters. Mar. Ecol. Prog. Ser. **412**: 69–84. doi:10.3354/meps08666

Martiny, A. C., C. T. A. Pham, F. W. Primeau, J. A. Vrugt, J. K. Moore, S. A. Levin, and M. W. Lomas. 2013. Strong latitudinal patterns in the elemental ratios of marine plankton and organic matter. Nat. Geosci. **6**: 279–283. doi:10.1038/ngeo1757

Menden-Deuer, S., and E. J. Lessard. 2000. Carbon to volume relationships for dinoflagellates, diatoms, and other protist plankton. Limnol. Oceanogr. **45**: 569–579. doi:10.4319/lo.2000.45.3.0569

Mignot, A., H. Claustre, J. Uitz, A. Poteau, F. D'Ortenzio, and X. Xing. 2014. Understanding the seasonal dynamics of phytoplankton biomass and the deep chlorophyll maximum in oligotrophic environments: A Bio-Argo float investigation. Glob. Biogeochem. Cycles **28**: 2013GB004781. doi:10.1002/2013GB004781

Minas, H. J., M. Minas, and T. T. Packard. 1986. Productivity in upwelling areas deduced from hydrographic and chemical fields. Limnol. Oceanogr. **31**: 1182–1206. doi:10.4319/lo.1986.31.6.1182

Moore, C. M., A. E. Hickman, A. J. Poulton, S. Seeyave, and M. I. Lucas. 2007. Iron–light interactions during the CROZet natural iron bloom and EXport experiment (CROZEX): II—Taxonomic responses and elemental stoichiometry. Deep Sea Res. Part II Top. Stud. Oceanogr. **54**: 2066–2084. doi:10.1016/j.dsr2.2007.06.015

Morel, A., and J.-F. Berthon. 1989. Surface pigments, algal biomass profiles, and potential production of the euphotic layer: Relationships reinvestigated in view of remote-sensing applications. Limnol. Oceanogr. **34**: 1545–1562. doi:10.4319/lo.1989.34.8.1545

Mosseri, J., B. Quéguiner, L. Armand, and V. Cornet-Barthaux. 2008. Impact of iron on silicon utilization by diatoms in the Southern Ocean: A case study of Si/N cycle decoupling in a naturally iron-enriched area. Deep Sea Res. Part II Top. Stud. Oceanogr. **55**: 801–819. doi:10.1016/j.dsr2.2007.12.003

Neveux, J., and F. Lantoine. 1993. Spectrofluorometric assay of chlorophylls and phaeopigments using the least squares approximation technique. Deep Sea Res. Part I Oceanogr. Res. Pap. **40**: 1747–1765. doi:10.1016/0967-0637(93)90030-7

Obernosterer, I., U. Christaki, D. Lefèvre, P. Catala, F. Van Wambeke, and P. Lebaron. 2008. Rapid bacterial mineralization of organic carbon produced during a phytoplankton bloom induced by natural iron fertilization in the Southern Ocean. Deep Sea Res. Part II Top. Stud. Oceanogr. **55**: 777–789. doi:10.1016/j.dsr2.2007.12.005

Obernosterer, I., P. Catala, P. Lebaron, and N. J. West. 2011. Distinct bacterial groups contribute to carbon cycling during a naturally iron fertilized phytoplankton bloom in the Southern Ocean. Limnol. Oceanogr. **56**: 2391–2401. doi:10.4319/lo.2011.56.6.2391

Park, Y.-H., E. Charriaud, D. R. Pino, and C. Jeandel. 1998. Seasonal and interannual variability of the mixed layer properties and steric height at station KERFIX, southwest of Kerguelen. J. Mar. Syst. **17**: 571–586. doi:10.1016/S0924-7963(98)00065-7

Park, J., I.-S. Oh, H.-C. Kim, and S. Yoo. 2010. Variability of SeaWiFS chlorophyll-a in the southwest Atlantic sector of the Southern Ocean: Strong topographic effects and weak seasonality. Deep Sea Res. Part I Oceanogr. Res. Pap. **57**: 604–620. doi:10.1016/j.dsr.2010.01.004

Park, Y.-H., J.-H. Lee, I. Durand, and C.-S. Hong. 2014. Validation of Thorpe-scale-derived vertical diffusivities against microstructure measurements in the Kerguelen region. Biogeosciences **11**: 6927–6937. doi:10.5194/bg-11-6927-2014

Parslow, J. S., P. W. Boyd, S. R. Rintoul, and F. B. Griffiths. 2001. A persistent subsurface chlorophyll maximum in the Interpolar Frontal Zone south of Australia: Seasonal progression and implications for phytoplankton-light-nutrient interactions. J. Geophys. Res. Oceans **106**: 31543–31557. doi:10.1029/2000JC000322

Pollard, R. T., H. J. Venables, J. F. Read, and J. T. Allen. 2007. Large-scale circulation around the Crozet Plateau controls an annual phytoplankton bloom in the Crozet Basin. Deep Sea Res. Part II Top. Stud. Oceanogr. **54**: 1915–1929. doi:10.1016/j.dsr2.2007.06.012

Poulton, A. J., C. Mark Moore, S. Seeyave, M. I. Lucas, S. Fielding, and P. Ward. 2007. Phytoplankton community composition around the Crozet Plateau, with emphasis on diatoms and Phaeocystis. Deep Sea Res. Part II Top. Stud. Oceanogr. **54**: 2085–2105. doi:10.1016/j.dsr2.2007.06.005

Price, N. M. 2005. The elemental stoichiometry and composition of an iron-limited diatom. Limnol. Oceanogr. **50**: 1159–1171. doi:10.4319/lo.2005.50.4.1159

Price, N. M., B. A. Ahner, and F. M. M. Morel. 1994. The equatorial Pacific Ocean: Grazer-controlled phytoplankton populations in an iron-limited ecosystem. Limnol. Oceanogr. **39**: 520–534. doi:10.4319/lo.1994.39.3.0520

Primeau, F. W., M. Holzer, and T. DeVries. 2013. Southern Ocean nutrient trapping and the efficiency of the biological pump. J. Geophys. Res. Oceans **118**: 2547–2564. doi:10.1002/jgrc.20181

Pujo-Pay, M., and P. Raimbault. 1994. Improvement of the wet-oxidation procedure for simultaneous determination of particulate organic nitrogen and phosphorus collected on filters. Mar. Ecol. Prog. Ser. **105**: 203–207. doi:10.3354/meps105203

Quéguiner, B. 2013. Iron fertilization and the structure of planktonic communities in high nutrient regions of the Southern Ocean. Deep Sea Res. Part II Top. Stud. Oceanogr. **90**: 43–54. doi:10.1016/j.dsr2.2012.07.024

Quéguiner, B., and M. A. Brzezinski. 2002. Biogenic silica production rates and particulate organic matter distribution in the Atlantic sector of the Southern Ocean during austral

spring 1992. Deep Sea Res. Part II Top. Stud. Oceanogr. **49**: 1765–1786. doi:10.1016/S0967-0645(02)00011-5

Quigg, A., and others. 2003. The evolutionary inheritance of elemental stoichiometry in marine phytoplankton. Nature **425**: 291–294. doi:10.1038/nature01953

Ragueneau, O., N. Savoye, Y. Del Amo, J. Cotten, B. Tardiveau, and A. Leynaert. 2005. A new method for the measurement of biogenic silica in suspended matter of coastal waters: Using Si:Al ratios to correct for the mineral interference. Cont. Shelf Res. **25**: 697–710. doi:10.1016/j.csr.2004.09.017

Redfield, A. C. 1958. The biological control of chemical factors in the environment. Am. Sci. **11**: 205–221.

Rembauville, M., S. Blain, L. Armand, B. Quéguiner, and I. Salter. 2015a. Export fluxes in a naturally iron-fertilized area of the Southern Ocean—Part 2: Importance of diatom resting spores and faecal pellets for export. Biogeosciences **12**: 3171–3195. doi:10.5194/bg-12-3171-2015

Rembauville, M., I. Salter, N. Leblond, A. Gueneugues, and S. Blain. 2015b. Export fluxes in a naturally iron-fertilized area of the Southern Ocean—Part 1: Seasonal dynamics of particulate organic carbon export from a moored sediment trap. Biogeosciences **12**: 3153–3170. doi:10.5194/bg-12-3153-2015

Rigual-Hernández, A. S., T. W. Trull, S. G. Bray, A. Cortina, and L. K. Armand. 2015. Latitudinal and temporal distributions of diatom populations in the pelagic waters of the Subantarctic and Polar Frontal zones of the Southern Ocean and their role in the biological pump. Biogeosciences **12**: 5309–5337. doi:10.5194/bg-12-5309-2015

Sabine, C. L., and others. 2004. The oceanic sink for anthropogenic CO$_2$. Science **305**: 367–371. doi:10.1126/science.1097403

Salter, I., and others. 2007. Estimating carbon, silica and diatom export from a naturally fertilised phytoplankton bloom in the Southern Ocean using PELAGRA: A novel drifting sediment trap. Deep Sea Res. Part II Top. Stud. Oceanogr. **54**: 2233–2259. doi:10.1016/j.dsr2.2007.06.008

Salter, I., A. E. S. Kemp, C. M. Moore, R. S. Lampitt, G. A. Wolff, and J. Holtvoeth. 2012. Diatom resting spore ecology drives enhanced carbon export from a naturally iron-fertilized bloom in the Southern Ocean. Global Biogeochem. Cycles **26**: GB1014. doi:10.1029/2010GB003977

Salter, I., R. Schiebel, P. Ziveri, A. Movellan, R. Lampitt, and G. A. Wolff. 2014. Carbonate counter pump stimulated by natural iron fertilization in the Polar Frontal Zone. Nat. Geosci. **7**: 885–889. doi:10.1038/ngeo2285

Sarmiento, J. L., N. Gruber, M. A. Brzezinski, and J. P. Dunne. 2004. High-latitude controls of thermocline nutrients and low latitude biological productivity. Nature **427**: 56–60. doi:10.1038/nature02127

Sarthou, G., K. R. Timmermans, S. Blain, and P. Tréguer. 2005. Growth physiology and fate of diatoms in the

ocean: A review. J. Sea Res. **53**: 25–42. doi:10.1016/j.seares.2004.01.007

Sarthou, G., D. Vincent, U. Christaki, I. Obernosterer, K. R. Timmermans, and C. P. D. Brussaard. 2008. The fate of biogenic iron during a phytoplankton bloom induced by natural fertilisation: Impact of copepod grazing. Deep Sea Res. Part II Top. Stud. Oceanogr. **55**: 734–751. doi:10.1016/j.dsr2.2007.12.033

Shih, L. H., J. R. Koseff, G. N. Ivey, and J. H. Ferziger. 2005. Parameterization of turbulent fluxes and scales using homogeneous sheared stably stratified turbulence simulations. J. Fluid Mech. **525**: 193–214. doi:10.1017/S0022112004002587

Smetacek, V. S. 1985. Role of sinking in diatom life-history cycles: Ecological, evolutionary and geological significance. Mar. Biol. **84**: 239–251. doi:10.1007/BF00392493

Smetacek, V., P. Assmy, and J. Henjes. 2004. The role of grazing in structuring Southern Ocean pelagic ecosystems and biogeochemical cycles. Antarct. Sci. **16**: 541–558. doi:10.1017/S0954102004002317

Sterner, R. W., and J. J. Elser. 2002. Ecological stoichiometry: The biology of elements from molecules to the biosphere. Princeton University Press.

Strzepek, R. F., K. A. Hunter, R. D. Frew, P. J. Harrison, and P. W. Boyd. 2012. Iron-light interactions differ in Southern Ocean phytoplankton. Limnol. Oceanogr. **57**: 1182–1200. doi:10.4319/lo.2012.57.4.1182

Tagliabue, A., J.-B. Sallée, A. R. Bowie, M. Lévy, S. Swart, and P. W. Boyd. 2014. Surface-water iron supplies in the Southern Ocean sustained by deep winter mixing. Nat. Geosci. **7**: 314–320. doi:10.1038/ngeo2101

Takeda, S. 1998. Influence of iron availability on nutrient consumption ratio of diatoms in oceanic waters. Nature **393**: 774–777. doi:10.1038/31674

Timmermans, K. R., W. Stolte, and H. J. W. de Baar. 1994. Iron-mediated effects on nitrate reductase in marine phytoplankton. Mar. Biol. **121**: 389–396. doi:10.1007/BF00346749

Toseland, A., and others. 2013. The impact of temperature on marine phytoplankton resource allocation and metabolism. Nat. Clim. Chang. **3**: 979–984. doi:10.1038/nclimate1989

Uitz, J., H. Claustre, F. B. Griffiths, J. Ras, N. Garcia, and V. Sandroni. 2009. A phytoplankton class-specific primary production model applied to the Kerguelen Islands region (Southern Ocean). Deep Sea Res. Part I Oceanogr. Res. Pap. **56**: 541–560. doi:10.1016/j.dsr.2008.11.006

Van Mooy, B. A. S., and others. 2009. Phytoplankton in the ocean use non-phosphorus lipids in response to phosphorus scarcity. Nature **458**: 69–72. doi:10.1038/nature07659

Venrick, E. L., J. A. McGowan, and A. W. Mantyla. 1973. Deep maxima of photosynthetic chlorophyll in Pacific Ocean. Fish. Bull. **71**: 41–52.

Particulate matter stoichiometry

Weber, T. S., and C. Deutsch. 2010. Ocean nutrient ratios governed by plankton biogeography. Nature **467**: 550–554. doi:10.1038/nature09403

Weston, K., L. Fernand, D. K. Mills, R. Delahunty, and J. Brown. 2005. Primary production in the deep chlorophyll maximum of the central North Sea. J. Plankton Res. **27**: 909–922. doi:10.1093/plankt/fbi064

Whitehouse, M. J., J. Priddle, and M. A. Brandon. 2000. Chlorophyll/nutrient characteristics in the water masses to the north of South Georgia, Southern Ocean. Polar Biol. **23**: 373–382. doi:10.1007/s003000050458

Acknowledgments

3.2   Composition of lipids in export fluxes (article 6)

In **article 2**, we have demonstrated that the biological assemblage of export (e. g. "carbon sinker", "silica sinker", faecal pellet type) impacts the BSi:POC stoichiometry of export fluxes. In **article 5**, we report that microplankton community (mainly diatoms vs. dinoflagellates) structure constrains the PON:POP signature of the particulate stock in the upper ocean. These papers focussed on the role of biology on the cycling of elements (C, N, Si) in the ocean. Here, we increase the analytical resolution and look at the lipid composition of organic matter exported in the vicinity of three island systems in the Southern Ocean: Kerguelen, Crozet and South Georgia.

The export of labile lipids (unsaturated compounds) is 2-4 times higher in the naturally fertilized sites (downstream of the islands) compared to the low productivity sites (upstream of the islands). The four orders of magnitude difference in total lipid flux normalized to organic carbon between the shallowest trap and the deepest trap highlights the preferential remineralization of lipids. There are strong geographical differences in the lipid composition of export fluxes. At Kerguelen (289 m), the abundance of mono- and polyunsaturated fatty acids reflects the contribution of diatoms to the export of fresh and labile organic matter. At Crozet (>3000 m), north of the Polar Front, the sterols assemblage indicates a more diversified phytoplankton community (diatoms, dinoflagellates, haptophytes). Moreover the presence of specific fatty acid methyl esters suggests the organic material was impacted by bacterial metabolism at these important depths. At South Georgia (1500 - 2000 m), the dominance of sterols (mainly cholesterol) indicates an important contribution by zooplankton faecal material. At Kerguelen, we compare the biological constituents of export and the lipid compounds over an annual cycle. In spring and summer, diatom resting spores drive an export of highly labile and energy-rich palmitoleic and eicosapentaenoic acids. In autumn, cholesterol is associated with a dominance of faecal pellet to carbon export. In winter alkenols, probably derived from zooplankton wax ester, highlight metabolic changes in the zooplanktonic community.

*All the lipid analyses presented here were performed by George A. Wolff at the University of Liverpool - School of Environmental Sciences. Sediment trap deployments and POC fluxes are previously presented in **articles 1, 4** and (Salter et al., 2012). The author analysed the data and wrote the manuscript.*

Lipid composition of export fluxes from contrasting productivity sites in the Southern Ocean

Manuscript in preparation

Introduction

The biological pump transfers organic carbon (OC) from photosynthetic production to the deep ocean (Volk and Hoffert, 1985) with important implications for the atmospheric CO_2 content (Sarmiento et al., 1988; Kwon et al., 2009). Only a minor fraction of the carbon fixed in the sunlit ocean reaches the deep ocean (Martin et al., 1987; Honjo et al., 2008), but this carbon and energy supply is essential for the functioning of benthic ecosystems (Billett et al., 1983, 2001; Ruhl and Smith, 2004; Ruhl et al., 2008). Understanding the factors influencing the functioning of the biological pump has been, and remains, a central question in biogeochemical oceanography (Boyd and Newton, 1995; Rivkin et al., 1996; Boyd and Trull, 2007; Guidi et al., 2016). Different approaches can be used to document the biological components of export fluxes. Moored sediment traps allow the direct quantification of sinking protists such as dinoflagellates (Harland and Pudsey, 1999), diatoms (Romero and Armand, 2010), radiolaria (Lampitt et al., 2009), silicoflagellates (Rigual-Hernández et al., 2010), foraminifer (King and Howard, 2005), and zooplankton faecal pellets (Lampitt et al., 1990; Wilson et al., 2008, 2013; Manno et al., 2015). Recent advances in sequencing techniques made possible the description of the bacterial community associated with the sinking matter (Fontanez et al., 2015). Another indirect approach uses biomarkers such as lipids and amino acids to identify the source (algal, zooplanktonic, bacterial) and diagenetic status (lability, degree of preservation) of the exported organic matter (OM, Wakeham, 1982; Wakeham et al., 1980, 1984, 1997; Kiriakoulakis et al., 2001; Lee et al., 2009; Wakeham et al., 2009; Salter et al., 2010). Although it is widely acknowledged that ecological vectors of flux are linked to the geochemical composition, studies providing a coupled description of biological components and organic matter composition of export fluxes remain relatively scarce (e. g. Budge and Parrish, 1998).

Southern Ocean island plateaus such as Kerguelen (Blain et al., 2007), Crozet (Pollard et al., 2009) and South Georgia (Tarling et al., 2012) provide a natural source of iron to the iron-poor waters of the Antarctic Circumpolar Current (de Baar et al., 1990; Martin et al., 1990). Currents and the topography of the sea floor lead to enrichment of iron in waters downstream of the islands which supports massive diatom-dominated phytoplankton blooms (Armand et al., 2008a; Korb et al., 2008; Quéguiner, 2013) that contrast with the high nutrient, low chlorophyll (HNLC, Minas et al., 1986) regime generally prevailing in Antarctic waters. The strong gradients in productivity that characterize these island systems offer a valuable framework to address the link between biological and geochemical composition of particle export. Iron-fertilized blooms in the Southern Ocean constitute
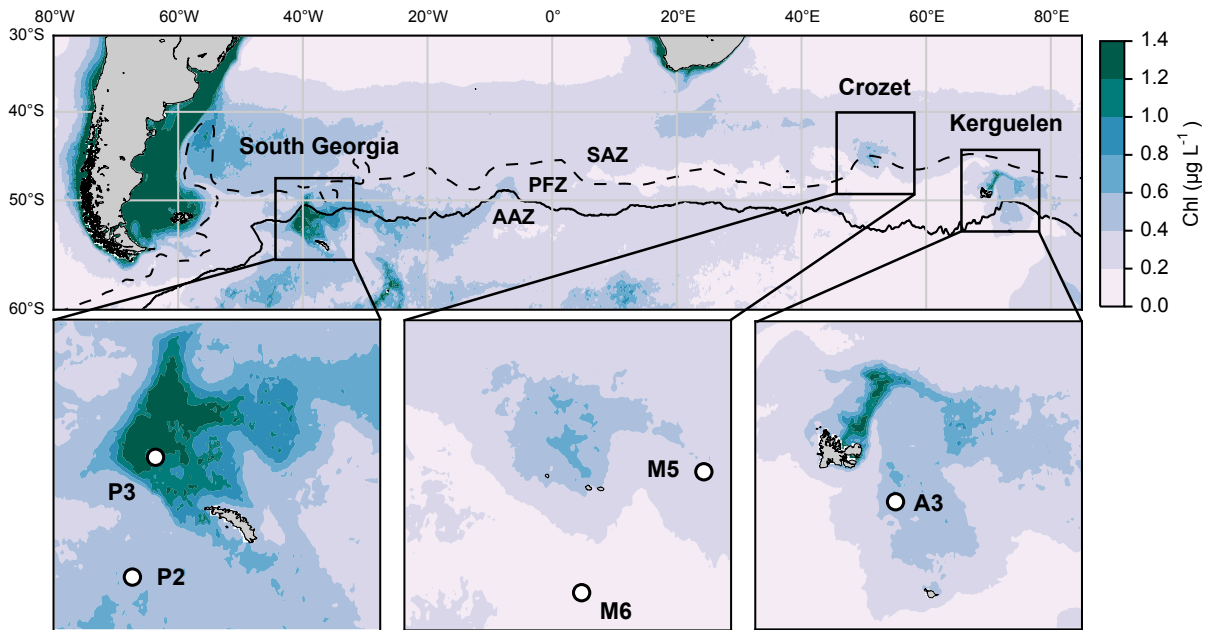
Figure 3.1: Location of the five annual sediment trap deployments in the Southern Ocean. Color refers to surface satellite-derived chlorophyll a climatology (MODIS 2002-2016 full mission product accessed at `http://oceancolor.gsfc.nasa.gov/cms/`). Dashed and continuous lines represent respectively the Subantarctic Front (SAF) and Polar Front (PF) from Sallée et al. (2008) . SAZ: Subantarctic Zone, PFZ: Polar Frontal Zone, AAZ: Antarctic Zone.

the basis of a food web generally considered as short where iconic species such as euphausiids efficiently transfer matter and energy to top predators (seabirds and mammals) (Murphy et al., 2012). Similarly strong patterns in the species composition and life-cycle stages of diatoms are evident across these iron-fertilized productivity gradients. For example, previous studies of Southern Ocean island plateaus have identified the significance of resting spore formation by neritic diatom species (*Eucampia antacrica* var. *antarctica*, *Chaetoceros Hyalochaete* and *Thalassiosira antarctica*) probably in response to nutrient limitation in mid-summer (Salter et al., 2012; Rembauville et al., 2015b, 2016a). The export of resting spores generally occurs during short and intense events but they can account for a significant fraction (40-60 %) of annual carbon flux out of the mixed layer at these naturally fertilized sites. This process contributes to the ∼2 fold increase in annual carbon export when compared to the HNLC sites (Salter et al., 2012; Rembauville et al., 2015b, 2016a).

Despite the general importance of resting spore ecology for POC export from naturally iron-fertilized systems in the Southern Ocean, there are some notable differences in the nature of export fluxes from Crozet, Kerguelen and South Georgia. At Crozet, in the Polar Front Zone (PFZ), the abundance of foraminifers and pteropods leads to a high inorganic to organic carbon export ratio (1 mol:mol, Salter et al., 2014). At Kerguelen, south of the

Polar Front in the Antarctic Zone (AAZ) the inorganic to organic ratio is lower (0.07) and mainly attributed to coccoliths (Rembauville et al., 2016b). At South Georgia (AAZ), the faecal pellet contribution to carbon export is higher (∼60 % in summer-autumn, Manno et al., 2015) when compared to Kerguelen (34 % at annual scale, Rembauville et al., 2015b). The impact of different carbon export vectors on the lability of the exported OM needs to be investigated to understand their importance for the pelagic-benthic coupling (Ruhl and Smith, 2004; Ruhl et al., 2008). High biomass of meio-, micro- and macrofauna in abyssal sediments of the Southern Ocean suggests a transfer of OM originating from photosynthetic autotrophs down to the seafloor (Brandt et al., 2007). This diversity and biomass is not geographically homogeneous, but rather constrained by the upper ocean productivity levels (Wolff et al., 2011; Lins et al., 2015). In this context, the comparison of lipid biomarkers in export fluxes originating from different sites in the Southern Ocean may help to understand how ecological processes at the origin of export flux also shape the magnitude and lability of OM supply to the deep benthic communities.

This study compiles lipid biomarkers from five annual sediment trap deployments in the vicinity of Southern Ocean Island plateaus in order to (i) compare the composition of lipid biomarkers in export fluxes collected in sites of various productivity levels and across different depths, (ii) identify how ecological export vectors shape the magnitude and lability of OC fluxes over a complete annual cycle over the central Kerguelen plateau and (iii) derive the potential implications of this link for the pelagic-benthic coupling.

Material and methods

Trap deployments and sample processing

We compile 5 long-term sediment trap deployments located in the vicinity of island plateaus in the Southern Ocean (Fig. 3.1, Table 3.1). Two sediment traps were located upstream of the islands in HNLC waters (M6 and P2 at Crozet and South Georgia, respectively) and three were located in naturally iron-fertilized and productive waters characterized by enhanced phytoplankton biomass (A3, M5 and P3 at Kerguelen, Crozet and South Georgia, respectively). The detailed hydrological settings of deployments and bulk chemical analyses of biogeochemical fluxes have been published previously (Table 3.1). After the retrieval of each sediment trap, swimmers (organisms actively entering the trap funnel) were manually removed from the samples and therefore do not contribute to the lipid fluxes we report.

Lipid analysis

Lipid analyses were performed on 1/8 wet aliquots resulting from the splitting of original samples. Because of the low amount of material collected in some cups, 1/8 wet aliquots were grouped prior to the lipid analyses (Appendix 1). Lipid analyses of Crozet sediment trap samples were performed as described in Kiriakoulakis et al. (2001) and Wolff

Location and reference	Trap model	Collection period	Total fluxes (mmol m^{-2})	
			POC	BSi
Kerguelen				
(Rembauville et al., 2015a)				
A3	Technicap	21/10/2011-07/09/2012		
50°38.30'S–72°02.60'E	PPS3/3	No sample lost	98	114
289 m	0.125 m^2	total 322 days		
Crozet				
(Salter et al., 2012)				
M5	McLane	28/12/2005-29/12/2005		
46°00.00'S–56°05.00'E	PARFLUX	No sample lost	40	165
3195 m	0.5 m^2	total 360 days		
M6		05/01/2005-03/01/2006		
49°00.03'S–51°30.59'E	idem	No sample lost	14	97
3160 m		total 359 days		
South Georgia				
(Rembauville et al., 2016a)				
P3		15/01/2012-01/12/2012		
52°43.40'S–40°05.83'E	idem	1 sample lost	41	46
2000 m		total 291 days		
P2		15/01/2012-01/12/2012		
55°11.99'S–41°07.42'E	idem	3 samples lost	26	39
3160 m		total 231 days		

Table 3.1: Information on sediment trap deployments and total fluxes of particulate organic carbon (POC) and biogenic silica (BSi) collected.

et al. (2011). For the Kerguelan and South Georgia samples a similar protocol was used. Briefly, separate 1/8 aliquots were spiked with an internal standard (5α(H)-cholestane), sonicated (filters, 45 min, dichloromethane:methanol 9:1), transmethylated (methanolic acetyl chloride) and silylated (bistrimethylsilyltrifluoroacetamide, 1 % trimethylsilane chloride, 30–50 µL, 40 °C, 0.5–1 h). GC-MS analyses were carried out using a GC Trace 1300 fitted with a split-splitless injector, using helium as a carrier gas (2 mL min^{-1}) and column DB-5MS (60 m x 0.25 mm i.d., film thickness 0.1 µm, non-polar solution of 5 % phenyl and 95 % methyl silicone). The GC oven was programmed after 1 min from 60 °C to 170 °C at 6 °C min^{-1}, then from 170 °C to 315 °C at 2.5 °C min^{-1} and held at 315 °C for 15 min. The eluent from the GC was transferred directly to the electron impact source of a Thermoquest ISQMS single quadrupole mass spectrometer. Typical operating conditions were: ionisation potential 70 eV, source temperature 215 °C, trap current 300 µA. Mass data were collected at a resolution of 600, cycling every second from 50–600 Thompsons and were processed using Xcalibur software. Compounds were identified either by comparison of their mass spectra and relative retention indices with those available in the literature and/or by comparison with authentic standards. Quantitative data were calculated by comparison of peak areas of the internal standard with those of the compounds of interest, using the total ion current (TIC) chromatogram. The relative response factors of the analytes were determined individually for 36 representative fatty acids, sterols and alkenones using authentic standards. Response factors for analytes where standards were unavailable were assumed to be identical to those of available compounds of the same class.

Statistical analyses

The lipid composition of sediment trap samples from the five sites was investigated with a principal component analysis (PCA) and the similarity of samples was studied using a clustering (Ward aggregation criteria) based on lipid classes. This methodology has been used previously to study the organic geochemistry of sinking particles in the ocean (Xue et al., 2011). Prior to both PCA and clustering, raw lipid fluxes were transformed by calculating the square root of their relative abundance within each sample. This transformation followed by the calculation of the Euclidian distance is also known as the Hellinger distance, which provides a good compromise between linearity and resolution in ordination analyses (Legendre and Legendre, 1998; Legendre and Gallagher, 2001).

Results

Lipid classes distribution and seasonality

The total lipid flux collected by sediment traps was five orders of magnitude higher in the shallow deployment at A3 (230 mg m^{-2} at 289 m), when compared to the deep sediment trap at M6 (44 µg m^{-2} at 3160 m, Fig. 3.2, Table 3.2). The contribution by labile lipids
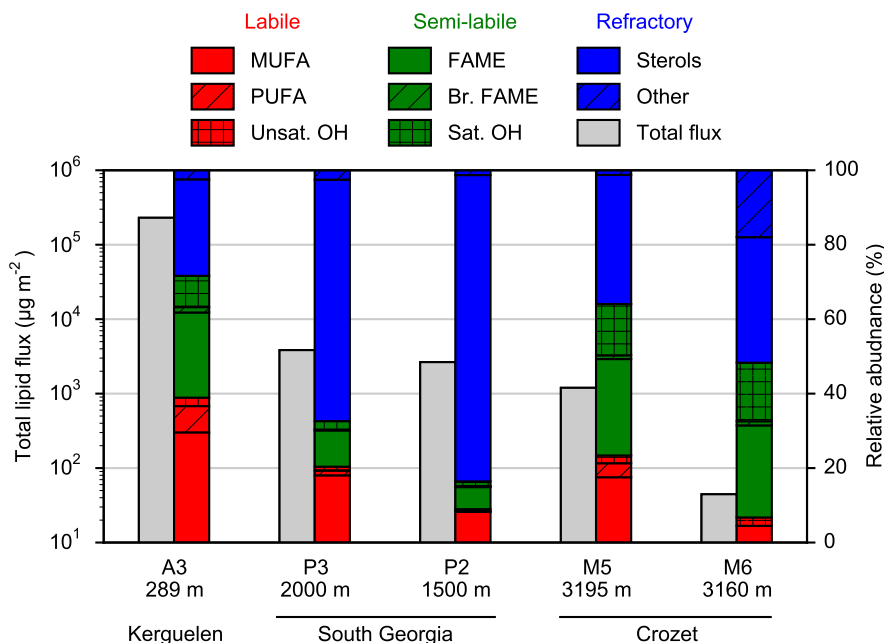
Figure 3.2: Annual total lipid fluxes (grey bars, left axis) and relative contribution of lipid classes (coloured bars, right axis) to the total flux from five moored sediment trap deployments in the Southern Ocean. Lability is defined according to Wolff et al. (2011).

(unsaturated fatty acids and alcohols, Wolff et al., 2011, , Table 3.2) to total lipids flux was 2-4 times higher in the naturally fertilized sites (20-40 % at A3, P3 and M5) when compared to the HNLC deployments (<10 % at P2 and M6). Unsaturated fatty acids were dominated (>75 %) by monounsaturated fatty acids (MUFA) at all sites. Semi-labile lipids (fatty acid methyl ester – FAMEs, and saturated fatty alkanols, Table 3.2) accounted for a small fraction (10-15 %) of total lipids at South Georgia, and a higher fraction (30-40 %) at Crozet. Semi-labile lipids where dominated by the FAME contribution ($\sim$70 %) at all sites. Sterols were the dominant lipids at South Georgia (65-85 %) and were less abundant (30-35 %) at the other sites.

The total lipid flux normalized by the OC flux decreased by four orders of magnitude between the shallowest (A3, 195.2 mg lipid g OC^{-1}) and the deepest (M6, 0.3 mg lipid g O^{-1}) deployment (Table 3.2). OC-normalized lipid flux in the shallow deployment at Kerguelen (A3) displayed high contribution from MUFAs (57.7 mg lipid g OC^{-1}), PUFAs (13.8 mg lipid g OC^{-1}) and FAMEs (44.6 mg lipid g OC^{-1}). All the other deployments (P3, P2, M5 and M6) had a much lower contribution from these labile and semi-labile compounds where sterols dominated (89.5 – 5 111.5 g lipid g OC^{-1}).

Samples from Crozet (M5 and M6) were positively projected on the first axis of the PCA together with FAME, C_{28} and C_{29} sterols and long chain unsaturated fatty acids (C_{22}, C_{24}) (Fig. 3.3a). Samples from South Georgia (P3 and P2) were negatively projected on the first axis, close to C_{27} sterols. Samples from Kerguelen (A3) were positively projected on the second axis and mainly associated with C_{16}-C_{20} unsaturated fatty acids.

Site	A3	P3	P2	M5	M6
Total lipid flux	230.01	3.84	2.65	1.2	0.04
$(\mathrm{mg\,m^{-2}})$					
Relative contribution (%)					
MUFA	29.6	18.1	8.2	17.5	4.5
PUFA	7.1	1.3	0.2	3.8	0
Unsat. OH	2.3	1.1	0.6	2.1	2.2
FAME	22.9	9.7	5.9	25.9	24.7
Br. FAME	1.4	0.2	0.3	1	1.1
OH	8.4	2.3	1.3	13.8	15.7
Sterols	25.9	64.9	82.3	34.7	33.7
Other	2.4	2.5	1.3	1.3	18
Normalized total lipid flux	195.2	7.9	8.4	2.5	0.3
(mg lipid g $\mathrm{OC^{-1}}$)					
Normalized lipid flux					
(μg lipid g $\mathrm{OC^{-1}}$)					
MUFA	57 758.2	1 422.8	689.6	437.5	11.9
PUFA	13 783.6	99.7	13	93.8	0
Unsat. OH	4 431.7	83.8	47.5	52.1	6
FAME	44 640.5	766.6	495	645.8	65.5
Br. FAME	2 807.7	18.9	23.1	25	3
OH	16 416.9	178.9	104.8	343.8	41.7
Sterols	50 580.6	5 111.5	6 878.4	864.6	89.3
Other	4 769.6	199.2	107.8	31.3	47.6

Table 3.2: Total annual lipid flux, relative composition of lipid classes and lipid flux normalized to POC flux for the five sediment trap deployments.

Four main clusters of sediment trap samples could be identified based on the largest distance break after the first node of the dendrogram (Fig. 3.3b). Cluster A contained most of the spring and summer samples from the naturally-fertilized sites of Kerguelen and Crozet (A3 and M5) characterized by the highest relative abundance of labile lipids (PUFAs and MUFAs). Cluster B was composed of summer and winter samples from A3 displaying a high abundance of unsaturated alkenols. Cluster C contained spring and summer samples from the naturally-fertilized site of South Georgia (P3) and few samples from Kerguelen and Crozet. They were characterized by a mixture of labile, semi-labile and refractory lipids (MUFAs, FAMEs and sterols). Finally, cluster D was mostly composed of samples from the HNLC site of South Georgia (P2) displaying a strict dominance of sterols.

Detailed lipid seasonality at A3

In spring, vegetative diatoms were the main contributors to the low POC flux, followed by cylindrical faecal pellets (Fig. 3.4a). Lipid fluxes were dominated by palmitoleic acid ($C_{16:1}$ (cis-9)), hexadecanoic acid (C_{16} FAME), eicosapentaenoic acid (EPA, $C_{20:5}$ (cis-5, 8, 11, 14, 17)), oleic acid ($C_{18:1}$ (cis-9)), and chlolesterol ($C_{27}\Delta^5$) that altogether contributed to >75 % of the total lipids (Fig. 3.4b). In summer, diatom resting spores dominated the POC flux, followed by cylindrical and ovoid faecal pellets (Fig. 3.4c). $C_{16:1}$ (cis-9) strongly dominated the lipid export (47 %), followed by $C_{18:1}$ (cis-9), $C_{27}\Delta^5$, C_{29} sterols and EPA (Fig. 3.4d). In autumn, when tabular faecal pellets dominated the export flux (Fig. 3.4e), $C_{27}\Delta^5$ was the major lipid exported followed by C_{16} FAME, $C_{18:1}$ (cis-9), eicosatrienoic acid ($C_{20:3}$ (cis-11)) and *n*-hexadecanol (C_{16} OH, Fig. 3.4f). In winter, large faecal pellets (tabular and ellipsoid shapes) dominated the carbon flux (Fig. 3.4g). Dominant lipids where eicosanol ($C_{20:1}$ OH) and octadecanol ($C_{18:1}$ OH) acids, followed by C_{16} FAME, $C_{27}\Delta^5$ and $C_{18:1}$ (cis-9) (Fig. 3.4h).

Discussion

Diversity of lipid export across the Southern Ocean island system

The annual lipid export in the naturally-fertilized sites of Kerguelen and South Georgia was characterized by relatively high fluxes of labile and semi-labile compounds when compared to the HNLC sites, in agreement with previous observations made at Crozet (Wolff et al., 2011). Labile lipids were dominated by MUFAs, and to a lesser extent PUFAs, two lipid classes (e. g. $C_{16:1}$ (cis-9) and EPA) long associated with diatoms (Kates and Volcani, 1966; Lee et al., 1971). These observations confirm that the large diatom-dominated phytoplankton blooms observed downstream of island plateaus (Armand et al., 2008a; Korb et al., 2008; Quéguiner, 2013) and supported by iron delivery (Blain et al., 2008a; Nielsdóttir et al., 2012; Bowie et al., 2015) leads to the export of labile lipids.

The PCA and clustering analyses reveal reveal that the dataset is strongly structured and highlight the specific association of lipids with a given island system. The first axis of
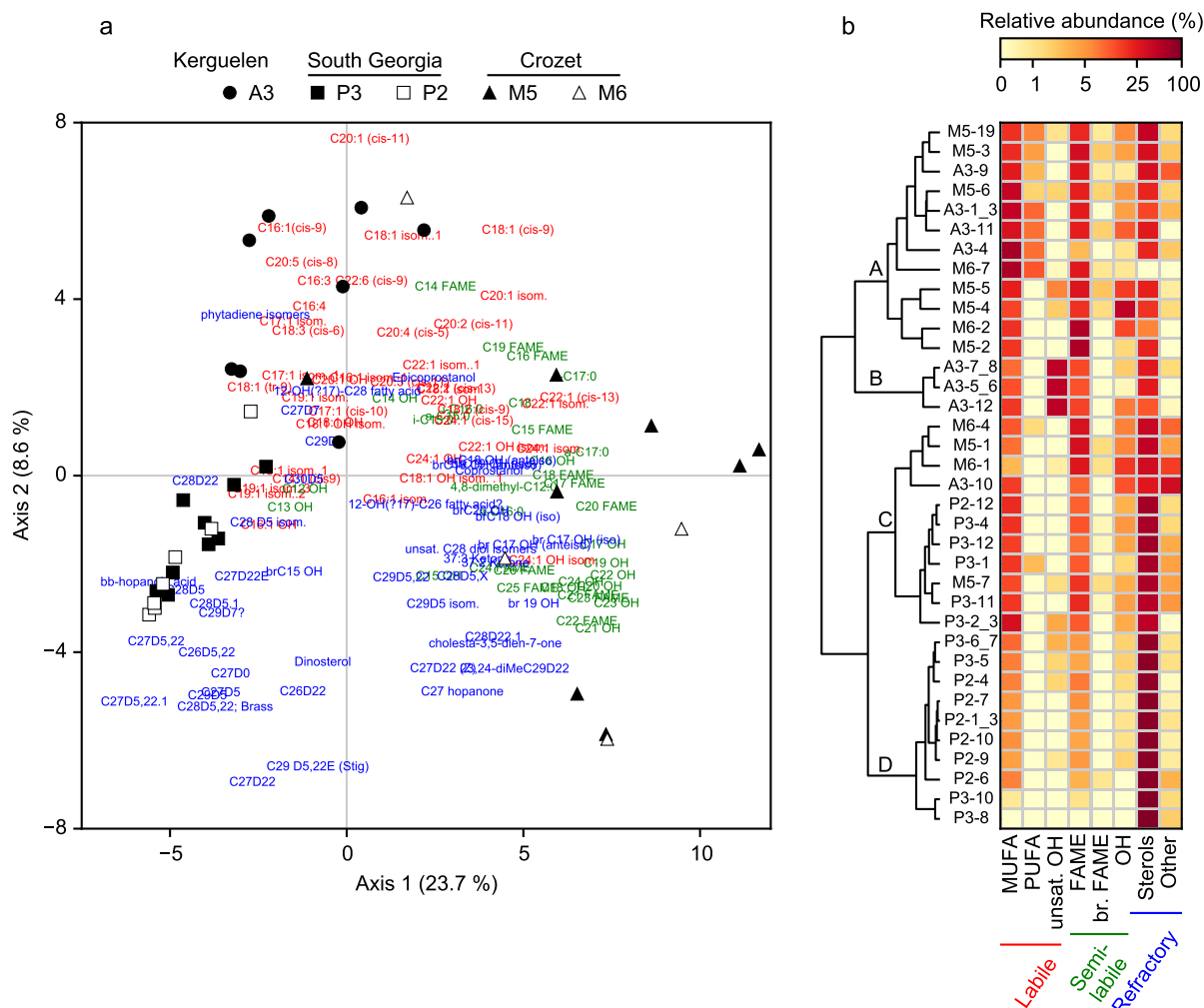
Figure 3.3: Association of lipid compounds with sediment trap samples. **a.** Principal component analysis of the relative abundance of lipids (n = 121). Black and white symbols represent respectively the naturally-fertilized and the low productivity sites. **b.** Clustering of the sediment trap samples based on the relative abundance of lipid classes (Euclidian distance, Ward aggregation criteria). Clusters A, B, C and D were defined based on the highest distance break after the first node. In **a.** and **b.**, color refers to the lability of lipids according to Wolff et al. (2011).

Figure 3.4: Seasonal evolution of carbon export vectors and associated lipid composition over the central Kerguelen Plateau (A3, 289 m). Left panels: carbon export vectors from (Rembauville et al., 2015b). Right panels: sorted relative abundance (coloured bars) and cumulative relative abundance (dots) of major lipids. **a.** and **b.** cups 1-3, **c.** and **d.** cup 9, **e.** and **f.** cup 11, **g.** and **h.** cup 12.

the PCA (23.7 % of variance) summarized the location of the trap deployments whereas the second axis represented somehow the depth of the trap. The P3 and P2 sites at South Georgia both display $\sim$2 times higher relative abundance of sterols compared to the Kerguelen (A3) and Crozet (M5 and M6) sites. Sterols are important components of the plasma membrane found in almost all eukaryotic organisms (Dufourc, 2008). Zooplankton uses dietary sterols of phytoplankton origin preferentially assimilating $C_{27}\Delta^5$, or converting phytosterols to $C_{27}\Delta^5$ (Volkman, 1986, 2003) that are ultimately egested in faecal pellets (Bradshaw and Eglinton, 1993; Prahl et al., 1984). An enrichment in $C_{27}\Delta^5$ (and other C_{27} sterols such as $C_{27}\Delta^{22}$ and $C_{27}\Delta^{5,22}$) in sinking OM may thus be interpreted as indicating a high contribution of faecal material (Ternois et al., 1998). The South Georgia Plateau is located in the Atlantic sector of the Southern Ocean that hosts the largest biomass of Antarctic krill (Atkinson et al., 2008, 2009). This could explain the higher contribution of faecal pellets to carbon export at South Georgia (Manno et al., 2015) compar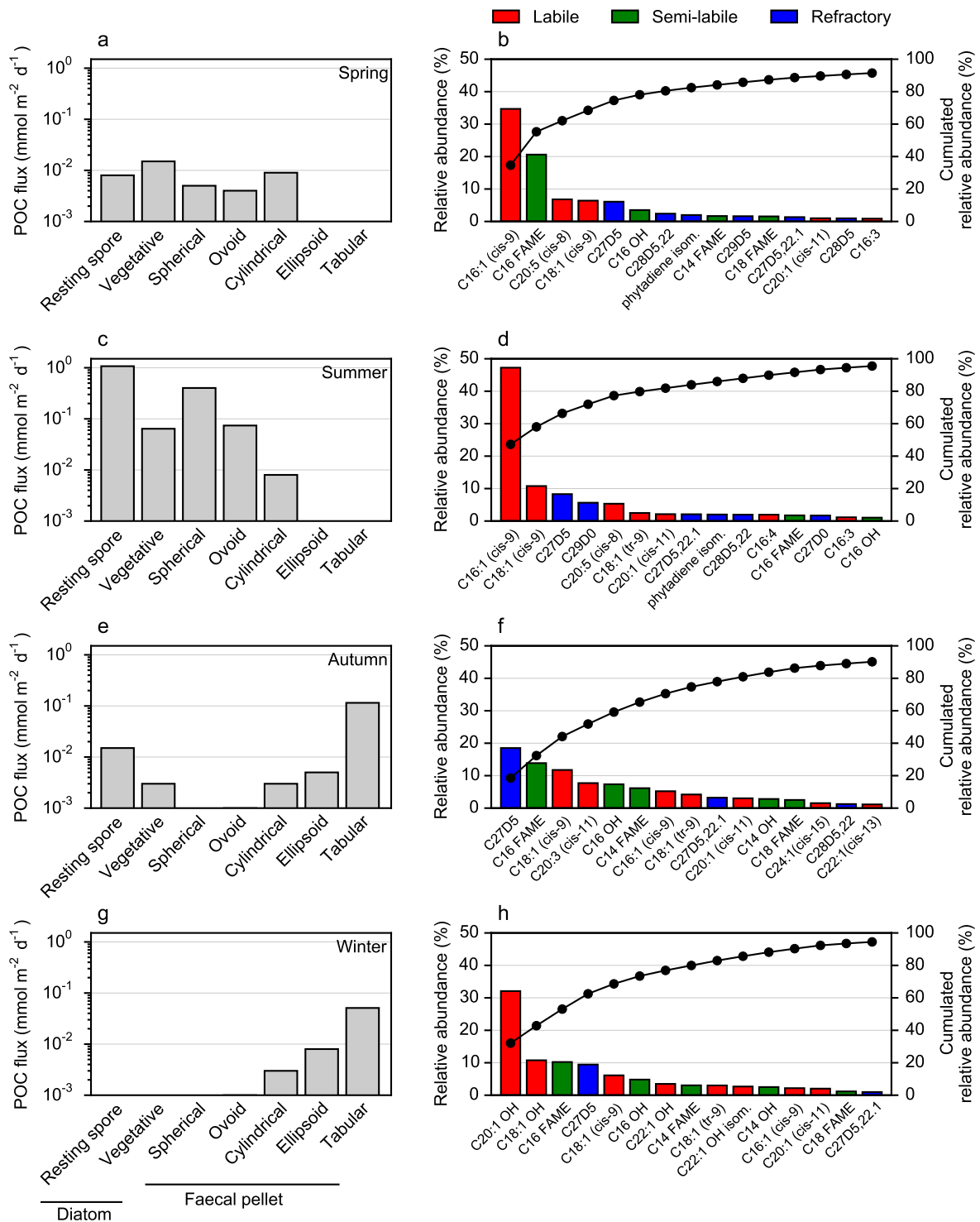ed to Kerguelen (Rembauville et al., 2015b), and explains the higher relative abundance of $C_{27}\Delta^5$, $C_{27}\Delta^{22}$ and $C_{27}\Delta^{5,22}$ in the exported lipids. The slightly higher OC-normalized sterol flux at P2 compared to P3 (6.9 vs.5.1 mg lipid g OC^{-1}) suggests that the influence of zooplankton faecal pellets is higher in the HNLC site. The high contribution of $C_{27}\Delta^5$ and $C_{28}\Delta^{5,22}$ at South Georgia reflects the dominance of diatoms at the base of the food web (Korb et al., 2010), whereas the higher contribution of $C_{29}\Delta^0$ and $C_{29}\Delta^{5,22}$ at Crozet suggests a more diversified phytoplankton community with possible contributions from chlorophyceae, haptophyceae and cyanobacteria (Volkman, 2003; Hernandez-Sanchez et al., 2011, 2012). Warmer waters of the Polar Frontal Zone (PFZ) at Crozet are known to host a more diversified phytoplankton community compared to the diatom-dominated waters of the Antarctic one (AAZ) at Kerguelen and South Georgia (Wright et al., 1996; Fiala et al., 2004; Poulton et al., 2007; Korb et al., 2012; Armand et al., 2008a).

The location of the sediment trap is not the only factor influencing the magnitude and composition of lipid fluxes. The decrease in the total lipid flux of five orders of magnitude between the shallowest (289 m) and the deepest (>3000 m) deployment is consistent with the trend generally observed in the global ocean (Wakeham and Lee, 1993; Wakeham et al., 1997, 2009). Moreover, the strong decrease in OC-normalized lipid flux suggests that lipids are selectively degraded/remineralized during the sinking of the OM. In the shallowest deployment (A3, 289 m), the high OC-normalized MUFAs flux and the abundance of diatom-derived essential PUFAs ($C_{16:3}$, $C_{18:6}$, $C_{20:4}$, $C_{20:5}$ and $C_{22:6}$) reflects the recent export of fresh and highly labile diatom-derived OM (Dunstan et al., 1993). By contrast, the presence of branched *iso-* and *anteiso-* C_{15} and C_{17} compounds in the deepest samples from Crozet (M5 and M6, >3000 m) can be attributed to the activity of bacteria reworking the particulate OM in the deep ocean (Kaneda, 1991; Wakeham et al., 1997).

Association of lipid with ecological export vectors

Seasonal changes in the exported lipids at the Kerguelen islands (station A3) can be compared in detail with the biological components of POC export reported previously by (Rembauville et al., 2015b).

In spring, the lipid flux is low ($0.3\,\mathrm{mg\,m^{-2}\,d^{-1}}$), as is the POC flux ($\sim 0.15\,\mathrm{mmol\,m^{-2}\,d^{-1}}$), which is mainly driven by vegetative diatoms belonging to the genera *Fragilariopsis*, *Pseudo-nitzschia* and *Thalassionema*, as well as small faecal pellets (Rembauville et al., 2015b).Diatoms are known to predominantly accumulate unsaturated fatty acids such as $C_{16:1}$ (cis-9), EPA and to a lesser extent $C_{18:1}$ (cis-9) (Kates and Volcani, 1966; Opute, 1974; Chen, 2012; Levitan et al., 2014). Diatoms also produce FAMEs, mainly the C_{16} homologue (Lee et al., 1971; Matsumoto et al., 2009; Liang et al., 2014). Although the lipid flux is very low, the lipid assemblage we report in spring ($C_{16:1}$ (cis-9), $C_{16:1}$ FAME, EPA and $C_{18:1}$ (cis-9)) is consistent with a diatom-dominated export.

In summer the intense export of diatom resting spores (*Chaetoceros Hyalochaete* spp. and to a lesser extent *Thalassiosira antarctica*) is associated with the highest export of total lipids ($2.5\,\mathrm{mg\,m^{-2}\,d^{-1}}$, Appendix 1) which are dominated by $C_{16:1}$ (cis-9) and $C_{18:1}$ (cis-9), and a marked contribution of EPA. Higher total lipid content were found in resting spores of *Chaetoceros Hyalochaete* and *Thalassiosira antarctica* when compared to vegetative cells (Doucette and Fryxell, 1983; Kuwata et al., 1993). Moreover, our results are consistent with the 8-12 fold increase in the content of $C_{16:1}$ (cis-9) and $C_{18:1}$ (cis-9) in *Chaetoceros pseudocurvisetus* resting spores when compared to the vegetative stages (Kuwata et al., 1993). An increase in the cell content of EPA acid during the formation of resting spore was also reported for *Chaetoceros salsugineus* (Zhukova and Aizdaicher, 2001). A resting spore stage is likely to be used by diatoms as a way to persist in environments where unfavorable conditions (e.g. light or nutrient limitation) occur during low productivity periods (Smetacek, 1985; French and Hargraves, 1985; McQuoid and Hobson, 1996). Lipids produce more energy per mass unit than polysaccharides and can be stored in concentrated forms by diatoms (Obata et al., 2013). The accumulation of energy-rich unsaturated fatty acid in the resting spore, associated with a reduced metabolism (Oku and Kamatani, 1999), probably increases the survival rate of the cell during adverse conditions.

Cholestrol ($C_{27}\Delta^5$) was present ($>10\,\%$ of total lipids) throughout the year and showed the highest contribution ($18\,\%$) in autumn when the contribution of faecal pellet to POC flux increased. Contrary to many eukaryotes, crustacean are incapable of *de novo* synthesis of sterols and show a simple sterol composition dominated by $C_{27}\Delta^5$ (Goad, 1981; Baker and Kerr, 1993; Kanazawa, 2001). Its presence throughout the year can be explained by the continuous export of spherical, ovoid and cylindrical faecal pellet, attributed to copepods, amphipods and euphausiids (Wilson et al., 2008, 2013). The summer sample differs from the others by the presence of a $C_{29}\Delta^0$ sterol. C_{29} sterols

are abundant in diatoms (Volkman, 2003), and can account for 60 % and 80 % of total lipids of *Navicula* sp., and *Eucampia antarctica* var. *antarctica*, respectively (Rampen et al., 2010), both of which showed a clear seasonality with a marked summer maximum (Rembauville et al., 2015b).

In winter, the lowest lipid flux contrasted with the other samples by the dominance of mono-unsaturated fatty alkenols ($C_{18:1}$ OH and $C_{20:1}$ OH). These compounds are generally absent in phytoplankton lipids but abundant in zooplankton wax ester (Lee et al., 1971), and are often utilized as a marker for zooplanktonic OM (Wakeham et al., 1997). More specifically, salp faecal pellets (tabular shape) have been shown to contain important amounts of $C_{18:1}$ OH and $C_{20:1}$ OH (Matsueda et al., 1986). This is in good agreement with the dominance of tabular faecal pellets to POC flux we report in winter. In summer and autumn, faecal material is present in export flux but fatty alkenols are minor constituents of lipid flux. To first order, this could be explained by the contribution of diatoms to export flux (as both single cells or present in faecal pellets), but also by changes in zooplankton lipid composition across the season (Lee et al., 2006). Indeed, wax esters are used as energy reserve (Lee et al., 1970) but also contribute to adjust buoyancy in cold and deep waters in winter (Pond and Tarling, 2011). The abundance of wax ester-derived compounds we report in winter is also consistent with observations from neritic areas of the Kerguelen Islands (Mayzaud et al., 2011). Another indicator of a seasonal shift from diatom (spring) to faecal pellet-dominated export system (autumn and winter) is the absence of long chain PUFAs in autumn and winter. It has been previously reported that this energy-rich compound is preferentially assimilated by zooplankton and absent in faecal pellets (Stübing et al., 2003).

Implications for pelagic-benthic coupling

The large export of resting spores in the three naturally fertilized sites (Salter et al., 2012; Rembauville et al., 2015b, 2016a) is associated with a high abundance of $C_{16:1}$ (cis-9). Given their resistance to grazing pressure (Kuwata and Tsuda, 2005) and important sinking speed (up to 30 times higher than for the vegetative stage, McQuoid and Hobson, 1996), it is likely that diatom resting spores are efficiently transferred to the seafloor (Crosta et al., 1997; Tsukazaki et al., 2013; Rembauville et al., 2016a). The oxidation of a MUFA such as $C_{16:1}$ (cis-9) produces more energy than for saturated fatty acids (Levitan et al., 2014). This energy-rich food supply to the seafloor is likely to have an important impact on benthic community structure and biomass. At Crozet, the biomass and abundance of abyssal megafaunal invertebrates increased respectively by a factor 3 and 6 between the M6 (HNLC) and the M5 (naturally-fertilized) site (Wolff et al., 2011). At South Georgia, Lins et al. (2015) have reported a 10 times higher nematode biomass in deep sediments (>3700 m) located in the naturally fertilized area (close to P3) compared to the HNLC area. Moreover, nematode fatty acids were significantly

enriched in palmitoleic and eicosapentaenoic fatty acids, two majors lipids we observe during diatom resting-spore dominated export events.

Deep sea ecosystems are strongly dependent on OM food supply originating from photosynthesis in the surface ocean (Billett et al., 1983, 2001; Ruhl and Smith, 2004; Ruhl et al., 2008). In the Southern Ocean, it has been demonstrated that upper ocean plankton community composition and associated ecological strategies influence the intensity and C:Si stoichiometry of the biological pump (Smetacek et al., 2004; Salter et al., 2012; Assmy et al., 2013; Rembauville et al., 2015b). The present study highlights that the composition of ecological export vectors (e. g. diatom resting spore versus faecal pellets), mediated by iron availability, also shapes the geochemical composition of export with potentially important implications for the energy supply to the benthic communities of the deep ocean.

4 | Carbonate export fluxes over the Kerguelen plateau
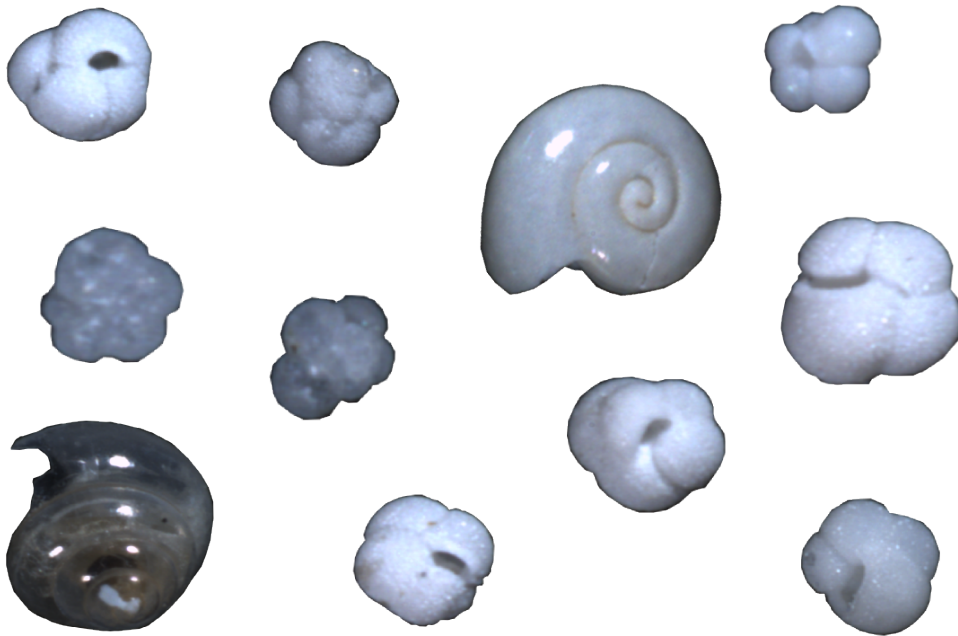
Contents

4.1 Planktic foraminifer and coccolith contribution to carbonate export fluxes over the central Kerguelen Plateau (article 7).

The impact of oceanic biological processes on the air-sea CO_2 exchange results from the net balance between the biological pump (CO_2 sink) and the carbonate counter pump (CO_2 source, Frankignoulle et al., 1994; Archer et al., 2000b; Zeebe, 2012). **Articles 1-4** aimed at identifying ecological vectors (e.g. diatoms, faecal pellets) of the biological pump. In contrast, very few studies have quantified the role of different calcifying organisms on the export of inorganic carbon. Salter et al. (2014) reported a dominance of foraminifer (30-50 %) to carbonate export fluxes in the Polar Frontal Zone close to the Crozet Islands. It is known that the Polar Front is a major hydrological discontinuity through which the abundance of calcifying organisms decreases (Winter et al., 1999; Hunt et al., 2008). The sediment trap deployment at station A3 (Antarctic Zone) was the opportunity to document the contribution of calcifying plankton to particulate inorganic carbon (PIC) export flux in a naturally fertilized area South of the Polar Front.

At Kerguelen, the annual PIC export is low ($6.6 \, \mathrm{mmol \, m^{-2} \, yr^{-1}}$) and leads to a low PIC:POC export ratio (0.07) compared to the one observed at Crozet ($\sim$1, Salter et al., 2014). Particle size measurement and size-fractionated Ca analysis suggest a dominance (85 %) of coccoliths contribution to PIC export and a much lower contribution of foraminifer. Microscopic qualitative observations reveal that *Emiliania huxleyi* coccoliths are the major components of the PIC flux, mainly exported in later summer (January-March) concomitant with the highest satellite-derived PIC concentration in surface water. Analysis of the foraminifer community structure shows a dominance of the polar species *Turborotalita quinqueloba* and *Neogloboquadrina pachyderma*. The compilation of test size-normalized weight (SNW) data from exported foraminifer communities at Crozet and Kerguelen reveals that SNW is species-specific. This demonstrates that the lower carbonate counter pump at Kerguelen ($\sim$ 5%) compared to Crozet (6-32%) results from both a change in the dominance of the calcifier type (coccolithophore versus foraminifer) and an export of polar foraminifer species with a lower SNW south of the Polar Front.

Foraminifer imaging, weighing and identification, fine fraction sieving and oxidation performed by the author. Bulk PIC analyses performed by N. Leblond, fine fractions PIC analyses performed by P. Ziveri.

Contents lists available at ScienceDirect

Deep-Sea Research I

Planktic foraminifer and coccolith contribution to carbonate export fluxes over the central Kerguelen Plateau

M. Rembauville [a,*], J. Meilland [b], P. Ziveri [c,d], R. Schiebel [b,e], S. Blain [a], I. Salter [a,f]

[a] Sorbonne Universités, UPMC Univ Paris 06, CNRS, Laboratoire d'Océanographie Microbienne (LOMIC), Observatoire Océanologique, F-66650 Banyuls/mer, France
[b] Université d'Angers, UMR CNRS 6112, LPG-BIAF-Bio-Indicateurs Actuels et Fossiles, 2 Boulevard Lavoisier, Angers 49045, France
[c] Universitat Autònoma de Barcelona, ICREA-ICTA, Edifici Z, Carrer de les columnes s/n, E-08193 Bellaterra, Barcelona, Spain
[d] Catalan Institution for Research and Advanced Studies, ICREA, Catalonia, Barcelona 08010, Spain
[e] Max-Planck-Institute for Chemistry, Hahn-Meitner-Weg 1, 55128 Mainz, Germany
[f] Alfred Wegener Institute, Helmholtz Centre for Polar and Marine Research, Am Handelshafen 12, 27570 Bremerhaven, Germany

ARTICLE INFO

ABSTRACT

We report the contribution of planktic foraminifers and coccoliths to the particulate inorganic carbon (PIC) export fluxes collected over an annual cycle (October 2011/September 2012) on the central Kerguelen Plateau in the Antarctic Zone (AAZ) south of the Polar Front (PF). The seasonality of PIC flux was decoupled from surface chlorophyll *a* concentration and particulate organic carbon (POC) fluxes and was characterized by a late summer (February) maximum. This peak was concomitant with the highest satellite-derived sea surface PIC and corresponded to a *Emiliania huxleyi* coccoliths export event that accounted for 85% of the annual PIC export. The foraminifer contribution to the annual PIC flux was much lower (15%) and dominated by *Turborotalita quinqueloba* and *Neogloboquadrina pachyderma*. Foraminifer export fluxes were closely related to the surface chlorophyll *a* concentration, suggesting food availability as an important factor regulating the foraminifer's biomass. We compared size-normalized test weight (SNW) of the foraminifers with previously published SNW from the Crozet Islands using the same methodology and found no significant difference in SNW between sites for a given species. However, the SNW was significantly species-specific with a threefold increase from *T. quinqueloba* to *Globigerina bulloides*. The annual PIC:POC molar ratio of 0.07 was close to the mean ratio for the global ocean and lead to a low carbonate counter pump effect ($\sim$5%) compared to a previous study north of the PF (6–32%). We suggest that lowers counter pump effect south of the PF despite similar productivity levels is due to a dominance of coccoliths in the PIC fluxes and a difference in the foraminifers species assemblage with a predominance of polar species with lower SNW.

© 2016 Elsevier Ltd. All rights reserved.

1. Introduction

The Southern Ocean is the largest high nutrient, low chlorophyll (HNLC, Minas et al., 1986) area of the global ocean (Martin et al., 1990; Minas and Minas, 1992). Downstream of Subantarctic island plateaus, iron input from shelf sediments and glacial melt water can alleviate iron limitation and support large scale and long-lasting phytoplankton blooms (Blain et al., 2001, 2007; Pollard et al., 2007; Tarling et al., 2012). These blooms are dominated by diatoms (Armand et al., 2008; Korb et al., 2008; Quéguiner, 2013) that respond to high macronutrient concentrations, marked turbulence, deep mixed layer depths and usually moderate light

levels (Smetacek, 1985; Boyd, 2002; Strzepek et al., 2012). Diatom blooms result in a major contribution of biogenic silica to biomineral production of Southern Ocean waters, although biogenic production of calcium carbonate by calcifying planktonic organisms such as coccolithophores, foraminifers and pteropods can also occur.

Although neglected for a long time, the presence of coccolithophores in the Southern Ocean has been diagnosed based on an increasing number of direct observations (Winter et al., 2014) and the development of remote sensing methods (Balch et al., 2005, 2011, 2014). Southern Ocean coccolithophore populations are dominated by the cosmopolitan species *Emiliania huxleyi* (Saavedra-Pellitero et al., 2014; Winter et al., 2014) that is thought to be the major component of the "great calcite belt" observed in the vicinity of the Subantarctic Front (SAF) and Polar Front (PF)

(Balch et al., 2014). Several studies have reported modern planktic foraminifer abundances and fluxes in the Southern Ocean from net tows (Asioli and Langone, 1997; Mortyn and Charles, 2003; Bergami et al., 2009; Meilland, 2015) and sediment traps (Donner and Wefer, 1994; King and Howard, 2003; Northcote and Neil, 2005; Salter et al., 2014). Foraminifer assemblages are characterized by a southward dominance of polar species *Neogloboquadrina pachyderma*. In a review, Hunt et al., (2008) compiled pteropod abundance in the Southern Ocean and reported a switch from a dominance of *Limacina retroversa australis* north of the PF to *Limacina helicina antarctica* south of the PF.

The presence of calcareous organisms has important implications not only for food web ecology of the Southern Ocean, but also for the cycling of carbon between the atmospheric, oceanic, and sedimentary reservoirs on various climatically relevant timescales. Two distinct carbon pumps operate to cycle carbon trough these different reservoirs (Volk and Hoffert, 1985). The soft tissue pump transfers particulate organic carbon (POC) originating from photosynthetic production to the ocean interior and plays a key role in the sequestration of atmospheric CO_2 (Sarmiento et al., 1988). The carbonate pump exports particulate inorganic carbon ($CaCO_3$, PIC) mainly as detrital calcareous shells (Volk and Hoffert, 1985). Calcification in the mixed layer decreases total alkalinity (TA) and dissolved inorganic carbon (DIC) with a ratio 2:1 and acts as a net source of CO_2 to the atmosphere over a seasonal timescale (Frankignoulle et al., 1994). If the PIC production is exported in the deep ocean below the permanent thermocline, the net impact on the atmospheric CO_2 occurs at a much longer timescale corresponding to the ocean mixing time (~ 1000 years, Zeebe, 2012). This phenomenon is known as the "carbonate counter pump" effect. Additionally, it has been suggested that during the last glaciation, lower PIC:POC export ratio due to increased organic carbon export may have contributed to higher dissolution of the deep-ocean carbonate sediments, leading to a decrease in pCO_2 compared to the interglacial periods (Archer and Maier-Reimer, 1994; Archer et al., 2000; Sigman and Boyle, 2000). Therefore the PIC:POC ratio of exported particles is likely to have a significant impact on the atmosphere-ocean CO_2 fluxes from seasonal to geological timescales (Matsumoto et al., 2002; Sarmiento et al., 2002). More recently, in the Subantarctic Southern Ocean, the strong response of calcifying organisms to natural iron fertilization has been observed to increase the PIC:POC export ratio leading to a strong carbonate counter pump, lowering the efficiency of CO_2 sequestration by the biological carbon pump (Salter et al., 2014).

Understanding how calcifying communities drive the carbonate counter pump requires a coupled description of the chemical composition and biological properties of different vectors driving $CaCO_3$ export fluxes. Sediment trap studies provide a tractable framework to link detailed analyses of the morphological and physiological properties of exported calcareous particles (e.g. species composition, test size and test weight) with seasonal and annual geochemical budgets. In this context, the study by Salter et al. (2014) quantified a carbonate counter pump effect accounting for 6–32% of measured POC fluxes with a notable contribution from foraminifer species (mainly *Globigerina bulloides* and *N. pachyderma*) in iron-fertilized waters downstream of the Crozet Islands. Several studies have reported geochemical transitions in particle stoichiometry across the Polar Front (Trull et al., 2001; Honjo et al., 2008), highlighting the importance of regional variability for a Southern Ocean carbonate counter pump that is partly linked to the biogeography of calcareous organisms (Salter et al., 2014).

The objectives of the present study are to (1) quantify the magnitude of PIC export and the carbonate counter pump in an iron fertilized area (the Kerguelen Plateau) south of the Polar Front (Antarctic Zone, AAZ), (2) determine the relative contribution of

foraminifer and coccolithophores to total PIC export in this regime, and (3) constrain the importance of species composition and test characteristics (size and size-normalized weight) for foraminifer-mediated PIC fluxes in iron fertilized blooms of the Southern Ocean.

2. Materials and methods

2.1. Sediment trap deployment and environmental data

As part of the KEOPS2 project (Kerguelen Ocean and Plateau compared study 2), a sediment trap (Technicap PPS3, 2.5 aspect ratio) was moored for 11 months (21 October 2011 to 7 September 2012) at 289 m over the central Kerguelen Plateau (seafloor depth 527 m) at station A3 (50 °38.3 S–72 °02.6 E, Fig. 1a,b). The carrousel comprised 12 sampling cups (250 mL) containing 5% formalin hypersaline solution buffered with sodium tetraborate (pH=8). A detailed description of the sample processing and particulate organic carbon (POC) analyses are provided in Rembauville et al. (2015b). Briefly, swimmers (zooplanktonic organisms actively entering the trap) were manually removed, samples were freeze-dried and the carbonate fraction was dissolved by the addition of acid before the organic carbon content was measured with a CHN analyzer.

Station A3 is characterized by a recurrent and large phytoplankton bloom induced by natural iron fertilization coming from the underlying plateau (Blain et al., 2007). Dissolved iron (dFe) is delivered to the mixed layer through two processes: winter mixing and entrainment of dFe from deeper waters and, to a less extend, vertical diapycnal diffusion of dFe in summer (Bowie et al., 2015). South of the Kerguelen Island, the polar front is permanent and non motile (Park et al., 2014) and therefore does not impact sediment trap deployment location. At the A3 station, the circulation is weak (< 3 cm s^{-1}) and primarily tidal-driven (Park et al., 2008). Physical data acquired during the sediment trap deployment suggest the record was not subject to major hydrodynamic biases (Rembauville et al., 2015b), allowing a detailed and quantitative discussion of the export fluxes.

Satellite-derived surface chlorophyll *a* and PIC concentration (MODIS 8 days product, accessed at http://oceancolor.gsfc.nasa.gov/cms/), and sea surface temperature (NOAA OISST, weakly product, Reynolds et al., 2007) were extracted for a 100 km radius around the trap location. Calcite saturation state was calculated in the vicinity of the trap location with the CO2sys toolbox using climatological fields of DIC and Alkalinity (GLODAP, Key et al., 2004) and temperature, salinity, silicate and phosphate (World Ocean Atlas 2013, Garcia et al., 2013). Constants recommended for best practice were used (Dickson et al., 2007) as suggested by Orr et al. (2015).

2.2. Calcium analyses in the bulk and fine fractions

For bulk particulate inorganic carbon analyses, 5 mg of freeze-dried material was weighed (Sartorius MC 210 P balance) into Teflon vials for the mineralization. 1 mL of 65% HNO_3 was added and samples were placed in an ultrasonication bath for 20 min. Samples were then dried overnight at 130 °C. 0.5 mL of 65% HNO_3 and 0.5 mL of 40% HF were added and samples were ultrasonicated a second time and dried overnight. The resulting residue was dissolved in 10 mL of 0.1 N HNO_3 and calcium content analyzed by inductively coupled plasma – optical emission spectrometry (ICP-OES, Perkin-Elmer Optima 2000). The efficiency of the mineralization procedure was estimated using reference material (GBW-07314) and was $> 96\%$.

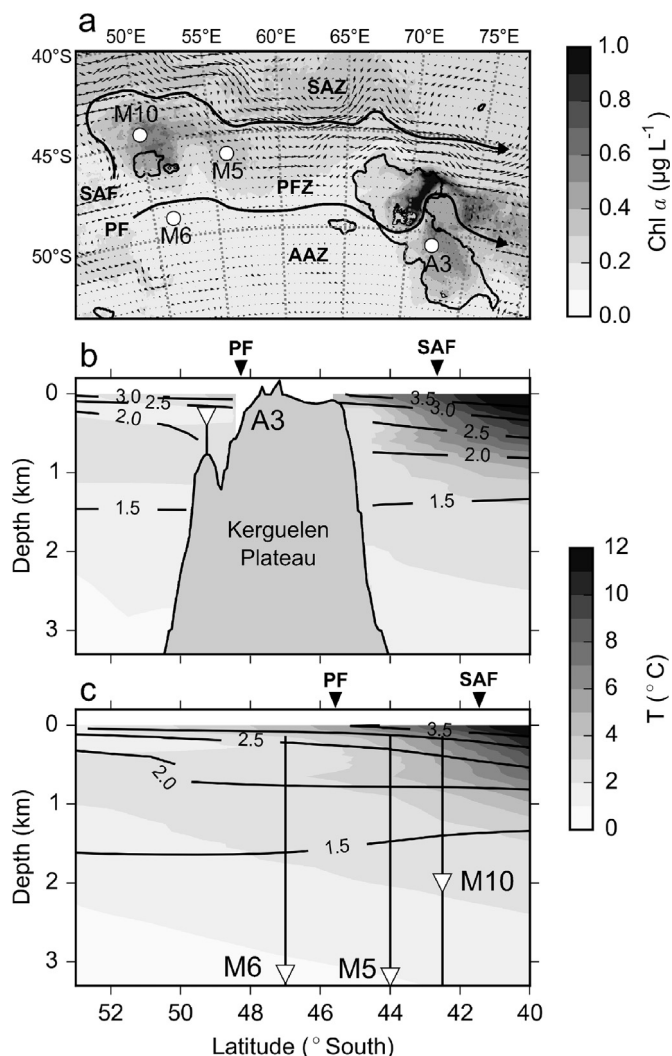For the fine fractions (20–63 μm and < 20 μm) Ca analyses, the

Fig. 1. (a) Map showing the locations of the sediment trap deployments in the Indian Sector of the Southern Ocean. Grey scale represents MODIS surface chlorophyll *a* climatology. Arrows are climatological altimetry-derived surface geostrophic currents (AVISO product). Dashed lines denote the Subantarctic Front (SAF) and Polar Front (PF). SAZ: Subantarctic Zone, PFZ: Polar Frontal Zone, AAZ: Antarctic Zone. The 1000 m isobath is shown as a black contour line. (b) Section of temperature (World Ocean Atlas 2013, grey scale) and calcite saturation state (black isolines) along the 70°E meridian. (c) Same as (b) along the 55 °E meridian.

membranes (0.4 μm pore size, 47 mm diameter). Filters were dried at 40 °C and the residue was leached in 10 mL 1% HNO_3, ultrasonicated for 10 min and left 12 h at room temperature before the Ca analysis. Ca concentration was analyzed by inductively coupled plasma-atomic emission spectrometry (ICP-AES, Perkin Elmer, Optima 4300DV). Overall accuracy amounted to better than 2% based on replicate analysis.

For the qualitative analyses of the coccolithophore species composition, samples were prepared in a similar way as for the fine fraction Ca analysis (oxidation and sieving) and then filtered on cellulose acetate membranes (Millipore, 0.45 μm pore size, 47 mm diameter). Filters were dried at 40 °C and observed under a polarized microscope at 1200 magnification.

2.3. Foraminifer carbonate flux estimation

Foraminifer quantification, morphometric measurements and weighing was performed following the methods outlined in Salter et al. (2014). One 1/8 aliquot was sieved on a 63 μm mesh with tap water and the > 63 μm fraction was dried overnight (40 °C). Dried particles were homogeneously placed on a glass tray. Images of the entire 1/8 sample were acquired with a fully automated incident light monocular microscope (Leica Z16 APO), and a motorized xy-stage with a Lstep-PCI controller (Märzhäuser). High-resolution images (1.4 μm^{-2} $pixel^{-1}$) were taken with a color camera (SIS CC12). Particle size (minimum test diameter, d_{min}) was automatically analyzed using analySIS FIVE software (SIS/Olympus with a MAS software add-in). Foraminifer species were manually counted and classified into morpho-species following the taxonomic concept of Hemleben et al. (1989). Eight species of planktic foraminifer were identified: *Neogloboquadrina pachyderma* (left coiling), *Neogloboquadrina incompta* (right coiling), *Turborotalita quinqueloba*, *Globigerinita uvula*, *Globigerinita glutinata*, *Globorotalia inflata*, *Globigerinoides ruber* (sensu stricto) and *Trilobatus sacculifer* (normal type). Only one empty shell of pteropod (*Limacina helicina*) was found in the samples and therefore pteropod's contribution to the passive carbonate flux was considered negligible. However, numerous pteropods were found as swimmers (distinguished by well preserved organic material) actively entering the trap in late summer (Rembauville et al., 2015b). Those shells were withdrawn from the samples as they were considered not to contribute to the passive flux. To determine size-weight relationships, individuals of *N. pachyderma* (n=23), *N. incompta* (n=10), *T. quinqueloba* (n=60) were manually picked from samples representative of different flux conditions (spring, summer and winter). Individuals were placed in aluminium cups and weighed (Mettler Toledo XP2U, 0.1 μg precision). Samples were acclimatized in the weighing room for at least 12 h before the analysis. Once the test weight was determined, the minimal diameter (d_{min}) of each individual was measured with the procedure described above. Size-weight relationships ($W = a \times d_{min}^{b}$) were constructed by fitting linear regressions to log-transformed data (Movellan et al., 2012). A species-specific relationship was developed for *N. pachyderma*, *N. incompta* and *T. quinqueloba*. For the other species, an average size-weight relationship was calculated by pooling the entire foraminifer dataset (n=93). Parameters of the size-weight relationships are given in Table 1. Foraminifer carbonate flux was then calculated using the abundance and size from the whole dataset and species or group-specific size-weight relationships. We refer to the sum of foraminifer and fine fractions (20–63 μm and < 20 μm) PIC as "calculated PIC".

2.4. Test size and size normalized weight comparison with assemblages from Crozet

Discrete measurements of the test size and weight of

original 1/8 split samples (Rembauville et al., 2015b) were further split into 1/80 aliquots with a rotary wet-splitter (McLane WSD-10) using purified water (Elix by Millipore purification system) buffered with ammonia as a rinse solution. Coccoliths in sinking particles captured in sediment trap samples may be contained in faecal pellets and/or phytoplankton aggregates. To improve the efficiency of size fraction separation by sieving it is necessary to oxidize the samples to disaggregate particles and retrieve the entire carbonate fine fraction (Bairbakhish et al., 1999; Broerse et al., 2000; Ziveri et al., 2000; Stoll et al., 2007). The 1/80 aliquots were placed in a 50 mL centrifugation tube for the oxidation steps using a method adapted from Bairbakhish et al. (1999). Samples were centrifuged (5000 rpm, 5 min) and the supernatant withdrawn. Subsequently, 3 mL of Elix water buffered with ammonia, 3 mL of 5% NaClO and 1.5 mL of 30% H_2O_2 were added and the samples were ultrasonicated for 10 s. Every 10 min, 2 mL of NaClO were added and samples were ultrasonicated for 10 s. This cycle was repeated for one hour. The oxidized aliquot was wet-sieved over a 63 μm and a 20 μm mesh, and the two resulting size fractions (20–63 μm and < 20 μm) were filtered on polycarbonate

Table 1
Parameters of the size-weight relationship (W (μg)$=a \times d_{min}$ (μm)^b) for the different foraminifer groups OR species considered. All the regressions are highly significant ($p < 0.01$).

Species	d_{min} range (μm)	W range (μg)	a	b	R^2
N. pachyderma (n=23)	102–300	0.3–5.5	5.26×10^{-7}	2.90	0.71
N. incompta (n=10)	128–230	0.9–3.0	3.98×10^{-4}	1.61	0.77
T. quinqueloba (n=60)	132–340	0.3–4.9	3.54×10^{-9}	3.85	0.71
Global (n=93)	102–340	0.3–5.5	1.25×10^{-7}	3.16	0.67

foraminifer individuals facilitate the calculation of size-normalized weight (SNW), a commonly used descriptor of test density/thickness (Bijma et al., 1999; Beer et al., 2010a; Marshall et al., 2013). The SNW was calculated for each individual by dividing the weight by the minimum test diameter (SNW (μg μm^{-1})$=W/d_{min}$). Given the good relationship between area and minimum diameter, this method is considered as an appropriate mean to characterize the test density (Beer et al., 2010b). We compared the Kerguelen dataset (station A3, AAZ) with previously published size and weight data using the same methodology from the Crozet Islands (Salter et al., 2014). Stations M10 and M5 are located in the PFZ (Pollard et al., 2007). Altimetry data suggest station M6 might be seasonally influenced by a weakly marked Polar Front (Park et al., 1993; Pollard et al., 2007), but the presence of a temperature minimum layer (1.6 °C at 200 m) strongly supports its belonging to the AAZ (Pollard et al., 2002; Planquette et al., 2007; Salter et al., 2014). Statistical differences in minimum diameter (d_{min}) and size-normalized weight (SNW) between the four study sites were tested for three species independently (*N. pachyderma*, *T. quinqueloba*, *G. bulloides*) using a non-parametric Kruskall-Wallis test. If the four sites constituted significantly different groups, a post-hoc Tuckey test was performed to identify which sites were significantly different from the others. If the four sites constituted a significantly homogeneous group, the data from the four sites were pooled for each species and differences between the three species were tested using a Kruskal-Wallis test followed by a Tuckey post-hoc test. All tests were performed at a significance level of 5%.

3. Results

3.1. Seasonality of POC and bulk PIC fluxes

Surface chlorophyll *a* concentration displayed two peaks (Fig. 2a). The major peak (2.5 μg L^{-1}) occurred during spring at the onset of thermal stratification (November 2011) and a second moderate peak (1 μg L^{-1}) in summer (January 2012). POC fluxes were characterized by two short (< 15 days) and intense (~ 1.5 mmol m^{-2} d^{-1}) export events lagging the chlorophyll *a* peaks by one month. These two POC export events comprised primarily *Thalassiosira antarctica* and *Chaetoceros Hyalochaete* resting spores (Rembauville et al., 2015a).

The satellite-derived mixed layer PIC concentration displayed a clear seasonal pattern (Fig. 2a) with moderate values in spring (0.4 μmol L^{-1} in October/November 2011) and a strong increase in summer to reach nearly 1 μmol L^{-1} in end January 2012. The PIC concentration decreased gradually after this summer peak to reach low values of 0.2 μmol L^{-1} in winter 2012. Total bulk PIC fluxes displayed a similar seasonality as the surface satellite-derived PIC concentration (Fig. 2b). A moderate peak of 33 μmol m^{-2} d^{-1} in the first cup (21 October to 4 November 2011) was followed by very low fluxes for the remainder of spring ($< 10\mu$mol m^{-2} d^{-1}). PIC fluxes gradually increased in the summer to 30 μmol m^{-2} d^{-1}
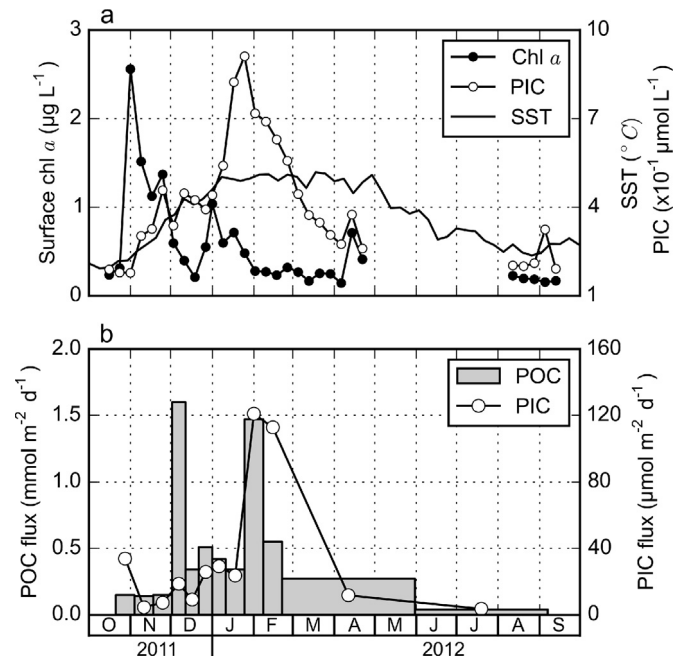
Fig. 2. (a) Satellite-derived surface chlorophyll *a* (black dots), particulate inorganic carbon (PIC, white dots) and sea surface temperature (SST, black line) averaged in a 100 km radius around the trap located at the A3 station. (b) Particulate organic carbon (POC) and bulk particulate inorganic carbon (PIC) fluxes from the A3 sediment trap.

before a clear maximum in late summer (110–120 μmol m^{-2} d^{-1}) that persisted for one month (25 January to 22 February 2015). Autumn and winter fluxes were very low (< 12 μmol m^{-2} d^{-1}). Assuming negligible PIC flux out of the collecting period (corresponding to the months of September and October characterized by low chlorophyll *a* concentration), the annual PIC export was low (6.6 mmol m^{-2} yr^{-1}). The annually-integrated PIC:POC molar ratio was equal to 0.07.

3.2. Seasonal dynamics of foraminifer and coccolith export fluxes

The seasonality of total foraminifer test flux closely followed chlorophyll *a* dynamics (Fig. 3a). A major peak of 800 indiv. m^{-2} d^{-1} was observed in spring. In December, when surface chlorophyll *a* concentrations were low, the total foraminifer flux was very low (15 indiv. m^{-2} d^{-1}). During the second surface chlorophyll *a* increase (January to mid-February), the total foraminifer flux increased again to reach values of 450–550 indiv. m^{-2} d^{-1}. Foraminifer flux was very low in autumn (30 indiv. m^{-2} d^{-1}) and negligible in winter. There was no major seasonal change in the foraminifer assemblage throughout the year. At an annual scale, 4 species dominated (> 95%) the foraminifer flux. The community assemblage was dominated by *T. quinqueloba* (31.8%), closely followed by *N. pachyderma* (30.8%) with lower contributions of *N. incompta* (18%) and *G. uvula* (15.3%) (Table 2).

Total and fine fractions (20–63 μm and < 20 μm) PIC fluxes are presented in Fig. 3c. The 20–63 μm fine fraction displayed very low fluxes (< 15 μmol m^{-2} d^{-1}) throughout the year with maximum in February 2012. The fine fraction < 20 μm fluxes followed a similar seasonal pattern as total PIC fluxes. Spring and summer (October to mid-January) were characterized by low fluxes with values < 25 μmol m^{-2} d^{-1} and peaked to the highest values ~ 100 μmol m^{-2} d^{-1} in late summer (February). In autumn and winter, the PIC fine fraction < 20 μm fluxes were < 15 μmol m^{-2} d^{-1}.

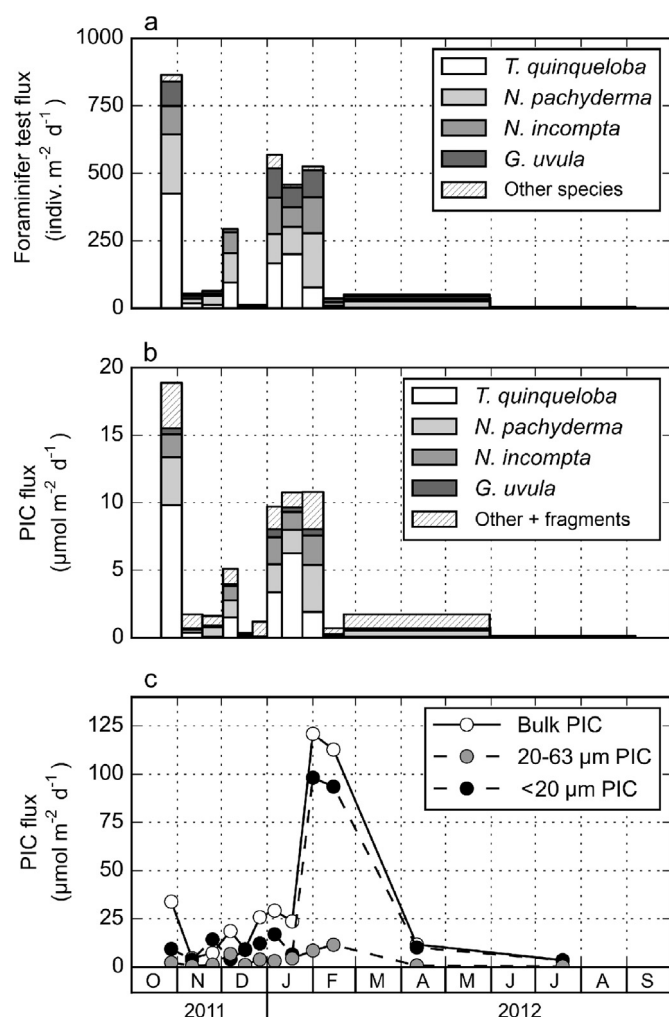**Fig. 3.** (a) Numerical test fluxes of planktic foraminifers recorded by the sediment trap at the A3 station. (b) Corresponding foraminifer PIC fluxes. (c) Fine fractions PIC fluxes (20–63 μm – grey dots, < 20 μm-black dots), and bulk PIC flux (circles).

Table 2
Relative contribution of foraminifer species to the annual numerical export and annual foraminifer PIC. Relative contribution of foraminifers and fine fractions (< 63 μm) to the calculated annual PIC export.

Species/group	Numerical for-aminifer flux (%)	Foraminifer PIC (%)	Calculated PIC (%)
N. pachyderma	30.8	22.6	3.3
N. incompta	18.0	11.9	1.8
T. quinqueloba	31.8	32.8	4.9
G. uvula	15.3	3.4	0.5
Other foraminifer species	4.1	10.3	1.4
Foraminifer fragments		19.0	2.8
Total foraminifers			14.8
< 63 μm			85.2
20–63 μm			10
< 20 μm			75.2

3.3. Relative contribution of foraminifers and coccoliths to carbonate export

The individual size-weight relationships were considered sufficiently reliable to calculate the contribution of each foraminifer species to the PIC export (all fits were highly significant, $R^2 > 0.66$, Table 1). The total foraminifer-mediated PIC export showed a seasonality comparable to the surface chlorophyll a with a strong peak in early spring (18 μmol m^{-2} d^{-1} in October 2011) and a secondary increase in late summer (11 μmol m^{-2} d^{-1} in Januray 2011). Fluxes were much lower the remainder of the year (< 5 μmol m^{-2} d^{-1}).The relative contribution of each foraminifer species/group to the total foraminifer PIC and the calculated PIC annual flux is reported in Table 2. The relative contribution of the major foraminifer species to the total foraminifer PIC fluxes was comparable to their contribution to numerical fluxes, and a notable fraction (19%) of foraminifer PIC was exported as unclassified test fragments. *T. quinqueloba* displayed the highest contribution to the calculated PIC (4.9%), followed by *N. pachyderma* (3.3%) and *N. incompta* (1.8%). The contribution of *G. uvula* was very low (0.5%). Microscopic observations of the fine size fractions after the organic oxidation step revealed the absence of juvenile foraminifers and calcareous dinophytes in the 20–63 μm size fraction and the presence of coccoliths aggregated to diatom frustules and unidentified CaCO$_3$ fragments. Therefore, the < 20 μm fine fraction represents a slight underestimation of coccolith calcite fluxes (Ziveri et al., 2007). The total contribution of foraminifer tests to the annual calculated PIC export was 14.8%. Conversely, the contribution of the coccolith fine fractions (< 20 μm and 20–63 μm) to the annual calculated PIC flux was high (85.2%), primarily due to their major contribution in the late summer export peak.

The relationship between the bulk and calculated PIC flux is presented in Fig. 4. Data points are close to the 1:1 relationship. A highly significant linear correlation (Pearson, n = 12, $p < 0.01$) existed between the bulk and calculated PIC. Regression suggested a slope close to 1 (0.94, $R^2 = 0.99$) and the annual calculated PIC export (6.5 mmol m^{-2}) was very close to the annual bulk PIC flux measured (6.6 mmol m^{-2}). These statistics ensure the analytical method was robust and the partitioning of PIC fluxes among the quantified biological vectors accounted for the majority of total PIC measured in the samples.

3.4. Foraminifer test size and SNW comparison with Crozet
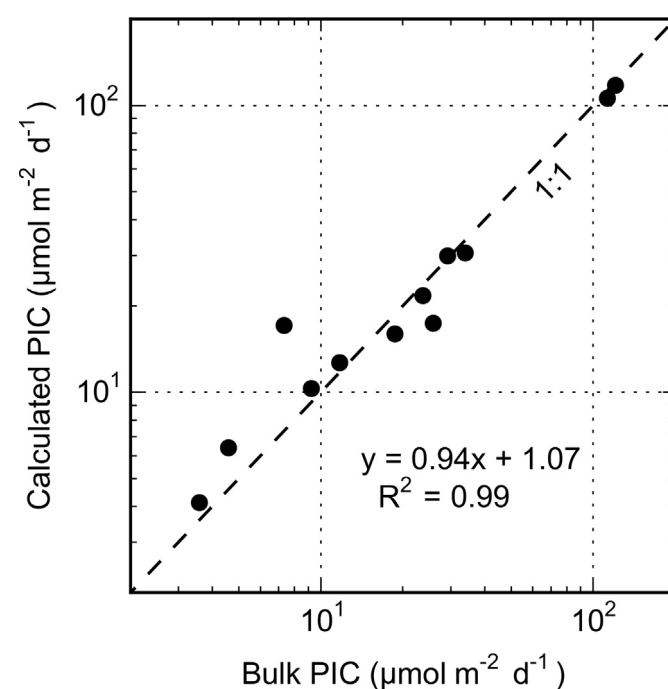

Fig. 4. Relationship between the measured bulk PIC flux and the calculated PIC flux (sum of the foraminifer, the 20–63 μm and the < 20 μm fine fractions PIC fluxes). Dashed line denotes the 1:1 relationship. The equation of the regression performed on the raw data is given.
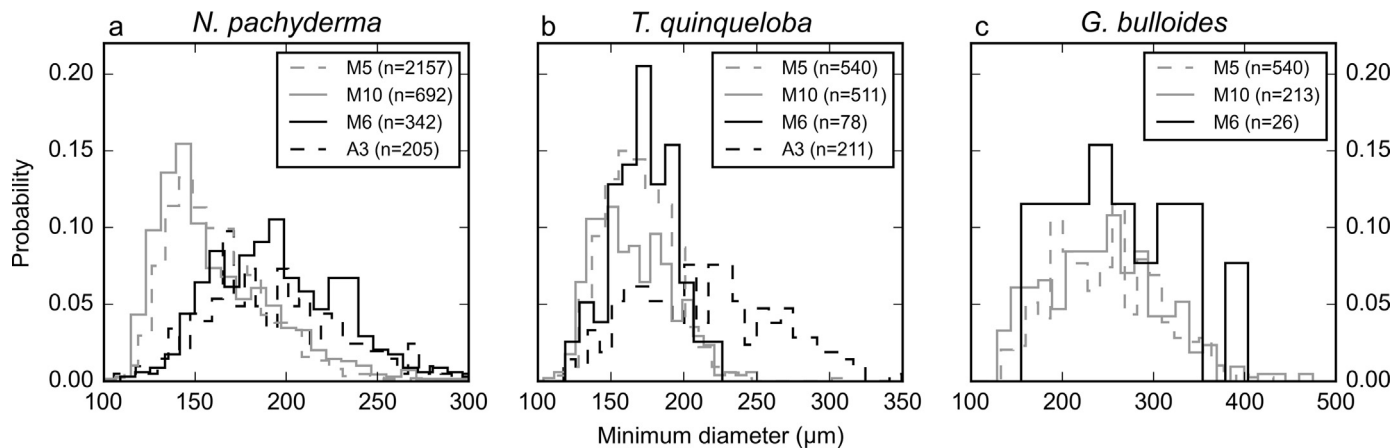
Fig. 5. Probability histogram of size distribution for three major species collected by the sediment traps at Crozet (M5, M6 and M10) and Kerguelen (A3): (a) *Neogloboquadrina pachyderma*, (b) *Turborotalita quinqueloba* and (c) *Globigerina bulloides*. Grey lines represent data from sediment traps located north of the Polar Front (PF) and black lines south of the PF.

assemblages

Probability histograms of size distribution at each site for *N. pachyderma*, *T. quinqueloba* and *G. bulloides* are presented in Figs. 5a, b and c, respectively. All the density functions displayed quasi-unimodal distributions. For *N. pachyderma*, d_{min} was significantly higher in the AAZ (M6 and A3 sites, 195 ± 39 μm, mean $\pm$ standard deviation) than the PFZ (M5 and M10 sites, 151 ± 30 μm). For *T. quinqueloba*, d_{min} was significantly higher at A3 (206 ± 51 μm) than at the three other sites (M5, M10 and M6, 167 ± 29 μm) that constituted a significantly homogeneous group. Only 5 g. *bulloides* were observed at A3 and therefore were not taken into account in the analysis. For *G. bulloides*, d_{min} was significantly homogeneous at the three Crozet sites (M5, M10 and M6, 244 ± 65 μm).

Boxplots of SNW are presented for the three species in Fig. 6. For each species, there was no significant difference in SNW among sites. Therefore, the data from all the sites were pooled by species. Each species SNW constituted a significantly homogeneous group different from the two others. *G. bulloides* SNW ($31 \pm 14 \times 10^{-3}$ μg μm^{-1}, mean $\pm$ standard deviation) was significantly higher than *N. pachyderma* SNW ($18 \pm 11 \times 10^{-3}$ μg μm^{-1}) that was also significantly higher than *T. quinqueloba* SNW ($10 \pm 4 \times 10^{-3}$ μg μm^{-1}) (Fig. 6).

4. Discussion

4.1. Foraminifer test flux amplitude and seasonality

We observed moderate planktic foraminifer test fluxes of 500–1000 indiv. m^{-2} d^{-1} despite high primary production levels in this naturally iron-fertilized area. The low test fluxes we report over the central Kerguelen Plateau, and the dominance of *N. pachyderma* and *T. quinqueloba* are consistent with the general decrease in flux from the SAZ to the AAZ that goes with a switch from a mixture of subpolar and polar water species to a dominance of the two aforementioned species. Donner and Wefer (1994) reported very low fluxes (~ 50 indiv. m^{-2} d^{-1}) in the Northern Weddell Sea and Bransfield Strait (AAZ) whereas fluxes where much higher at the Maud Rise ($\sim 1 \times 10^3$ indiv. m^{-2} d^{-1}) where *N. pachyderma* dominated the community assemblage, followed by *T. quinqueloba*. King and Howard (2003) reported foraminifer export fluxes south of Tasmania with highest numerical fluxes of $\sim 1 \times 10^4$ indiv. m^{-2} d^{-1} in the SAZ very close to the SAF and lower values (4×10^3 indiv. m^{-2} d^{-1}) in the PFZ. The transition from SAZ to PFZ was associated with a switch from temperate species to a dominance of *N. pachyderma* and *T. quinqueloba*. South of New Zealand, Northcote and Neil (2005) described fluxes of 5×10^3 indiv. m^{-2} d^{-1} with a major contribution of *G. inflata* in the SAZ. In the PFZ North of the Crozet Islands, foraminifer numerical export fluxes were

Fig. 6. Box-and-whisker plots representation of size-normalized weight for three major species collected by the sediment traps at Crozet (M5, M6 and M10) and Kerguelen (A3): (a) *Neogloboquadrina pachyderma*, (b) *Turborotalita quinqueloba*, (c) *Globigerina bulloides*. Box extends from the lower to upper quartile values of the data, with a line at the median. Whiskers extend from the quartiles to values comprised within a 1.5 inter-quartile distance. Black lines in the background are median (full line) and lower and upper quartile (dashed lines) calculated by grouping all samples for a given species.

$\sim 1 \times 10^4$ indiv. $m^{-2} d^{-1}$ and mostly represented by *N. pachyderma* with a notable contribution of the larger temperate species *G. bulloides* and *G. inflata* (Salter et al., 2014).

The seasonal dynamics of foraminifer test export flux at station A3 was characterized by two peaks in spring and summer closely related with surface chlorophyll *a* concentration, but were not particularly associated with SST dynamics. Jonkers and Kučera (2015) have analyzed the phenology of foraminifer export fluxes at global scale and demonstrated that a group composed of temperate and cold water species (comprising *N. pachyderma*, *N. incompta* and *T. quinqueloba*) displayed two export peaks in spring and summer. Our results are highly consistent with this general scheme and support the close link between primary production (assessed from surface chlorophyll *a*) and foraminifer production (Hemleben et al., 1989; Klaas, 2001; Schiebel et al., 2001; Kuroyanagi and Kawahata, 2004; Lombard et al., 2011) and subsequent export (Schiebel, 2002). At Crozet (M5 and M10 sites in PFZ) foraminifer test export occurred in one continuous event in summer from January to March (Salter et al., 2014) when SST was generally highest ($>8\,°C$) and chlorophyll *a* concentration was low ($0.5\,\mu g\,L^{-1}$, Salter et al., 2012). This strongly contrasts with the close link we observe between the chlorophyll *a* concentration and the foraminifer test export at A3. However, the comparison of flux seasonality must be treated with caution because of the different sediment trap deployment depths (289 m at A3 versus >2500 m for the M5 and M10 sites), increasing water depth might dampen seasonal particle flux signal. Our results from a shallow sediment trap at A3 suggest that food availability might be the major controlling factor for low temperature communities of the AAZ.

4.2. Foraminifer test size and SNW distribution

The calculation of the calcite saturation state is strongly dependent on the input variables of DIC and Alkalinity (a 1% change in one of these variables can drive a 10% change in saturations state, Orr et al., 2015). Given this uncertainty, the climatological field suggests that all of the sediment trap deployments around Crozet and Kerguelen were located in waters oversaturated with respect to CO_3^{2-} with a calcite saturation state >1 (Fig. 1b,c). Therefore it is unlikely that seawater carbonate chemistry has strongly affected test weight and size through dissolution during particle sinking. However, test dissolution would lead to an underestimation of the weight in the sediment trap material and therefore the SNW should be considered as a lower estimate compared to living individuals.

The compilation of the large dataset generated with the automated microscope from Crozet and Kerguelen samples revealed that location relative to the Polar Front had a significant impact on the size of *N. pachyderma* with smaller individuals in the PFZ (Fig. 5). This pattern was not evident for *T. quinqueloba* and *G. bulloides*. When food is not limiting, temperature is presumed a fundamental factor influencing foraminifer growth rate at the species level (Lombard et al., 2009). An explanation of the Bergmann's rule (larger individuals in colder environments) in plankton is that lower growth rate due to lower temperature leads to larger individuals at sexual maturity (von Bertalanffy, 1960; Atkinson, 1994). Under this hypothesis, colder SST south of the Polar Front might explain larger individuals of *N. pachyderma* at M6 and A3 sites. However the fact that Crozet communities of *T quinqueloba* and *G. bulloides* have a significantly homogeneous size in the PFZ and AAZ suggests that temperature is not the only factor at play and that population dynamics (Schiebel et al., 1997) and the availability of prey (Schmidt et al., 2004) as well as genetic diversity within a given morphospecies (Weiner et al., 2015) might also constrain planktonic foraminifer size.

SNW was originally considered as a proxy for $[CO_3^{2-}]$ (Lohmann, 1995; Bijma et al., 1999; Broecker and Clark, 2001; Barker and Elderfield, 2002; Bijma et al., 2002). Additionally, the comparison of foraminifer tests from modern sediment traps samples and Holocene sediments demonstrated the impact of ocean acidification and the lowering of $[CO_3^{2-}]$ on the reduction of the test weight at high southern latitudes (Moy et al., 2009). However, there is a growing number of observations suggesting that the relationship between the SNW and the $[CO_3^{2-}]$ is not homogeneous among foraminifer species (Beer et al., 2010a; Meilland, 2015), and the relationship is more robust for certain species than for others (Marshall et al., 2013). Our results show that for a given species, SNW is not statistically different regarding the hydrography but that SNW varies significantly between the dominant species *N. pachyderma*, *T. quinqueloba* and *G. bulloides*. This suggests that ecological conditions other than the carbon chemistry of ambient seawater at long (Weinkauf et al., 2013) and short time scale (de Villiers, 2004; Marshall et al., 2013), and species physiological characteristics and metabolism might be responsible for the three-fold SNW increase between *T. quinqueloba* and *G. bulloides*. This has potentially important implications for the carbon pumps because it implies that planktic foraminifer community composition together with the magnitude of the numerical flux (number of individuals) plays a role in the foraminifer-mediated PIC flux.

4.3. Seasonality and magnitude of the coccolith fine fraction export

The sediment trap record represents the first annual record of coccolith calcite export south of the Polar Front. Over the central Kerguelen Plateau, we observe a clear decoupling between the two chlorophyll *a* peaks (November and January) and the coccolith fine fraction ($<20\,\mu m$) export peak (February). The algorithm used to calculate PIC concentration based on satellite remote sensing reflectance is associated with a root mean square error (RMSE) of $1.2\,\mu mol\,L^{-1}$ (Balch et al., 2005). The maximum satellite-derived PIC concentration we report is $\sim 1\,\mu mol\,L^{-1}$ which is lower than the RMSE. Additionally, the sunlight penetration depth constraining satellite data is <20 m in such a productive area (Gordon and McCluney, 1975), preventing the detection of subsurface features. For this reason, we only consider the satellite-derived PIC as qualitative date product. The uncertainty on satellite-derived PIC concentration, the shallow sediment trap depth (289 m) and the sampling temporal resolution (15 days) prevent a robust calculation of coccolith sinking speed or turnover time. However, the satellite-derived PIC concentration displays a clear seasonal signal tightly coupled to the coccolith fine fraction export. This result suggests that the algorithm used to derive coccolithophore presence from satellite data (Gordon et al., 2001; Balch et al., 2005) is sensitive, if not quantitative, over the central Kerguelen Plateau.

Historical observations suggest a diatom to coccolithophore succession from spring to summer in various locations of the global ocean (Margalef, 1978; Holligan et al., 1983; Lochte et al., 1993; Ziveri et al., 1995; Thunell et al., 1996; Ziveri and Thunell, 2000; Schiebel et al., 2011). Using satellite hyperspectral measurements and the PhytoDOAS method, Sadeghi et al. (2012) built a climatology of coccolithophore biomass in the Southern Atlantic. They reported a recurrent coccolithophore bloom in February/March, in good agreement with our measurement of maximum fine fraction ($<20\,\mu m$) export flux in February. Sadeghi et al. (2012) highlighted the importance of SST maxima for the origination of a coccolithophore bloom in the high latitude ocean. Similarly, we report the highest coccolith calcite export flux during the period of highest SST ($\sim 5\,°C$), in agreement with the hypothesis of a temperature control on the coccolithophore bloom. More recently, Hopkins et al. (2015) used satellite-derived PIC as a proxy of coccolithophore biomass and concluded to a co-

occurrence of chlorophyll *a* and coccolithophore peaks in the Southern Ocean. The results at large spatial and temporal scales differ somewhat from the uncoupling we observe at our specific location. Such differences may be attributed to inter-annual variability in the seasonality of chlorophyll *a* concentrations and/ or the timing of coccolithophore production.

The qualitative microscopic observation of the $< 20\ \mu m$ and $20–63\ \mu m$ fractions indicate that *Emiliania huxleyi* represents $> 95\%$ of the coccolithophores assemblage with a minor contribution of *Helicosphaera carteri*. This finding is consistent with previous observations of a strict dominance of *E. huxleyi* with low abundances south of the PF (Saavedra-Pellitero et al., 2014; Winter et al., 2014). *E. huxleyi* is reported to bloom in waters with generally low silicic acid concentration resulting by its consumption by diatoms (Holligan et al., 1983; Townsend et al., 1994; Tyrrell and Merico, 2004). Additionally, this species has been shown to be tolerant to low iron concentration (Brand et al., 1983; Sunda and Huntsman, 1995; Muggli and Harrison, 1997; Findlay and Giraudeau, 2000; Holligan et al., 2010). In January, the silicic acid concentration at the station A3 reaches $< 2\ \mu mol\ L^{-1}$ (Mosseri et al., 2008) and iron concentration is $\sim 0.1\ nmol\ L^{-1}$ (Blain et al., 2008). Moreover, the high nitrate, phosphate and ammonium concentrations (Mosseri et al., 2008) and the highest SST in late summer might be favorable conditions for a *E. huxleyi* bloom. Nevertheless, despite the summer stratification, the SST of 5 °C is still in the lower end of the thermal niche of *E. huxleyi* (1–31 °C, McIntyre et al., 1970). This temperature is likely to result in relatively low growth rate (Fisher and Honjo, 1989; Fielding, 2013). This may explain why the magnitude of the bloom is weak and corresponds to low surface chlorophyll *a* concentration at this period of the season. This weak coccolithophore bloom drives most (85.2%) of the annual PIC export that appears very low ($6.6\ mmol\ m^{-2}\ y^{-1}$) compared to coccolith fine fraction export from the temperate ocean ($0.2–0.8\ mol\ m^{-2}\ y^{-1}$, Ziveri et al., 2007).

4.4. Southern Ocean carbonate counter pump affected by different planktonic calcifying organisms

The annually-integrated PIC:POC export ratio of 0.07 (mol:mol) is close to the mean ratio for the global ocean (0.06 ± 0.03, Sarmiento et al., 2002) and appears much lower than the ratio found in sediment traps of the PFZ and the SAZ (~ 1, from a data compilation by Salter et al., 2014). The annual POC export ($98.2\ mmol\ m^{-2}\ yr^{-1}$, Rembauville et al., 2015b) and the annual PIC export ($6.6\ mmol\ m^{-2}\ yr^{-1}$) at station A3 allow us to estimate the strength of the carbonate counter pump: the reduction of the CO_2 drawdown by the biological pump due to the CO_2 production during the calcification process in the mixed layer (Frankignoulle et al., 1994; Zeebe, 2012; Salter et al., 2014). As the trap depth (289 m) was close to the winter mixed layer depth (220 m in this region of the Southern Ocean (Park et al., 1998; de Boyer Montégut et al., 2004), POC fluxes were not corrected for attenuation with depth. The carbonate counter pump effect (CC_{pump}, %) was calculated from the annual fluxes as $CC_{pump} = (PIC_{flux} \times \Psi)/POC_{flux} \times 100$. Ψ is the mole of CO_2 emitted by mole of CO_3^{2-} precipitated during the calcification process and ranges 0.7–0.8 for seawater at 5 °C and a pCO_2 of 300–400 μatm (Frankignoulle et al., 1994). The calculation leads to a CC_{pump} of 4.7–5.4% at station A3. This value is consistent with the previously reported value at the M6 site also located in the AAZ (1–4%) and is significantly lower that the values in the PFZ at the M5 and M10 sites (6–32%) reported in Salter et al. (2014).

In the PFZ downstream Crozet, foraminifers were significant contributors to the production and export of PIC (30–50%), with a lower contribution of coccoliths (20%) and pteropods (5%, Salter et al., 2014). Conversely, foraminifers are minor contributors over the central Kerguelen plateau in the AAZ ($< 15\%$, Table 2). The similarity of the CC_{pump} between the M6 and A3 sites in the AAZ supports the idea that the position of productivity relative to the Polar Front (Salter et al., 2014) exerts a major control on the magnitude of the CC_{pump} through two processes: (1) changes in the relative abundance of heterotrophic calcifiers foraminifers/ pteropods to autotrophic coccolithophores, and (2) a change in the contribution of foraminifer species with different SNWs.

During the last two million years the glaciations have been characterized by lower CO_2 concentration in the atmosphere that has been explained by a combination of both biology (strengthening of the biological pump) and physics of the Southern Ocean (Sigman and Boyle, 2000; Kohfeld et al., 2005; Robinson et al., 2005; Martínez-Botí et al., 2015). The higher efficiency of the biological pump was likely linked to higher deposition of eolian iron and more complete utilization of nutrients at high latitudes (Mahowald et al., 2006; Martínez-García et al., 2014). Our results from naturally fertilized Southern Ocean blooms suggest that the magnitude of the associated carbonate counter pump (Salter et al., 2014) depends not only on the dominant calcifying planktonic organisms (foraminifers versus coccolithophores), but also on the species assemblage that responds to the increase in primary production.

Acknowledgements

References

Archer, D., Maier-Reimer, E., 1994. Effect of deep-sea sedimentary calcite preservation on atmospheric CO_2 concentration. Nature 367, 260–263. http://dx.doi.org/10.1038/367260a0.

Archer, D., Winguth, A., Lea, D., Mahowald, N., 2000. What caused the glacial/interglacial atmospheric pCO_2 cycles? Rev. Geophys. 38, 159–189. http://dx.doi.org/10.1029/1999RG000066.

Armand, L.K., Cornet-Barthaux, V., Mosseri, J., Quéguiner, B., 2008. Late summer diatom biomass and community structure on and around the naturally iron-fertilised Kerguelen Plateau in the Southern Ocean. Deep-Sea Res. II: Top. Stud. Oceanogr. 55, 653–676. http://dx.doi.org/10.1016/j.dsr2.2007.12.031.

Asioli, A., Langone, L., 1997. Relationship between recent Planktic Foraminifera and water mass properties in the Western Ross Sea (Antarctica). Geogr. Fis. Din. Quat. 20, 193–198.

Atkinson, D., 1994. Temperature and organism size – a biological law for ectotherms. Adv. Ecol. Res. 25, 1–58.

Bairbakhish, A.N., Bollmann, J., Sprengel, C., Thierstein, H.R., 1999. Disintegration of aggregates and coccospheres in sediment trap samples. Mar. Micropaleontol. 37, 219–223. http://dx.doi.org/10.1016/S0377-8398(99)00019-5.

Balch, W.M., Drapeau, D.T., Bowler, B.C., Lyczskowski, E., Booth, E.S., Alley, D., 2011. The contribution of coccolithophores to the optical and inorganic carbon budgets during the southern ocean gas exchange experiment: new evidence in support of the "Great calcite Belt" hypothesis. J. Geophys. Res. Oceans 116. http://dx.doi.org/10.1029/2011JC006941.

Balch, W.M., Drapeau, D.T., Bowler, B.C., Lyczskowski, E.R., Lubelczyk, L.C., Painter, S.C., Poulton, A.J., 2014. Surface biological, chemical, and optical properties of the Patagonian shelf coccolithophore bloom, the brightest Waters of the great calcite belt. Limnol. Oceanogr. 59, 1715–1732. http://dx.doi.org/10.4319/lo.2014.59.5.1715.

Balch, W.M., Gordon, H.R., Bowler, B.C., Drapeau, D.T., Booth, E.S., 2005. Calcium carbonate measurements in the surface global ocean based on moderate-resolution imaging Spectroradiometer data. J. Geophys. Res. Oceans, 110. http://dx.doi.org/10.1029/2004JC002560.

Barker, S., Elderfield, H., 2002. Foraminiferal calcification response to glacial-interglacial Changes in atmospheric CO_2. Science 297, 833–836. http://dx.doi.org/10.1126/science.1072815.

Beer, C.J., Schiebel, R., Wilson, P.A., 2010a. Testing planktic foraminiferal shell weight as a surface water [CO3 2−] proxy using plankton net samples. Geology 38, 103–106.

Beer, C.J., Schiebel, R., Wilson, P.A., 2010b. Technical note: on methodologies for determining the size-normalised weight of planktic foraminifera. Biogeosciences 7, 2193–2198. http://dx.doi.org/10.5194/bg-7-2193-2010.

Bergami, C., Capotondi, L., Langone, L., Giglio, F., Ravaioli, M., 2009. Distribution of living planktonic foraminifera in the Ross SEA and the pacific sector of the southern ocean (Antarctica). Mar. Micropaleontol. 73, 37–48. http://dx.doi.org/10.1016/j.marmicro.2009.06.007.

Bijma, J., Hönisch, B., Zeebe, R.E., 2002. Impact of the ocean carbonate chemistry on living foraminiferal shell weight: comment on "Carbonate ion concentration in glacial-age deep waters of the caribbean sea" by W.S. Broecker and E. Clark, Geochem. Geophys. Geosyst., 3, p. 1064. doi:10.1029/2002GC000388.

Bijma, J., Spero, H.J., Lea, D.W., 1999. Reassessing foraminiferal stable isotope geochemistry: impact of the oceanic carbonate system (experimental results). In: Fischer, D.G., Wefer, P.D.G. (Eds.), Use of Proxies in Paleoceanography. Springer, Berlin, Heidelberg, pp. 489–512.

Blain, S., Quéguiner, B., Armand, L., Belviso, S., Bombled, B., Bopp, L., Bowie, A., Brunet, C., Brussaard, C., Carlotti, F., Christaki, U., Corbière, A., Durand, I., Ebersbach, F., Fuda, J.-L., Garcia, N., Gerringa, L., Griffiths, B., Guigue, C., Guillerm, C., Jacquet, S., Jeandel, C., Laan, P., Lefèvre, D., Lo Monaco, C., Malits, A., Mosseri, J., Obernosterer, I., Park, Y.-H., Picheral, M., Pondaven, P., Remenyi, T., Sandrini, V., Sarthou, G., Savoye, N., Scouarnec, L., Souhaut, M., Thuiller, D., Timmermans, K., Trull, T., Uitz, J., van Beek, P., Veldhuis, M., Vincent, D., Viollier, E., Vong, L., Wagener, T., 2007. Effect of natural iron fertilization on carbon sequestration in the southern ocean. Nature 446, 1070–1074. http://dx.doi.org/10.1038/nature05700.

Blain, S., Sarthou, G., Laan, P., 2008. Distribution of dissolved iron during the natural iron-fertilization experiment KEOPS (Kerguelen plateau, southern ocean). Deep Sea Res. Part II Top. Stud. Oceanogr. 55, 594–605. http://dx.doi.org/10.1016/j.dsr2.2007.12.028, KEOPS: Kerguelen Ocean and Plateau compared Study.

Blain, S., Tréguer, P., Belviso, S., Bucciarelli, E., Denis, M., Desabre, S., Fiala, M., Martin Jézéquel, V., Le Fèvre, J., Mayzaud, P., Marty, J.-C., Razouls, S., 2001. A biogeochemical study of the island Mass effect in the context of the iron hypothesis: Kerguelen Islands Southern Ocean. Deep-Sea Res. I: Oceanogr. Res. Pap. 48, 163–187. http://dx.doi.org/10.1016/S0967-0637(00)00047-9.

Bowie, A.R., van der Merwe, P., Quéroué, F., Trull, T., Fourquez, M., Planchon, F., Sarthou, G., Chever, F., Townsend, A.T., Obernosterer, I., Sallée, J.-B., Blain, S., 2015. Iron budgets for three distinct biogeochemical sites around the Kerguelen archipelago (Southern Ocean) during the natural fertilisation study, KEOPS-2. Biogeosciences 12, 4421–4445. http://dx.doi.org/10.5194/bg-12-4421-2015.

Boyd, P.W., 2002. Environmental factors controlling phytoplankton processes in the Southern Ocean1. J. Phycol. 38, 844–861. http://dx.doi.org/10.1046/j.1529-8817.2002.t01-1-01203.x.

Brand, L.E., Sunda, W.G., Guillard, R.R.L., 1983. Limitation of marine phytoplankton reproductive rates by zinc, manganese, and iron1. Limnol. Oceanogr. 28, 1182–1198. http://dx.doi.org/10.4319/lo.1983.28.6.1182.

Broecker, W.S., Clark, E., 2001. Reevaluation of the $CaCO_3$ size index paleocarbonate ion proxy. Paleoceanography 16, 669–671. http://dx.doi.org/10.1029/2001PA000660.

Broerse, A.T.C., Ziveri, P., van Hinte, J.E., Honjo, S., 2000. Coccolithophore export production, species composition, and coccolith-$CaCO_3$ fluxes in the NE Atlantic (34°N 21°W and 48°N 21°W). Deep Sea Res. II: Top. Stud. Oceanogr. 47, 1877–1905. http://dx.doi.org/10.1016/S0967-0645(00)00010-2.

de Boyer Montégut, C., Madec, G., Fischer, A.S., Lazar, A., Iudicone, D., 2004. Mixed layer depth over the global ocean: an examination of profile data and a profile-based climatology. J. Geophys. Res. Oceans 109, C12003. http://dx.doi.org/10.1029/2004JC002378.

de Villiers, S., 2004. Optimum growth conditions as opposed to calcite saturation as a control on the calcification rate and shell-weight of marine foraminifera. Mar. Biol. 144, 45–49. http://dx.doi.org/10.1007/s00227-003-1183-8.

Dickson, A.G., Sabine, C.L., Christian, J.R., 2007. Guide to Best Practices for Ocean CO_2 Measurements. PICES Special Publication 3.

Donner, B., Wefer, G., 1994. Flux and stable isotope composition of Neogloboquadrina pachyderma and other planktonic foraminifers in the southern ocean (Atlantic sector). Deep Sea Res. I: Oceanogr. Res. Pap. 41, 1733–1743. http://dx.doi.org/10.1016/0967-0637(94)90070-1.

Fielding, S.R., 2013. Emiliania huxleyi specific growth rate dependence on temperature. Limnol. Oceanogr. 58, 663–666. http://dx.doi.org/10.4319/lo.2013.58.2.0663.

Findlay, C.S., Giraudeau, J., 2000. Extant calcareous nannoplankton in the Australian sector of the southern ocean (austral summers 1994 and 1995). Mar. Micropaleontol. 40, 417–439. http://dx.doi.org/10.1016/S0377-8398(00)00046-3.

Fisher, N.S., Honjo, S., 1989. Intraspecific differences in temperature and salinity responses in the coccolithophore Emiliania huxleyi. Biol. Ocean. 6, 355–361. http://dx.doi.org/10.1080/01965581.1988.10749537.

Frankignoulle, M., Canon, C., Gattudo, J.-P., 1994. Marine calcification as a source of carbon dioxide : positive deedback of increasing atmospheric CO_2. Limnol.

Oceanogr. 39, 458–462.

Garcia, H.E., Locarini, R.A., Boyer, T.P., Antonov, J.I., Baranova, O.K., Zweng, M.M., Reagan, J.R., Johnson, D.R., 2013. World Ocean Atlas 2013, In: S. Levitus(Eds.), A. Mishonov Technical Ed., Dissolved Inorganic Nutrients (phosphate, nitrate, silicate), Vol. 4.

Gordon, H.R., Boynton, G.C., Balch, W.M., Groom, S.B., Harbour, D.S., Smyth, T.J., 2001. Retrieval of coccolithophore calcite concentration from SeaWiFS imagery. Geophys. Res. Lett. 28, 1587–1590. http://dx.doi.org/10.1029/2000GL012025.

Gordon, H.R., McCluney, W.R., 1975. Estimation of the depth of sunlight penetration in the SEA for remote sensing. Appl. Opt. 14, 413–416.

Hemleben, C., Spindler, O., Anderson, R., 1989. Modern Planktonic Foraminifera, ed. Springer-Verlag, New-York.

Holligan, P.M., Charalampopoulou, A., Hutson, R., 2010. Seasonal distributions of the coccolithophore, Emiliania huxleyi, and of particulate inorganic carbon in surface waters of the scotia sea. J. Mar. Syst. 82, 195–205. http://dx.doi.org/10.1016/j.jmarsys.2010.05.007.

Holligan, P.M., Viollier, M., Harbour, D.S., Camus, P., Champagne-Philippe, M., 1983. Satellite and ship studies of coccolithophore production along a continental shelf edge. Nature 304, 339–342. http://dx.doi.org/10.1038/304339a0.

Honjo, S., Manganini, S.J., Krishfield, R.A., Francois, R., 2008. Particulate organic carbon fluxes to the ocean interior and factors controlling the biological pump: a synthesis of global sediment trap programs since 1983. Prog. Oceanogr. 76, 217–285. http://dx.doi.org/10.1016/j.pocean.2007.11.003.

Hopkins, J., Henson, S.A., Painter, S.C., Tyrrell, T., Poulton, A.J., 2015. Phenological characteristics of global coccolithophore blooms. Glob. Biogeochem. Cycles 29. http://dx.doi.org/10.1002/2014GB004919.

Hunt, B.P.V., Pakhomov, E.A., Hosie, G.W., Siegel, V., Ward, P., Bernard, K., 2008. Pteropods in southern ocean ecosystems. Prog. Oceanogr. 78, 193–221. http://dx.doi.org/10.1016/j.pocean.2008.06.001.

Jonkers, L., Kučera, M., 2015. Global analysis of seasonality in the shell flux of extant planktonic Foraminifera. Biogeosciences 12, 2207–2226. http://dx.doi.org/10.5194/bg-12-2207-2015.

Key, R.M., Kozyr, A., Sabine, C.L., Lee, K., Wanninkhof, R., Bullister, J.L., Feely, R.A., Millero, F.J., Mordy, C., Peng, T.-H., 2004. A global ocean carbon climatology: results from global data analysis project (GLODAP). Glob. Biogeochem. Cycles 18, GB4031. http://dx.doi.org/10.1029/2004GB002247.

King, A.L., Howard, W.R., 2003. Planktonic foraminiferal flux seasonality in subantarctic sediment traps: a test for paleoclimate reconstructions. Paleoceanography 18, 1019. http://dx.doi.org/10.1029/2002PA000839.

Klaas, C., 2001. Spring distribution of larger (> 64 μm) protozoans in the Atlantic sector of the southern ocean. Deep-Sea Res. I: Oceanogr. Res. Pap. 48, 1627–1649. http://dx.doi.org/10.1016/S0967-0637(00)00088-1.

Kohfeld, K.E., Quéré, C.L., Harrison, S.P., Anderson, R.F., 2005. Role of marine biology in glacial-interglacial CO_2 cycles. Science 308, 74–78. http://dx.doi.org/10.1126/science.1105375.

Korb, R.E., Whitehouse, M.J., Atkinson, A., Thorpe, S.E., 2008. Magnitude and maintenance of the phytoplankton bloom at South Georgia: a naturally iron-replete environment. Mar. Ecol. Prog. Ser. 368, 75–91. http://dx.doi.org/10.3354/meps07525.

Kuroyanagi, A., Kawahata, H., 2004. Vertical distribution of living planktonic foraminifera in the seas around Japan. Mar. Micropaleontol. 53, 173–196. http://dx.doi.org/10.1016/j.marmicro.2004.06.001.

Lochte, K., Ducklow, H.W., Fasham, M.J.R., Stienen, C., 1993. Plankton succession and carbon cycling at 47-degrees-N-20-degrees-W during the Jgofs north-Atlantic bloom experiment. Deep-Sea Res. II: Top. Stud. Oceanogr. 40, 91–114.

Lohmann, G.P., 1995. A model for variation in the chemistry of planktonic foraminifera due to secondary calcification and selective dissolution. Paleoceanography 10, 445–457. http://dx.doi.org/10.1029/95PA00059.

Lombard, F., Labeyrie, L., Michel, E., Bopp, L., Cortijo, E., Retailleau, S., Howa, H., Jorissen, F., 2011. Modelling planktic foraminifer growth and distribution using an ecophysiological multi-species approach. Biogeosciences 8, 853–873. http://dx.doi.org/10.5194/bg-8-853-2011.

Lombard, F., Labeyrie, L., Michel, E., Spero, H.J., Lea, D.W., 2009. Modelling the temperature dependent growth rates of planktic foraminifera. Mar. Micropaleontol. 70, 1–7. http://dx.doi.org/10.1016/j.marmicro.2008.09.004.

Mahowald, N.M., Muhs, D.R., Levis, S., Rasch, P.J., Yoshioka, M., Zender, C.S., Luo, C., 2006. Change in atmospheric mineral aerosols in response to climate: last glacial period, preindustrial, modern, and doubled carbon dioxide climates. J. Geophys. Res. Atmos. 111, D10202. http://dx.doi.org/10.1029/2005JD006653.

Margalef, R., 1978. Life-forms of phytoplankton as survival alternatives in an unstable environment. Oceanol. Acta 1, 493–509.

Marshall, B.J., Thunell, R.C., Henehan, M.J., Astor, Y., Wejnert, K.E., 2013. Planktonic foraminiferal area density as a proxy for carbonate ion concentration: a calibration study using the Cariaco basin ocean time series. Paleoceanography 28, 363–376. http://dx.doi.org/10.1002/palo.20034.

Martínez-Botí, M.A., Marino, G., Foster, G.L., Ziveri, P., Henehan, M.J., Rae, J.W.B., Mortyn, P.G., Vance, D., 2015. Boron isotope evidence for oceanic carbon dioxide leakage during the last deglaciation. Nature 518, 219–222. http://dx.doi.org/10.1038/nature14155.

Martínez-García, A., Sigman, D.M., Ren, H., Anderson, R.F., Straub, M., Hodell, D.A., Jaccard, S.L., Eglinton, T.I., Haug, G.H., 2014. Iron fertilization of the subantarctic ocean during the last ICE age. Science 343, 1347–1350. http://dx.doi.org/10.1126/science.1246848.

Martin, J.H., Gordon, R.M., Fitzwater, S.E., 1990. Iron in Antarctic waters. Nature 345, 156–158. http://dx.doi.org/10.1038/345156a0.

Matsumoto, K., Sarmiento, J.L., Brzezinski, M.A., 2002. Silicic acid leakage from the

southern ocean: a possible explanation for glacial atmospheric pCO₂. Glob. Biogeochem. Cycles 16. http://dx.doi.org/10.1029/2001GB001442.

Meilland, J., 2015. The Role of Planktonic foraminifera in the Marine Carbon Cycle at High Latitudes (Souther, Indian Ocean) (Ph.D Thesis). University of Angers, France.

McIntyre, A., Bé, A.W.H., Roche, M.B., 1970. Modern pacific coccolithophorida: a paleontological thermometer. Trans. N. Y. Acad. Sci. 32, 720–731. http://dx.doi.org/10.1111/j.2164-0947.1970.tb02746.x.

Minas, H.J., Minas, M., Packard, T.T., 1986. Productivity in upwelling areas deduced from hydrographic and chemical fields. Limnol. Oceanogr. 31, 1182–1206. http://dx.doi.org/10.4319/lo.1986.31.6.1182.

Minas, H., Minas, M., 1992. Net community production in High nutrient-low chlorophyll waters of the tropical and Antarctic oceans-grazing vs iron hypothesis. Oceanol. Acta 15, 145–162.

Mortyn, P.G., Charles, C.D., 2003. Planktonic foraminiferal depth habitat and δ18O calibrations: plankton TOW results from the Atlantic sector of the southern ocean. Paleoceanography 18, 1037. http://dx.doi.org/10.1029/2001PA000637.

Mosseri, J., Quéguiner, B., Armand, L., Cornet-Barthaux, V., 2008. Impact of iron on silicon utilization by diatoms in the southern ocean: a case study of Si/N cycle decoupling in a naturally iron-enriched area. Deep-Sea Res. II: Top. Stud. Oceangr. 55, 801–819. http://dx.doi.org/10.1016/j.dsr2.2007.12.003.

Movellan, A., Schiebel, R., Zubkov, M.V., Smyth, A., Howa, H., 2012. Protein biomass quantification of unbroken individual foraminifers using nano-spectro-photometry. Biogeosciences 9, 3613–3623. http://dx.doi.org/10.5194/bg-9-3613-2012.

Moy, A.D., Howard, W.R., Bray, S.G., Trull, T.W., 2009. Reduced calcification in modern southern ocean planktonic foraminifera. Nat. Geosci. 2, 276–280. http://dx.doi.org/10.1038/ngeo460.

Muggli, D.L., Harrison, P.J., 1997. Effects of iron on two oceanic phytoplankters grown in natural NE subarctic pacific seawater with no artificial chelators present. J. Exp. Mar. Biol. Ecol. 212, 225–237. http://dx.doi.org/10.1016/S0022-0981(96)02752-9.

Northcote, L.C., Neil, H.L., 2005. Seasonal variations in foraminiferal flux in the southern ocean, Campbell Plateau, New Zealand. Mar. Micropaleontol. 56, 122–137. http://dx.doi.org/10.1016/j.marmicro.2005.05.001.

Orr, J.C., Epitalon, J.-M., Gattuso, J.-P., 2015. Comparison of ten packages that compute ocean carbonate chemistry. Biogeosciences 12, 1483–1510. http://dx.doi.org/10.5194/bg-12-1483-2015.

Park, Y.-H., Charriaud, E., Pino, D.R., Jeandel, C., 1998. Seasonal and interannual variability of the mixed layer properties and steric height at station KERFIX, southwest of Kerguelen. J. Mar. Syst. 17, 571–586. http://dx.doi.org/10.1016/S0924-7963(98)00065-7.

Park, Y.-H., Durand, I., Kestenare, E., Rougier, G., Zhou, M., d'Ovidio, F., Cotté, C., Lee, J.-H., 2014. Polar Front around the Kerguelen Islands: An up-to-date determination and associated circulation of surface/subsurface waters. J. Geophys. Res.-Oceans 119, 6575–6592, http://dx.doi.org/10.1002/2014JC010061.

Park, Y.-H., Gamberoni, L., Charriaud, E., 1993. Frontal structure, water masses, and circulation in the Crozet basin. J. Geophys. Res. Oceans 98, 12361–12385. http://dx.doi.org/10.1029/93JC00938.

Park, Y.-H., Roquet, F., Durand, I., Fuda, J.-L., 2008. Large-scale circulation over and around the northern Kerguelen plateau. Deep Sea Res. II: Top. Stud. Oceangr. 55, 566–581. http://dx.doi.org/10.1016/j.dsr2.2007.12.030.

Planquette, H., Statham, P.J., Fones, G.R., Charette, M.A., Moore, C.M., Salter, I., Nédélec, F.H., Taylor, S.L., French, M., Baker, A.R., Mahowald, N., Jickells, T.D., 2007. Dissolved iron in the vicinity of the Crozet Islands, Southern Ocean. Deep Sea Res. II: Top. Stud. Oceangr. 54, 1999–2019. http://dx.doi.org/10.1016/j.dsr2.2007.06.019.

Pollard, R., Lucas, M., Read, J., 2002. Physical controls on biogeochemical zonation in the southern ocean. Deep Sea Res. II: Top. Stud. Oceangr. 49, 3289–3305. http://dx.doi.org/10.1016/S0967-0645(02)00084-X.

Pollard, R., Sanders, R., Lucas, M., Statham, P., 2007. The Crozet natural iron bloom and export experiment (CROZEX). Deep-Sea Res. II: Top. Stud. Oceangr. 54, 1905–1914. http://dx.doi.org/10.1016/j.dsr2.2007.07.023.

Pollard, R.T., Venables, H.J., Read, J.F., Allen, J.T., 2007. Large-scale circulation around the Crozet plateau controls an annual phytoplankton bloom in the Crozet basin. Deep Sea Res. II: Top. Stud. Oceangr. 54, 1915–1929. http://dx.doi.org/10.1016/j.dsr2.2007.06.012.

Quéguiner, B., 2013. Iron fertilization and the structure of planktonic communities in high nutrient regions of the southern ocean. Deep-Sea Res. II: Top. Stud. Oceangr. 90, 43–54. http://dx.doi.org/10.1016/j.dsr2.2012.07.024.

Rembauville, M., Blain, S., Armand, L., Quéguiner, B., Salter, I., 2015a. Export fluxes in a naturally iron-fertilized area of the southern ocean – Part 2: importance of diatom resting spores and faecal pellets for export. Biogeosciences 12, 3171–3195. http://dx.doi.org/10.5194/bg-12-3171-2015.

Rembauville, M., Salter, I., Leblond, N., Gueneugues, A., Blain, S., 2015b. Export fluxes in a naturally iron-fertilized area of the southern ocean – Part 1: seasonal dynamics of particulate organic carbon export from a moored sediment trap. Biogeosciences 12, 3153–3170. http://dx.doi.org/10.5194/bg-12-3153-2015.

Reynolds, R.W., Smith, T.M., Liu, C., Chelton, D.B., Casey, K.S., Schlax, M.G., 2007. Daily high-resolution-blended analyses for SEA surface temperature. J. Clim. 20, 5473–5496. http://dx.doi.org/10.1175/2007JCLI1824.1.

Robinson, R.S., Sigman, D.M., DiFiore, P.J., Rohde, M.M., Mashiotta, T.A., Lea, D.W., 2005. Diatom-bound 15N/14N: new support for enhanced nutrient consumption in the ICE age subantarctic. Paleoceanography 20, PA3003. http://dx.doi.org/10.1029/2004PA001114.

Saavedra-Pellitero, M., Baumann, K.-H., Flores, J.-A., Gersonde, R., 2014.

Biogeographic distribution of living coccolithophores in the pacific sector of the southern ocean. Mar. Micropaleontol. 109, 1–20. http://dx.doi.org/10.1016/j.marmicro.2014.03.003.

Sadeghi, A., Dinter, T., Vountas, M., Taylor, B., Altenburg-Soppa, M., Bracher, A., 2012. Remote sensing of coccolithophore blooms in selected oceanic regions using the phytoDOAS method applied to hyper-spectral satellite data. Biogeosciences 9, 2127–2143. http://dx.doi.org/10.5194/bg-9-2127-2012.

Salter, I., Kemp, A.E.S., Moore, C.M., Lampitt, R.S., Wolff, G.A., Holtvoeth, J., 2012. Diatom resting spore ecology drives enhanced carbon export from a naturally iron-fertilized bloom in the southern ocean. Glob. Biogeochem. Cycles 26, GB1014. http://dx.doi.org/10.1029/2010GB003977.

Salter, I., Schiebel, R., Ziveri, P., Movellan, A., Lampitt, R., Wolff, G.A., 2014. Carbonate counter pump stimulated by natural iron fertilization in the polar frontal zone. Nat. Geosci. 7, 885–889. http://dx.doi.org/10.1038/ngeo2285.

Sarmiento, J.L., Dunne, J., Gnanadesikan, A., Key, R.M., Matsumoto, K., Slater, R., 2002. A new estimate of the CaCO₃ to organic carbon export ratio. Glob. Biogeochem. Cycles 16, 1107. http://dx.doi.org/10.1029/2002GB001919.

Sarmiento, J.L., Toggweiler, J.R., Najjar, R., Webb, D.J., Jenkins, W.J., Wunsch, C., Elderfield, H., Whitfield, M., Minster, J.-F., 1988. Ocean carbon-cycle dynamics and atmospheric CO₂ [and discussion]. Philos. Trans. R. Soc. Lond. Math. Phys. Eng. Sci. 325, 3–21. http://dx.doi.org/10.1098/rsta.1988.0039.

Schiebel, R., 2002. Planktic foraminiferal sedimentation and the marine calcite budget. Glob. Biogeochem. Cycles 16, 1065. http://dx.doi.org/10.1029/2001GB001459.

Schiebel, R., Bijma, J., Hemleben, C., 1997. Population dynamics of the planktic foraminifer globigerina bulloides from the eastern north Atlantic. Deep-Sea Res. I: Oceanogr. Res. Pap. 44, 1701–1713. http://dx.doi.org/10.1016/S0967-0637(97)00036-8.

Schiebel, R., Brupbacher, U., Schmidtko, S., Nausch, G., Waniek, J.J., Thierstein, H.-R., 2011. Spring coccolithophore production and dispersion in the temperate eastern north Atlantic ocean. J. Geophys. Res. Oceans 116, C08030. http://dx.doi.org/10.1029/2010JC006841.

Schiebel, R., Waniek, J., Bork, M., Hemleben, C., 2001. Planktic foraminiferal production stimulated by chlorophyll redistribution and entrainment of nutrients. Deep-Sea Res. I: Oceanogr. Res. Pap. 48, 721–740. http://dx.doi.org/10.1016/S0967-0637(00)00065-0.

Schmidt, D.N., Thierstein, H.R., Bollmann, J., Schiebel, R., 2004. Abiotic forcing of plankton evolution in the Cenozoic. Science 303, 207–210. http://dx.doi.org/10.1126/science.1090592.

Sigman, D.M., Boyle, E.A., 2000. Glacial/interglacial variations in atmospheric carbon dioxide. Nature 407, 859–869. http://dx.doi.org/10.1038/35038000.

Smetacek, V.S., 1985. Role of sinking in diatom life-history cycles: ecological, evolutionary and geological significance. Mar. Biol. 84, 239–251. http://dx.doi.org/10.1007/BF00392493.

Stoll, H.M., Ziveri, P., Shimizu, N., Conte, M., Theroux, S., 2007. Relationship between coccolith Sr/CA ratios and coccolithophore production and export in the Arabian Sea and sargasso Sea. Deep-Sea Res. Part II Top. Stud. Oceangr. 54, 581–600. http://dx.doi.org/10.1016/j.dsr2.2007.01.003, The Role of Marine Organic Carbon and Calcite Fluxes in Driving Global Climate Change, Past and Future.

Strzepek, R.F., Hunter, K.A., Frew, R.D., Harrison, P.J., Boyd, P.W., 2012. Iron-light interactions differ in southern ocean phytoplankton. Limnol. Oceanogr. 57, 1182–1200. http://dx.doi.org/10.4319/lo.2012.57.4.1182.

Sunda, W.G., Huntsman, S.A., 1995. Iron uptake and growth limitation in oceanic and coastal phytoplankton. Mar. Chem. 50, 189–206. http://dx.doi.org/10.1016/0304-4203(95)00035-P, The Chemistry of Iron in Seawater and its Interaction with Phytoplankton.

Tarling, G.A., Ward, P., Atkinson, A., Collins, M.A., Murphy, E.J., 2012. DISCOVERY 2010: spatial and temporal variability in a dynamic polar ecosystem. Deep-Sea Res. II: Top. Stud. Oceangr. 59–60, 1–13. http://dx.doi.org/10.1016/j.dsr2.2011.10.001.

Thunell, R., Pride, C., Ziveri, P., Muller-Karger, F., Sancetta, C., Murray, D., 1996. Plankton response to physical forcing in the gulf of California. J. Plankton Res. 18, 2017–2026. http://dx.doi.org/10.1093/plankt/18.11.2017.

Townsend, D.W., Keller, M.D., Holligan, P.M., Ackleson, S.G., Balch, W.M., 1994. Blooms of the coccolithophore Emiliania huxleyi with respect to hydrography in the gulf of Maine. Cont. Shelf Res. 14, 979–1000. http://dx.doi.org/10.1016/0278-4343(94)90060-4.

Trull, T.W., Bray, S.G., Manganini, S.J., Honjo, S., François, R., 2001. Moored sediment trap measurements of carbon export in the subantarctic and polar frontal zones of the southern ocean, south of Australia. J. Geophys. Res. Oceans 106, 31489–31509. http://dx.doi.org/10.1029/2000JC000308.

Tyrrell, T., Merico, A., 2004. Emiliania huxleyi: bloom observations and the conditions that induce them. In: Thierstein, P.D.H.R., Young, D.J.R. (Eds.), Coccolithophores. Springer, Berlin, Heidelberg, pp. 75–97.

Volk, T., Hoffert, M.I., 1985. Ocean carbon pumps: analysis of relative strengths and efficiencies in ocean-driven atmospheric CO₂ changes. In: Sundquist, E.T., Broecker, W.S. (Eds.), Geophysical Monograph SeriesAmerican Geophysical Union, Washington, D.C, pp. 99–110.

L., von Bertalanffy, 1960. Principles and theory of growth, in: Fundamental Aspects of Normal and Malignant Growth. Norwinksi, D.D.

Weiner, A.K.M., Weinkauf, M.F.G., Kurasawa, A., Darling, K.F., Kucera, M., 2015. Genetic and morphometric evidence for parallel evolution of the Globigerinella calida morphotype. Mar. Micropaleontol. 114, 19–35. http://dx.doi.org/10.1016/j.marmicro.2014.10.003.

Weinkauf, M.F.G., Moller, T., Koch, M.C., Kučera, M., 2013. Calcification intensity in

planktonic Foraminifera reflects ambient conditions irrespective of environmental stress. Biogeosciences 10, 6639–6655. http://dx.doi.org/10.5194/bg-10-6639-2013.

Winter, A., Henderiks, J., Beaufort, L., Rickaby, R.E.M., Brown, C.W., 2014. Poleward expansion of the coccolithophore Emiliania huxleyi. J. Plankton Res. 36, 316–325. http://dx.doi.org/10.1093/plankt/fbt110.

Zeebe, R.E., 2012. History of seawater carbonate chemistry, atmospheric CO_2, and ocean acidification. Annu. Rev. Earth Planet. Sci. 40, 141–165. http://dx.doi.org/10.1146/annurev-earth-042711-105521.

Ziveri, P., Broerse, A.T.C., van Hinte, J.E., Westbroek, P., Honjo, S., 2000. The fate of coccoliths at 48°N 21°W, Northeastern Atlantic. Deep-Sea Res. II: Top. Stud. Oceangr. 47, 1853–1875. http://dx.doi.org/10.1016/S0967-0645(00)00009-6.

Ziveri, P., de Bernardi, B., Baumann, K.-H., Stoll, H.M., Mortyn, P.G., 2007. Sinking of coccolith carbonate and potential contribution to organic carbon ballasting in the deep ocean. Deep-Sea Res. II: Top. Stud. Oceanogr. 54, 659–675. http://dx.doi.org/10.1016/j.dsr2.2007.01.006, The Role of Marine Organic Carbon and Calcite Fluxes in Driving Global Climate Change, Past and Future.

Ziveri, P., Thunell, R.C., 2000. Coccolithophore export production in Guaymas basin, gulf of California: response to climate forcing. Deep-Sea Res. II: Top. Stud. Oceangr. 47, 2073–2100. http://dx.doi.org/10.1016/S0967-0645(00)00017-5.

Ziveri, P., Thunell, R.C., Rio, D., 1995. Export production of coccolithophores in an upwelling region: results from San Pedro basin, southern California borderlands. Mar. Micropaleontol. 24, 335–358. http://dx.doi.org/10.1016/0377-8398(94)00017-H.

5 | Conclusions and perspectives

Contents

5.1   General conclusion

5.1.1   Synthesis of the main results

Pioneering work synthesizing export data at global scale (Armstrong et al., 2002; Klaas and Archer, 2002; Francois et al., 2002), followed by more recent studies including numerical estimation of primary production (Honjo et al., 2008; Henson et al., 2012) have converged towards a common scheme of the biological pump functioning (Fig. 5.2a). However, the mechanisms underpinning such function, and more specifically the impact of ecological processes have been poorly characterized to date. During this PhD, I have studied how plankton community influences particulate matter export in environments of contrasting productivity in the Southern Ocean. This section summarizes the main findings and compares them with previous conclusions from the literature (Fig. 5.2b.)

On the contribution of diatoms and faecal pellets to export fluxes
It is widely accepted that diatoms are efficient vectors for carbon export out of the mixed layer (Smetacek, 1985; Michaels and Silver, 1988; Boyd and Newton, 1995). It was observed from both shallow (300 m, Kerguelen) and deep (1500-2000 m, South Georgia) sediment trap deployments in diatom-dominated ecosystems that vegetative diatoms are predominantly exported as empty frustules, leading to low PE_{eff} and T_{eff}. Therefore, diatom vegetative stages do not appear to efficiently transport carbon to the deep Southern Ocean. Conversely, resting spores contribute significantly to diatom-mediated carbon export, and their increasing relative contribution with depth suggests a high T_{eff}. Furthermore, during a summer survey, a dominance of *Chaetoceros Hyalochaete* resting spores to POC stocks at 250 m over the central Kerguelen Plateau further supported its key role in exporting carbon from the mixed layer to the mesopelagic ocean.

The relationship between the fraction of empty diatom and the BSi:POC ratio found at Kerguelen confirms that diatom ecology significantly impacts the preferential export of silicon and carbon (Smetacek et al., 2004; Assmy et al., 2013). Additionally, consistent patterns arise from the comparison of full and empty diatom species exported at Kerguelen and South Georgia (Fig. 5.1). In both island systems a high relative abundance of preferentially empty cells of *Fragilariopsis kerguelensis* and *Thalassionema nitzschioides* are observed, highlighting these species as preferential "silica sinkers". Conversely, *Chaetoceros Hyalochaete* resting spores (CRS) and *Thalassiosira antarctica* resting spores (TRS) are exported as full cells in productive environments (P3 and A3) and strongly contribute to POC export. Between these two end members, certain species were exported with moderate relative abundance (∼1 %), such as *Navicula directa* and *Thalassiothrix antarctica* show an empty:full ratio increasing with the sampling depth (300 m at A3, 2000 m at P2). Massive deposition of *T. antarctica* in marine sediments suggested that this large di-

atom may strongly contribute to carbon export during intense "fall dump" events (Kemp et al., 2000, 2006). However, if the cell carbon is quickly remineralized during its sinking through the mesopelagic ocean (leading to an increase in the empty:full cell ratio), then the contribution of this species to carbon export may be limited. The statistical approach used at the KERFIX HNLC site also identifies CRS, *Eucampia antarctica*, *Navicula directa*, *Pseudo-nitzschia* spp. and *Thalassiothrix antarctica* as species positively associated with POC export. Although this approach is not quantitative, this cluster is consistent with other observations from the SAZ and PFZ South of Tasmania (Rigual-Hernández et al., 2015b). The role of these species on POC export might be valid in both HNLC and naturally-fertilized productive areas.
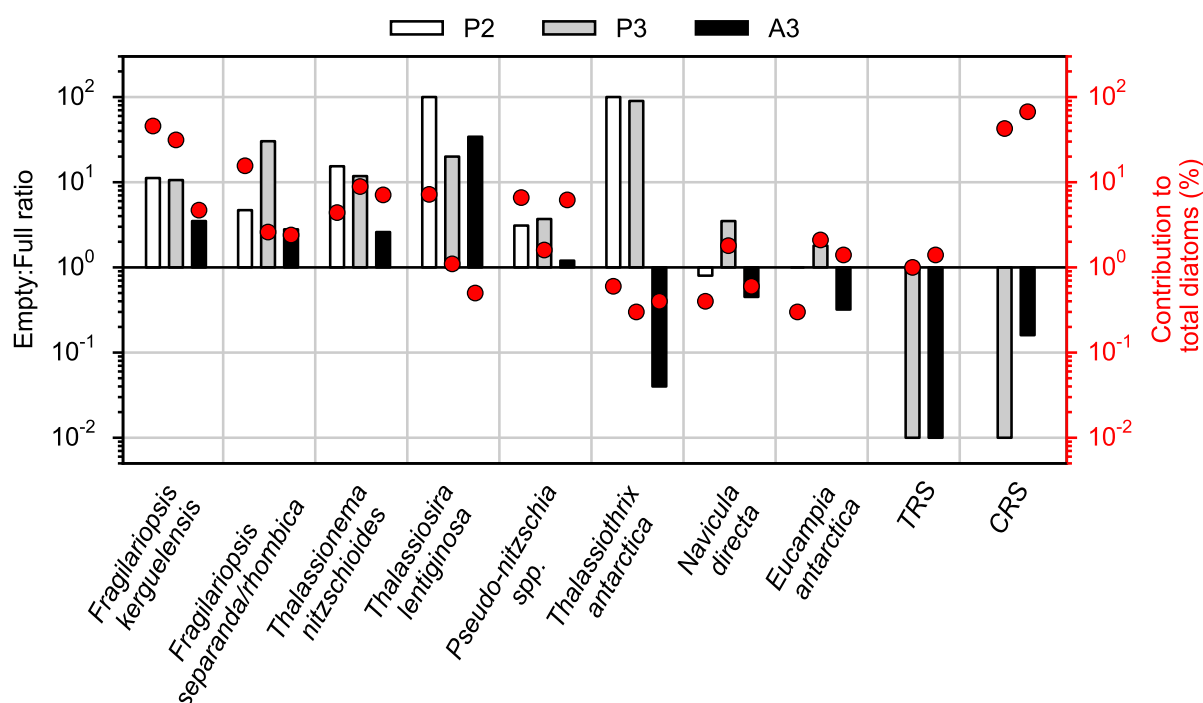
Figure 5.1: Annually integrated empty:full ratio (bars, left axis) and total (full + empty) relative abundance (red dots, right axis) of major diatom taxa exported at South Georgia (P2 - low productivity, P3 - high productivity) and Kerguelen (A3 - high productivity). CRS: *Chaetoceros Hyalochaete* resting spore, TRS: *Thalassiosira antarctica* resting spore.
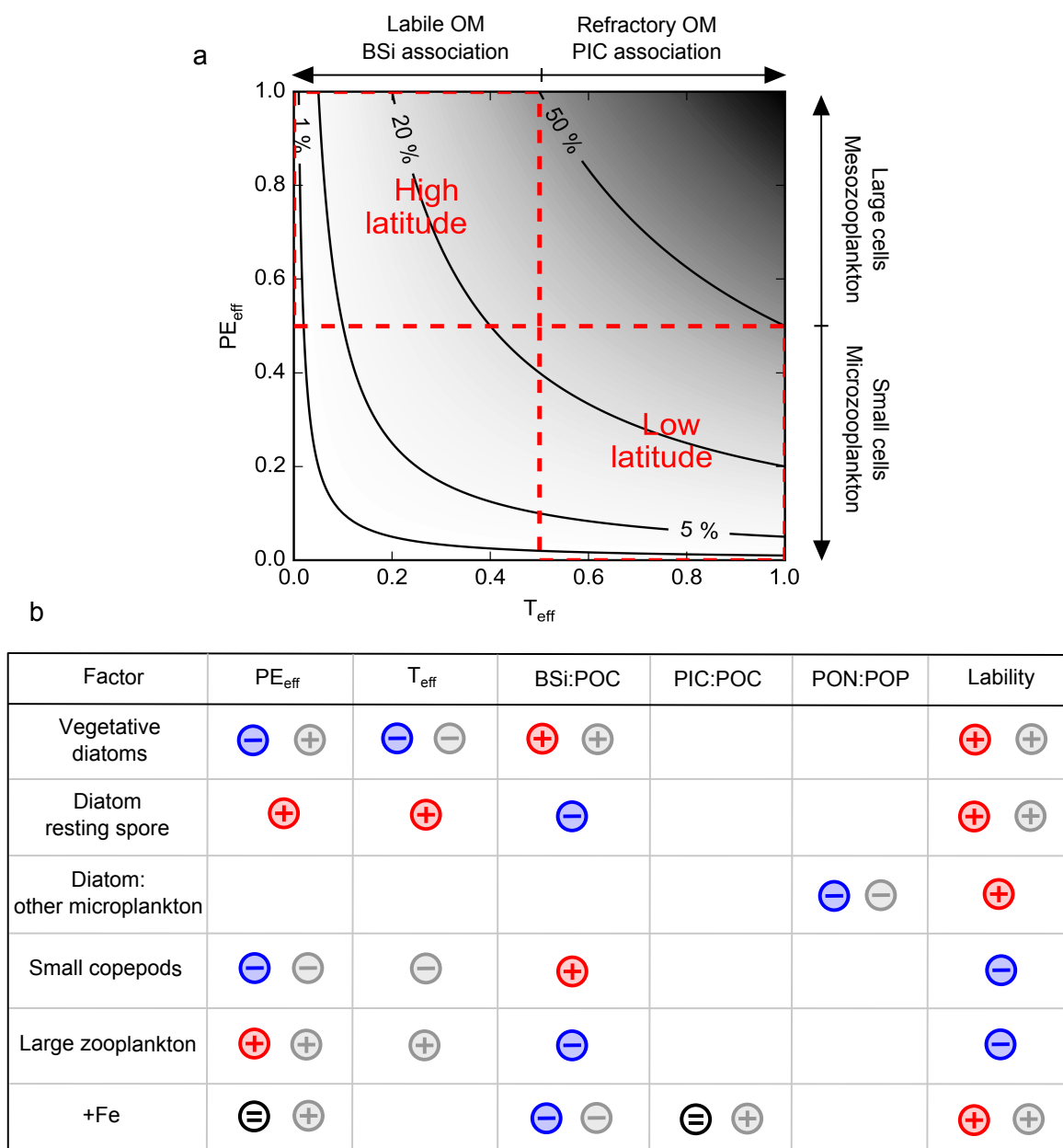
Figure 5.2: **a.** Summary of the relationship between ecosystem structure and the functionning of the biological pump from the literature. Isolines and grey scale represent the biological pump efficiency (fraction of net primary production exported). **b.** Table synthesizing the main results obtained during the PhD (coloured symbols). Positive relationships shown in red, negative in blue, no effect in black. Grey symbols represent the relationships suggested by the literature.

The enumeration and measurement of faecal pellets exported at Kerguelen, coupled with the description of zooplankton communities during KEOPS1 and KEOPS2 allow an estimation of the potential influence of zooplankton groups on export. The highest BSi:POC ratio, associated with the lowest POC export, is observed in spring when faecal pellets are mostly represented by small spherical shapes and the zooplankton community is dominated by small calanoid copepods (e.g. *Oithona*, Carlotti et al., 2015). This is consistent with the essential role of small copepods in recycling carbon within the mixed layer through feeding on suspended particles and coprophagy (Gonzalez and Smetacek, 1994; Iversen and Poulsen, 2007), leading to low PE$_{eff}$ (Lam and Bishop, 2007). Conversely, faecal material from large zooplankton (large copepods, euphausiids, salps) dominates the autumn and winter export and drives a substantial fraction of annual POC export (∼30% at Kerguelen). This is also in good agreement with previous findings suggesting that large zooplankton is a major contributor to faecal pellet-driven export because of the strong and fast-sinking faecal pellets they produce (Lebrato and Jones, 2009; Wilson et al., 2013; Smith et al., 2014; Cavan et al., 2015). At South Georgia, the contribution of diatoms to carbon flux is 46 % and 2% in the productive and HNLC sites, respectively. This indicates that non-diatom components, and possibly faecal pellets, are important vectors for carbon export at greater (>1500 m) depths (Wilson et al., 2008; Manno et al., 2015). The high abundance of sterols in the exported organic matter at this site when compared to Kerguelen and Crozet also supports an important role of zooplankton in organic matter export.

On plankton diversity and particulate matter stoichiometry and lability
During a summer survey, we observe that diatom biomass relative to that of dinoflagellates drives most of the variability in PON:POP ratio. This is consistent with previous findings from culture experiments (Ho et al., 2003; Quigg et al., 2003) and is a potential factor explaining the latitudinal pattern of the PON:POP ratio at global scale (Martiny et al., 2013a). Additionally, Si:C uncoupling was observed to occur in transition layers of the AAZ through two mechanisms: (1) the accumulation of empty diatom frustules (dominated by *F. kerguelensis*) within this interface and (2) high vertical silicic acid diffusive fluxes likely to sustain silicification despite very low primary production at these depths (∼100 m).

The 2-4 fold increase in labile lipids (unsaturated fatty acids) in the naturally-fertilized sites compared to the HNLC sites is attributed to the dominance of diatom, and more specifically resting spores, in the export fluxes. These findings corroborate previous results restricted to Crozet (Wolff et al., 2011). Diatoms accumulate palmitoleic acid during resting spore formation, and their efficient transfer to the seafloor is likely to deliver this energy-rich compound to the deep-sea benthic communities. The HNLC sites display a higher relative abundance of sterols accumulated in zooplankton faecal pellets. At station

A3, the coupled description of biological export vectors and lipid composition of export fluxes demonstrates that ecological processes (e.g. resting spore formation, seasonal shifts in zooplankton community composition) strongly affect the lability of the exported organic matter. Thus, ecological processes not only impact the magnitude and Si:C stoichiometry of the biological pump but also constrain the lability of export with potentially important implications for the energy flow to the deep ocean (Ruhl and Smith, 2004; Ruhl et al., 2008).

On natural iron fertilization and the carbon pumps

The comparison of the three naturally fertilized island systems of South Georgia, Crozet, and Kerguelen (Fig 5.3) lead to several conclusions concerning the relative impact of natural iron fertilization on the biological pump and carbonate counter pump. The biological pump intensity is 1.5 to 2.5 times higher in the naturally fertilized waters compared to the HNLC waters. However, in the productive sites, POC fluxes remain low ($< 100\,\mathrm{mmol\,m^{-2}\,yr^{-1}}$) regardless of the depth considered (289 - 2000 m). The difference in POC export between the HNLC and productive sites is mostly explained by the late summer export of diatom resting spores. At Kerguelen, the fraction of NCP exiting the mixed layer is low (<2 %) and similar in the HNLC (KERFIX) and productive (A3) waters. These results suggests that natural iron fertilization increases the production and export of organic matter (Blain et al., 2007; Pollard et al., 2009; Manno et al., 2015) but that it does not increase the efficiency of the biological pump (i. e. it does not increase the fraction of NCP exported). However, iron fertilization has a significant impact on the chemical composition of the exported organic matter with a 2-4 fold increase in the fraction of labile lipids (energy-rich unsaturated fatty acids). Thus the effect of iron fertilization is not restricted to the cycling of major elements, but also shapes the energy supply to the deep sea communities.

Contrary to what was observed at Crozet by Salter et al. (2014), the carbonate flux is very low in the naturally fertilized waters downstream of Kerguelen, leading to a weak carbonate counter pump (4.7-5.3 % of POC export). This is due to a much lower contribution by foraminifer to the carbonate flux, most of it (85 %) being attributed to a moderate bloom of *Emiliania huxleyi*. Although the composition of the calcifying plankton in the HNLC KERFIX sediment trap is not available, the annual PIC export appears similar to what is observed at A3. Therefore natural iron fertilization does not lead to a stronger carbonate counter pump South of the Polar Front. This phenomenon appears to be explained by a difference in the community structure of calcifying organisms. South of the Polar Front, a lower abundance of cold water foraminifer species with lower size-normalized test weight (SNW) is observed. Conversely, north of the Polar front, higher abundances of cold water and temperate foraminifer species (Salter et al., 2014) with higher SNW respond to the increased food availability driven by natural iron-fertilization.
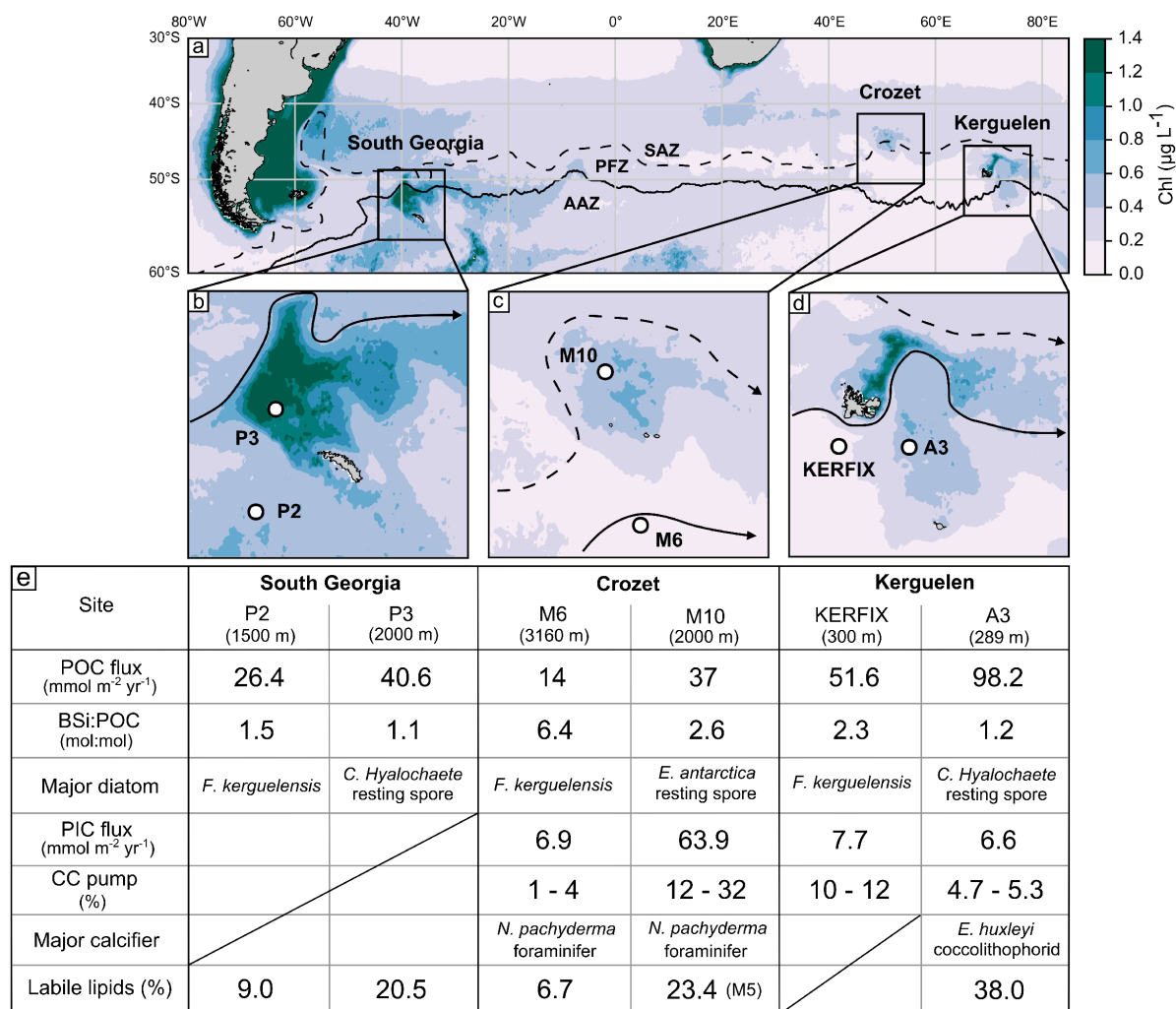
Figure 5.3: **a.** Climatology of surface chlorophyll *a* concentration in the Southern Ocean (MODIS aqua full mission), dashed and continuous lines represent the Subantarctic and Polar Front, respectively (Sallée et al., 2008). SAZ: Subantarctic Zone, PFZ: Polar Frontal Zone, AAZ: Antarctic Zone. **b.- d.** Detailed view of annual sediment trap deployments in the vicinity of island systems. **e.** Table summarizing the biogeochemical fluxes and major plankton groups from sediment trap deployments. Crozet data from Salter et al. (2012, 2014) and Wolff et al. (2011). Labile lipids are the sum of unsaturated fatty acids.

5.1.2   Implications

Diatoms as a paleoproxy for carbon and silicon export

Numerous studies have used the modern analogue technique to reconstruct the past water hydrology based on diatom taxa distribution in sediment cores (e.g. Leventer et al., 1993; Zielinski and Gersonde, 1997; Crosta et al., 1998; Ferry et al., 2015). This methodology was applied on sediment trap samples and diatom frustules have been used as indicators of carbon export (Grigorov et al., 2014; Rigual-Hernández et al., 2015b). At South Georgia, it was demonstrated that the composition of the diatom community is deeply modified from the mixed layer to the sediments. Moreover, the majority of diatom taxa were exported as empty frustules and therefore did not contribute significantly to POC export. Therefore associating increased diatom frustule fluxes in sediment traps, or diatom accumulation rates in sediments, to increased POC export is not straightforward. In line with these findings, a recent study demonstrated that an increase in diatom accumulation rate is not necessarily coupled with an increase in primary production or export efficiency over geological time scales (Lopes et al., 2015). It is suggested that a more precise consideration of diatom species/groups is necessary in light of their distinct role on carbon or silicon export. Additionally, although the micropaleontological counting technique is used for sediments samples, the comparative analysis of methods conducted in the present thesis (Appendix 2) suggests that a biological counting technique, coupled with efficient preservative in sediment trap samples, is better adapted to understand the relative contribution of diatom taxa to carbon export.

> *Our results discount the importance of temperature as a sole control of carbon remineralization and illustrate dominant ecosystem control of carbon export.* - (Lopes et al., 2015).

Based on suggestions by Smetacek et al. (2004) and Assmy et al. (2013) the present work links the empty:full ratio of diatom export assemblages to the BSi:POC stoichiometry of the biological pump. However, in the present study these conclusions are based on statistical techniques that address co-occurrence. Consequently they do not provide a quantitative framework between diatom taxa and BSi export. Relationships between cell volume and silica content have been proposed (Conley et al., 1989). Using such allometric relationships would in theory allow one to partition BSi fluxes among the main diatom species and confirm their respective role as preferential silica sinker. However, more recent studies demonstrate that an interplay of factors such as salinity (Vrieling et al., 1999), iron (Takeda, 1998; Hutchins and Bruland, 1998) and silicic acid availability (Jungandreas et al., 2012) influences the silica content of the frustule at the species level. Fixed allometric relationships do not take into account such variability. To overcome this issue, modern techniques such as synchrotron X-ray fluorescence or Fourier transform infrared

spectroscopy (FTIR) provide the possibility to derive the silica and carbon content of diatoms at the cellular level in heterogenous samples (Jungandreas et al., 2012; Sackett et al., 2014; Twining et al., 2014). A quantitative representation of how species composition and phenotypic plasticity impacts the export and preservation of silicon throughout the water column would further increase our mechanistic understanding of the ecological processes regulating silicon trapping in the Southern Ocean (Chase et al., 2015).

Oceanic carbon pumps during the last glacial maximum

Based on sedimentary records in the ACC, Abelmann et al. (2006) suggested that extensive blooms of spore-forming diatoms in naturally iron-fertilized waters of the Southern Ocean during the last glacial maximum (LGM) may have driven a more intense organic carbon burial. The authors concluded their study by highlighting "*the need for longer-term, species-oriented, in situ iron fertilization experiments to further validate proxies and test hypotheses linking biogeochemical and ecological processes*". The regional studies of naturally iron-fertilized blooms presented in this thesis have made significant progress in quantifying the role of diatom resting spores for POC export. However, one must be cautious in extending this conclusion to the Southern Ocean during glacial times. The environmental factors favouring spore-forming species, and the triggers for resting spore formation in the field are still poorly characterized.

Higher iron deposition leading to a more efficient biological pump in the Southern Ocean has been commonly evoked to contribute to the lower atmospheric pCO$_2$ during the LGM (Martin, 1990; Sigman and Boyle, 2000). The efficiency of iron fertilization is usually quantified as the ratio of net CO$_2$ drawdown to iron input (de Baar et al., 2005), assuming that CO$_2$ drawdown reflects net community production (NCP) and that NCP is close to export production under steady state conditions (Eppley and Peterson, 1979). At Kerguelen, we report that the fraction of seasonal NCP exported as POC is similar in iron-fertilized and HNLC waters. A recent study based on paleo-oceanographic data reports lower export efficiency during the LGM resulting from an uncoupling between primary production and export efficiency (Lopes et al., 2015). This study adds to a growing body of evidence demonstrating that the relationship between iron availability, primary production and POC export is not straightforward (Lam et al., 2011; Jacquet et al., 2011; Maiti et al., 2013; Cavan et al., 2015; Laurenceau-Cornec et al., 2015a). It seems that although iron increases primary production, ecosystem structure is the ultimate factor imposing the efficiency of the carbon transfer to the seafloor. More sediment trap deployments coupled with estimations of seasonal NCP in a variety of Southern Ocean environments are still required to effectively evaluate the uncoupling and evaluate ecological factors responsible for flux attenuation.

Natural iron fertilization south of the Polar Front does not appear to enhance the carbonate counter pump to the same degree as in the Polar Frontal Zone. We describe

an important shift in calcifying plankton community composition is observed when crossing the Polar Front, with a dominance of coccolithophore contribution to PIC export in the AAZ. This leads to a lower PIC export resulting in a lower carbonate counter-pump compared to the PFZ. Numerous biotic and abiotic factors were evoked to explain the 80 ppmv difference in pCO_2 partial pressure between the pre-industrial area and the LGM (Archer et al., 2000a; Sigman and Boyle, 2000), and biology itself is thought to account for less than 50 % in this process (Kohfeld et al., 2005). Paleo-oceanographic records suggest a 5° northward shift of the ACC fronts during the LGM (Francois et al., 1997; Gersonde et al., 2003). In this context, a lower carbonate counter pump at the Southern Ocean scale due to an extended AAZ may have impacted the atmospheric pCO_2.

Where does the carbon go ?

The imbalance between NCP and export in the Southern Ocean have already been reported during artificial iron fertilization experiments (Martin et al., 2013), and a recent study came to the same conclusion in the naturally-fertilized waters of the Western Antarctic Peninsula (Stukel et al., 2015). Numerous studies have used on-going measurements of oxygen isotopes and/or O_2/Ar to derive NCP and the associated export in the Southern Ocean (Cassar et al., 2011; Jonsson et al., 2013; Chang et al., 2014). Our results at Kerguelen suggest a strong uncoupling between NCP and POC export. If such uncoupling is commonly evoked (Hamme et al., 2012; Jonsson et al., 2013; Estapa et al., 2015), the ecological factors responsible for it are not determined. Emerson (2014) proposed that the export due to vertical migration of motile organisms was enough to close the carbon budget in low latitude ecosystems. In the Southern Ocean, the significant biomass of predators (fishes, birds, marine mammals) is likely to play a role in the carbon budget (Huntley et al., 1991; Banse, 1995) but is not considered as part of the "community" in NCP estimates made by biogeochemists. For example, top predator carbon consumption at Kerguelen is estimated to be 1.6×10^6 $mol\,yr^{-1}$ (Guinet et al., 1996). Assuming that predation occurs in the phytoplankton bloom area ($\sim 45\,000\,km^2$), the mean carbon consumption by top predators is $0.36\,mol\,m^{-2}\,yr^{-1}$. Although important uncertainties are associated with this calculation, it represents a notable fraction of the annual net air-sea CO_2 flux estimated at $\sim 1\,mol\,m^{-2}\,yr^{-1}$ (Blain, pers. comm.).

Taking into account carbon transfer to higher trophic levels is therefore a new challenge to fully understand the carbon cycle in the Southern Ocean. The main limits are the estimation of the higher trophic levels biomass and feeding strategies (Guinet et al., 1996; Murphy et al., 2012). Studies combining biogeochemical data on production and export, coupled with higher trophic levels biomass estimation (from hydroacoustic to marine mammals) and identification of food web structure (stable isotopes, lipids) may help to better understand end-to-end carbon pathways.

The scientific value of sediment trap deployments

Most of the long term moored sediment trap (MST) deployments in the Southern Ocean occurred during the JGOFS period (1990-2000, Fig. 5.4) and contributed to increase our understanding of the functioning of the biological pump (Boyd and Trull, 2007; Honjo et al., 2008). The deployment of a MST is logistically complex and expensive, and not all the moorings are easily retrieved. Moreover, the development of chemical and optical proxies of export may have contributed to the decrease in long term MST deployments in the Southern Ocean over the last two decades (Fig. 5.4). Long time series (several decades) of biogeochemical properties are needed to detect significant trends possibly associated to climate change, and the Southern Ocean is particularly poorly covered by long term observatories (Henson, 2014; Henson et al., 2016). Short term estimates of export with proxies cannot document long term changes. In this context, long term deployments of MST, although associated with many uncertainties in the efficiency of flux collection, appear as the only available tool to document a change in export fluxes (Salter et al., 2010; Nodder et al., 2016) and understand the driving biological mechanisms. The decrease in MST deployments in the Southern Ocean challenges our ability to document and understand future changes in export fluxes.
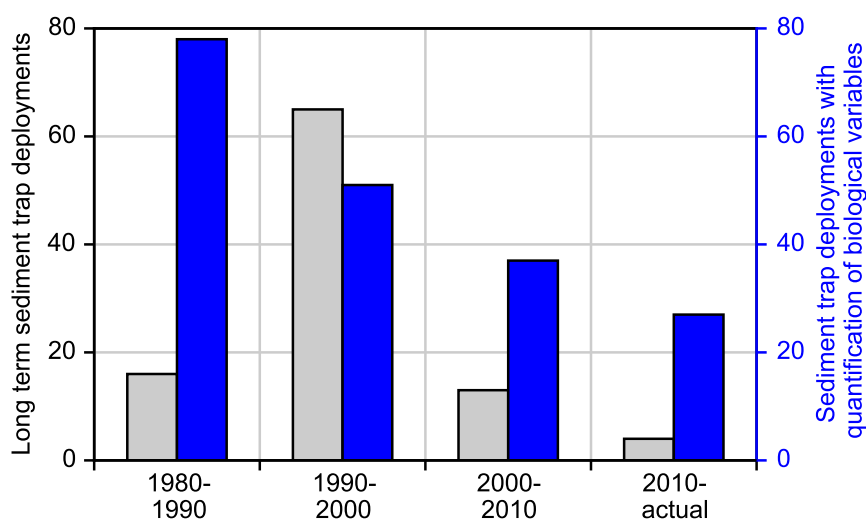
Figure 5.4: History of sediment trap deployments in the Southern Ocean (South of 40°S). Grey bars represent the number of long term (>250 days) sediment trap deployments per decade in the Southern Ocean. Blue bars represent the number of short- and long-term sediment trap deployments in which a biological variable (e.g. diatom, faecal pellet, calcifying plankton) was quantified. Multiple sediment traps on the same mooring were considered as independent deployments.

Three decades ago, sediment traps were used to document temporal and vertical variability in diatom assemblages in the seasonal ice zone (Leventer and Dunbar, 1987). The present manuscript emphasizes the importance to take into account the biological components of export fluxes to understand their magnitude and stoichiometry. A recent

study have statistically linked mixed layer plankton community structure (derived from DNA sequencing) to export at 150 m (derived from an optical proxy), although authors suggested that the correlation between the two did not imply causal relationship (Guidi et al., 2016). To date, sediment traps remain the only tools able to quantitatively attribute fluxes to biological components. There is a constant decrease in the quantification of biological variables in sediment trap samples in the Southern Ocean (Fig. 5.4). Given the strong uncertainties still existing on the intensity of the biological pump at global scale and the associated biological processes (Burd et al., 2010; Henson et al., 2012), it appears important to adopt a coupled chemical and biological approach in future sediment trap studies.

5.2 Perspectives

5.2.1 Quantifying other variables in sediment trap samples

The present manuscript focused on the biological components regulating the export of major elements (C, N, Si). The quantification of particulate trace metal export, and more specifically iron, is necessary to fully understand the cycle of these major elements. Several studies have reported particulate iron (PFe) fluxes in the Southern Ocean in the context of natural or artificial fertilization (Frew et al., 2006; Bowie et al., 2009; Planquette et al., 2011; Ellwood et al., 2014). These fluxes have been derived from short term sediment trap deployments and thus do not allow one to describe PFe export over a complete seasonal cycle. For example, at station A3 during KEOPS2, the PFe export flux in spring was far greater than the dissolved Fe supply (Bowie et al., 2015). Using a similar approach as for major elements, a coupled description of biological vectors and export of trace elements using a moored sediment trap would greatly aid our understanding of their cycling at seasonal and annual scale. As part of the SOCLIM project (`www.soclim.com`), a moored sediment trap dedicated to quantifying the export of trace metals will be deployed at station A3 from October to March 2016.

Diatoms and faecal pellets can be identified and enumerated with relatively simple optical tools. However, other components of the microbial food web such as bacteria are important actors in the biological pump attenuating the organic carbon flux. Only a few studies have reported the bacterial communities associated with sinking particles during short term sediment trap deployments (Röske et al., 2008; LeCleir et al., 2014; Fontanez et al., 2015). No preservatives were used in the sediment trap samples, the 16S RNA gene was sequenced and sequences were assigned to bacterial taxa. Fontanez et al. (2015) reported that specific bacterial lineages were associated with eukaryotic organisms, suggesting that particle flux composition might constrain the diversity, and probably activity, of heterotrophic bacteria.

Assigning sequences to operational taxonomic units (OTU) is poorly quantitative and provides prokaryotic community structure as a relative contribution to total identified sequences. Alternatively, catalyzed reported deposition - fluorescent in situ hybridization (CARD-FISH) allows identification of targeted bacterial taxa in the particles (Sekar et al., 2003; Orsi et al., 2015; Thiele et al., 2015). Multiple CARD-FISH performed on the same particle using different probes can provide information on the preferential association of bacterial groups with particle types (Fig. 5.5). However, only the cells on the surface of the particle can be enumerated, probably biasing the view of the total bacterial community. Additionally, autofluorescence of phytoplanktonic cells present in particles render the quantification of labelled bacterial cells difficult. Although the multiple CARD-FISH protocol is functional (Fig. 5.5), it clearly needs to be adapted to the study of parti-

cles containing phytoplanktonic cells. For example, fluorochromes emitting in different wavelength than phytoplanktonic pigments could be used.
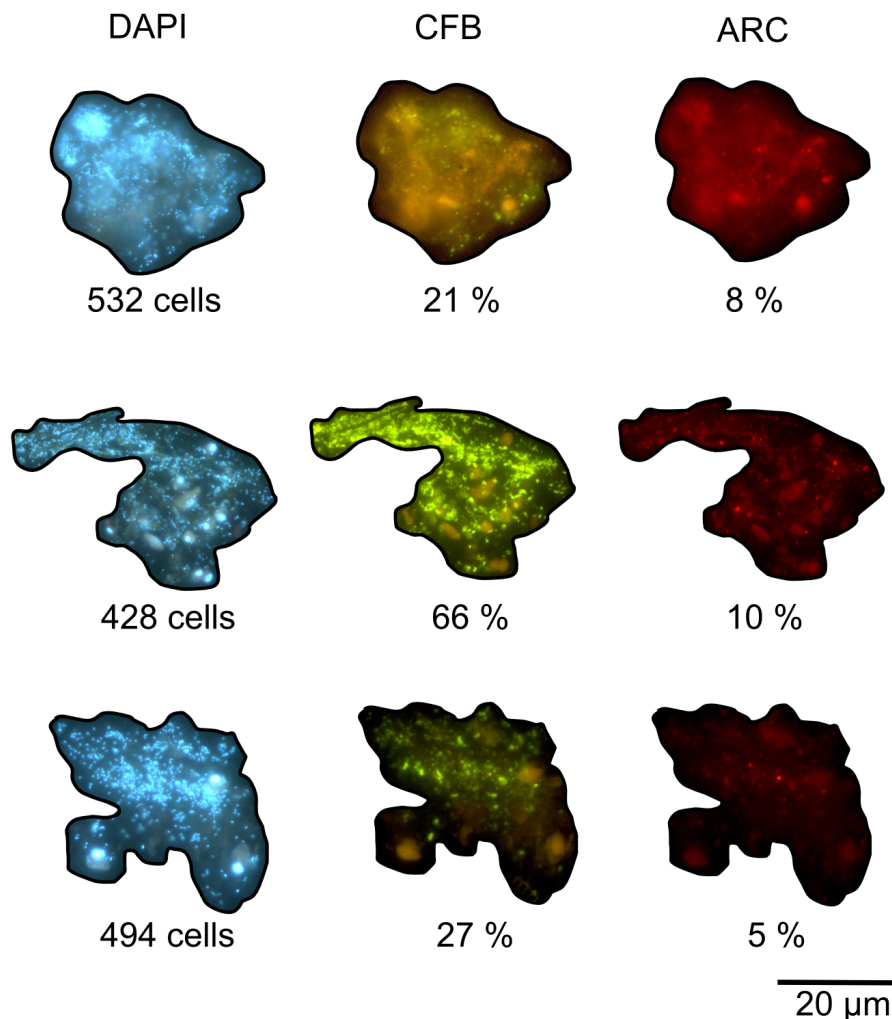
Figure 5.5: Examples of double CARD-FISH performed on sediment trap samples collected over the central Kerguelen Plateau. On each particle, total bacterial cells are stained with DAPI in blue, Cytophaga-Flavobacterium-Bacteroides (CFB) in green, and Archae (ARC) in red.

5.2.2 The bio-optical approach: example in the vicinity of Kerguelen

Sediment trap deployments provide valuable time series of the chemical and biological components of export. However, the coarse temporal resolution (cup collection period of several days to month) does not allow the study of short events such as resting spore formation (articles 2 and 4). Moreover, the findings are extrapolated over large areas, neglecting the spatial variability at small scale due to hydrodynamics and/or patchiness in the distribution of biological constituents of the ocean. The recent development of autonomous oceanographic platforms (profiling floats, gliders) equipped with bio-optical
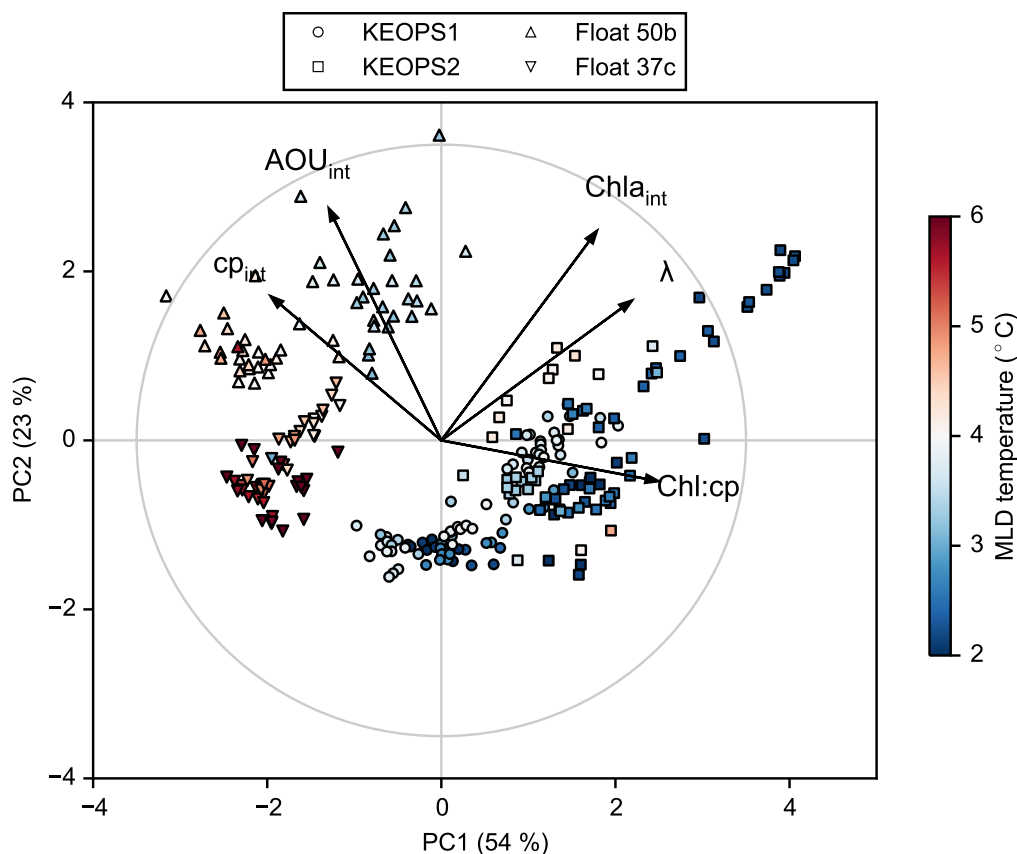
Figure 5.6: Projection on the first two axes of a principal component analysis (PCA) of the CTD- and bio-argo float derived variables collected in the vicinity of the Kerguelen Plateau. The marker of the profile projection refers to the platform (cruises or floats) and the color refers to the mean temperature within the mixed layer depth (MLD).

sensors opens up new perspectives for the study of biogeochemical cycles with a high spatial and temporal resolution (Johnson et al., 2009; Claustre et al., 2010). Several examples of direct applications have been given in section 1.3.3. More specifically, the perspective of autonomous observation in the Southern Ocean is particularly relevant since meteorological conditions and sea-ice strongly restrict research cruises to spring and summer periods (Meredith et al., 2013). For example, first deployments of autonomous bio-optical platforms in the SAZ have developed our understanding of processes regulating the spring bloom initiation (Thomalla et al., 2015).

Here I present a first attempt at scaling the relative importance of mesozooplankton and microbial communities in attenuating the particle stock with depth over a seasonal cycle (Figure A.6). The methods are fully described in **Appendix 3**. The association of λ (a metric for POC stock attenuation with increasing isopycnals) with the $Chl : c_p$ ratio highlights a stronger attenuation in spring when particles are dominated by algal biomass. Two principal factors can be responsible for particle stock attenuation: (1) an intense heterotrophic microbial respiration in response to an increase in labile organic carbon availability (Obernosterer et al., 2008) and (2) an efficient consumption and retention of

carbon within the mixed layer by zooplankton (Smetacek et al., 2004; Lam and Bishop, 2007). Intense microbial heterotrophic activity would lead to an increase in the oxygen utilisation. However, AOU_{int} (apparent oxygen utilization integrated between the MLD and 300 m) is not associated with λ, suggesting that microbial activity is not the dominant process in the relatively cold waters in spring. During KEOPS2, a negative relationship was observed between zooplankton biomass and the carbon export efficiency (Laurenceau-Cornec et al., 2015a). Moreover, the diatom communities exported at 300 m in spring were strictly dominated by empty frustules (Rembauville et al., 2015a), an indication of intense grazing activity (Smetacek et al., 2004; Assmy et al., 2013). We select the hyopthesis of enhanced grazing activity in response to a high fraction of algal biomass to total particles in spring to explain the important stock attenuation. This supports the functioning of the productive Kerguelen Plateau as a high biomass, low export regime (Lam and Bishop, 2007; Lam et al., 2011). In Autumn, the $c_{p\ int}$ is highest but the $Chl : c_p$ is low. This indicates that the total particle abundance is important but contains a low fraction of algal biomass. The important AOU_{int} may result from intense heterotrophic microbial remineralization of this mainly detrital organic matter pool in warmer waters.

As part of the SOCLIM project, multiple CTD casts and bio-argo float deployments will take place in October 2016 and March 2017 in both the HNLC and productive waters around Kerguelen. A coupled description of the bio-optical properties and phytoplankton community (from cytometry to microplankton taxonomy, including biovolume calculation to derive contributions to total POC) and the associated particulate stoichiometry (POC/PON/POP/PIC/BSi) will help to build quantitative relationships between the bio-optical signals and the structure of the planktonic ecosystem. These relationships will be specific to the considered region and will then be used to interpret signals provided by the autonomous instruments over longer time scales.

5.2.3   The modelling approach: taking into account resting spore formation

Articles 2 and 4 highlight the importance of resting spore formation for the export of carbon out of the mixed layer in naturally fertilized areas around Kerguelen and South Georgia. Consistent with the observations made around the Crozet Plateau (Salter et al., 2012), these results suggest that an accurate description of export cannot be made in these productive areas without taking into account diatom life cycles. Several global circulation/biogeochemical coupled models have been used to study the biological pump at global scale (Bopp et al., 2005; Lima et al., 2014; Henson et al., 2014). Although these models may include several plankton functional types (Le Quéré et al., 2005), the export of particulate matter is mainly driven by its association with minerals, following the "ballast hypothesis", and/or aggregation. The aim of this section is to build a very
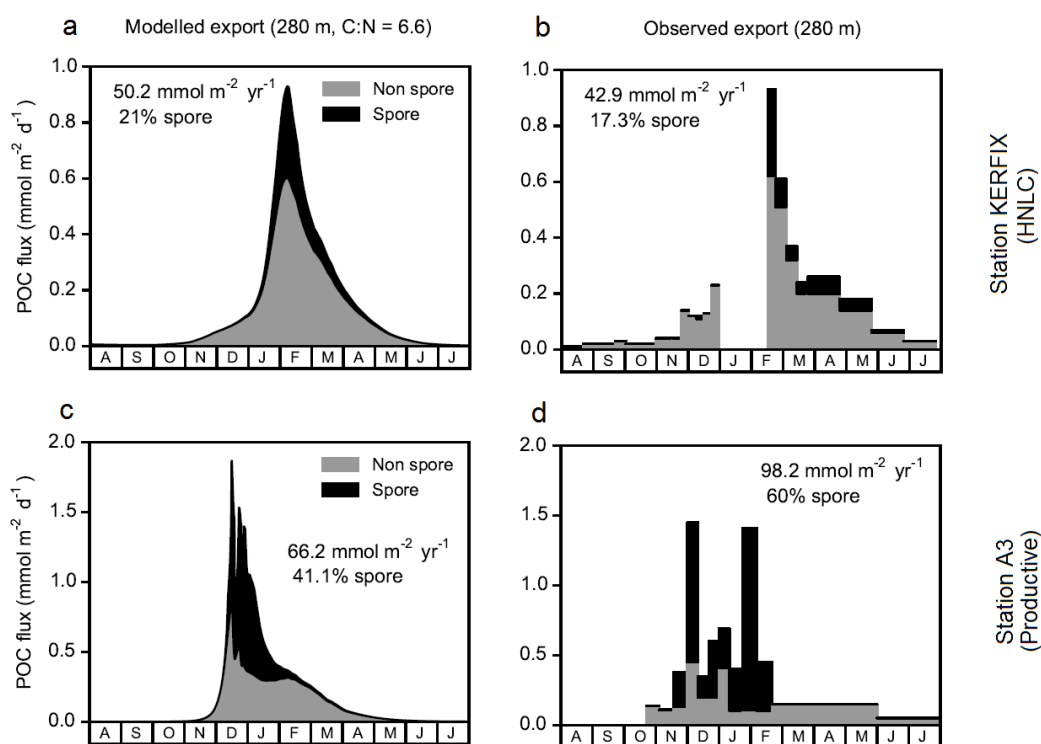
Figure 5.7: Comparison of the observed (right pannels) and modelled (left pannels) export at stations KERFIX (top pannels) and A3 (bottom pannels). Black area denotes carbon export attributed to diatom resting spore.

simple mixed layer NPZD model and test formulations for resting spore formation. The model is then used in environments of contrasted iron availability (A3 and KERFIX) and compared to observations of export. The model structure, parametrization, physical forcing and results are fully described in **Appendix 4**.

A simple formulation for resting spore formation appears efficient in reproducing the resting spore contribution to carbon export in terms of both amplitude and seasonality (Figure 5.7). In article 4, it was suggested that diatom resting spores had a very high T_{eff} (their relative contribution to the total diatom assemblage increases with depth). The resting spore formation strategy is generally associated with neritic diatom populations (McQuoid and Hobson, 1996). However, the sedimentary distribution of *Chaetoceros Hyalochaete* resting spores in the Southern Ocean suggests that the export of resting spores is not restricted to neritic areas (Crosta et al., 1997). The widespread resting spore sedimentary distribution might be due to advection and dilution of a coastal signal by the circumpolar current. Under this hypothesis, it only contributes to the biological pump in the location where the bloom of the vegetative stages occurs. Conversely, if this distribution results from the very efficient transfer of resting spores from the surface waters where spore-forming diatoms do not dominate the diatom community (such as the HNLC waters), then it is a key aspect of the biological pump even in areas remote from the shelf.

To answer this question, two complementary approaches can be adopted. Firstly, by increasing the coupled description of the chemical and biological composition of export fluxes in the ocean, together with an autonomous observation of the mixed layer processes. This will increase our understanding of *in situ* triggering factors for resting spore formation. Secondly, by including resting spore formation in a biogeochemical-circulation coupled model to scale its importance in the biological pump at global scale. High abundances of *Eucampia antarctica* and *Chaetoceros Hyalocahete* resting stages are found in sediment cores during the LGM in the Atlantic sector of the Southern Ocean (Abelmann et al., 2006; Jacot Des Combes et al., 2008). A global biogeochemical/circulation model including resting spores during the LGM would allow us to test if the increase in diatom resting spores have influenced the intensity or efficiency of the biological pump, contributing to lower atmospheric $p\mathrm{CO_2}$. Finally, if it is proved that the mechanisms of resting spore formation have a significant impact on atmospheric $p\mathrm{CO_2}$, then its response to climate change have to be taken into account to assess the future role of the Southern Ocean as a carbon sink (Bopp et al., 2005; Wang and Moore, 2012; Hauck et al., 2015).

A | Appendices
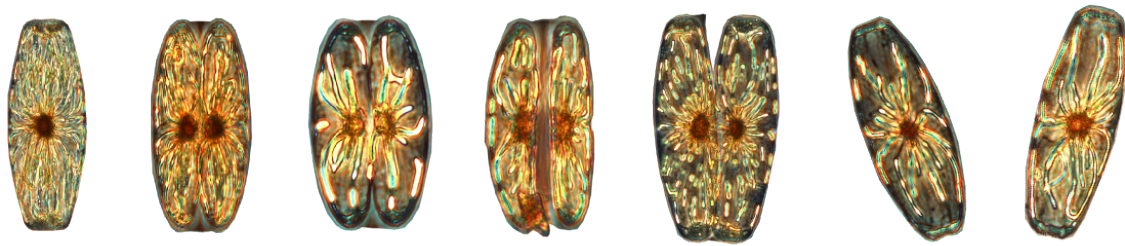
A.1 Comparison of the kinetic and triple extraction methods for the BSi measurement

Methods

Four samples from a sediment trap deployment over the central Kerguelen Plateau (Rembauville et al., 2015a) were used to compare the kinetic (DeMaster, 1981) and triple extraction (Ragueneau et al., 2005) methods for biogenic silicon (BSi) quantification. Sample cups corresponding to high fluxes (cup 4 and 9), moderate flux (cup 8) and low flux (cup 11) were selected.

For the kinetic method, 2-5 mg of freeze-dried material was weighed and placed in centrifuge tubes with $40\,\text{mL}$ of ultrapure sodium hydroxide (NaOH, 0.2 N). The samples were placed in a water bath at $95\,°\text{C}$ and $200\,\mu\text{L}$ of solution were removed after 1, 2, 3 and 4 h, placed into scintillation vials and made up to $10\,\text{mL}$ with milli-Q water. The BSi content was determined by fitting a linear regression to silicic acid concentration as a function of extraction time. The intercept of this relationship is the BSi content corrected for lithogenic silica leaching (DeMaster, 1981).

For the triple extraction method, 2-5 mg of freeze-dried material were weighed and placed into centrifuge tubes. $4\,\text{mL}$ of ultrapure sodium hydroxide (NaOH, 0.2 N) were added and samples were placed in a water bath at $95\,°\text{C}$ for 45 minutes. Samples were then immediately placed in ice and $1\,\text{mL}$ of hydrochloric acid (HCl, 1 N) was added to to stop the reaction and neutralise the pH. Samples were centrifuged (3000 rpm, 10 minutes) and two aliquots of $500\,\mu\text{L}$ were withdrawn for the measurement of dissolved silicon and aluminium ($[\text{Si}]_1$ and $[\text{Al}]_1$). Samples were then rinsed by adding $12\,\text{mL}$ of milli-Q water, vortexing, centrifuging, and withdrawing $12\,\text{mL}$ of the supernatant. This step was repeated 3 times. Samples were then dried at $60\,°\text{C}$ overnight. A second leaching was performed (similar to the first extraction) to obtain $[\text{Si}]_2$ and $[\text{Al}]_2$. After a rinsing and drying procedure, a third extraction for the determination of lithogenic silicon (LSi) was performed by adding $0.2\,\text{mL}$ of hydrofluoric acid (HF, 2.9 N). Samples were left at room temperature for 48h before $9.8\,\text{mL}$ of boric acid (H_3BO_3, saturated, $60\,\text{g\,L}^{-1}$) was added to stop the reaction. This solution was used for the determination of $[\text{Si}]_3$.

For both methods, Si(OH)_4 resulting from NaOH extractions was measured automatically on a Skalar 5100 autoanalyzer whereas Si(OH)_4 resulting from HF extraction was measured manually on a Milton Roy Spectronic 401 spectrophotometer. Si(OH)_4 analyses were performed colorimetrically following Aminot and Kerouel (2007). Standards for the analysis of samples from the HF extraction were prepared in an $\text{HF/H}_3\text{BO}_3$, matrix, ensuring the use of an appropriate calibration factor that differs from Milli-Q water. Aluminum concentrations were measured by spectrophotometry (Howard et al., 1986). The BSi content of the sediment ($\mu\text{mol\,mg}^{-1}$) was calculated assuming all the BSi was digested

during the first leaching, and corrected for the LSi leaching using the Al/Si ratio from the second extraction (Ragueneau et al., 2005):

$$BSi = \left([Si]_1 V_1 - \frac{[Si]_2}{[Al]_2} \times [Al]_1 V_1 \right) \times \frac{1}{m} \qquad \text{(A.1)}$$

The LSi content (result not shown here) was calculated by summing the contribution of the three extractions:

$$LSi = \left(\frac{[Si]_2}{[Al]_2} \times [Al]_1 V_1 + [Si]_2 V_2 + [Si]_3 V_3 \right) \times \frac{1}{m} \qquad \text{(A.2)}$$

Where V_i is the extraction volume of step i and m is the mass of freeze-dried sediment used for the extraction. Both techniques were performed in triplicates.
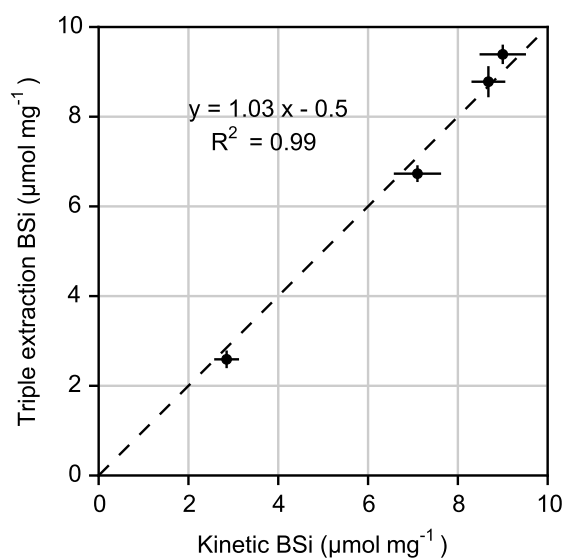
Figure A.1: Comparision of two BSi quantification methods used in this manuscript. Kinetic method from DeMaster (1981), triple extraction from Ragueneau et al. (2005). Circles and errorbars are respectively the mean and standard deviation from triplicates measurements.

Result and discussion

The two methods showed a very good agreement with a highly linear relation ($R^2 = 0.99$) very close to the 1:1 relationship (Fig. A.1). Therefore, studies using different methods can be compared such as in **article 2** and **article 3**. However, the kinetic method produced a higher standard error (range 4.0-8.8 %, mean 6.4 %) compared to the triple extraction procedure (range 2.0-6.4 %, mean 3.6 %). The estimation of the BSi in the triple extraction procedure depends on the quality of the linear fitting of silicon extracted along time (the intercept being the BSi content). The uncertainty on the silicon content from each extraction time may impact the quality of the fit and lead to a dispersion on

the intercept between the triplicates. However, the average standard error from the four samples remains <10 %.

The mean standard error from the triple extraction method is lower. This method appears more precise but takes more time: the kinetic extraction can be performed in one day, the triple extraction procedure takes at least 3 days. Moreover, if the BSi content of the sample is high (which is the case for exported particles in the Southern Ocean), some BSi may remain in the sample after the first NaOH extraction step, which can be diagnosed from a very high $[Si]_2:[Al]_2$ ratio (see **article 2**). To overcome this issue, a longer extraction time can be used for the first NaOH extraction step, although the choice of the duration is somewhat subjective. Another solution is to use a lower quantity of freeze-dried material ($\sim$1 mg), which requires a high precision balance. Finally, a characteristic crustal Si:Al ratio (e.g. Taylor and McClennan, 1986) can be used to correct for the LSi contribution to the first extraction step. This method has been previously used to correct for the lithogenic origin of various elements (Cardinal et al., 2001; Trull et al., 2001).

In conclusion, the triple extraction procedure appears more precise (lower standard error) than the kinetic method. However, the kinetic method is faster and does not require the measurement of aluminium, which is an important consideration when dealing with large sample numbers (e.g. Mosseri et al., 2005). Finally, if the triple extraction procedure is chosen, an appropriate initial sample mass must be used in order to digest the entirety of the BSi during the first NaOH extraction step.

A.2 Comparison of the micropaleontological and biological techniques for diatom enumeration

Introduction

The enumeration of diatoms from raw sediment trap samples can be performed with two different techniques. A micropaleontological technique, originally developed for marine sediments, has been used since the early sediment trap studies (Gersonde and Wefer, 1987) and is still widely used (Rigual-Hernández et al., 2015a). This technique is based on the oxidation of organic matter and dissolution of the carbonate phase in order to facilitate the observation of the siliceous microfossils (Funkhouser and Evitt, 1959). To assess the contribution of each diatom taxa to carbon export, it is necessary to make the distinction between the cells exported as empty frustules and full cells with clearly identifiable organelles (Rembauville et al., 2015a). The micropaleontological technique eliminates the organic material and therefore prevents the identification of taxa contributing to carbon export. Alternative to the micropaleontological technique, a biological technique developed to study live plankton communities can be used (Salter et al., 2007, 2012). This simple method consists in the dilution of the original sample and its subsequent observation with a microscope. This method has proven to be efficient to document the contribution of diatom taxa to carbon export (**articles 2 and 4**). A comparison between the two methods is necessary to describe their advantages and drawbacks and estimate if they provide comparable results.

Methods

We compared the two methods on samples coming from two sediment trap deployments in the productive environments of Kerguelen (**article 2**) and South Georgia (**article 4**). We selected 12 samples from each sediment trap deployment including periods of low, moderate and high export fluxes.

For the biological technique, samples from $1/8^{th}$ aliquots were gently homogenised and $2\,mL$ were diluted in a final volume of $20\,mL$ of artificial seawater (S=34). $1\,mL$ of this diluted solution was placed in a Sedgewick Rafter counting chamber (Pyser-SGI S52) for the microscopic observation.

For the micropaleontological technique, samples were first oxidized following the methodology used in Romero et al. (1999). Samples from $1/8^{th}$ aliquots were centrifuged (1800 rpm, 8 minutes) and their volume reduced to $30\,mL$. Samples were then transferred into a $500\,mL$ beaker and settled for $24\,h$. The supernatant was withdrawn to a final volume of $10\,mL$. Then $10\,mL$ of potassium permanganate ($KMnO_4$, $65\,g\,L^{-1}$) were added and samples were left for oxidation at room temperature for $24\,h$. Beakers were then placed in a $95\,°C$ water bath and $50\,mL$ of hydrochloric acid (HCl, 37%) was added to dissolve

the carbonate phase during 15 minutes. Then 40 mL of hydrogen peroxide (H_2O_2, 35 %) were added for 15 minutes. Beakers were removed from the water bath and 20 mL of milli-Q water was added. Sampled were let to settle for 24 h at room temperature. The supernatant was removed and the resulting 10 mL were placed in centrifuge tubes and made up to 50 mL with milli-Q water. In order to reach a close-to-neutral pH, several steps of centrifugation (1800 rpm, 8 minutes) and rinsing (supernatant withdrawn and replaced with milli-Q water) were performed until the pH of the sample reached that of the milli-Q water.

The preparation of slides for the microscopic observation was performed following the random settling method outlined by Bárcena and Abrantes (1998). A slide cover glass was placed in the center of petri dishes (6 cm diameter) and 0.5 to 1.5 mL of the oxidized sample (depending on the abundance of material) was placed on the cover glass. The petri dish was then filled with milli-Q water using random movements of the squeeze bottle. Samples were left to settle and evaporate for several days until the petri dish was perfectly dry. The cover glass was then retrieved with tweezers and glued on glass slides with optical glue (Norland NOA 61) and dried with UV light. Slides were prepared in triplicates.

The counting chamber and the slides were observed under an inverted microscope with phase contrast (Olympus IX70) at respectively 400 and 1000X magnification. Pictures were acquired with an Olympyus DP71 camera. In both cases a minimum of 400 diatoms were counted. Diatom species were identified following Hasle and Syvertsen (1997). For the biological technique, diatom valve flux (F, valve $m^{-2}\,d^{-1}$) was calculated as follows:

$$F = 2 \times n \times f \times d \times 8 \times V \times \frac{1}{D \times t} \tag{A.3}$$

Where n is the number of cells counted (1 cell = two valves), f is the fraction of the counting chamber that was observed (1/4 to 1/2 depending on the diatom abundance), d is the dilution factor from the original $1/8^{th}$ split (here 10), 8 is the number of splits, V is the volume of the split (mL), D is the diameter of the trap ($0.125\,m^2$ for the technicap PPS3 trap at Kerguelen, $0.5\,m^2$ for the McLane Parflux trap at South Georgia) and t is the collection time for the sample cup (days).

For the micropaleontological technique, diatom valve flux was calculated as follow:

$$F = n \times 8 \times \frac{A}{a} \times \frac{V}{v} \times \frac{1}{D \times t} \tag{A.4}$$

Where A is the area of the petri dish, a is the area of the field observed with the microscope, v is the volume used in the random settling step (0.5 to 1.5 mL). The area a is calculated by multiplying the number of field of view by the area of one field of view at a given magnification (calibrated with a graduated reticule).

Results

Qualitative comparison

Pictures of diatoms from both methods are shown in Figure A.2. The oxidation and slide preparation technique allowed observations at higher magnification in the case of the micropaleontologic technique. This facilitated the detailed observation of diatom frustule characteristics, such as aerolations and processes (e.g. for *Thalassiosira* species, Fig. A.2a-c.). Detailed observations ensured a precise taxonomic description. Because the high temperature oxidation separates the two frustules, all diatoms were observed as individual valves (e. g. *Eucampia antarctica* var. *antacrtica* and *Fragilariopsis kerguelensis*, Fig. A.2d-e). Large and long diatoms (e.g. *Proboscia, Rhizosolenia*) were absent as entire frustules but observed as damaged small fractions, only recognizable when the apex fraction was kept intact (e.g. *Proboscia inermis*, Fig. A.2f). Finally, no entire cells of *Dactyliosolen antarcticus* could be observed, but rather numerous girdle bands (Fig. A.2g).

In the case of the biological technique, the lower magnification and the presence of organic material sometimes obscuring the valve made the taxonomic identification more difficult and less detailed. For example, *Fragilariopsis separanda* and *F. rhombica* were difficult to differentiate.It was also the case for *Pseudo-nitzschia lineola* and *P-N. heimii*. However, the two valves of the frustule were present is the vast majority of the cases, and the difference between the empty and full cells can clearly be made (Fig. A.2h-k). The formation of resting spore by *Thalassisoira antarctica* could be observed (Fig. A.2i). Long and large diatoms were intact (Fig. A.2n-o), and chains were also frequently observed (Fig. A.2h,i,p). This ensures the sample preparation procedures did not damage the natural assemblage of diatom cells.

Quantitative comparison

A highly significant correlation existed between the total valve flux calculated from the two techniques (Pearson's correlation test, $p<0.01$). The values were close to the 1:1 relationship, although for the lowest fluxes (10^5-10^6 valve$\,$m$^{-2}\,$d^{-1}), values from the micropaleontological where higher than for the biological technique (Fig. A.3a).

In order to estimate if the two techniques provided homogeneous results for different diatom species, fluxes were grouped by genera. Two metrics were used to estimate (1) if the techniques provided similar absolute valve fluxes within samples (i.e. do both techniques provide a similar seasonality for a given genera?) and (2) if some genera were more represented in one technique compared to the other (asymmetry between techniques). In the first case, the Pearson correlation coefficient (r) was calculated on the absolute valve flux (n=24). In the second case, the asymmetry was estimated by calculating the ratio of the total valve flux summed among all samples (valve$\,$m^{-2}) from one technique over the
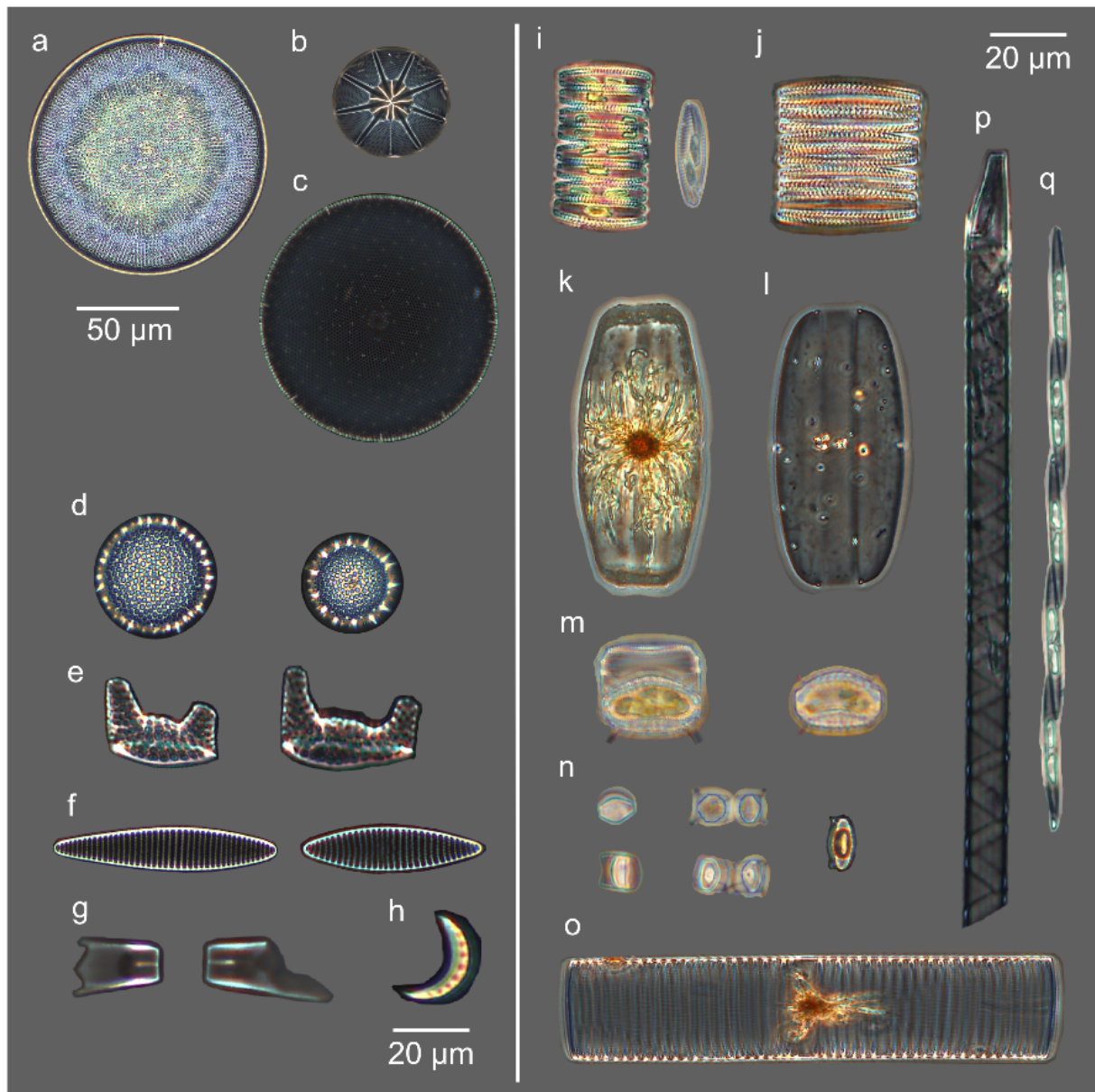
Figure A.2:   Left panel: diatom pictures from slides prepared with the micropaleontological technique. **a.** *Thalassiosira lentiginosa*, **b.** Asteromphalus hookeri, **c.** *Thalassiosira tumida*, **d.** *Thalassiosira antarctica* resting spore, **e.** *Eucampia antarctica* var. *antarctica*, **f.** *Fragilariopsis kerguelensis*, **g.** apex of *Proboscia inermis*, **h.** girdle band of *Dactyliosolen antarcticus*.

Right panel: diatom pictures from samples prepared with the biological technique. **i.** chain of full *F. kerguelensis* cells, **j.** chain of empty *F. kerguelensis* cells, **k.** full *Membraneis* sp. cell, **l.** empty *Membraneis* sp. cell, **m.** *T. antarctica* resting spores, **n.** *Chaetoceros Hyalochaete* resting spores, **o.** full *D. antarcticus* cell (cytoplasm concentrated around the nucleus), **p.** empty *P. inermis* cell, **q.** chain of full *Pseudo-nitzschia heimii* cells.

other. An asymmetry of 10 means the genera is ten times more abundant in the biological technique compared to the micropaleontological one.

The following genera/group displayed low absolute asymmetry and highly significant correlation of absolute valve flux: *Thalassiosira antarctica* resting spore, *Chaetoceros Hyalochaete* resting spore, *Fragilariopsis*, *Thalassionema nitzscioides*, *Thalassiosira* and *Asteromphalus*. Conversely, some genera were poorly correlated and associated to a strong asymmetry with a higher representation with the biological technique compared to the micropaleontological one. This was notably the case of *Corethron*, *Pseudo-nitzschia*, *Pleurosigma*, *Thalassiothrix*, *Chaetoceros* subgenus Phaeoceros, *Rhizosolenia* and *Eucampia*. Finally, the genera *Navicula* and *Proboscia* were highly correlated (both techniques provided the same seasonality) but were ∼5 times more abundant as derived from the biological technique compared to the micropaleontological one.
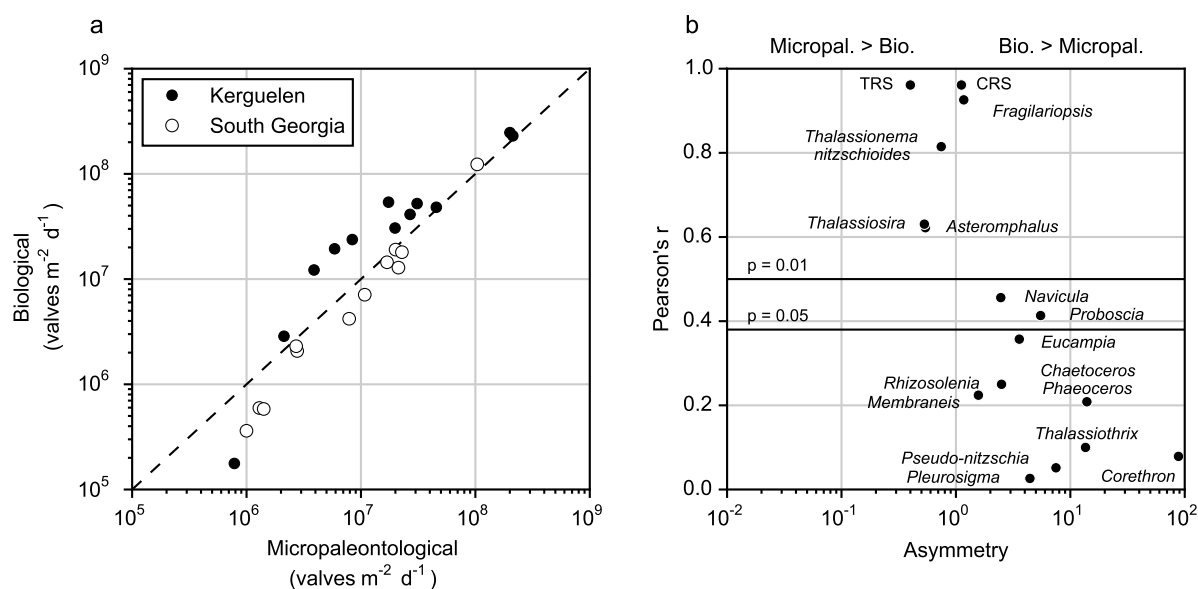
Figure A.3: **a.** Comparison of the total valve flux from 24 samples from the Kerguelen (A3) and South Georgia (P2 and P3) sediment trap using the micropaleontological and biological counting techniques. The dashed line represents a 1:1 relationship. **b.** Comparison of the two techniques for the major diatom genera. The Pearson correlation coefficient r (y axis) is calculated on absolute fluxes from 24 samples for each genera. The r value for n=24 and a significance level of 1 and 5% are shown by horizontal lines. See the text for the definition of asymmetry.

Discussion

Despite a highly significant relationship between the absolute fluxes derived from the two methods (Fig. A.3a), higher fluxes are obtained with the micropaleontological technique for the lowest range of the fluxes ($< 10^6$ valve $\mathrm{m^{-2}\,d^{-1}}$). The reason for this difference can first be tested by studying the uncertainty in the calculations. We can attribute relative uncertainties on each of the parameters of the calculations. In Eq. A.2, f, D and t have negligible uncertainties. The dilution d depends on the micropipette precision (5 %) and

the volume estimation by weighing the sample (2 %). The calculation of error propagation leads to a final uncertainty of 5.4%. In Eq. A.2, uncertainty is associated to the area of the petri dish (A, 2 %), the total area of the field of view (a, 5 %), the volume used for the random settling (v, 5 %) and the volume of the oxidized sample (2 %). The total relative error is 7.6 % for the micropaleontological technique. Therefore, both techniques are characterized by a similar uncertainty (5.4 vs. 7.6 %), and the difference observed for the lowest flux is probably due to biases occurring during the sample preparation and/or counting. Indeed, for samples with low diatom abundance, the absence of organic material makes the rare frustules easier to find in the case of the micropaleontological technique. Conversely, in the biological technique, the observer might miss some rare frustules hidden/obscured by the presence of organic matter. Another explanation would be the presence of diatom frustules within faecal pellets during faecal pellet export events (Nöthig and von Bodungen, 1989; Voss, 1991). In the case of the biological technique, frustules inside faecal pellets are not quantified whereas the oxidation from micropaleontological technique liberates frustules from the faecal pellets. This could explain why the fluxes are higher for the micropaleontological technique when the total diatom valve flux is low (i. e. the relative contribution of faecal pellets to export fluxes is higher).

It was often pointed out that *Pseudo-nitzschia* species were under-represented in sediment trap studies compared to their abundance in the mixed layer (Grigorov et al., 2014; Rigual-Hernández et al., 2015a,b). All of these studies used the micropalontological technique. The strong asymmetry (higher abundance with the biological technique) and low correlation we obtained for *Pseudo-nitzschia* suggest this lightly-silicified genus might be prone to fragmentation and dissolution during the oxidation and centrifugation steps. We found the highest asymmetry and a very low correlation for the *Corethron* genus. Interestingly, thus genus is most of the time reported as absent (Grigorov et al., 2014; Rigual-Hernández et al., 2015a) or as a very poor contributor to the diatom export assemblage (Rigual-Hernández et al., 2015b) estimated with the micropaleontological technique. Our comparison suggests these results are due to the selective breaking and dissolution of this genus during the processing of samples. Diatoms of the *Corethron* genus are large (>300 μm) and weakly silicified. Moreover, they exhibit large and numerous processes and spines, very likely to be damaged during the centrifugation steps. A selective dissolution or damaging of some diatom genera might have important implications because the micropaleontological technique is used to analyse microfossil composition to reconstruct past ocean properties (sea ice extent, sea surface temperature, e.g. Ferry et al., 2015). Some of the transfer functions are built with modern analogues, which are live diatoms quantified with a method close to the biological technique. A bias introduced by the two different methods might render the transfer function difficult to apply to microfossil records.

Conclusion

Both methods provided comparable results for the total valve flux, suggesting that different sediment trap studies using different methods can be compared. The choice of one method over the other will depend on the question asked. If the aim of the study is to provide a highly detailed description of the taxonomic composition of the diatom community, then the micropaleontological method is adequate. It allows the detailed observation at high magnification of the valve's morphological characteristics (e. g. aerolations, processes, pseudonodulus). However, it must be kept in mind that the high temperature oxidation procedure followed by centrifugation steps is highly likely to selectively damage/dissolve the lightly silicified species and/or the long and thin species. Thereby, the diatom assemblage might not be representative of the original community with an underestimation of the contribution of the aforementioned species. Conversely, due to the presence of organic material and the lower magnification, the biological technique does not allow one to reach the level of taxonomic detail obtained with the micropaleontological technique. However, the enumeration of full and empty frustules makes the estimation of diatoms contribution to carbon fluxes possible. Moreover, the absence of chemical and physical treatment suggests the diatom community derived from the biological technique is more representative of the natural assemblage. Finally, the user must keep in mind that the oxidation step from the micropaleontological technique liberates frustules from faecal pellets and thereby the observed community comprises diatoms sinking as single cells or chains and diatoms within faecal pellets and aggregates.

A.3 The bio-optical approach: example in the vicinity of Kerguelen

The SOCLIM project (www.soclim.com) aims at coupling autonomous observation (bio-argo floats) with moorings (sediment traps, autosampler, T/S, pCO_2 and gas tension sensors, ADCP) in the vicinity of the Kerguelen Plateau to document production and export at high temporal resolution over a seasonal scale in the AAZ. Six bio-argo floats have already been deployed around the Kerguelen Islands in January 2015. In this section we compile physical, chemical and bio-optical data from the KEOPS cruises together with the bio-argo floats data around the Kerguelen Islands. We introduce a metric (λ) to quantify the attenuation of particle stock with depth. Secondly, we evaluate how λ evolves seasonally and use a mutlivariate approach to identify the parameters likely to influence the attenuation of particle stock.
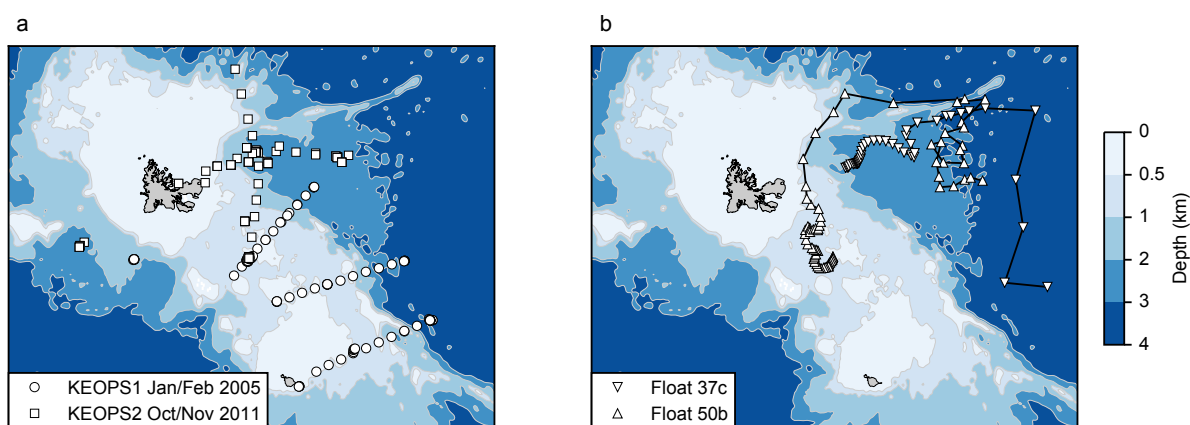
Figure A.4: **a.** Location of the KEOPS1 (January/February 2005) and KEOPS2 (October/November 2011) CTD profiles. **b.** Location of the profiles from two bio-argo floats deployed from January to May 2015. Colors correspond to bathymetry.

Methods

We compiled the temperature/salinity, fluorescence, beam attenuation coefficient and oxygen profiles from the KEOPS1 (121 profiles, January/February 2005) and KEOPS2 (115 profiles, October/November 2011) cruises together with the data acquired from January to May 2015 by two bio-argo floats (float 37c, 57 profiles and float 50b, 70 profiles). The location of the profiles considered is shown in Fig. A.4.

Data from both CTD and float upcasts were first low-pass filtered to remove spikes and high frequency variability. Although spikes from raw instrument records might be informative on biological processes (Briggs et al., 2011, 2013), we focussed on the main signal for our synoptic approach. Quadratic fit was applied on 20 m intervals and root mean squared error (RMS) was calculated. Data away from the fit by more than one

RMS were discarded. Profiles were then linearly interpolated with a 1 m resolution.

Non-photochemical quenching (NPQ, decrease in the fluorescence when light exceeds the excitation potential of pigments) affects the fluorescence profiles within the penetration depth and leads to an underestimation of the algal biomass (Müller et al., 2001; Behrenfeld et al., 2009). A way to correct for NPQ is to assume an homogeneous fluorescence profile through the mixed layer and extrapolate the deep fluorescence value toward the surface (Xing et al., 2012). However, direct measurements of chlorophyll *a* suggested the phytoplankton biomass and associated pigment concentration is sometimes not homogeneous within the mixed layer in the Southern Ocean (Kopczynska et al., 2001; Holm-Hansen and Hewes, 2004; Holm-Hansen et al., 2005; Gomi et al., 2010). Therefore, we choose an alternative way to correct NPQ. A linear regression was applied between the beam attenuation coefficient c_p and the fluorescence between 50-100 m. The slope of the regression was then used to retrieve the fluorescence in the 0-50 m interval. The high coefficient of determination of the regressions ($R^2 = 0.96 \pm 0.03$) gave confidence in the robustness of the method. An example of the different steps is given in Fig. A.5a.

Chlorophyll *a* concentration was retrieved from the CTD-derived fluorescence (KEOPS cruises) based on *in situ* HPLC measurments and non-linear calibration. For the bio-argo float data, Chlorophyll *a* concentration was retrieved from the fluorescence and the downward irradiance at 490 nm using a method described in Xing et al. (2011). Briefly, the method uses the downward irradiance attenuation coefficient as a proxy for chlorophyll *a* concentration, allowing the fluorescence signal to be calibrated in absolute units.

To correct for the drift in c_p, the mean value at depth >1000 m (when available) was subtracted from the c_p profile, assuming negligible particle concentration at this depth compared to the productive layer. The efficiency of particle export from the mixed layer can be estimated by comparing POC stock decrease with depth (Lam et al., 2011). The strong correlation between POC and c_p suggests the latter is a good proxy for POC (Cetinić et al., 2012). To quantify the attenuation of particle stock, the c_p within the first 300 m was first normalized to filter-out the information on absolute particle abundance and focus on the shape of the particle distribution.

$$c_{p\ norm} = \frac{c_p - c_{p\ min}}{c_{p\ max} - c_{p\ min}}$$

The $c_{p\ norm}$ attenuation was quantified as a function of density rather than depth to correct for vertical displacements of isopycnals due to internal waves oner the Kerguelen Plateau (Park et al., 2008a). The downward attenuation was quantified by fitting an exponential law on $c_{p\ norm}$ versus potential density (σ_θ), starting from a σ_θ value where $c_{p\ norm} = 1$ (i.e. where the particle abundance is maximal, hereafter refereed to as σ_θ^{ini}). An example is provided in Fig. A.5b.

$$c_{p\ norm} = \exp[-\lambda(\sigma_\theta - \sigma_\theta^{ini})]$$
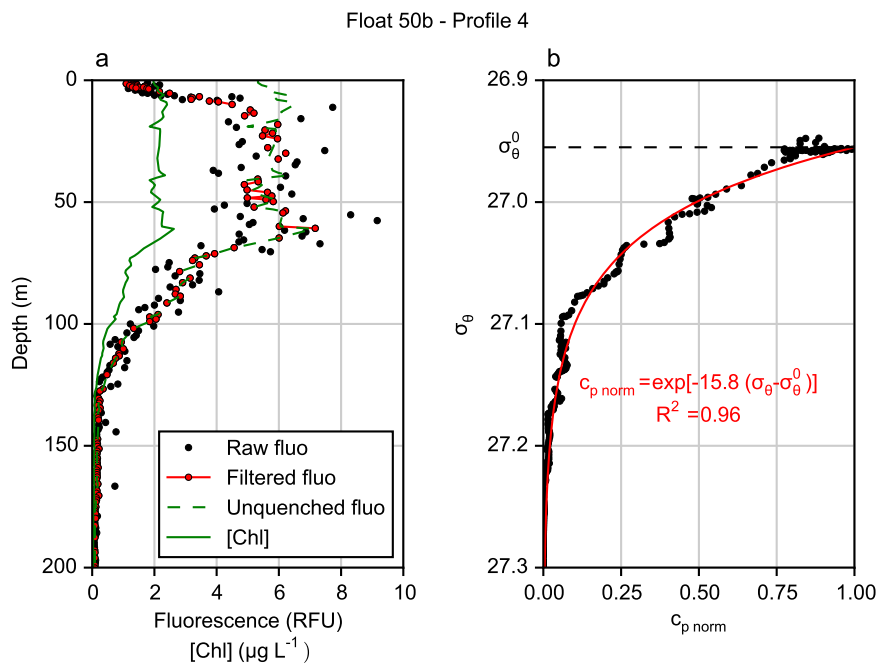
Figure A.5: Example of fluorescence and c_p profiles treatment **a.** Low pass filtering, unquenching of the fluorescence profile and chlorophyll a retrieval. **b.** Estimation of the particle stock attenuation coefficient ($\lambda = 15.8$) as a function of potential density anomaly. See the methods for the explanation of λ.

λ is a dimensionless parameter quantifying the attenuation of particle stock with increasing isopycnals. λ can be compared between profiles because it is not impacted by the absolute c_p value. All the fits were highly significant, with a $R^2 > 0.80$. Other variables likely to be linked to λ were considered: the integrated c_p from 0-300 meters ($c_{p\ int}$, an estimator of the total carbon biomass), the integrated chlorophyll a from 0 to 300 m (Chl_{int}, an estimator of the total phytoplankton biomass), the chlorophyll a to c_p ratio averaged within 50-100 m ($Chl : c_p$, an estimator of the fraction of algal biomass), and the apparent oxygen utilisation (calculated using the oxygen solubility from Garcia and Gordon, 1992) integrated between the mixed depth and 300 m (AOU_{int}, an estimator of the heterotrophic microbial remineralization below the mixed layer). A principal component analysis (PCA) was performed on the data from the KEOPS cruises and the floats to identify the variables potentially influencing the λ parameter.

Results and discussion

The first two principal components of the PCA accounted for 77% of the variance of the dataset (Fig. A.6). Axis 1 described a seasonal gradient opposing the profiles from spring (KEOPS2), to autumn (float 37c and 50b). Axis 2 described a lower fraction of the variance (23%) and described somehow a spatial gradient with profiles close to the plateau (KEOPS1 and first profiles from float 50b) opposed to the data acquired away from the plateau (KEOPS2 and most of the profiles from float 37c). The temperature

Figure A.6: Projection on the first two axes of a principal component analysis (PCA) of the CTD- and float derived variables. The marker of the profile projection refers to the platform (cruises or floats) and the color refers to the mean temperature within the mixed layer depth (MLD).

was not used as forcing variable in the PCA to avoid the weight of hydrological variability (e. g. fronts, submesoscale dynamics). However a consistent thermal structure emerges and results from both seasonality (lower temperature in spring than summer) and spatial variability (higher temperature in locations influenced by the polar front than in locations strictly in the Antarctic zone).

The $Chl : c_p$ ratio, Chl_{int} and λ were positively projected on axis 1, close to the spring (KEOPS2) profiles projection. Conversely, the $c_{p\ int}$ and AOU_{int} were negatively projected along axis 1, close to the autumn (floats) profile projection. The opposition between $c_{p\ int}$ and the $Chl : c_p$ ratio confirms that the normalisation of the c_p signal was efficient (i. e. the higher stock attenuation does not result from a higher particle stock in the mixed layer). The strong collinearity between the first principal component and λ suggests that seasonality, and probably the ecological successions associated with this seasonality, is the major factor influencing the particle stock attenuation. Although the $Chl : c_p$ ratio can be used as an indicator of photoacclimatisation (Geider et al., 1998; Behrenfeld and Boss, 2003, 2006), it is considered here as a simple proxy of the contribution of algal biomass to the total particle stock (Sathyendranath et al., 2009).

Implications and future work

There are several limits to this non-quantitative approach. Firstly, the difference in the time of sampling precludes intercalibration of the instruments on the CTD and the floats. Secondly the presence of frontal structures along the bio-argo float trajectories render the interpretation of the AOU signal difficult. They are associated with abrupt changes in the age and origin of the water masses (d'Ovidio et al., 2015), which might drive an AOU signal that does not originate from the observed particle stock attenuation. Finally, if some recent studies have proposed a link between the optical signals reported by autonomous platforms and the biological constituents of the phytoplankton communities (Cetinić et al., 2015), the interpretation of these signals is not homogeneous among the scientific community. For example, the $Chl : c_p$ ratio is influenced from both phytoplankton community structure and physiology (photoacclimation) (Behrenfeld and Boss, 2003).
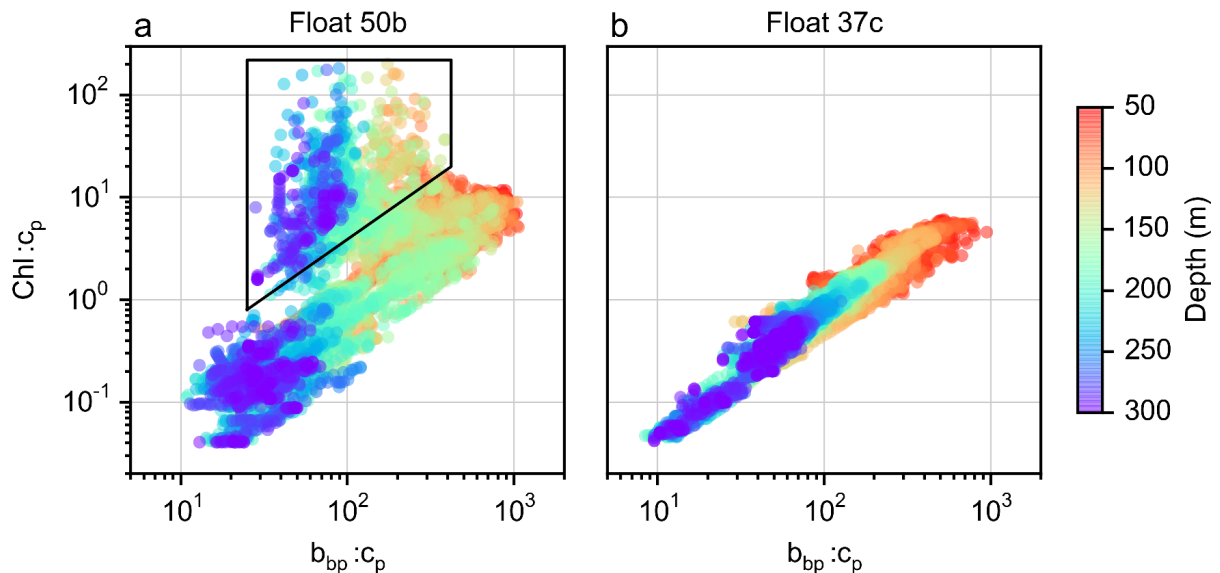
Figure A.7: Bio-optical ratios reported by two bio-argo floats deployed in the vicinity of the Kerguelen islands (data from January to May are represented). Float 50b was deployed at the reference productive station A3.

Float 50b, deployed at the productive reference station A3, reported a distinct bio-optical signal when compared to float 37c (Fig. A.7). High $Chl : c_p$ and $b_{bp} : c_p$ are observed between 150 and 300 m, below the mixed layer depth. High $Chl : c_p$ suggests important algal contribution to this particle pool. Backward scattering (b_{bp}) has been suggested to be an indicator of small ($\sim$1 μm), non algal particles according to the physical Mie theory (Stramski and Kiefer, 1991; Morel and Ahn, 1991). However, field and laboratory studies have shown that phytoplanktonic cells > 100 μm could contribute significantly to b_{bp} (Stramski et al., 2004; Dall'Olmo et al., 2009; Whitmire et al., 2010). At station A3, carbon export in late summer (Januray - March) is driven by resting spore formation by the diatoms *Chaetoceros* subgenus *Hyalochaete* and *Thalassiosira antarctica*

(Rembauville et al., 2015a). Moreover, in February 2014, diatom resting spores were the major contributors to POC stock at 250 m at the A3 station (article 5). These small (10 - 20 µm) and robust cells might contribute to the distinct optical signal observed by float 50b. If a quantitative relationship between c_p, b_{bp}, Chl and the structure of the microplankton community could be established, autonomous platforms equipped with bio-optical sensors would become a potential tool to track ecological processes such as changes in phytoplankton community structure or resting spore formation.

A.4 The modelling approach: taking into account resting spore formation

Model structure

The simple Nutrient-Phytoplankton-Zooplankton-Detritus-Spore (NPZD-S) model contains three nutrients (N, Fe, Si), two phytoplankton groups (diatom P1 and nanophytoplankton P2), a detritus pool (D), and one generalist grazer (Z) able to feed on the two phytoplankton groups and the detritus (Fig. A.8). The model only represents mixed layer processes in the sense of Fasham et al. (1990).
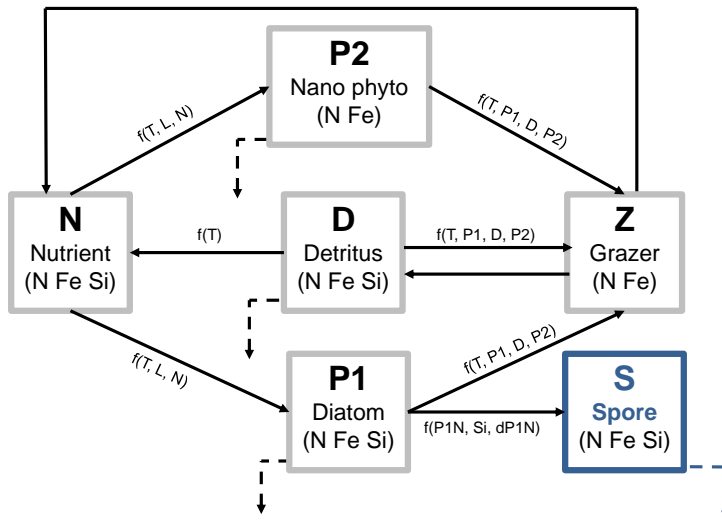
Figure A.8: Scheme of a simple NPZD model used to test formulations of resting spore formation. Continuous arrows represent the flux of matter and dashed arrows represent the sinking of components.

Differential equations

$$\frac{dP1}{dt} = (\mu_{P1} - m_{P1} - p_{spore})P1 - g_{P1}Z - \frac{(m+h+w_{P1})}{MLD}P1$$

$$\frac{dP2}{dt} = (\mu_{P2} - m_{P2})P2 - g_{P2}Z - \frac{(m+h+w_{P2})}{MLD}P2$$

$$\frac{dZ}{dt} = (g_{P1} + g_{P2} + g_D - m_Z - e)Z - p_Z Z^2 - \frac{h}{MLD}Z$$

$$\frac{dD}{dt} = m_{P1}P1 + m_{P2}P2 + m_Z Z - g_D Z - rD - \frac{(m+h+w_D)}{MLD}D$$

$$\frac{dN}{dt} = -\mu_{P1}1P1 - \mu_{P2}P2 + rD + eZ + (N_{deep} - N_{surf})\frac{(h+m)}{MLD}$$

Phytoplankton growth

Phytoplankton growth rate μ_{P1} depends on light, temperature and nutrient availability.

$$\mu_{P1} = \mu_{opt} lim_T lim_N$$

The optimal growth rate depends on light (Peeters and Eilers, 1978).

$$\mu_{opt} = \frac{\mu_{max}I}{I + \frac{\mu_{max}}{\alpha}\left(\frac{I}{I_{opt}}-1\right)^2}$$

The temperature limitation follows the cardinal temperature model with inflexion developed by Rosso et al. (1993) and adapted to phytoplankton by Bernard and Rémond (2012).

$$lim_T = \begin{cases} 0 & if \ T < t_{min} \ or \ T > T_{max} \\ \phi(T) & \text{otherwise} \end{cases}$$

$$\phi(T) = \frac{(T-T_{max})(T-T_{min})}{(T_{opt}-T_{min})\Big[(T_{opt}-T_{min})(T-T_{opt})-(T_{opt}-T_{max})(T_{opt}+T_{min}-2T)\Big]}$$

Nutrient limitation follows a minimum law on simple Michaelis-Menten formulations.

$$lim_N = min(\frac{NO3}{km_{NO3}+NO3}, \ \frac{dFe}{km_{dFe}+dFe}, \ \frac{Si(OH)4}{km_{Si(OH)4}+Si(OH)4})$$

For P1, the Si:N uptake ratio depends on the iron limitation (Takeda, 1998; Hutchins and Bruland, 1998).

$$Si:N = Si:N_{min} + (Si:N_{max} - Si:N_{min})(1 - lim_{Fe})$$

Zooplankton grazing

Zooplankton grazing on any prey X $\in$(P1, P2, D) depends on its preference for this prey. The preference for diatoms depends on their silicification level (e. g. if P1 is highly silicified, then the preference for P2 and D increases).

$$gX = g_{T0}z_{Q10}^{T/10} \ \frac{pref_X X}{km_Z + pref_X X + pref_Y Y + pref_Z Z}$$

$$pref_{P1} = pref_{p1min} + \frac{(pref_{p1max} - pref_{p1min})}{1 + exp\Big(s_{Si:N}(Si:N - t_{Si:N})\Big)}$$

$$pref_{P2, \ D} = \frac{1 - pref_{P1}}{2}$$

Nutrient remineralization

The remineralization rate of nutrients (r) depends on temperature. NO_{3Q10} and dFe_{Q10} are bacterial $Q10$, whereas $Si(OH)4_{Q10}$ is a physical $Q10$. For any nutrient X $\in$(NO3, Si(OH)4, dFe):

$$r_X = r_{XT0} \ x_{Q10}^{T/10}$$

Resting spore formation

The formulation of resting spore formation is based on several constraints, observations and hypotheses:

- In order to facilitate its integration into pre-existing general circulation/biogeochemical models, no new plankton functional type is created, but spores are rather formed from the pre-existing diatom class.

- Spore forming diatoms are generally observed in very productive neritic environments (McQuoid and Hobson, 1996). Therefore the maximum fraction of spore forming diatoms (p_{max}) is scaled to the total diatom biomass.

- It is hypothesized that silicate limitation is the main triggering factor for resting spore formation in the Southern Ocean (Salter et al., 2012; Rembauville et al., 2015a), represented by p_{Si}.

- Resting spore formation occurs at the end of summer when diverse environmental conditions (light, temperature, nutrient) become unfavourable for diatom growth (McQuoid and Hobson, 1996). An integrator of these unfavourable conditions is the diatom biomass decrease (p_{dP1}).

- Resting spores have a very high transfer efficiency (Article 4) represented by an important sinking speed (w_S) and the absence of grazing on the spore (Kuwata and Tsuda, 2005).

- Resting spore formation is an abrupt and continuous process that can occur within 48 hours (Kuwata et al., 1993; Oku and Kamatani, 1997). Hense, probabilities of resting spore formation follow sigmoid formulations (Fig. A.9).

$$p_{spore} = p_{max} \times p_{Si} \times p_{dP1}$$

$$p_{spore} = \frac{P1}{\sigma} \times \frac{1}{1+exp\left(s_{Si} \times (Si - t_{Si})\right)} \times \frac{1}{1+exp\left(s_{dP1} \times (\frac{dP1}{dt} - t_{dP1})\right)}$$

$$\frac{dS}{dt} = p_{spore} \times P1 - \frac{(m+h+wS)}{MLD} \times S$$
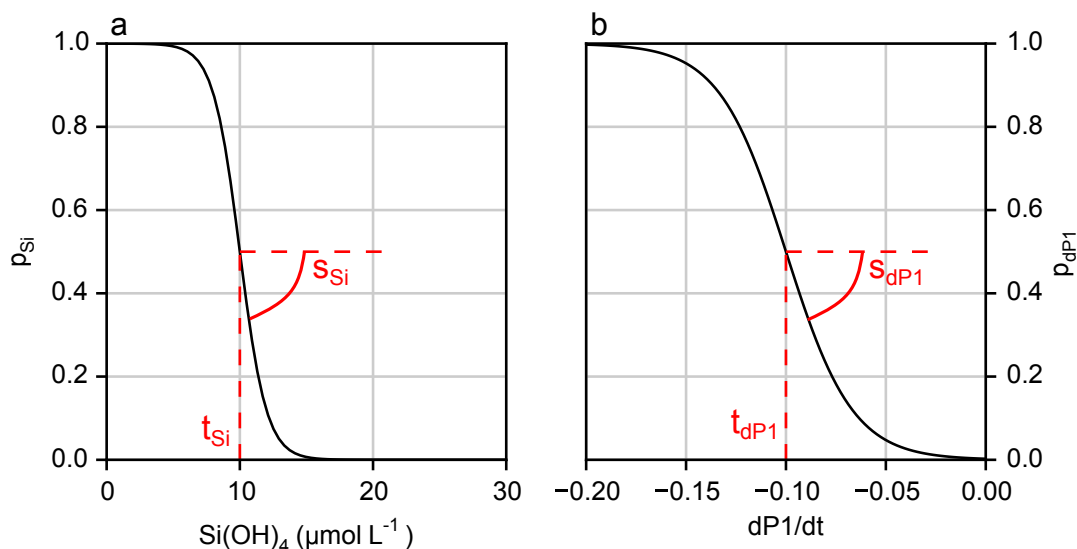
Figure A.9: Representation of the probability to form a resting stage as a function of silicic acid concentration and diatom biomass variation.

Export

The export not driven by the spores (E) is the sum of P1 and P2 single cells sinking and the detritus sinking (w), mixing (m) and detrainment (h) out of the mixed layer.

$$E = \frac{w_{P1}P1 + w_{P2}P2 + w_D D + (m+h)(P1+P2+D)}{MLD}$$

The export driven by the spores (ES) follows the same expression:

$$ES = \frac{(m+h+w_S)S}{MLD}$$

To compare the results with observed export at $300\,\mathrm{m}$, E is attenuated by a Martin et al. (1987) formulation where E_{z0} is the export at the basis of the mixed layer and b is the flux attenuation coefficient. A value of 1 is appropriate for the Southern Ocean (Guidi et al., 2015).

$$E_z = E_{z0}\left(\tfrac{z}{z0}\right)^{-b}$$

Physical forcing

The mixed layer rate of variation is calculated following Fasham et al. (1990).

$$h = max\left(0, \tfrac{dMLD}{dt}\right)$$

Mixing by diffusion through the mixed layer is kept constant with the artificial mixing coefficient m. Each particulate component has a specific sinking speed w. The mean light within the mixed layer is used to calculate the optimal phytoplankton growth. Light attenuation within the mixed layer depends on the chlorophyll concentration according to Morel (1988).

$$I = \int_0^{MLD} I_0 e^{-Kdz} \tfrac{1}{MLD}$$

$$Kd = Kd_w + 0.121 Chl^{0.428}$$

Param.	Value	Unit	Description	Reference
P1 Diatoms				
$P1_N ini$	0.02	$\mu mol\,L^{-1}$	initial biomass	
μ_{maxP1}	0.8	d^{-1}	maximum growth rate	Boyd et al. (2013)
km_{SiP1}	10	$\mu mol\,L^{-1}$	$Si(OH)_4$ half saturation	Mosseri et al. (2008)
km_{NP1}	0.6	$\mu mol\,L^{-1}$	NO_3^- half saturation	Eppley et al. (1969)
km_{FeP1}	1	$nmol\,L^{-1}$	dFe half saturation	Timmermans et al. (2004)
α_{P1}	0.2		initial P vs. I slope	
I_{optP1}	3	$mol\,m^{-2}\,d^{-1}$	optimal irradiance	
T_{optP1}	5	$^\circ C$	opt. temperature	Boyd et al. (2013)
T_{minP1}	1	$^\circ C$	min. temperature	Boyd et al. (2013)
T_{maxP1}	7	$^\circ C$	max. temperature	Boyd et al. (2013)
$Si:N_{min}$	1	$mol\,mol^{-1}$	min. Si:N uptake ratio	Hutchins and Bruland (1998)
$Si:N_{max}$	2.5	$mol\,mol^{-1}$	max. Si:N uptake ratio	Hutchins and Bruland (1998)
$Fe:N_{P1}$	0.03	$mmol\,mol^{-1}$	Fe:N uptake ratio	Strzepek et al. (2012)
$Chl:N_{P1}$	0.8	$\mu g\,\mu mol^{-1}$	Chl:N ratio	Behrenfeld et al. (2005)
w_{P1}	2	$m\,d^{-1}$	cell sinking speed	Laurenceau-Cornec et al. (2015b)
σ_1	50	$1/\mu mol\,L^{-1}$	mortality scaling	
P2 Nanophytoplankton				
$P2_{Nini}$	0.02	$\mu mol\,L^{-1}$	initial biomass	
μ_{maxP2}	1	d^{-1}	max. growth rate	Boyd et al. (2013)
km_{NP2}	0.4	$\mu mol\,L^{-1}$	NO_3^- half saturation	Eppley et al. (1969)
km_{FeP2}	0.6	$nmol\,L^{-1}$	dFe half saturation	Timmermans et al. (2004)
α_{P2}	0.2		initial P vs. I slope	
I_{optP2}	3	$mol\,m^{-2}\,d^{-1}$	optimal irradiance	
T_{optP2}	6	$^\circ C$	optimal temperature	
T_{minP2}	3	$^\circ C$	min. temperature	
T_{maxP2}	10	$^\circ C$	max. temperature	
$Fe:N_{P2}$	0.06	$mmol\,mol^{-1}$	Fe:N uptake ratio	Strzepek et al. (2012)
$Chl:N_{P2}$	0.4	$\mu g\,\mu mol^{-1}$	Chl:N ratio	Behrenfeld et al. (2005)
w_{P2}	1	$m\,d^{-1}$	cell sinking speed	Laurenceau-Cornec et al. (2015b)
σ_{P2}	50	$1/\mu mol\,L^{-1}$	mortality scaling	

Table A.1: Parameter values for the NPZD-S model.

Param.	Value	Unit	Description	Reference
Z Zooplankton				
Z_{Nini}	0.02	$\mu mol\,L^{-1}$	initial biomass	
g_0	0.2	d^{-1}	grazing rate at $0\,°C$	Hirst and Bunker (2003)
q_{Q10}	2		grazing Q_{10}	Mayzaud and Pakhomov (2014)
e	0.02	d^{-1}	excretion rate	
km_Z	1	$\mu mol\,L^{-1}$	grazing half saturation	Chen et al. (2014)
$s_{Si:N}$	10		preference slope	
$t_{Si:N}$	2.2		preference Si:N threshold	
$pref_{P1min}$	0.4		min. diatom preference	
$pref_{P1min}$	0.8		max. diatom preference	
pZ	0.02	d^{-1}	predation rate	
σ_Z	10	$1/\mu mol\,L^{-1}$	mortality scaling	
D Detritus				
D_{Nini}	0.02	$\mu mol\,L^{-1}$	initial biomass	
r_{NT0}	0.4		N remin. at $0\,°C$	
r_{SiT0}	0.4		Si remin. at $0\,°C$	
N_{Q10}	5		remin. sensivity to T	Adams et al. (2010)
Si_{Q10}	1		remin. sensivity to T	
w_D	100	$m\,s^{-1}$	sinking speed	Laurenceau-Cornec et al. (2015b)
S Spore				
σ	10	$1/\mu mol\,L^{-1}$	P1 scaling factor	
t_{Si}	15	$\mu mol\,L^{-1}$	$Si(OH)_4$ sigmoid threshold	
s_{Si}	1	$1/\mu mol\,L^{-1}$	$Si(OH)_4$ sigmoid slope	
t_{dP1}	-0.15	$\mu mol\,L^{-1}\,d^{-1}$	dP1 sigmoid threshold	
s_{dP1}	8	$1/\mu mol\,L^{-1}\,d^{-1}$	dP1 sigmoid slope	
w_S	250	$m\,s^{-1}$	sinking speed	
Physical parameters				
Kd_w	0.0384	m^{-1}	water att. coef.	Morel (1988)
m	0.1	d^{-1}	turb. mix.	

Table A.2: Parameter values for the NPZD-S model (continued).

Runs in environments of contrasted productivity

Two runs were performed at two stations where observations of POC export and the associated diatom communities are available: the low productivity station KERFIX (article 3) and the highly productive station A3 (articles 1 and 2). A 13 year climatology of PAR (MODIS) and SST (ECMWF) was calculated for the A3 and KERFIX stations. A climatological MLD based on ARGO float and elephant seal data (J.B. Sallée, pers. comm.) was used at A3 whereas the mean MLD cycle from a three year record was used at KERFIX (Park et al., 1998). Initial (winter) dFe concentration was set to 0.25 and $0.5\,\mathrm{nmol\,L^{-1}}$ at KERFIX and A3, respectively (Blain et al., 2008b). The model was run for 20 years with a time step of 1 hour. The last year is discussed hereafter.

The results for the run at KERFIX are shown in Figure A.10. The model accurately reproduced the nutrient consumption starting in December, although the phytoplankton bloom occurred one month later than in the observations. The model produced an accurate amplitude of both chlorophyll a and zooplankton biomass. The comparison with the observed export must be taken with caution since the sediment trap deployment took place in mid-February (the observations from August to December correspond to the second half of the record). The model showed one export peak starting in December, reaching $0.9\,\mathrm{mmol\,m^{-2}\,d^{-1}}$ and decreasing to $<0.1\,\mathrm{mmol\,m^{-2}\,d^{-1}}$ in June. This pattern was comparable to the observations in terms of both amplitude and timing. The slightly higher annual export in the model ($50.2\,\mathrm{mmol\,m^{-2}\,yr^{-1}}$) compared to the observations ($42.9\,\mathrm{mmol\,m^{-2}\,yr^{-1}}$) can be explain by the missing observations in January and part of February. The contribution of *Chaetoceros Hyalochaete* resting spores (CRS) to carbon export in the observations was calculated assuming that all the CRS were exported as full cells with a carbon content of $227\,\mathrm{pg\,cell^{-1}}$ (articles 2 and 4). The modeled annual contribution of resting spores to carbon export (21%) was close to the observations (17.3 %)

The results for the run at A3 is shown in Figure A.11. The observations are a composite of the KEOPS1 (summer 2004/2005) and KEOPS2 (spring 2011) cruises and may include inter annual variability. This could explain part of the difference in seasonality between the observations and the model. The model performed well at representing $\mathrm{Si(OH)_4}$ seasonality, but summer $\mathrm{NO_3^-}$ concentration were low compared to the observations during KEOPS1. This might be due to the absence of nitrification in the model, a process that could explain the high nitrate concentration despite high primary production levels (Dehairs et al., 2015). The low dissolved iron (dFe) concentration in summer was accurately reproduced by the model, but the dFe consumption in spring occurred later than in the observations. The modeled amplitude in phytoplankton and zooplankton biomass was consistent with observations. The model reported one export peak early in December reaching $1.6\,\mathrm{mmol\,m^{-2}\,d^{-1}}$, in good agreement with the observations. The second spore-dominated export event observed in February was not represented by the model. This

feature may result from a second $Si(OH)_4$ limitation event following nutrient injection by a mid-summer mixing event (articles 1 and 2). The climatological MLD cycle does not reproduce this event. This may explain the 30% lower annual carbon export reported by the model ($66.2\,\mathrm{mmol\,m^{-2}\,yr^{-1}}$) compared to the observations ($98.2\,\mathrm{mmol\,m^{-2}\,yr^{-1}}$).
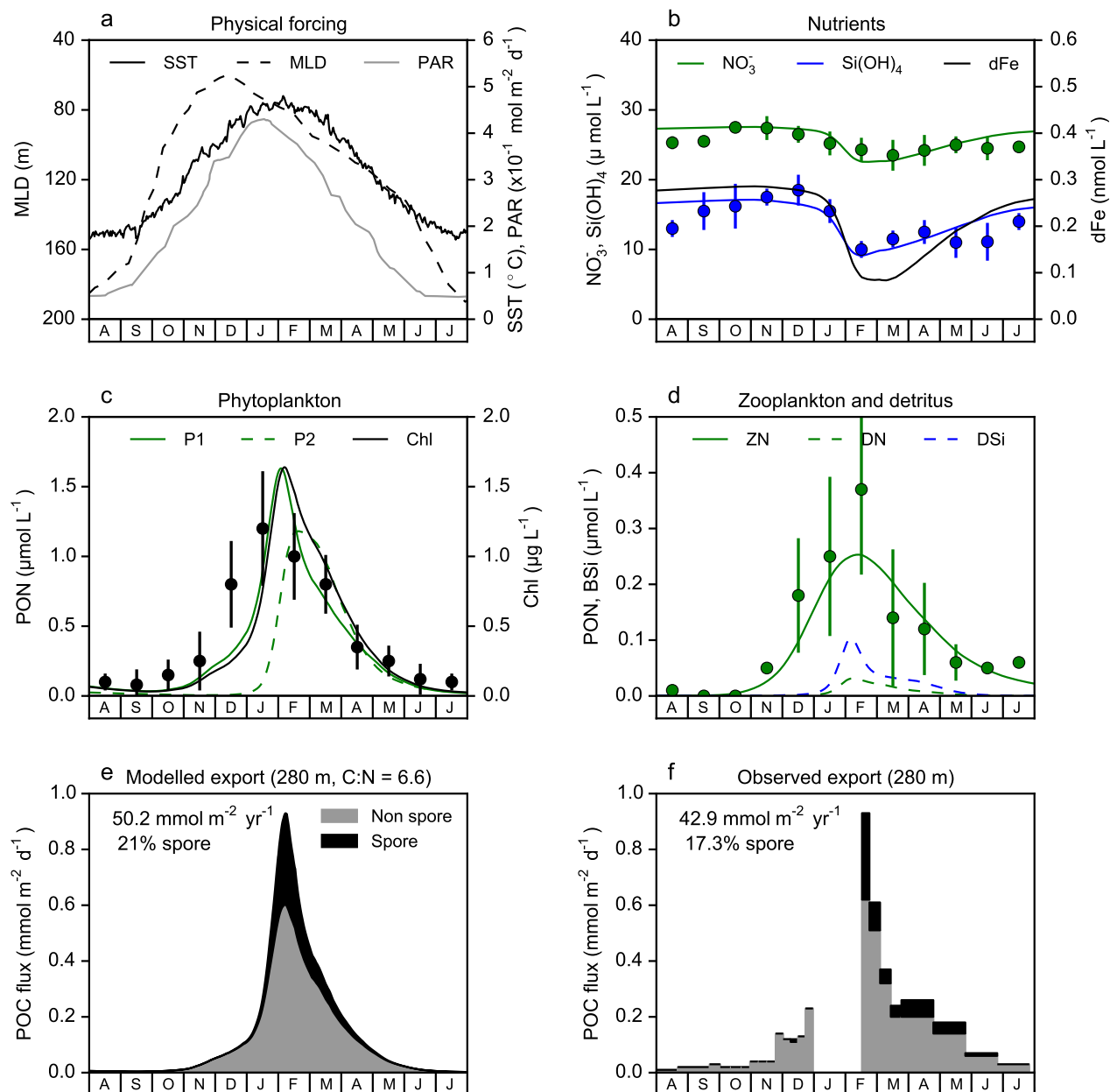
Figure A.10: Simulation from the NPZD-S model at the KERFIX station. Dots and error bars are respectively the monthly mean and range from the three year record during the KERFIX project (Jeandel et al., 1998). The observed export is presented in Article 3.
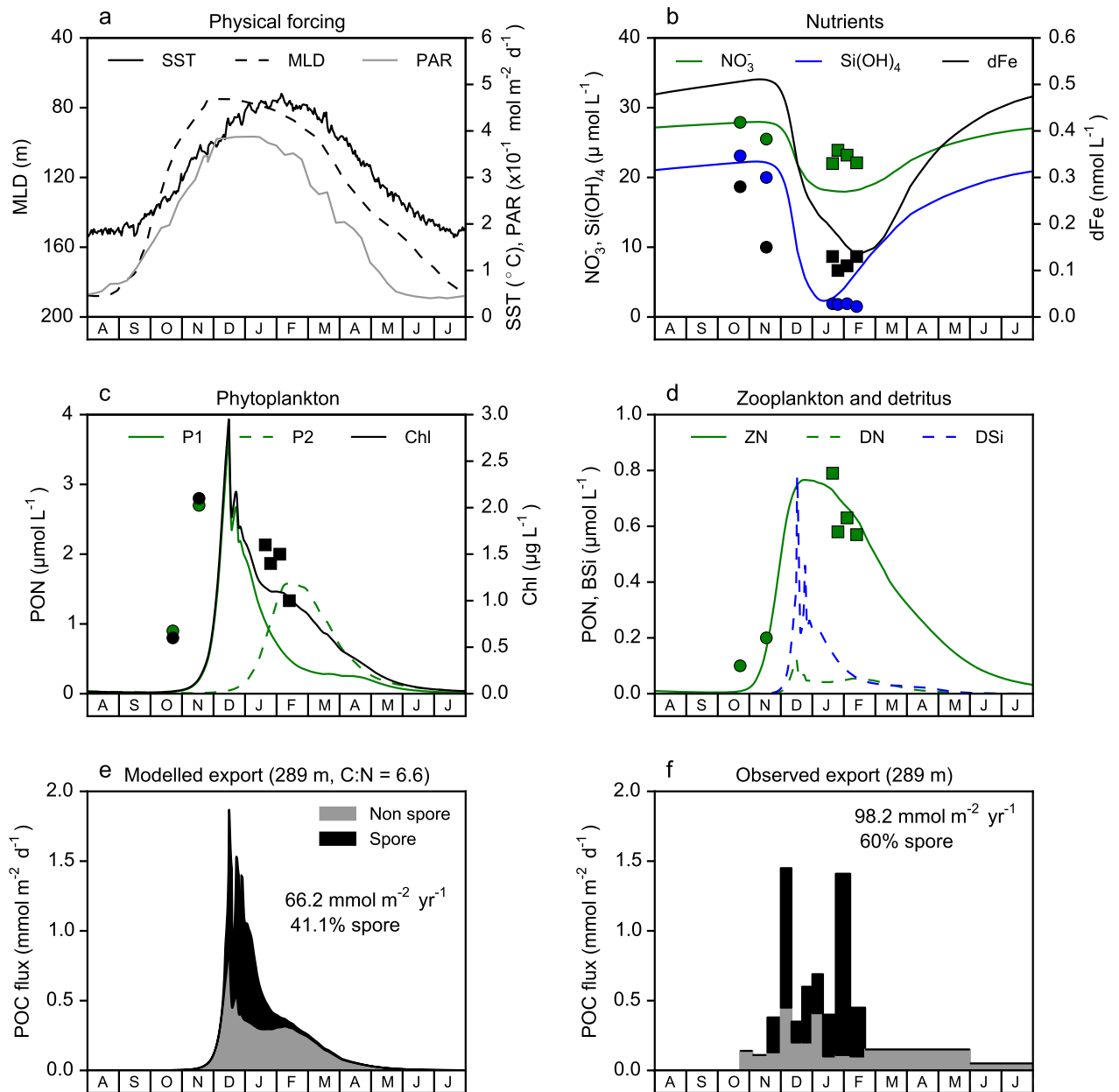
Figure A.11: Simulation from the NPZD-S model at the A3 station. Squares correspond to observations during the KEOPS1 cruise (Blain et al., 2008a), and circles for the KEOPS2 cruise. The observed export comes from Article 2.

A.5 Lipid data

Sample cup	A3-1_3	A3_4	A3-5_6	A3-7_9	A3_9	A3_10	A3_11	A3_12
Start	21/10/2011	04/11/2011	12/12/2011	22/12/2012	21/01/2012	08/02/2012	22/02/2012	31/05/2012
Stop	04/11/2011	12/12/2011	22/12/2011	11/01/2012	08/02/2012	22/02/2012	31/05/2012	07/09/2012
Total lipid flux (µg/m2/d)	26.1	562.0	247.3	127.5	2408.5	210.8	1770.6	21.2
Relative abund. (%)								
C14:1 (cis-9)	0.0	0.0	0.0	0.0	0.0	0.5	0.0	0.0
C16:1 (cis-9)	34.8	47.3	2.7	1.8	5.0	2.4	5.2	2.2
C16:1 isom.	0.2	0.0	0.0	0.0	0.0	0.0	0.2	0.0
C16:1 isom.	0.0	0.7	0.1	0.0	0.0	0.0	0.2	0.0
C17:1 (cis-10)	0.8	0.1	0.0	0.0	0.0	0.0	0.0	0.0
C17:1 isom.	0.1	0.0	0.0	0.0	0.0	0.0	0.1	0.0
C17:1 isom.	0.0	0.1	0.0	0.0	0.0	0.0	0.0	0.0
C18:1 (cis-9)	6.4	10.8	3.0	0.4	7.8	6.0	11.8	6.1
C18:1 (tr-9)	0.5	2.5	2.6	3.2	3.7	2.0	4.2	3.0
C18:1 isom.	0.0	0.0	0.0	0.0	0.2	0.1	0.3	0.0
C18:1 isom.	0.0	0.0	0.0	0.0	5.2	0.0	0.6	0.3
C19:1 isom.	0.0	0.0	0.0	0.0	0.1	0.0	0.0	0.0
C19:1 isom.	0.0	0.0	0.0	0.0	0.0	0.0	0.0	0.0
C19:1 isom.	0.0	0.0	0.0	0.0	0.1	0.6	0.0	0.7
C19:1 isom.	0.0	0.0	0.0	0.0	0.0	0.2	0.0	0.2
C20:1 (cis-11)	1.0	2.1	3.2	3.0	2.6	0.7	3.0	2.0
C20:1 isom.	0.0	0.1	0.3	0.2	0.7	0.3	0.7	0.7
C22:1 isom.	0.1	0.0	0.0	0.0	0.3	0.3	1.0	0.6
C22:1 (cis-13)	0.1	0.3	0.1	0.1	0.3	0.4	1.1	0.6
C22:1 isom.	0.0	0.0	0.0	0.0	0.0	0.0	0.2	0.0
C24:1 isom.	0.0	0.1	0.0	0.0	0.1	0.0	0.2	0.2
C24:1 (cis-15)	0.0	0.2	0.0	0.0	0.4	2.6	1.5	0.2
Σ MUFA	44.1	64.3	12.0	8.8	26.5	16.1	30.4	16.9
C16:3	0.9	1.1	0.0	0.0	0.0	0.0	0.0	0.0
C16:4	0.8	2.0	0.0	0.0	0.0	0.0	0.0	0.0
C18:2 (cis-9)	0.8	0.0	0.0	0.0	0.0	0.0	0.0	0.0
C18:3 (cis-6)	0.4	0.0	0.0	0.0	0.1	0.0	0.0	0.0
C20:2 (cis-11)	0.1	0.0	0.0	0.0	0.3	0.0	0.0	0.0
C20:3 (cis-11)	0.0	0.0	0.1	0.0	0.0	0.0	7.7	0.0
C20:4 (cis-5)	0.4	0.1	0.0	0.0	0.1	0.0	0.0	0.0
C20:5 (cis-8)	6.8	5.3	0.0	0.1	0.2	0.0	0.0	0.0
C22:2 (cis-13)	0.0	0.0	0.0	0.0	0.0	0.0	0.6	0.0
C22:6 (cis-9)	0.0	0.0	0.0	0.0	2.3	0.0	0.1	0.0
Σ PUFA	10.2	8.5	0.1	0.1	2.9	0.0	8.4	0.0
C16:1 OH	0.0	0.0	0.0	0.0	0.0	0.0	0.0	0.0
C18:1 OH	0.1	0.0	0.2	0.0	0.0	0.0	0.1	10.8
C18:1 OH isom.	0.0	0.0	9.2	4.7	0.0	0.0	0.0	0.0
C18:1 OH isom.	0.0	0.0	0.0	0.0	0.0	0.0	0.0	0.0
C20:1 OH	0.0	0.0	40.0	43.8	0.0	0.0	0.0	32.1
C22:1 OH	0.0	0.0	0.0	0.0	0.0	0.0	0.0	3.5
C22:1 OH isom.	0.0	0.0	0.0	0.0	0.0	0.0	0.0	2.7
C24:1 OH	0.0	0.0	0.0	0.0	0.0	0.0	0.0	0.2
C24:1 OH isom.	0.0	0.0	0.0	0.0	0.0	0.0	0.0	0.0
Σ unsat. OH	0.1	0.0	49.5	48.5	0.0	0.0	0.1	49.2
C14 FAME	1.7	0.6	3.2	2.6	0.7	0.9	6.1	3.0
C15 FAME	0.5	0.0	0.0	0.0	0.1	0.1	0.4	0.1
C16 FAME	20.7	1.7	7.9	9.8	26.3	6.7	13.9	10.2
C17 FAME	0.1	0.1	0.0	0.0	0.1	0.1	0.1	0.0
C18 FAME	1.6	0.1	0.7	0.8	0.6	1.8	2.5	1.2
C19 FAME	0.0	0.0	0.0	0.0	0.0	0.0	0.0	0.0
C20 FAME	0.1	0.0	0.0	0.0	0.0	0.0	0.3	0.0
C21 FAME	0.0	0.0	0.0	0.0	0.0	0.0	0.0	0.0
C22 FAME	0.0	0.0	0.0	0.0	0.0	0.0	0.0	0.0
C23 FAME	0.0	0.0	0.0	0.0	0.0	0.0	0.0	0.0
C24 FAME	0.0	0.0	0.0	0.0	0.0	0.1	0.0	0.0
C25 FAME	0.0	0.0	0.0	0.0	0.0	0.0	0.0	0.0
C26 FAME	0.0	0.0	0.0	0.0	0.0	0.0	0.0	0.0
Σ FAME	24.6	2.6	11.8	13.2	27.7	9.6	23.5	14.6

Figure A.12: Complete lipid dataset for the Kerguelen sediment trap deployment at station A3 (289 m).

4,8-dimethyl-C12:0	0.0	0.0	0.0	0.0	0.0	0.0	0.0	0.0
i-C15:0	0.1	0.2	0.0	0.0	0.1	0.1	0.6	0.1
a-C15:0	0.1	0.0	0.0	0.0	0.1	0.0	0.2	0.0
i-C16:0	0.0	0.0	0.0	0.0	0.1	0.0	0.0	0.0
a-C16:0	0.0	0.0	0.0	0.0	0.0	0.0	0.2	0.0
i-C17:0	0.1	0.1	0.0	0.0	0.3	0.1	0.3	0.0
a-C17:0	0.0	0.0	0.0	0.0	0.1	0.0	0.2	0.0
i-C18:0	0.0	0.0	0.0	0.0	0.2	0.0	0.2	0.0
Σ br. FAME	0.2	0.3	0.1	0.0	0.8	0.2	1.7	0.1
C12 OH	0.0	0.0	0.0	0.0	0.0	0.1	0.0	0.0
C13 OH	0.0	0.0	0.0	0.0	0.0	0.0	0.0	0.0
C14 OH	0.6	0.0	0.1	0.8	0.2	3.5	2.8	2.5
C15 OH	0.0	0.0	0.0	0.0	0.0	0.0	0.0	0.0
C16 OH	3.5	1.0	0.4	1.1	0.5	7.7	7.3	4.8
C17 OH	0.0	0.0	0.0	0.0	0.0	0.0	0.0	0.0
C18 OH	0.1	0.0	0.0	0.0	0.1	0.7	0.3	0.2
C19 OH	0.0	0.0	0.0	0.0	0.0	0.0	0.0	0.0
C20 OH	0.0	0.0	0.0	0.0	0.0	0.0	0.0	0.0
C21 OH	0.0	0.0	0.0	0.0	0.0	0.0	0.0	0.0
C22 OH	0.0	0.0	0.0	0.0	0.0	0.0	0.0	0.0
C23 OH	0.0	0.0	0.0	0.0	0.0	0.0	0.0	0.0
C24 OH	0.0	0.0	0.0	0.0	0.0	0.0	0.0	0.0
Σ OH	4.3	1.0	0.5	1.9	0.8	12.1	10.5	7.6
C26Δ22	0.0	0.1	0.1	0.1	0.0	0.0	0.0	0.0
C26Δ5,22	0.0	1.0	1.2	0.7	0.4	0.6	0.5	0.1
Coprostanol	0.0	0.0	0.0	0.0	1.5	0.0	0.0	0.0
Epicoprostanol	0.0	0.0	0.0	0.0	11.7	0.0	0.0	0.0
C27Δ22 (Z)	0.0	0.0	0.0	0.0	0.0	0.0	0.0	0.0
C27Δ5,22	0.0	0.0	0.0	0.0	0.0	0.1	0.1	0.0
C27Δ22E	0.0	0.0	0.0	0.0	0.0	0.0	0.0	0.0
C27Δ5,22	1.3	2.1	3.7	4.4	3.5	4.4	3.2	1.0
C27Δ22	0.1	0.0	0.2	0.2	0.0	0.2	0.0	0.0
C27Δ5	6.1	8.3	16.0	16.2	12.1	15.2	18.5	9.4
C27Δ0	0.1	1.7	0.3	0.4	0.4	0.3	0.1	0.1
C28Δ5,22	2.4	2.0	2.1	3.6	2.7	4.6	1.2	0.5
C28Δ22	0.1	0.3	0.0	0.3	0.1	0.4	0.0	0.0
C27Δ7	0.0	0.0	0.0	0.2	0.1	0.1	0.0	0.0
C28Δ5	0.8	0.0	0.8	0.0	0.0	0.0	0.0	0.0
C28Δ5 isom.	0.0	0.0	0.0	0.0	0.0	0.0	0.3	0.0
C28Δ5	1.0	0.0	0.0	0.0	0.0	0.8	0.1	0.0
C28Δ22	0.0	0.0	0.0	0.0	0.0	0.0	0.1	0.0
C28Δ5,X	0.0	0.0	0.0	0.0	0.0	0.0	0.0	0.0
C29Δ5,22	0.0	0.0	0.0	0.0	0.0	0.0	0.0	0.0
C29 Δ5,22	0.0	0.0	0.2	0.0	0.0	0.0	0.0	0.0
C29Δ5 isom.	0.0	0.0	0.0	0.0	0.6	0.0	0.0	0.0
C29Δ5	1.6	0.0	0.0	0.0	0.0	0.0	0.2	0.0
C29Δ0	0.2	5.6	1.1	0.0	0.2	0.0	0.7	0.0
Dinosterol	0.0	0.0	0.0	0.0	0.1	0.0	0.0	0.0
C29Δ7	0.0	0.0	0.0	0.0	0.0	0.0	0.0	0.0
C30Δ5	0.0	0.0	0.0	0.0	0.0	0.0	0.0	0.0
Σ Sterols	13.8	21.2	25.7	26.1	33.5	26.6	25.0	11.2
br. C15 OH	0.0	0.0	0.0	0.0	0.0	0.0	0.0	0.0
phytadiene isomers	2.0	2.0	0.2	0.9	0.2	0.1	0.3	0.2
br. 19 OH	0.0	0.0	0.0	0.0	0.0	0.1	0.0	0.0
br. C17 OH (iso)	0.0	0.0	0.0	0.0	0.0	0.0	0.0	0.0
br. C17 OH (anteiso)	0.0	0.0	0.0	0.0	0.0	0.0	0.0	0.0
br. C18 OH (iso)	0.0	0.0	0.0	0.0	0.0	0.0	0.0	0.0
br. C18 OH (anteiso)	0.0	0.0	0.0	0.0	0.0	0.0	0.0	0.0
br. C19 OH (iso)	0.0	0.0	0.0	0.0	0.0	0.0	0.0	0.0
br. C19 OH (anteiso)	0.0	0.0	0.0	0.0	0.0	0.0	0.0	0.0
br. C20 OH	0.0	0.0	0.0	0.0	0.0	0.0	0.0	0.0
C27 hopanone	0.0	0.0	0.0	0.0	0.0	0.0	0.0	0.0
cholesta-3,5-dien-7-one	0.0	0.0	0.0	0.0	0.0	0.0	0.0	0.0
12-OH(ω17)-C26	0.0	0.0	0.0	0.3	2.2	9.9	0.0	0.0
unsat. C28 diol isom.	0.0	0.0	0.0	0.0	3.4	12.1	0.0	0.0
12-OH(ω17)-C28	0.0	0.0	0.0	0.0	1.9	5.9	0.0	0.0
bb-hopanoic acid	0.7	0.0	0.1	0.2	0.0	0.0	0.0	0.3
37:3 Ketone	0.0	0.0	0.0	0.0	0.0	4.2	0.0	0.0
37:2 Ketone	0.0	0.0	0.0	0.0	0.0	3.1	0.0	0.0
Σ Other	2.7	2.0	0.4	1.4	7.8	35.3	0.3	0.5

Figure A.13: Complete lipid dataset for the Kerguelen sediment trap deployment at station A3 (289 m) - continued.

Sample cup	P3-1	P3-2_3	P3-4	P3-5	P3-6_7	P3-8	P3-10	P3-11	P3-12
Start	15/01/2012	01/02/2012	01/03/2012	01/04/2012	01/05/2012	01/07/2012	01/09/2012	01/10/2012	01/11/2012
Stop	01/02/2012	01/03/2012	01/04/2012	01/05/2012	01/07/2012	01/08/2012	01/10/2012	01/11/2012	01/12/2012
Total lipid flux (µg/m2/d)	122.3	38.6	11.5	7.5	3.9	3.2	5.7	4.8	4.8
Relative abund. (%)									
C14:1 (cis-9)	0.0	2.2	0.0	0.0	0.0	0.0	0.0	0.0	0.0
C16:1 (cis-9)	10.2	18.1	4.8	1.3	2.1	0.0	0.2	5.2	3.3
C16:1 isom.	0.1	0.5	0.3	0.0	0.2	0.0	0.0	0.2	0.1
C16:1 isom.	0.3	0.4	0.5	0.0	0.1	0.0	0.0	0.4	0.1
C17:1 (cis-10)	0.2	0.2	0.4	0.0	0.1	0.0	0.0	0.8	0.6
C17:1 isom.	0.0	0.1	0.0	0.0	0.1	0.0	0.0	0.3	0.0
C17:1 isom.	0.1	0.0	0.5	0.0	0.0	0.0	0.0	0.0	0.0
C18:1 (cis-9)	1.9	3.5	4.9	1.8	4.2	0.3	0.4	3.4	2.0
C18:1 (tr-9)	2.3	6.5	4.3	0.9	1.7	0.1	0.2	0.5	3.4
C18:1 isom.	0.0	0.0	0.0	0.0	0.1	0.0	0.0	0.2	0.1
C18:1 isom.	0.0	0.0	0.0	0.0	0.0	0.0	0.0	0.0	0.0
C19:1 isom.	0.0	0.0	0.0	0.0	0.0	0.0	0.0	0.0	0.0
C19:1 isom.	0.0	0.0	0.0	0.0	0.0	0.0	0.0	0.0	0.0
C19:1 isom.	0.0	0.0	1.6	2.2	0.0	0.0	0.0	3.7	3.8
C19:1 isom.	0.0	0.0	0.4	0.6	0.0	0.0	0.0	0.9	0.9
C20:1 (cis-11)	0.3	0.4	0.4	0.1	0.2	0.0	0.0	0.4	0.3
C20:1 isom.	0.1	0.1	0.0	0.0	0.0	0.0	0.0	0.0	0.0
C22:1 isom.	0.2	0.0	0.0	0.0	0.0	0.0	0.0	0.0	0.0
C22:1 (cis-13)	0.1	0.0	0.1	0.0	0.0	0.0	0.0	0.0	0.0
C22:1 isom.	0.0	0.0	0.1	0.0	0.0	0.0	0.0	0.0	0.0
C24:1 isom.	0.0	0.0	0.0	0.0	0.0	0.0	0.0	0.0	0.0
C24:1 (cis-15)	0.7	0.2	0.3	0.1	0.1	0.0	0.0	0.6	0.3
Σ MUFA	16.5	32.1	18.4	7.0	8.9	0.3	0.9	16.7	15.0
C16:3	0.0	0.0	0.0	0.0	0.0	0.0	0.0	0.0	0.0
C16:4	0.0	0.0	0.0	0.0	0.0	0.0	0.0	0.0	0.0
C18:2 (cis-9)	0.0	0.0	0.0	0.2	0.3	0.0	0.0	0.0	0.0
C18:3 (cis-6)	0.0	0.0	0.0	0.0	0.0	0.0	0.0	0.0	0.0
C20:2 (cis-11)	0.0	0.0	0.0	0.0	0.0	0.0	0.0	0.0	0.0
C20:3 (cis-11)	0.0	0.0	0.0	0.0	0.0	0.0	0.0	0.0	0.0
C20:4 (cis-5)	0.1	0.0	0.0	0.0	0.0	0.0	0.0	0.0	0.0
C20:5 (cis-8)	2.4	0.2	0.1	0.0	0.0	0.0	0.0	0.1	0.0
C22:2 (cis-13)	0.0	0.0	0.0	0.0	0.0	0.0	0.0	0.0	0.0
C22:6 (cis-9)	0.2	0.1	0.1	0.0	0.0	0.0	0.0	0.0	0.0
Σ PUFA	2.7	0.3	0.2	0.2	0.3	0.0	0.0	0.1	0.0
C16:1 OH	0.0	0.9	0.0	0.5	0.8	0.0	0.0	0.0	0.0
C18:1 OH	0.0	1.8	0.0	0.6	1.4	0.0	0.4	0.0	0.2
C18:1 OH isom.	0.0	0.5	0.0	0.1	0.3	0.0	0.0	0.0	0.0
C18:1 OH isom.	0.0	0.0	0.0	0.0	0.0	0.0	0.0	0.0	0.0
C20:1 OH	0.0	0.3	0.0	0.1	0.7	0.0	0.0	0.0	0.0
C22:1 OH	0.0	0.0	0.0	0.0	0.0	0.0	0.0	0.0	0.0
C22:1 OH isom.	0.0	0.0	0.0	0.0	0.0	0.0	0.0	0.0	0.0
C24:1 OH	0.0	0.0	0.0	0.3	0.0	0.0	0.0	0.0	0.0
C24:1 OH isom.	0.0	0.0	0.0	0.0	0.0	0.0	0.0	0.0	0.0
Σ unsat. OH	0.0	3.5	0.0	1.5	3.1	0.0	0.4	0.0	0.2
C14 FAME	3.9	2.0	0.9	0.0	0.2	0.0	0.0	0.6	0.7
C15 FAME	0.1	0.1	0.2	0.0	0.0	0.0	0.0	0.0	0.1
C16 FAME	6.0	8.4	9.3	3.4	3.9	0.0	0.7	8.9	6.2
C17 FAME	0.0	0.0	0.2	0.0	0.0	0.0	0.0	0.1	0.1
C18 FAME	0.4	0.3	0.9	0.3	0.8	0.3	0.3	6.5	1.1
C19 FAME	0.0	0.0	0.0	0.0	0.0	0.0	0.0	0.0	0.0
C20 FAME	0.1	0.0	0.1	0.0	0.2	0.0	0.0	0.1	0.0
C21 FAME	0.0	0.0	0.0	0.0	0.0	0.0	0.0	0.0	0.0
C22 FAME	0.1	0.0	0.0	0.0	0.0	0.0	0.0	0.1	0.0
C23 FAME	0.0	0.0	0.0	0.0	0.0	0.0	0.0	0.0	0.0
C24 FAME	0.3	0.0	0.1	0.0	0.0	0.0	0.0	3.6	0.1
C25 FAME	0.0	0.0	0.0	0.0	0.0	0.0	0.0	0.0	0.0
C26 FAME	0.0	0.0	0.0	0.0	0.0	0.0	0.0	0.0	0.0
Σ FAME	10.9	10.9	11.6	3.7	5.0	0.3	1.0	19.9	8.4

Figure A.14: Complete lipid dataset for the South Georgia sediment trap deployment at station P3 (2000 m).

4,8-dimethyl-C12:0	0.0	0.0	0.0	0.0	0.0	0.0	0.0	0.0	0.0
i-C15:0	0.2	0.1	0.2	0.0	0.0	0.0	0.0	0.3	0.2
a-C15:0	0.1	0.0	0.1	0.0	0.0	0.0	0.0	0.1	0.1
i-C16:0	0.0	0.0	0.0	0.0	0.0	0.0	0.0	0.0	0.0
a-C16:0	0.0	0.0	0.0	0.0	0.0	0.0	0.0	0.0	0.0
i-C17:0	0.0	0.0	0.0	0.0	0.0	0.0	0.0	0.0	0.1
a-C17:0	0.0	0.0	0.1	0.0	0.0	0.0	0.0	0.1	0.0
i-C18:0	0.0	0.0	0.0	0.0	0.0	0.0	0.0	0.0	0.0
Σ br. FAME	0.3	0.1	0.5	0.0	0.1	0.0	0.0	0.5	0.4
C12 OH	0.0	0.0	0.2	0.0	0.0	0.0	0.0	0.0	0.0
C13 OH	0.0	0.0	0.1	0.0	0.0	0.0	0.0	0.0	0.1
C14 OH	0.4	0.5	0.5	0.2	0.1	0.0	0.0	0.5	0.4
C15 OH	0.0	0.0	0.1	0.2	0.0	0.0	0.0	0.1	2.4
C16 OH	0.8	2.8	2.9	1.1	1.2	0.0	0.0	2.1	0.0
C17 OH	0.0	0.0	0.0	0.0	0.0	0.0	0.0	0.0	0.0
C18 OH	0.2	0.2	1.0	0.2	0.3	0.2	0.1	1.5	1.0
C19 OH	0.0	0.0	0.0	0.0	0.0	0.0	0.0	0.0	0.0
C20 OH	0.0	0.0	0.1	0.0	0.0	0.0	0.0	0.1	0.0
C21 OH	0.0	0.0	0.0	0.0	0.0	0.0	0.0	0.0	0.0
C22 OH	0.0	0.0	0.0	0.0	0.0	0.0	0.0	0.0	0.0
C23 OH	0.0	0.0	0.0	0.0	0.0	0.0	0.0	0.0	0.0
C24 OH	0.1	0.0	0.0	0.0	0.0	0.0	0.0	0.0	0.0
Σ OH	1.4	3.4	5.0	1.7	1.7	0.2	0.1	4.3	4.0
C26Δ22	0.6	1.2	0.1	0.1	0.1	0.1	0.0	0.1	0.1
C26Δ5,22	4.7	1.1	0.8	2.1	1.3	0.9	0.5	0.7	0.3
Coprostanol	0.0	0.0	0.0	0.0	0.0	0.0	0.0	0.0	0.0
Epicoprostanol	0.0	0.0	0.0	0.0	0.0	0.0	0.0	0.0	0.0
C27Δ22 (Z)	0.0	0.0	0.0	0.0	0.0	0.0	0.0	0.0	0.2
C27Δ5,22	0.2	0.3	0.4	0.9	0.6	0.3	0.3	0.2	0.0
C27Δ22E	0.0	0.2	0.0	0.0	0.0	0.0	0.0	0.0	0.0
C27Δ5,22	10.3	6.1	7.7	11.1	7.0	11.1	11.0	4.9	3.9
C27Δ22	1.0	1.1	0.3	0.5	0.4	0.3	0.5	0.3	0.4
C27Δ5	17.7	23.5	33.1	48.4	58.6	79.4	67.9	37.7	51.7
C27Δ0	1.5	0.9	1.0	1.6	1.2	1.0	2.3	1.2	0.9
C28Δ5,22	7.7	7.0	10.7	12.7	6.2	0.0	8.2	3.2	3.9
C28Δ22	0.3	1.2	0.0	0.0	0.0	0.0	0.6	0.0	0.7
C27Δ7	0.0	0.0	0.0	0.0	0.0	0.0	0.0	0.0	0.0
C28Δ5	1.0	1.6	0.0	2.4	1.3	0.0	1.0	0.0	0.0
C28Δ5 isom.	0.0	0.0	1.8	0.0	0.0	0.0	0.0	0.0	1.0
C28Δ5	5.5	1.0	1.1	1.6	0.8	0.8	0.9	0.0	0.5
C28Δ22	0.0	1.1	0.0	0.0	0.0	0.0	0.0	0.0	0.0
C28Δ5,X	0.0	0.0	0.0	0.0	0.0	0.0	0.0	0.0	0.0
C29Δ5,22	0.4	0.0	0.5	0.0	0.0	0.0	0.0	0.0	0.0
C29 Δ5,22	2.6	0.0	0.0	0.8	0.6	0.5	0.5	0.0	0.8
C29Δ5 isom.	0.6	0.0	0.0	0.0	0.0	0.0	0.0	0.0	0.0
C29Δ5	3.7	2.1	2.5	2.2	1.4	2.2	2.2	3.5	2.8
C29Δ0	0.0	0.0	0.0	0.0	0.0	0.1	0.0	0.4	0.0
Dinosterol	2.1	0.0	1.8	0.4	0.2	0.2	0.4	1.4	1.1
C29Δ7	3.5	0.8	0.4	0.0	0.0	0.2	0.0	0.0	0.5
C30Δ5	0.6	0.0	0.6	0.0	0.0	0.0	0.0	0.0	0.0
Σ Sterols	64.1	49.4	62.9	84.7	79.7	97.0	96.3	53.5	68.7
br. C15 OH	0.0	0.0	0.0	0.0	0.1	0.0	0.0	0.0	0.0
phytadiene isomers	4.0	0.1	0.2	0.0	0.0	0.0	0.0	3.1	1.0
br. 19 OH	0.0	0.0	0.0	0.0	0.0	0.0	0.0	0.0	0.0
br. C17 OH (iso)	0.0	0.0	0.0	0.0	0.0	0.0	0.0	0.0	0.0
br. C17 OH (anteiso)	0.0	0.0	0.0	0.0	0.0	0.0	0.0	0.0	0.0
br. C18 OH (iso)	0.0	0.0	0.0	0.0	0.0	0.0	0.0	0.0	0.0
br. C18 OH (anteiso)	0.0	0.0	0.0	0.0	0.0	0.0	0.0	0.0	0.0
br. C19 OH (iso)	0.0	0.0	0.0	0.0	0.0	0.0	0.0	0.0	0.0
br. C19 OH (anteiso)	0.0	0.0	0.0	0.0	0.0	0.0	0.0	0.0	0.0
br. C20 OH	0.0	0.0	0.0	0.0	0.0	0.0	0.0	0.0	0.0
C27 hopanone	0.0	0.0	0.0	0.0	0.0	0.0	0.0	0.0	0.0
cholesta-3,5-dien-7-one	0.0	0.0	0.0	0.0	0.0	0.0	0.0	0.0	0.0
12-OH(ω17)-C26	0.0	0.0	0.0	0.0	0.0	0.0	0.0	0.0	0.0
unsat. C28 diol isom.	0.0	0.0	0.0	0.0	0.0	0.0	0.0	0.0	0.0
12-OH(ω17)-C28	0.0	0.0	0.0	0.0	0.0	0.0	0.0	0.0	0.0
bb-hopanoic acid	0.0	0.2	1.2	1.1	0.9	2.2	1.3	1.9	2.4
37:3 Ketone	0.0	0.0	0.0	0.0	0.0	0.0	0.0	0.0	0.0
37:2 Ketone	0.0	0.0	0.0	0.0	0.0	0.0	0.0	0.0	0.0
Σ Other	4.0	0.4	1.5	1.1	1.1	2.2	1.3	5.0	3.4

Figure A.15: Complete lipid dataset for the South Georgia sediment trap deployment at station P3 (2000 m) - continued.

Sample cup	P2-1_3	P2-4	P2-6	P2-7	P2-9	P2-10	P2-12
Start	15/01/2012	01/03/2012	01/05/2012	01/06/2012	01/08/2012	01/09/2012	01/11/2012
Stop	01/03/2012	01/04/2012	01/06/2012	01/07/2012	01/09/2012	01/10/2012	01/12/2012
Total lipid flux (µg/m2/d)	4.1	26.0	20.2	6.6	7.8	9.7	17.2
Relative abund. (%)							
C14:1 (cis-9)	0.0	0.0	0.0	0.0	0.0	0.0	0.0
C16:1 (cis-9)	0.8	1.7	2.1	1.5	1.2	1.5	5.1
C16:1 isom.	0.0	0.1	0.1	0.0	0.1	0.1	0.2
C16:1 isom.	0.0	0.1	0.0	0.0	0.0	0.0	0.2
C17:1 (cis-10)	0.0	0.3	0.4	0.0	0.0	0.0	0.3
C17:1 isom.	0.0	0.1	0.0	0.0	0.0	0.0	0.0
C17:1 isom.	0.0	0.0	0.0	0.0	0.0	0.0	0.7
C18:1 (cis-9)	1.5	1.8	1.5	0.7	1.2	0.7	3.5
C18:1 (tr-9)	2.3	1.5	2.2	2.7	1.7	3.2	6.2
C18:1 isom.	0.0	0.0	0.0	0.0	0.0	0.0	0.0
C18:1 isom.	0.0	0.0	0.0	0.0	0.0	0.0	0.0
C19:1 isom.	0.0	0.0	0.0	0.0	0.0	0.0	0.0
C19:1 isom.	0.0	0.0	0.0	0.0	0.0	0.0	0.0
C19:1 isom.	0.0	0.6	0.1	0.0	0.0	0.0	0.0
C19:1 isom.	0.0	0.2	0.0	0.0	0.0	0.0	0.0
C20:1 (cis-11)	0.0	0.2	0.1	0.0	0.1	0.3	1.9
C20:1 isom.	0.0	0.0	0.0	0.0	0.0	0.0	0.0
C22:1 isom.	0.0	0.0	0.0	0.0	0.0	0.0	0.1
C22:1 (cis-13)	0.0	0.0	0.0	0.0	0.0	0.0	0.1
C22:1 isom.	0.0	0.0	0.0	0.0	0.0	0.0	0.0
C24:1 isom.	0.0	0.0	0.0	0.0	0.0	0.0	0.0
C24:1 (cis-15)	0.0	0.1	0.0	0.0	0.0	0.0	1.0
Σ MUFA	4.6	6.8	6.5	5.0	4.2	5.7	19.4
C16:3	0.0	0.0	0.0	0.0	0.0	0.0	0.0
C16:4	0.0	0.0	0.0	0.0	0.0	0.0	0.0
C18:2 (cis-9)	0.0	0.1	0.2	0.0	0.0	0.0	0.0
C18:3 (cis-6)	0.0	0.0	0.0	0.0	0.0	0.0	0.0
C20:2 (cis-11)	0.0	0.0	0.0	0.0	0.0	0.0	0.0
C20:3 (cis-11)	0.0	0.0	0.0	0.0	0.0	0.0	0.0
C20:4 (cis-5)	0.0	0.0	0.0	0.0	0.0	0.0	0.0
C20:5 (cis-8)	0.0	0.1	0.0	0.0	0.0	0.0	0.1
C22:2 (cis-13)	0.0	0.0	0.0	0.0	0.0	0.0	0.0
C22:6 (cis-9)	0.0	0.1	0.1	0.0	0.0	0.0	0.2
Σ PUFA	0.0	0.3	0.3	0.0	0.0	0.0	0.4
C16:1 OH	0.0	0.0	0.0	0.0	0.2	0.1	0.0
C18:1 OH	0.1	0.2	0.0	0.1	0.4	0.0	0.0
C18:1 OH isom.	0.1	0.0	0.0	0.0	0.1	0.0	0.0
C18:1 OH isom.	0.0	0.0	0.0	0.0	0.0	0.0	0.0
C20:1 OH	0.0	1.3	0.0	0.0	0.2	0.2	0.0
C22:1 OH	0.0	0.0	0.0	0.0	0.0	0.0	0.0
C22:1 OH isom.	0.0	0.0	0.0	0.0	0.0	0.0	0.0
C24:1 OH	0.0	0.0	0.0	0.0	0.0	0.0	0.0
C24:1 OH isom.	0.0	0.0	0.0	0.0	0.0	0.0	0.0
Σ unsat. OH	0.2	1.6	0.0	0.1	0.9	0.3	0.0
C14 FAME	0.1	0.0	0.3	0.0	0.1	0.2	0.6
C15 FAME	0.0	0.0	0.0	0.0	0.0	0.0	0.1
C16 FAME	3.5	6.7	2.4	4.6	4.3	3.6	5.1
C17 FAME	0.0	0.0	0.0	0.0	0.0	0.0	0.1
C18 FAME	0.7	0.7	0.3	1.1	0.4	0.0	0.5
C19 FAME	0.0	0.0	0.0	0.0	0.0	0.0	0.0
C20 FAME	0.0	0.0	0.0	0.0	0.0	0.0	0.0
C21 FAME	0.0	0.0	0.0	0.0	0.0	0.0	0.0
C22 FAME	0.0	0.0	0.0	0.0	0.0	0.0	0.1
C23 FAME	0.0	0.0	0.0	0.0	0.0	0.0	0.0
C24 FAME	0.0	0.0	0.0	0.0	0.0	0.0	3.6
C25 FAME	0.0	0.0	0.0	0.0	0.0	0.0	0.0
C26 FAME	0.0	0.0	0.0	0.0	0.0	0.0	0.0
Σ FAME	4.3	7.4	3.0	5.7	4.8	3.9	9.9

Figure A.16: Complete lipid dataset for the South Georgia sediment trap deployment at station P2 (1500 m).

4,8-dimethyl-C12:0	0.0	0.0	0.0	0.0	0.0	0.0	0.0
i-C15:0	0.0	0.1	0.5	0.0	0.1	0.0	0.1
a-C15:0	0.0	0.0	0.1	0.0	0.0	0.0	0.0
i-C16:0	0.0	0.0	0.0	0.0	0.0	0.1	0.0
a-C16:0	0.0	0.0	0.0	0.0	0.0	0.0	0.0
i-C17:0	0.0	0.0	0.1	0.0	0.0	0.0	0.0
a-C17:0	0.0	0.0	0.1	0.0	0.0	0.0	0.0
i-C18:0	0.0	0.0	0.0	0.0	0.0	0.0	0.0
Σ br. FAME	0.0	0.2	0.8	0.0	0.1	0.1	0.3
C12 OH	0.0	0.0	0.0	0.0	0.0	0.0	0.0
C13 OH	0.0	0.0	0.0	0.0	0.0	0.0	0.0
C14 OH	0.1	0.2	0.4	0.0	0.2	0.2	0.6
C15 OH	0.0	0.0	0.0	0.0	0.3	0.0	0.0
C16 OH	0.8	0.9	1.4	0.6	0.9	0.7	2.0
C17 OH	0.0	0.0	0.0	0.0	0.0	0.0	0.0
C18 OH	0.2	0.3	0.3	0.1	0.1	0.2	0.5
C19 OH	0.0	0.0	0.0	0.0	0.0	0.0	0.0
C20 OH	0.0	0.0	0.0	0.0	0.0	0.0	0.0
C21 OH	0.0	0.0	0.0	0.0	0.0	0.0	0.0
C22 OH	0.0	0.0	0.0	0.0	0.0	0.0	0.0
C23 OH	0.0	0.0	0.0	0.0	0.0	0.0	0.0
C24 OH	0.0	0.0	0.0	0.0	0.0	0.0	0.0
Σ OH	1.0	1.3	2.1	0.7	1.6	1.1	3.1
C26Δ22	0.1	0.1	0.2	0.2	0.1	0.1	0.5
C26Δ5,22	0.9	1.9	1.4	1.3	2.8	0.4	3.2
Coprostanol	0.0	0.0	0.0	0.0	0.0	0.0	0.0
Epicoprostanol	0.0	0.0	0.0	0.0	0.0	0.0	0.0
C27Δ22 (Z)	0.0	0.0	0.0	0.0	0.0	0.0	0.0
C27Δ5,22	0.8	2.1	0.9	0.8	3.0	0.1	0.1
C27Δ22E	0.0	0.0	0.1	0.1	0.0	0.0	0.0
C27Δ5,22	11.9	13.4	13.2	13.2	14.1	8.0	6.5
C27Δ22	0.5	0.3	0.6	1.0	0.4	0.5	0.0
C27Δ5	27.4	29.1	26.7	47.1	28.3	69.5	25.7
C27Δ0	1.5	0.7	1.0	1.8	1.1	3.7	5.3
C28Δ5,22	14.2	16.8	15.3	13.5	20.7	2.8	6.1
C28Δ22	0.7	0.3	0.6	0.0	0.0	0.3	1.0
C27Δ7	0.0	0.0	0.2	0.0	0.0	0.0	0.0
C28Δ5	1.8	0.0	0.0	4.0	2.2	1.0	0.0
C28Δ5 isom.	0.0	2.5	2.9	0.0	0.0	0.0	0.0
C28Δ5	0.0	0.9	0.9	0.7	1.2	0.0	0.0
C28Δ22	0.0	0.0	0.0	0.0	0.0	0.0	0.0
C28Δ5,X	0.0	0.0	0.0	0.0	0.0	0.0	0.0
C29Δ5,22	0.0	0.0	0.0	0.0	0.0	0.0	0.0
C29 Δ5,22	2.1	1.5	1.2	0.5	2.2	0.0	0.0
C29Δ5 isom.	0.0	0.3	0.4	0.0	0.0	0.0	0.0
C29Δ5	11.7	11.2	13.9	2.9	0.4	1.7	0.0
C29Δ0	0.5	0.0	0.0	0.2	10.0	0.0	17.5
Dinosterol	0.0	0.1	0.4	0.0	0.0	0.0	0.0
C29Δ7	15.1	0.6	4.1	0.7	1.0	0.0	0.0
C30Δ5	0.0	0.0	0.0	0.0	0.0	0.0	0.0
Σ Sterols	89.0	81.8	84.3	87.9	87.7	88.2	65.6
br. C15 OH	0.1	0.2	2.6	0.0	0.0	0.0	0.0
phytadiene isomers	0.0	0.0	0.0	0.0	0.0	0.0	1.4
br. 19 OH	0.0	0.0	0.0	0.0	0.0	0.0	0.0
br. C17 OH (iso)	0.0	0.0	0.0	0.0	0.0	0.0	0.0
br. C17 OH (anteiso)	0.0	0.0	0.0	0.0	0.0	0.0	0.0
br. C18 OH (iso)	0.0	0.0	0.0	0.0	0.0	0.0	0.0
br. C18 OH (anteiso)	0.0	0.0	0.0	0.0	0.0	0.0	0.0
br. C19 OH (iso)	0.0	0.0	0.0	0.0	0.0	0.0	0.0
br. C19 OH (anteiso)	0.0	0.0	0.0	0.0	0.0	0.0	0.0
br. C20 OH	0.0	0.0	0.0	0.0	0.0	0.0	0.0
C27 hopanone	0.0	0.0	0.0	0.0	0.0	0.0	0.0
cholesta-3,5-dien-7-one	0.0	0.0	0.0	0.0	0.0	0.0	0.0
12-OH(ω17)-C26	0.0	0.0	0.0	0.0	0.0	0.0	0.0
unsat. C28 diol isom.	0.0	0.0	0.0	0.0	0.0	0.0	0.0
12-OH(ω17)-C28	0.0	0.0	0.0	0.0	0.0	0.0	0.0
bb-hopanoic acid	0.8	0.3	0.4	0.7	0.9	0.6	0.0
37:3 Ketone	0.0	0.0	0.0	0.0	0.0	0.0	0.0
37:2 Ketone	0.0	0.0	0.0	0.0	0.0	0.0	0.0
Σ Other	0.9	0.5	3.0	0.7	0.9	0.7	1.4

Figure A.17: Complete lipid dataset for the South Georgia sediment trap deployment at station P2 (1500 m) - continued.

Sample cup	M5-1	M5-2	M5-3	M5-4	M5-5	M5-6	M5-7	M5-19
Start	28/12/2004	09/01/2005	23/01/2005	06/02/2005	27/02/2005	27/03/2005	24/04/2005	18/12/2005
Stop	09/01/2005	23/01/2005	06/02/2005	27/02/2005	27/03/2005	24/04/2005	22/05/2005	11/01/2006
Total lipid flux (µg/m2/d)	5.9	5.6	9.1	9.0	11.4	0.9	2.8	285.8
Relative abund. (%)								
C14:1 (cis-9)	0.0	0.0	0.0	0.0	0.0	0.0	0.0	0.0
C16:1 (cis-9)	1.6	5.4	1.2	0.9	2.1	1.5	1.3	2.8
C16:1 isom.	0.3	0.0	0.0	0.0	0.1	0.2	0.0	0.1
C16:1 isom.	0.2	0.0	0.0	0.0	0.6	0.2	0.0	0.4
C17:1 (cis-10)	0.2	0.0	0.2	0.0	0.1	0.1	0.0	0.1
C17:1 isom.	0.0	0.0	0.0	0.0	0.0	0.0	0.0	0.0
C17:1 isom.	0.0	0.0	0.0	0.0	0.0	0.0	0.0	0.0
C18:1 (cis-9)	4.7	8.1	9.4	3.3	9.7	23.2	5.7	8.7
C18:1 (tr-9)	0.5	2.1	2.6	1.0	3.1	0.0	1.3	1.4
C18:1 isom.	0.0	0.0	0.0	0.0	0.0	2.8	0.0	0.8
C18:1 isom.	0.0	0.0	0.2	0.3	0.0	0.0	0.0	0.3
C19:1 isom.	0.0	0.0	0.0	0.0	0.0	0.0	0.0	0.0
C19:1 isom.	0.0	0.0	0.0	0.0	0.0	0.0	0.0	0.0
C19:1 isom.	0.0	0.0	0.0	0.0	0.0	0.0	0.0	0.0
C19:1 isom.	0.0	0.0	0.0	0.0	0.0	0.0	0.0	0.0
C20:1 (cis-11)	0.2	1.8	1.8	0.1	0.1	3.1	0.8	0.5
C20:1 isom.	0.1	0.0	0.4	1.6	3.4	0.3	0.3	0.1
C22:1 isom.	0.0	0.0	0.0	1.2	1.2	0.6	1.4	0.4
C22:1 (cis-13)	0.2	0.0	3.6	2.4	0.9	7.3	1.1	1.2
C22:1 isom.	0.0	0.0	0.0	0.2	0.1	0.0	0.0	0.0
C24:1 isom.	0.1	0.0	0.0	1.9	0.5	0.3	0.7	0.2
C24:1 (cis-15)	0.3	0.0	0.0	1.0	0.6	3.2	0.4	1.3
Σ MUFA	8.4	17.4	19.4	13.9	22.5	42.8	12.9	18.3
C16:3	0.0	0.0	0.0	0.0	0.0	0.0	0.0	0.0
C16:4	0.0	0.0	0.0	0.0	0.0	0.0	0.0	0.0
C18:2 (cis-9)	0.0	0.0	0.3	0.1	0.2	0.3	0.2	0.1
C18:3 (cis-6)	0.0	0.0	0.0	0.0	0.0	0.0	0.0	0.0
C20:2 (cis-11)	0.0	0.0	0.1	0.0	0.1	0.1	0.1	1.2
C20:3 (cis-11)	0.0	0.0	0.0	0.0	0.0	0.0	0.0	5.0
C20:4 (cis-5)	0.0	0.0	0.0	0.0	0.7	0.1	0.0	0.0
C20:5 (cis-8)	0.0	0.0	0.0	0.0	0.0	0.1	0.0	0.2
C22:2 (cis-13)	0.0	0.0	0.9	0.0	0.0	1.2	0.0	0.0
C22:6 (cis-9)	0.0	0.0	3.3	0.0	0.0	0.0	0.0	0.0
Σ PUFA	0.0	0.0	4.6	0.1	1.0	1.8	0.3	6.5
C16:1 OH	0.0	0.0	0.0	0.0	0.0	0.0	0.0	0.1
C18:1 OH	0.0	0.0	0.0	0.1	1.3	0.1	0.1	0.2
C18:1 OH isom.	0.0	0.0	0.0	0.2	1.0	0.2	0.1	0.1
C18:1 OH isom.	0.0	0.0	0.0	0.0	0.1	0.0	0.0	0.1
C20:1 OH	0.1	0.0	0.1	0.4	2.2	0.4	0.3	0.2
C22:1 OH	0.0	0.0	0.0	0.2	0.4	0.1	0.1	0.1
C22:1 OH isom.	0.1	0.0	0.0	0.3	1.2	1.0	0.5	0.0
C24:1 OH	0.0	0.0	0.0	0.1	0.1	0.0	0.0	0.1
C24:1 OH isom.	0.1	0.0	0.0	0.5	0.2	0.6	0.3	0.0
Σ unsat. OH	0.2	0.0	0.1	1.9	6.6	2.3	1.4	1.0
C14 FAME	2.5	4.5	3.5	1.6	3.5	0.0	1.1	1.8
C15 FAME	0.8	1.4	0.7	0.3	0.7	0.0	0.4	0.4
C16 FAME	21.2	46.0	23.9	10.5	19.0	16.0	11.0	15.2
C17 FAME	0.5	0.6	0.5	0.3	0.4	0.6	0.5	0.2
C18 FAME	3.7	4.9	3.7	3.8	2.9	4.6	3.1	2.7
C19 FAME	0.0	0.0	0.0	0.1	0.1	0.1	0.0	0.0
C20 FAME	0.4	0.2	0.5	0.5	0.5	0.4	0.4	0.2
C21 FAME	0.2	0.0	0.0	0.0	0.7	0.1	0.0	0.0
C22 FAME	0.6	0.0	0.5	0.2	0.3	0.3	0.4	0.1
C23 FAME	0.2	0.0	0.1	0.0	0.1	0.1	0.1	0.1
C24 FAME	1.4	1.1	0.8	0.3	0.5	0.5	0.6	0.2
C25 FAME	0.3	0.0	0.1	0.1	0.0	0.0	0.1	0.1
C26 FAME	0.5	0.0	0.6	0.1	0.0	0.0	0.3	0.1
Σ FAME	32.3	58.7	34.9	17.8	28.7	22.6	17.9	21.1

Figure A.18: Complete lipid dataset for the Crozet sediment trap deployment at station M5 (3195 m).

4,8-dimethyl-C12:0	0.1	0.0	0.1	0.0	0.1	0.0	0.0	0.2
i-C15:0	0.4	0.0	0.3	0.2	0.6	0.0	0.2	0.1
a-C15:0	0.2	0.0	0.1	0.1	0.2	0.0	0.1	0.1
i-C16:0	0.0	0.0	0.3	0.0	0.1	0.0	0.0	0.0
a-C16:0	0.0	0.0	0.0	0.0	0.2	0.3	0.2	0.1
i-C17:0	0.3	0.0	0.7	0.2	0.5	0.5	0.2	0.2
a-C17:0	0.3	0.0	0.4	0.2	0.3	0.5	0.3	0.1
i-C18:0	0.0	0.0	0.0	0.5	0.2	0.1	0.2	0.0
Σ br. FAME	1.3	0.0	1.9	1.2	2.2	1.4	1.1	0.8
C12 OH	0.0	0.0	0.0	0.0	0.0	0.0	0.0	0.0
C13 OH	0.0	0.0	0.0	0.0	0.0	0.0	0.0	0.0
C14 OH	0.7	0.3	0.5	0.0	0.5	0.0	0.0	0.3
C15 OH	0.1	0.3	0.1	0.3	0.1	0.1	0.1	0.1
C16 OH	3.7	0.9	2.6	36.2	8.3	4.2	1.6	4.7
C17 OH	0.0	0.0	0.0	0.4	0.4	0.1	0.0	0.0
C18 OH	1.2	0.0	0.4	7.8	5.0	0.7	0.8	0.6
C19 OH	0.0	0.0	0.0	0.1	0.2	0.0	0.0	0.0
C20 OH	0.2	0.0	0.2	0.6	0.4	0.1	0.1	0.2
C21 OH	0.1	0.0	0.0	0.0	0.3	0.0	0.1	0.0
C22 OH	0.2	0.0	0.2	0.4	0.4	0.1	0.2	0.1
C23 OH	0.1	0.0	0.1	0.1	0.1	0.1	0.1	0.1
C24 OH	0.2	0.0	0.1	0.3	0.0	0.2	0.1	0.0
Σ OH	6.6	1.6	4.1	46.3	15.7	5.6	3.1	6.2
C26Δ22	0.5	0.0	0.0	0.0	0.2	0.0	0.8	0.1
C26Δ5,22	2.0	1.0	0.0	0.0	0.5	0.0	2.2	0.6
Coprostanol	0.2	0.0	0.1	0.2	0.1	0.0	0.1	0.1
Epicoprostanol	0.7	0.0	0.5	0.3	0.2	0.4	0.0	0.0
C27Δ22 (Z)	0.1	0.0	0.0	0.0	0.0	0.0	0.1	0.1
C27Δ5,22	0.0	0.0	0.0	0.0	0.0	0.0	0.0	0.0
C27Δ22E	0.0	0.0	0.0	0.0	0.0	0.0	0.0	0.0
C27Δ5,22	4.4	4.2	0.0	0.0	2.3	1.2	7.3	1.0
C27Δ22	0.8	0.0	0.0	0.0	0.4	0.1	0.8	0.1
C27Δ5	19.4	12.6	25.1	11.4	15.2	15.2	33.3	39.1
C27Δ0	1.0	0.2	0.0	0.5	0.6	0.7	1.1	0.6
C28Δ5,22	9.4	4.3	6.3	3.0	2.0	2.5	7.4	1.4
C28Δ22	0.0	0.0	0.0	0.0	0.0	0.0	0.0	0.0
C27Δ7	0.0	0.0	0.0	0.0	0.0	0.0	0.0	0.0
C28Δ5	0.0	0.0	0.0	0.0	0.0	0.0	0.0	0.0
C28Δ5 isom.	0.0	0.0	0.0	0.0	0.0	0.0	0.0	0.0
C28Δ5	0.0	0.0	0.0	0.4	0.0	0.0	0.5	0.1
C28Δ22	0.9	0.0	0.0	0.0	0.4	0.3	1.4	0.3
C28Δ5,X	0.9	0.0	0.0	0.0	0.0	0.3	0.0	0.2
C29Δ5,22	0.9	0.0	0.0	0.0	0.0	0.2	0.0	0.1
C29 Δ5,22	0.9	0.0	0.4	0.6	0.3	0.3	0.8	0.2
C29Δ5 isom.	2.4	0.0	0.0	1.0	0.0	0.0	0.0	0.3
C29Δ5	0.7	0.0	0.2	0.0	0.0	0.9	2.8	0.2
C29Δ0	1.6	0.0	0.3	0.1	0.3	0.1	0.1	0.1
Dinosterol	0.5	0.0	0.0	0.0	0.2	0.0	0.6	0.1
C29Δ7	0.0	0.0	0.0	0.0	0.0	0.0	0.0	0.0
C30Δ5	0.0	0.0	0.0	0.0	0.0	0.0	0.0	0.0
Σ Sterols	47.3	22.3	33.0	17.5	22.7	22.2	59.3	44.6
br. C15 OH	0.0	0.0	0.0	0.1	0.0	0.0	0.0	0.0
phytadiene isomers	0.0	0.0	0.0	0.0	0.0	0.0	0.0	0.0
br. 19 OH	0.1	0.0	0.0	0.0	0.0	0.1	0.0	0.2
br. C17 OH (iso)	0.0	0.0	0.0	0.2	0.1	0.0	0.0	0.0
br. C17 OH (anteiso)	0.0	0.0	0.1	0.0	0.1	0.1	0.0	0.0
br. C18 OH (iso)	0.0	0.0	0.0	0.1	0.1	0.1	0.1	0.0
br. C18 OH (anteiso)	0.0	0.0	0.0	0.1	0.1	0.1	0.0	0.0
br. C19 OH (iso)	0.0	0.0	0.0	0.1	0.0	0.0	0.0	0.0
br. C19 OH (anteiso)	0.0	0.0	0.0	0.0	0.0	0.0	0.0	0.0
br. C20 OH	0.0	0.0	0.0	0.0	0.0	0.1	0.0	0.0
C27 hopanone	0.6	0.0	0.0	0.0	0.0	0.0	1.4	0.0
cholesta-3,5-dien-7-one	0.3	0.0	0.0	0.0	0.0	0.1	0.3	0.8
12-OH(ω17)-C26	0.4	0.0	0.2	0.1	0.0	0.0	0.2	0.0
unsat. C28 diol isom.	1.0	0.0	0.4	0.2	0.1	0.3	0.7	0.0
12-OH(ω17)-C28	0.0	0.0	0.0	0.0	0.0	0.0	0.0	0.0
bb-hopanoic acid	0.0	0.0	0.0	0.0	0.0	0.0	0.0	0.0
37:3 Ketone	0.7	0.0	0.6	0.2	0.1	0.2	0.5	0.1
37:2 Ketone	0.6	0.0	0.8	0.2	0.1	0.2	0.7	0.2
Σ Other	3.9	0.0	2.1	1.3	0.8	1.2	3.9	1.4

Figure A.19: Complete lipid dataset for the Crozet sediment trap deployment at station M5 (3195 m) - continued.

Sample cup	M6-1	M6-2	M6-4	M6-7
Start	05/01/2005	16/01/2005	13/02/2005	01/05/2005
Stop	16/01/2005	30/01/2005	06/03/2005	29/05/2005
Total lipid flux	5.7	0.5	0.8	61.0
(µg/m2/d)				
Relative abund. (%)				
C14:1 (cis-9)	0.0	0.0	0.0	0.0
C16:1 (cis-9)	0.4	1.3	1.8	9.0
C16:1 isom.	0.0	2.0	0.0	0.0
C16:1 isom.	0.0	0.0	0.0	0.3
C17:1 (cis-10)	0.0	0.1	0.4	0.2
C17:1 isom.	0.0	0.0	0.0	0.6
C17:1 isom.	0.0	0.0	0.0	0.0
C18:1 (cis-9)	1.6	9.5	6.9	26.5
C18:1 (tr-9)	0.2	1.0	0.2	0.0
C18:1 isom.	0.0	0.3	0.0	0.0
C18:1 isom.	0.0	0.0	0.0	1.0
C19:1 isom.	0.0	0.0	0.0	0.0
C19:1 isom.	0.0	0.0	0.0	0.0
C19:1 isom.	0.0	0.0	0.0	0.0
C19:1 isom.	0.0	0.0	0.0	0.0
C20:1 (cis-11)	0.1	0.0	0.1	6.8
C20:1 isom.	0.0	0.0	0.0	0.5
C22:1 isom.	0.2	0.7	0.0	0.0
C22:1 (cis-13)	0.1	2.7	0.6	0.0
C22:1 isom.	0.0	0.0	0.0	0.0
C24:1 isom.	0.0	0.0	0.0	0.0
C24:1 (cis-15)	0.1	0.0	0.1	0.0
Σ MUFA	2.7	17.6	10.1	44.8
C16:3	0.0	0.0	0.0	0.0
C16:4	0.0	0.0	0.0	0.0
C18:2 (cis-9)	0.0	1.3	0.4	1.0
C18:3 (cis-6)	0.0	0.0	0.0	0.0
C20:2 (cis-11)	0.0	0.0	0.0	0.9
C20:3 (cis-11)	0.0	0.2	0.0	0.0
C20:4 (cis-5)	0.0	0.0	0.0	0.0
C20:5 (cis-8)	0.0	0.0	0.0	1.7
C22:2 (cis-13)	0.0	0.0	0.4	0.0
C22:6 (cis-9)	0.0	0.0	0.0	6.0
Σ PUFA	0.0	1.6	0.9	9.6
C16:1 OH	0.0	0.0	0.0	0.0
C18:1 OH	0.0	0.1	0.0	0.1
C18:1 OH isom.	0.0	0.0	0.0	0.0
C18:1 OH isom.	0.0	0.0	0.0	0.0
C20:1 OH	0.1	0.3	0.2	0.0
C22:1 OH	0.2	0.0	0.0	0.1
C22:1 OH isom.	0.2	0.0	0.0	0.1
C24:1 OH	0.0	0.0	0.0	0.0
C24:1 OH isom.	0.1	0.0	0.0	0.0
Σ unsat. OH	0.6	0.3	0.2	0.4
C14 FAME	1.2	0.6	0.0	2.0
C15 FAME	0.3	1.3	0.9	0.2
C16 FAME	18.3	28.5	18.1	13.5
C17 FAME	0.3	2.5	1.6	0.5
C18 FAME	3.1	18.6	5.5	3.3
C19 FAME	0.0	0.0	0.0	0.1
C20 FAME	0.3	1.1	0.5	0.1
C21 FAME	0.3	0.2	0.1	0.0
C22 FAME	1.0	1.2	1.0	0.0
C23 FAME	0.3	0.5	0.2	0.1
C24 FAME	2.7	2.6	2.5	0.1
C25 FAME	0.0	0.6	0.0	0.0
C26 FAME	0.0	0.4	0.0	0.0
Σ FAME	27.7	58.2	30.4	19.8

Figure A.20: Complete lipid dataset for the Crozet sediment trap deployment at station M6 (3160 m).

4,8-dimethyl-C12:0	0.1	0.0	0.0	0.2
i-C15:0	0.1	0.0	0.0	0.1
a-C15:0	0.1	0.0	0.0	0.1
i-C16:0	0.0	0.0	0.0	0.0
a-C16:0	0.1	0.0	0.0	0.0
i-C17:0	0.4	0.2	0.0	0.3
a-C17:0	0.2	0.1	0.0	0.1
i-C18:0	0.0	0.0	0.0	0.0
Σ br. FAME	1.0	0.3	0.0	0.7
C12 OH	0.0	0.0	0.0	0.0
C13 OH	0.0	0.0	0.0	0.0
C14 OH	1.4	1.5	0.7	0.0
C15 OH	0.1	0.5	0.3	0.0
C16 OH	11.9	4.1	2.6	0.3
C17 OH	0.1	0.1	0.1	0.0
C18 OH	1.7	3.9	1.4	0.1
C19 OH	0.0	0.2	0.1	0.0
C20 OH	0.4	0.9	0.5	0.1
C21 OH	0.4	0.2	0.1	0.0
C22 OH	0.3	1.0	0.3	0.1
C23 OH	0.1	0.3	0.0	0.0
C24 OH	0.1	0.7	0.3	0.0
Σ OH	16.6	13.4	6.4	0.7
C26Δ22	0.6	0.0	0.0	0.0
C26Δ5,22	1.0	0.0	0.0	0.2
Coprostanol	0.4	0.0	0.0	0.0
Epicoprostanol	0.3	0.0	0.0	0.0
C27Δ22 (Z)	0.1	0.0	0.0	0.0
C27Δ5,22	0.0	0.0	0.0	0.0
C27Δ22E	0.0	0.0	0.0	0.0
C27Δ5,22	2.1	0.2	5.5	0.1
C27Δ22	0.9	0.0	0.0	0.0
C27Δ5	22.9	7.1	28.6	23.7
C27Δ0	1.1	0.1	0.5	0.1
C28Δ5,22	3.3	0.2	5.1	0.0
C28Δ22	0.0	0.0	0.0	0.0
C27Δ7	0.0	0.0	0.0	0.0
C28Δ5	0.0	0.0	0.0	0.0
C28Δ5 isom.	0.0	0.0	0.0	0.0
C28Δ5	0.0	0.0	0.0	0.0
C28Δ22	0.8	0.0	0.0	0.0
C28Δ5,X	0.0	0.0	0.0	0.0
C29Δ5,22	0.0	0.0	0.0	0.0
C29 Δ5,22	0.8	0.0	0.5	0.0
C29Δ5 isom.	0.6	0.0	0.0	0.0
C29Δ5	0.3	0.0	1.6	0.0
C29Δ0	0.2	0.0	0.0	0.0
Dinosterol	0.8	0.0	0.0	0.0
C29Δ7	0.0	0.0	0.0	0.0
C30Δ5	0.0	0.0	0.0	0.0
Σ Sterols	36.1	7.7	41.9	24.0
br. C15 OH	0.0	0.0	0.0	0.0
phytadiene isomers	0.0	0.0	0.0	0.0
br. 19 OH	0.5	0.0	0.1	0.0
br. C17 OH (iso)	0.0	0.1	0.1	0.0
br. C17 OH (anteiso)	0.0	0.6	0.7	0.0
br. C18 OH (iso)	0.0	0.0	0.0	0.0
br. C18 OH (anteiso)	0.0	0.0	0.0	0.0
br. C19 OH (iso)	0.0	0.0	0.0	0.0
br. C19 OH (anteiso)	0.0	0.0	0.0	0.0
br. C20 OH	0.0	0.0	0.0	0.0
C27 hopanone	0.7	0.0	0.0	0.0
cholesta-3,5-dien-7-one	0.6	0.0	0.0	0.0
12-OH(ω17)-C26	2.5	0.0	4.2	0.0
unsat. C28 diol isom.	9.7	0.3	5.1	0.0
12-OH(ω17)-C28	0.0	0.0	0.0	0.0
bb-hopanoic acid	0.0	0.0	0.0	0.0
37:3 Ketone	0.8	0.0	0.0	0.0
37:2 Ketone	0.5	0.0	0.0	0.0
Σ Other	15.3	1.0	10.1	0.0

Figure A.21: Complete lipid dataset for the Crozet sediment trap deployment at station M6 (3160 m) - continued.

A.6 Posters from conferences

ASLO Aquatic Science Meeting, Granada, February 2015.

Our Common Future Under Climate Change, Paris, June 2015.

Autonomous observations with Bio-Argo floats in the Southern Ocean

Stéphane Blain[1], Hervé Claustre[2], Sabrina Speich[3], Julia Uitz[3],
Antoine Poteau[3], Grigor Obolensky[3], Mathieu Rembauville[1]

[1]Laboratoire d'Océanographie Microbienne, Banyuls sur mer, [2]Laboratoire d'Océanographie de Villefranche sur mer,
[3]Laboratoire de Météorologie Dynamique, Paris

OUR UNDER
COMMON CLIMATE
FUTURE CHANGE

Paris 7-10 Juillet 2015

Context:

The Southern Ocean (SO) is the most remote and the least understood of the world's oceans, although it plays a crucial role in past and present climate state and changes. It is unique in being the only zonally unbounded ocean. For this reason, it is the major link by which water properties are exchanged among the other oceans. Moreover, the SO is a major source of natural CO_2 due to the upwelling of CO_2-rich deep waters and a major sink of anthropogenic CO_2 due to the formation of intermediate and bottom waters. For all these reasons, the SO plays a critical role in the control of the Earth's climate. In turn it is very sensitive to climate variability. Given its critical role, changes in the SO have global ramifications. In fact, such changes are already under way. But at present, the SO remains particularly under-explored. The SO extends over a vast area of the Earth's surface and it is located far away from the other continents and most of the research facilities. Extreme weather conditions and significant sea-ice coverage prevail over most of the year. This results in a scarcity of oceanographic data that limits our ability to understand key climatic-relevant processes and document ongoing changes.
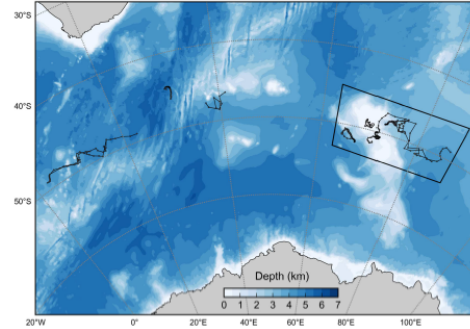
Map of the Indian sector of the Southern Ocean with the trajectories of the 12 bio-argo floats deployed in 2015.

The SOCLIM (Southern Ocean and Climate) project intends to implement a cutting-edge approach that will qualitatively and quantitatively improve the observation of the SO *via* via a combination of pioneering as well as existing in situ data acquisition, including Bio-Argo profiling floats, moorings and sediment traps.

Bio-Argo floats acquisition in the high chlorophyll region around Kerguelen Island.

Panels a & b : location of profiles acquired by 6 Bio-Argo floats superimposed on the mean chlorophyll concentration in surface water derived from satellite observations (MODIS).

Panels c-f : vertical distributions of parameters measured by the Bio-Argo float 50b. Three differents periods were considered. The dark or white lines denotes the mixed layer depth. The gray lines on panel c denote the isopycnals.

The float caught the decline of the bloom on the Kerguelen Plateau. The most interesting feature was the establishment of a deep chlorophyll maximum at the base of the mixed layer.

More data at: http://soclim.com/interactive-map-en.php
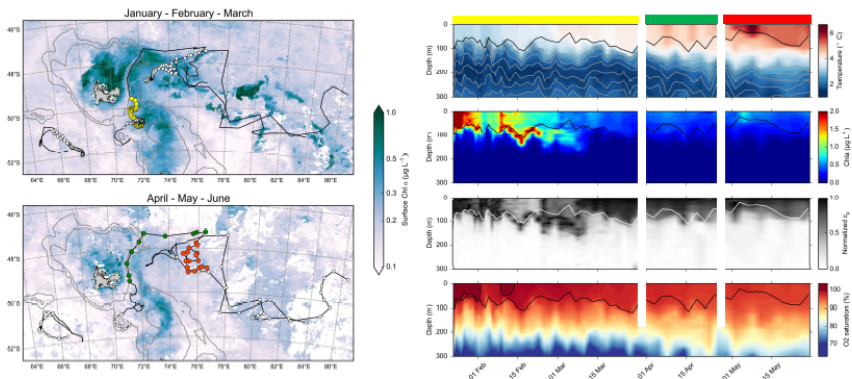
Contrasted vertical distribution of particulate material above and outside the Kerguelen Plateau.

Two floats were equiped with transmissiometers. Vertical profiles of the attenuation coefficient c_p, are used to compare the attenuation of the stock of particles above and outside the plateau. c_p are normalized using the equation :

$$c_{pnorm} = \frac{c_p - \min(c_p)}{\max(c_p) - \min(c_p)}$$

The variations of c_{pnorm} with potential density anomaly (σ_θ) are fitted with the equation :

$$c_{pnorm} = \exp(\lambda(\sigma_\theta - \sigma_{\theta 1}))$$

λ represent the attenuation of the stock of particles. The two fold difference observed for λ above and outside the plateau, suggests that different processes, or same processes with different magnitudes are acting at the two differents sites. This processes remain to be identified. This critical because they may also impact the vertical flux of particulate matter.
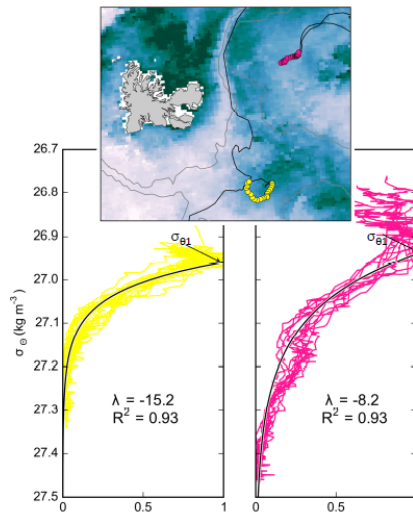
Perspectives :

The next step for SOCLIM will be the deployment of new floats in the Kerguelen region in October 2016. Two of these floats will be equiped with new instruments dedicated to the study of the bio-optical anomaly in the Southern Ocean. During this cruise different moorings will be also deployed on the Kerguelen plateau. Instrumented packages for the measurements of CO_2, O_2, chlorophyll, and a remote autonomous sampler will be deployed in the mixed layer to follow the dynamics of the bloom and its impact CO_2 uptake. Sediment traps will collect at the same site sinking material to quantify the carbon flux and identify the main ecological vectors of export in relation with the bloom dynamics in the surface layer.

LEFE-CYBER workshop on modelling, Marseille, November 2015.

Plankton ecology and particulate matter export in the Southern Ocean: a step forward

Mathieu Rembauville[1], Ian Salter[1,2], and Stéphane Blain[1]
[1]Sorbonne Universités, UPMC Univ Paris 06, CNRS, Laboratoire d'Océanographie Microbienne (LOMIC), Observatoire Océanologique, F-66650, Banyuls/mer, France
[2]Alfred Wegener Institute for Polar and Marine Research, Bremerhaven, Germany

Observations

- Moored sediment traps allow the coupled description of the chemical and biological composition of export

- Higher carbon export in productive areas is associated with the formation of diatom resting spores in summer: 40-60 % of annual POC export

- Higher BSi:POC ratio in the less productive area is linked to the dominance of *F. kerguelensis*

- Resting spore formation is an ecological strategy mainly perfomed by neritic diatom species but spores are found in sediments remote from the shelf

- Diatom resting spores exhibit a high carbon content and are efficently transfered to the seafloor. They apprear as efficient vectors for carbon export
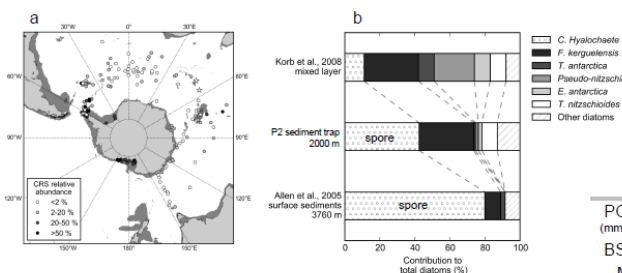

Figure 2: (a) Relative abundance of *Chaetoceros Hyalocahete* resting spores in superficial sediments of the Southern Ocean. Stars denote the sediment trap records of massive export events of diatom spores. Shelves areas (<1000 m) are represented in dark grey. **(b)** Evolution of the diatom community composition from the mixed layer to the seafloor at the P3 site (downstream South Georgia).
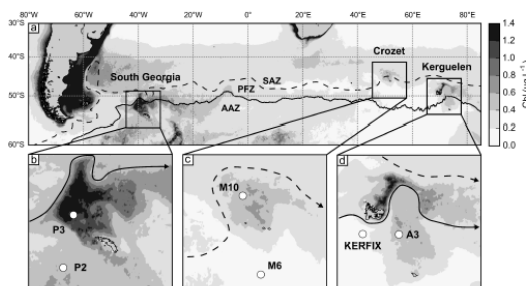

Figure 1: (a) Location of three subantarctic island systems. Dotted line denotes the Subantarctic front (Orsi et al., 1995) and continuous line represents the Polar Front (Moore et al., 1999). **(b)** to **(d)** Detailed view of the location of six annual sediment trap deployments. Grey levels represent climatological surface chlorophyll *a* (MODIS full mission).

	South Georgia[#]		Crozet[§]		Kerguelen[‡]	
	P2 (1500m)	P3 (2000 m)	M6 (3160 m)	M10 (2000 m)	KERFIX (280 m)	A3 (289 m)
POC flux (mmol m⁻² yr⁻¹)	26.4	40.6	14	37	51.6	98.2
BSi:POC	1.5	1.1	6.4	2.6	2.3	1.2
Major diatom	*F. kerguelensis*	*Chaetoceros Hyalochaete* spore	*F. kerguelensis*	*Eucampia antarctica* spore	*F. kerguelensis*	*Chaetoceros Hyalochaete* spore

[#] Rembauville et al., in prep. Samples, POC and BSi data courtesy of C. Manno and G. Tarling (BAS)
[§] Salter et al., 2012
[‡] Rembauville et al., 2015a,b

Including resting spores in models – basic approach

Hypotheses and constraints

- Spore-forming diatoms (e.g. *Chaetoceros Hyalocahete*) present in productive neritic environments (p_{max})

- Silicate limitation drives resting spore formation in the Southern Ocean (p_{Si})

- Spore formation occurs in summer when diatom biomass is declining (p_{dP1})

- Resting spores are endospores: half of the BSi remains in the vegetative stage

- Resting spores are not grazed and sink rapidly (wS ~300 m d⁻¹)

- No PFT additon: a fraction of the diatom community forms spores

- Abrupt (~48h) but continuous process: sigmoid formulation with slope (s_{Si}, s_{dP1}) and threshold (t_{Si}, t_{dP1})

Fasham-like mixed layer model

- Diatom and nanophyto (Primesiophyceae, cocco + phaeocystis)
- Self shading
- Natural mortality f(P1 and P2 biomass)
- Variable Si:N uptake f(Fe)
- Different Si and N/Fe remineralization kinetic
- Generalist grazer: preference for preys depends on the level of silicification of diatom
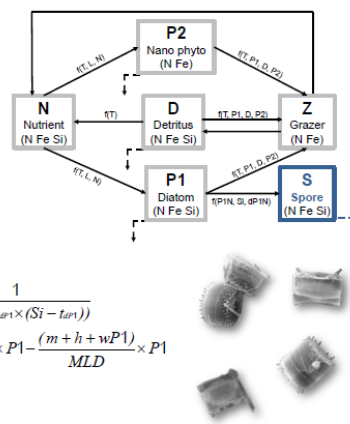
Spore formation formulation

$$p_{spore} = p_{max} \times p_{Si} \times p_{dP1}$$

$$p_{spore} = \frac{P1N}{\alpha} \times \frac{1}{1 + exp(s_{Si} \times (Si - t_{Si}))} \times \frac{1}{1 + exp(s_{dP1} \times (Si - t_{dP1}))}$$

$$\frac{dP1N}{dt} = (\mu P1 - mP1) \times P1 - gZ1 \times Z1 - p_{spore} \times P1 - \frac{(m + h + wP1)}{MLD} \times P1$$

$$\frac{dSN}{dt} = p_{spore} \times P1N - \frac{(m + h + wS)}{MLD} \times SN$$
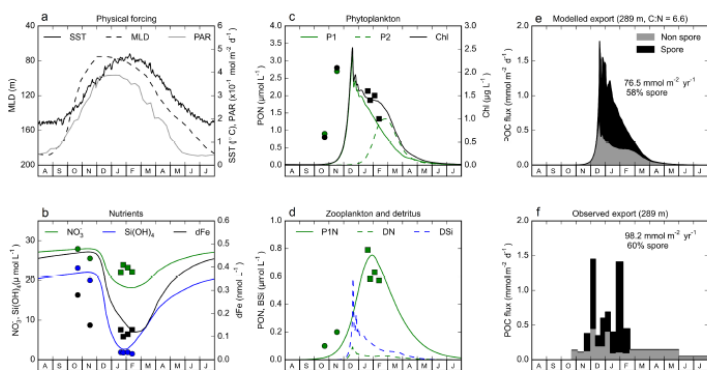
Simulation

Figure 3: (a) Physical forcing for the mixed-layer model corresponding to the A3 site. MLD from argo float and elephant seals data. **(b)** to **(e)** model results from the last year of a 10 years simulation. Dots and squares correpond respectively to the KEOPS2 and KEOPS1 data. **(f)** Oberved export from a sediment trap at the A3 site (Rembauville et al., 2015a)

First results

- Overall good representation of key parameters

- Export magnitude and timing consistent with the sediment trap record

- Obervations suggest two spore export events: hyopthesis of a mixing event in January

Going further

- Include spore formation in GCM models

- Compare with resting spore sedimentary distribution

References

Moore, J.K., Abbott, M.R., Richman, J.G., 1999. Location and dynamics of the Antarctic Polar Front from satellite sea surface temperature data. J. Geophys. Res. 104, 3059–3073.
Orsi, A.H., Whitworth III, T., Nowlin Jr., W.D., 1995. On the meridional extent and fronts of the Antarctic Circumpolar Current. Deep Sea Research Part I: Oceanographic Research Papers 42, 641–673.
Rembauville, M., Blain, S., Armand, L., Gueguiner, B., Salter, I., 2015a. Export fluxes in a naturally iron-fertilized area of the Southern Ocean – Part 2: importance of diatom resting spores and faecal pellets for export. Biogeosciences 12, 3171–3195.
Rembauville, M., Salter, I., Lebiond, N., Gueneugues, A., Blain, S., 2015b. Export fluxes in a naturally iron-fertilized area of the Southern Ocean – Part 1: Seasonal dynamics of particulate organic carbon export from a moored sediment trap. Biogeosciences 12, 3153–3170.
Salter, I., Kemp, A.E.S., Moore, C.M., Lampitt, R.S., Wolff, G.A., Holtvoeth, J., 2012. Diatom resting spore ecology drives enhanced carbon export from a naturally iron-fertilized bloom in the Southern Ocean. Global Biogeochem. Cycles 26, GB1014.

A.7 Manuscript on Si isotopes submitted in Biogeosciences.

Unveiling the Si cycle using isotopes in an iron fertilized zone of the Southern Ocean: from mixed layer supply to export

Ivia Closset[1], Damien Cardinal[1], Mathieu Rembauville[2], François Thil[3], Stéphane Blain[2]

[1]Sorbonne Universités (UPMC, Univ Paris 06)-CNRS-IRD-MNHN, LOCEAN Laboratory, 4 place Jussieu, F-75005 Paris, France

[2]Sorbonne Universités (UPMC, Univ Paris 06)-CNRS, Laboratoire d'Océanographie Microbienne (LOMIC), Observatoire Océanologique, F-66650 Banyuls/mer, France

[3]Laboratoire des Sciences du Climat et de l'Environnement, CNRS 91190 Gif-sur-Yvette, France

Correspondence to: Ivia Closset (ivia.closset@locean-ipsl.upmc.fr)

Abstract. A massive diatom-bloom is observed annually in the surface waters of the naturally Fe-fertilized Kerguelen Plateau (Southern Ocean). In this study, silicon isotopic signatures (δ^{30}Si) of silicic acid (DSi) and suspended biogenic silica (BSi) were investigated in the whole water column with an unprecedented spatial resolution in this region, during the KEOPS-2 experiment (spring 2011). We use δ^{30}Si measurements to track the silicon sources that fuel the bloom, and investigate the seasonal evolution of Si biogeochemical cycle in the iron fertilized area. We compare the results from a HNLC reference station with stations characterized by different degrees of iron enrichment and bloom conditions. Dissolved and particulate δ^{30}Si signatures were generally highly variable in the upper 500 m, reflecting the effect of the intense silicon utilization in spring, while they were quite homogeneous in deeper waters. The Si-isotopic and mass balance identified a unique WW Si-source for the iron-fertilized area originating from the southeastern Kerguelen Plateau and spreading northward. However, when reaching a retroflection of the Polar Front (PF), the δ^{30}Si composition of WW silicic acid pool was getting progressively heavier. This would result from sequential diapycnal mixings between these initial WW and ML water masses, highlighting the strong circulation of surface waters that defined this zone. When comparing the results from the two KEOPS expeditions, the relationship between DSi depletion, BSi production and their isotopic composition appears decoupled in the iron fertilized area. This seasonal decoupling could help to explain the low apparent fractionation factor observed here in the ML at the end of summer. Taking into account these considerations, we refined the seasonal net BSi production in the ML of the iron-fertilized area to 3.0 ± 0.3 mol Si m^{-2} y^{-1}, that was exclusively sustained by surface water phytoplankton populations. These insights confirm that the isotopic composition of dissolved and particulate silicon is a promising tool to improve our understanding on the Si-biogeochemical cycle since the isotopic and mass balance allows resolving the processes involved i.e. uptake, dissolution, mixing.

References

Abelmann, A. and Gersonde, R.: Biosiliceous particle flux in the Southern Ocean, Marine Chemistry, 35, 503–536, doi:10.1016/S0304-4203(09)90040-8, URL http://www.sciencedirect.com/science/article/pii/S0304420309900408, 1991.

Abelmann, A., Gersonde, R., Cortese, G., Kuhn, G., and Smetacek, V.: Extensive phytoplankton blooms in the Atlantic sector of the glacial Southern Ocean, Paleoceanography, 21, doi:10.1029/2005PA001199, URL http://onlinelibrary.wiley.com/doi/10.1029/2005PA001199/abstract, 2006.

Adams, H. E., Crump, B. C., and Kling, G. W.: Temperature controls on aquatic bacterial production and community dynamics in arctic lakes and streams, Environmental Microbiology, 12, 1319–1333, doi:10.1111/j.1462-2920.2010.02176.x, URL http://onlinelibrary.wiley.com/doi/10.1111/j.1462-2920.2010.02176.x/abstract, 2010.

Ainley, D. G., Ballard, G., Jones, R. M., Jongsomjit, D., Pierce, S. D., Smith, W. O., Jr, and Veloz, S.: Trophic cascades in the western Ross Sea, Antarctica: revisited, Marine Ecology Progress Series, 534, 1–16, doi:10.3354/meps11394, URL http://www.int-res.com/abstracts/meps/v534/p1-16/, 2015.

Alldredge, A. L. and Gotschalk, C.: In situ settling behavior of marine snow, Limnology and Oceanography, 33, 339–351, doi:10.4319/lo.1988.33.3.0339, URL http://onlinelibrary.wiley.com/doi/10.4319/lo.1988.33.3.0339/abstract, 1988.

Alvain, S., Moulin, C., Dandonneau, Y., and Loisel, H.: Seasonal distribution and succession of dominant phytoplankton groups in the global ocean: A satellite view, Global Biogeochemical Cycles, 22, GB3001, doi:10.1029/2007GB003154, URL http://onlinelibrary.wiley.com/doi/10.1029/2007GB003154/abstract, 2008.

Aminot, A. and Kerouel, R.: Dosage automatique des nutriments dans les eaux marines: méthodes en flux continu, Ifremer, Plouzané, France, 2007.

Andersen, K. H., Aksnes, D. L., Berge, T., Fiksen, y., and Visser, A.: Modelling emergent trophic strategies in plankton, Journal of Plankton Research, 37, 862–868, doi:10.1093/plankt/fbv054, URL http://plankt.oxfordjournals.org/content/early/2015/08/04/plankt.fbv054, 2015.

Anderson, L. W. J. and Sweeney, B. M.: Role of Inorganic Ions in Controlling Sedimentation Rate of a Marine Centric Diatom Ditylum Brightwelli1,2, Journal of Phycology, 14, 204–214, doi:10.1111/j.1529-8817.1978.tb02450.x, URL http://onlinelibrary.wiley.com/doi/10.1111/j.1529-8817.1978.tb02450.x/abstract, 1978.

Anderson, O. R.: The Ultrastructure and Cytochemistry of Resting Cell Formation in Amphora Coffaeformis (bacillariophyceae), Journal of Phycology, 11, 272–281, doi:10.1111/j.1529-8817.1975.tb02778.x, URL http://onlinelibrary.wiley.com/doi/10.1111/j.1529-8817.1975.tb02778.x/abstract, 1975.

Antia, A. N.: Solubilization of particles in sediment traps: revising the stoichiometry of mixed layer export, Biogeosciences, 2, 189–204, doi:10.5194/bg-2-189-2005, URL http://www.biogeosciences.net/2/189/2005/, 2005.

Archer, D. and Maier-Reimer, E.: Effect of deep-sea sedimentary calcite preservation on atmospheric CO2 concentration, Nature, 367, 260–263, doi:10.1038/367260a0, URL http:

//www.nature.com/nature/journal/v367/n6460/abs/367260a0.html, 1994.

Archer, D., Winguth, A., Lea, D., and Mahowald, N.: What caused the glacial/interglacial atmospheric pCO2 cycles?, Reviews of Geophysics, 38, 159–189, doi:10.1029/1999RG000066, URL http://onlinelibrary.wiley.com/doi/10.1029/1999RG000066/abstract, 2000a.

Archer, D. E., Eshel, G., Winguth, A., Broecker, W., Pierrehumbert, R., Tobis, M., and Jacob, R.: Atmospheric pCO2 sensitivity to the biological pump in the ocean, Global Biogeochemical Cycles, 14, 1219–1230, doi:10.1029/1999GB001216, URL http://onlinelibrary.wiley.com/doi/10.1029/1999GB001216/abstract, 2000b.

Armand, L. K., Cornet-Barthaux, V., Mosseri, J., and Quéguiner, B.: Late summer diatom biomass and community structure on and around the naturally iron-fertilised Kerguelen Plateau in the Southern Ocean, Deep Sea Research Part II: Topical Studies in Oceanography, 55, 653–676, doi:10.1016/j.dsr2.2007.12.031, URL http://www.sciencedirect.com/science/article/pii/S0967064508000179, 2008a.

Armand, L. K., Crosta, X., Quéguiner, B., Mosseri, J., and Garcia, N.: Diatoms preserved in surface sediments of the northeastern Kerguelen Plateau, Deep Sea Research Part II: Topical Studies in Oceanography, 55, 677–692, doi:10.1016/j.dsr2.2007.12.032, URL http://www.sciencedirect.com/science/article/pii/S0967064508000192, 2008b.

Armstrong, R. A., Lee, C., Hedges, J. I., Honjo, S., and Wakeham, S. G.: A new, mechanistic model for organic carbon fluxes in the ocean based on the quantitative association of POC with ballast minerals, Deep Sea Research Part II: Topical Studies in Oceanography, 49, 219–236, doi:10.1016/S0967-0645(01)00101-1, URL http://www.sciencedirect.com/science/article/pii/S0967064501001011, 2002.

Arrigo, K. R. and Alderkamp, A.-C.: Shedding dynamic light on Fe limitation (DynaLiFe), Deep Sea Research Part II: Topical Studies in Oceanography, 71–76, 1–4, doi:10.1016/j.dsr2.2012.03.004, URL http://www.sciencedirect.com/science/article/pii/S0967064512000410, 2012.

Arrigo, K. R. and van Dijken, G. L.: Phytoplankton dynamics within 37 Antarctic coastal polynya systems, Journal of Geophysical Research: Oceans, 108, 3271, doi:10.1029/2002JC001739, URL http://onlinelibrary.wiley.com/doi/10.1029/2002JC001739/abstract, 2003.

Assmy, P., Henjes, J., Klaas, C., and Smetacek, V.: Mechanisms determining species dominance in a phytoplankton bloom induced by the iron fertilization experiment EisenEx in the Southern Ocean, Deep Sea Research Part I: Oceanographic Research Papers, 54, 340–362, doi:10.1016/j.dsr.2006.12.005, URL http://www.sciencedirect.com/science/article/pii/S096706370600330X, 2007.

Assmy, P., Smetacek, V., Montresor, M., Klaas, C., Henjes, J., Strass, V. H., Arrieta, J. M., Bathmann, U., Berg, G. M., Breitbarth, E., Cisewski, B., Friedrichs, L., Fuchs, N., Herndl, G. J., Jansen, S., Krägefsky, S., Latasa, M., Peeken, I., Röttgers, R., Scharek, R., Schüller, S. E., Steigenberger, S., Webb, A., and Wolf-Gladow, D.: Thick-shelled, grazer-protected diatoms decouple ocean carbon and silicon cycles in the iron-limited Antarctic Circumpolar Current, Proceedings of the National Academy of Sciences, 110, 20 633–20 638, doi:10.1073/pnas.1309345110, URL http://www.pnas.org/content/110/51/20633, 2013.

Atkinson, A., Siegel, V., Pakhomov, E. A., Rothery, P., Loeb, V., Ross, R. M., Quetin, L. B., Schmidt, K., Fretwell, P., Murphy, E. J., Tarling, G. A., and Fleming, A. H.: Oceanic circumpolar habitats of Antarctic krill, Marine Ecology Progress Series, 362, 1–23, doi:10.3354/meps07498, URL http://www.int-res.com/abstracts/meps/v362/p1-23/, 2008.

Atkinson, A., Siegel, V., Pakhomov, E. A., Jessopp, M. J., and Loeb, V.: A re-appraisal of the total biomass and annual production of Antarctic krill, Deep Sea Research Part I: Oceanographic Research Papers, 56, 727–740, doi:10.1016/j.dsr.2008.12.007, URL http://www.sciencedirect.com/science/article/pii/S0967063708002513, 2009.

Aumont, O. and Bopp, L.: Globalizing results from ocean in situ iron fertilization stud-

ies, Global Biogeochemical Cycles, 20, GB2017, doi:10.1029/2005GB002591, URL http://onlinelibrary.wiley.com/doi/10.1029/2005GB002591/abstract, 2006.

Baker, B. J. and Kerr, R. G.: Biosynthesis of marine sterols, in: Marine Natural Products — Diversity and Biosynthesis, edited by Scheuer, P. P. J., no. 167 in Topics in Current Chemistry, pp. 1–31, Springer Berlin Heidelberg, URL http://link.springer.com/chapter/10.1007/BFb0034369, dOI: 10.1007/BFb0034369, 1993.

Baker, E. T., Milburn, H. B., and Tennant, D. A.: Field assessment of sediment trap efficiency under varying flow conditions, Journal of Marine Research, 46, 573–592, doi:10.1357/002224088785113522, URL http://www.pmel.noaa.gov/publications/search_abstract.php?fmContributionNum=999, 1988.

Balch, W. M., Gordon, H. R., Bowler, B. C., Drapeau, D. T., and Booth, E. S.: Calcium carbonate measurements in the surface global ocean based on Moderate-Resolution Imaging Spectroradiometer data, Journal of Geophysical Research: Oceans, 110, doi:10.1029/2004JC002560, URL http://onlinelibrary.wiley.com/doi/10.1029/2004JC002560/abstract, 2005.

Balch, W. M., Drapeau, D. T., Bowler, B. C., Lyczskowski, E., Booth, E. S., and Alley, D.: The contribution of coccolithophores to the optical and inorganic carbon budgets during the Southern Ocean Gas Exchange Experiment: New evidence in support of the "Great Calcite Belt" hypothesis, Journal of Geophysical Research: Oceans, 116, C00F06, doi:10.1029/2011JC006941, URL http://onlinelibrary.wiley.com/doi/10.1029/2011JC006941/abstract, 2011.

Banse, K.: New views on the degradation and disposition of organic particles as collected by sediment traps in the open sea, Deep Sea Research Part A. Oceanographic Research Papers, 37, 1177–1195, doi:10.1016/0198-0149(90)90058-4, URL http://www.sciencedirect.com/science/article/pii/0198014990900584, 1990.

Banse, K.: Antarctic marine top predators revisited: homeotherms do not leak much CO2 to the air, Polar Biology, 15, 93–104, doi:10.1007/BF00241047, URL http://link.springer.com/article/10.1007/BF00241047, 1995.

Bar-Zeev, E., Avishay, I., Bidle, K. D., and Berman-Frank, I.: Programmed cell death in the marine cyanobacterium Trichodesmium mediates carbon and nitrogen export, The ISME journal, 7, 2340–2348, doi:10.1038/ismej.2013.121, 2013.

Battaglia, G., Steinacher, M., and Joos, F.: Aprobabilistic assessment of calcium carbonate export and dissolution in the modern ocean, Biogeosciences, 13, 2823–2848, doi:10.5194/bg-13-2823-2016, URL http://www.biogeosciences.net/13/2823/2016/, 2016.

Beaufort, L. and Heussner, S.: Coccolithophorids on the continental slope of the Bay of Biscay – production, transport and contribution to mass fluxes, Deep Sea Research Part II: Topical Studies in Oceanography, 46, 2147–2174, doi:10.1016/S0967-0645(99)00058-2, URL http://www.sciencedirect.com/science/article/pii/S0967064599000582, 1999.

Beaugrand, G., Edwards, M., Raybaud, V., Goberville, E., and Kirby, R. R.: Future vulnerability of marine biodiversity compared with contemporary and past changes, Nature Climate Change, 5, 695–701, doi:10.1038/nclimate2650, URL http://www.nature.com/nclimate/journal/v5/n7/full/nclimate2650.html?message-global=remove, 2015.

Behrenfeld, M. J. and Boss, E.: The beam attenuation to chlorophyll ratio: an optical index of phytoplankton physiology in the surface ocean?, Deep Sea Research Part I: Oceanographic Research Papers, 50, 1537–1549, doi:10.1016/j.dsr.2003.09.002, URL http://www.sciencedirect.com/science/article/pii/S0967063703001559, 2003.

Behrenfeld, M. J. and Boss, E.: Beam attenuation and chlorophyll concentration as alternative optical indices of phytoplankton biomass, Journal of Marine Research, 64, 431–451, doi:10.1357/002224006778189563, 2006.

Behrenfeld, M. J., Boss, E., Siegel, D. A., and Shea, D. M.: Carbon-based ocean productivity and phytoplankton physiology from space, Global Biogeochemical Cycles, 19, GB1006, doi:10.1029/2004GB002299, URL http://onlinelibrary.wiley.com/doi/10.1029/2004GB002299/abstract, 2005.

Behrenfeld, M. J., Westberry, T. K., Boss, E. S., O'Malley, R. T., Siegel, D. A., Wiggert, J. D., Franz, B. A., McClain, C. R., Feldman, G. C., Doney, S. C., Moore, J. K., Dall'Olmo, G., Milligan, A. J., Lima, I., and Mahowald, N.: Satellite-detected fluorescence reveals global physiology of ocean phytoplankton, Biogeosciences, 6, 779–794, doi:10.5194/bg-6-779-2009, URL http://www.biogeosciences.net/6/779/2009/, 2009.

Benitez-Nelson, C. R., O. Buesseler, K., and Crossin, G.: Upper ocean carbon export, horizontal transport, and vertical eddy diffusivity in the southwestern Gulf of Maine, Continental Shelf Research, 20, 707–736, doi:10.1016/S0278-4343(99)00093-X, URL http://www.sciencedirect.com/science/article/pii/S027843439900093X, 2000.

Bergami, C., Capotondi, L., Langone, L., Giglio, F., and Ravaioli, M.: Distribution of living planktonic foraminifera in the Ross Sea and the Pacific sector of the Southern Ocean (Antarctica), Marine Micropaleontology, 73, 37–48, doi:10.1016/j.marmicro.2009.06.007, URL http://www.sciencedirect.com/science/article/pii/S0377839809000747, 2009.

Berger, W. H.: Sedimentation of planktonic foraminifera, Marine Geology, 11, 325–358, doi:10.1016/0025-3227(71)90035-1, URL http://www.sciencedirect.com/science/article/pii/0025322771900351, 1971.

Bernard, O. and Rémond, B.: Validation of a simple model accounting for light and temperature effect on microalgal growth, Bioresource Technology, 123, 520–527, doi:10.1016/j.biortech.2012.07.022, URL http://www.sciencedirect.com/science/article/pii/S0960852412010693, 2012.

Bhat, S., Krishnaswamy, S., Lal, D., Rama, and Moore, W.: 234Th/238U ratios in the ocean, Earth and Planetary Science Letters, 5, 483–491, doi:10.1016/S0012-821X(68)80083-4, URL http://www.sciencedirect.com/science/article/pii/S0012821X68800834, 1968.

Bianchi, D., Galbraith, E. D., Carozza, D. A., Mislan, K. a. S., and Stock, C. A.: Intensification of open-ocean oxygen depletion by vertically migrating animals, Nature Geoscience, 6, 545–548, doi:10.1038/ngeo1837, URL http://www.nature.com/ngeo/journal/v6/n7/abs/ngeo1837.html, 2013a.

Bianchi, D., Stock, C., Galbraith, E. D., and Sarmiento, J. L.: Diel vertical migration: Ecological controls and impacts on the biological pump in a one-dimensional ocean model, Global Biogeochemical Cycles, 27, 478–491, doi:10.1002/gbc.20031, URL http://onlinelibrary.wiley.com/doi/10.1002/gbc.20031/abstract, 2013b.

Billett, D. S. M., Lampitt, R. S., Rice, A. L., and Mantoura, R. F. C.: Seasonal sedimentation of phytoplankton to the deep-sea benthos, Nature, 302, 520–522, doi:10.1038/302520a0, URL http://www.nature.com/nature/journal/v302/n5908/abs/302520a0.html, 1983.

Billett, D. S. M., Bett, B. J., Rice, A. L., Thurston, M. H., Galéron, J., Sibuet, M., and Wolff, G. A.: Long-term change in the megabenthos of the Porcupine Abyssal Plain (NE Atlantic), Progress in Oceanography, 50, 325–348, doi:10.1016/S0079-6611(01)00060-X, URL http://www.sciencedirect.com/science/article/pii/S007966110100060X, 2001.

Bishop, J. K. B. and Wood, T. J.: Year-round observations of carbon biomass and flux variability in the Southern Ocean, Global Biogeochemical Cycles, 23, GB2019, doi:10.1029/2008GB003206, URL http://onlinelibrary.wiley.com/doi/10.1029/2008GB003206/abstract, 2009.

Bishop, J. K. B., Wood, T. J., Davis, R. E., and Sherman, J. T.: Robotic Observations of Enhanced Carbon Biomass and Export at 55S During SOFeX, Science, 304, 417–420, doi:10.1126/science.1087717, URL http://www.sciencemag.org/content/304/5669/417, 2004.

Blain, S., Tréguer, P., Belviso, S., Bucciarelli, E., Denis, M., Desabre, S., Fiala, M., Martin Jézéquel, V., Le Fèvre, J., Mayzaud, P., Marty, J.-C., and Razouls, S.: A biogeochemical study of the island mass effect in the context of the iron hypothesis: Kerguelen Islands, Southern Ocean, Deep Sea Research Part I: Oceanographic Research Papers, 48, 163–187, doi:10.1016/S0967-0637(00)00047-9, URL http://www.sciencedirect.com/science/article/pii/S0967063700000479, 2001.

Blain, S., Quéguiner, B., Armand, L., Belviso, S., Bombled, B., Bopp, L., Bowie, A., Brunet, C., Brussaard, C., Carlotti, F., Christaki, U., Corbière, A., Durand, I., Ebersbach, F., Fuda, J.-L., Garcia, N., Gerringa, L., Griffiths, B., Guigue, C., Guillerm, C., Jacquet, S., Jeandel, C., Laan, P., Lefèvre, D., Lo Monaco, C., Malits, A., Mosseri, J., Obernosterer, I., Park, Y.-H., Picheral, M., Pondaven, P., Remenyi, T., Sandroni, V., Sarthou, G., Savoye, N., Scouarnec, L., Souhaut, M., Thuiller, D., Timmermans, K., Trull, T., Uitz, J., van Beek, P., Veldhuis, M., Vincent, D., Viollier, E., Vong, L., and Wagener, T.: Effect of natural iron fertilization on carbon sequestration in the Southern Ocean, Nature, 446, 1070–1074, doi:10.1038/nature05700, URL http://www.nature.com/nature/journal/v446/n7139/abs/nature05700.html, 2007.

Blain, S., Quéguiner, B., and Trull, T.: The natural iron fertilization experiment KEOPS (KErguelen Ocean and Plateau compared Study): An overview, Deep Sea Research Part II: Topical Studies in Oceanography, 55, 559–565, doi:10.1016/j.dsr2.2008.01.002, URL http://www.sciencedirect.com/science/article/pii/S096706450800009X, 2008a.

Blain, S., Sarthou, G., and Laan, P.: Distribution of dissolved iron during the natural iron-fertilization experiment KEOPS (Kerguelen Plateau, Southern Ocean), Deep Sea Research Part II: Topical Studies in Oceanography, 55, 594–605, doi:10.1016/j.dsr2.2007.12.028, URL http://www.sciencedirect.com/science/article/pii/S096706450800012X, 2008b.

Blain, S., Capparos, J., Guéneuguès, A., Obernosterer, I., and Oriol, L.: Distributions and stoichiometry of dissolved nitrogen and phosphorus in the iron-fertilized region near Kerguelen (Southern Ocean), Biogeosciences, 12, 623–635, doi:10.5194/bg-12-623-2015, URL http://www.biogeosciences.net/12/623/2015/, 2015.

Bodungen, B. v.: Phytoplankton growth and krill grazing during spring in the Bransfield Strait, Antarctica — Implications from sediment trap collections, Polar Biology, 6, 153–160, doi:10.1007/BF00274878, URL http://link.springer.com/article/10.1007/BF00274878, 1986.

Bopp, L., Kohfeld, K. E., Le Quéré, C., and Aumont, O.: Dust impact on marine biota and atmospheric CO2 during glacial periods, Paleoceanography, 18, 1046, doi:10.1029/2002PA000810, URL http://onlinelibrary.wiley.com/doi/10.1029/2002PA000810/abstract, 2003.

Bopp, L., Aumont, O., Cadule, P., Alvain, S., and Gehlen, M.: Response of diatoms distribution to global warming and potential implications: A global model study, Geophysical Research Letters, 32, L19 606, doi:10.1029/2005GL023653, URL http://onlinelibrary.wiley.com/doi/10.1029/2005GL023653/abstract, 2005.

Bowen, G. J.: Up in smoke: A role for organic carbon feedbacks in Paleogene hyperthermals, Global and Planetary Change, 109, 18–29, doi:10.1016/j.gloplacha.2013.07.001, URL http://www.sciencedirect.com/science/article/pii/S0921818113001550, 2013.

Bowie, A. R., Lannuzel, D., Remenyi, T. A., Wagener, T., Lam, P. J., Boyd, P. W., Guieu, C., Townsend, A. T., and Trull, T. W.: Biogeochemical iron budgets of the Southern Ocean south of Australia: Decoupling of iron and nutrient cycles in the subantarctic zone by the summertime supply, Global Biogeochemical Cycles, 23, GB4034, doi:10.1029/2009GB003500, URL http://onlinelibrary.wiley.com/doi/10.1029/2009GB003500/abstract, 2009.

Bowie, A. R., Trull, T. W., and Dehairs, F.: Estimating the sensitivity of the subantarctic zone to environmental change: The SAZ-Sense project, Deep Sea Research Part II: Topical Studies in Oceanography, 58, 2051–2058, doi:10.1016/j.dsr2.2011.05.034, URL http://ecite.utas.edu.au/76785, 2011.

Bowie, A. R., van der Merwe, P., Quéroué, F., Trull, T., Fourquez, M., Planchon, F., Sarthou, G., Chever, F., Townsend, A. T., Obernosterer, I., Sallée, J.-B., and Blain, S.: Iron budgets for three distinct biogeochemical sites around the Kerguelen Archipelago (Southern Ocean) during the natural fertilisation study, KEOPS-2, Biogeosciences, 12, 4421–4445, doi:10.5194/bg-12-4421-2015, URL http://www.biogeosciences.net/12/4421/2015/, 2015.

Boyd, C. and Gradmann, D.: Impact of osmolytes on buoyancy of marine phytoplankton, Marine Biology, 141, 605–618, doi:10.1007/s00227-002-0872-z, URL http://link.springer.com/

article/10.1007/s00227-002-0872-z, 2002.

Boyd, P. and Newton, P.: Evidence of the potential influence of planktonic community structure on the interannual variability of particulate organic carbon flux, Deep Sea Research Part I: Oceanographic Research Papers, 42, 619–639, doi:10.1016/0967-0637(95)00017-Z, URL http://www.sciencedirect.com/science/article/pii/096706379500017Z, 1995.

Boyd, P. and Newton, P.: Does planktonic community structure determine downward particulate organic carbon flux in different oceanic provinces?, Deep Sea Research Part I: Oceanographic Research Papers, 46, 63–91, doi:10.1016/S0967-0637(98)00066-1, URL http://www.sciencedirect.com/science/article/pii/S0967063798000661, 1999.

Boyd, P. W.: Environmental Factors Controlling Phytoplankton Processes in the Southern Ocean, Journal of Phycology, 38, 844–861, doi:10.1046/j.1529-8817.2002.t01-1-01203.x, URL http://onlinelibrary.wiley.com/doi/10.1046/j.1529-8817.2002.t01-1-01203.x/abstract, 2002.

Boyd, P. W. and Trull, T. W.: Understanding the export of biogenic particles in oceanic waters: Is there consensus?, Progress in Oceanography, 72, 276–312, doi:10.1016/j.pocean.2006.10.007, URL http://www.sciencedirect.com/science/article/pii/S0079661106001340, 2007.

Boyd, P. W., Watson, A. J., Law, C. S., Abraham, E. R., Trull, T., Murdoch, R., Bakker, D. C. E., Bowie, A. R., Buesseler, K. O., Chang, H., Charette, M., Croot, P., Downing, K., Frew, R., Gall, M., Hadfield, M., Hall, J., Harvey, M., Jameson, G., LaRoche, J., Liddicoat, M., Ling, R., Maldonado, M. T., McKay, R. M., Nodder, S., Pickmere, S., Pridmore, R., Rintoul, S., Safi, K., Sutton, P., Strzepek, R., Tanneberger, K., Turner, S., Waite, A., and Zeldis, J.: A mesoscale phytoplankton bloom in the polar Southern Ocean stimulated by iron fertilization, Nature, 407, 695–702, doi:10.1038/35037500, URL http://www.nature.com/nature/journal/v407/n6805/abs/407695a0.html, 2000.

Boyd, P. W., Jickells, T., Law, C. S., Blain, S., Boyle, E. A., Buesseler, K. O., Coale, K. H., Cullen, J. J., Baar, H. J. W. d., Follows, M., Harvey, M., Lancelot, C., Levasseur, M., Owens, N. P. J., Pollard, R., Rivkin, R. B., Sarmiento, J., Schoemann, V., Smetacek, V., Takeda, S., Tsuda, A., Turner, S., and Watson, A. J.: Mesoscale Iron Enrichment Experiments 1993-2005: Synthesis and Future Directions, Science, 315, 612–617, doi:10.1126/science.1131669, URL http://www.sciencemag.org/content/315/5812/612, 2007.

Boyd, P. W., Rynearson, T. A., Armstrong, E. A., Fu, F., Hayashi, K., Hu, Z., Hutchins, D. A., Kudela, R. M., Litchman, E., Mulholland, M. R., Passow, U., Strzepek, R. F., Whittaker, K. A., Yu, E., and Thomas, M. K.: Marine Phytoplankton Temperature versus Growth Responses from Polar to Tropical Waters – Outcome of a Scientific Community-Wide Study, PLoS ONE, 8, e63 091, doi:10.1371/journal.pone.0063091, URL http://dx.doi.org/10.1371/journal.pone.0063091, 2013.

Bradshaw, S. A. and Eglinton, G.: Marine Invertebrate Feeding and the Sedimentary Lipid Record, in: Organic Geochemistry, edited by Engel, M. H. and Macko, S. A., no. 11 in Topics in Geobiology, pp. 225–235, Springer US, URL http://link.springer.com/chapter/10.1007/978-1-4615-2890-6_10, dOI: 10.1007/978-1-4615-2890-6_10, 1993.

Bramlette, M. N.: Significance of Coccolithophorids in Calcium-Carbonate Deposition, Geological Society of America Bulletin, 69, 121, doi:10.1130/0016-7606(1958)69[121:SOCICD]2.0.CO;2, URL http://adsabs.harvard.edu/abs/1958GSAB...69..121B, 1958.

Brand, L. E., Sunda, W. G., and Guillard, R. R. L.: Limitation of marine phytoplankton reproductive rates by zinc, manganese, and iron1, Limnology and Oceanography, 28, 1182–1198, doi:10.4319/lo.1983.28.6.1182, URL http://onlinelibrary.wiley.com/doi/10.4319/lo.1983.28.6.1182/abstract, 1983.

Brandt, A., Gooday, A. J., Brandão, S. N., Brix, S., Brökeland, W., Cedhagen, T., Choudhury, M., Cornelius, N., Danis, B., De Mesel, I., Diaz, R. J., Gillan, D. C., Ebbe, B., Howe, J. A., Janussen, D., Kaiser, S., Linse, K., Malyutina, M., Pawlowski, J., Raupach, M., and Vanreusel, A.: First insights into the biodiversity and biogeography of the Southern Ocean

deep sea, Nature, 447, 307–311, doi:10.1038/nature05827, URL http://www.nature.com/nature/journal/v447/n7142/abs/nature05827.html, 2007.

Bárcena, M. A. and Abrantes, F.: Evidence of a high-productivity area off the coast of Málaga from studies of diatoms in surface sediments, Marine Micropaleontology, 35, 91–103, doi:10.1016/S0377-8398(98)00012-7, URL http://www.sciencedirect.com/science/article/pii/S0377839898000127, 1998.

Bressac, M., Guieu, C., Doxaran, D., Bourrin, F., Desboeufs, K., Leblond, N., and Ridame, C.: Quantification of the lithogenic carbon pump following a simulated dust-deposition event in large mesocosms, Biogeosciences, 11, 1007–1020, doi:10.5194/bg-11-1007-2014, URL http://www.biogeosciences.net/11/1007/2014/, 2014.

Briggs, N., Perry, M. J., Cetinić, I., Lee, C., D'Asaro, E., Gray, A. M., and Rehm, E.: High-resolution observations of aggregate flux during a sub-polar North Atlantic spring bloom, Deep Sea Research Part I: Oceanographic Research Papers, 58, 1031–1039, doi:10.1016/j.dsr.2011.07.007, URL http://www.sciencedirect.com/science/article/pii/S0967063711001361, 2011.

Briggs, N. T., Slade, W. H., Boss, E., and Perry, M. J.: Method for estimating mean particle size from high-frequency fluctuations in beam attenuation or scattering measurements, Applied Optics, 52, 6710–6725, doi:10.1364/AO.52.006710, URL http://www.osapublishing.org/abstract.cfm?uri=ao-52-27-6710, 2013.

Broecker, W. S.: Ocean chemistry during glacial time, Geochimica et Cosmochimica Acta, 46, 1689–1705, doi:10.1016/0016-7037(82)90110-7, URL http://www.sciencedirect.com/science/article/pii/0016703782901107, 1982.

Broecker, W. S.: The great ocean conveyor, Oceanography, 4, 79–89, URL http://www-pord.ucsd.edu/~ltalley/sio210/readings/broecker_1991_ocean_conveyor.pdf, 1991.

Brzezinski, M. A., Pride, C. J., Franck, V. M., Sigman, D. M., Sarmiento, J. L., Matsumoto, K., Gruber, N., Rau, G. H., and Coale, K. H.: A switch from silicate to nitrate depletion in the glacial Southern Ocean, Geophysical Research Letters, 29, 1564, doi:10.1029/2001GL014349, URL http://onlinelibrary.wiley.com/doi/10.1029/2001GL014349/abstract, 2002.

Budge, S. M. and Parrish, C. C.: Lipid biogeochemistry of plankton, settling matter and sediments in Trinity Bay, Newfoundland. II. Fatty acids, Organic Geochemistry, 29, 1547–1559, doi:10.1016/S0146-6380(98)00177-6, URL http://www.sciencedirect.com/science/article/pii/S0146638098001776, 1998.

Buesseler, K. O.: The decoupling of production and particulate export in the surface ocean, Global Biogeochemical Cycles, 12, 297–310, doi:10.1029/97GB03366, URL http://onlinelibrary.wiley.com/doi/10.1029/97GB03366/abstract, 1998.

Buesseler, K. O., Steinberg, D. K., Michaels, A. F., Johnson, R. J., Andrews, J. E., Valdes, J. R., and Price, J. F.: A comparison of the quantity and composition of material caught in a neutrally buoyant versus surface-tethered sediment trap, Deep Sea Research Part I: Oceanographic Research Papers, 47, 277–294, doi:10.1016/S0967-0637(99)00056-4, URL http://www.sciencedirect.com/science/article/pii/S0967063799000564, 2000.

Buesseler, K. O., Andrews, J. E., Pike, S. M., and Charette, M. A.: The Effects of Iron Fertilization on Carbon Sequestration in the Southern Ocean, Science, 304, 414–417, doi:10.1126/science.1086895, URL http://www.sciencemag.org/content/304/5669/414, 2004.

Buesseler, K. O., Benitez-Nelson, C. R., Moran, S. B., Burd, A., Charette, M., Cochran, J. K., Coppola, L., Fisher, N. S., Fowler, S. W., Gardner, W. D., Guo, L. D., Gustafsson, ., Lamborg, C., Masque, P., Miquel, J. C., Passow, U., Santschi, P. H., Savoye, N., Stewart, G., and Trull, T.: An assessment of particulate organic carbon to thorium-234 ratios in the ocean and their impact on the application of 234Th as a POC flux proxy, Marine Chemistry, 100, 213–233, doi:10.1016/j.marchem.2005.10.013, URL http://www.sciencedirect.com/science/article/pii/S0304420305002148, 2006.

Buesseler, K. O., Antia, A. N., Chen, M., Fowler, S. W., Gardner, W. D., Gustafsson, r., Harada,

K., Michaels, A. F., Rutgers v. d. Loeff, M., Sarin, M., Steinberg, D. K., and Trull, T.: An assessment of the use of sediment traps for estimating upper ocean particle fluxes, Journal of Marine Research, 65, 345–416, URL http://epic.awi.de/12944/, 2007.

Buesseler, K. O., McDonnell, A. M. P., Schofield, O. M. E., Steinberg, D. K., and Ducklow, H. W.: High particle export over the continental shelf of the west Antarctic Peninsula, Geophysical Research Letters, 37, L22 606, doi:10.1029/2010GL045448, URL http://onlinelibrary.wiley.com/doi/10.1029/2010GL045448/abstract, 2010.

Burd, A. B. and Jackson, G. A.: Particle Aggregation, Annual Review of Marine Science, 1, 65–90, doi:10.1146/annurev.marine.010908.163904, URL http://www.annualreviews.org/doi/abs/10.1146/annurev.marine.010908.163904, 2009.

Burd, A. B., Hansell, D. A., Steinberg, D. K., Anderson, T. R., Arístegui, J., Baltar, F., Beaupré, S. R., Buesseler, K. O., DeHairs, F., Jackson, G. A., Kadko, D. C., Koppelmann, R., Lampitt, R. S., Nagata, T., Reinthaler, T., Robinson, C., Robison, B. H., Tamburini, C., and Tanaka, T.: Assessing the apparent imbalance between geochemical and biochemical indicators of meso- and bathypelagic biological activity: What the @$! is wrong with present calculations of carbon budgets?, Deep Sea Research Part II: Topical Studies in Oceanography, 57, 1557–1571, doi:10.1016/j.dsr2.2010.02.022, URL http://www.sciencedirect.com/science/article/pii/S0967064510000883, 2010.

Cardinal, D., Dehairs, F., Cattaldo, T., and André, L.: Geochemistry of suspended particles in the Subantarctic and Polar Frontal zones south of Australia: Constraints on export and advection processes, Journal of Geophysical Research: Oceans, 106, 31 637–31 656, doi:10.1029/2000JC000251, URL http://onlinelibrary.wiley.com/doi/10.1029/2000JC000251/abstract, 2001.

Carlotti, F., Thibault-Botha, D., Nowaczyk, A., and Lefèvre, D.: Zooplankton community structure, biomass and role in carbon fluxes during the second half of a phytoplankton bloom in the eastern sector of the Kerguelen Shelf (January–February 2005), Deep Sea Research Part II: Topical Studies in Oceanography, 55, 720–733, doi:10.1016/j.dsr2.2007.12.010, URL http://www.sciencedirect.com/science/article/pii/S0967064508000210, 2008.

Carlotti, F., Jouandet, M.-P., Nowaczyk, A., Harmelin-Vivien, M., Lefèvre, D., Richard, P., Zhu, Y., and Zhou, M.: Mesozooplankton structure and functioning during the onset of the Kerguelen phytoplankton bloom during the KEOPS2 survey, Biogeosciences, 12, 4543–4563, doi:10.5194/bg-12-4543-2015, URL http://www.biogeosciences.net/12/4543/2015/, 2015.

Cassar, N., DiFiore, P. J., Barnett, B. A., Bender, M. L., Bowie, A. R., Tilbrook, B., Petrou, K., Westwood, K. J., Wright, S. W., and Lefevre, D.: The influence of iron and light on net community production in the Subantarctic and Polar Frontal Zones, Biogeosciences, 8, 227–237, doi:10.5194/bg-8-227-2011, URL http://www.biogeosciences.net/8/227/2011/, 2011.

Cavagna, A. J., Fripiat, F., Elskens, M., Mangion, P., Chirurgien, L., Closset, I., Lasbleiz, M., Florez-Leiva, L., Cardinal, D., Leblanc, K., Fernandez, C., Lefèvre, D., Oriol, L., Blain, S., Quéguiner, B., and Dehairs, F.: Production regime and associated N cycling in the vicinity of Kerguelen Island, Southern Ocean, Biogeosciences, 12, 6515–6528, doi:10.5194/bg-12-6515-2015, URL http://www.biogeosciences.net/12/6515/2015/, 2015.

Cavan, E. L., Le Moigne, F., Poulton, A. J., Tarling, G. A., Ward, P., Daniels, C. J., Fragoso, G., and Sanders, R. J.: Zooplankton fecal pellets control the attenuation of particulate organic carbon flux in the Scotia Sea, Southern Ocean, Geophysical Research Letters, p. 2014GL062744, doi:10.1002/2014GL062744, URL http://onlinelibrary.wiley.com/doi/10.1002/2014GL062744/abstract, 2015.

Cermeño, P., Falkowski, P. G., Romero, O. E., Schaller, M. F., and Vallina, S. M.: Continental erosion and the Cenozoic rise of marine diatoms, Proceedings of the National Academy of Sciences, 112, 4239–4244, doi:10.1073/pnas.1412883112, URL http://www.pnas.org/content/112/14/4239, 2015.

Cetinić, I., Perry, M. J., Briggs, N. T., Kallin, E., D'Asaro, E. A., and Lee, C. M.: Particulate organic carbon and inherent optical properties during 2008 North Atlantic Bloom Experiment, Journal of Geophysical Research: Oceans, 117, C06 028, doi:10.1029/2011JC007771, URL http://onlinelibrary.wiley.com/doi/10.1029/2011JC007771/abstract, 2012.

Cetinić, I., Perry, M. J., D'Asaro, E., Briggs, N., Poulton, N., Sieracki, M. E., and Lee, C. M.: A simple optical index shows spatial and temporal heterogeneity in phytoplankton community composition during the 2008 North Atlantic Bloom Experiment, Biogeosciences, 12, 2179–2194, doi:10.5194/bg-12-2179-2015, URL http://www.biogeosciences.net/12/2179/2015/, 2015.

Chang, C.-H., Johnson, N. C., and Cassar, N.: Neural network-based estimates of Southern Ocean net community production from in situ O2 / Ar and satellite observation: a methodological study, Biogeosciences, 11, 3279–3297, doi:10.5194/bg-11-3279-2014, URL http://www.biogeosciences.net/11/3279/2014/, 2014.

Charette, M. A. and Buesseler, K. O.: Does iron fertilization lead to rapid carbon export in the Southern Ocean?, Geochemistry, Geophysics, Geosystems, 1, 2000GC000 069, doi:10.1029/2000GC000069, URL http://onlinelibrary.wiley.com/doi/10.1029/2000GC000069/abstract, 2000.

Chase, Z., Kohfeld, K. E., and Matsumoto, K.: Controls on biogenic silica burial in the Southern Ocean, Global Biogeochemical Cycles, 29, 2015GB005 186, doi:10.1002/2015GB005186, URL http://onlinelibrary.wiley.com/doi/10.1002/2015GB005186/abstract, 2015.

Chen, B., Laws, E. A., Liu, H., and Huang, B.: Estimating microzooplankton grazing half-saturation constants from dilution experiments with nonlinear feeding kinetics, Limnology and Oceanography, 59, 639–644, doi:10.4319/lo.2014.59.3.0639, URL http://onlinelibrary.wiley.com/doi/10.4319/lo.2014.59.3.0639/abstract, 2014.

Chen, J. H., Lawrence Edwards, R., and Wasserburg, G. J.: 238U, 234U and 232Th in seawater, Earth and Planetary Science Letters, 80, 241–251, doi:10.1016/0012-821X(86)90108-1, URL http://adsabs.harvard.edu/abs/1986E%26PSL..80..241C, 1986.

Chen, Y.-C.: The biomass and total lipid content and composition of twelve species of marine diatoms cultured under various environments, Food Chemistry, 131, 211–219, doi:10.1016/j.foodchem.2011.08.062, URL http://www.sciencedirect.com/science/article/pii/S0308814611012118, 2012.

Chever, F., Sarthou, G., Bucciarelli, E., Blain, S., and Bowie, A. R.: An iron budget during the natural iron fertilisation experiment KEOPS (Kerguelen Islands, Southern Ocean), Biogeosciences, 7, 455–468, doi:10.5194/bg-7-455-2010, URL http://www.biogeosciences.net/7/455/2010/, 2010.

Chisholm, S. W., Falkowski, P. G., and Cullen, J. J.: Dis-Crediting Ocean Fertilization, Science, 294, 309–310, doi:10.1126/science.1065349, URL http://www.sciencemag.org/content/294/5541/309, 2001.

Chuecas, L. and Riley, J. P.: Component Fatty Acids of the Total Lipids of Some Marine Phytoplankton, Journal of the Marine Biological Association of the United Kingdom, 49, 97–116, doi:10.1017/S0025315400046439, URL http://journals.cambridge.org/article_S0025315400046439, 1969.

Claustre, H., Antoine, D., Boehme, L., Boss, E., D'Ortenzio, F., Fanton D'Andon, O., Guinet, C., Gruber, N., Handegard, N. O., Hood, M., Johnson, K., Kortzinger, A., Lampitt, R., LeTraon, P.-Y., Le Quere, C., Lewis, M., Perry, M.-J., Platt, T., Roemmich, D., Sathyendranath, S., Send, U., Testor, P., and Yoder, J.: Guidelines towards an integrated ocean observation system for ecosystems and biogeochemical cycles, in: Proceedings of OceanObs'09: Sustained Ocean Observations and Information for Society, Vol. 1, edited by Hall, J., Harrison, D. E., and Stammer, D., pp. 593–612, European Space Agency, URL http://eprints.soton.ac.uk/340375/, 2010.

Coale, K. H., Johnson, K. S., Chavez, F. P., Buesseler, K. O., Barber, R. T., Brzezinski,

M. A., Cochlan, W. P., Millero, F. J., Falkowski, P. G., Bauer, J. E., Wanninkhof, R. H., Kudela, R. M., Altabet, M. A., Hales, B. E., Takahashi, T., Landry, M. R., Bidigare, R. R., Wang, X., Chase, Z., Strutton, P. G., Friederich, G. E., Gorbunov, M. Y., Lance, V. P., Hilting, A. K., Hiscock, M. R., Demarest, M., Hiscock, W. T., Sullivan, K. F., Tanner, S. J., Gordon, R. M., Hunter, C. N., Elrod, V. A., Fitzwater, S. E., Jones, J. L., Tozzi, S., Koblizek, M., Roberts, A. E., Herndon, J., Brewster, J., Ladizinsky, N., Smith, G., Cooper, D., Timothy, D., Brown, S. L., Selph, K. E., Sheridan, C. C., Twining, B. S., and Johnson, Z. I.: Southern Ocean Iron Enrichment Experiment: Carbon Cycling in High- and Low-Si Waters, Science, 304, 408–414, doi:10.1126/science.1089778, URL http://www.sciencemag.org/content/304/5669/408, 2004.

Cochran, J. K. and Masqué, P.: Short-lived U/Th Series Radionuclides in the Ocean: Tracers for Scavenging Rates, Export Fluxes and Particle Dynamics, Reviews in Mineralogy and Geochemistry, 52, 461–492, doi:10.2113/0520461, URL http://rimg.geoscienceworld.org/content/52/1/461, 2003.

Conley, D. J., Kilham, S. S., and Theriot, E.: Differences in silica content between marine and freshwater diatoms, Limnology and Oceanography, 34, 205–212, doi:10.4319/lo.1989.34.1.0205, URL http://onlinelibrary.wiley.com/doi/10.4319/lo.1989.34.1.0205/abstract, 1989.

Conway, T. J. and Tans, P. P.: Trends in atmospheric carbon dioxide, URL http://www.esrl.noaa.gov/gmd/ccgg/trends/index.html, 2015.

Coppola, L., Roy-Barman, M., Wassmann, P., Mulsow, S., and Jeandel, C.: Calibration of sediment traps and particulate organic carbon export using 234Th in the Barents Sea, Marine Chemistry, 80, 11–26, doi:10.1016/S0304-4203(02)00071-3, URL http://www.sciencedirect.com/science/article/pii/S0304420302000713, 2002.

Cox, P. A.: The Elements: Their Origin, Abundance and Distribution, Oxford, UK, oxford university press edn., 1989.

Crosta, X., Pichon, J.-J., and Labracherie, M.: Distribution of Chaetoceros resting spores in modern peri-Antarctic sediments, Marine Micropaleontology, 29, 283–299, doi:10.1016/S0377-8398(96)00033-3, URL http://www.sciencedirect.com/science/article/pii/S0377839896000333, 1997.

Crosta, X., Pichon, J.-J., and Burckle, L. H.: Application of modern analog technique to marine Antarctic diatoms: Reconstruction of maximum sea-ice extent at the Last Glacial Maximum, Paleoceanography, 13, 284–297, doi:10.1029/98PA00339, URL http://onlinelibrary.wiley.com/doi/10.1029/98PA00339/abstract, 1998.

Cubillos, J. C., Wright, S. W., Nash, G., Salas, M. F. d., Griffiths, B., Tilbrook, B., Poisson, A., and Hallegraeff, G. M.: Calcification morphotypes of the coccolithophorid Emiliania huxleyi in the Southern Ocean: changes in 2001 to 2006 compared to historical data, Marine Ecology Progress Series, 348, 47–54, doi:10.3354/meps07058, URL http://www.int-res.com/abstracts/meps/v348/p47-54/, 2007.

D'Alelio, D., d'Alcalà, M. R., Dubroca, L., , D. S., Zingone, A., and Montresor, M.: The time for sex: A biennial life cycle in a marine planktonic diatom, Limnology and Oceanography, 55, 106–114, doi:10.4319/lo.2010.55.1.0106, URL http://onlinelibrary.wiley.com/doi/10.4319/lo.2010.55.1.0106/abstract, 2010.

Dall'Olmo, G. and Mork, K. A.: Carbon export by small particles in the Norwegian Sea, Geophysical Research Letters, 41, 2921–2927, doi:10.1002/2014GL059244, URL http://onlinelibrary.wiley.com/doi/10.1002/2014GL059244/abstract, 2014.

Dall'Olmo, G., Westberry, T. K., Behrenfeld, M. J., Boss, E., and Slade, W. H.: Significant contribution of large particles to optical backscattering in the open ocean, Biogeosciences, 6, 947–967, doi:10.5194/bg-6-947-2009, URL http://www.biogeosciences.net/6/947/2009/, 2009.

Dalsgaard, J., St. John, M., Kattner, G., Müller-Navarra, D., and Hagen, W.: Fatty acid

trophic markers in the pelagic marine environment, vol. 46, pp. 225–340, Academic Press, URL http://www.sciencedirect.com/science/article/pii/S0065288103460057, 2003.

Davison, P. C., Checkley Jr., D. M., Koslow, J. A., and Barlow, J.: Carbon export mediated by mesopelagic fishes in the northeast Pacific Ocean, Progress in Oceanography, 116, 14–30, doi:10.1016/j.pocean.2013.05.013, URL http://www.sciencedirect.com/science/article/pii/S0079661113000554, 2013.

de Baar, H. J. W., Buma, A. G. J., Nolting, R. F., Cadée, G. C., Jacques, G., and Tréguer, P.: On iron limitation of the Southern Ocean: experimental observations in the Weddell and Scotia Seas, Marine Ecology Progress Series, 65, 105–122, doi:10.3354/meps065105, 1990.

de Baar, H. J. W., de Jong, J. T. M., Bakker, D. C. E., Löscher, B. M., Veth, C., Bathmann, U., and Smetacek, V.: Importance of iron for plankton blooms and carbon dioxide drawdown in the Southern Ocean, Nature, 373, 412–415, doi:10.1038/373412a0, URL http://www.nature.com/nature/journal/v373/n6513/abs/373412a0.html, 1995.

de Baar, H. J. W., Boyd, P. W., Coale, K. H., Landry, M. R., Tsuda, A., Assmy, P., Bakker, D. C. E., Bozec, Y., Barber, R. T., Brzezinski, M. A., Buesseler, K. O., Boyé, M., Croot, P. L., Gervais, F., Gorbunov, M. Y., Harrison, P. J., Hiscock, W. T., Laan, P., Lancelot, C., Law, C. S., Levasseur, M., Marchetti, A., Millero, F. J., Nishioka, J., Nojiri, Y., van Oijen, T., Riebesell, U., Rijkenberg, M. J. A., Saito, H., Takeda, S., Timmermans, K. R., Veldhuis, M. J. W., Waite, A. M., and Wong, C.-S.: Synthesis of iron fertilization experiments: From the Iron Age in the Age of Enlightenment, Journal of Geophysical Research: Oceans, 110, C09S16, doi:10.1029/2004JC002601, URL http://onlinelibrary.wiley.com/doi/10.1029/2004JC002601/abstract, 2005.

de Vargas, C., Audic, S., Henry, N., Decelle, J., Mahé, F., Logares, R., Lara, E., Berney, C., Bescot, N. L., Probert, I., Carmichael, M., Poulain, J., Romac, S., Colin, S., Aury, J.-M., Bittner, L., Chaffron, S., Dunthorn, M., Engelen, S., Flegontova, O., Guidi, L., Horák, A., Jaillon, O., Lima-Mendez, G., Lukeš, J., Malviya, S., Morard, R., Mulot, M., Scalco, E., Siano, R., Vincent, F., Zingone, A., Dimier, C., Picheral, M., Searson, S., Kandels-Lewis, S., Coordinators, T. O., Acinas, S. G., Bork, P., Bowler, C., Gorsky, G., Grimsley, N., Hingamp, P., Iudicone, D., Not, F., Ogata, H., Pesant, S., Raes, J., Sieracki, M. E., Speich, S., Stemmann, L., Sunagawa, S., Weissenbach, J., Wincker, P., Karsenti, E., Boss, E., Follows, M., Karp-Boss, L., Krzic, U., Reynaud, E. G., Sardet, C., Sullivan, M. B., and Velayoudon, D.: Eukaryotic plankton diversity in the sunlit ocean, Science, 348, 1261 605, doi:10.1126/science.1261605, URL http://www.sciencemag.org/content/348/6237/1261605, 2015.

Decelle, J., Probert, I., Bittner, L., Desdevises, Y., Colin, S., Vargas, C. d., Galí, M., Simó, R., and Not, F.: An original mode of symbiosis in open ocean plankton, Proceedings of the National Academy of Sciences, 109, 18 000–18 005, doi:10.1073/pnas.1212303109, URL http://www.pnas.org/content/109/44/18000, 2012.

Dehairs, F., Jeandel, C., Cattaldo, T., Tachikawa, K., and Goeyens, L.: Barium-barite as a tracer of export production: some information from the water column, in: Proceedings of the symposium OPALEO, pp. 175–192, Brest, ragueneau et al. edn., 1996.

Dehairs, F., Fripiat, F., Cavagna, A.-J., Trull, T. W., Fernandez, C., Davies, D., Roukaerts, A., Fonseca Batista, D., Planchon, F., and Elskens, M.: Nitrogen cycling in the Southern Ocean Kerguelen Plateau area: evidence for significant surface nitrification from nitrate isotopic compositions, Biogeosciences, 12, 1459–1482, doi:10.5194/bg-12-1459-2015, URL http://www.biogeosciences.net/12/1459/2015/, 2015.

DeMaster, D. J.: The supply and accumulation of silica in the marine environment, Geochimica et Cosmochimica Acta, 45, 1715–1732, doi:10.1016/0016-7037(81)90006-5, URL http://www.sciencedirect.com/science/article/pii/0016703781900065, 1981.

Desboeufs, K., Leblond, N., Wagener, T., Bon Nguyen, E., and Guieu, C.: Chemical fate and settling of mineral dust in surface seawater after atmospheric deposition observed from

dust seeding experiments in large mesocosms, Biogeosciences, 11, 5581–5594, doi:10.5194/bg-11-5581-2014, URL http://www.biogeosciences.net/11/5581/2014/, 2014.

Doucette, G. J. and Fryxell, G. A.: Thalassiosira antarctica: vegetative and resting stage chemical composition of an ice-related marine diatom, Marine Biology, 78, 1–6, doi:10.1007/BF00392964, URL http://link.springer.com/article/10.1007/BF00392964, 1983.

d'Ovidio, F., Della Penna, A., Trull, T. W., Nencioli, F., Pujol, M.-I., Rio, M.-H., Park, Y.-H., Cotté, C., Zhou, M., and Blain, S.: The biogeochemical structuring role of horizontal stirring: Lagrangian perspectives on iron delivery downstream of the Kerguelen Plateau, Biogeosciences, 12, 5567–5581, doi:10.5194/bg-12-5567-2015, URL http://www.biogeosciences.net/12/5567/2015/, 2015.

Dufourc, E. J.: Sterols and membrane dynamics, Journal of Chemical Biology, 1, 63–77, doi:10.1007/s12154-008-0010-6, URL http://www.ncbi.nlm.nih.gov/pmc/articles/PMC2698314/, 2008.

Dugdale, R. C. and Goering, J. J.: Uptake of New and Regenerated Forms of Nitrogen in Primary Productivity, Limnology and Oceanography, 12, 196–206, URL http://www.jstor.org/stable/2833031, 1967.

Dunne, J. P., Armstrong, R. A., Gnanadesikan, A., and Sarmiento, J. L.: Empirical and mechanistic models for the particle export ratio, Global Biogeochemical Cycles, 19, GB4026, doi:10.1029/2004GB002390, URL http://onlinelibrary.wiley.com/doi/10.1029/2004GB002390/abstract, 2005.

Dunstan, G. A., Volkman, J. K., Barrett, S. M., Leroi, J.-M., and Jeffrey, S. W.: Essential polyunsaturated fatty acids from 14 species of diatom (Bacillariophyceae), Phytochemistry, 35, 155–161, doi:10.1016/S0031-9422(00)90525-9, URL http://www.sciencedirect.com/science/article/pii/S0031942200905259, 1993.

Durkin, C. A., Estapa, M. L., and Buesseler, K. O.: Observations of carbon export by small sinking particles in the upper mesopelagic, Marine Chemistry, 175, 72–81, doi:10.1016/j.marchem.2015.02.011, URL http://www.sciencedirect.com/science/article/pii/S0304420315000390, 2015.

Ebersbach, F. and Trull, T. W.: Sinking particle properties from polyacrylamide gels during the KErguelen Ocean and Plateau compared Study (KEOPS): Zooplankton control of carbon export in an area of persistent natural iron inputs in the Southern Ocean, Limnology and Oceanography, 53, 212–224, doi:10.4319/lo.2008.53.1.0212, URL http://ecite.utas.edu.au/54193, 2008.

Ellwood, M. J., Nodder, S. D., King, A. L., Hutchins, D. A., Wilhelm, S. W., and Boyd, P. W.: Pelagic iron cycling during the subtropical spring bloom, east of New Zealand, Marine Chemistry, 160, 18–33, doi:10.1016/j.marchem.2014.01.004, URL http://www.sciencedirect.com/science/article/pii/S030442031400005X, 2014.

Emerson, S.: Annual net community production and the biological carbon flux in the ocean, Global Biogeochemical Cycles, 28, 2013GB004 680, doi:10.1002/2013GB004680, URL http://onlinelibrary.wiley.com/doi/10.1002/2013GB004680/abstract, 2014.

Emerson, S., Quay, P., Karl, D., Winn, C., Tupas, L., and Landry, M.: Experimental determination of the organic carbon flux from open-ocean surface waters, Nature, 389, 951–954, doi:10.1038/40111, URL http://www.nature.com/nature/journal/v389/n6654/abs/389951a0.html, 1997.

Engel, A.: The role of transparent exopolymer particles (TEP) in the increase in apparent particle stickiness () during the decline of a diatom bloom, Journal of Plankton Research, 22, 485–497, doi:10.1093/plankt/22.3.485, URL http://plankt.oxfordjournals.org/content/22/3/485, 2000.

Eppley, R., Rogers, J., and McCarthy, J.: Half_saturation constants for uptake of nitrate and ammonium by marine phytoplankton, Limnology and Oceanography, 14, 912–920, 1969.

Eppley, R. W. and Peterson, B. J.: Particulate organic matter flux and planktonic new

production in the deep ocean, Nature, 282, 677–680, doi:10.1038/282677a0, URL `http://www.nature.com/nature/journal/v282/n5740/abs/282677a0.html`, 1979.

Estapa, M. L., Siegel, D. A., Buesseler, K. O., Stanley, R. H. R., Lomas, M. W., and Nelson, N. B.: Decoupling of net community and export production on submesoscales in the Sargasso Sea, Global Biogeochemical Cycles, 29, 2014GB004 913, doi:10.1002/2014GB004913, URL `http://onlinelibrary.wiley.com/doi/10.1002/2014GB004913/abstract`, 2015.

Fabry, V. J.: Shell growth rates of pteropod and heteropod molluscs and aragonite production in the open ocean: Implications for the marine carbonate system, Journal of Marine Research, 48, 209–222, doi:10.1357/002224090784984614, URL `http://www.ingentaconnect.com/content/jmr/jmr/1990/00000048/00000001/art00009`, 1990.

Fabry, V. J., Seibel, B. A., Feely, R. A., and Orr, J. C.: Impacts of ocean acidification on marine fauna and ecosystem processes, ICES Journal of Marine Science: Journal du Conseil, 65, 414–432, doi:10.1093/icesjms/fsn048, URL `http://icesjms.oxfordjournals.org/content/65/3/414`, 2008.

Fasham, M. J. R., Ducklow, H. W., and McKelvie, S. M.: A nitrogen-based model of plankton dynamics in the oceanic mixed layer, Journal of Marine Research, 48, 591–639, 1990.

Feely, R., Doney, S., and Cooley, S.: Ocean Acidification: Present Conditions and Future Changes in a High-CO2 World, Oceanography, 22, 36–47, doi:10.5670/oceanog.2009.95, URL `http://www.tos.org/oceanography/archive/22-4_feely.html`, 2009.

Ferry, A. J., Prvan, T., Jersky, B., Crosta, X., and Armand, L. K.: Statistical modeling of Southern Ocean marine diatom proxy and winter sea ice data: Model comparison and developments, Progress in Oceanography, 131, 100–112, doi:10.1016/j.pocean.2014.12.001, URL `http://www.sciencedirect.com/science/article/pii/S0079661114002031`, 2015.

Fiala, M., Kopczynska, E. E., Jeandel, C., Oriol, L., and Vetion, G.: Seasonal and inter-annual variability of size-fractionated phytoplankton biomass and community structure at station Kerfix, off the Kerguelen Islands, Antarctica, Journal of Plankton Research, 20, 1341–1356, doi:10.1093/plankt/20.7.1341, URL `http://plankt.oxfordjournals.org/content/20/7/1341`, 1998.

Fiala, M., Kopczynska, E. E., Oriol, L., and Machado, M.-C.: Phytoplankton variability in the Crozet Basin frontal zone (Southwest Indian Ocean) during austral summer, Journal of Marine Systems, 50, 243–261, doi:10.1016/j.jmarsys.2004.01.008, URL `http://www.sciencedirect.com/science/article/pii/S0924796304001083`, 2004.

Field, n., Behrenfeld, n., Randerson, n., and Falkowski, n.: Primary production of the biosphere: integrating terrestrial and oceanic components, Science (New York, N.Y.), 281, 237–240, 1998.

Fontanez, K. M., Eppley, J. M., Samo, T. J., Karl, D. M., and DeLong, E. F.: Microbial community structure and function on sinking particles in the North Pacific Subtropical Gyre, Frontiers in Microbiology, 6, 469, doi:10.3389/fmicb.2015.00469, URL `http://www.ncbi.nlm.nih.gov/pmc/articles/PMC4436931/`, 2015.

Forster, P. M., Andrews, T., Good, P., Gregory, J. M., Jackson, L. S., and Zelinka, M.: Evaluating adjusted forcing and model spread for historical and future scenarios in the CMIP5 generation of climate models, Journal of Geophysical Research: Atmospheres, 118, 1139–1150, doi:10.1002/jgrd.50174, URL `http://onlinelibrary.wiley.com/doi/10.1002/jgrd.50174/abstract`, 2013.

Francois, R., Altabet, M. A., Yu, E.-F., Sigman, D. M., Bacon, M. P., Frank, M., Bohrmann, G., Bareille, G., and Labeyrie, L. D.: Contribution of Southern Ocean surface-water stratification to low atmospheric CO2 concentrations during the last glacial period, Nature, 389, 929–935, doi:10.1038/40073, URL `http://www.nature.com/nature/journal/v389/n6654/abs/389929a0.html`, 1997.

Francois, R., Honjo, S., Krishfield, R., and Manganini, S.: Factors controlling the flux of organic carbon to the bathypelagic zone of the ocean, Global Biogeochemical Cycles, 16, 1087, doi:10.1029/2001GB001722, URL `http://onlinelibrary.wiley.com/doi/10.1029/`

`2001GB001722/abstract`, 2002.

Frankignoulle, M., Canon, C., and Gattudo, J.-P.: Marine calcification as a source of carbon dioxide : Positive deedback of increasing atmospheric CO2, Limnology and Oceanography, 39, 458–462, 1994.

French, F. W. and Hargraves, P. E.: Spore Formation in the Life Cycles of the Diatoms Chaetoceros Diadema and Leptocylindrus Danicus, Journal of Phycology, 21, 477–483, doi: 10.1111/j.0022-3646.1985.00477.x, URL `http://onlinelibrary.wiley.com/doi/10.1111/j.0022-3646.1985.00477.x/abstract`, 1985.

Frew, R. D., Hutchins, D. A., Nodder, S., Sanudo-Wilhelmy, S., Tovar-Sanchez, A., Leblanc, K., Hare, C. E., and Boyd, P. W.: Particulate iron dynamics during Fe-Cycle in subantarctic waters southeast of New Zealand, Global Biogeochemical Cycles, 20, GB1S93, doi:10.1029/2005GB002558, URL `http://onlinelibrary.wiley.com/doi/10.1029/2005GB002558/abstract`, 2006.

Friedrichs, L., Hrnig, M., Schulze, L., Bertram, A., Jansen, S., and Hamm, C.: Size and biomechanic properties of diatom frustules influence food uptake by copepods, Marine Ecology Progress Series, 481, 41–51, doi:10.3354/meps10227, URL `http://www.int-res.com/abstracts/meps/v481/p41-51/`, 2013.

Frölicher, T. L., Sarmiento, J. L., Paynter, D. J., Dunne, J. P., Krasting, J. P., and Winton, M.: Dominance of the Southern Ocean in Anthropogenic Carbon and Heat Uptake in CMIP5 Models, Journal of Climate, 28, 862–886, doi:10.1175/JCLI-D-14-00117.1, URL `http://journals.ametsoc.org/doi/abs/10.1175/JCLI-D-14-00117.1`, 2014.

Fryxell, G. A. and Prasad, A. K. S. K.: Eucampia antarctica var. recta (Mangin) stat. nov. (Biddulphiaceae, Bacillariophyceae): life stages at the Weddell Sea ice edge, Phycologia, 29, 27–38, doi:10.2216/i0031-8884-29-1-27.1, URL `http://phycologia.org/doi/abs/10.2216/i0031-8884-29-1-27.1`, 1990.

Funkhouser, J. W. and Evitt, W. R.: Preparation Techniques for Acid-Insoluble Microfossils, Micropaleontology, 5, 369–375, doi:10.2307/1484431, URL `http://www.jstor.org/stable/1484431`, 1959.

Garcia, H. E. and Gordon, L. I.: Oxygen solubility in seawater: Better fitting equations, Limnology and Oceanography, 37, 1307–1312, doi:10.4319/lo.1992.37.6.1307, URL `http://onlinelibrary.wiley.com/doi/10.4319/lo.1992.37.6.1307/abstract`, 1992.

Garcia, H. E., Locarini, R. A., Boyer, T. P., Antonov, J. I., Baranova, O. K., Zweng, M. M., Reagan, J. R., and Johnson, D. R.: World Ocean Atlas 2013, Volume 4: Dissolved Inorganic Nutrients (phosphate, nitrate, silicate), S. Levitus, a. mishonov technical ed. edn., URL `https://www.nodc.noaa.gov/OC5/woa13/`, 2013.

Gardner, W., Richardson, M. J., Walsh, I., and Berglund, B.: In-Situ Optical Sensing of Particles for Determination of Oceanic Processes: What Satellites Can't See, But Tranmissometers Can, Oceanography, 3, 11–17, doi:10.5670/oceanog.1990.02, URL `http://www.tos.org/oceanography/archive/3-2_gardner.html`, 1990.

Gardner, W. D.: Field assessment of sediment traps, Journal of Marine Research, 38, 41–52, URL `http://geotest.tamu.edu/userfiles/135/GardnerTrapCalField80.pdf`, 1980.

Gast, R. J. and Caron, D. A.: Photosymbiotic associations in planktonic foraminifera and radiolaria, Hydrobiologia, 461, 1–7, doi:10.1023/A:1012710909023, URL `http://link.springer.com/article/10.1023/A%3A1012710909023`, 2001.

Gauld, D. T.: A Peritrophic Membrane in Calanoid Copepods, Nature, 179, 325–326, doi:10.1038/179325a0, URL `http://www.nature.com/nature/journal/v179/n4554/abs/179325a0.html`, 1957.

Geider, R. J., Maclntyre, H. L., and Kana, T. M.: A dynamic regulatory model of phytoplanktonic acclimation to light, nutrients, and temperature, Limnology and Oceanography, 43, 679–694, doi:10.4319/lo.1998.43.4.0679, URL `http://onlinelibrary.wiley.com/doi/10.4319/lo.1998.43.4.0679/abstract`, 1998.

Gerringa, L. J., Alderkamp, A.-C., Laan, P., Thuróczy, C.-E., De Baar, H. J., Mills, M. M., van Dijken, G. L., Haren, H. v., and Arrigo, K. R.: Iron from melting glaciers fuels the phytoplankton blooms in Amundsen Sea (Southern Ocean): Iron biogeochemistry, Deep Sea Research Part II: Topical Studies in Oceanography, 71–76, 16–31, doi:10.1016/j.dsr2.2012.03.007, URL http://www.sciencedirect.com/science/article/pii/S0967064512000446, 2012.

Gerringa, L. J. A., Blain, S., Laan, P., Sarthou, G., Veldhuis, M. J. W., Brussaard, C. P. D., Viollier, E., and Timmermans, K. R.: Fe-binding dissolved organic ligands near the Kerguelen Archipelago in the Southern Ocean (Indian sector), Deep Sea Research Part II: Topical Studies in Oceanography, 55, 606–621, doi:10.1016/j.dsr2.2007.12.007, URL http://www.sciencedirect.com/science/article/pii/S0967064508000131, 2008.

Gersonde, R. and Wefer, G.: Sedimentation of biogenic siliceous particles in Antarctic waters from the Atlantic sector, Marine Micropaleontology, 11, 311–332, doi:10.1016/0377-8398(87)90004-1, URL http://www.sciencedirect.com/science/article/pii/0377839887900041, 1987.

Gersonde, R., Abelmann, A., Brathauer, U., Becquey, S., Bianchi, C., Cortese, G., Grobe, H., Kuhn, G., Niebler, H.-S., Segl, M., Sieger, R., Zielinski, U., and Fütterer, D. K.: Last glacial sea surface temperatures and sea-ice extent in the Southern Ocean (Atlantic-Indian sector): A multiproxy approach, Paleoceanography, 18, 1061, doi:10.1029/2002PA000809, URL http://onlinelibrary.wiley.com/doi/10.1029/2002PA000809/abstract, 2003.

Giering, S. L. C., Sanders, R., Lampitt, R. S., Anderson, T. R., Tamburini, C., Boutrif, M., Zubkov, M. V., Marsay, C. M., Henson, S. A., Saw, K., Cook, K., and Mayor, D. J.: Reconciliation of the carbon budget in the ocean/'s twilight zone, Nature, 507, 480–483, doi:10.1038/nature13123, URL http://www.nature.com/nature/journal/v507/n7493/full/nature13123.html, 2014.

Goad, L. J.: Sterol biosynthesis and metabolism in marine invertebrates, Pure and Applied Chemistry, 53, 837–852, doi:10.1351/pac198153040837, URL http://www.degruyter.com/view/j/pac.1981.53.issue-4/pac198153040837/pac198153040837.xml, 1981.

Gomi, Y., Fukuchi, M., and Taniguchi, A.: Diatom assemblages at subsurface chlorophyll maximum layer in the eastern Indian sector of the Southern Ocean in summer, Journal of Plankton Research, 32, 1039–1050, doi:10.1093/plankt/fbq031, URL http://plankt.oxfordjournals.org/content/32/7/1039, 2010.

Gonzalez, H. E. and Smetacek, V.: The possible role of the cyclopoid copepod Oithona in retarding vertical flux of zooplankton faecal material, Marine Ecology-Progress Series, 113, 233–246, URL http://epic.awi.de/1010/, 1994.

Gorsky, G., Picheral, M., and Stemmann, L.: Use of the Underwater Video Profiler for the Study of Aggregate Dynamics in the North Mediterranean, Estuarine, Coastal and Shelf Science, 50, 121–128, doi:10.1006/ecss.1999.0539, URL http://www.sciencedirect.com/science/article/pii/S0272771499905395, 2000.

Grigorov, I., Rigual-Hernandez, A. S., Honjo, S., Kemp, A. E. S., and Armand, L. K.: Settling fluxes of diatoms to the interior of the Antarctic circumpolar current along 170W, Deep Sea Research Part I: Oceanographic Research Papers, 93, 1–13, doi:10.1016/j.dsr.2014.07.008, URL http://www.sciencedirect.com/science/article/pii/S096706371400137X, 2014.

Guidi, L., Jackson, G. A., Stemmann, L., Miquel, J. C., Picheral, M., and Gorsky, G.: Relationship between particle size distribution and flux in the mesopelagic zone, Deep Sea Research Part I: Oceanographic Research Papers, 55, 1364–1374, doi:10.1016/j.dsr.2008.05.014, URL http://www.sciencedirect.com/science/article/pii/S0967063708001209, 2008.

Guidi, L., Legendre, L., Reygondeau, G., Uitz, J., Stemmann, L., and Henson, S. A.: A new look at ocean carbon remineralization for estimating deepwater sequestration, Global Biogeochemical Cycles, 29, 1044–1059, doi:10.1002/2014GB005063, URL http://onlinelibrary.wiley.com/doi/10.1002/2014GB005063/abstract, 2015.

Guidi, L., Chaffron, S., Bittner, L., Eveillard, D., Larhlimi, A., Roux, S., Darzi, Y., Audic, S.,

Berline, L., Brum, J., Coelho, L. P., Espinoza, J. C. I., Malviya, S., Sunagawa, S., Dimier, C., Kandels-Lewis, S., Picheral, M., Poulain, J., Searson, S., Tara Oceans Consortium Coordinators, Stemmann, L., Not, F., Hingamp, P., Speich, S., Follows, M., Karp-Boss, L., Boss, E., Ogata, H., Pesant, S., Weissenbach, J., Wincker, P., Acinas, S. G., Bork, P., de Vargas, C., Iudicone, D., Sullivan, M. B., Raes, J., Karsenti, E., Bowler, C., and Gorsky, G.: Plankton networks driving carbon export in the oligotrophic ocean, Nature, advance online publication, doi:10.1038/nature16942, URL http://www.nature.com/nature/journal/vaop/ncurrent/full/nature16942.html, 2016.

Guieu, C., Aumont, O., Paytan, A., Bopp, L., Law, C. S., Mahowald, N., Achterberg, E. P., Marañón, E., Salihoglu, B., Crise, A., Wagener, T., Herut, B., Desboeufs, K., Kanakidou, M., Olgun, N., Peters, F., Pulido-Villena, E., Tovar-Sanchez, A., and Völker, C.: The significance of the episodic nature of atmospheric deposition to Low Nutrient Low Chlorophyll regions, Global Biogeochemical Cycles, 28, 2014GB004 852, doi:10.1002/2014GB004852, URL http://onlinelibrary.wiley.com/doi/10.1002/2014GB004852/abstract, 2014.

Guinet, C., Cherel, Y., Ridoux, V., and Jouventin, P.: Consumption of marine resources by seabirds and seals in Crozet and Kerguelen waters: changes in relation to consumer biomass 1962–85, Antarctic Science, 8, 23–30, doi:10.1017/S0954102096000053, URL http://journals.cambridge.org/article_S0954102096000053, 1996.

Hamm, C. E., Merkel, R., Springer, O., Jurkojc, P., Maier, C., Prechtel, K., and Smetacek, V.: Architecture and material properties of diatom shells provide effective mechanical protection, Nature, 421, 841–843, doi:10.1038/nature01416, URL http://www.nature.com/nature/journal/v421/n6925/abs/nature01416.html, 2003.

Hamme, R. C., Cassar, N., Lance, V. P., Vaillancourt, R. D., Bender, M. L., Strutton, P. G., Moore, T. S., DeGrandpre, M. D., Sabine, C. L., Ho, D. T., and Hargreaves, B. R.: Dissolved O2/Ar and other methods reveal rapid changes in productivity during a Lagrangian experiment in the Southern Ocean, Journal of Geophysical Research: Oceans, 117, C00F12, doi:10.1029/2011JC007046, URL http://onlinelibrary.wiley.com/doi/10.1029/2011JC007046/abstract, 2012.

Hansell, D.: Marine Dissolved Organic Matter and the Carbon Cycle, Oceanography, 14, 41–49, doi:10.5670/oceanog.2001.05, URL http://www.tos.org/oceanography/archive/14-4_hansell.html, 2001.

Hansell, D. A.: Recalcitrant Dissolved Organic Carbon Fractions, Annual Review of Marine Science, 5, 421–445, doi:10.1146/annurev-marine-120710-100757, URL http://dx.doi.org/10.1146/annurev-marine-120710-100757, 2013.

Haren, H. v. and Compton, T. J.: Diel Vertical Migration in Deep Sea Plankton Is Finely Tuned to Latitudinal and Seasonal Day Length, PLOS ONE, 8, e64 435, doi:10.1371/journal.pone.0064435, URL http://journals.plos.org/plosone/article?id=10.1371/journal.pone.0064435, 2013.

Harland, R. and Pudsey, C. J.: Dinoflagellate cysts from sediment traps deployed in the Bellingshausen, Weddell and Scotia seas, Antarctica, Marine Micropaleontology, 37, 77–99, doi:10.1016/S0377-8398(99)00016-X, URL http://www.sciencedirect.com/science/article/pii/S037783989900016X, 1999.

Hasle, G. R. and Syvertsen, E. E.: Chapter 2 - Marine Diatoms, in: Identifying Marine Phytoplankton, edited by Tomas, C. R., pp. 5–385, Academic Press, San Diego, URL http://www.sciencedirect.com/science/article/pii/B9780126930184500045, 1997.

Hauck, J., Völker, C., WolfGladrow, D. A., Laufkötter, C., Vogt, M., Aumont, O., Bopp, L., Buitenhuis, E. T., Doney, S. C., Dunne, J., Gruber, N., Hashioka, T., John, J., Quéré, C. L., Lima, I. D., Nakano, H., Séférian, R., and Totterdell, I.: On the Southern Ocean CO2 uptake and the role of the biological carbon pump in the 21st century, Global Biogeochemical Cycles, 29, 1451–1470, doi:10.1002/2015GB005140, URL http://onlinelibrary.wiley.com/doi/10.1002/2015GB005140/abstract, 2015.

Hawley, N.: Flow in Cylindrical Sediment Traps, Journal of Great Lakes Research, 14, 76–88, doi: 10.1016/S0380-1330(88)71534-8, URL http://www.sciencedirect.com/science/article/pii/S0380133088715348, 1988.

Henson, S. A.: Slow science: the value of long ocean biogeochemistry records, Philosophical Transactions of the Royal Society of London A: Mathematical, Physical and Engineering Sciences, 372, 20130 334, doi:10.1098/rsta.2013.0334, URL http://rsta.royalsocietypublishing.org/content/372/2025/20130334, 2014.

Henson, S. A., Sanders, R., and Madsen, E.: Global patterns in efficiency of particulate organic carbon export and transfer to the deep ocean, Global Biogeochemical Cycles, 26, GB1028, doi:10.1029/2011GB004099, URL http://onlinelibrary.wiley.com/doi/10.1029/2011GB004099/abstract, 2012.

Henson, S. A., Yool, A., and Sanders, R.: Variability in efficiency of particulate organic carbon export: A model study, Global Biogeochemical Cycles, 29, GB4965, doi:10.1002/2014GB004965, URL http://onlinelibrary.wiley.com.biblioplanets.gate.inist.fr/doi/10.1002/2014GB004965/abstract, 2014.

Henson, S. A., Beaulieu, C., and Lampitt, R.: Observing climate change trends in ocean biogeochemistry: when and where, Global Change Biology, 22, 1561–1571, doi:10.1111/gcb.13152, URL http://onlinelibrary.wiley.com/doi/10.1111/gcb.13152/abstract, 2016.

Hernandez-Sanchez, M. T., Mills, R. A., Planquette, H., Pancost, R. D., Hepburn, L., Salter, I., and FitzGeorge-Balfour, T.: Quantifying export production in the Southern Ocean: Implications for the Baxs proxy, Paleoceanography, 26, PA4222, doi:10.1029/2010PA002111, URL http://onlinelibrary.wiley.com/doi/10.1029/2010PA002111/abstract, 2011.

Hernandez-Sanchez, M. T., Holtvoeth, J., Mills, R. A., Fisher, E. H., Wolff, G. A., and Pancost, R. D.: Signature of organic matter exported from naturally Fe-fertilised oceanic waters, Deep Sea Research Part I: Oceanographic Research Papers, 65, 59–72, doi: 10.1016/j.dsr.2012.02.007, URL http://www.sciencedirect.com/science/article/pii/S096706371200057X, 2012.

Herndl, G. J. and Reinthaler, T.: Microbial control of the dark end of the biological pump, Nature Geoscience, 6, 718–724, doi:10.1038/ngeo1921, URL http://www.nature.com/ngeo/journal/v6/n9/full/ngeo1921.html, 2013.

Hirst, A. G. and Bunker, A. J.: Growth of marine planktonic copepods: Global rates and patterns in relation to chlorophyll a, temperature, and body weight, Limnology and Oceanography, 48, 1988–2010, doi:10.4319/lo.2003.48.5.1988, URL http://onlinelibrary.wiley.com/doi/10.4319/lo.2003.48.5.1988/abstract, 2003.

Ho, T.-Y., Quigg, A., Finkel, Z. V., Milligan, A. J., Wyman, K., Falkowski, P. G., and Morel, F. M. M.: The Elemental Composition of Some Marine Phytoplankton, Journal of Phycology, 39, 1145–1159, doi:10.1111/j.0022-3646.2003.03-090.x, URL http://onlinelibrary.wiley.com/doi/10.1111/j.0022-3646.2003.03-090.x/abstract, 2003.

Hobson, L. A.: Seasonal variations in maximum photosynthetic rates of phytoplankton in Saanich Inlet, Vancouver Island, British Columbia, Journal of Experimental Marine Biology and Ecology, 52, 1–13, doi:10.1016/0022-0981(81)90166-0, URL http://www.sciencedirect.com/science/article/pii/0022098181901660, 1981.

Holm-Hansen, O. and Hewes, C. D.: Deep chlorophyll-a maxima (DCMs) in Antarctic waters. I. Relationships between DCMs and the physical, chemical, and optical conditions in the upper water column, Polar Biology, 27, 699–710, doi:10.1007/s00300-004-0641-1, URL http://link.springer.com/article/10.1007/s00300-004-0641-1, 2004.

Holm-Hansen, O., Kahru, M., and Hewes, C.: Deep chlorophyll a maxima (DCMs) in pelagic Antarctic waters. II. Relation to bathymetric features and dissolved iron concentrations, Marine Ecology Progress Series, 297, 71–81, doi:10.3354/meps297071, URL https://bora.uib.no/handle/1956/4270, 2005.

Holzer, M., Primeau, F. W., DeVries, T., and Matear, R.: The Southern Ocean sil-

icon trap: Data-constrained estimates of regenerated silicic acid, trapping efficiencies, and global transport paths, Journal of Geophysical Research: Oceans, 119, 313–331, doi:10.1002/2013JC009356, URL http://onlinelibrary.wiley.com/doi/10.1002/2013JC009356/abstract, 2014.

Honjo, S.: Coccoliths: Production, transportation and sedimentation, Marine Micropaleontology, 1, 65–79, doi:10.1016/0377-8398(76)90005-0, URL http://linkinghub.elsevier.com/retrieve/pii/0377839876900050, 1976.

Honjo, S., Manganini, S. J., Krishfield, R. A., and Francois, R.: Particulate organic carbon fluxes to the ocean interior and factors controlling the biological pump: A synthesis of global sediment trap programs since 1983, Progress in Oceanography, 76, 217–285, doi:10.1016/j.pocean.2007.11.003, URL http://www.sciencedirect.com/science/article/pii/S0079661108000025, 2008.

Howard, A. G., Coxhead, A. J., Potter, I. A., and Watt, A. P.: Determination of dissolved aluminium by the micelle-enhanced fluorescence of its lumogallion complex, Analyst, 111, 1379–1382, doi:10.1039/AN9861101379, URL http://pubs.rsc.org/en/content/articlelanding/1986/an/an9861101379, 1986.

Härnström, K., Ellegaard, M., Andersen, T. J., and Godhe, A.: Hundred years of genetic structure in a sediment revived diatom population, Proceedings of the National Academy of Sciences, 108, 4252–4257, doi:10.1073/pnas.1013528108, URL http://www.pnas.org/content/108/10/4252, 2011.

Hunt, B. P. V., Pakhomov, E. A., Hosie, G. W., Siegel, V., Ward, P., and Bernard, K.: Pteropods in Southern Ocean ecosystems, Progress in Oceanography, 78, 193–221, doi:10.1016/j.pocean.2008.06.001, URL http://www.sciencedirect.com/science/article/pii/S0079661108001183, 2008.

Huntley, M. E., Lopez, M. D., and Karl, D. M.: Top predators in the Southern ocean: a major leak in the biological carbon pump, Science, 253, 64–66, doi:10.1126/science.1905841, URL http://science.sciencemag.org/content/253/5015/64, 1991.

Hutchins, D. A. and Bruland, K. W.: Iron-limited diatom growth and Si:N uptake ratios in a coastal upwelling regime, Nature, 393, 561–564, doi:10.1038/31203, URL http://www.nature.com/nature/journal/v393/n6685/abs/393561a0.html, 1998.

IPCC: Carbon and Other Biogeochemical Cycles, in: Climate Change 2013: the physical Science Basis, URL http://www.ipcc.ch/report/ar5/wg1/, 2013.

Ito, T., Woloszyn, M., and Mazloff, M.: Anthropogenic carbon dioxide transport in the Southern Ocean driven by Ekman flow, Nature, 463, 80–83, doi:10.1038/nature08687, URL http://www.nature.com/nature/journal/v463/n7277/full/nature08687.html, 2010.

Ito, T., Bracco, A., Deutsch, C., Frenzel, H., Long, M., and Takano, Y.: Sustained growth of the Southern Ocean carbon storage in a warming climate, Geophysical Research Letters, 42, 2015GL064 320, doi:10.1002/2015GL064320, URL http://onlinelibrary.wiley.com/doi/10.1002/2015GL064320/abstract, 2015.

Ittekkot, V.: The abiotically driven biological pump in the ocean and short-term fluctuations in atmospheric CO2 contents, Global and Planetary Change, 8, 17–25, doi:10.1016/0921-8181(93)90060-2, URL http://www.sciencedirect.com/science/article/pii/0921818193900602, 1993.

Iversen, M. H. and Poulsen, L. K.: Coprorhexy, coprophagy, and coprochaly in the copepods Calanus helgolandicus, Pseudocalanus elongatus, and Oithona similis, Marine Ecology Progress Series, 350, 79–89, doi:10.3354/meps07095, URL http://www.int-res.com/abstracts/meps/v350/p79-89/, 2007.

Jackson, G. and Kiørboe, T.: Maximum phytoplankton concentrations in the sea, Limnology and Oceanography, 53, 395–399, URL http://aslo.org.globalproxy.cvt.dk/lo/toc/vol_53/issue_1/0395.pdf, 2008.

Jackson, G. A.: A model of the formation of marine algal flocs by physical coagulation pro-

cesses, Deep Sea Research Part A. Oceanographic Research Papers, 37, 1197–1211, doi: 10.1016/0198-0149(90)90038-W, URL http://www.sciencedirect.com/science/article/pii/019801499090038W, 1990.

Jackson, G. A.: Flux feeding as a mechanism for zooplankton grazing and its implications for vertical particulate flux 1, Limnology and Oceanography, 38, 1328–1331, doi:10.4319/lo.1993.38.6.1328, URL http://onlinelibrary.wiley.com/doi/10.4319/lo.1993.38.6.1328/abstract, 1993.

Jackson, G. A. and Burd, A. B.: A model for the distribution of particle flux in the mid-water column controlled by subsurface biotic interactions, Deep Sea Research Part II: Topical Studies in Oceanography, 49, 193–217, doi:10.1016/S0967-0645(01)00100-X, URL http://www.sciencedirect.com/science/article/pii/S096706450100100X, 2001.

Jackson, G. A., Waite, A. M., and Boyd, P. W.: Role of algal aggregation in vertical carbon export during SOIREE and in other low biomass environments, Geophysical Research Letters, 32, L13 607, doi:10.1029/2005GL023180, URL http://onlinelibrary.wiley.com/doi/10.1029/2005GL023180/abstract, 2005.

Jacot Des Combes, H., Esper, O., De La Rocha, C. L., Abelmann, A., Gersonde, R., Yam, R., and Shemesh, A.: Diatom 13C, 15N, and C/N since the Last Glacial Maximum in the Southern Ocean: Potential impact of Species Composition, Paleoceanography, 23, PA4209, doi:10.1029/2008PA001589, URL http://onlinelibrary.wiley.com/doi/10.1029/2008PA001589/abstract, 2008.

Jacquet, S., Lam, P., Trull, T., and Dehairs, F.: Carbon export production in the subantarctic zone and polar front zone south of Tasmania, Deep Sea Research Part II: Topical Studies in Oceanography, 58, 2277–2292, doi:10.1016/j.dsr2.2011.05.035, URL http://www.sciencedirect.com/science/article/pii/S0967064511001615, 2011.

Jeandel, C., Ruiz-Pino, D., Gjata, E., Poisson, A., Brunet, C., Charriaud, E., Dehairs, F., Delille, D., Fiala, M., Fravalo, C., Carlos Miquel, J., Park, Y.-H., Pondaven, P., Quéguiner, B., Razouls, S., Shauer, B., and Tréguer, P.: KERFIX, a time-series station in the Southern Ocean: a presentation, Journal of Marine Systems, 17, 555–569, doi:10.1016/S0924-7963(98)00064-5, URL http://www.sciencedirect.com/science/article/pii/S0924796398000645, 1998.

Jeong, H. J., Yoo, Y. D., Kim, J. S., Seong, K. A., Kang, N. S., and Kim, T. H.: Growth, feeding and ecological roles of the mixotrophic and heterotrophic dinoflagellates in marine planktonic food webs, Ocean Science Journal, 45, 65–91, doi:10.1007/s12601-010-0007-2, URL http://link.springer.com/article/10.1007/s12601-010-0007-2, 2010.

Jiao, N., Herndl, G. J., Hansell, D. A., Benner, R., Kattner, G., Wilhelm, S. W., Kirchman, D. L., Weinbauer, M. G., Luo, T., Chen, F., and Azam, F.: Microbial production of recalcitrant dissolved organic matter: long-term carbon storage in the global ocean, Nature Reviews Microbiology, 8, 593–599, doi:10.1038/nrmicro2386, URL http://www.nature.com/nrmicro/journal/v8/n8/abs/nrmicro2386.html, 2010.

Jiao, N., Robinson, C., Azam, F., Thomas, H., Baltar, F., Dang, H., Hardman-Mountford, N. J., Johnson, M., Kirchman, D. L., Koch, B. P., Legendre, L., Li, C., Liu, J., Luo, T., Luo, Y.-W., Mitra, A., Romanou, A., Tang, K., Wang, X., Zhang, C., and Zhang, R.: Mechanisms of microbial carbon sequestration in the ocean – future research directions, Biogeosciences, 11, 5285–5306, doi:10.5194/bg-11-5285-2014, URL http://www.biogeosciences.net/11/5285/2014/, 2014.

Johnson, K., Berelson, W., Boss, E., Chase, Z., Claustre, H., Emerson, S., Gruber, N., Körtzinger, A., Perry, M. J., and Riser, S.: Observing Biogeochemical Cycles at Global Scales with Profiling Floats and Gliders: Prospects for a Global Array, Oceanography, 22, 216–225, doi:10.5670/oceanog.2009.81, URL http://www.tos.org/oceanography/archive/22-3_johnson.html, 2009.

Jonsson, B. F., Doney, S. C., Dunne, J., and Bender, M.: Evaluation of the Southern Ocean O2/Ar-based NCP estimates in a model framework, Journal of Geophysical Research: Bio-

geosciences, 118, 385–399, doi:10.1002/jgrg.20032, URL http://onlinelibrary.wiley.com/doi/10.1002/jgrg.20032/abstract, 2013.

Jouandet, M. P., Blain, S., Metzl, N., Brunet, C., Trull, T. W., and Obernosterer, I.: A seasonal carbon budget for a naturally iron-fertilized bloom over the Kerguelen Plateau in the Southern Ocean, Deep Sea Research Part II: Topical Studies in Oceanography, 55, 856–867, doi:10.1016/j.dsr2.2007.12.037, URL http://www.sciencedirect.com/science/article/pii/S0967064508000209, 2008.

Jouandet, M.-P., Trull, T. W., Guidi, L., Picheral, M., Ebersbach, F., Stemmann, L., and Blain, S.: Optical imaging of mesopelagic particles indicates deep carbon flux beneath a natural iron-fertilized bloom in the Southern Ocean, Limnology and Oceanography, 56, 1130–1140, doi:10.4319/lo.2011.56.3.1130, URL http://www.aslo.org/lo/toc/vol_56/issue_3/1130.html, 2011.

Jouandet, M.-P., Jackson, G. A., Carlotti, F., Picheral, M., Stemmann, L., and Blain, S.: Rapid formation of large aggregates during the spring bloom of Kerguelen Island: observations and model comparisons, Biogeosciences, 11, 4393–4406, doi:10.5194/bg-11-4393-2014, URL http://www.biogeosciences.net/11/4393/2014/, 2014.

Jungandreas, A., Wagner, H., and Wilhelm, C.: Simultaneous Measurement of the Silicon Content and Physiological Parameters by FTIR Spectroscopy in Diatoms with Siliceous Cell Walls, Plant and Cell Physiology, 53, 2153–2162, doi:10.1093/pcp/pcs144, URL http://pcp.oxfordjournals.org/content/53/12/2153, 2012.

Kanazawa, A.: Sterols in marine invertebrates, Fisheries Science, 67, 997–1007, doi:10.1046/j.1444-2906.2001.00354.x, URL http://onlinelibrary.wiley.com/doi/10.1046/j.1444-2906.2001.00354.x/abstract, 2001.

Kaneda, T.: Iso- and anteiso-fatty acids in bacteria: biosynthesis, function, and taxonomic significance., Microbiological Reviews, 55, 288–302, URL http://www.ncbi.nlm.nih.gov/pmc/articles/PMC372815/, 1991.

Karleskind, P., Lévy, M., and Memery, L.: Subduction of carbon, nitrogen, and oxygen in the northeast Atlantic, Journal of Geophysical Research: Oceans, 116, C02 025, doi:10.1029/2010JC006446, URL http://onlinelibrary.wiley.com/doi/10.1029/2010JC006446/abstract, 2011.

Kates, M. and Volcani, B. E.: Lipid components of diatoms, Biochimica et Biophysica Acta (BBA) - Lipids and Lipid Metabolism, 116, 264–278, doi:10.1016/0005-2760(66)90009-9, URL http://www.sciencedirect.com/science/article/pii/0005276066900099, 1966.

Keeling, R. F., Körtzinger, A., and Gruber, N.: Ocean Deoxygenation in a Warming World, Annual Review of Marine Science, 2, 199–229, doi:10.1146/annurev.marine.010908.163855, URL http://dx.doi.org/10.1146/annurev.marine.010908.163855, 2010.

Kemp, A. E., Pike, J., Pearce, R. B., and Lange, C. B.: The "Fall dump" — a new perspective on the role of a "shade flora" in the annual cycle of diatom production and export flux, Deep Sea Research Part II: Topical Studies in Oceanography, 47, 2129–2154, doi:10.1016/S0967-0645(00)00019-9, URL http://www.sciencedirect.com/science/article/pii/S0967064500000199, 2000.

Kemp, A. E. S., Pearce, R. B., Grigorov, I., Rance, J., Lange, C. B., Quilty, P., and Salter, I.: Production of giant marine diatoms and their export at oceanic frontal zones: Implications for Si and C flux from stratified oceans, Global Biogeochemical Cycles, 20, GB4S04, doi:10.1029/2006GB002698, URL http://onlinelibrary.wiley.com/doi/10.1029/2006GB002698/abstract, 2006.

Khatiwala, S., Primeau, F., and Hall, T.: Reconstruction of the history of anthropogenic CO2 concentrations in the ocean, Nature, 462, 346–349, doi:10.1038/nature08526, URL http://www.nature.com/nature/journal/v462/n7271/full/nature08526.html, 2009.

King, A. L. and Howard, W. R.: Planktonic foraminiferal flux seasonality in Subantarctic sediment traps: A test for paleoclimate reconstructions, Paleoceanography, 18,

1019, doi:10.1029/2002PA000839, URL http://onlinelibrary.wiley.com/doi/10.1029/2002PA000839/abstract, 2003.

King, A. L. and Howard, W. R.: 18O seasonality of planktonic foraminifera from Southern Ocean sediment traps: Latitudinal gradients and implications for paleoclimate reconstructions, Marine Micropaleontology, 56, 1–24, doi:10.1016/j.marmicro.2005.02.008, URL http://www.sciencedirect.com/science/article/pii/S0377839805000174, 2005.

Kiørboe, T., Lundsgaard, C., Olesen, M., and Hansen, J. L. S.: Aggregation and sedimentation processes during a spring phytoplankton bloom: A field experiment to test coagulation theory, Journal of Marine Research, 52, 297–323, doi:10.1357/0022240943077145, 1994.

Kiriakoulakis, K., Stutt, E., Rowland, S. J., Vangriesheim, A., Lampitt, R. S., and Wolff, G. A.: Controls on the organic chemical composition of settling particles in the Northeast Atlantic Ocean, Progress in Oceanography, 50, 65–87, doi:10.1016/S0079-6611(01)00048-9, URL http://www.sciencedirect.com/science/article/pii/S0079661101000489, 2001.

Klaas, C. and Archer, D. E.: Association of sinking organic matter with various types of mineral ballast in the deep sea: Implications for the rain ratio, Global Biogeochemical Cycles, 16, 1116, doi:10.1029/2001GB001765, URL http://onlinelibrary.wiley.com/doi/10.1029/2001GB001765/abstract, 2002.

Klausmeier, C. A., Litchman, E., Daufresne, T., and Levin, S. A.: Optimal nitrogen-to-phosphorus stoichiometry of phytoplankton, Nature, 429, 171–174, doi:10.1038/nature02454, URL http://www.nature.com/nature/journal/v429/n6988/abs/nature02454.html, 2004.

Kohfeld, K. E., Quéré, C. L., Harrison, S. P., and Anderson, R. F.: Role of Marine Biology in Glacial-Interglacial CO2 Cycles, Science, 308, 74–78, doi:10.1126/science.1105375, URL http://www.sciencemag.org/content/308/5718/74, 2005.

Kopczynska, E. E., Dehairs, F., Elskens, M., and Wright, S.: Phytoplankton and microzooplankton variability between the Subtropical and Polar Fronts south of Australia: Thriving under regenerative and new production in late summer, Journal of Geophysical Research: Oceans, 106, 31 597–31 609, doi:10.1029/2000JC000278, URL http://onlinelibrary.wiley.com/doi/10.1029/2000JC000278/abstract, 2001.

Kopczyńska, E. E., Fiala, M., and Jeandel, C.: Annual and interannual variability in phytoplankton at a permanent station off Kerguelen Islands, Southern Ocean, Polar Biology, 20, 342–351, doi:10.1007/s003000050312, URL http://link.springer.com/article/10.1007/s003000050312, 1998.

Korb, R. E., Whitehouse, M. J., Atkinson, A., and Thorpe, S. E.: Magnitude and maintenance of the phytoplankton bloom at South Georgia: a naturally iron-replete environment, Marine Ecology Progress Series, 368, 75–91, doi:10.3354/meps07525, URL http://www.int-res.com/abstracts/meps/v368/p75-91/, 2008.

Korb, R. E., Whitehouse, M. J., Gordon, M., Ward, P., and Poulton, A. J.: Summer microplankton community structure across the Scotia Sea: implications for biological carbon export, Biogeosciences, 7, 343–356, doi:10.5194/bg-7-343-2010, URL http://www.biogeosciences.net/7/343/2010/, 2010.

Korb, R. E., Whitehouse, M. J., Ward, P., Gordon, M., Venables, H. J., and Poulton, A. J.: Regional and seasonal differences in microplankton biomass, productivity, and structure across the Scotia Sea: Implications for the export of biogenic carbon, Deep Sea Research Part II: Topical Studies in Oceanography, 59–60, 67–77, doi:10.1016/j.dsr2.2011.06.006, URL http://www.sciencedirect.com/science/article/pii/S0967064511001792, 2012.

Kroeker, K. J., Kordas, R. L., Crim, R., Hendriks, I. E., Ramajo, L., Singh, G. S., Duarte, C. M., and Gattuso, J.-P.: Impacts of ocean acidification on marine organisms: quantifying sensitivities and interaction with warming, Global Change Biology, 19, 1884–1896, doi:10.1111/gcb.12179, URL http://onlinelibrary.wiley.com/doi/10.1111/gcb.12179/abstract, 2013.

Kuwata, A. and Takahashi, M.: Life-form population responses of a marine planktonic di-

atom,Chaetoceros pseudocurvisetus, to oligotrophication in regionally upwelled water, Marine Biology, 107, 503–512, doi:10.1007/BF01313435, URL http://link.springer.com/article/10.1007/BF01313435, 1990.

Kuwata, A. and Tsuda, A.: Selection and viability after ingestion of vegetative cells, resting spores and resting cells of the marine diatom, Chaetoceros pseudocurvisetus, by two copepods, Journal of Experimental Marine Biology and Ecology, 322, 143–151, doi:10.1016/j.jembe.2005.02.013, URL http://www.sciencedirect.com/science/article/pii/S0022098105001127, 2005.

Kuwata, A., Hama, T., and Takahashi, M.: Ecophysiological characterization of two life forms, resting spores and resting cells, of a marine planktonic diatom, Marine Ecology Progress Series, 102, 245–255, URL http://www.int-res.com/abstracts/meps/v102/, 1993.

Kwon, E. Y., Primeau, F., and Sarmiento, J. L.: The impact of remineralization depth on the air–sea carbon balance, Nature Geoscience, 2, 630–635, doi:10.1038/ngeo612, URL http://www.nature.com/ngeo/journal/v2/n9/abs/ngeo612.html, 2009.

Lam, P. J. and Bishop, J. K.: High biomass, low export regimes in the Southern Ocean, Deep Sea Research Part II: Topical Studies in Oceanography, 54, 601–638, doi:10.1016/j.dsr2.2007.01.013, URL http://www.sciencedirect.com/science/article/pii/S0967064507000380, 2007.

Lam, P. J., Doney, S. C., and Bishop, J. K. B.: The dynamic ocean biological pump: Insights from a global compilation of particulate organic carbon, CaCO3, and opal concentration profiles from the mesopelagic, Global Biogeochemical Cycles, 25, GB3009, doi:10.1029/2010GB003868, URL http://onlinelibrary.wiley.com/doi/10.1029/2010GB003868/abstract, 2011.

Lampitt, R. S., Noji, T., and Bodungen, B. v.: What happens to zooplankton faecal pellets? Implications for material flux, Marine Biology, 104, 15–23, doi:10.1007/BF01313152, URL http://link.springer.com/article/10.1007/BF01313152, 1990.

Lampitt, R. S., Boorman, B., Brown, L., Lucas, M., Salter, I., Sanders, R., Saw, K., Seeyave, S., Thomalla, S. J., and Turnewitsch, R.: Particle export from the euphotic zone: Estimates using a novel drifting sediment trap, 234Th and new production, Deep Sea Research Part I: Oceanographic Research Papers, 55, 1484–1502, doi:10.1016/j.dsr.2008.07.002, URL http://www.sciencedirect.com/science/article/pii/S0967063708001453, 2008.

Lampitt, R. S., Salter, I., and Johns, D.: Radiolaria: Major exporters of organic carbon to the deep ocean, Global Biogeochemical Cycles, 23, GB1010, doi:10.1029/2008GB003221, URL http://onlinelibrary.wiley.com/doi/10.1029/2008GB003221/abstract, 2009.

Landschützer, P., Gruber, N., Haumann, F. A., Rödenbeck, C., Bakker, D. C. E., Heuven, S. v., Hoppema, M., Metzl, N., Sweeney, C., Takahashi, T., Tilbrook, B., and Wanninkhof, R.: The reinvigoration of the Southern Ocean carbon sink, Science, 349, 1221–1224, doi:10.1126/science.aab2620, URL http://www.sciencemag.org/content/349/6253/1221, 2015.

Laurenceau-Cornec, E. C., Trull, T. W., Davies, D. M., Bray, S. G., Doran, J., Planchon, F., Carlotti, F., Jouandet, M.-P., Cavagna, A.-J., Waite, A. M., and Blain, S.: The relative importance of phytoplankton aggregates and zooplankton fecal pellets to carbon export: insights from free-drifting sediment trap deployments in naturally iron-fertilised waters near the Kerguelen Plateau, Biogeosciences, 12, 1007–1027, doi:10.5194/bg-12-1007-2015, URL http://www.biogeosciences.net/12/1007/2015/, 2015a.

Laurenceau-Cornec, E. C., Trull, T. W., Davies, D. M., Rocha, C. L. D. L., and Blain, S.: Phytoplankton morphology controls on marine snow sinking velocity, Marine Ecology Progress Series, 520, 35–56, doi:10.3354/meps11116, URL http://www.int-res.com/abstracts/meps/v520/p35-56/, 2015b.

Law, C. S.: Predicting and monitoring the effects of large-scale ocean iron fertilization on marine trace gas emissions, Marine Ecology Progress Series, 364, 283–288, doi:10.3354/meps07549, URL http://www.int-res.com/abstracts/meps/v364/p283-288/, 2008.

Laws, E. A., Falkowski, P. G., Smith, W. O., Ducklow, H., and McCarthy, J. J.: Temperature effects on export production in the open ocean, Global Biogeochemical Cycles, 14, 1231–1246, doi:10.1029/1999GB001229, URL http://onlinelibrary.wiley.com/doi/10.1029/1999GB001229/abstract, 2000.

Laws, E. A., D'Sa, E., and Naik, P.: Simple equations to estimate ratios of new or export production to total production from satellite-derived estimates of sea surface temperature and primary production, Limnology and Oceanography: Methods, 9, 593–601, doi:10.4319/lom.2011.9.593, URL http://onlinelibrary.wiley.com/doi/10.4319/lom.2011.9.593/abstract, 2011.

Le Moigne, F. A. C., Henson, S. A., Sanders, R. J., and Madsen, E.: Global database of surface ocean particulate organic carbon export fluxes diagnosed from the 234Th technique, Earth System Science Data, 5, 295–304, doi:10.5194/essd-5-295-2013, URL http://www.earth-syst-sci-data.net/5/295/2013/, 2013a.

Le Moigne, F. A. C., Villa-Alfageme, M., Sanders, R. J., Marsay, C., Henson, S., and García-Tenorio, R.: Export of organic carbon and biominerals derived from 234Th and 210Po at the Porcupine Abyssal Plain, Deep Sea Research Part I: Oceanographic Research Papers, 72, 88–101, doi:10.1016/j.dsr.2012.10.010, URL http://www.sciencedirect.com/science/article/pii/S0967063712002075, 2013b.

Le Quéré, C., Harrison, S. P., Colin Prentice, I., Buitenhuis, E. T., Aumont, O., Bopp, L., Claustre, H., Cotrim Da Cunha, L., Geider, R., Giraud, X., Klaas, C., Kohfeld, K. E., Legendre, L., Manizza, M., Platt, T., Rivkin, R. B., Sathyendranath, S., Uitz, J., Watson, A. J., and Wolf-Gladrow, D.: Ecosystem dynamics based on plankton functional types for global ocean biogeochemistry models, Global Change Biology, 11, 2016–2040, doi:10.1111/j.1365-2486.2005.1004.x, URL http://onlinelibrary.wiley.com/doi/10.1111/j.1365-2486.2005.1004.x/abstract, 2005.

le Quéré, C., Rödenbeck, C., Buitenhuis, E. T., Conway, T. J., Langenfelds, R., Gomez, A., Labuschagne, C., Ramonet, M., Nakazawa, T., Metzl, N., Gillett, N., and Heimann, M.: Saturation of the Southern Ocean CO2 Sink Due to Recent Climate Change, Science, 316, 1735–1738, doi:10.1126/science.1136188, URL http://www.sciencemag.org/content/316/5832/1735, 2007.

Le Quéré, C., Andres, R. J., Boden, T., Conway, T., Houghton, R. A., House, J. I., Marland, G., Peters, G. P., van der Werf, G. R., Ahlström, A., Andrew, R. M., Bopp, L., Canadell, J. G., Ciais, P., Doney, S. C., Enright, C., Friedlingstein, P., Huntingford, C., Jain, A. K., Jourdain, C., Kato, E., Keeling, R. F., Klein Goldewijk, K., Levis, S., Levy, P., Lomas, M., Poulter, B., Raupach, M. R., Schwinger, J., Sitch, S., Stocker, B. D., Viovy, N., Zaehle, S., and Zeng, N.: The global carbon budget 1959–2011, Earth System Science Data, 5, 165–185, doi:10.5194/essd-5-165-2013, URL http://www.earth-syst-sci-data.net/5/165/2013/essd-5-165-2013.html, 2013.

Lebrato, M. and Jones, D. O. B.: Mass deposition event of Pyrosoma atlanticum carcasses off Ivory Coast (West Africa), Limnology and Oceanography, 54, 1197–1209, doi:10.4319/lo.2009.54.4.1197, URL http://onlinelibrary.wiley.com/doi/10.4319/lo.2009.54.4.1197/abstract, 2009.

LeCleir, G. R., DeBruyn, J. M., Maas, E. W., Boyd, P. W., and Wilhelm, S. W.: Temporal changes in particle-associated microbial communities after interception by nonlethal sediment traps, FEMS Microbiology Ecology, 87, 153–163, doi:10.1111/1574-6941.12213, URL http://onlinelibrary.wiley.com/doi/10.1111/1574-6941.12213/abstract, 2014.

Lee, C., Peterson, M. L., Wakeham, S. G., Armstrong, R. A., Cochran, J. K., Miquel, J. C., Fowler, S. W., Hirschberg, D., Beck, A., and Xue, J.: Particulate organic matter and ballast fluxes measured using time-series and settling velocity sediment traps in the northwestern Mediterranean Sea, Deep Sea Research Part II: Topical Studies in Oceanography, 56, 1420–1436, doi:10.1016/j.dsr2.2008.11.029, URL http://www.sciencedirect.com/science/

article/pii/S0967064508004177, 2009.

Lee, R. F., Nevenzel, J. C., and Paffenhöfer, G.-A.: Wax Esters in Marine Copepods, Science, 167, 1510–1511, doi:10.1126/science.167.3924.1510, URL http://science.sciencemag.org/content/167/3924/1510, 1970.

Lee, R. F., Hirota, J., and Barnett, A. M.: Distribution and importance of wax esters in marine copepods and other zooplankton, Deep Sea Research and Oceanographic Abstracts, 18, 1147–1165, doi:10.1016/0011-7471(71)90023-4, URL http://www.sciencedirect.com/science/article/pii/0011747171900234, 1971.

Lee, R. F., Hagen, W., and Kattner, G.: Lipid storage in marine zooplankton, Marine Ecology Progress Series, 307, 273–306, doi:10.3354/meps307273, URL http://www.int-res.com/abstracts/meps/v307/p273-306/, 2006.

Legendre, L. and le Fèvre, J.: Hydrodynamical singularities as controls of recycled versus export production in oceans, in: Productivity of the oceans: present and past, pp. 49–63, Berger, W. H., Smetacek, V. S., Wefer, G., wiley edn., 1989.

Legendre, L., Rivkin, R. B., Weinbauer, M. G., Guidi, L., and Uitz, J.: The microbial carbon pump concept: Potential biogeochemical significance in the globally changing ocean, Progress in Oceanography, 134, 432–450, doi:10.1016/j.pocean.2015.01.008, URL http://www.sciencedirect.com/science/article/pii/S0079661115000105, 2015.

Legendre, P. and Gallagher, E. D.: Ecologically meaningful transformations for ordination of species data, Oecologia, 129, 271–280, doi:10.1007/s004420100716, URL http://link.springer.com/article/10.1007/s004420100716, 2001.

Legendre, P. and Legendre, L.: Numerical Ecology, Elsevier Science, Amsterdam ; New York, Édition: 2 edn., 1998.

Leventer, A.: Sediment trap diatom assemblages from the northern Antarctic Peninsula region, Deep Sea Research Part I. Oceanographic Research Papers, 38, 1127–1143, doi:10.1016/0198-0149(91)90099-2, URL http://www.sciencedirect.com/science/article/pii/019801499190092, 1991.

Leventer, A. and Dunbar, R. B.: Diatom flux in McMurdo Sound, Antarctica, Marine Micropaleontology, 12, 49–64, doi:10.1016/0377-8398(87)90013-2, URL http://www.sciencedirect.com/science/article/pii/0377839887900132, 1987.

Leventer, A., Dunbar, R. B., and DeMaster, D. J.: Diatom Evidence for Late Holocene Climatic Events in Granite Harbor, Antarctica, Paleoceanography, 8, 373–386, doi:10.1029/93PA00561, URL http://onlinelibrary.wiley.com/doi/10.1029/93PA00561/abstract, 1993.

Levitan, O., Dinamarca, J., Hochman, G., and Falkowski, P. G.: Diatoms: a fossil fuel of the future, Trends in Biotechnology, 32, 117–124, doi:10.1016/j.tibtech.2014.01.004, URL http://www.cell.com/article/S0167779914000055/abstract, 2014.

Levy, M., Bopp, L., Karleskind, P., Resplandy, L., Ethe, C., and Pinsard, F.: Physical pathways for carbon transfers between the surface mixed layer and the ocean interior, Global Biogeochemical Cycles, 27, 1001–1012, doi:10.1002/gbc.20092, URL http://onlinelibrary.wiley.com/doi/10.1002/gbc.20092/abstract, 2013.

Lewis, Jr., W. M.: The Diatom Sex Clock and Its Evolutionary Significance, The American Naturalist, 123, 73–80, URL http://www.jstor.org/stable/2460887, 1984.

Liang, Y., Maeda, Y., Yoshino, T., Matsumoto, M., and Tanaka, T.: Profiling of fatty acid methyl esters from the oleaginous diatom Fistulifera sp. strain JPCC DA0580 under nutrition-sufficient and -deficient conditions, Journal of Applied Phycology, 26, 2295–2302, doi:10.1007/s10811-014-0265-y, URL http://link.springer.com/article/10.1007/s10811-014-0265-y, 2014.

Lima, I. D., Lam, P. J., and Doney, S. C.: Dynamics of particulate organic carbon flux in a global ocean model, Biogeosciences, 11, 1177–1198, doi:10.5194/bg-11-1177-2014, URL http://www.biogeosciences.net/11/1177/2014/, 2014.

Lins, L., da Silva, M. C., Hauquier, F., Esteves, A. M., and Vanreusel, A.: Nematode community

composition and feeding shaped by contrasting productivity regimes in the Southern Ocean, Progress in Oceanography, 134, 356–369, doi:10.1016/j.pocean.2015.03.006, URL http://www.sciencedirect.com/science/article/pii/S0079661115000476, 2015.

Logan, B. E., Passow, U., Alldredge, A. L., Grossartt, H.-P., and Simont, M.: Rapid formation and sedimentation of large aggregates is predictable from coagulation rates (half-lives) of transparent exopolymer particles (TEP), Deep Sea Research Part II: Topical Studies in Oceanography, 42, 203–214, doi:10.1016/0967-0645(95)00012-F, URL http://www.sciencedirect.com/science/article/pii/096706459500012F, 1995.

Loisel, H. and Morel, A.: Light scattering and chlorophyll concentration in case 1 waters: A re-examination, Limnology and Oceanography, 43, 847–858, doi:10.4319/lo.1998.43.5.0847, URL http://onlinelibrary.wiley.com/doi/10.4319/lo.1998.43.5.0847/abstract, 1998.

Lombard, F., Labeyrie, L., Michel, E., Bopp, L., Cortijo, E., Retailleau, S., Howa, H., and Jorissen, F.: Modelling planktic foraminifer growth and distribution using an ecophysiological multi-species approach, Biogeosciences, 8, 853–873, doi:10.5194/bg-8-853-2011, URL http://www.biogeosciences.net/8/853/2011/, 2011.

Lopes, C., Kucera, M., and Mix, A. C.: Climate change decouples oceanic primary and export productivity and organic carbon burial, Proceedings of the National Academy of Sciences, 112, 332–335, doi:10.1073/pnas.1410480111, URL http://www.pnas.org/content/112/2/332, 2015.

Louanchi, F., Ruiz-Pino, D. P., Jeandel, C., Brunet, C., Schauer, B., Masson, A., Fiala, M., and Poisson, A.: Dissolved inorganic carbon, alkalinity, nutrient and oxygen seasonal and interannual variations at the Antarctic Ocean JGOFS-KERFIX site, Deep Sea Research Part I: Oceanographic Research Papers, 48, 1581–1603, doi:10.1016/S0967-0637(00)00086-8, URL http://www.sciencedirect.com/science/article/pii/S0967063700000868, 2001.

Lovenduski, N. S., Long, M. C., Gent, P. R., and Lindsay, K.: Multi-decadal trends in the advection and mixing of natural carbon in the Southern Ocean, Geophysical Research Letters, 40, 139–142, doi:10.1029/2012GL054483, URL http://onlinelibrary.wiley.com/doi/10.1029/2012GL054483/abstract, 2013.

Lovenduski, N. S., Fay, A. R., and McKinley, G. A.: Observing multidecadal trends in Southern Ocean CO2 uptake: What can we learn from an ocean model?, Global Biogeochemical Cycles, 29, 2014GB004 933, doi:10.1002/2014GB004933, URL http://onlinelibrary.wiley.com/doi/10.1002/2014GB004933/abstract, 2015.

Lundsgaard, C.: Use of high viscosity medium in studies of aggregates, Sediment Trap Studies in the Nordic Countries. Symposium Proc., Mar. Biol. Lab., Helsingør, Denmark, pp. 141–152, 1994.

Lutz, M., Dunbar, R., and Caldeira, K.: Regional variability in the vertical flux of particulate organic carbon in the ocean interior, Global Biogeochemical Cycles, 16, 11–1–11–18, doi:10.1029/2000GB001383, URL http://onlinelibrary.wiley.com/doi/10.1029/2000GB001383/abstract, 2002.

Lutz, M. J., Caldeira, K., Dunbar, R. B., and Behrenfeld, M. J.: Seasonal rhythms of net primary production and particulate organic carbon flux to depth describe the efficiency of biological pump in the global ocean, Journal of Geophysical Research: Oceans, 112, C10 011, doi:10.1029/2006JC003706, URL http://onlinelibrary.wiley.com/doi/10.1029/2006JC003706/abstract, 2007.

Ma, Z., Gray, E., Thomas, E., Murphy, B., Zachos, J., and Paytan, A.: Carbon sequestration during the Palaeocene-Eocene Thermal Maximum by an efficient biological pump, Nature Geoscience, 7, 382–388, doi:10.1038/ngeo2139, URL http://www.nature.com/ngeo/journal/v7/n5/full/ngeo2139.html, 2014.

Madin, L. P.: Production, composition and sedimentation of salp fecal pellets in oceanic waters, Marine Biology, 67, 39–45, doi:10.1007/BF00397092, URL http://link.springer.com/article/10.1007/BF00397092, 1982.

Mahowald, N. M., Baker, A. R., Bergametti, G., Brooks, N., Duce, R. A., Jickells, T. D., Kubilay, N., Prospero, J. M., and Tegen, I.: Atmospheric global dust cycle and iron inputs to the ocean, Global Biogeochemical Cycles, 19, GB4025, doi:10.1029/2004GB002402, URL http://onlinelibrary.wiley.com/doi/10.1029/2004GB002402/abstract, 2005.

Maiti, K., Charette, M. A., Buesseler, K. O., and Kahru, M.: An inverse relationship between production and export efficiency in the Southern Ocean, Geophysical Research Letters, 40, 1557–1561, doi:10.1002/grl.50219, URL http://onlinelibrary.wiley.com/doi/10.1002/grl.50219/abstract, 2013.

Manno, C., Stowasser, G., Enderlein, P., Fielding, S., and Tarling, G. A.: The contribution of zooplankton faecal pellets to deep-carbon transport in the Scotia Sea (Southern Ocean), Biogeosciences, 12, 1955–1965, doi:10.5194/bg-12-1955-2015, URL http://www.biogeosciences.net/12/1955/2015/, 2015.

Maraldi, C., Lyard, F., Testut, L., and Coleman, R.: Energetics of internal tides around the Kerguelen Plateau from modeling and altimetry, Journal of Geophysical Research: Oceans, 116, C06004, doi:10.1029/2010JC006515, URL http://onlinelibrary.wiley.com/doi/10.1029/2010JC006515/abstract, 2011.

Marchetti, A., Parker, M. S., Moccia, L. P., Lin, E. O., Arrieta, A. L., Ribalet, F., Murphy, M. E. P., Maldonado, M. T., and Armbrust, E. V.: Ferritin is used for iron storage in bloom-forming marine pennate diatoms, Nature, 457, 467–470, doi:10.1038/nature07539, URL http://www.nature.com/nature/journal/v457/n7228/abs/nature07539.html, 2009.

Margalef, R.: Temporal succession and spatial heterogeneity in phytoplankton., in: Perspective in marine biology., pp. 323–349, Buzzat-Traverso, A. A., Berkley and Los Angeles, univeristy of california press edn., 1958.

Marshall, J. and Speer, K.: Closure of the meridional overturning circulation through Southern Ocean upwelling, Nature Geoscience, 5, 171–180, doi:10.1038/ngeo1391, URL http://www.nature.com/ngeo/journal/v5/n3/full/ngeo1391.html, 2012.

Martin, J. H.: Glacial-interglacial CO2 change: The Iron Hypothesis, Paleoceanography, 5, 1–13, doi:10.1029/PA005i001p00001, URL http://onlinelibrary.wiley.com/doi/10.1029/PA005i001p00001/abstract, 1990.

Martin, J. H., Knauer, G. A., Karl, D. M., and Broenkow, W. W.: VERTEX: carbon cycling in the northeast Pacific, Deep Sea Research Part A. Oceanographic Research Papers, 34, 267–285, doi:10.1016/0198-0149(87)90086-0, URL http://www.sciencedirect.com/science/article/pii/0198014987900860, 1987.

Martin, J. H., Gordon, R. M., and Fitzwater, S. E.: Iron in Antarctic waters, Nature, 345, 156–158, doi:10.1038/345156a0, URL http://www.nature.com/nature/journal/v345/n6271/abs/345156a0.html, 1990.

Martin, P., van der Loeff, M. R., Cassar, N., Vandromme, P., d'Ovidio, F., Stemmann, L., Rengarajan, R., Soares, M., González, H. E., Ebersbach, F., Lampitt, R. S., Sanders, R., Barnett, B. A., Smetacek, V., and Naqvi, S. W. A.: Iron fertilization enhanced net community production but not downward particle flux during the Southern Ocean iron fertilization experiment LOHAFEX, Global Biogeochemical Cycles, 27, 871–881, doi:10.1002/gbc.20077, URL http://onlinelibrary.wiley.com/doi/10.1002/gbc.20077/abstract, 2013.

Martiny, A. C., Pham, C. T. A., Primeau, F. W., Vrugt, J. A., Moore, J. K., Levin, S. A., and Lomas, M. W.: Strong latitudinal patterns in the elemental ratios of marine plankton and organic matter, Nature Geoscience, 6, 279–283, doi:10.1038/ngeo1757, URL http://www.nature.com/ngeo/journal/v6/n4/full/ngeo1757.html, 2013a.

Martiny, A. C., Vrugt, J. A., Primeau, F. W., and Lomas, M. W.: Regional variation in the particulate organic carbon to nitrogen ratio in the surface ocean, Global Biogeochemical Cycles, 27, 723–731, doi:10.1002/gbc.20061, URL http://onlinelibrary.wiley.com/doi/10.1002/gbc.20061/abstract, 2013b.

Matsueda, H., Handa, N., Inoue, I., and Takano, H.: Ecological significance of salp fecal pellets

collected by sediment traps in the eastern North Pacific, Marine Biology, 91, 421–431, doi:10.1007/BF00428636, URL http://link.springer.com/article/10.1007/BF00428636, 1986.

Matsumoto, K., Sarmiento, J. L., and Brzezinski, M. A.: Silicic acid leakage from the Southern Ocean: A possible explanation for glacial atmospheric pCO2, Global Biogeochemical Cycles, 16, 5–1, doi:10.1029/2001GB001442, URL http://onlinelibrary.wiley.com/doi/10.1029/2001GB001442/abstract, 2002.

Matsumoto, M., Sugiyama, H., Maeda, Y., Sato, R., Tanaka, T., and Matsunaga, T.: Marine Diatom, Navicula sp. Strain JPCC DA0580 and Marine Green Alga, Chlorella sp. Strain NKG400014 as Potential Sources for Biodiesel Production, Applied Biochemistry and Biotechnology, 161, 483–490, doi:10.1007/s12010-009-8766-x, URL http://link.springer.com/article/10.1007/s12010-009-8766-x, 2009.

Mayzaud, P. and Pakhomov, E. A.: The role of zooplankton communities in carbon recycling in the Ocean: the case of the Southern Ocean, Journal of Plankton Research, 36, 1543–1556, doi:10.1093/plankt/fbu076, URL http://plankt.oxfordjournals.org/content/36/6/1543, 2014.

Mayzaud, P., Lacombre, S., and Boutoute, M.: Seasonal and growth stage changes in lipid and fatty acid composition in the multigeneration copepod Drepanopus pectinatus from Iles Kerguelen, Antarctic Science, 23, 3–17, doi:10.1017/S0954102010000519, URL http://journals.cambridge.org/article_S0954102010000519, 2011.

McCave, I. N.: Vertical flux of particles in the ocean, Deep-sea Research, 22, 491–502, doi:10.1016/0011-7471(75)90022-4, 1975.

McDonnell, A. M. P. and Buesseler, K. O.: Variability in the average sinking velocity of marine particles, Limnology and Oceanography, 55, 2085–2096, doi:10.4319/lo.2010.55.5.2085, URL http://onlinelibrary.wiley.com/doi/10.4319/lo.2010.55.5.2085/abstract, 2010.

McDonnell, A. M. P. and Buesseler, K. O.: A new method for the estimation of sinking particle fluxes from measurements of the particle size distribution, average sinking velocity, and carbon content, Limnology and Oceanography: Methods, 10, 329–346, doi:10.4319/lom.2012.10.329, URL http://onlinelibrary.wiley.com/doi/10.4319/lom.2012.10.329/abstract, 2012.

McEwen, G. F., Johnson, M. W., and Folsom, T. R.: A statistical analysis of the performance of the folsom plankton sample splitter, based upon test observations, Archives for Meteorology Geophysics and Bioclimatology Series A Meteorology and Atmopsheric Physics, 7, 502–527, doi:10.1007/BF02277939, URL http://adsabs.harvard.edu/abs/1954AMGBA...7..502M, 1954.

McQuoid, M. R. and Hobson, L. A.: Diatom Resting Stages, Journal of Phycology, 32, 889–902, doi:10.1111/j.0022-3646.1996.00889.x, URL http://onlinelibrary.wiley.com/doi/10.1111/j.0022-3646.1996.00889.x/abstract, 1996.

Meijers, A. J. S.: The Southern Ocean in the Coupled Model Intercomparison Project phase 5, Philosophical Transactions of the Royal Society of London A: Mathematical, Physical and Engineering Sciences, 372, 20130296, doi:10.1098/rsta.2013.0296, URL http://rsta.royalsocietypublishing.org/content/372/2019/20130296, 2014.

Meredith, M. P., Schofield, O., Newman, L., Urban, E., and Sparrow, M.: The vision for a Southern Ocean Observing System, Current Opinion in Environmental Sustainability, 5, 306–313, doi:10.1016/j.cosust.2013.03.002, URL http://www.sciencedirect.com/science/article/pii/S1877343513000262, 2013.

Merlivat, L., Boutin, J., and Antoine, D.: Roles of biological and physical processes in driving seasonal air–sea CO2 flux in the Southern Ocean: New insights from CARIOCA pCO2, Journal of Marine Systems, 147, 9–20, doi:10.1016/j.jmarsys.2014.04.015, URL http://www.sciencedirect.com/science/article/pii/S0924796314001018, 2015.

Michaels, A. F. and Silver, M. W.: Primary production, sinking fluxes and the microbial food web, Deep Sea Research Part A. Oceanographic Research Papers, 35, 473–490, doi:10.1016/0198-0149(88)90126-4, URL http://www.sciencedirect.com/science/article/

pii/0198014988901264, 1988.

Mikaloff Fletcher, S. E., Gruber, N., Jacobson, A. R., Doney, S. C., Dutkiewicz, S., Gerber, M., Follows, M., Joos, F., Lindsay, K., Menemenlis, D., Mouchet, A., Müller, S. A., and Sarmiento, J. L.: Inverse estimates of anthropogenic CO2 uptake, transport, and storage by the ocean, Global Biogeochemical Cycles, 20, GB2002, doi:10.1029/2005GB002530, URL http://onlinelibrary.wiley.com/doi/10.1029/2005GB002530/abstract, 2006.

Mikaloff Fletcher, S. E., Gruber, N., Jacobson, A. R., Gloor, M., Doney, S. C., Dutkiewicz, S., Gerber, M., Follows, M., Joos, F., Lindsay, K., Menemenlis, D., Mouchet, A., Müller, S. A., and Sarmiento, J. L.: Inverse estimates of the oceanic sources and sinks of natural CO2 and the implied oceanic carbon transport, Global Biogeochemical Cycles, 21, GB1010, doi:10.1029/2006GB002751, URL http://onlinelibrary.wiley.com/doi/10.1029/2006GB002751/abstract, 2007.

Miklasz, K. A. and Denny, M. W.: Diatom sinkings speeds: Improved predictions and insight from a modified Stokes' law, Limnology and Oceanography, 55, 2513–2525, doi:10.4319/lo.2010.55.6.2513, URL http://onlinelibrary.wiley.com/doi/10.4319/lo.2010.55.6.2513/abstract, 2010.

Minas, H. and Minas, M.: Net community production in high nutrient-low chlorophyll waters of the tropical and antarctic oceans - grazing vs iron hypothesis, Oceanologica Acta, 15, 145–162, URL http://archimer.ifremer.fr/doc/00100/21149/, 1992.

Minas, H. J., Minas, M., and Packard, T. T.: Productivity in upwelling areas deduced from hydrographic and chemical fields, Limnology and Oceanography, 31, 1182–1206, doi:10.4319/lo.1986.31.6.1182, URL http://onlinelibrary.wiley.com/doi/10.4319/lo.1986.31.6.1182/abstract, 1986.

Miquel, J. C., Fowler, S. W., La Rosa, J., and Buat-Menard, P.: Dynamics of the downward flux of particles and carbon in the open northwestern Mediterranean Sea, Deep Sea Research Part I: Oceanographic Research Papers, 41, 243–261, doi:10.1016/0967-0637(94)90002-7, URL http://www.sciencedirect.com/science/article/pii/0967063794900027, 1994.

Mitra, A., Flynn, K. J., Burkholder, J. M., Berge, T., Calbet, A., Raven, J. A., Granéli, E., Glibert, P. M., Hansen, P. J., Stoecker, D. K., Thingstad, F., Tillmann, U., Våge, S., Wilken, S., and Zubkov, M. V.: The role of mixotrophic protists in the biological carbon pump, Biogeosciences, 11, 995–1005, doi:10.5194/bg-11-995-2014, URL http://www.biogeosciences.net/11/995/2014/, 2014.

Müller, P., Li, X.-P., and Niyogi, K. K.: Non-Photochemical Quenching. A Response to Excess Light Energy, Plant Physiology, 125, 1558–1566, doi:10.1104/pp.125.4.1558, URL http://www.plantphysiol.org/content/125/4/1558, 2001.

Müller-Navarra, D. C., Brett, M. T., Liston, A. M., and Goldman, C. R.: A highly unsaturated fatty acid predicts carbon transfer between primary producers and consumers, Nature, 403, 74–77, doi:10.1038/47469, URL http://www.nature.com/nature/journal/v403/n6765/full/403074a0.html, 2000.

Moore, C. M., Hickman, A. E., Poulton, A. J., Seeyave, S., and Lucas, M. I.: Iron–light interactions during the CROZet natural iron bloom and EXport experiment (CROZEX): II—Taxonomic responses and elemental stoichiometry, Deep Sea Research Part II: Topical Studies in Oceanography, 54, 2066–2084, doi:10.1016/j.dsr2.2007.06.015, URL http://www.sciencedirect.com/science/article/pii/S0967064507001555, 2007.

Moore, J. and Abbott, M. R.: Surface chlorophyll concentrations in relation to the Antarctic Polar Front: seasonal and spatial patterns from satellite observations, Journal of Marine Systems, 37, 69–86, doi:10.1016/S0924-7963(02)00196-3, URL http://www.sciencedirect.com/science/article/pii/S0924796302001963, 2002.

Moore, J. K. and Abbott, M. R.: Phytoplankton chlorophyll distributions and primary production in the Southern Ocean, Journal of Geophysical Research: Oceans, 105, 28 709–28 722, doi:10.1029/1999JC000043, URL http://onlinelibrary.wiley.com/doi/10.1029/

1999JC000043/abstract, 2000.

Moore, J. K. and Villareal, T. A.: Size-ascent rate relationships in positively buoyant marine diatoms, Limnology and Oceanography, 41, 1514–1520, doi:10.4319/lo.1996.41.7.1514, URL http://onlinelibrary.wiley.com/doi/10.4319/lo.1996.41.7.1514/abstract, 1996.

Mora, C., Tittensor, D. P., Adl, S., Simpson, A. G. B., and Worm, B.: How Many Species Are There on Earth and in the Ocean?, PLoS Biol, 9, e1001 127, doi:10.1371/journal.pbio.1001127, URL http://dx.doi.org/10.1371/journal.pbio.1001127, 2011.

Morel, A.: Optical modeling of the upper ocean in relation to its biogenous matter content (case I waters), Journal of Geophysical Research: Oceans, 93, 10 749–10 768, doi:10.1029/JC093iC09p10749, URL http://onlinelibrary.wiley.com/doi/10.1029/JC093iC09p10749/abstract, 1988.

Morel, A. and Ahn, Y.-H.: Optics of heterotrophic nanoflagellates and ciliates: A tentative assessment of their scattering role in oceanic waters compared to those of bacterial and algal cells, Journal of Marine Research, 49, 177–202, doi:10.1357/002224091784968639, 1991.

Mortyn, P. G. and Charles, C. D.: Planktonic foraminiferal depth habitat and 18O calibrations: Plankton tow results from the Atlantic sector of the Southern Ocean, Paleoceanography, 18, 1037, doi:10.1029/2001PA000637, URL http://onlinelibrary.wiley.com/doi/10.1029/2001PA000637/abstract, 2003.

Mosseri, J., Quéguiner, B., Rimmelin, P., Leblond, N., and Guieu, C.: Silica fluxes in the northeast Atlantic frontal zone of Mode Water formation (38–45N, 16–22W) in 2001–2002, Journal of Geophysical Research: Oceans, 110, C07S19, doi:10.1029/2004JC002615, URL http://onlinelibrary.wiley.com/doi/10.1029/2004JC002615/abstract, 2005.

Mosseri, J., Quéguiner, B., Armand, L., and Cornet-Barthaux, V.: Impact of iron on silicon utilization by diatoms in the Southern Ocean: A case study of Si/N cycle decoupling in a naturally iron-enriched area, Deep Sea Research Part II: Topical Studies in Oceanography, 55, 801–819, doi:10.1016/j.dsr2.2007.12.003, URL http://www.sciencedirect.com/science/article/pii/S0967064508000301, 2008.

Muggli, D. L. and Harrison, P. J.: Effects of iron on two oceanic phytoplankters grown in natural NE subarctic pacific seawater with no artificial chelators present, Journal of Experimental Marine Biology and Ecology, 212, 225–237, doi:10.1016/S0022-0981(96)02752-9, URL http://www.sciencedirect.com/science/article/pii/S0022098196027529, 1997.

Murphy, E. J., Cavanagh, R. D., Hofmann, E. E., Hill, S. L., Constable, A. J., Costa, D. P., Pinkerton, M. H., Johnston, N. M., Trathan, P. N., Klinck, J. M., Wolf-Gladrow, D. A., Daly, K. L., Maury, O., and Doney, S. C.: Developing integrated models of Southern Ocean food webs: Including ecological complexity, accounting for uncertainty and the importance of scale, Progress in Oceanography, 102, 74–92, doi:10.1016/j.pocean.2012.03.006, URL http://www.sciencedirect.com/science/article/pii/S0079661112000237, 2012.

Nelson, D. M. and Brzezinski, M. A.: Diatom growth and productivity in an oligo-trophic midocean gyre: A 3-yr record from the Sargasso Sea near Bermuda, Limnology and Oceanography, 42, 473–486, doi:10.4319/lo.1997.42.3.0473, URL http://onlinelibrary.wiley.com/doi/10.4319/lo.1997.42.3.0473/abstract, 1997.

Nelson, D. M., Tréguer, P., Brzezinski, M. A., Leynaert, A., and Quéguiner, B.: Production and dissolution of biogenic silica in the ocean: Revised global estimates, comparison with regional data and relationship to biogenic sedimentation, Global Biogeochemical Cycles, 9, 359–372, doi:10.1029/95GB01070, URL http://onlinelibrary.wiley.com/doi/10.1029/95GB01070/abstract, 1995.

Nielsdóttir, M. C., Bibby, T. S., Moore, C. M., Hinz, D. J., Sanders, R., Whitehouse, M., Korb, R., and Achterberg, E. P.: Seasonal and spatial dynamics of iron availability in the Scotia Sea, Marine Chemistry, 130–131, 62–72, doi:10.1016/j.marchem.2011.12.004, URL http://www.sciencedirect.com/science/article/pii/S0304420311001320, 2012.

Nodder, S. D. and Alexander, B. L.: The effects of multiple trap spacing, baffles and brine

volume on sediment trap collection efficiency, Journal of Marine Research, 57, 537–559, doi:
10.1357/002224099764805183, 1999.

Nodder, S. D. and Waite, A. M.: Is Southern Ocean organic carbon and biogenic silica export
enhanced by iron-stimulated increases in biological production? Sediment trap results from
SOIREE, Deep Sea Research Part II: Topical Studies in Oceanography, 48, 2681–2701, doi:
10.1016/S0967-0645(01)00014-5, URL http://www.sciencedirect.com/science/article/
pii/S0967064501000145, 2001.

Nodder, S. D., Charette, M. A., Waite, A. M., Trull, T. W., Boyd, P. W., Zeldis, J.,
and Buesseler, K. O.: Particle transformations and export flux during an in situ iron-
stimulated algal bloom in the Southern Ocean, Geophysical Research Letters, 28, 2409–
2412, doi:10.1029/2001GL013008, URL http://onlinelibrary.wiley.com/doi/10.1029/
2001GL013008/abstract, 2001.

Nodder, S. D., Chiswell, S. M., and Northcote, L. C.: Annual cycles of deep-ocean biogeochemical
export fluxes in subtropical and subantarctic waters, southwest Pacific Ocean, Journal of
Geophysical Research: Oceans, doi:10.1002/2015JC011243, URL http://onlinelibrary.
wiley.com/doi/10.1002/2015JC011243/abstract, 2016.

Nöthig, E.-M. and von Bodungen, B.: Occurrence and vertical flux of faecal pellets of probably
protozoan origin in the southeastern Weddell Sea (Antarctica), Marine ecology-progress series,
56, 281–289, URL http://epic.awi.de/2271/, 1989.

Obata, T., Fernie, A. R., and Nunes-Nesi, A.: The Central Carbon and Energy Metabolism
of Marine Diatoms, Metabolites, 3, 325–346, doi:10.3390/metabo3020325, URL http://www.
ncbi.nlm.nih.gov/pmc/articles/PMC3901268/, 2013.

Obernosterer, I., Christaki, U., Lefèvre, D., Catala, P., Van Wambeke, F., and Lebaron, P.:
Rapid bacterial mineralization of organic carbon produced during a phytoplankton bloom
induced by natural iron fertilization in the Southern Ocean, Deep Sea Research Part II:
Topical Studies in Oceanography, 55, 777–789, doi:10.1016/j.dsr2.2007.12.005, URL http:
//www.sciencedirect.com/science/article/pii/S0967064508000246, 2008.

Oku, O. and Kamatani, A.: Resting spore formation and phosphorus composition of the ma-
rine diatom Chaetoceros pseudocurvisetus under various nutrient conditions, Marine Biol-
ogy, 123, 393–399, doi:10.1007/BF00353630, URL http://link.springer.com/article/
10.1007/BF00353630, 1995.

Oku, O. and Kamatani, A.: Resting spore formation of the marine planktonic diatom Chaeto-
ceros anastomosans induced by high salinity and nitrogen depletion, Marine Biology, 127,
515–520, doi:10.1007/s002270050040, URL http://link.springer.com/article/10.1007/
s002270050040, 1997.

Oku, O. and Kamatani, A.: Resting spore formation and biochemical composition of the marine
planktonic diatom Chaetoceros pseudocurvisetus in culture: ecological significance of de-
creased nucleotide content and activation of the xanthophyll cycle by resting spore formation,
Marine Biology, 135, 425–436, doi:10.1007/s002270050643, URL http://link.springer.
com/article/10.1007/s002270050643, 1999.

Omand, M. M., D'Asaro, E. A., Lee, C. M., Perry, M. J., Briggs, N., Cetinić, I., and Mahadevan,
A.: Eddy-driven subduction exports particulate organic carbon from the spring bloom, Sci-
ence, 348, 222–225, doi:10.1126/science.1260062, URL http://science.sciencemag.org/
content/348/6231/222, 2015.

O'Neill, L. P., Benitez-Nelson, C. R., Styles, R. M., Tappa, E., and Thunell, R. C.: Diagenetic
effects on particulate phosphorus samples collected using formalin poisoned sediment traps,
Limnology and Oceanography: Methods, 3, 308–317, doi:10.4319/lom.2005.3.308, URL http:
//aslo.info/lomethods/free/2005/0308.html, 2005.

Opute, F. K.: Lipid and Fatty-acid Composition of Diatoms, Journal of Experimental Botany,
25, 823–835, URL http://www.jstor.org/stable/23688816, 1974.

Orr, J. C., Fabry, V. J., Aumont, O., Bopp, L., Doney, S. C., Feely, R. A., Gnanadesikan, A.,

Gruber, N., Ishida, A., Joos, F., Key, R. M., Lindsay, K., Maier-Reimer, E., Matear, R., Monfray, P., Mouchet, A., Najjar, R. G., Plattner, G.-K., Rodgers, K. B., Sabine, C. L., Sarmiento, J. L., Schlitzer, R., Slater, R. D., Totterdell, I. J., Weirig, M.-F., Yamanaka, Y., and Yool, A.: Anthropogenic ocean acidification over the twenty-first century and its impact on calcifying organisms, Nature, 437, 681–686, doi:10.1038/nature04095, URL http://www.nature.com/nature/journal/v437/n7059/abs/nature04095.html, 2005.

Orsi, A. H., Whitworth III, T., and Nowlin Jr., W. D.: On the meridional extent and fronts of the Antarctic Circumpolar Current, Deep Sea Research Part I: Oceanographic Research Papers, 42, 641–673, doi:10.1016/0967-0637(95)00021-W, URL http://www.sciencedirect.com/science/article/pii/096706379500021W, 1995.

Orsi, W. D., Smith, J. M., Wilcox, H. M., Swalwell, J. E., Carini, P., Worden, A. Z., and Santoro, A. E.: Ecophysiology of uncultivated marine euryarchaea is linked to particulate organic matter, The ISME Journal, 9, 1747–1763, doi:10.1038/ismej.2014.260, URL http://www.nature.com/ismej/journal/v9/n8/full/ismej2014260a.html, 2015.

Pahlow, M., Riebesell, U., and Wolf-Gladrow, D. A.: Impact of cell shape and chain formation on nutrient acquisition by marine diatoms, Limnology and Oceanography, 42, 1660–1672, doi:10.4319/lo.1997.42.8.1660, URL http://onlinelibrary.wiley.com/doi/10.4319/lo.1997.42.8.1660/abstract, 1997.

Park, Y.-H., Charriaud, E., Pino, D., and Jeandel, C.: Seasonal and interannual variability of the mixed layer properties and steric height at station KERFIX, southwest of Kerguelen, Journal of Marine Systems, 17, 571–586, doi:10.1016/S0924-7963(98)00065-7, URL http://www.sciencedirect.com/science/article/pii/S0924796398000657, 1998.

Park, Y.-H., Fuda, J.-L., Durand, I., and Naveira Garabato, A. C.: Internal tides and vertical mixing over the Kerguelen Plateau, Deep Sea Research Part II: Topical Studies in Oceanography, 55, 582–593, doi:10.1016/j.dsr2.2007.12.027, URL http://www.sciencedirect.com/science/article/pii/S0967064508000118, 2008a.

Park, Y.-H., Roquet, F., Durand, I., and Fuda, J.-L.: Large-scale circulation over and around the Northern Kerguelen Plateau, Deep Sea Research Part II: Topical Studies in Oceanography, 55, 566–581, doi:10.1016/j.dsr2.2007.12.030, URL http://www.sciencedirect.com/science/article/pii/S0967064508000106, 2008b.

Patrick, R.: Factors effecting the distribution of diatoms, The Botanical Review, 14, 473–524, doi:10.1007/BF02861575, URL http://link.springer.com/article/10.1007/BF02861575, 1948.

Pedrós-Alió, C.: Marine microbial diversity: can it be determined?, Trends in Microbiology, 14, 257–263, doi:10.1016/j.tim.2006.04.007, 2006.

Peeters, J. C. H. and Eilers, P.: The relationship between light intensity and photosynthesis—A simple mathematical model, Hydrobiological Bulletin, 12, 134–136, doi:10.1007/BF02260714, URL http://link.springer.com/article/10.1007/BF02260714, 1978.

Peloquin, J., Hall, J., Safi, K., Smith Jr., W. O., Wright, S., and van den Enden, R.: The response of phytoplankton to iron enrichment in Sub-Antarctic HNLCLSi waters: Results from the SAGE experiment, Deep Sea Research Part II: Topical Studies in Oceanography, 58, 808–823, doi:10.1016/j.dsr2.2010.10.021, URL http://www.sciencedirect.com/science/article/pii/S0967064510002997, 2011.

Peters, E. and Thomas, D. N.: Prolonged nitrate exhaustion and diatom mortality: a comparison of polar and temperate Thalassiosira species, Journal of Plankton Research, 18, 953–968, doi:10.1093/plankt/18.6.953, URL http://plankt.oxfordjournals.org/content/18/6/953, 1996.

Petit, J. R., Jouzel, J., Raynaud, D., Barkov, N. I., Barnola, J.-M., Basile, I., Bender, M., Chappellaz, J., Davis, M., Delaygue, G., Delmotte, M., Kotlyakov, V. M., Legrand, M., Lipenkov, V. Y., Lorius, C., PÉpin, L., Ritz, C., Saltzman, E., and Stievenard, M.: Climate and atmospheric history of the past 420,000 years from the Vostok ice core, Antarctica,

Nature, 399, 429–436, doi:10.1038/20859, URL http://www.nature.com/nature/journal/v399/n6735/abs/399429a0.html, 1999.

Picheral, M., Guidi, L., Stemmann, L., Karl, D. M., Iddaoud, G., and Gorsky, G.: The Underwater Vision Profiler 5: An advanced instrument for high spatial resolution studies of particle size spectra and zooplankton, Limnology and Oceanography: Methods, 8, 462–473, doi:10.4319/lom.2010.8.462, URL http://onlinelibrary.wiley.com/doi/10.4319/lom.2010.8.462/abstract, 2010.

Pilskaln, C. H., Manganini, S. J., Trull, T. W., Armand, L., Howard, W., Asper, V. L., and Massom, R.: Geochemical particle fluxes in the Southern Indian Ocean seasonal ice zone: Prydz Bay region, East Antarctica, Deep Sea Research Part I: Oceanographic Research Papers, 51, 307–332, doi:10.1016/j.dsr.2003.10.010, URL http://www.sciencedirect.com/science/article/pii/S0967063703001985, 2004.

Planchon, F., Ballas, D., Cavagna, A.-J., Bowie, A. R., Davies, D., Trull, T., Laurenceau-Cornec, E. C., Van Der Merwe, P., and Dehairs, F.: Carbon export in the naturally iron-fertilized Kerguelen area of the Southern Ocean based on the 234Th approach, Biogeosciences, 12, 3831–3848, doi:10.5194/bg-12-3831-2015, URL http://www.biogeosciences.net/12/3831/2015/, 2015.

Planquette, H., Sanders, R. R., Statham, P. J., Morris, P. J., and Fones, G. R.: Fluxes of particulate iron from the upper ocean around the Crozet Islands: A naturally iron-fertilized environment in the Southern Ocean, Global Biogeochemical Cycles, 25, GB2011, doi:10.1029/2010GB003789, URL http://onlinelibrary.wiley.com/doi/10.1029/2010GB003789/abstract, 2011.

Pollard, R., Sanders, R., Lucas, M., and Statham, P.: The Crozet Natural Iron Bloom and Export Experiment (CROZEX), Deep Sea Research Part II: Topical Studies in Oceanography, 54, 1905–1914, doi:10.1016/j.dsr2.2007.07.023, URL http://www.sciencedirect.com/science/article/pii/S0967064507001452, 2007.

Pollard, R. T., Salter, I., Sanders, R. J., Lucas, M. I., Moore, C. M., Mills, R. A., Statham, P. J., Allen, J. T., Baker, A. R., Bakker, D. C. E., Charette, M. A., Fielding, S., Fones, G. R., French, M., Hickman, A. E., Holland, R. J., Hughes, J. A., Jickells, T. D., Lampitt, R. S., Morris, P. J., Nédélec, F. H., Nielsdóttir, M., Planquette, H., Popova, E. E., Poulton, A. J., Read, J. F., Seeyave, S., Smith, T., Stinchcombe, M., Taylor, S., Thomalla, S., Venables, H. J., Williamson, R., and Zubkov, M. V.: Southern Ocean deep-water carbon export enhanced by natural iron fertilization, Nature, 457, 577–580, doi:10.1038/nature07716, URL http://www.nature.com/nature/journal/v457/n7229/full/nature07716.html, 2009.

Pond, D. W. and Tarling, G. A.: Phase transitions of wax esters adjust buoyancy in diapausing Calanoides acutus, Limnology and Oceanography, 56, 1310–1318, doi:10.4319/lo.2011.56.4.1310, URL http://onlinelibrary.wiley.com/doi/10.4319/lo.2011.56.4.1310/abstract, 2011.

Pondaven, P., Fravalo, C., Ruiz-Pino, D., Tréguer, P., Quéguiner, B., and Jeandel, C.: Modelling the silica pump in the Permanently Open Ocean Zone of the Southern Ocean, Journal of Marine Systems, 17, 587–619, doi:10.1016/S0924-7963(98)00066-9, URL http://www.sciencedirect.com/science/article/pii/S0924796398000669, 1998.

Pondaven, P., Ruiz-Pino, D., Fravalo, C., Tréguer, P., and Jeandel, C.: Interannual variability of Si and N cycles at the time-series station KERFIX between 1990 and 1995 – a 1-D modelling study, Deep Sea Research Part I: Oceanographic Research Papers, 47, 223–257, doi:10.1016/S0967-0637(99)00053-9, URL http://www.sciencedirect.com/science/article/pii/S0967063799000539, 2000.

Poulsen, L. K. and Iversen, M. H.: Degradation of copepod fecal pellets: key role of protozooplankton, Marine Ecology Progress Series, 367, 1–13, doi:10.3354/meps07611, URL http://www.int-res.com/abstracts/meps/v367/p1-13/, 2008.

Poulton, A. J., Mark Moore, C., Seeyave, S., Lucas, M. I., Fielding, S., and Ward, P.: Phyto-

plankton community composition around the Crozet Plateau, with emphasis on diatoms and Phaeocystis, Deep Sea Research Part II: Topical Studies in Oceanography, 54, 2085–2105, doi: 10.1016/j.dsr2.2007.06.005, URL http://www.sciencedirect.com/science/article/pii/S0967064507001567, 2007.

Prahl, F. G., Eglinton, G., Corner, E. D. S., and O'hara, S. C. M.: Copepod Fecal Pellets as a Source of Dihydrophytol in Marine Sediments, Science, 224, 1235–1237, doi:10.1126/science.224.4654.1235, URL http://science.sciencemag.org/content/224/4654/1235, 1984.

Quéguiner, B.: Iron fertilization and the structure of planktonic communities in high nutrient regions of the Southern Ocean, Deep Sea Research Part II: Topical Studies in Oceanography, 90, 43–54, doi:10.1016/j.dsr2.2012.07.024, URL http://www.sciencedirect.com/science/article/pii/S0967064512001105, 2013.

Quigg, A., Finkel, Z. V., Irwin, A. J., Rosenthal, Y., Ho, T.-Y., Reinfelder, J. R., Schofield, O., Morel, F. M. M., and Falkowski, P. G.: The evolutionary inheritance of elemental stoichiometry in marine phytoplankton, Nature, 425, 291–294, doi:10.1038/nature01953, URL http://www.nature.com/nature/journal/v425/n6955/full/nature01953.html, 2003.

Ragueneau, O., Savoye, N., Del Amo, Y., Cotten, J., Tardiveau, B., and Leynaert, A.: A new method for the measurement of biogenic silica in suspended matter of coastal waters: using Si:Al ratios to correct for the mineral interference, Continental Shelf Research, 25, 697–710, doi:10.1016/j.csr.2004.09.017, URL http://www.sciencedirect.com/science/article/pii/S0278434304002468, 2005.

Ragueneau, O., Schultes, S., Bidle, K., Claquin, P., and Moriceau, B.: Si and C interactions in the world ocean: Importance of ecological processes and implications for the role of diatoms in the biological pump, Global Biogeochemical Cycles, 20, GB4S02, doi:10.1029/2006GB002688, URL http://onlinelibrary.wiley.com/doi/10.1029/2006GB002688/abstract, 2006.

Rampen, S. W., Abbas, B. A., Schouten, S., and Sinninghe Damste, J. S.: A comprehensive study of sterols in marine diatoms (Bacillariophyta): Implications for their use as tracers for diatom productivity, Limnology and Oceanography, 55, 91–105, doi:10.4319/lo.2010.55.1.0091, URL http://onlinelibrary.wiley.com/doi/10.4319/lo.2010.55.1.0091/abstract, 2010.

Raven, J. A. and Falkowski, P. G.: Oceanic sinks for atmospheric CO2, Plant, Cell & Environment, 22, 741–755, doi:10.1046/j.1365-3040.1999.00419.x, URL http://onlinelibrary.wiley.com/doi/10.1046/j.1365-3040.1999.00419.x/abstract, 1999.

Razouls, S., Réau, G. D., Guillot, P., Maison, J., and Jeandel, C.: Seasonal abundance of copepod assemblages and grazing pressure in the Kerguelen Island area (Southern Ocean), Journal of Plankton Research, 20, 1599–1614, doi:10.1093/plankt/20.8.1599, URL http://plankt.oxfordjournals.org/content/20/8/1599, 1998.

Rembauville, M., Blain, S., Armand, L., Quéguiner, B., and Salter, I.: Export fluxes in a naturally iron-fertilized area of the Southern Ocean – Part 2: Importance of diatom resting spores and faecal pellets for export, Biogeosciences, 12, 3171–3195, doi:10.5194/bg-12-3171-2015, URL http://www.biogeosciences.net/12/3171/2015/, 2015a.

Rembauville, M., Salter, I., Leblond, N., Gueneugues, A., and Blain, S.: Export fluxes in a naturally iron-fertilized area of the Southern Ocean – Part 1: Seasonal dynamics of particulate organic carbon export from a moored sediment trap, Biogeosciences, 12, 3153–3170, doi:10.5194/bg-12-3153-2015, URL http://www.biogeosciences.net/12/3153/2015/, 2015b.

Rembauville, M., Manno, C., Tarling, G. A., Blain, S., and Salter, I.: Strong contribution of diatom resting spores to deep-sea carbon transfer in naturally iron-fertilized waters downstream of South Georgia, Deep Sea Research Part I: Oceanographic Research Papers, 115, 22–35, doi:10.1016/j.dsr.2016.05.002, URL http://www.sciencedirect.com/science/article/pii/S0967063716300036, 2016a.

Rembauville, M., Meilland, J., Ziveri, P., Schiebel, R., Blain, S., and Salter, I.: Planktic foraminifer and coccolith contribution to carbonate export fluxes over the central Kergue-

len Plateau, Deep Sea Research Part I: Oceanographic Research Papers, 111, 91–101, doi: 10.1016/j.dsr.2016.02.017, URL http://www.sciencedirect.com/science/article/pii/S0967063715301837, 2016b.

Rigual-Hernández, A. S., Bárcena, M. A., Sierro, F. J., Flores, J. A., Hernández-Almeida, I., Sanchez-Vidal, A., Palanques, A., and Heussner, S.: Seasonal to interannual variability and geographic distribution of the silicoflagellate fluxes in the Western Mediterranean, Marine Micropaleontology, 77, 46–57, doi:10.1016/j.marmicro.2010.07.003, URL http://www.sciencedirect.com/science/article/pii/S0377839810000642, 2010.

Rigual-Hernández, A. S., Trull, T. W., Bray, S. G., Closset, I., and Armand, L. K.: Seasonal dynamics in diatom and particulate export fluxes to the deep sea in the Australian sector of the southern Antarctic Zone, Journal of Marine Systems, 142, 62–74, doi:10.1016/j.jmarsys.2014.10.002, URL http://www.sciencedirect.com/science/article/pii/S0924796314002322, 2015a.

Rigual-Hernández, A. S., Trull, T. W., Bray, S. G., Cortina, A., and Armand, L. K.: Latitudinal and temporal distributions of diatom populations in the pelagic waters of the Subantarctic and Polar Frontal zones of the Southern Ocean and their role in the biological pump, Biogeosciences, 12, 5309–5337, doi:10.5194/bg-12-5309-2015, URL http://www.biogeosciences.net/12/5309/2015/, 2015b.

Rivkin, R. B., Legendre, L., Deibel, D., Tremblay, J.-r., Klein, B., Crocker, K., Roy, S., Silverberg, N., Lovejoy, C., Mesplé, F., Romero, N., Anderson, M. R., Matthews, P., Savenkoff, C., Vézina, A., Therriault, J.-C., Wesson, J., Bérubé, C., and Ingram, R. G.: Vertical Flux of Biogenic Carbon in the Ocean: Is There Food Web Control?, Science, 272, 1163–1166, doi:10.1126/science.272.5265.1163, URL http://science.sciencemag.org/content/272/5265/1163, 1996.

Robinson, C., Steinberg, D. K., Anderson, T. R., Arístegui, J., Carlson, C. A., Frost, J. R., Ghiglione, J.-F., Hernández-León, S., Jackson, G. A., Koppelmann, R., Quéguiner, B., Ragueneau, O., Rassoulzadegan, F., Robison, B. H., Tamburini, C., Tanaka, T., Wishner, K. F., and Zhang, J.: Mesopelagic zone ecology and biogeochemistry – a synthesis, Deep Sea Research Part II: Topical Studies in Oceanography, 57, 1504–1518, doi:10.1016/j.dsr2.2010.02.018, URL http://www.sciencedirect.com/science/article/pii/S0967064510000846, 2010.

Romero, O., Lange, C., Fisher, G., Treppke, U., and Wefer, G.: Variability in export production documented by downward fluxes and species composition of marine planktonic diatoms: observations from the tropical and equatorial Atlantic., in: The Use of Proxies in Paleoceanography, Examples from the South Atlantic, pp. 365–392, Heidelberg, Berlin, springer edn., 1999.

Romero, O. E. and Armand, L.: Marine diatoms as indicators of modern changes in oceanographic conditions. In: 2nd Edition The Diatoms: Applications for the Environmental and Earth Sciences,, Cambridge University Press, pp. 373–400, 2010.

Rosselló-Mora, R. and Amann, R.: The species concept for prokaryotes, FEMS Microbiology Reviews, 25, 39–67, doi:10.1111/j.1574-6976.2001.tb00571.x, URL http://onlinelibrary.wiley.com/doi/10.1111/j.1574-6976.2001.tb00571.x/abstract, 2001.

Rosso, L., Lobry, J. R., and Flandrois, J. P.: An Unexpected Correlation between Cardinal Temperatures of Microbial Growth Highlighted by a New Model, Journal of Theoretical Biology, 162, 447–463, doi:10.1006/jtbi.1993.1099, URL http://www.sciencedirect.com/science/article/pii/S0022519383710994, 1993.

Round, F. E., Crawford, R. M., and Mann, D. G.: Diatoms: Biology and Morphology of the Genera, Cambridge University Press, URL http://www.cambridge.org/us/academic/subjects/life-sciences/plant-science/diatoms-biology-and-morphology-genera, 2007.

Röske, K., Röske, I., and Uhlmann, D.: Characterization of the bacterial population and chemistry in the bottom sediment of a laterally subdivided drinking water reser-

voir system, Limnologica - Ecology and Management of Inland Waters, 38, 367–377, doi:10.1016/j.limno.2008.06.005, URL http://www.sciencedirect.com/science/article/pii/S0075951108000388, 2008.

Ruhl, H. A. and Smith, K. L.: Shifts in Deep-Sea Community Structure Linked to Climate and Food Supply, Science, 305, 513–515, doi:10.1126/science.1099759, URL http://science.sciencemag.org/content/305/5683/513, 2004.

Ruhl, H. A., Ellena, J. A., and Smith, K. L.: Connections between climate, food limitation, and carbon cycling in abyssal sediment communities, Proceedings of the National Academy of Sciences, doi:10.1073/pnas.0803898105, URL http://www.pnas.org/content/early/2008/10/29/0803898105, 2008.

Rynearson, T. A., Richardson, K., Lampitt, R. S., Sieracki, M. E., Poulton, A. J., Lyngsgaard, M. M., and Perry, M. J.: Major contribution of diatom resting spores to vertical flux in the sub-polar North Atlantic, Deep Sea Research Part I: Oceanographic Research Papers, 82, 60–71, doi:10.1016/j.dsr.2013.07.013, URL http://www.sciencedirect.com/science/article/pii/S0967063713001477, 2013.

Ryther, J. H.: Photosynthesis and Fish Production in the Sea, Science, 166, 72–76, doi:10.1126/science.166.3901.72, URL http://www.sciencemag.org/content/166/3901/72, 1969.

Saavedra-Pellitero, M., Baumann, K.-H., Flores, J.-A., and Gersonde, R.: Biogeographic distribution of living coccolithophores in the Pacific sector of the Southern Ocean, Marine Micropaleontology, 109, 1–20, doi:10.1016/j.marmicro.2014.03.003, URL http://www.sciencedirect.com/science/article/pii/S0377839814000310, 2014.

Sabine, C. L., Feely, R. A., Gruber, N., Key, R. M., Lee, K., Bullister, J. L., Wanninkhof, R., Wong, C. S., Wallace, D. W. R., Tilbrook, B., Millero, F. J., Peng, T.-H., Kozyr, A., Ono, T., and Rios, A. F.: The Oceanic Sink for Anthropogenic CO2, Science, 305, 367–371, doi:10.1126/science.1097403, URL http://www.sciencemag.org/content/305/5682/367, 2004.

Sackett, O., Armand, L., Beardall, J., Hill, R., Doblin, M., Connelly, C., Howes, J., Stuart, B., Ralph, P., and Heraud, P.: Taxon-specific responses of Southern Ocean diatoms to Fe enrichment revealed by synchrotron radiation FTIR microspectroscopy, Biogeosciences, 11, 5795–5808, doi:10.5194/bg-11-5795-2014, URL http://www.biogeosciences.net/11/5795/2014/, 2014.

Sadeghi, A., Dinter, T., Vountas, M., Taylor, B., Altenburg-Soppa, M., and Bracher, A.: Remote sensing of coccolithophore blooms in selected oceanic regions using the PhytoDOAS method applied to hyper-spectral satellite data, Biogeosciences, 9, 2127–2143, doi:10.5194/bg-9-2127-2012, URL http://www.biogeosciences.net/9/2127/2012/, 2012.

Sala, O. E., Chapin, F. S., Iii, Armesto, J. J., Berlow, E., Bloomfield, J., Dirzo, R., Huber-Sanwald, E., Huenneke, L. F., Jackson, R. B., Kinzig, A., Leemans, R., Lodge, D. M., Mooney, H. A., Oesterheld, M., Poff, N. L., Sykes, M. T., Walker, B. H., Walker, M., and Wall, D. H.: Global Biodiversity Scenarios for the Year 2100, Science, 287, 1770–1774, doi:10.1126/science.287.5459.1770, URL http://www.sciencemag.org/content/287/5459/1770, 2000.

Sallée, J. B., Speer, K., and Morrow, R.: Response of the Antarctic Circumpolar Current to Atmospheric Variability, Journal of Climate, 21, 3020–3039, doi:10.1175/2007JCLI1702.1, URL http://journals.ametsoc.org/doi/abs/10.1175/2007JCLI1702.1, 2008.

Sallée, J.-B., Matear, R. J., Rintoul, S. R., and Lenton, A.: Localized subduction of anthropogenic carbon dioxide in the Southern Hemisphere oceans, Nature Geoscience, 5, 579–584, doi:10.1038/ngeo1523, URL http://www.nature.com/ngeo/journal/v5/n8/full/ngeo1523.html, 2012.

Salter, I., Lampitt, R. S., Sanders, R., Poulton, A., Kemp, A. E. S., Boorman, B., Saw, K., and Pearce, R.: Estimating carbon, silica and diatom export from a naturally fertilised phytoplankton bloom in the Southern Ocean using PELAGRA: A novel drifting sediment trap, Deep Sea Research Part II: Topical Studies in Oceanography, 54, 2233–2259, doi:10.1016/j.dsr2.2007.06.008, URL http://www.sciencedirect.com/science/article/pii/

S0967064507001622, 2007.

Salter, I., Kemp, A. E. S., Lampitt, R. S., and Gledhill, M.: The association between biogenic and inorganic minerals and the amino acid composition of settling particles, Limnology and Oceanography, 55, 2207–2218, doi:10.4319/lo.2010.55.5.2207, URL http://aslo.org/lo/toc/vol_55/issue_5/2207.html, 2010.

Salter, I., Kemp, A. E. S., Moore, C. M., Lampitt, R. S., Wolff, G. A., and Holtvoeth, J.: Diatom resting spore ecology drives enhanced carbon export from a naturally iron-fertilized bloom in the Southern Ocean, Global Biogeochemical Cycles, 26, GB1014, doi:10.1029/2010GB003977, URL http://onlinelibrary.wiley.com/doi/10.1029/2010GB003977/abstract, 2012.

Salter, I., Schiebel, R., Ziveri, P., Movellan, A., Lampitt, R., and Wolff, G. A.: Carbonate counter pump stimulated by natural iron fertilization in the Polar Frontal Zone, Nature Geoscience, 7, 885–889, doi:10.1038/ngeo2285, URL http://www.nature.com/ngeo/journal/v7/n12/abs/ngeo2285.html, 2014.

Sanders, R., Morris, P. J., Poulton, A. J., Stinchcombe, M. C., Charalampopoulou, A., Lucas, M. I., and Thomalla, S. J.: Does a ballast effect occur in the surface ocean?, Geophysical Research Letters, 37, L08 602, doi:10.1029/2010GL042574, URL http://onlinelibrary.wiley.com/doi/10.1029/2010GL042574/abstract, 2010.

Sarmiento, J. L. and Gruber, N.: Ocean Biogeochemical Dynamics, Princeton University Press, Princeton, URL http://press.princeton.edu/titles/8223.html, 2006.

Sarmiento, J. L. and Orr, J. C.: Three-dimensional simulations of the impact of Southern Ocean nutrient depletion on atmospheric CO2 and ocean chemistry, Limnology and Oceanography, 36, 1928–1950, doi:10.4319/lo.1991.36.8.1928, URL http://onlinelibrary.wiley.com/doi/10.4319/lo.1991.36.8.1928/abstract, 1991.

Sarmiento, J. L. and Toggweiler, J. R.: A new model for the role of the oceans in determining atmospheric pCO2, Nature, 308, 621–624, doi:10.1038/308621a0, URL http://www.nature.com/nature/journal/v308/n5960/abs/308621a0.html, 1984.

Sarmiento, J. L., Toggweiler, J. R., Najjar, R., Webb, D. J., Jenkins, W. J., Wunsch, C., Elderfield, H., Whitfield, M., and Minster, J.-F.: Ocean Carbon-Cycle Dynamics and Atmospheric pCO2, Philosophical Transactions of the Royal Society of London A: Mathematical, Physical and Engineering Sciences, 325, 3–21, doi:10.1098/rsta.1988.0039, URL http://rsta.royalsocietypublishing.org/content/325/1583/3, 1988.

Sarmiento, J. L., Hughes, T. M. C., Stouffer, R. J., and Manabe, S.: Simulated response of the ocean carbon cycle to anthropogenic climate warming, Nature, 393, 245–249, doi:10.1038/30455, URL http://www.nature.com/nature/journal/v393/n6682/abs/393245a0.html, 1998.

Sarmiento, J. L., Gruber, N., Brzezinski, M. A., and Dunne, J. P.: High-latitude controls of thermocline nutrients and low latitude biological productivity, Nature, 427, 56–60, doi:10.1038/nature02127, URL http://www.nature.com/nature/journal/v427/n6969/abs/nature02127.html, 2004.

Sarthou, G., Timmermans, K. R., Blain, S., and Tréguer, P.: Growth physiology and fate of diatoms in the ocean: a review, Journal of Sea Research, 53, 25–42, doi:10.1016/j.seares.2004.01.007, URL http://www.sciencedirect.com/science/article/pii/S1385110104000644, 2005.

Sathyendranath, S., Stuart, V., Nair, A., Oka, K., Nakane, T., Bouman, H., Forget, M., Maass, H., and Platt, T.: Carbon-to-chlorophyll ratio and growth rate of phytoplankton in the sea, Marine Ecology Progress Series, 383, 73–84, doi:10.3354/meps07998, URL http://www.int-res.com/abstracts/meps/v383/p73-84/, 2009.

Savoye, N., Benitez-Nelson, C., Burd, A. B., Cochran, J. K., Charette, M., Buesseler, K. O., Jackson, G. A., Roy-Barman, M., Schmidt, S., and Elskens, M.: 234Th sorption and export models in the water column: A review, Marine Chemistry, 100, 234–249, doi:10.1016/j.marchem.2005.10.014, URL http://www.sciencedirect.com/science/article/

pii/S030442030500215X, 2006.

Savoye, N., Trull, T. W., Jacquet, S. H. M., Navez, J., and Dehairs, F.: 234Th-based export fluxes during a natural iron fertilization experiment in the Southern Ocean (KEOPS), Deep Sea Research Part II: Topical Studies in Oceanography, 55, 841–855, doi: 10.1016/j.dsr2.2007.12.036, URL http://www.sciencedirect.com/science/article/pii/S0967064508000325, 2008.

Schiebel, R.: Planktic foraminiferal sedimentation and the marine calcite budget, Global Biogeochemical Cycles, 16, 1065, doi:10.1029/2001GB001459, URL http://onlinelibrary.wiley.com/doi/10.1029/2001GB001459/abstract, 2002.

Schnack-Schiel, S. and Isla, E.: The role of zooplankton in the pelagic-benthic coupling of the Southern Ocean, Scientia Marina, 69 (Suppl. 2), 39–55, 2005.

Schrader, H. J. and Gersonde, R.: Diatoms and silicofagellates. Micropaleontological counting methods and techniques: an exercise on an eight metres section of the Lower Pliocene of Capo Rosello, Sicily., Utrecht Micropaleontological Bulletins, pp. 129–176, 1978.

Schulz, M. and Mudelsee, M.: REDFIT: estimating red-noise spectra directly from unevenly spaced paleoclimatic time series, Computers & Geosciences, 28, 421–426, doi: 10.1016/S0098-3004(01)00044-9, URL http://www.sciencedirect.com/science/article/pii/S0098300401000449, 2002.

Sekar, R., Pernthaler, A., Pernthaler, J., Warnecke, F., Posch, T., and Amann, R.: An Improved Protocol for Quantification of Freshwater Actinobacteria by Fluorescence In Situ Hybridization, Applied and Environmental Microbiology, 69, 2928–2935, doi:10.1128/AEM.69.5.2928-2935.2003, URL http://aem.asm.org/content/69/5/2928, 2003.

Sell, D. W. and Evans, M. S.: A statistical analysis of subsampling and an evaluation of the Folsom plankton splitter, Hydrobiologia, 94, 223–230, doi:10.1007/BF00016403, URL http://link.springer.com/article/10.1007/BF00016403, 1982.

Sigman, D. M. and Boyle, E. A.: Glacial/interglacial variations in atmospheric carbon dioxide, Nature, 407, 859–869, doi:10.1038/35038000, URL http://www.nature.com/nature/journal/v407/n6806/abs/407859a0.html, 2000.

Sigman, D. M., Hain, M. P., and Haug, G. H.: The polar ocean and glacial cycles in atmospheric CO2 concentration, Nature, 466, 47–55, doi:10.1038/nature09149, URL http://www.nature.com/nature/journal/v466/n7302/full/nature09149.html, 2010.

Smetacek, V.: Diatoms and the ocean carbon cycle, Protist, 150, 25–32, doi:10.1016/S1434-4610(99)70006-4, 1999.

Smetacek, V.: A watery arms race, Nature, 411, 745–745, doi:10.1038/35081210, URL http://www.nature.com/nature/journal/v411/n6839/full/411745a0.html, 2001.

Smetacek, V., Assmy, P., and Henjes, J.: The role of grazing in structuring Southern Ocean pelagic ecosystems and biogeochemical cycles, Antarctic Science, 16, 541–558, doi:10.1017/S0954102004002317, URL http://journals.cambridge.org/article_S0954102004002317, 2004.

Smetacek, V., Klaas, C., Strass, V. H., Assmy, P., Montresor, M., Cisewski, B., Savoye, N., Webb, A., d'Ovidio, F., Arrieta, J. M., Bathmann, U., Bellerby, R., Berg, G. M., Croot, P., Gonzalez, S., Henjes, J., Herndl, G. J., Hoffmann, L. J., Leach, H., Losch, M., Mills, M. M., Neill, C., Peeken, I., Röttgers, R., Sachs, O., Sauter, E., Schmidt, M. M., Schwarz, J., Terbrüggen, A., and Wolf-Gladrow, D.: Deep carbon export from a Southern Ocean iron-fertilized diatom bloom, Nature, 487, 313–319, doi:10.1038/nature11229, URL http://www.nature.com/nature/journal/v487/n7407/full/nature11229.html, 2012.

Smetacek, V. S.: Role of sinking in diatom life-history cycles: ecological, evolutionary and geological significance, Marine Biology, 84, 239–251, doi:10.1007/BF00392493, URL http://link.springer.com/article/10.1007/BF00392493, 1985.

Smith, Jr., K. L., Sherman, A. D., Huffard, C. L., McGill, P. R., Henthorn, R., Von Thun, S., Ruhl, H. A., Kahru, M., and Ohman, M. D.: Large salp bloom export from the up-

per ocean and benthic community response in the abyssal northeast Pacific: Day to week resolution, Limnology and Oceanography, 59, 745–757, doi:10.4319/lo.2014.59.3.0745, URL http://onlinelibrary.wiley.com/doi/10.4319/lo.2014.59.3.0745/abstract, 2014.

Smith, W. O. and Nelson, D. M.: Phytoplankton Bloom Produced by a Receding Ice Edge in the Ross Sea: Spatial Coherence with the Density Field, Science, 227, 163–166, doi: 10.1126/science.227.4683.163, URL http://science.sciencemag.org/content/227/4683/163, 1985.

Smith, Jr., W. O. and Nelson, D. M.: Importance of Ice Edge Phytoplankton Production in the Southern Ocean, BioScience, 36, 251–257, doi:10.2307/1310215, URL http://www.jstor.org/stable/1310215, 1986.

Speer, K., Rintoul, S. R., and Sloyan, B.: The Diabatic Deacon Cell, Journal of Physical Oceanography, 30, 3212–3222, doi:10.1175/1520-0485(2000)030⟨3212:TDDC⟩2.0.CO;2, URL http://journals.ametsoc.org/doi/abs/10.1175/1520-0485(2000)030%3C3212%3ATDDC%3E2.0.CO%3B2, 2000.

Stübing, D., Hagen, W., and Schmidt, K.: On the use of lipid biomarkers in marine food web analyses: An experimental case study on the Antarctic krill, Euphausia *superba*, Limnology and Oceanography, 48, 1685–1700, doi:10.4319/lo.2003.48.4.1685, URL http://doi.wiley.com/10.4319/lo.2003.48.4.1685, 2003.

Steinberg, D. K., Goldthwait, S. A., and Hansell, D. A.: Zooplankton vertical migration and the active transport of dissolved organic and inorganic nitrogen in the Sargasso Sea, Deep Sea Research Part I: Oceanographic Research Papers, 49, 1445–1461, doi: 10.1016/S0967-0637(02)00037-7, URL http://www.sciencedirect.com/science/article/pii/S0967063702000377, 2002.

Steinberg, D. K., Van Mooy, B. A. S., Buesseler, K. O., Boyd, P. W., Kobari, T., and Karl, D. M.: Bacterial vs. zooplankton control of sinking particle flux in the ocean's twilight zone, Limnology and Oceanography, 53, 1327–1338, doi:10.4319/lo.2008.53.4.1327, URL http://aslo.org/lo/toc/vol_53/issue_4/1327.html, 2008.

Stemmann, L., Jackson, G. A., and Ianson, D.: A vertical model of particle size distributions and fluxes in the midwater column that includes biological and physical processes—Part I: model formulation, Deep Sea Research Part I: Oceanographic Research Papers, 51, 865–884, doi:10.1016/j.dsr.2004.03.001, URL http://www.sciencedirect.com/science/article/pii/S0967063704000433, 2004.

Stephens, B. B. and Keeling, R. F.: The influence of Antarctic sea ice on glacial–interglacial CO$_2$ variations, Nature, 404, 171–174, doi:10.1038/35004556, URL http://www.nature.com/nature/journal/v404/n6774/full/404171a0.html, 2000.

Stoecker, D. K.: Mixotrophy among Dinoflagellates, Journal of Eukaryotic Microbiology, 46, 397–401, doi:10.1111/j.1550-7408.1999.tb04619.x, URL http://onlinelibrary.wiley.com/doi/10.1111/j.1550-7408.1999.tb04619.x/abstract, 1999.

Stoecker, D. K., Taniguchi, A., and Michaels, A. E.: Abundance of autotrophic, mixotrophic and heterotrophic planktonic ciliates in shelf and slope waters, Marine Ecology Progress Series, 50, 241–254, URL http://www.int-res.com/articles/meps/50/m050p255.pdf, 1989.

Stramski, D. and Kiefer, D. A.: Light scattering by microorganisms in the open ocean, Progress in Oceanography, 28, 343–383, doi:10.1016/0079-6611(91)90032-H, URL http://www.sciencedirect.com/science/article/pii/007966119190032H, 1991.

Stramski, D., Boss, E., Bogucki, D., and Voss, K. J.: The role of seawater constituents in light backscattering in the ocean, Progress in Oceanography, 61, 27–56, doi:10.1016/j.pocean.2004.07.001, URL http://www.sciencedirect.com/science/article/pii/S0079661104000692, 2004.

Strzepek, R. F., Hunter, K. A., Frew, R. D., Harrison, P. J., and Boyd, P. W.: Iron-light interactions differ in Southern Ocean phytoplankton, Limnology and Oceanography, 57, 1182–1200, doi:10.4319/lo.2012.57.4.1182, URL http://aslo.org/lo/toc/vol_57/issue_

4/1182.html, 2012.

Stukel, M. R., Asher, E., Couto, N., Schofield, O., Strebel, S., Tortell, P., and Ducklow, H. W.: The imbalance of new and export production in the western Antarctic Peninsula, a potentially "leaky" ecosystem, Global Biogeochemical Cycles, 29, 2015GB005 211, doi:10.1002/2015GB005211, URL http://onlinelibrary.wiley.com/doi/10.1002/2015GB005211/abstract, 2015.

Suess, E.: Particulate organic carbon flux in the oceans—surface productivity and oxygen utilization, Nature, 288, 260–263, doi:10.1038/288260a0, URL http://www.nature.com/nature/journal/v288/n5788/abs/288260a0.html, 1980.

Sugie, K. and Kuma, K.: Resting spore formation in the marine diatom Thalassiosira nordenskioeldii under iron- and nitrogen-limited conditions, Journal of Plankton Research, 30, 1245–1255, doi:10.1093/plankt/fbn080, URL http://plankt.oxfordjournals.org/content/30/11/1245, 2008.

Sunda, W. G. and Hardison, D. R.: Evolutionary tradeoffs among nutrient acquisition, cell size, and grazing defense in marine phytoplankton promote ecosystem stability, Marine Ecology Progress Series, 401, 63–76, doi:10.3354/meps08390, URL http://www.int-res.com/abstracts/meps/v401/p63-76/, 2010.

Sundquist, E. T.: Geologic Analogs: Their Value and Limitations in Carbon Dioxide Research, in: The Changing Carbon Cycle, edited by Trabalka, J. R. and Reichle, D. E., pp. 371–402, Springer New York, URL http://link.springer.com/chapter/10.1007/978-1-4757-1915-4_19, 1986.

Suzuki, H., Sasaki, H., and Fukuchi, M.: Short-term variability in the flux of rapidly sinking particles in the Antarctic marginal ice zone, Polar Biology, 24, 697–705, doi:10.1007/s003000100271, URL http://link.springer.com/article/10.1007/s003000100271, 2001.

Swan, B. K., Martinez-Garcia, M., Preston, C. M., Sczyrba, A., Woyke, T., Lamy, D., Reinthaler, T., Poulton, N. J., Masland, E. D. P., Gomez, M. L., Sieracki, M. E., DeLong, E. F., Herndl, G. J., and Stepanauskas, R.: Potential for Chemolithoautotrophy Among Ubiquitous Bacteria Lineages in the Dark Ocean, Science, 333, 1296–1300, doi:10.1126/science.1203690, URL http://science.sciencemag.org/content/333/6047/1296, 2011.

Takahashi, T., Sutherland, S. C., Sweeney, C., Poisson, A., Metzl, N., Tilbrook, B., Bates, N., Wanninkhof, R., Feely, R. A., Sabine, C., Olafsson, J., and Nojiri, Y.: Global sea–air CO2 flux based on climatological surface ocean pCO2, and seasonal biological and temperature effects, Deep Sea Research Part II: Topical Studies in Oceanography, 49, 1601–1622, doi:10.1016/S0967-0645(02)00003-6, URL http://www.sciencedirect.com/science/article/pii/S0967064502000036, 2002.

Takahashi, T., Sutherland, S. C., Wanninkhof, R., Sweeney, C., Feely, R. A., Chipman, D. W., Hales, B., Friederich, G., Chavez, F., Sabine, C., Watson, A., Bakker, D. C., Schuster, U., Metzl, N., Yoshikawa-Inoue, H., Ishii, M., Midorikawa, T., Nojiri, Y., Körtzinger, A., Steinhoff, T., Hoppema, M., Olafsson, J., Arnarson, T. S., Tilbrook, B., Johannessen, T., Olsen, A., Bellerby, R., Wong, C., Delille, B., Bates, N., and de Baar, H. J.: Climatological mean and decadal change in surface ocean pCO2, and net sea–air CO2 flux over the global oceans, Deep Sea Research Part II: Topical Studies in Oceanography, 56, 554–577, doi:10.1016/j.dsr2.2008.12.009, URL http://www.sciencedirect.com/science/article/pii/S0967064508004311, 2009.

Takeda, S.: Influence of iron availability on nutrient consumption ratio of diatoms in oceanic waters, Nature, 393, 774–777, doi:10.1038/31674, URL http://www.nature.com/nature/journal/v393/n6687/abs/393774a0.html, 1998.

Tarling, G. A., Ward, P., Atkinson, A., Collins, M. A., and Murphy, E. J.: DISCOVERY 2010: Spatial and temporal variability in a dynamic polar ecosystem, Deep Sea Research Part II: Topical Studies in Oceanography, 59–60, 1–13, doi:10.1016/j.dsr2.2011.10.001, URL http://www.sciencedirect.com/science/article/pii/S0967064511002323, 2012.

Taylor, S. R. and McClennan, S. M.: The continental crust: Its composition and evolution, Geological Journal, 21, 85–86, doi:10.1002/gj.3350210116, URL http://onlinelibrary.wiley.com/doi/10.1002/gj.3350210116/abstract, 1986.

Ternois, Y., Sicre, M.-A., Boireau, A., Beaufort, L., Miquel, J.-C., and Jeandel, C.: Hydrocarbons, sterols and alkenones in sinking particles in the Indian Ocean sector of the Southern Ocean, Organic Geochemistry, 28, 489–501, doi:10.1016/S0146-6380(98)00008-4, URL http://www.sciencedirect.com/science/article/pii/S0146638098000084, 1998.

Ternon, E., Guieu, C., Loÿe-Pilot, M.-D., Leblond, N., Bosc, E., Gasser, B., Miquel, J.-C., and Martín, J.: The impact of Saharan dust on the particulate export in the water column of the North Western Mediterranean Sea, Biogeosciences, 7, 809–826, doi:10.5194/bg-7-809-2010, URL http://www.biogeosciences.net/7/809/2010/, 2010.

Thackeray, S. J., Sparks, T. H., Frederiksen, M., Burthe, S., Bacon, P. J., Bell, J. R., Botham, M. S., Brereton, T. M., Bright, P. W., Carvalho, L., Clutton-Brock, T., Dawson, A., Edwards, M., Elliott, J. M., Harrington, R., Johns, D., Jones, I. D., Jones, J. T., Leech, D. I., Roy, D. B., Scott, W. A., Smith, M., Smithers, R. J., Winfield, I. J., and Wanless, S.: Trophic level asynchrony in rates of phenological change for marine, freshwater and terrestrial environments, Global Change Biology, 16, 3304–3313, doi:10.1111/j.1365-2486.2010.02165.x, URL http://onlinelibrary.wiley.com/doi/10.1111/j.1365-2486.2010.02165.x/abstract, 2010.

Thiele, S., Fuchs, B. M., Amann, R., and Iversen, M. H.: Colonization in the Photic Zone and Subsequent Changes during Sinking Determine Bacterial Community Composition in Marine Snow, Applied and Environmental Microbiology, 81, 1463–1471, doi:10.1128/AEM.02570-14, URL http://aem.asm.org/content/81/4/1463, 2015.

Thomalla, S. J., Poulton, A. J., Sanders, R., Turnewitsch, R., Holligan, P. M., and Lucas, M. I.: Variable export fluxes and efficiencies for calcite, opal, and organic carbon in the Atlantic Ocean: A ballast effect in action?, Global Biogeochemical Cycles, 22, GB1010, doi:10.1029/2007GB002982, URL http://onlinelibrary.wiley.com/doi/10.1029/2007GB002982/abstract, 2008.

Thomalla, S. J., Racault, M.-F., Swart, S., and Monteiro, P. M. S.: High-resolution view of the spring bloom initiation and net community production in the Subantarctic Southern Ocean using glider data, ICES Journal of Marine Science: Journal du Conseil, 72, 1999–2020, doi:10.1093/icesjms/fsv105, URL http://icesjms.oxfordjournals.org/content/72/6/1999, 2015.

Thuróczy, C.-E., Alderkamp, A.-C., Laan, P., Gerringa, L. J., Mills, M. M., Van Dijken, G. L., De Baar, H. J., and Arrigo, K. R.: Key role of organic complexation of iron in sustaining phytoplankton blooms in the Pine Island and Amundsen Polynyas (Southern Ocean), Deep Sea Research Part II: Topical Studies in Oceanography, 71–76, 49–60, doi:10.1016/j.dsr2.2012.03.009, URL http://www.sciencedirect.com/science/article/pii/S096706451200046X, 2012.

Timmermans, K. R., Wagt, B. v. d., and de Baar, H. J. W.: Growth rates, half saturation constants, and silicate, nitrate, and phosphate depletion in relation to iron availability of four large open-ocean diatoms from the Southern Ocean, Limnology and Oceanography, 49, 2141–2151, doi:10.4319/lo.2004.49.6.2141, URL http://www.aslo.org/lo/toc/vol_49/issue_6/2141.html, 2004.

Toggweiler, J. R.: Variation of atmospheric CO2 by ventilation of the ocean's deepest water, Paleoceanography, 14, 571–588, doi:10.1029/1999PA900033, URL http://onlinelibrary.wiley.com/doi/10.1029/1999PA900033/abstract, 1999.

Toggweiler, J. R., Murnane, R., Carson, S., Gnanadesikan, A., and Sarmiento, J. L.: Representation of the carbon cycle in box models and GCMs, 2, Organic pump, Global Biogeochemical Cycles, 17, 1027, doi:10.1029/2001GB001841, URL http://onlinelibrary.wiley.com/doi/10.1029/2001GB001841/abstract, 2003.

Toseland, A., Daines, S. J., Clark, J. R., Kirkham, A., Strauss, J., Uhlig, C., Lenton, T. M., Valentin, K., Pearson, G. A., Moulton, V., and Mock, T.: The impact of temperature on

marine phytoplankton resource allocation and metabolism, Nature Climate Change, 3, 979–984, doi:10.1038/nclimate1989, URL http://www.nature.com/nclimate/journal/v3/n11/full/nclimate1989.html, 2013.

Tréguer, P., Nelson, D. M., Bennekom, A. J. V., DeMaster, D. J., Leynaert, A., and Quéguiner, B.: The Silica Balance in the World Ocean: A Reestimate, Science, 268, 375–379, doi:10.1126/science.268.5209.375, URL http://www.sciencemag.org/content/268/5209/375, 1995.

Trull, T. W., Bray, S. G., Manganini, S. J., Honjo, S., and François, R.: Moored sediment trap measurements of carbon export in the Subantarctic and Polar Frontal zones of the Southern Ocean, south of Australia, Journal of Geophysical Research: Oceans, 106, 31 489–31 509, doi:10.1029/2000JC000308, URL http://onlinelibrary.wiley.com/doi/10.1029/2000JC000308/abstract, 2001.

Tsukazaki, C., Ishii, K.-I., Saito, R., Matsuno, K., Yamaguchi, A., and Imai, I.: Distribution of viable diatom resting stage cells in bottom sediments of the eastern Bering Sea shelf, Deep Sea Research Part II: Topical Studies in Oceanography, 94, 22–30, doi:10.1016/j.dsr2.2013.03.020, URL http://www.sciencedirect.com/science/article/pii/S0967064513001185, 2013.

Turner, J. T.: Zooplankton fecal pellets, marine snow and sinking phytoplankton blooms, Aquatic Microbial Ecology, 27, 57–102, doi:10.3354/ame027057, URL http://www.int-res.com/abstracts/ame/v27/n1/p57-102/, 2002.

Twining, B. S., Nodder, S. D., King, A. L., Hutchins, D. A., LeCleir, G. R., DeBruyn, J. M., Maas, E. W., Vogt, S., Wilhelm, S. W., and Boyd, P. W.: Differential remineralization of major and trace elements in sinking diatoms, Limnology and Oceanography, 59, 689–704, doi:10.4319/lo.2014.59.3.0689, URL http://onlinelibrary.wiley.com/doi/10.4319/lo.2014.59.3.0689/abstract, 2014.

Tyrrell, T., Merico, A., Waniek, J. J., Wong, C. S., Metzl, N., and Whitney, F.: Effect of seafloor depth on phytoplankton blooms in high-nitrate, low-chlorophyll (HNLC) regions, Journal of Geophysical Research: Biogeosciences, 110, G02 007, doi:10.1029/2005JG000041, URL http://onlinelibrary.wiley.com/doi/10.1029/2005JG000041/abstract, 2005.

Venables, H. and Moore, C. M.: Phytoplankton and light limitation in the Southern Ocean: Learning from high-nutrient, high-chlorophyll areas, Journal of Geophysical Research: Oceans, 115, C02 015, doi:10.1029/2009JC005361, URL http://onlinelibrary.wiley.com/doi/10.1029/2009JC005361/abstract, 2010.

Villareal, T. A.: Positive buoyancy in the oceanic diatom Rhizosolenia debyana H. Peragallo, Deep Sea Research Part A. Oceanographic Research Papers, 35, 1037–1045, doi:10.1016/0198-0149(88)90075-1, URL http://www.sciencedirect.com/science/article/pii/0198014988900751, 1988.

Villareal, T. A.: Buoyancy properties of the giant diatom Ethmodiscus, Journal of Plankton Research, 14, 459–463, doi:10.1093/plankt/14.3.459, URL http://plankt.oxfordjournals.org/content/14/3/459, 1992.

Volk, T. and Hoffert, M. I.: Ocean carbon pumps: Analysis of relative strengths and efficiencies in ocean-driven atmospheric CO2 changes, in: Geophysical Monograph Series, edited by Sundquist, E. T. and Broecker, W. S., vol. 32, pp. 99–110, American Geophysical Union, Washington, D. C., URL http://www.agu.org/books/gm/v032/GM032p0099/GM032p0099.shtml, 1985.

Volkman, J. K.: A review of sterol markers for marine and terrigenous organic matter, Organic Geochemistry, 9, 83–99, doi:10.1016/0146-6380(86)90089-6, URL http://www.sciencedirect.com/science/article/pii/0146638086900896, 1986.

Volkman, J. K.: Sterols in microorganisms, Applied Microbiology and Biotechnology, 60, 495–506, doi:10.1007/s00253-002-1172-8, 2003.

von Bodungen, B., Fischer, G., Nöthig, E.-M., and Wefer, G.: Sedimentation of krill faeces during spring development of phytoplankton in Bransfield Strait, Antarctica, Mitt Geol Paläont Inst Univ Hamburg, SCOPE/UNEP Sonderbd., 62, 243–257, URL http://epic.awi.de/

370/, 1987.

Voss, M.: Content of copepod faecal pellets in relation to food supply in Kiel Bight and its effect on sedimentation rate, Marine Ecology Progress Series, 75, 217–225, URL http://www.int-res.com/abstracts/meps/v75/, 1991.

Vrieling, E. G., Poort, L., Beelen, T. P., and Gieskes, W. W.: Growth and silica content of the diatoms Thalassiosira weissflogii and Navicula salinarum at different salinities and enrichments with aluminium, European Journal of Phycology, 34, 307–316, doi:10.1080/09670269910001736362, URL http://journals.cambridge.org/article_S0967026299002206, 1999.

Waite, A. M., Safi, K. A., Hall, J. A., and Nodder, S. D.: Mass sedimentation of picoplankton embedded in organic aggregates, Limnology and Oceanography, 45, 87–97, doi:10.4319/lo.2000.45.1.0087, URL http://onlinelibrary.wiley.com/doi/10.4319/lo.2000.45.1.0087/abstract, 2000.

Wakeham, S. G.: Organic matter from a sediment trap experiment in the equatorial north Atlantic: wax esters, steryl esters, triacylglycerols and alkyldiacylglycerols, Geochimica et Cosmochimica Acta, 46, 2239–2257, doi:10.1016/0016-7037(82)90198-3, URL http://www.sciencedirect.com/science/article/pii/0016703782901983, 1982.

Wakeham, S. G. and Lee, C.: Production, Transport, and Alteration of Particulate Organic Matter in the Marine Water Column, in: Organic Geochemistry, edited by Engel, M. H. and Macko, S. A., no. 11 in Topics in Geobiology, pp. 145–169, Springer US, URL http://link.springer.com/chapter/10.1007/978-1-4615-2890-6_6, dOI: 10.1007/978-1-4615-2890-6_6, 1993.

Wakeham, S. G., Farrington, J. W., Gagosian, R. B., Lee, C., DeBaar, H., Nigrelli, G. E., Tripp, B. W., Smith, S. O., and Frew, N. M.: Organic matter fluxes from sediment traps in the equatorial Atlantic Ocean, Nature, 286, 798–800, doi:10.1038/286798a0, URL http://www.nature.com/nature/journal/v286/n5775/abs/286798a0.html, 1980.

Wakeham, S. G., Lee, C., Farrington, J. W., and Gagosian, R. B.: Biogeochemistry of particulate organic matter in the oceans: results from sediment trap experiments, Deep Sea Research Part A. Oceanographic Research Papers, 31, 509–528, doi:10.1016/0198-0149(84)90099-2, URL http://www.sciencedirect.com/science/article/pii/0198014984900992, 1984.

Wakeham, S. G., Hedges, J. I., Lee, C., Peterson, M. L., and Hernes, P. J.: Compositions and transport of lipid biomarkers through the water column and surficial sediments of the equatorial Pacific Ocean, Deep Sea Research Part II: Topical Studies in Oceanography, 44, 2131–2162, doi:10.1016/S0967-0645(97)00035-0, URL http://www.sciencedirect.com/science/article/pii/S0967064597000350, 1997.

Wakeham, S. G., Lee, C., Peterson, M. L., Liu, Z., Szlosek, J., Putnam, I. F., and Xue, J.: Organic biomarkers in the twilight zone—Time series and settling velocity sediment traps during MedFlux, Deep Sea Research Part II: Topical Studies in Oceanography, 56, 1437–1453, doi:10.1016/j.dsr2.2008.11.030, URL http://www.sciencedirect.com/science/article/pii/S0967064508004189, 2009.

Walsh, J. J.: A carbon budget for overfishing off Peru, Nature, 290, 300–304, doi:10.1038/290300a0, URL http://www.nature.com/nature/journal/v290/n5804/abs/290300a0.html, 1981.

Wang, S. and Moore, J. K.: Variability of primary production and air-sea CO2 flux in the Southern Ocean, Global Biogeochemical Cycles, 26, GB1008, doi:10.1029/2010GB003981, URL http://onlinelibrary.wiley.com/doi/10.1029/2010GB003981/abstract, 2012.

Ward, Jr., J. H.: Hierarchical Grouping to Optimize an Objective Function, Journal of the American Statistical Association, 58, 236–244, doi:10.2307/2282967, URL http://www.jstor.org/stable/2282967, 1963.

Wassmann, P.: Retention versus export food chains: processes controlling sinking loss from marine pelagic systems, Hydrobiologia, 363, 29–57, doi:10.1023/A:1003113403096, URL http:

//link.springer.com/article/10.1023/A%3A1003113403096, 1997.

Wefer, G., Fischer, G., Füetterer, D., and Gersonde, R.: Seasonal particle flux in the Bransfield Strait, Antartica, Deep Sea Research Part A. Oceanographic Research Papers, 35, 891–898, doi:10.1016/0198-0149(88)90066-0, URL http://www.sciencedirect.com/science/article/pii/0198014988900660, 1988.

Weiss, R. F.: Carbon dioxide in water and seawater: the solubility of a non-ideal gas, Marine Chemistry, 2, 203–215, doi:10.1016/0304-4203(74)90015-2, URL http://www.sciencedirect.com/science/article/pii/0304420374900152, 1974.

Westberry, T. K., Behrenfeld, M. J., Milligan, A. J., and Doney, S. C.: Retrospective satellite ocean color analysis of purposeful and natural ocean iron fertilization, Deep Sea Research Part I: Oceanographic Research Papers, 73, 1–16, doi:10.1016/j.dsr.2012.11.010, URL http://www.sciencedirect.com/science/article/pii/S0967063712002300, 2013.

Whitmire, A. L., Pegau, W. S., Karp-Boss, L., Boss, E., and Cowles, T. J.: Spectral backscattering properties of marine phytoplankton cultures, Optics Express, 18, 15 073, doi:10.1364/OE.18.015073, URL https://www.osapublishing.org/oe/abstract.cfm?uri=oe-18-14-15073, 2010.

Wilson, S. E., Steinberg, D. K., and Buesseler, K. O.: Changes in fecal pellet characteristics with depth as indicators of zooplankton repackaging of particles in the mesopelagic zone of the subtropical and subarctic North Pacific Ocean, Deep Sea Research Part II: Topical Studies in Oceanography, 55, 1636–1647, doi:10.1016/j.dsr2.2008.04.019, URL http://www.sciencedirect.com/science/article/pii/S0967064508001458, 2008.

Wilson, S. E., Ruhl, H. A., and Smith, K. L., J.: Zooplankton fecal pellet flux in the abyssal northeast Pacific: A 15 year time-series study, Limnology and Oceanography, 58, 881–892, doi:10.4319/lo.2013.58.3.0881, URL http://onlinelibrary.wiley.com/doi/10.4319/lo.2013.58.3.0881/abstract, 2013.

Winter, A., Elbrächter, M., and Krause, G.: Subtropical coccolithophores in the Weddell Sea, Deep Sea Research Part I: Oceanographic Research Papers, 46, 439–449, doi:10.1016/S0967-0637(98)00076-4, URL http://www.sciencedirect.com/science/article/pii/S0967063798000764, 1999.

Winter, A., Henderiks, J., Beaufort, L., Rickaby, R. E. M., and Brown, C. W.: Poleward expansion of the coccolithophore Emiliania huxleyi, Journal of Plankton Research, 36, 316–325, doi:10.1093/plankt/fbt110, URL http://plankt.oxfordjournals.org/content/36/2/316, 2014.

Wolf-Gladrow, D. A., Riebesell, U., Burkhardt, S., and Bijma, J.: Direct effects of CO2 concentration on growth and isotopic composition of marine plankton, Tellus B, 51, 461–476, doi:10.1034/j.1600-0889.1999.00023.x, URL http://onlinelibrary.wiley.com/doi/10.1034/j.1600-0889.1999.00023.x/abstract, 1999.

Wolff, E. W., Fischer, H., Fundel, F., Ruth, U., Twarloh, B., Littot, G. C., Mulvaney, R., Röthlisberger, R., de Angelis, M., Boutron, C. F., Hansson, M., Jonsell, U., Hutterli, M. A., Lambert, F., Kaufmann, P., Stauffer, B., Stocker, T. F., Steffensen, J. P., Bigler, M., Siggaard-Andersen, M. L., Udisti, R., Becagli, S., Castellano, E., Severi, M., Wagenbach, D., Barbante, C., Gabrielli, P., and Gaspari, V.: Southern Ocean sea-ice extent, productivity and iron flux over the past eight glacial cycles, Nature, 440, 491–496, doi:10.1038/nature04614, URL http://www.nature.com/nature/journal/v440/n7083/abs/nature04614.html, 2006.

Wolff, G. A., Billett, D. S. M., Bett, B. J., Holtvoeth, J., FitzGeorge-Balfour, T., Fisher, E. H., Cross, I., Shannon, R., Salter, I., Boorman, B., King, N. J., Jamieson, A., and Chaillan, F.: The Effects of Natural Iron Fertilisation on Deep-Sea Ecology: The Crozet Plateau, Southern Indian Ocean, PLoS ONE, 6, e20 697, doi:10.1371/journal.pone.0020697, URL http://dx.doi.org/10.1371/journal.pone.0020697, 2011.

Wright, S. W., Thomas, D. P., Marchant, H. J., Higgins, H. W., Mackey, M. D., and Mackey, D. J.: Analysis of phytoplankton of the Australian sector of the Southern Ocean: com-

parisons of microscopy and size frequency data with interpretations of pigment HPLC data using the 'CHEMTAX' matrix factorisation program, Marine Ecology Progress Series, 144, 285–298, doi:10.3354/meps144285, URL http://www.int-res.com/abstracts/meps/v144/p285-298/, 1996.

Xing, X., Morel, A., Claustre, H., Antoine, D., D'Ortenzio, F., Poteau, A., and Mignot, A.: Combined processing and mutual interpretation of radiometry and fluorimetry from autonomous profiling Bio-Argo floats: Chlorophyll a retrieval, Journal of Geophysical Research: Oceans, 116, C06 020, doi:10.1029/2010JC006899, URL http://onlinelibrary.wiley.com/doi/10.1029/2010JC006899/abstract, 2011.

Xing, X., Claustre, H., Blain, S., D'Ortenzio, F., Antoine, D., Ras, J., and Guinet, C.: Quenching correction for in vivo chlorophyll fluorescence acquired by autonomous platforms: A case study with instrumented elephant seals in the Kerguelen region (Southern Ocean), Limnology and Oceanography: Methods, 10, 483–495, doi:10.4319/lom.2012.10.483, URL http://www.aslo.org/lomethods/free/2012/0483.html, 2012.

Xing, X., Claustre, H., Uitz, J., Mignot, A., Poteau, A., and Wang, H.: Seasonal variations of bio-optical properties and their interrelationships observed by Bio-Argo floats in the subpolar North Atlantic, Journal of Geophysical Research: Oceans, 119, 7372–7388, doi:10.1002/2014JC010189, URL http://onlinelibrary.wiley.com/doi/10.1002/2014JC010189/abstract, 2014.

Xue, J., Lee, C., Wakeham, S. G., and Armstrong, R. A.: Using principal components analysis (PCA) with cluster analysis to study the organic geochemistry of sinking particles in the ocean, Organic Geochemistry, 42, 356–367, doi:10.1016/j.orggeochem.2011.01.012, URL http://www.sciencedirect.com/science/article/pii/S0146638011000301, 2011.

Yoon, W., Kim, S., and Han, K.: Morphology and sinking velocities of fecal pellets of copepod, molluscan, euphausiid, and salp taxa in the northeastern tropical Atlantic, Marine Biology, 139, 923–928, doi:10.1007/s002270100630, URL http://link.springer.com/article/10.1007/s002270100630, 2001.

Zeebe, R. E.: History of Seawater Carbonate Chemistry, Atmospheric CO2, and Ocean Acidification, Annual Review of Earth and Planetary Sciences, 40, 141–165, doi:10.1146/annurev-earth-042711-105521, URL http://www.annualreviews.org/doi/abs/10.1146/annurev-earth-042711-105521, 2012.

Zeebe, R. E. and Archer, D.: Feasibility of ocean fertilization and its impact on future atmospheric CO2 levels, Geophysical Research Letters, 32, L09 703, doi:10.1029/2005GL022449, URL http://onlinelibrary.wiley.com/doi/10.1029/2005GL022449/abstract, 2005.

Zhou, M., Zhu, Y., Measures, C. I., Hatta, M., Charette, M. A., Gille, S. T., Frants, M., Jiang, M., and Greg Mitchell, B.: Winter mesoscale circulation on the shelf slope region of the southern Drake Passage, Deep Sea Research Part II: Topical Studies in Oceanography, 90, 4–14, doi:10.1016/j.dsr2.2013.03.041, URL http://www.sciencedirect.com/science/article/pii/S0967064513001392, 2013.

Zhukova, N. V. and Aizdaicher, N. A.: Lipid and Fatty Acid Composition during Vegetative and Resting Stages of the Marine Diatom Chaetoceros salsugineus, Botanica Marina, 44, doi:10.1515/BOT.2001.037, URL http://www.degruyter.com/view/j/botm.2001.44.issue-3/bot.2001.037/bot.2001.037.xml, 2001.

Zielinski, U. and Gersonde, R.: Diatom distribution in Southern Ocean surface sediments (Atlantic sector): Implications for paleoenvironmental reconstructions, Palaeogeography, Palaeoclimatology, Palaeoecology, 129, 213–250, doi:10.1016/S0031-0182(96)00130-7, URL http://www.sciencedirect.com/science/article/pii/S0031018296001307, 1997.